Shenzhen River Regulation Office of Municipal Government

ENVIRONMENTAL IMPACT ASSESSMENT STUDY ON SHENZHEN RIVER REGULATION PROJECT

FINAL EIA STUDY REPORT (II)

Lead Consultant *Peking University*

Sub-Consultant(HK) *Axis Environmental Consultants Ltd.*
Consultant in Environmental Science(Asia) Ltd.

Other Consultant *Tsinghua University*
Xiamen University
Shenzhen Station of Environmental Monitoring
South China Institute of Environmental Science
Neilingding-Futian National Nature Reserve
The World Wide Fund for Nature Hong Kong(WWF)

APPENDICES

A5 AIR QUALITY BASELINE

A5.1 Results of Air Quality Baseline Monitoring
A5.2 Air Quality Model

A6 NOISE BASELINE

A6.1 Noise Baseline Monitoring
A6.2 Noise Model

A7 MODELING

A7.1 Hydrodynamic Modelling
A7.2 Sediment Transport Modelling
A7.3 1-D Steady State Water Quality Model
A7.4 Dynamic Water Quality Modelling

A8 WATER QUALITY BASELINE AND ASSESSMENT INDEX

A8.1 Water Quality Baseline of Deep Bay
A8.2 Water Quality Baseline of the Shenzhen River
A8.3 Pollution Sharing Rate
A8.4 Estimation of Deep Bay Topography Using Remote Sensing and GIS Technique

A9 SEDIMENT QUALITY AND SEDIMENTATION RATE

A9.1 Soil and Sediment Quality
A9.2 Vertical Distribution of Metal and Pesticide Contents along Sediment Profile
A9.3 Hakanson's Sediment Assessment Method
A9.4 Sedimentation Rates in Shenzhen River Estuary

APPENDIX 5 AIR QUALITY BASELINE

A5.1 Results of Air Quality Baseline Monitoring

Air quality monitoring were carried out at 2 sites on Shenzhen side and the sampling locations are shown in Figure 4.1. Five parameters measured were wind speed, wind direction, RSP, TSP, and dust. The results are stored in Database Management System in diskette format and listed in Table A5.1.

Table A5.1 Result of air quality baseline monitoring, 1994

Sampling Time		Yumin Village (A1)			Zhuan Matou (A2)		
		RSP (mg/m^3)	TSP (mg/m^3)	DUST ($t/km^2 \cdot mon$)	RSP (mg/m^3)	TSP (mg/m^3)	DUST ($mg/km^2 \cdot mon$)
94.03.23	AM	0.005		10.13	0.003		9.94
	PM	0.005	0.225		0.002	0.091	
94.03.24	AM	0.008		(94.03.24 - 94.04.25)	0.004		(94.03.24 - 94.04.25)
	PM	0.006	0.204		0.002	0.049	
94.03.25	AM	0.007			0.003		
	PM	0.006	0.218		0.002	0.175	
94.03.26	AM	0.002			0.003		
	PM	0.004	0.144		0.002	0.104	
94.03.27	AM	0.003			0.003		
	PM	0.003	0.111		0.003	0.106	
94.05.24	AM	0.002		13.68	0.002		reading lost
	PM	0.002	0.222		0.002	0.128	
94.05.25	AM	0.003		(94.04.30 - 94.05.30)	0.004		
	PM	0.004	0.219		0.003	0.111	
94.05.26	AM	0.002			0.002		
	PM	0.001	0.205		0.003	0.155	
94.05.27	AM	0.002			0.001		
	PM	0.005	0.221		0.003	0.164	
94.05.28	AM	0.004			0.003		
	PM	0.003	0.239		0.003	0.113	

A5.2 Air Quality Model

A5.2.1 Introduction

The Fugitive Dust Model(FDM) was used for air quality assessment of the Shenzhen River Training EIA project. It has been used within and outside the US Environmental Protection Agency(EPA) in regulatory applications, The model has undergone extensive reviews and peer revisions to correct and improve its technical features. It has been approved and recommended by the Hong Kong Government and applied in many major construction projects in Hong Kong.

A5.2.2 Model Description

The Fugitive Dust Model (FDM) is designed for the purpose of estimation of concentrations and

deposition impacts from fugitive dust sources. FDM can treat both turbulent and gravitational removal mechanisms for particulates. Concentrations are calculated according to the standard Gaussian plume formula. For deposition, the model uses the advanced gradient-transfer algorithm based on equations developed by Ermak. Up to 20 particle size classes can be analyzed. For each particle class, FDM requires a gravitational setting velocity and a deposition velocity, which can either be calculated by the model or defined by the user. The method uses friction velocity (which is a function od wind speed) and surface roughness heights as inputs.

A5.2.3 Data Requirements

Data requirements are show in Table A5.2.

Table A5.2 Basic work data for emission inventory calculations

	Total Working Site Area Stock Piling Area Barge Loading Area Total Permanent Haul Road Length Maximum Annual Reclamations(mg/yr) Description	Source of Data
1	Load from front load shovel to haul truck Material silt content(%) Drop height(m) Material moisture content(%) Shovel capacity(cu/m)	 from AP-42 from Engineer from Engineer from Engineer
2	Haul truck on unpaved site road Silt content of road surface material(%) Mean vehicle speed(km/hr) Mean vehicle weight(Mg) Mean number of wheel Number of days with > =0.254mm Average trip distance to and fro(lm) No. of vehicle trip per year	from AP-42 from Engineer from Engineer from Engineer from RO data from Engineer from Engineer
3	Site erosion Silt content(%) No. of day with > = 0.25mm rainfall Time with > 5.4m/s wind speed(%) Percentage active operating area(%)	from AP-42 from AP-42 from RO data of 1990 from Engineer

A5.2.4 Experience/ validation

Validation studies show that FDM Model performs well in charaterising dust concentrations in the vicinity of the fugitive dust source.

A5.2.5 Limitations

Sources are modelled as continuous. Complex terrain is not addressed.

A5.2.6 Technical Description of the FDM

The Fugitive Dust Model (FDM) is an analytical air quality model specifically designed for

the analysis of the dispersion of fugitive dust. The model incorporates a detailed deposition routine based on the equations of Ermak(1977). The basic equations as developed by Ermak are described in the remainder of this section. The general equation governing pollutant transport and dispersion in the atmosphere, when the pollutant is composed of uniformly-sized particles is as follows:

$$\frac{\partial \chi}{\partial t} = \frac{\partial}{\partial x} K_x \frac{\partial \chi}{\partial x} + u\frac{\partial \chi}{\partial x} + \frac{\partial}{\partial y} K_y \frac{\partial \chi}{\partial y} + \frac{\partial}{\partial z} K_z \frac{\partial \chi}{\partial z} + V_g \frac{\partial \chi}{\partial z} \qquad \text{(A5.1)}$$

where:

χ	=	concentration(g/m^3)
K_x, K_y, K_z	=	eddy diffusivity in the x, y and z directions(m^2/sec)
t	=	time(sec)
x,y,z	=	coordinates in three dimension space where x is parallel with the wind direction, y is perpendicular to x and parallel with the surface and z is perpendicular to both x and the surface(m)
u	=	wind speed(m/sec)
V_g	=	gravitational setting velocity(m/sec) where positive is in the downward direction

To solve equation(5.1), several simplifying assumptions are made. First the diffusion in the x direction is assumed to be small compared with the advection by the wind speed in that direction. This assumption eliminates the need consider any cases other than steady state. Second, the eddy diffusivities are assumed to be functions only of downwind distance (as will later be seen, further constraints are placed on the eddy diffusivity to obtain the gradient-transfer solution). The resulting diffusion equation is greatly simplified from equation (5.1):

$$u\frac{\partial \chi}{\partial x} = K_y \frac{\partial^2 \chi}{\partial y^2} + K_z \frac{\partial^2 \chi}{\partial z^2} + V_g \frac{\partial \chi}{\partial z} \qquad \text{(A5.2)}$$

A further assumption regarding the eddy diffusivity is made which generally means that the eddy diffusivity must be constant for all space and time. Actually, to obtain the solution, it is only necessary that the eddy diffusivity have the same functional dependance on the downwind distance as V_g. Since V_g is generally a constant, the eddy diffusivity in all directions is also assumed to be represented by a single parameter denoted by K. The relationship between K and the more commonly-seen diffusion parameter, the stand8ard deviation of the concentration in the y and z directions, σ_y and σ_z is as follows:

$$\sigma^2(x) = \frac{2}{u}\int_0^x K dx \qquad \text{(5.3)}$$

since K is to be assumed constant with x, it is obvious that the solution to be obtained is only strictly valid for cases where the σ varies as function of downwind distance to the 0.5 power. The equation thus obtained is:

$$X = \frac{Q}{2\pi\sigma_y\sigma_z u} e^{-\frac{y^2}{2\sigma_y^2}} e^{\left[-\frac{V_g(z-h)}{2k} - \frac{V_g^2\sigma_y^2}{8k^2}\right]}$$

$$[e^{-\frac{(z+h)^2}{2\sigma_z^2}} + e^{-\frac{(z+h)^2}{2\sigma_x^2}} - \sqrt{2\pi}\frac{V_1\sigma_z}{k}e^{[\frac{V(z+h)}{k}+\frac{v_1^2\sigma_z^2}{2k^2}]}erfc[\frac{V_1\sigma_z}{\sqrt{2}k} + \frac{z+h}{\sqrt{2}\sigma_z}]\,] \qquad (5.4)$$

where

χ	=	concentration in g/m^3
Q	=	Emission rate(g/sec)
u	=	wind speed(m/sec)
σ_y,σ_z	=	standard deviation of concentration in the y and z direction(m)
x,y,z	=	coordinates of the receptor(m)
V_g	=	gravitational settling velocity(m/sec)
h	=	plume centerline height(m)
K	=	eddy diffusivity(m^2/sec)
v_1	=	$U_d.V_g/2$
U_d	=	deposition velocity(m/sec).

A basic assumption in the solution of this equation is that deposition will be proportional to concentration at the surface. The deposition velocity is the proportionality constant (see equation (5.8) below). [Note: Ermak's original paper contained some typographical errors in the equation which have been corrected here]

With the assumption that K is constant and the assumption from equation(5.3) above, we can assume.

$$K = \frac{\sigma_z^2 u}{2x} \qquad (5.5)$$

The following two substitutions are made for convenience:

$$\gamma = \frac{v_1\sqrt{2}x}{\sigma_z u} + \frac{z+h}{\sqrt{2}\sigma_z} \qquad (5.6)$$

$$\beta = \frac{x}{\sqrt{2}\sigma_z} \qquad (5.7)$$

Whit these substitutions, equation(5.4) can be written in the form:

$$\chi = \frac{Q}{2\pi\sigma_y\sigma_{zu}}e^{[-\frac{v_g(z-h)\sqrt{2}\beta}{\sigma^2}-v_y^2\beta^2]}[e^{-\frac{(z-h)^2}{2\sigma_z^2}} - e^{-\frac{(z+h)^2}{2\sigma_z^2}} - 4\sqrt{\pi}V_1\beta\, e^{-\frac{(z+h)^2}{2\sigma_x^2}}\, e\gamma^2 erfc(\gamma)] \qquad (5.8)$$

The assumption regarding the behavior of K with respect to x leads to some inconsistencies when equation (5.4) is used with the standard Turner σ_y and σ_z curves. The inconsistency presents itself as a failure to conserve mass as the plume travels downwind. A numerical integration technique was used to calculate a correction term for modifying the concentration predictions of equation (5.4) to ensure that conservation of mass is obtained. The details of the development of the mass conservation correction factors are presented in the remainder of this section. The basic equation which defines the deposition algorithm is that

of this section. The basic equation which defines the deposition algorithm is that

$$D = U_d \chi|_{x=0} \tag{5.9}$$

where

D	=	Deposition rate
U_d	=	Deposition velocity
χ	=	Concentration

We can define corrected concentrations as the concentrations above, multiplied by some function of x, which we will call here q(x):

$$C = \chi q(x) \tag{5.10}$$

$$D = U_d q(x) c|_{x=0} \tag{5.11}$$

The requirement for mass conservation can be written as follows:

$$\int_0^k \int D dy dx + u \int\int C dy dz = Q \tag{5.12}$$

Substituting, we obtain the olowig fom ofthe aboe equatio:

$$\int_0^k u_d q(x) C_{cwi}|_{y=0} dx + u q(x) \int_0^\infty C_{cwi} dz = Q \tag{5.13}$$

where

$$C_{cwi} = \int c dy \tag{5.14}$$

Differentiating both sides of the equation by x we obtain:

$$u_0 q(x) C_{cwi} + u \frac{\partial}{\partial x} [q(x) (\int_0^\infty C_{cwi} dz)] = 0 \tag{5.15}$$

Reforming, we obtain a first-order differential equation in x:

$$\frac{\partial q(x)}{\partial x} u \int_0^\infty C_{cwi} dz + q(x) [u_d C_{cwi}|_{z=0} + u \frac{\partial}{\partial x} (\int_0^{inf C_{ww}} dz)] = 0 \tag{5.16}$$

The above equation was solved using a third-order Runge-Kutta integration process as follows:

$$LecA(x) = \int_0^\infty C_{cwi} dz \tag{5.17}$$

Then

$$\frac{\partial q(x)}{\partial x} u A(x) + q(x) [u_d C_{cwi}|_{z=0} + u \frac{\partial A(x)}{\partial x}] = 0 \tag{5.18}$$

$$\frac{\partial q(x)}{\partial x} = \frac{-q(x)[u_d C_{cwi_{x=0}} + u\frac{\partial A(x)}{\partial x}]}{uA(x)} \tag{5.19}$$

$$dq(x) = \frac{-q(x)\left|u_d C_{cwi_{x=0}} + u\frac{\partial A(x)}{\partial x}\right|}{uA(x)}dx \tag{5.20}$$

$$k_1 = \frac{-q_{x=x_1}\left(u_d C_{cwi_{x=x_1,z=0}} + u\frac{A|_{x=x_1}+\frac{dx}{2} - A|_{x=x_1}-\frac{dx}{2}}{dx}\right)}{uA_{x=x_1}}dx \tag{5.21}$$

$$k_2 = \frac{-q_{x=x_1}+\frac{k_1}{2}\left(u_d C_{cwi|_{x=x_1+\frac{dx}{2},z=0}} + u\frac{A|_{x=x_1+dx} - A|_{x=x_1}}{dx}\right)}{uA_{x=x_1+\frac{dx}{2}}}dx \tag{5.22}$$

$$k_3 = \frac{-(q_{x=x-1} + 2k_2 - k_1)\left(u_d C_{cwi|_{x=x_1+dx,z=0}} + u\frac{A|_{x=x_1+\frac{dx}{2}} - A|_{x=x_1+\frac{dx}{2}}}{dx}\right)}{uA_{x=x_1+dx}}dx \tag{5.23}$$

$$q_{x=x_1+dx} = q_{x=x_1} + \frac{k_1+4k_2+k_3}{6} \tag{5.24}$$

A variable step length (dx) was used for using the above numerical integration scheme to determine q(x). A total of 100 steps from 1 meter to 50,000 meters was used in the numerical integration. From these 100 values of downwind distance and q(x), a least squares fit was performed for an equation of the form:

$$\log(q(x)) = b_0+b_1\log(x)+b_2(\log(x))^2+b_3(\log(x))^3+b_4(\log(x))^4 \tag{5.25}$$

Separate values of $b_0 \cdots b_4$ were calculated for the combination of 6 different wind speeds. 6 different stability classes. 6 different particle size classes and 5 different release 2 heights. Over 1000 values of $b_0 \cdots b_4$ were computed and entered into the FDM code.

APPENDIX 6 NOISE BASELINE

A6.1 Noise Baseline Monitoring

Noise baseline monitoring has been carried out twice during March-April and May-June. Six sites are all on Shenzhen side and are given in Figure 4.1. The results are provided in the Database Management System in diskette format attached to this report and the statistics are tabulated in Table A6.1 and Table A6.2.

Table A6.1 Results of noise baseline monitoring during March-April, 1994

Site	Survey	Time	LeqD	LeqN	LeqdN	Leq(24)
N1	I	94.03.26-27	60.7	55.4	62.9	59.6
	II	94.03.27-28	61.4	55.5	63.2	60.1
N2	I	94.03.28-29	60.8	55.4	63.0	59.7
	II	94.03.29-30	61.3	63.3*	69.1	62.1
N3	I	94.03.31-01	60.0	58.1	64.5	59.4
	II	94.04.04-05	63.2	65.2*	70.9	64.0
N4	I	94.03.31-01	56.8	51.8	59.2	55.6
	II	94.04.04-05	50.5	49.6	55.8	50.3
N5	I	94.04.06-07	60.8	64.4*	70.0	62.3
	II	94.04.08-09	64.1	57.6	65.6	62.8
N6	I	94.04.07-08	49.5	47.8	49.0	48.9
	II	94.04.09-10	53.1	34.1	53.5	53.5

* monitoring were influenced by construction or navigation

Table A6.2 Result of noise baseline monitoring during May-June, 1994

Site	Survey	Time	LeqD	LeqN	LeqdN	Leq(24)
N1	I	94.05.24-25	62.0	58.7	65.5	61.1
	II	94.05.26-27	62.0	58.8	65.6	61.2
N2	I	94.06.06	60.5	54.6	62.3	59.3
	II	94.06.16	65.4	50.1	64.2	63.7
N3	I	94.06.16-17	60.0	58.1	64.5	59.4
	II	94.06.22-23	57.3	55.8	*	56.8**
N4	I	94.05.24-25	52.8	49.7	56.4	52.0
	II	94.05.27-28	55.4	53.0	59.5	54.7
N5	I	94.05.30-31	57.4	57.7	64.1	58.9
	II	94.06.01-02	61.7	57.1	64.4	60.6
N6	I	94.05.30-31	50.0	46.9	53.6	49.2
	II	94.06.06-07	49.8	54.0	59.6	51.7

* Reading lost
** Leq(23)

A6.2 Noise Model

Noise from construction and from construction traffic will be considered in the study.

A6.2.1 Construction noise

Construction noise from PME

Summary of procedures for the determination and the assessment of construction noise is as follows:

1) Location of the most effected the Noise Sensitive Receivers
2) Determination of the Area Sensitive Rating
3) Determination of Basic Noise Level
4) Correction for the duration of the Construction Noise Permit
5) Correction for multiple site situations
6) Determination of the Acceptable Noise Level
7) Location of items of PME
8) SWLs for items of PME
9) Distance attenuation and summation of noise levels
10) Corrections for the effect of barriers
11) Correction for acoustic reflections
12) Correction Noise Level at the Noise Sensitive Receivers

SWLs of the equipment were taken from Table 3 of the Technical Memoranda on Noise from Construction Work other than Percussive Piling. Where no SWL was supplied in this Technical Memorandum, then reference was made to British Standard (BS5228).

Attenuation for distances over 300m are not provided using the standard acoustical principles, the attenuation for distance was calculated by the following formula:

$$\textit{Distane Attenuation in } dB(A) = 20\log(D) + B \qquad (6.1)$$

where D is the distance in meters.

Noise from Percussive Piling

Procedures for the assessment of noise levels from percussive piling at the Noise Sensitive Receivers are summarized as

1) Location of the most affected Noise Sensitive Receiver
2) Determination of the Acceptable Noise Levels for the Noise Sensitive Receiver
3) SWL for percussive piling
4) Summation of noise levels
5) Distance attenuation
6) Corrections for the effect of barriers
7) Correction for the acoustic reflections

8) Corrected Noise level at the Noise Sensitive Receiver
9) Determination of the permitted hours of operation

A6.2.2 Construction traffic noise

Construction traffic can be divided into two categories:(a) construction traffic within the site area; and (b) construction traffic outside the side area.

Construction traffic noise within the site area

Noise levels generated from the mobile plant on haul road can be predicted by the following formula:

$$L_{eq} + L_w = 33 + 10\log_{10}Q - 10\log_{10}V - 10\log_{10}d \qquad (6.2)$$

where
L_w is the sound power level of the plant (dB);
Q is the number of vehicles per hour;
V is the average vehicle speed (km/hr)
d is the distance of receiving position from the centre of haul road (m).

The resultant noise levels at the Noise Sensitive Receivers can be estimated by incorporating the screening and reflection effects and the percentage of the assessment period for which activities takes place into the noise level obtained from the above formula.

Construction traffic noise outside the site area

Calculations were carried out using the UK Department of Transport Calculation of Road Traffic Noise, 1988(CRTN) which provides a general method for predicting noise levels at a distance from a highway, taking into account different traffic parameters, intervening ground cover, road configuration and site layout. However, prediction based on the CRTN method will constitute the preferred calculation technique but in a small number of cases traffic conditions may fall outside the scope of the prediction method and it will then be necessary to resort to measurement.

CRTN method of predicting noise at reception point from a road scheme consists of five main parts:

1) divide the road scheme into segments such that the variation of noise within the segment is small;
2) calculate the basic noise level at a reference distance of 10 m away from the near side carriageway edge for each segment;
3) assess for each segment the noise level at the reception point taking into account distance attenuation and screening of the source;
4) correct the noise level at the reception point to take into account site layout features including reflections from buildings and facades, and the size of the source segment; and

5) combine the contributions from all segments to give the predicted noise level at the reception point for the whole road scheme.

APPENDIX 7.1 HYDRODYNAMIC MODELLING

7.1.1 Introduction

The prime objective of the modelling is to provide a quantitative assessment of the hydrodynamic behaviours in both Shenzhen River and Deep Bay before and after the Stage 2 work. The 1—D flow model for Shenzhen River is based on the De Venant equation and Pressmann Scheme is adopted for numerical computation;the 2—D flow model for the Deep Bay is based on the horizontal two dimensional shallow flow equations.

7.1.2 1—D Flow Model for Shenzhen River

7.1.2.1 Basic Equations

The proposed 1-D model is consitituted with the unsteady flow model. The basic equations read: Continuity equation for flow

$$\frac{\partial Z}{\partial t}+\frac{1}{B}\frac{\partial Q}{\partial x}=0 \qquad (A7.1)$$

and momentum equation for flow

$$\frac{\partial Q}{\partial t}+\frac{\partial}{\partial x}\left(\frac{Q^2}{A}\right)+gA\left(\frac{\partial z}{\partial x}+\frac{Q|Q|}{k^2}\right)=0 \qquad (A7.2)$$

Where x and t are spatial and temporal variables; z, water level; B, flow width; Q, flow discharge; A, area of cross-section; K, discharge modulus; g, gravitational acceleration.

7.1.2.2 Computation Scheme

Equations (A7.1) and (A7.2) for th flow is discretized with the Preissmann four-point eccentric pattern as shown in Fig. A7.1. Thus,the equations after the transformation become

$$A_{1j}\triangle Q_j+B_{1j}\triangle z_j+C_{1j}\triangle Q_{j+1}+D_{1j}\triangle z_{j+1}=E_{1j} \qquad (A7.3)$$

and

$$A_{2j}\triangle Q_j+B_{2j}\triangle z_j+C_{2j}\triangle Q_{j+1}+D_{2j}\triangle z_{j+1}=E_{2j} \qquad (A7.4)$$

respectively. Where

$$A_{1j}=-\frac{4\theta\triangle t}{\triangle x\,(B_j^n+B_{j+1}^n)} \qquad (A7.5)$$

$$B_{1j} = 1 - \frac{4\theta\triangle t(Q^n_{j+1} - Q^n_j)}{\triangle x\,(B^n_{j+1} + B^n_j)^2} \cdot \frac{d\,B^n_j}{d\,z^n_j} \tag{A7.6}$$

$$C_{1j} = -\frac{4\theta\triangle t}{\triangle x\,(B^n_{j+1} + B^n_j)} \tag{A7.7}$$

$$D_{1j} = 1 - \frac{4\theta\triangle t(Q^n_{j+1} - Q^n_j)}{\triangle x\,(B^n_{j+1} + B^n_j)^2} \cdot \frac{d\,B^n_{j+1}}{d\,z^n_{j+1}} \tag{A7.8}$$

$$E_{1j} = -\frac{4\triangle t(Q^n_{j+1} - Q^n_j)}{\triangle x\,(B^n_j + B^n_{j+1})} \tag{A7.9}$$

$$A_{2j} = 1 - \frac{4\theta\triangle t}{\triangle x}\left(\frac{Q^n_j}{A^n_j}\right) + 2\triangle t g\theta\,\frac{A^n_j|Q^n_j|}{(k^n_j)^2} \tag{A7.10}$$

$$B_{2j} = \frac{\theta\triangle t}{\triangle x}\left[\frac{2(Q^n_j)^2 B^n_j}{(A^n_j)^2} - g\,(A^n_{j+1} + A^n_j) + g\,(z^n_{j+1} - z^n_j)B^n_j\right] + g\theta\triangle t\,\frac{Q^n_j|Q^n_j|}{(k^n_j)^2}\left[B^n_j - \frac{2A^n_j d\,k^n_j}{k^n_j d\,z^n_j}\right] \tag{A7.11}$$

$$C_{2j} = 1 + \frac{4\triangle t\theta Q^n_{j+1}}{\triangle x\,A^n_{j+1}}) + 2g\theta\triangle t\,\frac{A^n_{j+1}|Q^n_{j+1}|}{(k^n_{j+1})^2} \tag{A7.12}$$

$$D_{2j} = \frac{\theta\triangle t}{\triangle x}\left[-\frac{2(Q^n_{j+1})^2 B^n_{j+1}}{(A^n_{j+1})^2} + g\,(A^n_{j+1} + A^n_j) + g\,(z^n_{j+1} - z^n_j)B^n_{j+1}\right] + g\theta\triangle t\,\frac{Q^n_{j+1}|Q^n_{j+1}|}{(k^n_{j+1})^2}\left[B^n_{j+1} - \frac{2A^n_{j+1}d\,k^n_{j+1}}{(k^n_{j+1}d\,z^n_{j+1}}\right] \tag{A7.13}$$

$$E_{2j} = \frac{\triangle t}{\triangle x}\left[-\frac{2(Q^n_{j+1})^2}{A^n_{j+1}} + \frac{2(Q^n_j)^2}{A^n_j} - g\,(A^n_{j+1} + A^n_j)(z^n_{j+1} - z^n_j)\right] - g\,\triangle t\left[\frac{A^n_{j+1}Q^n_{j+1}|Q^n_{j+1}|}{(k^n_{j+1})^2} + \frac{Q^n_j|Q^n_j|A^n_j}{(k^n_j)^2}\right] \tag{A7.14}$$

Then, the solutions of Eqs. (A7.3) and (A7.4), by means of Runing-After Method, are

$$\triangle Q_j = F_j\triangle z_j + G_j \tag{A7.15}$$

$$\triangle z_j = H_j \triangle Q_{j+1} + I_j \triangle z_{j+1} + J_j \qquad (A7.16)$$

In which

$$H_j = \frac{-C_{1j}}{A_{1j}F_j + B_{1j}} \qquad (A7.17)$$

$$I_j = \frac{-D_{1j}}{A_{1j}F_j + B_{1j}} \qquad (A7.18)$$

$$J_j = \frac{E_{1j} - A_{1j}G_j}{A_{1j}F_j + B_{1j}} \qquad (A7.19)$$

$$F_{j+1} = -\frac{\alpha I_j + D_{2j}}{\alpha H_j + C_{2j}} \qquad (A7.20)$$

$$G_{j+1} = \frac{E_{2j} - \alpha J_j - A_{2j}G_j}{\alpha H_j + C_{2j}} \qquad (A7.21)$$

$$\alpha = A_{2j}F_j + B_{2j} \qquad (A7.22)$$

7.1.2.3 Input Information

The total area of the catchment of Shenzhen River is 312.5 km^2. The area within PRC is 187.5 km^2, and that in Hong Kong side is 125 km^2. There was no hydrologic monitoring station within the catchment and no data were available on flow and sediment characteristics. However, hydrologic calculations for the catchment should be carried out in terms of non-discharge conditions. In order to supply the input information such as runoff from different sub-catchments of Shenzhen River for the hydrodynamic modeling, the following calculations are needed.

There are two meteorological stations with relatively long-term records for the catchment. One is at Baoan Station on Shenzhen side which maintained records from July 1952 to 1993. The second is the Emperor Meteorological Station on Hong Kong side, which maintained records from 1884 to date (excepting 1940-1946).

The designed storm frequencies in the catchment were deduced from analysis of precipitation data. In 1982 the deduction method was used for hydrologic calculation of the preliminary design of the Shenzhen Flood Control and Engineering Works (Guangdong Institute of Hydraulic and Elec-

tric Survey and Design, 1982). The peak discharge of the designed flood as well as its occurrence time were predicted. In 1984 the synthetic unit line method (Shenzhen Office of Flood Control Planning 1994) was used for the same predictions. Comparison of the results from the two different methods shows that predicted peak discharges under different flood frequencies from the latter method are often larger than those from the former method.

The designed peak discharge deduced from the two different methods for Sha Wan River, Lian Tao River, and the Shang Shui River were basically the same. However, the designed peak discharge was increased 17-27 percent using the synthetic unit line prediction method. In the upper reaches of the Buji River (Sun Gang detention basin) the 1994 cross sectional area of the channel and the flood volume over 24 hours were essentially the same as those in 1982. However, the flood volume over 6 hours increased 50 percent. This implies that the runoff convergence process is faster owing to urbanization of the catchment.

It is necessary to know the inflow process of the tributaries during one flood between San Cha River and the Shenzhen River estuary so that flood routing of Shenzhen River can be carried out. The principal tributaries of the Shenzhen River in the study reach include the ShangShui, Buji, Futian, and Huang Gang Rivers. The Buji River receives flows from Sun Gang Detention Basin, Bijia Mountain, and Caiwu Wui. The flow from Chi Wui is too small to be considered. The comparison of the peak discharge predictions from the aforementioned two methods is given in Table A7—1.

Table A7—1 Peak discharges under different design frequencies by two calculattion methods

Q (m^3/s) Sta \ P	P=2%		P=5%		P=10%		P=20%	
	1982	1994	1982	1994	1982	1994	1982	1994
Sancha River	1014	1019	819	840	657	702	550	562
Shangshui River	745	768	603	632	486	528	408	422
Buji River	661	658	536	542	432	454	342	364
Futian River	188	199	154	165	125	139		112
Huanggang River	254	259	208	214	170	180		145

Table A7—2 The designed peak discharge(P=2%) with consideration of detention (m^3/s)

Section	Sancha River	Shangshui River	Buji River	Futian River	Huanggang River
1982	869	570	359	127	165
1994	895	566	389		

When predicting peak flood discharge the influence of the management alternatives of Shenzhen Reservoir and the Sun Gang Detention Basin should be considered. Also,the flood hydrographs for the junctions of Shenzhen River with Shang Shui River, Futian River and Huang Gang River are different from those designed since the overbank flow was not discounted in the design. Thus, the real peak discharges should be smaller than those from the designed peak discharges. The peak discharges at the junctions (P=2%) after consideration of flood adjustment are given in Table A7—2. The difference between the peak discharges in 1982 and those in 1994 are very small as shown in Table A7—1, thus both can meet the requirements for flood routing.

On the basis of the 1982 data (Table A7—2) the present study gives all the flood hydrographs at different tributary junctions along the Shenzhen River under four design alternatives corresponding to frequencies of 2, 5, 10, and 20%, respectively. The calculated results are given in Figures A7—2 to A7—6 in the Stage 1 report, and the peak discharges are listed in Table A7—3.

Table A7—3 Peak discharges from Sancha River and its principal tributaries

Q (m^3/s) Sta \ P	P=2%	P=5%	P=10%	P=20%
Sancha River	869	747	657	55
Shangshui River	570	442	360	253
Buji River	359	339	322	300
Futian River	127	103	83	66
Huanggang River	165	134	108	86

7.1.2.4 Verification and Predication

In 1—D model, the time steps are taken as 60 seconds for flood and 600 seconds (or 900

seconds) for tide flow. Cross sections along the river are derived from the topographic map of the channel measured in 1985. Within the study reach from Sacha River section to the Shenzhen estuary, 168 cross sections are divided for the existing channel and 148 ones for the channel after realignment. The roughness along the river are from the designed values suggested by Guang Dong Institute of Hydraulic and Electric Survey and Design, as shown in Table A7—4.

Table A7—4 Roughness of Shenzhen River

Area	Estuary— Yunong village	Yunong village —Lowu	Lowu— Sancha River
main flume	0. 020	0. 025	0. 0275
floodplain	0. 0267	0. 0333	0. 0367

1. Verification

The preliminary model runs have assumed the design parameters included in the Outline Design. This reflects the early stage of modelling work and is appropriate as any changes made to the channel design will have greatest influence on Stage 2 works.

The tributaries are simply considered as the inflow sources into Shenzhen River because of the paucity of the basic data. When small frequency flood appears in a tributary, the inflow is estimated according to the fullbank discharge. The verification of the flood level in the main channel is based on the record of the flood trace at five locations along the river, provided by the joint survey of Shenzhen Sanfang Office and Guangdong Institute of Hydraulic and Electric Survey and Designing (May 1989). The recorded actual tide type at Tsim Bei Tsui(as the boundary condition of the lower end) on the same day is used to match the flood equivelant to that with the return period of 1—in—5 years. The data measured at Yumin Village and Wenjindo in 1983 (typical tide from April to May and November) are used for the verification of the tide level. The results of verification are shown in Table A7—5 and Fig. A7—7 in the Stage 1 report.

2. Calculated Results

The modelling results based on 3 designed conditions with P equals to 2%, 5%, 10%, are obtained and shown in Fig. A7—2 to Fig. 7—4, including the water level and discharge variation before and after the stage 2 works. In Fig. A7—5, the modelling results based on both steady flow and unsteady flow model are also given, from which the greement of the predicted results from both models is clearly shown. The calculated results show that the water surface level will decrease owing to the stage 2 works, and the increase of tidal discharge is up to 1/3.

7. 1. 3 2—D Flow Model for Deep Bay

7. 1 . 3. 1 Basic Equations

The basic equations for the 2-D depth-integrated model consists of momentum and mass conservations, namely

$$\frac{\partial Z}{\partial t}+\frac{\partial Q}{\partial x}+\frac{\partial P}{\partial y}=s \qquad (A7.23)$$

$$\frac{\partial Q}{\partial t}+\frac{\partial uQ}{\partial x}+\frac{\partial vQ}{\partial y}+F'Q-\Omega P+gH\frac{\partial Z}{\partial x}=\nabla(K\nabla Q)+S_{mx} \qquad (A7.24)$$

$$\frac{\partial P}{\partial t}+\frac{\partial uP}{\partial x}+\frac{\partial vP}{\partial y}+F'P-\Omega Q+gH\frac{\partial Z}{\partial y}=\nabla(K\nabla P)+S_{my} \qquad (A7.25)$$

where z, water surface elevation; Q=uH; P=vH; H, the water depth; u and v, the velocity components in x and y directions, respectively; K, the momentum diffusion coefficient; Ω, the Coriolis coefficient; S, S_{mx} and S_{my}, source terms with respect to mass and momentum in x and y directions. In these equations, F′ is the resistant coefficient with the consideration of local energy loss due to rapid change in bathymetry and is expressed by

$$F'=\left(1+\zeta_s\frac{C_h^2\left|\bar{n}_Q\cdot\nabla H\right|}{g}\right)\frac{g\sqrt{Q^2+P^2}}{C_h^2H^2} \qquad (A7.26)$$

where $\vec{n}_Q$ is a unit vector of velocity; ∇H, water depth gradient; C_h, Chezy coefficient; ζ_s, an empirical parameter. At the land boundary, the resultant component of discharge normal to the boundary should vanish, i.e. $Q_n=0$. The flow boundary conditions are usually water stage or discharge hydrographs. When only one boundary condition is given on the water boundary (e.g. the stage hydrograph) and when the flow directs into the zone of computation, the assumption is tacitly made that the advective terms may be neglected. This amounts to the linearization of the momentum equations at the boundary. However, the error will increase obviously when the advection terms become large. In this case, adopting discharge hydrography as the condition on the water boundary has some merits. By applying the splitting technique, the basic equations (A7.23) to (A7.24) may be split into three sets of component equations:

$$\frac{\partial Q}{\partial t}+u\frac{\partial Q}{\partial x}+v\frac{\partial Q}{\partial y}=0 \qquad (A7.27)$$

$$\frac{\partial P}{\partial t}+u\frac{\partial P}{\partial x}+v\frac{\partial P}{\partial y}=0 \qquad (A7.28)$$

For this step, only one boundary condition needs to be given when the flow is directed into the zone of computation.

$$\frac{\partial Q}{\partial t} = \nabla(K\nabla Q) \qquad (A7.29)$$

$$\frac{\partial P}{\partial t} = \nabla(K\nabla P) \qquad (A7.30)$$

The initial state for this step is given by the results of the advection step. The boundary condition are $Q_n=0$ at the land boundary and the given hydrographs of Q and P at the water boundary. It is convenient to assume $\frac{\partial(Q,P)}{\partial n}=0$ at the downstream boundary for this step.

$$\frac{\partial Q}{\partial t} + F'Q - \Omega P + gH\frac{\partial z}{\partial x} = S_{mx} \qquad (A7.31)$$

$$\frac{\partial P}{\partial t} + F'P + \Omega Q + gH\frac{\partial z}{\partial y} = S_{my} \qquad (A7.32)$$

$$\frac{\partial z}{\partial t} + \frac{\partial Q}{\partial x} + \frac{\partial P}{\partial y} = S \qquad (A7.33)$$

The initial conditions for this step are defined by the values of Q and P obtained in the previous steps and the previous surface elevation. On the given boundary, stages or surface slope $\frac{\partial z}{\partial n}$ computed from given discharges may be taken as boundary conditions. The land boundary conditions is again $Q_n=0$, where n is the direction perpendicular to the boundary.

7.1.3.2 Computation Scheme

In order to integrate Eqs. (A7.27) to (A7.33) numerically, some preliminary derivations have to be done for the component equations (A7.30) to (A7.34) in a domain or local element as shown in Fig. A7—7. If the coefficient K in (A7.30) or (A7.31) is assumed to be constant and equal to the value at the center point C, and the two derivatives $\frac{\partial Q}{\partial t}$ and $\frac{\partial P}{\partial t}$ are replaced by finite differences, then the following relations may be derived from eqs. (A7.30) and (A7.31)

$$(\nabla_1^2 - \sigma_i^2)\bar{\Phi} + \sigma_i^2\bar{\Phi}_o = 0 \qquad (A7.34)$$

where

$\bar{\Phi}=(Q,P)^T$; $\nabla_1^2=\frac{\partial^2}{\partial\zeta^2}+\frac{\partial^2}{\partial\eta^2}$, local Laplace Operator; $\sigma_0^2=\triangle z^2/(K\cdot\triangle T)$, side length of a square grid; ζ and η, the local nondimensional coordinates. Subscript "o" refers to the initial status. For water surface elevation, we have

$$(\nabla_1^2 - \sigma^2)z + \sigma^2 S_r = 0 \qquad (A7.35)$$

and for Q and P:

$$Q=-\frac{\sqrt{gH_0}}{\sigma^2C_r^2(1+F_0)}\left[C_r(1+F_0)\frac{\partial z}{\partial\zeta}+C_r\omega\frac{\partial z}{\partial\eta}+(1+F_0)P_x+\omega P_y\right] \quad (A7.36)$$

$$P=-\frac{\sqrt{gH_0}}{\sigma^2C_r^2(1+F_0)}\left[C_r(1+F_0)\frac{\partial z}{\partial\eta}+C_r\omega\frac{\partial z}{\partial\zeta}+(1+F_0)P_y-\omega P_x\right] \quad (A7.37)$$

where

$$\sigma^2=\left[(1+F_0)^2+\omega^2\right]/C_r(1+F_0)$$

$$S_p=Z_0+S\triangle T+\left[\frac{\partial}{\partial\zeta}(\alpha_s P_y+P_x/C_r)+\frac{\partial}{\partial\eta}(P_y/C_r-\alpha_s P_x)\right]/\sigma^2$$

$$\alpha_s=\omega/(1+F_0)C_r$$

$$P_x=(\sigma_t^x F_0\zeta+\sigma_t^y F_0\eta-1)\frac{Q_0}{\sqrt{gH_0}}+C_r(\sigma_H^x\zeta+\sigma_H^y\eta)\frac{\partial Z_0}{\partial\zeta}-S_{mx}\triangle T$$

$$P_y=(\sigma_t^x F_0\zeta+\sigma_t^y F_0\eta-1)\frac{P_0}{\sqrt{gH_0}}+C_r(\sigma_H^x\zeta+\sigma_H^y\eta)\frac{\partial Z_0}{\partial\eta}-S_{my}\triangle T$$

$$\sigma_H^x=\frac{1}{H_0}\frac{\partial H_0}{\partial\zeta},\ \sigma_H^y=\frac{1}{H_0}\frac{\partial H_0}{\partial\eta}$$

$$\sigma_t^x=(Q_0\frac{\partial Q_0}{\partial\zeta}+P_0\frac{\partial P_0}{\partial\zeta})/(Q_0^2+P_0^2)-\frac{7}{3}\sigma_H^x$$

$$\sigma_t^y=(Q_0\frac{\partial Q_0}{\partial\eta}+P_0\frac{\partial P_0}{\partial\eta})/(Q_0^2+P_0^2)-\frac{7}{3}\sigma_H^y$$

where C_r is Courant number and the subscript "o" denotes the variables of the known state. CAS for the numerical solution of eqs. (A7.27) and (A7.28) in addition to the equation, $(\nabla_1^2-\sigma^2)\Phi+\sigma^2S_p=0$, further discusions are given as follows.

a) Application of the characteristic theory

Applying the theory of characteristics, one may obtain the following equations from the nonlinear hyperbolic eqs. (A7.27) and (A7.28), or

$$\frac{dQ}{dt}=\frac{\partial Q}{\partial t}+\frac{dx}{dt}\frac{\partial Q}{\partial x}+\frac{dy}{dt}\frac{\partial Q}{\partial y}=0 \quad (A7.38)$$

$$\frac{dP}{dt}=\frac{\partial P}{\partial t}+\frac{dx}{dt}\frac{\partial P}{\partial x}+\frac{dy}{dt}\frac{\partial P}{\partial y}=0 \quad (A7.39)$$

$$\frac{dx}{dt} = \frac{Q}{H} \qquad (A7.40)$$

$$\frac{dy}{dt} = \frac{P}{H} \qquad (A7.41)$$

As shown in Fig. A7—8, $M(x_o, y_o)$ is the point of intersection of characteristics extending from a point P to the previous time plane. Discharges Q and P remain unchanged along the line PM, so that

$$Q_p = Q(x, y, t) = Q(x_0, y_0, 0) \qquad (A7.42)$$

and

$$P_p = P(x, y, t) = P(x_0, y_0, 0) \qquad (A7.43)$$

Now suppose ξ, η be the local nondimensional coordinates and the water depth be replaced by the bilinear interpolation of the grid values, then point M is determined by

$$\zeta = \frac{\triangle T \cdot Q_0(\zeta, \eta)}{\triangle X \cdot H_{s1}(\zeta, \eta)} \qquad (A7.44)$$

$$\eta = \frac{\triangle T \cdot P_0(\zeta, \eta)}{\triangle y \cdot H_{s2}(\zeta, \eta)} \qquad (A7.45)$$

where

$$H_{s1} = H_1(\xi - \zeta^2/2)(1-\eta) + H_2\zeta^2(1-\eta)/2 + H_3\zeta^2\eta/2 + H_4(\zeta - \zeta^2/2)\eta$$

$$H_{s2} = H_1(1-\zeta)(\eta - \eta^2/2) + H_2\zeta(\eta - \eta^2/2) + H_3\zeta\eta^2/2 + H_4(1-\zeta)\eta^2/2$$

Q_o, P_o can evaluated with either bilinear interpolation or the interpolation method proposed by Holly and Preissmann. Eqs. (A7.44) and (A7.45) are nonlinear algebraic equations and can be solved with Newton method or Newton-Rophson method.

b)Finite analytical method

According to the finite analytical method (Chen), the common equation

$$(\nabla_1^2 - \sigma^2)\Phi + \sigma^2 S_p = 0 \qquad (A7.46)$$

can be solved analytically in the subdomain within the domain of computation if coefficient is fixed and the boundary function is assigned with the grid values of Φ_{NE}, Φ_{SE}……Φ_{NC} by parabolic inter-

polation. The general solution may be written:

$$\Phi = f(\Phi_N(\zeta), \Phi_S(\zeta), \Phi_E(\eta), \Phi_W(\eta), \triangle x, \triangle y, \zeta, \eta, \sigma^2, S_r) \qquad (A7.47)$$

Substituting the interpolation functions $\Phi_N(\zeta)$, $\Phi_S(\zeta)$, $\Phi_E(\eta)$, $\Phi_W(\eta)$ into the foregoing equation, yields

$$\Phi = f(\Phi_{NE}, \Phi_{SE}, \cdots\cdots \Phi_{NC}, \triangle x, \triangle y, \zeta, \eta, \sigma^2, S_r) \qquad (A7.48)$$

The actual form of Eq. (A7.48) has been given in Zhou(1988). Let $\zeta=\eta=0$, the algebraic relationship for Φ_p with the eight surrounding grid points becomes:

$$\Phi_r = C_{EC}\Phi_{EC} + C_{WC}\Phi_{WC} + \cdots\cdots + C_{SW}\Phi_{SW} + C_{SE}\Phi_{SE} + C_P S_P \qquad (A7.49)$$

where C_{EC}, C_{SC}, ... C_{NE} are known coefficients. Since the equation is symmetrical in form and $\triangle_x=\triangle_y$, the coefficients satisfy the relations of $C_{EC}=C_{SC}=C_{WC}=C_{NC}=C_0$ and $C_{NE}=C_{SE}=C_{SW}=C_{NW}=C_d$. C_o, C_d and C_p may be further evaluated by the following equations

$$C_0 = 2\sum_{n=1}^{\infty} \frac{(-1)^{n+1}}{\lambda_{2n-1}^3 \cosh \beta_{2n-1}}$$

$$C_d = \sum_{n=1}^{\infty} (-1)^{n+1}\left(1 - \frac{2}{\lambda_{2n-1}^2}\right) \frac{1}{\lambda_{2n-1}\cosh(\beta_{2n-1})}$$

and

$$C_r = \sum_{m=1}^{\infty}\sum_{n=1} \frac{4(-1)^{m+n}}{(\sigma^2 + \lambda_{2n-1}^2 + \lambda_{2m-1}^2)\lambda_{2n-1}\lambda_{2m-1}}$$

where $\lambda_m = n\pi/2$, $\beta_n = \sqrt{\lambda_n^2 + \sigma^2}$

7.1.3.3 Basic Requirements of the Model

The range of modelling is from the upper end of Shenzhen Estuary to the mouth of Deep Bay bordered Chi Wan and Black Point. 100x100m square grid is used and the time steps are 40 seconds. Fluctuating boundary method is used to simulate the change of intertidal areas due to the rise and fall of the tide flow.

The boundary condition of water level at the mouth of Deep Bay is obtained by the interpolation method using the measured tide level data in Chi Wan and Black Point. In the estuary of Shenzhen River, the flow discharge boundary condition are calculated according to the tidal flow discharge hydrograph offered by 1—D calculation model.

Since there is no overall sea—chart on Deep Bay for recent years, and the existing chart of 1: 50000 can not be used to simulate the topography of river mouth and the mud flat, additional measures are adopted as such:

a) The data of CED Model with 300m×300mm grid from Hong Kong is used.

These data give the detailed description on the major part of Deep Bay, but can not show the micratopography change in river mouth area, even can not show the elevation of the two main channels in river mouth (the major course of Shenzhen River for sea transportation).

b) The remote sensing photograph of satellite (at 9:00 in Dec. 21, 1992) is used for improvement treatment of the bathymetry.

The photographs are used to recover the topography of the river mouth of Shenzhen River and mud flat around it, and the elevation of these areas are obtained. These data show the precise of 30m in plane, and the error of the predicted depth is within 10 cm. The microtopography of the river mouth area is also clear in the graph.

The final bed elevation of the Deep Bay obtained from the two group data is shown in Fig. A7—9.

The data measured in Mar. 1—4, 1994 is used to verify the hydrodynamic model. The measurement of water level was made both in Black point and river mouth. The data for Chi Wan during this period is obtained from Ocean Observation Station. Through analysis, we can find that the character istics of tide level in Chi Wan and Black Point are basicly the same. The phase lag of tide flow at Chi Wan is 600 seconds behind that at Black Point.

The data of spring, average and neap tide in July 1994 are used for the basis of predictions. At the same time, according to the former analysis, the tide level of Black Point are believed the same as that of Chi Wan but with a 600 second advance. The typical tide types used here in are depicted in Fig. A7—10.

Considering the difference of sea bed of intertidal areas of Deep Bay and deep water area, roughness over different areas is used in the calculation. Because of the effects of shell on water flow, shallow water areas shows high roughness. The distribution of roughness is presented in Fig. A7—11. The data of roughness are calibrated with the flow field calculation.

7.1.3.4 Verification and Predication

1. Verification

The verification of the model has been made in the Stage 1 report.

2. Modelling Results

The modelling results indicate that the flow discharge entering Deep Bay from Shenzhen River have no significant difference pre and post the Project for all the combination of tide types and seasons. Therefore, the hydrodynamic condition changes little pre and post the Project. The flow field from the modelling results for different runs are shown in Figs. A7—12 to A7—14.

APPENDIX 7. 2 SEDIMENT TRANSPORT MODELLING

7. 2. 1 Introduction

The principal purpose of the modelling is to study the sediment erosion and deposition in Shenzhen River and Deep Bay, especially in the areas of Futian, Mai Po and the inter—tital mud flats at the mouth of Shenzhen River.

The concern is primarily for the long term impact of the changes in the depositional environment resulting from the regulation works and any future maintenance dredging.

7. 2. 2. 1 Basic Equations

The proposed 1—D sediment model is constituted with the unsteady flow model and the nonequilibrium transport model of suspended load without considering the bed load due to the paucity of primary data. The basic equations are as follows.

The proposed 1-D model is consitituted with the unsteady flow model. The basic equations read: Continuity equation for flow

$$\frac{\partial Z}{\partial t} + \frac{1}{B}\frac{\partial Q}{\partial x} = 0 \qquad (A7.50)$$

Momentum equation for flow

$$\frac{\partial Q}{\partial t} + \frac{\partial}{\partial x}\left(\frac{Q^2}{A}\right) + gA\left(\frac{\partial z}{\partial x} + \frac{Q|Q|}{k^2}\right) = 0 \qquad (A7.51)$$

Continuity equation for suspended sediment

$$\frac{\partial (Qs)}{\partial x} + \frac{\partial (As)}{\partial t} = -\alpha\omega B(s - s_*) \qquad (A7.52)$$

Sediment-laden capacity

$$s_* = k\left(\frac{u^3}{gh\omega}\right)^m \qquad (A7.53)$$

Bed deformation equation

$$\rho' \frac{\partial z_0}{\partial t} = \alpha\omega(s - s_*) \qquad (A7.54)$$

in which s_*, sediment-laden capacity; ω, settling velocity of sediment particles; z_0, average bed elevation; ρ', dry specific gravity of sediment; α, sediment saturation recovery coefficient; k and m, coefficient and exponential index in Eq. (A7.54).

7.2.2.2 Computation Scheme

With the same computation scheme for flow, sediment continuity equation (A7.54) and bed deformation equation (A7.52) are written as follows in accordance with the finite—difference scheme, that is

$$s_j^{n+1}=\frac{\Delta t\alpha_j^{n+1}\beta_j^{n+1}\omega_j^{n+1}s_{*j}^{n+1}+A_j^n s_j^n+\frac{\Delta t}{\Delta x_{j-1}}Q_{j-1}^{n+1}s_{j-1}^{n+1}}{A_j^{n+1}+\Delta t\alpha_j^{n+1}B_j^{n+1}\omega_j^{n+1}+\frac{\Delta t}{\Delta x_{j-1}}Q_j^{n+1}}Q\geqslant 0 \qquad (A7.55)$$

$$s_j^{n+1}=\frac{\Delta t\alpha_j^{n+1}\beta_j^{n+1}\omega_j^{n+1}s_{*j}^{n+1}+A_j^n s_j^n-\frac{\Delta t}{\Delta x_j}Q_{j+1}^{n+1}s_{j+1}^{n+1}}{A_j^{n+1}+\Delta t\alpha_j^{n+1}B_j^{n+1}\omega_j^{n+1}-\frac{\Delta t}{\Delta x_j}Q_{j+1}^{n+1}}Q>o \qquad (A7.56)$$

Correspondingly, the bed deformation equation is changed to

$$\Delta z_0=\frac{\Delta t}{\rho'}[\alpha_j^{n+1}\omega_j^{n+1}(s_j^{n+1}-S_{*j}^{n+1})] \qquad (A7.57)$$

All the calculations in the 1-D model are based on the equations mentioned above. the scheme is shown in Fig. A7—15.

7.2.2.3 Basic Requirements of the Model

1. Estimation of the Sediment Volume Entering the Shenzhen River

There are few available data on sediment yield for the entire Shenzhen River catchment. In addition, dramatic recent changes in the natural geographic conditions of the catchment in Shenzhen make it even more difficult to estimate the sediment yield. The following calculation was carried out primarily based on the limited data which were specially collected for this study.

The data available for estimation of sediment yield included sediment yield records from Hong Kong and monitoring data on suspended solids (SS) in Shenzhen River. The former were drawn from BMP (Basin Management Planning, Hong Kong) reports in which sediment yield in three small basins (Basins 10, 11, and 12) were given in Table. A7—5. The latter database is from regular monitoring of SS in Shenzhen River and its tributaries since 1985. The statistical results are listed in Table A7—6 and shown in Figures A7—36 to A7—39 in the Stage 1 report.

$$\alpha_* = \frac{R_*^4(R_* + 6)}{p_0(R_* + 6)R_*^3 - 12R_*(R_* + 3)(R_* - 2\theta_* - 0.25R_*^3) + 12(6\theta_* - 3 + R_*^2 - 0.2R_*^4)(R_* + 2)} \tag{A7.63}$$

where

$$\theta_n = 1 - \frac{(1 - e^{-R_n})}{R_n}, p_n = \begin{cases} 1 & S_n > \Phi_n \\ e^{-R_n} & S_n \leqslant \Phi_n \end{cases}$$

$R_n = \frac{6\omega_n}{\kappa u_*}$ herein is the Rouse number and κ, the von Karmann universal constant; u_*, friction velocity.

The equation of bed deformation due to nonumiform sediment erosion or deposition is obtained from the theorum of the solid mass conservation

$$\frac{\partial \eta}{\partial t} = \sum_{n=1}^{N_0} \alpha_n \omega_n \frac{S_n - \Phi_n}{\gamma_m} \tag{A7.64}$$

where η is the depth of bed deformation ($\eta < 0$ for erosion) and γ_m is the dry unit weight. In Eq (A7.62), S_n^* is proportional S^*, which is the transport capacity of flow corresponding to the mean size of sediment, i.e.,

$$S_n^* = P_n^* S^* \tag{A7.65}$$

where P_n^* is the percentage of concentration of group n under equilibrium condition; ω_m, mean settling velocity of the sediment, which is evaluated by

$$\omega_m = \left(\sum_{n=1}^{N_0} P_n^* \omega_n^{m_0}\right)^{\frac{1}{m_0}} \tag{A7.66}$$

According to the widely used formula in China, S^* may be well predicted by

$$S^* = K_s\left(\frac{U^3}{g H \omega_m}\right)^{m_0} \tag{A7.67}$$

where K_s and m_0 are empirical constants. The percentage of concentration P_n^* in Eq. (A7.65) is expressed as

$$P_n^* = a_n P_{bn} / \sum_{n=1}^{N_0} a_n P_{bn} \qquad (n = 1, 2, \cdots\cdots N_0) \tag{A7.68}$$

in which

$$a_s = (1 - A_s)\frac{1 - e^{-R_s}}{\omega_s}, A_s = \frac{\omega_s}{\frac{u_*}{\sqrt{2\pi}} e^{-\frac{\omega_s^2}{2u_*^2}} + \omega_s \psi(\frac{\omega_s}{u_*})}, \psi(x) = \int_{-\infty}^{x} \frac{1}{\sqrt{2\pi}} e^{-\frac{t^2}{2}} dt$$

In the process of nonuniform sediment transport, the bed material is unceasingly alternating itself and it has to be known before computations of each time step. It is easy when all groups of sediment are in deposition, but it would be rather complicated if only some groups of sediment are eroded from the bed. In the present study, a potential depth is used, which is proportional to the actual erosion depth during the former time step, or $\triangle_b = \beta\alpha_e$, where β ranges from 2.0 to 2.5. The bed material distribution is then computed with

$$P_{bs} = \frac{P_{bs}^0 \triangle_b + \delta_s}{\triangle_b + \delta_d - \delta_e} \tag{A7.69}$$

in which, $\alpha_d = \sum_{\delta_n > 0} \delta_n, \delta_e = -\sum_{\delta_n < 0} \delta_n$ For most of the practical cases, lateral erosion should also be considered. A simple relation is suggested for the evaluation of the lateral erosion rate

$$\frac{d\triangle}{dt} = \frac{\Psi}{\gamma_s v^2}(\tau - \tau_c)\tau \tag{A7.70}$$

where $\triangle$ is the width being washed away; τ, the tangent shear force of the flow acting on the wall; and τ_c, the incipient shear force. In practical computations, the laterally eroded material is assumed to be stacked on the closeast grid which is under the water surface and may be washed away in the next step.

7.2.3.2. Computation Scheme

By appling the split-operator method, the basic equation for suspended sediment may be split into two sets of component equations, i.e.,

$$\frac{\partial S_s}{\partial t} + \frac{\partial u S_s}{\partial x} + \frac{\partial v S_s}{\partial y} = 0 \tag{A7.71}$$

For this step only inflow sediment concentration is needed as boundary condition and the concentration of the previous time step is taken as initial condition.

$$\frac{\partial S_s}{\partial t} = \frac{\partial}{\partial x} K_x \frac{\partial S_s}{\partial x} + \frac{\partial}{\partial y} K_Y \frac{\partial S_s}{\partial y} \tag{A7.72}$$

The initial state for this step is given by the results of i) and the land boundary condition is $\frac{\partial S_n}{\partial n} = 0$

$$\frac{\partial S_s}{\partial t} = -\alpha_s \omega_s \frac{S_s - \Phi_s}{H} \tag{A7.73}$$

Characteristic coordinates scheme is adopted to decomposite eq. (A7.71). As a result, it is transformed into

$$\frac{\partial S_s}{\partial t} + \frac{\partial u_\xi S_s}{\partial \xi} + \frac{\partial u_\eta S_s}{\partial \eta} = 0 \qquad (A7.74)$$

By droping the term $\frac{\partial u_n S_n}{\partial \eta}$, representing the mass around point P, the finite difference equation yields

$$S_s = S_s^0 + \frac{\Delta T_s}{\Delta l}(U_p S_s - U_{M\xi} S_{sM}) \qquad (A7.75)$$

The subcripts A, B, C, D, P and M denote the points shown in Fig. A7—54. In eq. (A7.67), Δl, U_p, $U_{m\xi}$ are defined, respectively

$$\Delta l = M\bar{P}, U_p = \sqrt{u_p + V_p}, U_{M\xi} = \sqrt{u_M + V_m} cos\gamma \qquad (A7.76)$$

As for the equation (A7.73), a simple solution is avaialble.

$$S_s = \Phi_s(1 - e^{\frac{-\alpha_s \omega_s \Delta T_s}{H}}) + S_s^0 e^{-\frac{\alpha_s \omega_s \Delta T_s}{H}} \qquad (A7.77)$$

7.2.3.3 Basic Requirements of the Model

Time step for both 1—D and 2—D models is 80 seconds. Other requirements are the same as those described in Appendix 7.2.3.3 in the Stage 1 report.

7.2.3.4 Modelling Results

Although the sediment concentration in the river mouth region increases apparently during the construction of Stage 2 works, it decreases in all the cases after Stage 2 works. In general, the works has little effect on the region beyond the river mouth. The modelling results of maximum sediment concentration, mean concentration and deposition thickness in Deep Bay within 2 days during the construction of Stage 2 works are shown in Fig. A7—20～A7—22.

Those corresponding to the runs after Stage 2 works are shown in Fig. A7—23～A7—25.

APPENDIX 7. 3 1—D STEADY STATE WATER QUALITY MODEL

7. 3. 1 Introduction

The principal purpose of the present model is to study the time—averaged water quality of the Shenzhen River and Estuary over tidal cycles before and after the Stage 2 works.

For the assessment of the environmental impact of Shenzhen River training works, a 1-D estuary water quality model with BOD_5-DO coupling is applied to simulate and estimate the time-averaged water quality of Shenzhen River over tidal cycles. Then, single-component water quality models are used for the modeling and prediction of other contaminants such as TN, TP and heavy metals. In each of these 1-D models, finite-reach method is adopted to divide the 1-D estuary into reaches of finite length, so that for each reach the mass conservation principle can be applied to derive the water quality model acounting the hydrodynamic behavior of the river flow. This type of models has been widely applied to the planning and assessment of water quality and environmental impact.

Descretization of Shenzhen River estuary region by using number of volumes of finite length are reqired in order to apply the 1- D steady state estuary finite- reach model of finite- reaches. An additional restrict condition for the model application is the assumption of water in each reach being well-mixed. According to the topographical, hydrological and geological data as well as the needs for the assessment of environmental impact of the training works of Shenzhen River, totally 10 reaches as shown in Fig. A7—26 are adopted to discretize the estuary region, with reach No. 1 to No. 6 for Shenzhen River and No. 8 to No. 10 for Deep Bay. In the Fig. A7—26, the length of each reach and the locations of each tributary and the sewage-releasing works are shown. Shorter reaches are used for the middle part of Shenzhen River with the consideration of the facts that a greater concentration gradient is easily to occur in this region and that the inflows of tributaries including Shangshui Tributary and Buji Tributary often carry a great amount of contaminants into the region considered. Only 4 reaches are used for the part of Deep Bay due to several reasons. The first reason is that the concentration gradient is relatively small in the bay region;the second important reason is that flow recirculation causing currents in the transverse direction should be avoided with a simple 1-D model, so that the main stream of each reach could be kept as mornal to its upstream and downstream control-faces as possible. In addition, the water depth should not vary too much between two neighboring reaches.

7. 3. 2 Basic Equations

7. 3. 2. 1 1-D Analytical Solution

If C represents the time-average concentration of contaminant over tidal cycles, then the 1-D estuary water quality model may be written as

$$D_x \frac{\partial^2 C}{\partial x^2} - \frac{\partial (u_x \cdot C)}{\partial x} + r + s = 0 \qquad (A7.78)$$

where r, decay rate of the contaminant; s, input rate of the contaminant into the system under consideration; D_x, streamwise dispersion coefficient; u_x, flow velocity (m/s); c, concentration of the contaminant (mg/l); x, distance from the starting cross-section.

For the case of no time-variation in cross-sectional area and fresh water runoff, O'Connor obtained, by assuming s=0 and r=-KC, the analytical solution of the 1-D model, as follows

$$\frac{C}{C_0} = exp(j_1 \cdot x) \qquad (A7.79)$$

for x<0 (upstream of the releasing location) and

$$\frac{C}{C_0} = exp(j_2 \cdot x) \qquad (A7.80)$$

for x>0 (downstream of the releasing location)
In (A7.79) and (A7.80),

$$j_1 = \frac{u_x}{2D_x}(1 + \sqrt{1 + \frac{4KD_x}{u_x^2}}) \qquad (A7.81)$$

$$j_2 = \frac{u_x}{2D_x}(1 - \sqrt{1 + \frac{4KD_x}{u_x^2}}) \qquad (A7.82)$$

C_0, the contaminant concentration at x= 0, may calculated by the following formula

$$C_0 = W/(Q\sqrt{1 + \frac{4KD_x}{u_x^2}}) \qquad (A7.83)$$

where W, amount of contaminant discharge per unit time; Q, time-averaged fresh water runoff. The streamwise dispersion coefficient may be estimated by the following empirical formula

$$D_x = 63nu_m R^{5/6} \qquad (A7.84)$$

where n, Manning's roughness coefficient; u_M, velocity of the primary tide; R, hydaulic radius of the estuary cross-section.

The dispersion coefficent of the estuary is obtained by measuring, at a downstream location, the time variation of the concentration of the tracer that is released instantly into the river flow. For the case of salt-water intrusion, salt of the sea water may be used as the tracer. In this situation, the mass variation of the salt follows the conservation principle, and if r=0 and s=0 could be assumed, then the analytical solution of (A7.78) becomes

$$ln\frac{C}{C_0} = \frac{u_x}{D_x} \cdot x \qquad (A7.85)$$

where x is the distance measured towards the upstream, and $x<0$. Hence, the dispersion coefficient

$$D_x = x u_x/(lnC - lnC_0) \qquad (A7.86)$$

In the present study, two methods are adopted to estimate D_x, by using empirical formula and by using salt-tracer for estimation, so that the results can be verified by each other.

7.3.2.2 BOD-DO Coupled Model

For the 1-D steady state problem, the governing equation for oxygen deficit (D) may be written as

$$D_x \frac{\partial^2 D}{\partial x^2} - u_x \frac{\partial D}{\partial x} - Ka \cdot D + Kd \cdot L = 0 \qquad (A7.87)$$

If the boundry condition $D=0$ at $x=\pm\infty$ could be assumed, the solution of above equation can be obtained as

$$D = \frac{Kd \cdot W}{(Ka-Kd)Q}(A_1 - B_1) \qquad (A7.88)$$

for $x<0$ (upstream of the discharge point) and

$$D = \frac{Kd \cdot W}{(Ka-Kd)Q}(A_2 - B_2) \qquad (A7.89)$$

for $x>0$ (downstream of the discharge point)
where

$$A_1 = exp\left[\frac{u_x}{2D_x}(1 + j_3) \cdot x\right]/j_3 \qquad (A7.90)$$

$$A_2 = exp\left[\frac{u_x}{2D_x}(1 + j_4) \cdot x\right]/j_4 \qquad (A7.91)$$

$$B_1 = exp\left[\frac{u_x}{2D_x}(1-j_3) \cdot x\right]/j_3 \qquad (A7.92)$$

$$B_2 = exp\left[\frac{u_x}{2D_x}(1-j_4) \cdot x\right]/j_4 \qquad (A7.93)$$

$$j_3 = \sqrt{1 + \frac{4Kd \cdot D_x}{u_x^2}} \qquad j_4 = \sqrt{1 + \frac{4Ka \cdot D_x}{u_x^2}}$$

7. 3. 3 Computational Scheme

With the finite-reach model, a number of reaches of finite length being sequentially located in the stramwise direction are used in the replacement of the original continuous reach. For each of the finite reaches, water body is assumed being fully-mixed or being able to be described by a 0-D model, so that the entire estuary can be simulated by a 1-D model. With the finite reach-model, the modeled quantities, including the state variables and model parameters, represent the time average over tidal cycles, and the flow rate of the model is the net river runoff.

7.3.3.1 BOD Model

For any of the river reaches, the mass transport is related to three phenomena of convection, dispersion and material decay.

The amount of transport of the i-th reach due to convection is

$$Q_{i-1}L_{j-1} - Q_iL_j$$

where, net inflow and outflow of the i-th reach, respectively; L_{i-1}, L_i, BOD concentration of inflow and outflow of the ith reach, repectively; The contribution of dispersion effect to the mass variation of the i-th reach is

$$D_{j-1,i}A_{i-1,i}\frac{L_{i-1}-L_i}{\triangle x_{j-1,j}} - D_{j,i+1}A_{i,i+1}\frac{L_j-L_{j+1}}{\triangle x_{j,i+1}}$$

$$\triangle x_{ij} = \frac{1}{2}(\triangle x_i + \triangle x_j)$$

where D_{ij}, dispersion coefficient between the i-th and j-th reaches; A_{ij}, area of the interface between the i-th and j-th reaches; Δx_{ij}, distance between the centers of the i-th and j-th reaches.
The BOD_5 dacay rate of the i-th reach is

$$V_i \cdot Kd_i \cdot L_i$$

where V_i, volume of the i-th reach; K_{di}, decay coefficient of BOD_5.
Hence, the mass balance for each reach may be written as

$$V_j\frac{dL_j}{dt} = Q_{i-1}\cdot L_{i-1} - Q_iL_j + D_{i-1,j}\cdot A_{j-1,i}\cdot\frac{L_{j-1,j}-L_j}{\triangle x_{j-1,i}} - D_{j,i+1}\cdot A_{j,i+1}\frac{L_i-L_{j+1}}{\triangle x_{j,i+1}} - V_iKd_j\cdot L_j + W_i' \qquad (A7.94)$$

If $D_{ij}=D_{ij}\cdot A_{ij}/\Delta x_{ij}$ is used, then eq. (A7.94) may be rewritten as

$$V_i \frac{dL_j}{dt} = Q_{j-1} \cdot L_{i-1} - Q_i \cdot L_j + D'_{j-1,j}(L_{i-1} - L_j)$$
$$-D_{i,j+1}(L_i - L_{i+1}) - V_i K d_i \cdot L_i + W_i^L \qquad (A7.95)$$

In eqs. (A7.94) and (A7.95), W_j^L, inflow rate of BOD to the i-th reOach from outside.

If D_j stands for the the oxygen deficit of the i-th reach, then the related mass-balance equation becomes

$$V_i \frac{dD_j}{dt} = Q_{i-1} \cdot D_{j-1} - Q_i D_j + D'_{i-1,j}(D_{j-1} - D_j)$$
$$- D'_{j,j+1}(D_j - D_{j+1}) + V_j K d_j \cdot L_j - V_j K_{ai} D_i + W_j^D \qquad (A7.96)$$

where K_{ai}, oxygen-recover coefficient; W_{iD}, input of oxygen deficit from outside.
The time-averaged state over tidal cycles may be considered as a steady state, that is, $dL_i/dt=0$. The BOD_5 distribution of the estuary may be calculated by applying eq. (A7.95) and rewritting it in matrix form

$$G\vec{L} = \vec{W}^L \qquad (A7.97)$$

where $\vec{L}$, a vector of n-components representing the BOD_5 values of all the reaches; $\vec{W}_L$, a vector of n-components representing the values of BOD_5 input to the reaches.

In eq. (A7.97), the elements g_{ij} of n-dimensional matrix G at the i-th row and j-th colum are calculated by the following,

for j=i, $g_{ij}=Q_i+D'_{j-1,j}+D'_{i,j+1}+V_iKd_j$
for j=i-1. $g_{ij}=-Q_{j-1}-D'_{j-1,j}$
for j=i+1, $g_{ij}=-D'_{j,j+1}$
and for the other elements, $g_{ij}=0$

If W_{iL}, the pollution source, are known, then it is not difficult to calculate the distribution of BOD_5 in the estuary region with

$$\vec{L} = G^{-1} \cdot \vec{W^L} \qquad (A7.98)$$

7.3.3.2 DO Model

For the oxygen deficit, a similar equation in matrix form may written as

$$H\vec{D} = F\vec{L} + \vec{W^D} \qquad (A7.99)$$

where $\vec{D}$, a vector of n-components representing the oxygen deficit of all the reaches; $\vec{W}_D$, a vector of n-components representing the values of oxygen deficit input to the reaches.

Both H and F are matrices of n-dimensions, and their elements may be obtained by using eqn. (A7.97),

for $j=i$, $h_{ij}=Q_i+D'_{i-1,i}+D'_{i,j+1}+V_iK_{ai}$

for $j=i-1$, $h_{ij}=-Q_{i-1}-D'_{j-1,i}$
for $j=i+1$, $h_{ij}=-D'_{i,j+1}$

and for the other elements, $h_{ij}=0$; for $j=i$, $f_{ij}=V_iKd_i$, and the other elements of matrix F, $f_{ij}=0$.

The distribution of oxygen deficit in the estuary region may be obtained by sustituting (A7.98) into (A7.99) and finding the inverse of H,

$$\vec{D} = H^{-1} \cdot F \cdot G^{-1} \cdot \vec{W^L} + H^{-1} \cdot \vec{W^D} \qquad (A7.100)$$

Eqs. (A7.98) to (A7.100) are the set of governing equations of the steady-state BOD-DO coupling model for the time average over tidal cycles, which has a wide application to the simulation and prediction of water quality in the estuary region. The matrix G^{-1} of this model is called as BOD response matrix of a 1-D estuary, $H^{-1} \cdot F \cdot G^{-1}$ called as oxygen-deficit response matrix to BOD_5 of an estuary, and H^{-1} called as oxygen-deficit response matrix to oxygen-deficit input of an estuary.

7.3.3.3 Upstream and Downstream Boundary Conditions

The boundary conditions of the upstream and downstream estuary boundaries may calculated as the follows.

For the 1-st reach at the upstream end,

$$\begin{aligned} &Q_1L_1 + D'_{0,1}L_1 + D'_{1,2}L_1 - D'_{1,2}L_2 + V_1Kd_1 \cdot L_1 \\ &\quad = W_1^L + Q_0 \cdot L_0 - D'_{0,1}L_0 \end{aligned} \qquad (A7.101)$$

and

$$\begin{aligned} &Q_1D_1 + D'_{0,1}D_1 + D'_{1,2}D_1 - D'_{1,2}D_2 - V_1Kd_1 \cdot L_1 + V_1 \cdot K_{a1} \cdot D_1 \\ &\quad = W_1^D + Q_0 \cdot D_0 - D'_{0,1}D_0 \end{aligned} \qquad (A7.102)$$

hold. When the values of inflow rate Q_0, BOD_5 concentration L_0, oxygen deficit D'_0 and dispersion coefficient D'_0 are prescribed at the upstream end, source terms may be used to acount for the contributions of all the terms at the right-hand side of the above two equations, that is,

$$W_1^L := W_1^L + Q_0 L_0 - D'_{0,1} \cdot L_0 \tag{A7.103}$$

and

$$W_1^D := W_1^D + Q_0 D_0 - D'_{0,1} \cdot D_0 \tag{A7.104}$$

are the source terms for the upsteam 1-st reach.

For the last reach at the downstream end,

$$\begin{aligned} &Q_{n-1}L_{n-1} - Q_n L_n + D'_{n-1,n}(L_{n-1} - L_n) - D'_{n,n+1}(L_n - L_{n+1}) \\ &\quad - V_n K_{dn} L_n + W_n^L = 0 \end{aligned} \tag{A7.105}$$

and

$$\begin{aligned} &Q_{n-1}D_{n-1} - Q_n D_n + D'_{n-1,n}(D_{n-1} - D_n) - D'_{n,n+1}(D_n - D_{n+1}) + \\ &\quad V_n K_{dn} L_n - V_n K_{dn} D_n + W_n^L = 0 \end{aligned} \tag{A7.106}$$

hold.

It should be noticed that, two unknowns L_{n+1} and D_{n+1} need to be found for the last downstream reach. To solve this problem, two methods available may be applied.

i) In the outlet part of the estuary region, the water quality should be quite stable since the water body is close to the sea. In this case, L_{n+1} and D_{n+1} can be taken as given constants that could be acounted in the source term $W_{nL}W_{nL}$.

ii) If the last reach downstream is far away enough from the contaminant source, then the concentration gradient is approximately zero, or $L_{n+1}=L_n$ and $D_{n+1}=D_n$.

The determination of boundary conditions for the single-component models is the same as the BOD_5 model, its detailed description is dropped out here.

7.3.4 Basic Requirements

7.3.4.1 Input Information

The average water level over a tide cycle is calculated according to the measured water level hydrograph at each cross section in March, 1994.

$$H = \sum H(t_i)\Delta t_i / \sum \Delta t_i \tag{A7.107}$$

in which:

$H(t_i)$—water level (m) at ti

$\triangle t_i$—time in terval
H—average water level (m)

Based on the relationship between average waterlevels and river widths over cross—section, the average river width over a tide cycle is derived by interpolation.

The width in the realignment reach of the river is derived based on design document, while other parts of the river channel are derived as before.

The average water depth connected with average width before the river channel realignment is derived based on the data of all cross sections in the river channel. The average water depth over a tide cycle of the realignment part after the realignment is determined by the design documents.

The cross section intervals are derived based on the map. The average flow discharge over tide cycle is designated based on the hydrograph of tide flow

$$Q = \sum Q(t_i)\triangle t_i / \sum \triangle t_i \qquad (A7-108)$$

in which
Q—average flow discharge over tide cycle
$Q(t_i)$—tide flow discharge at t_i
$\triangle t_i$—time interval

Table A7—13 shows the monitoring results of pollution sources in Shenzhen side offered by the Lead Consultant. In order to meet the need of the model, we generalized all pollutant outlet locations and the locations of tributaries into relevant cross sections (Table A7—14). In order to estimate the parameters, the concentrations of pollutants from each cross section are calculated according to the average value from the continuous monitoring:

$$C = 1/n \sum_{i=1}^{n} C_{ij} \qquad (A7-109)$$

in which
C_i—average concentration for i cross section
C_{ij}—j times monitoring concentrations for i cross section

Table A7—15 and A7—16 show data statistical results before and after the river channel realignment. The pollution sources in Hong Kong side offered by Lead Consultant (including Shang Shui River and Yuan Lang River) is also considered.

Table A7—13 Water Polluttant Sources in Shenzhen River and Deep Bay

Location	Point	Time	T ℃	COD_{Mn}	BOD_5	TN	TP	Col.	Cu	Pb	SS	Q m^3/s
Buji River	1#	07.20 9:00	29.0	17.96	38.0	14.97	1.688	2.4×10^7	0.030	0.057	32.0	11.00+
		07.20 12:30	29.0	23.43	30.4	17.39	1.358	1.7×10^7	0.024	Y	72.0	12.10+
		07.20 15:00	30.0	25.32	52.3	13.86	2.322	1.7×10^7	0.030	0.038	300.0	7.20+
		07.20 18:15	28.0	23.81	61.0	13.36	2.441	4.8×10^6	0.024	0.038	404.4	12.00+
		07.20 21:00	28.0	23.81	55.0	14.77	1.695	2.8×10^6	0.036	0.038	81.5	7.15+
Lu dan Village I	2#	07.20 9:10	29.0	14.94	22.2	10.99	1.801	2.2×10^5	Y	0.038	37.5	0.07+
Lu dan Village II	3#	07.20 9:22	29.5	12.87	9.2	3.33	0.718	3.2×10^5	0.042	Y	9.6	0.22+
Bin Jiang	4#	07.20 11:40	29.0	13.06	13.2	16.58	2.844	3.3×10^5	Y	Y	6.5	0.40+
Xia Bu Biao I	5#	07.20 10:00	29.5	27.21	35.4	20.41	3.061	3.2×10^6	Y	0.113	63.0	0.05+
Xia Bu Biao II	6#	07.20 10:10	29.0	18.53	22.0	12.40	1.820	3.5×10^7	Y	0.075	68.7	0.10+
Zhuan Ma Tou	7#	07.20 9:50	29.0	16.83	35.5	13.81	2.032	3.2×10^5	Y	Y	52.0	0.11+
Futian River	8#	07.20 9:10	29.5	19.85	33.1	13.5	1.860	8.2×10^6	0.030	Y	34.0	3.12+
		07.20 12:10	29.5	14.94	16.4	19.07	1.484	8.4×10^6	0.018	0.038	30.0	4.68+
		07.20 15:20	32.0	25.32	34.0	12.60	2.025	4.4×10^7	0.084	0.038	78.9	3.36+
		07.20 18:30	30.0	25.32	37.0	12.10	1.880	1.4×10^8	0.060	Y	132.0	2.77+
		07.20 21:10	29.0	25.32	48.4	12.80	1.721	2.2×10^8	0.030	Y	80.0	3.17+
Huanggang River	9#	07.20 9:00	29.0	14.38	15.6	7.41	1.843	1.7×10^7	Y	0.057	60.00	3.17+
		07.20 12:00	29.5	15.70	17.4	11.49	1.814	1.0×10^7	0.018	0.057	61.8	3.30+
		07.20 15:00	31.0	35.89	48.8	14.87	3.794	4.7×10^8	0.018	0.189	489.6	0.75+
		07.20 18:20	30.0	28.34	27.8	7.86	1.880	3.2×10^7	0.084	0.057	124.5	0.54+
		07.20 21:00	29.0	22.30	31.6	3.58	2.467	2.5×10^8	Y	Y	440.0	0.54—
Xin Zhou River	10#	07.20 10:55	29.5	32.87	55.6	29.94	3.820	9.1×10^7	0.048	Y	74.0	1.07—
Jinxiu Zhonghua	11#	07.20 16:15	30.0	29.47	115	21.77	2.929	1.6×10^8	0.030	Y	32.4	0.07+
Da Shahe	12#	07.19 9:00	28.5	9.47	10.2	4.08	0.619	2.4×10^6	Y	Y	49.0	1.66+
Ma Queling	13#	07.19 16:10	31.0	21.55	28.4	6.10	1.220	1.4×10^9	0.102	Y	400.0	0.18+
Shenzhen Univ.	14#	07.19 15:50	29.0	7.02	5.0	4.64	0.639	8.7×10^5	Y	0.094	15.0	0.01+
Bali Mei	15#	07.19 15:20	20.5	44.94	232	14.47	2.837	1.4×10^9	0.251	0.057	54.3	0.01+
Guang Jin	16#	07.19 15:00	29.0	77.77	75.6	23.54	1.840	5.9×10^5	Y	Y	44.0	0.02+
Shekou I	17#	07.19 13:00	29.3	35.89	69.5	19.76	2.639	1.7×10^7	1.250	0.038	47.4	1.13+
Sea world	18#	07.19 14:00	28.4	31.66	19.4	9.78	2.230	9.1×10^8	0.191	0.057	463.8	0.44+
Nanhai Hotel	19#	07.19 13:25	31.0	5.51	17.8	3.63	0.698	3.2×10^5	Y	0.113	135.3	0.06+
Shekou II	20#	07.19 13:45	27.0	5.13	13.1	16.37	0.448	2.7×10^4	Y	0.038	4.0	0.01+

Note: "+"stands for flows entering Shenzhen River

"—"stands for flows entering tributaries

Table A7—14 General view of the Pollutants outlets

Section No.	No. of pollutant outlet
Yumin village	1#
Buji estuary	2# 3# 4#
Futian	5# 6# 7# 8#
Yunong village	9#
Shenzhen estuary	10#
Yaying shan	11#
Shenzhen Univ.	12# 13# 14#
Shekou	14#15#16#17#18#19#
Chiwan	20#

Table A7—15 Input data(before the realignment)

Location	NO.	L (m)	B (m)	H (m)	QL (m3/s)	CODMn (mg/l)	BOD5 (mg/l)	TN (mg/l)	TP (mg/l)	Col.	Cu (mg/l)	Pb (mg/l)	SS (mg/l)	Q (m3/s)	水温	DO (mg/l)
Sancha River	1	394.5	24.90	0.98										3.35		
Luohu bridge	2	828	41.34	1.35	2.12	23.0	12.0	3.31	0.61	1.0×10⁷	0.057	0.012	25		29.0	0.2
Yumin village	3	1883	48.16	1.65	9.87	22.87	47.34	14.87	1.901	1.9×10⁶	0.0288	0.0062	177.98		28.8	0.2
Buji estuary	4	2958	54.50	1.76	0.69	13.19	12.84	11.79	2.06	3.2×10⁷	0.013	0.004	10.63	17.02	29.2	0.2
Futian	5	3290	66.07	1.89	3.68	21.96	33.53	12.19	1.818	7.9×10⁷	0.041	0.018	70.86		29.5	0.2
Yunong village	6	3219	79.51	2.02	2.21	23.32	28.24	9.04	2.358	1.6×10⁸	0.024	0.072	235.18	24.39	29.7	0.2
Shenzhen esteary	7	2952	2444	1.81	1.27	47.63	66.80	28.06	4.01	9.1×10⁸	0.044	0.003	79.24	31.05	29.5	0.2
Yayingshan	8	6000	6310	1.93	0.07	29.47	115.0	21.77	2.929	1.6×10⁸	0.03	0.00	32.4		30.0	0.2
Shenzhen Univ.	9	3075	7110	2.46	1.85	10.63	11.92	4.28	0.678	1.4×10⁷	0.01	0.00	82.97		29.5	0.2
Shekoushan	10	5400	6646	4.18	1.66	34.23	55.40	16.54	2.452	2.6×10⁷	0.90	0.045	160.95		29.4	0.2
Chiwan					0.01	5.13	13.10	16.37	0.448	2.7×10⁴	0.00	0.038	4.00		27.0	0.2

Note: L, length; B, width; H, dept; QL, input Volume

Table A7—16 Input data (After the realignment)

Location	No.	L (m)	B (m)	H (m)	QL (m3/s)	CODMn (mg/l)	BOD5 (mg/l)	TN (mg/l)	TP (mg/l)	Col.	Cu (mg/l)	Pb (mg/l)	SS (mg/l)	Q (m3/s)	水温	DO (mg/l)
Sancha River	1	3945	43.90	4.64										3.35		
Luohu bridge	2	200	51.15	4.66	2.12	23.0	12.0	3.31	0.61	1.0×10⁷	0.057	0.012	25		29.0	0.2
Yumin village	3	1030	66.16	4.71	9.87	22.87	47.34	14.87	1.901	1.9×10⁶	0.0288	0.0062	177.98		28.8	0.2
Buji estuary	4	2958	97.50	4.86	0.69	13.19	12.84	11.79	2.06	3.2×10⁷	0.013	0.004	10.63	17.02	29.2	0.2
Futian	5	1120	102.7	5.02	3.68	21.96	33.53	12.19	1.818	7.9×10⁷	0.041	0.018	70.86		29.5	0.2
Yunong village	6	3219	120.1	5.16	2.21	23.32	28.24	9.04	2.358	1.6×10⁸	0.024	0.072	235.18	24.39	29.7	0.2
Shenzhen esteary	7	2952	2444	1.81	1.27	47.63	66.80	28.06	4.01	9.1×10⁸	0.044	0.003	79.24	31.05	29.5	0.2
Yayingshan	8	6000	6310	1.93	0.07	29.47	115.0	21.77	2.929	1.6×10⁸	0.03	0.00	32.4		30.0	0.2
Shenzhen Univ.	9	3075	7110	2.46	1.85	10.63	11.92	4.28	0.678	1.4×10⁷	0.01	0.00	82.97		29.5	0.2
Shekoushan	10	5400	6646	4.18	1.66	34.23	55.40	16.54	2.452	2.6×10⁷	0.90	0.045	160.95		29.4	0.2
Chiwan					0.01	5.13	13.10	16.37	0.448	2.7×10⁴	0.00	0.038	4.00		27.0	0.2

7.3.4.2 Parameter Estimation

Dispersive coefficient is estimated by Salinity Method

$$D_{xi} = X_i U_{xi}/(lnC_i - LnC_0)$$

in which:

D_{xi}—Dispersion coefficient in ith cross section (m^2/s)

X_i—The distance between tide mouse and i cross section (m)

U_{xi}—Average velocity in ith cross section (m/s)

C_i—Salinity in ith cross section (mg/l) from the modelling monitoring

C_0—Salinity in Bay Mouth (mg/l) from the modelling monitoring

Since the monitoring data of Salinity Obtained in June are "unusual ow than that in normal case", as commented in the monitoring report supplied by Shenzhen Environmental Monitoring Station, other methods methods must be resorted in order to give the proper estimation of the parameters. The so called Comprehensive Search Method is used for such purposes. With a target function formulated as:

$$J_i(D_{xi}, K_{di}, K_{si}) = \sum_{j=1}^{i} [\lambda(L_{ij} - L'_{ij})^2 + (1 - \lambda)(D_{ij} - D'_{ij})^2] \qquad (A7.110)$$

in which:

L_{ij}—Measured BOD_5

L'_{ij}—calculated BOD_5

D_{ij}—Measured DO

D'_{ij}—Calculated DO

λ—The weights of BOD_5 and DO

After the search, the target function will arrive at

$$J_i((D_{xi}*, K_{di}*, K_{si}*) = min \sum_{j=1}^{i} [\lambda(L_{ij} - L_{ij})^2 + (1 - \lambda)(D_{ij} - D'_{ij})^2] \qquad (A7-111)$$

in which, D_{xi}, K_{di}, K_{si} are the results of estimation (Table7—6).

Table A7—17 Estimation of dispersive coefficient

Section	Distance(m)	Velocity(m/s)	Salinity(mg/g)	$D_x(m^2/s)$
Sancha River	—24547.5	0.215	0.0044	888.7
Yumin village	—23325.0	0.145	0.0077	617.8
Yunong village	—15194.0	0.09	0.1474	563.3
Shenzhen estuary	—11975.0	0.087	0.5765	979.2
Chivan	0	/	1.67	/

Table A7—18 Estimation of parameters for BOD_5—DO model

Section	1#	2#	3#	4#	5#	6#	7#	8#	9#	10#
K_d(1/d)	0.246	0.204	0.143	0.146	0.184	0.756	0.325	0.264	0.203	0.283
K_a(1/d)	0.556	0.568	0.625	0.628	0.525	0.264	0.566	0.566	0.656	0.632
D_x(m^2/s)	186	65.0	300	210	400	487	58	60	64	70

Table A7—19 Decay coefficient for different pollutants (1/d)

Section	1#	2#	3#	4#	5#	6#	7#	8#	9#	10#
COD	0.08	0.08	0.08	0.08	0.05	0.05	0.01	0.01	0.01	0.01
TN	0.1	0.1	0.1	0.1	0.05	0.05	0.01	0.01	0.01	0.01
TP	0.001	0.001	0.001	0.001	0.001	0.001	0.001	0.001	0.001	0.001
Col.	2550	2580	2420	3000	2800	20000	20000	20000	20000	20000
Cu	1.94	2.82	1.19	0.407	0.154	0.782	0.744	0.456	0.643	0.533
Pb	0.834	0.832	0.739	0.729	0.424	0.142	0.144	0.162	0.043	0.033

7.3.4.3 Verification and Prediction

Comparisons of the calculated resullts and the measured ones are listed in Table A7—20 and A7—21 as well as Fig. A7—27 to A7—34. The relative errors are less than 26.7 percent.

Table A7—20 Verification of BOD—DO model

Index	Section	1#	2#	3#	4#	5#	6#	7#	8#	9#	10#
BOD_5 (mg/l)	A	21.28	35.47	33.37	31.76	26.64	19.23	4.53	1.07	0.98	1.05
	B	/	37.09	/	/	24.41	17.56	4.04	/	/	1.05
	C(%)	/	−4.37	/	/	9.14	9.51	12.1	/	/	0.0
DO (mg/l)	A	0.38	0.18	0.10	0.11	0.23	0.27	4.71	6.98	7.01	6.63
	B	/	0.16	/	/	0.25	0.25	5.25	/	/	6.68
	C(%)	/	12.5	/	/	−8.0	8.0	−10.3	/	/	−0.7

Note: A, calculated; B, measured; C, error.

Table A7—21 Verification of other models

Index	Section	1#	2#	3#	4#	5#	6#	7#	8#	9#	10#
COD (mg/l)	A	17.60	20.83	19.90	19.79	18.90	17.06	11.03	6.14	4.37	3.05
	B	/	19.82	/	/	21.90	17.08	/	5.79	/	3.2
	C(%)	/	2.8	/	/	−13.7	−0.1	/	6.0		−4.7
TN (mg/l)	A	8.74	12.14	11.87	11.59	10.07	9.60	5.98	2.98	1.87	1.05
	B	/	12.70	/	/	12.51	11.47	/	2.54	/	1.03
	C(%)	/	−4.4	/	/	−14.5	−16.3	/	17.3	/	1.9
TP (mg/l)	A	1.48	1.72	1.73	1.74	1.69	1.52	0.97	0.46	0.25	0.084
	B	/	1.98	/	/	2.12	2.2	/	0.40	/	0.083
	C(%)	/	−13.1	/	/	−20.3	−30.9	/	15.0	/	1.2
Cu (mg/l)	A	2.65	2.39	1.23	1.54	1.62	1.13	0.158	0.079	0.24	0.10
	B	/	2.1	/	/	2.2	0.86	/	0.075	/	0.12
	C(%)	/	13.8	/	/	−26.4	31.4	/	5.3	/	20
Pb (mg/l)	A	8.91	7.19	7.230	8.46	11.1	8.31	2.98	1.06	1.18	1.10
	B	/	6.9	/	/	9.40	10.6	/	1.2	/	1.10
	C(%)	/	4.2	/	/	15.3	−21.6	/	−11.7	/	0.0
Col.	A	6913	13734	5295	29545	26375	9660	1.89	1.53	3.48	1.03
	B	/	13985	/	/	26145	9400	/	1.39	/	1.03
	C(%)	/	−1.8	/	/	0.88	2.8	/	10.07	/	0.0

Note: A, calculated; B, measured; C, error.

The detailed modelling results of Shenzhen River and Deep Bay before and after the Stage 2 works are shown in Tablle A7—22 and A7—23 as well as in Figs A7—43~A7—50. Predicted results for the planning year of 2000 are also given in Table A7—24 and in Figures from A7—35 to A7—42. The prediction results of the pollution sources are still taken as 75% larger than the existing ones in each polllutant outlet.

Table A7—22 Verification of BOD_5—DO coupling model

Index	Sec. No.	1#	2#	3#	4#	5#	6#	7#	8#	9#	10#
BOD_5 (mg/l)	Calculated	19.22	34.18	32.37	30.94	26.13	18.96	4.51	1.07	0.98	1.05
	Measured	/	36.39	/	/	24.95	18.93	2.91	/	/	1.05
	Error(%)	/	−6.11	/	/	4.73	0.16	55.0	/	/	0.0
DO (mg/l)	Calculated	0.51	0.25	0.17	0.19	0.30	0.34	4.72	6.98	7.01	6.63
	Measured	/	0.15	/	/	0.22	0.25	5.10	/	/	6.68
	Error(%)	/	66.7	/	/	36.4	36.0	−7.45	/	/	−0.7

Table A7—23 Verification of other WQ models

Index	Sec.	1#	2#	3#	4#	5#	6#	7#	8#	9#	10#
COD (mg/l)	Calculated	15.77	19.58	19.21	19.22	18.45	16.73	10.90	6.10	4.35	3.05
	Measured	/	19.24	/	/	23.37	18.41	/	5.94	/	3.28
	Error(%)	/	1.77	/	/	−21.1	−9.13	/	2.69	/	−7.0
TN (mg/l)	Calculated	7.98	11.71	11.50	11.29	10.48	9.44	5.92	2.96	1.86	1.05
	Measured	/	12.15	/	/	12.02	12.00	/	2.17	/	1.04
	Error(%)	/	−3.62	/	/	−12.8	-21.33	/	36.4	/	0.96
TP (mg/l)		1.48	1.71	1.73	1.73	1.69	1.53	0.98	0.46	0.25	0.084
	Measured	/	1.82	/	/	2.17	2.21	/	0.283	/	0.085
	Error(%)	/	−6.04	/	/	−22.1	−30.8	/	62.5	/	1.2
Cu (mg/l)	Calculated	3.03	2.55	1.32	1.60	1.67	1.17	0.168	0.080	0.224	0.10
	Measured	/	1.8	/	/	1.4	0.77	/	0.097	/	0.117
	Error(%)	/	41.7	/	/	17.1	51.9	/	−17.5	/	−14.5
Pb (mg/l)	Calculated	12.0	8.57	8.340	9.30	11.7	8.80	3.18	1.11	1.19	1.10
	Measured	/	7.7	/	/	9.80	11.6	/	2.3	/	1.50
	Error(%)	/	11.3	/	/	19.4	−24.1	/	−51.7	/	−26.7
Col. 1/l	Calculated	6918	13732	5296	29545	26375	9661	1.89	1.53	3.48	1.03
	Measured	/	12967	/	/	25667	10067	/	1.17	/	0.81
	Error(%)	/	5.90	/	/	2.76	−4.03	/	30.8	/	27.2

Table A7—24 Prediction of BOD5—DO with and without works in 2000

Index	Sec.		1#	2#	3#	4#	5#	6#	7#	8#	9#	10#
BOD (mg/l)	pre	Current	21.28	35.47	33.37	31.76	26.64	19.23	4.53	1.07	0.98	1.05
		2000	28.76	58.48	55.27	53.02	44.68	32.34	7.59	1.67	1.29	1.05
	post	Current	21.68	25.84	21.49	18.09	12.79	9.05	3.69	0.93	0.94	1.05
		2000	33.66	42.68	35.69	30.22	21.45	15.21	6.17	1.43	1.22	1.05
DO (mg/l)	pre	Current	0.380	0.180	0.100	0.110	0.230	0.270	4.71	6.98	7.01	6.63
		2000	0.01	0.01	0.01	0.01	0.01	0.010	2.66	6.54	6.68	6.63
	post	Current	0.240	0.620	1.150	1.630	2.300	2.590	4.95	7.06	7.03	6.63
		2000	0.01	0.01	0.01	0.01	0.01	0.01	3.06	6.68	6.69	6.63

Table 7—25 Prediiction of other pollutants with and without works

Index	Sec.	1#	2#	3#	4#	5#	6#	7#	8#	9#	10#
COD	pre	17.60	20.38	19.90	19.79	18.90	17.06	11.03	6.14	4.37	3.05
(mg/l)	post	17.19	17.86	16.56	15.60	14.10	12.93	10.40	5.90	4.27	3.05
TN	pre	8.74	12.14	11.87	11.59	10.70	9.60	5.98	2.98	1.87	1.05
(mg/l)	post	9.27	10.26	9.41	8.71	7.70	7.03	5.53	2.80	1.80	1.05
TP	pre	1.48	1.72	1.73	1.74	1.69	1.52	0.97	0.46	0.25	0.0840
(mg/l)	post	1.55	1.60	1.53	1.46	1.33	1.22	0.97	0.46	0.25	0.084
Col.	pre	6.9×10^5	1.4×10^4	5.3×10^3	3.0×10^4	2.6×10^4	9.7×10^3	1.89	1.53	3.48	1.03
(1/l)	post	9.1×10^2	1.3×10^4	2.5×10^3	6.7×10^3	1.9×10^4	2.5×10^3	1.87	1.53	3.48	1.03
Cu	pre	0.027	0.024	0.012	0.015	0.016	0.011	0.002	0.00079	0.002	0.001
(mg/l)	post	0.012	0.014	0.012	0.011	0.009	0.006	0.002	0.006	0.002	0.001
Pb	pre	0.0089	0.0072	0.0072	0.0085	0.011	0.0083	0.003	0.001	0.001	0.0011
(mg/l)	post	0.005	0.005	0.005	0.005	0.005	0.004	0.002	0.0007	0.001	0.001

Table 7—26 Prediction of other pollutants with and without works in 2000

Index	Sec.	1#	2#	3#	4#	5#	6#	7#	8#	9#	10#
COD	pre	24.97	33.34	32.77	32.88	31.48	28.28	17.64	8.87	5.56	3.05
(mg/l)	post	26.47	28.92	26.95	25.47	22.95	20.93	16.49	8.42	5.38	3.05
TN	pre	11.03	19.44	19.18	18.94	17.57	17.56	9.60	4.45	2.51	1.05
(mg/l)	post	13.84	16.45	15.20	14.15	12.52	11.39	8.84	4.16	2.39	1.05
TP	pre	1.82	2.68	2.24	2.79	2.75	2.48	1.57	0.71	0.36	0.0840
(mg/l)	post	2.25	2.50	2.43	2.34	2.14	1.97	1.56	0.71	0.35	0.084
Col.	pre	1.2×1042	$.4\times1049$	$.3\times1035$	$.2\times1044$	$.6\times1041$	$.7\times104$	3.31	2.68	6.09	1.03
(1/l)	post	1.5×1032	$.3\times1044$	$.4\times1031$	$.2\times1043$	$.3\times1044$	$.4\times103$	3.27	2.68	6.09	1.03
Cu	pre	0.037	0.039	0.020	0.026	0.027	0.009	0.003	0.013	0.004	0.001
(mg/l)	post	0.018	0.024	0.020	0.018	0.015	0.010	0.003	0.010	0.004	0.001
Pb	pre	0.012	0.011	0.011	0.014	0.019	0.014	0.005	0.002	0.002	0.001
(mg/l)	post	0.007	0.008	0.008	0.008	0.009	0.007	0.004	0.010	0.001	0.001

APPENDIX 7.4 DYNAMIC WATER QUALITY MODELLING

7.4.1 Introduction

The purpose of the dynamic water quality modelling is to provide a quantitative assessment of the dynamic behaviours of water quality in Shenzhen River and Deep Bay before and after the Stage 2 works or in the planning year of 2000. A 1—D model is used for Shenzhen River and 2—D model for the Bay with the connection of the two models in the river mouth. The pollutants modeled are BOD_5, DO, COD, TN, TP, Cu, Pb and Col.

7.4.2 1—D Model for Shenzhen River

7.4.2.1 Basic Equations

The proposed 1—D model is constituted with the unsteady flow model. The basic equations include:

Continuity equation for flow

$$\frac{\partial Z}{\partial t} + \frac{1}{B}\frac{\partial Q}{\partial x} = 0 \qquad (A7.112)$$

Momentum equation for flow:

$$\frac{\partial Q}{\partial t} + \frac{\partial}{\partial x}\left(\frac{Q^2}{A}\right) + gA\left(\frac{\partial Z}{\partial x} + \frac{Q|Q|}{K^2}\right) = 0 \qquad (A7.113)$$

Equations for tranference and transformation of pollutants such as COD, TN, TP, Cu, Pb and Col.

$$\frac{\partial(AC)}{\partial t} + \frac{\partial(QC)}{\partial x} = \frac{\partial}{\partial x}\left(AE\frac{\partial C}{\partial x}\right) + R_c - K_c C \qquad (A7.114)$$

BOD-DO coupling equation

$$\frac{\partial(AB)}{\partial t} + \frac{\partial(QB)}{\partial x} = \frac{\partial}{\partial x}\left(AE\frac{\partial C}{\partial x}\right) + R_B - K_d B \qquad (A7.115)$$

$$\frac{\partial(AD)}{\partial t} + \frac{\partial(QD)}{\partial x} = \frac{\partial}{\partial x}\left(AE\frac{\partial D}{\partial x}\right) - R_0 + K_d B - K_a D \qquad (A7.116)$$

Where Z, water level; t, time; x, spatial variable; B, river width; Q, flow discharge; A, area of cross section; K, discharge modula; g, gravitational acceleration; $E=5.93Hg^{1/2}|u|/C_h$, disper-

sive coefficient; $C_h=\frac{1}{n}H^{1/6}$, H, flow depth; u, flow velocity; C_h, Chezy coefficient; n, roughness of the bed.

7. 4. 2. 2 **Computation Scheme**

The aforementioned equations may be further discretized with the Preissmann scheme as such

$$A_i\frac{C_i^{n+1}-C_i^n}{\Delta t}+u_i^{n+1}A_i\left[\frac{\frac{1+P}{2}C_{i+1}^n+PC_i^n-\frac{1+P}{2}C_{i-1}^n}{\Delta x}\cdot\beta+(1-\beta)\frac{\frac{1-P}{2}C_{i+1}^{n+1}+PC_i^{n+1}\frac{1-P}{2}C_{i-1}^{n+1}}{\Delta x}\right]$$

$$=D_i^nA_i\cdot\left[\beta\cdot\frac{C_{i+1}^n-2C_i^n+C_{i-1}^n}{\Delta x^2}+(1-\beta)\frac{C_{i+1}^{n+1}-2C_i^{n+1}-C_{i-1}^{n+1}}{\Delta x^2}\right]+R_e-K_iC_i^n \quad (A7.117)$$

in which

$$P=sing\,(u_i^{n+1})=\begin{cases}1 & u>0\\ -1 & u<0\end{cases} \quad (A7.118)$$

and $\beta=0.75$.

7. 4. 2. 3 **Basic Requirements**

The flow data and topographic information required are the same as those described in the hydrodynamic model. Pollution source data are the same as described in Appendix 7. 3.

7. 4. 2. 4 **Verification and Prediction**

1. Verification

The 1—D model for Shenzhen River is verified with the monitoring data aquired in dry season (March 1—4, 1994) and wet season (June 29—July 1,1994) as shown in Table A7—27 and A7—13.

The comparisons of modelling and measured results for most circumstances show a maximum error of 30% for all the pollutants. Detailed modelling results are given in Figures from A7—51 to A7—58.

2. Prediction

The model runs for five combinations as follows:

(1) Variations of COD,BOD,DO,TN,TP,Cu,Pb and Col. in dry season after Stage 1 works.
(2) Variations of the aforementioned index in wet season after Stage 1 works.
(3) Variation in dry season after Stage 2 works.
(4) Variation in wet season after Stage 2 works.

(5) Variation in dry season 2000

Relevant modelling results are shown in figures from A7—59 to A7—70.

Table A7—27 Monitoring results for Shenzhen River and Deep Bay

Location	NO.	Q (m^3/s)	COD_{Mn} (mg/l)	BOD_5 (mg/l)	T—N (mg/l)	T—P (mg/l)	Col. (mil./l)	Cu (mg/l)	Pb (mg/l)	SS (mg/l)
Buji estuary	1	3.30	9.51	50.5	15.58	2.45	12.80	0.04	0.03	67.3
Ludan village I	2	0.07	26.47	190.0	29.76	5.27	21.00	0.01	0.03	214.6
Ludan village II	3	0.28	25.18	134.0	24.88	5.22	1160.0	0.13	0.03	106.0
Bin jiang	4	0.03	719.19	736.0	141.50	40.00	570.00	0.02	0.21	7748.0
Xia bu muao I	5	0.13	32.00	184.0	31.53	5.31	320.00	0.01	0.03	70.0
Xia bu muao II	6	0.10	29.35	124.0	21.25	3.44	401.00	0.01	0.03	96.7
Zhuan Ma To	7	0.11	15.59	75.4	30.48	4.73	64.80	0.01	0.03	42.9
Futian River	8	2.44	19.65	69.0	33.51	3.98	78.00	0.05	0.03	185.9
Huang Gang River	9	1.12	68.83	139.0	19.25	5.07	160.00	0.05	0.15	796.0
Xin Zhou River	10	0.86	45.53	142.0	38.79	4.63	287.00	0.14	0.03	72.0
Jinxou Zhonghua	11	0.18	56.88	204.0	30.44	4.96	4.00	0.02	0.03	156.0
Da Shahe	12	0.53	17.99	16.1	8.00	0.60	7.00	0.01	0.05	54.2
Ma Queling	13	0.05	36.98	55.8	18.02	2.36	520.00	0.56	0.03	38.0
Shenzhen Univ.	14	0.03	26.73	112.0	11.85	2.24	52.80	0.02	0.09	70.0
Bali Mei	15	0.02	31.82	59.0	26.29	2.49	2.00	13.00	0.08	69.2
Guang Jin	16	0.05	23.34	45.0	20.40	2.43	28.80	0.01	0.03	113.3
She Kou I	17	0.08	35.87	133.0	27.30	3.64	3.00	4.29	0.06	205.3
See world	18	0.30	14.12	11.4	15.14	0.84	13.10	0.27	0.08	85.3
Nanhai Hotol	19	0.26	24.81	16.0	5.91	0.64	7.00	0.06	0.32	33.8
Shekou I	20	0.10	15.96	10.0	3.00	0.96	9.00	0.05	0.33	19.5

7.4.3 2—D Water Quality Modelling for Deep Bay

7.4.3.1 Basic Equations

The prime equations for tide flow in Deep Bay include:

Continuity equation for flows

$$\frac{\partial \xi}{\partial t}+\frac{\partial[(\xi+h)u]}{\partial x}+\frac{\partial[(\xi+h)v]}{\partial y} \tag{A7.119}$$

Momentum equation for flows

$$\frac{\partial u}{\partial t}+u\frac{\partial u}{\partial x}+v\frac{\partial v}{\partial y}-fu+y\frac{\partial \xi}{\partial x}+gu\frac{\sqrt{u^2+v^2}}{(\xi+h)C^2}=0 \tag{A7.120}$$

$$\frac{\partial v}{\partial t}+u\frac{\partial u}{\partial x}+v\frac{\partial v}{\partial y}-fv+g\frac{\partial \xi}{\partial y}+gv\frac{\sqrt{u^2+v^2}}{(\xi+h)C^2}=0 \tag{A7.121}$$

and the equation for transference and transformation of pollutants such as COD, TN, TP, Cu, Pb and Col.

$$\frac{\partial(HP_c)}{\partial t}+\frac{\partial HuP_c}{\partial x}+\frac{\partial(HvP_c)}{\partial y}=R_c+\frac{\partial}{\partial x}(HD_x\frac{\partial P_c}{\partial x})+\frac{\partial}{\partial y}(HD_y\frac{\partial P_c}{\partial y})-K_cP_c \tag{A7.122}$$

in which, h, average depth for the sea surface; ξ, temporal depth above or below the average surface; $H=h+\xi$, observed depth; P_c, pollutant concentration; K_c, decay coefficient; R_c, pollutant volume discharged into unit sea area; D_x, D_y, the dispersive coefficients in x and y directions, respectively, which are determined by Elder formula:

$$D_x=\frac{5.93Hg^{1/2}|u|}{C}$$

$$D_y=\frac{5.93Hg^{1/2}|v|}{C}$$

BOD_5—DO coupling equation

$$\frac{\partial(HB)}{\partial t}+\frac{\partial HuB}{\partial x}+\frac{\partial(HvB)}{\partial y}=R_B+\frac{\partial}{\partial x}(HD_x\frac{\partial B}{\partial x})+\frac{\partial}{\partial y}(HD_y\frac{\partial B}{\partial y})-K_1B \tag{A7.123}$$

$$\frac{\partial(HD)}{\partial t}+\frac{\partial HuD}{\partial x}+\frac{\partial(HvD)}{\partial y}=-R_0+\frac{\partial}{\partial x}(HD_x\frac{\partial D}{\partial x})+\frac{\partial}{\partial y}(HD_y\frac{\partial D}{\partial y})+K_1B-K_2D \tag{A7.124}$$

in which, B, stands for BOD; D=O_s−O, oxygen deficency; O,DO concentration; O_s,Saturated dissolved oxygen, which is expressed as

$$O_s = \frac{468}{31.6 + T}$$

for fresh water, and expressed as

$$O_s = 14.6244 - 0.367134T + 0.0044972T^2 - 0.09665 + 0.00205ST + 0.0002739S^2$$

for sea water. Where T, temperature; K_1 coefficient for oxygen dissipation; K_2, coefficient for oxygen recovery; R_B and R_O, volumes of BOD and DO discharged into unit sea area per unit time, respectively.

7.4.3.2 Computation Scheme

According to the ADI finite difference scheme, the equations of transference and transformation for the pollutants are discretized (for the afore—half time step P$\triangle$t→(P+$\frac{1}{2}$)$\triangle$t) as follows

$$A_{m-1,n}S^{p+1/2}_{m-1,n} + B_{m,n}S^{p+1/2}_{m,n} + C_{m+1,n}S^{p+1/2}_{m+1,n} = F_{m,n} \qquad (A7.125)$$

$$A_{m-1,n} = -\frac{\triangle t}{4\triangle l}(h_{m-1/2,n-1/2} + h_{m-1/2,n+1/2} + \zeta^{p+1/2}_{m-1,n} + \zeta^{p+1/2}_{m,n})[\beta U^{p+1/2}_{m-1/2,n} + \frac{1}{\triangle l}(K_x)^{p+1/2}_{m-1/2,n}] \qquad (A7.126)$$

$$B_{m,n} = \zeta^{p+1/2}_{m,n} + \frac{1}{4}(h_{m-1/2,n-1/2} + h_{m+1/2,n-1/2} + h_{m-1/2,n+1/2} + h_{m+1/2,n+1/2}) + \frac{t}{4l}(h_{m+1/2,n-1/2} + h_{m+1/2,n+1/2} + \zeta^{p+1/2}_{m,n} + \zeta^{p+1/2}_{m+1,n}) \times (\alpha U^{p+1/2}_{m+1/2,n} + \frac{1}{4l}(K_x)^{p+1/2}_{m+1/2,n}) - \frac{t}{4l}(h_{m-1/2,n-1/2} + h_{m-1/2,n+1/2} + \zeta^{p+1/2}_{m-1,n} + \zeta^{p+1/2}_{m,n}) \times [(1-\beta)U^{p+1/2}_{m-1/2,n} - \frac{1}{4l}(K_x)^{p+1/2}_{m-1/2,n}] \qquad (A7.127)$$

$$C_{m+1,n} = \frac{1}{4l}(h_{m+1/2,n-1/2} + h_{m+1/2,n+1/2} + \zeta^{p+1/2}_{m,n} + \zeta^{p+1/2}_{m+1,n}) \times [(1-\alpha)U^{p+1/2}_{m+1/2,n} - \frac{1}{4l}(K_x)^{p+1/2}_{m+1/2,n}] \qquad (A7.128)$$

$$F_{m,n} = \frac{\triangle t}{4\triangle l}S^{p}_{m,n-1}(h_{m-1/2,n-1/2} + h_{m+1/2,n-1/2} + \zeta^{p}_{m,n-1} + \zeta^{p}_{m,n}) \times [\delta V^{p}_{m,n-1/2} + \frac{1}{\triangle l}(K_y)^{p}_{m,n-1/2}]$$

$$+S^n_{m,n}\{\zeta^A_{m,n}+\frac{1}{4}(h_{m-1/2,n-1/2}+h_{m+1/2,n-1/2}+h_{m-1/2,n+1/2}+h_{m+1/2,n+1/2})-\frac{\triangle t}{4\triangle l}(h_{m-1/2,n+1/2}$$

$$+h_{m+1/2,n+1/2}+\zeta^n_{m,n}+\zeta^n_{m,n+1})\times[\gamma V^n_{m,n+1/2}+\frac{1}{\triangle l}(K_y)^n_{m,n+1/2}]+\frac{\triangle t}{4\triangle l}(h_{m-1/2,n-1/2}$$

$$+h_{m+1/2,n-1/2}+\zeta^n_{m,n-1}+\zeta^n_{m,n})\times[(1-\delta)V^n_{m,n-1/2}-\frac{1}{\triangle l}(K_y)^n_{m,n-1/2}]\}-\frac{\triangle t}{4\triangle l}S^n_{m,n+1/2}$$

$$\times(h_{m-1/2,n+1/2}+h_{m+1/2,n+1/2}+\zeta^n_{m,n}\zeta^n_{m,n+1})\times[(1-\gamma)V^n_{m,n+1/2}-\frac{1}{\triangle l}(K_y)^n_{m,n+1/2}]+\frac{\triangle t}{2}[M]_{m,n}$$

(A7.129)

where m and n stand for the grid number in x and y directions, respectively; other parameters, or the varible weighted coefficient are determined as such

$$\begin{aligned}
&\alpha=1 && (U^{n+1/2}_{m+1/2,n}\geqslant 0)\\
&\alpha=0 && (U^{n+1/2}_{m+1/2,n}<0)\\
&\beta=1 && (U^{n+1/2}_{m-1/2,n}\geqslant 0)\\
&\beta=0 && (U^{n+1/2}_{m-1/2,n}<0)\\
&\gamma=1 && (U^{n}_{m,n+1/2}\geqslant 0)\\
&\gamma=0 && (U^{n}_{m,n+1/2}<0)\\
&\delta=1 && (U^{n}_{m,n-1/2}\geqslant 0)\\
&\delta=0 && (U^{n}_{m,n-1/2}<0)
\end{aligned}$$

Similarly, the discretized formulas may be derived for the post—half time step.

7.4.3.3 Basic Requirements

The boundary condition for the contaminants are

$$\begin{aligned}
&\frac{\partial P}{\partial t}+u\frac{\partial P}{\partial x}=0 && \textit{for ebb tide}\\
&P=P_0 && \textit{for flood tide}
\end{aligned}$$

Where P_0 is the average of monitoring results of the contaminants at the bay mouth.

The close boundary condition for the contaminants are

$$u_n=0$$

$$D_n\frac{\partial P}{\partial n}=0$$

7.4.3.4 Verification and Prediction

With the time step of 30 seconds, the model runs for four designed conditions, i.e., modelling of the water quality in Deep Bay in July 1994, after the Stage 1 and Stage 2 works, and in 2000.

The comparison of the monitoring results and the modelling ones show that the error between them is less than 25% for most runs.

The modelling results are shown in figures from A7—71 to A7—86.

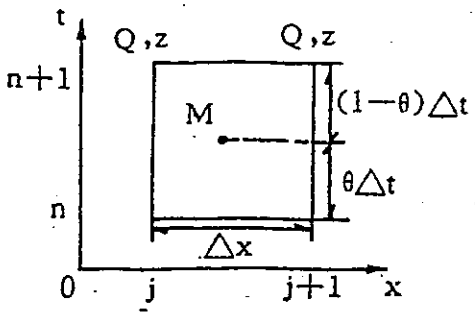

FIG. A7−1 Preissmann Scheme

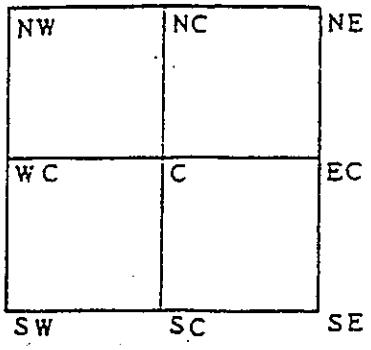

FIG. A7−7 Sketch of the computation scheme

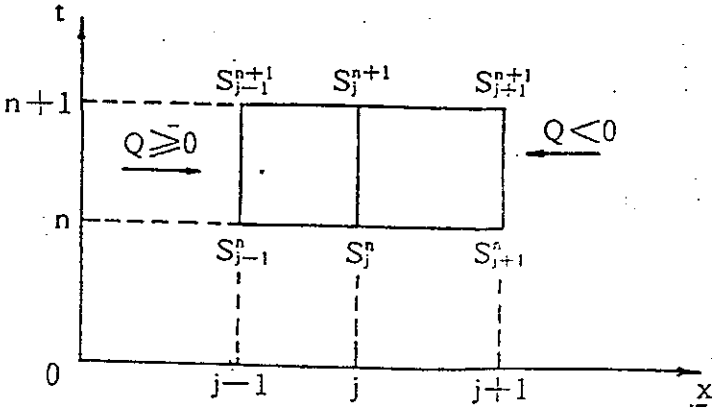

FIG. A7−15 Finite difference scheme for sediment transport

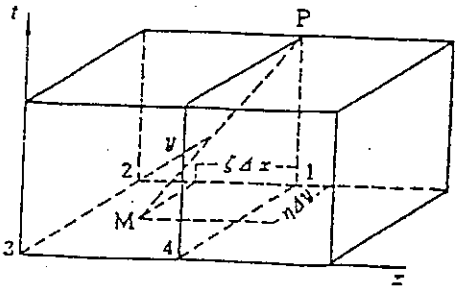

FIG. A7−8 Notation of the spatial characteristics

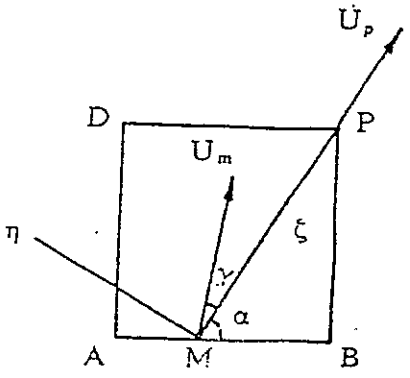

FIG. A7−19 Sketch of characteristic coordinate system

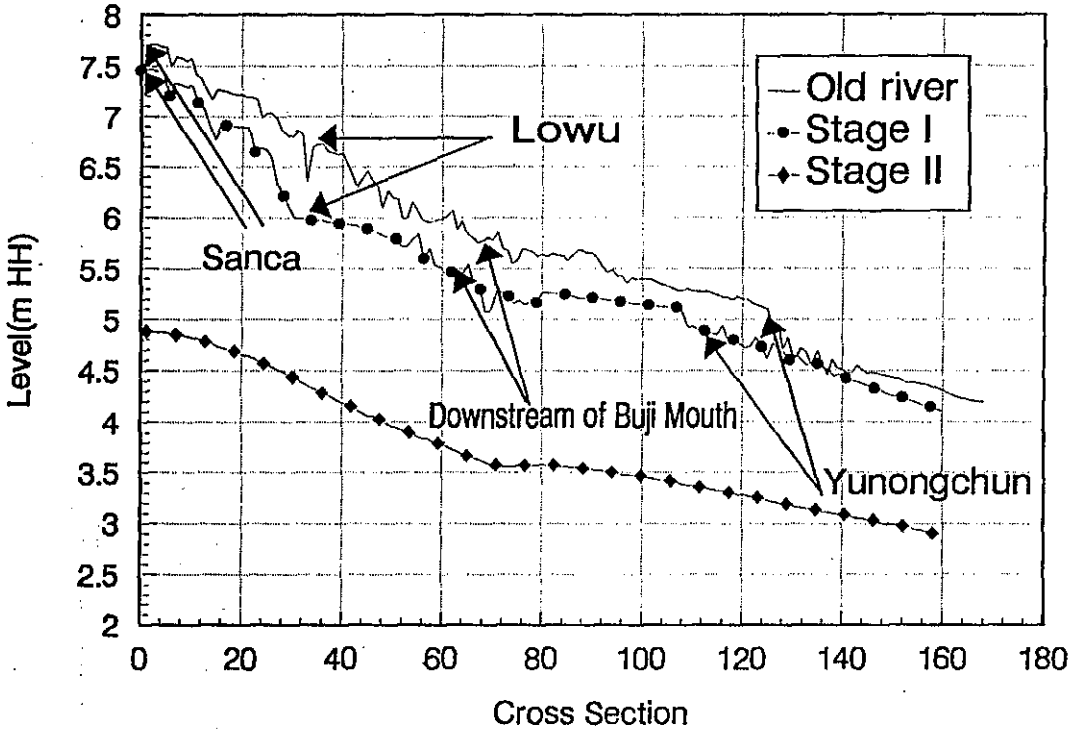

FIG. A7—2 Comparison of water levels during different stages (P=2%)

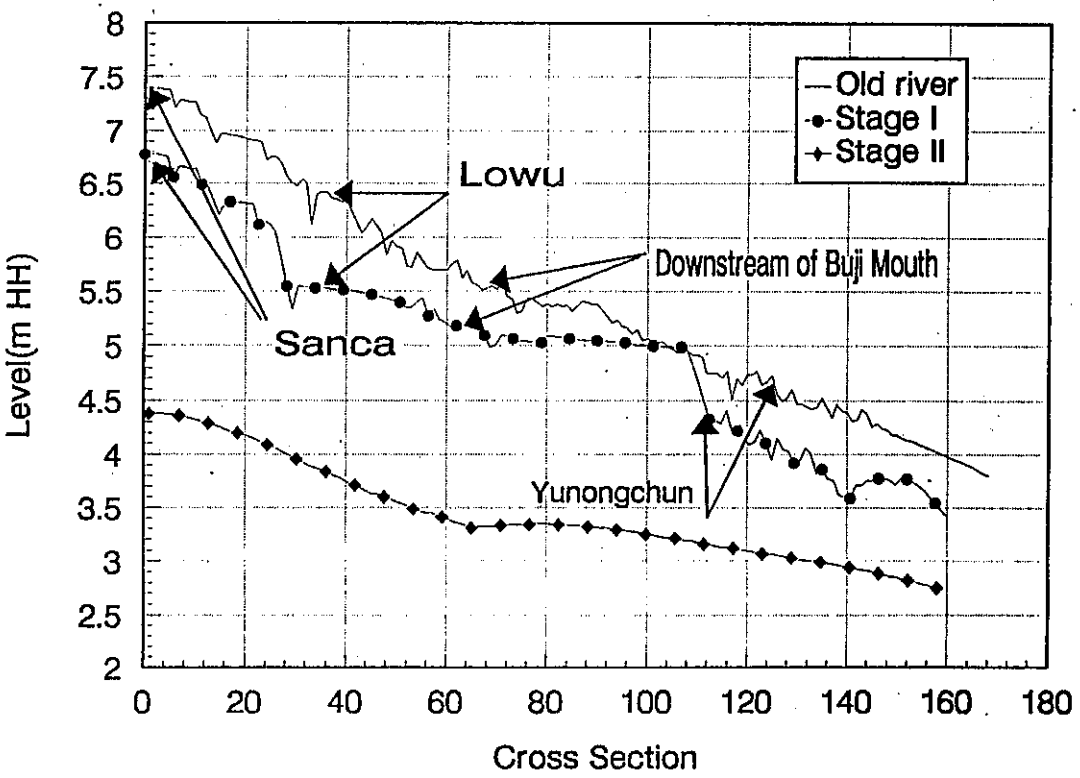

FIG. A7－3 **Comparison of water levels during different stages (P＝5％)**

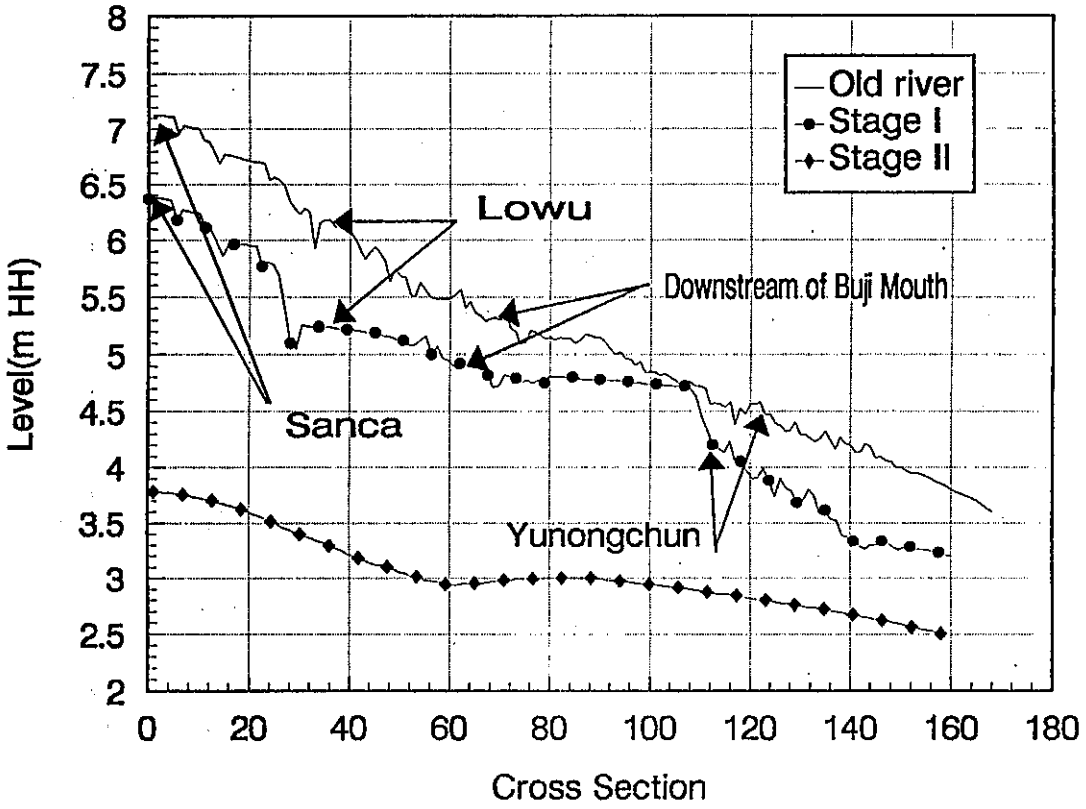

FIG. A7—4 Comparison of water levels during different stages (P=10%)

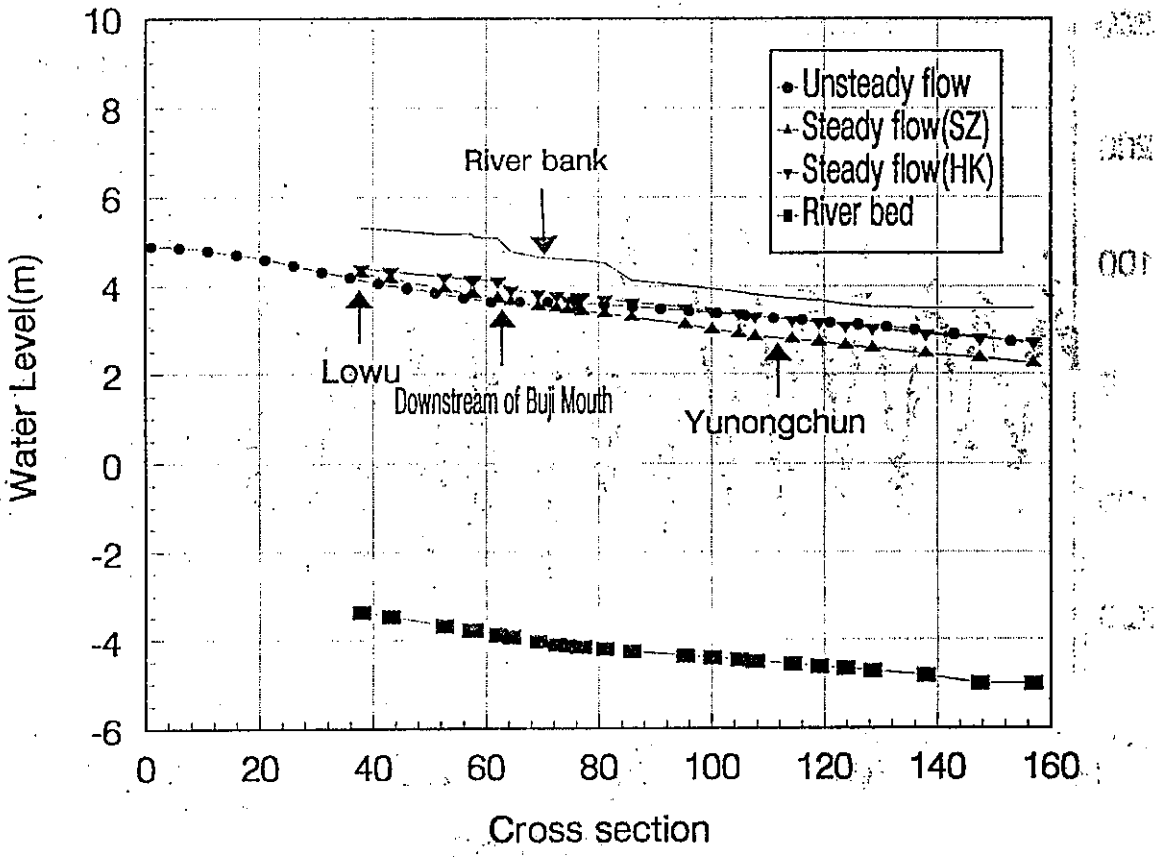

FIG. A7—5 Comparison of water levels from different models (P=2%)

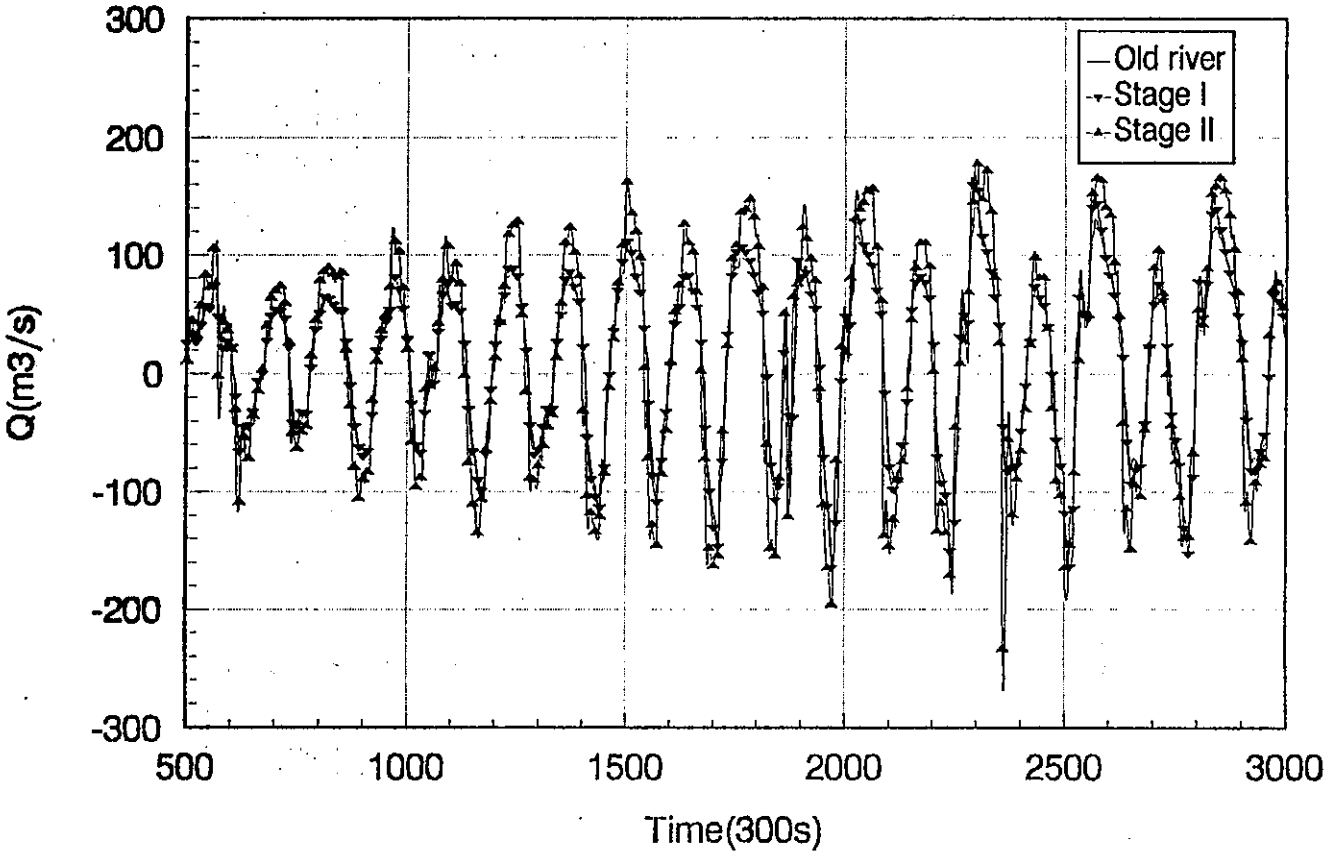

FIG. A7—6 Comparison of tide levels at the river mouth during different stages

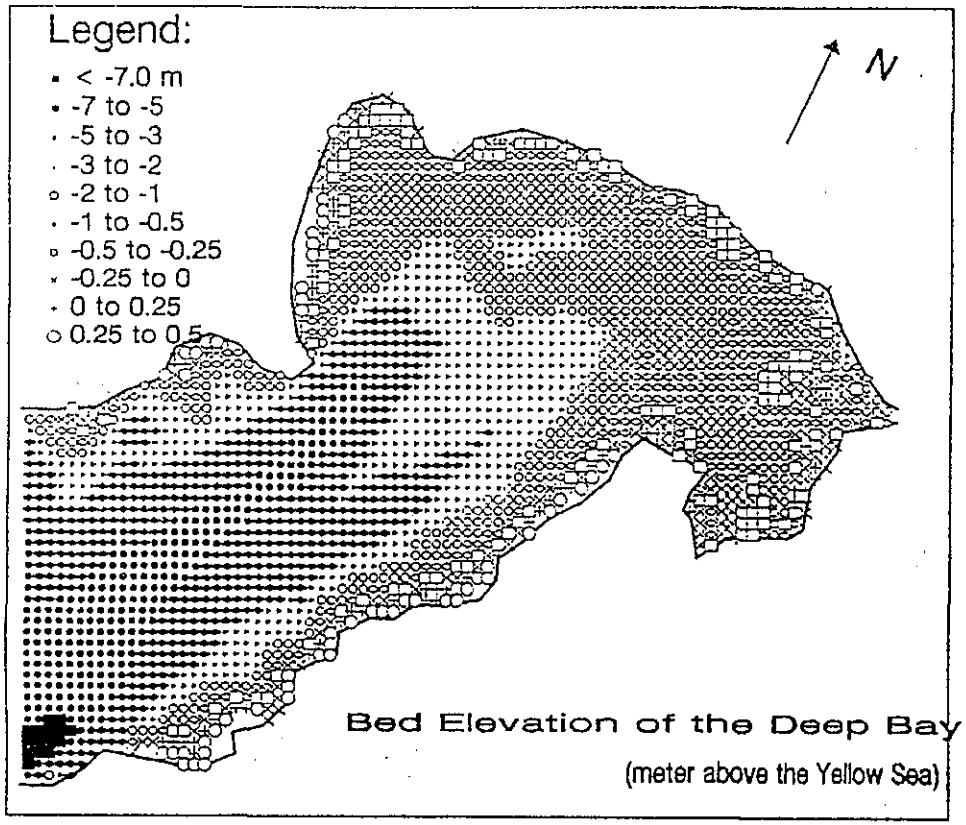
Legend:
< -7.0 m
-7 to -5
-5 to -3
-3 to -2
-2 to -1
-1 to -0.5
-0.5 to -0.25
-0.25 to 0
0 to 0.25
0.25 to 0.5
N
Bed Elevation of the Deep Bay
(meter above the Yellow Sea)

FIG. A7—9

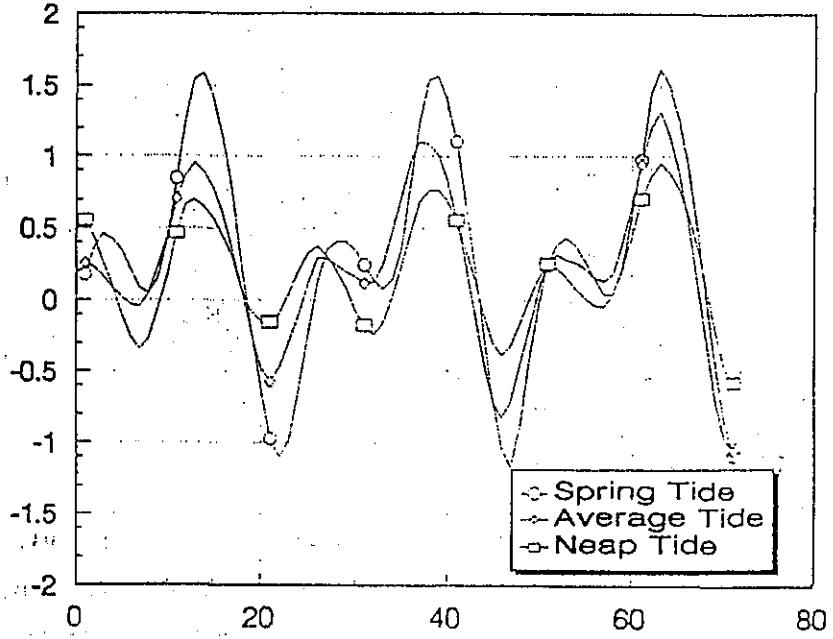

FIG. A7—10 Typical tides used in the modelling

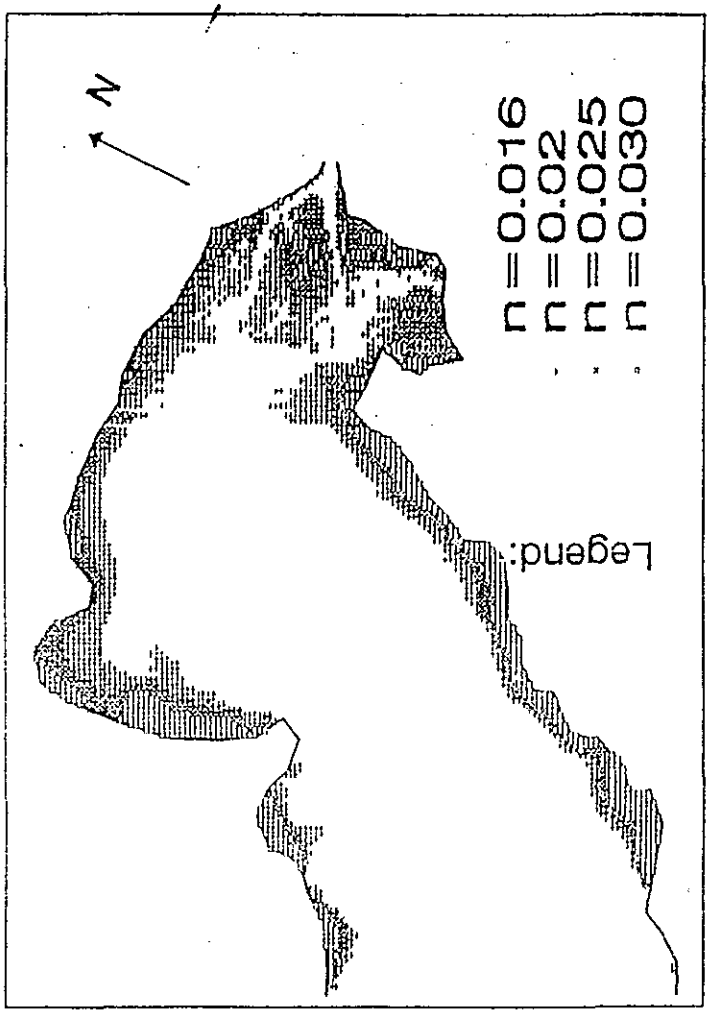

FIG. A7—11 Roughness distribution in Deep Bay

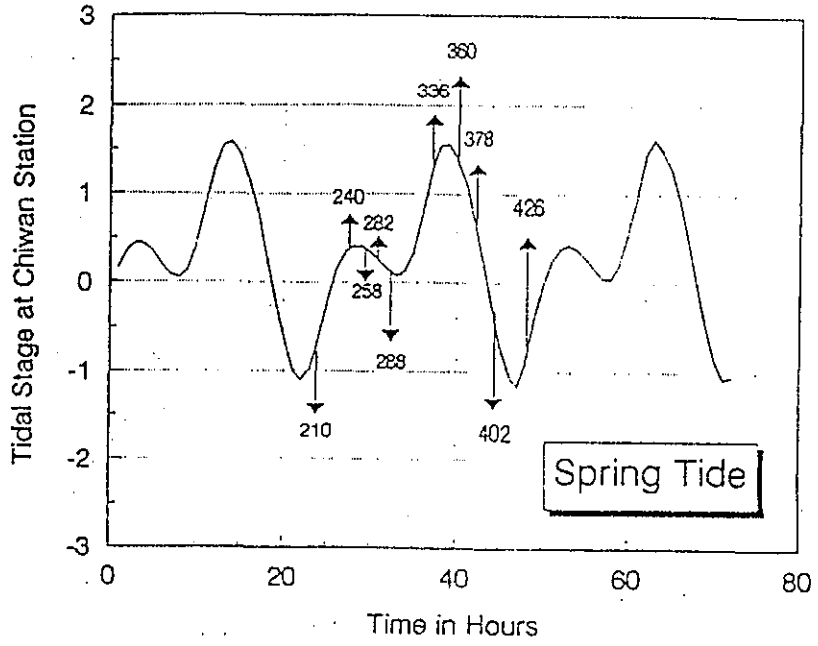

FIG. A7−12(a) Typical tide level process and time sequence (Spring Tide)

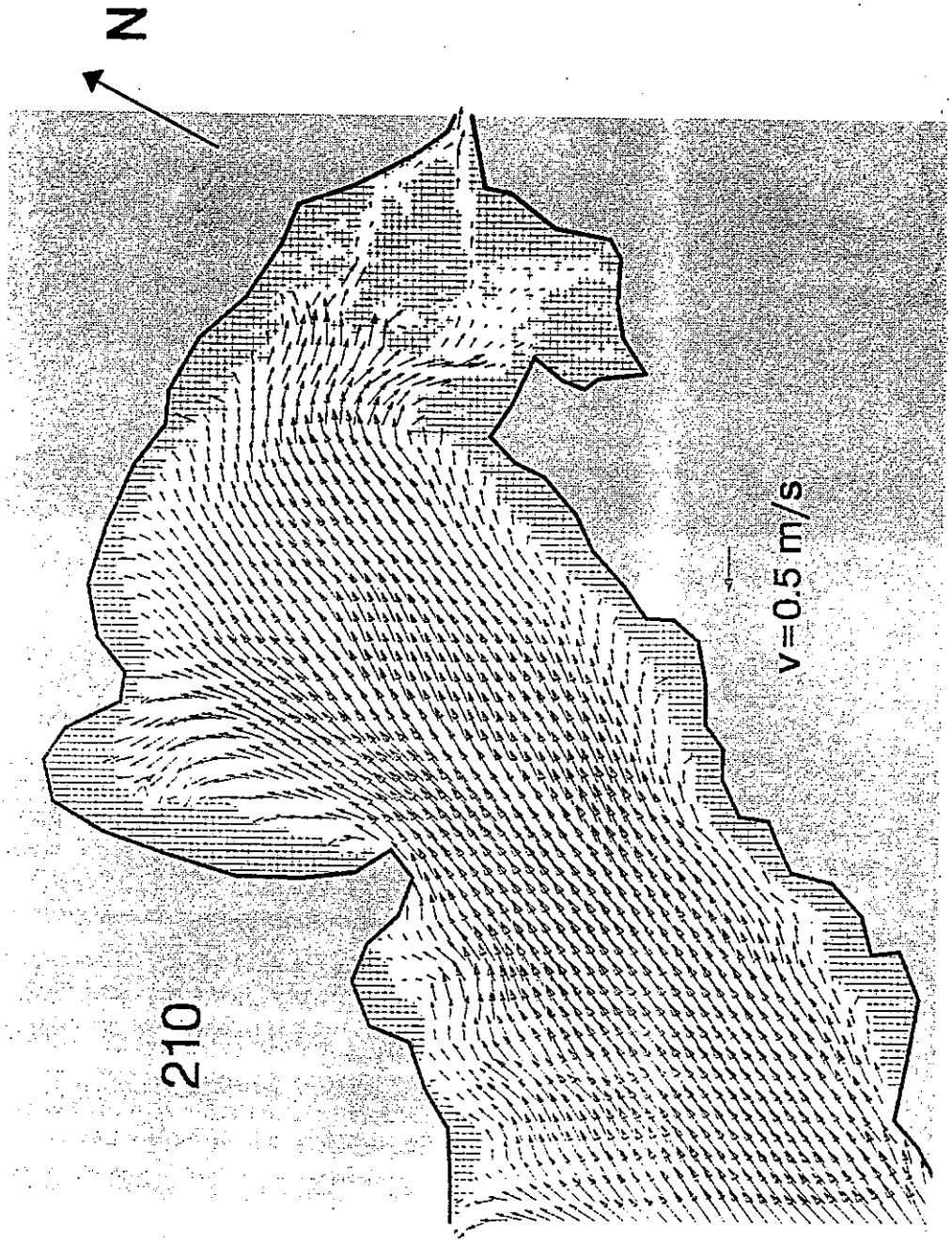

FIG. A7—12(b) Flow field in Deep Bay (Spring Tide)

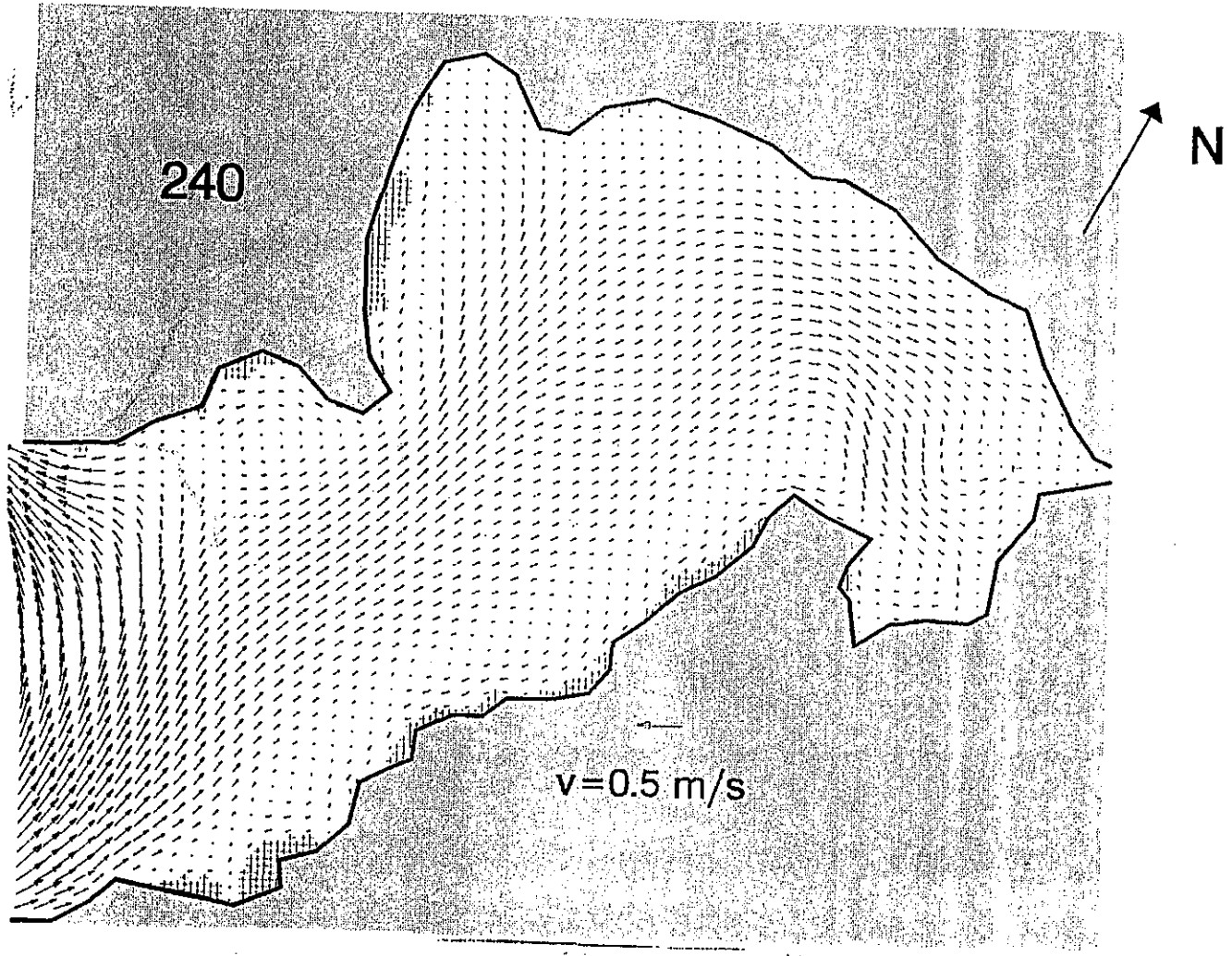

FIG. A7—12(c) Flow field in Deep Bay (Spring Tide)

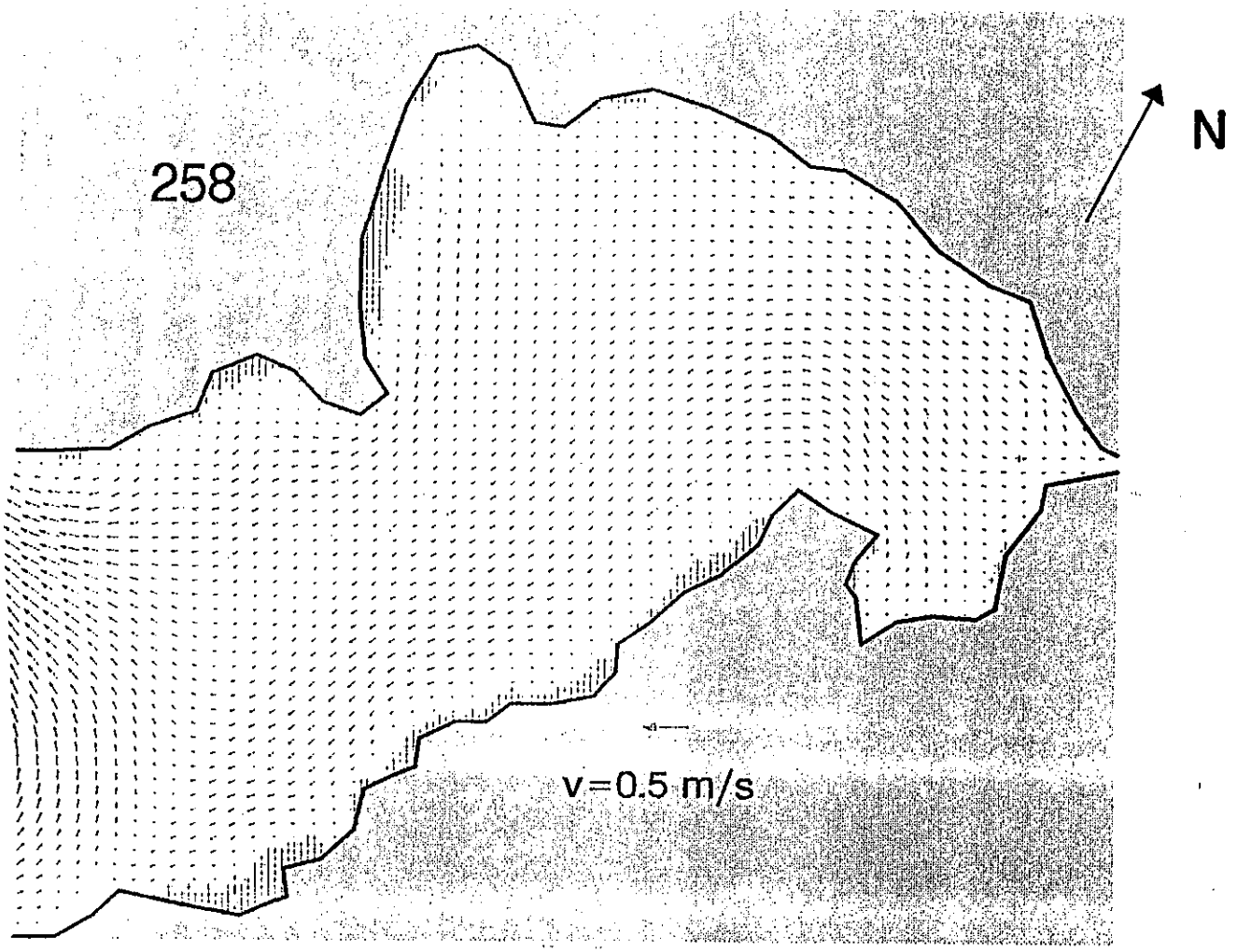

FIG. A7−12(d) **Flow field in Deep Bay (Spring Tide)**

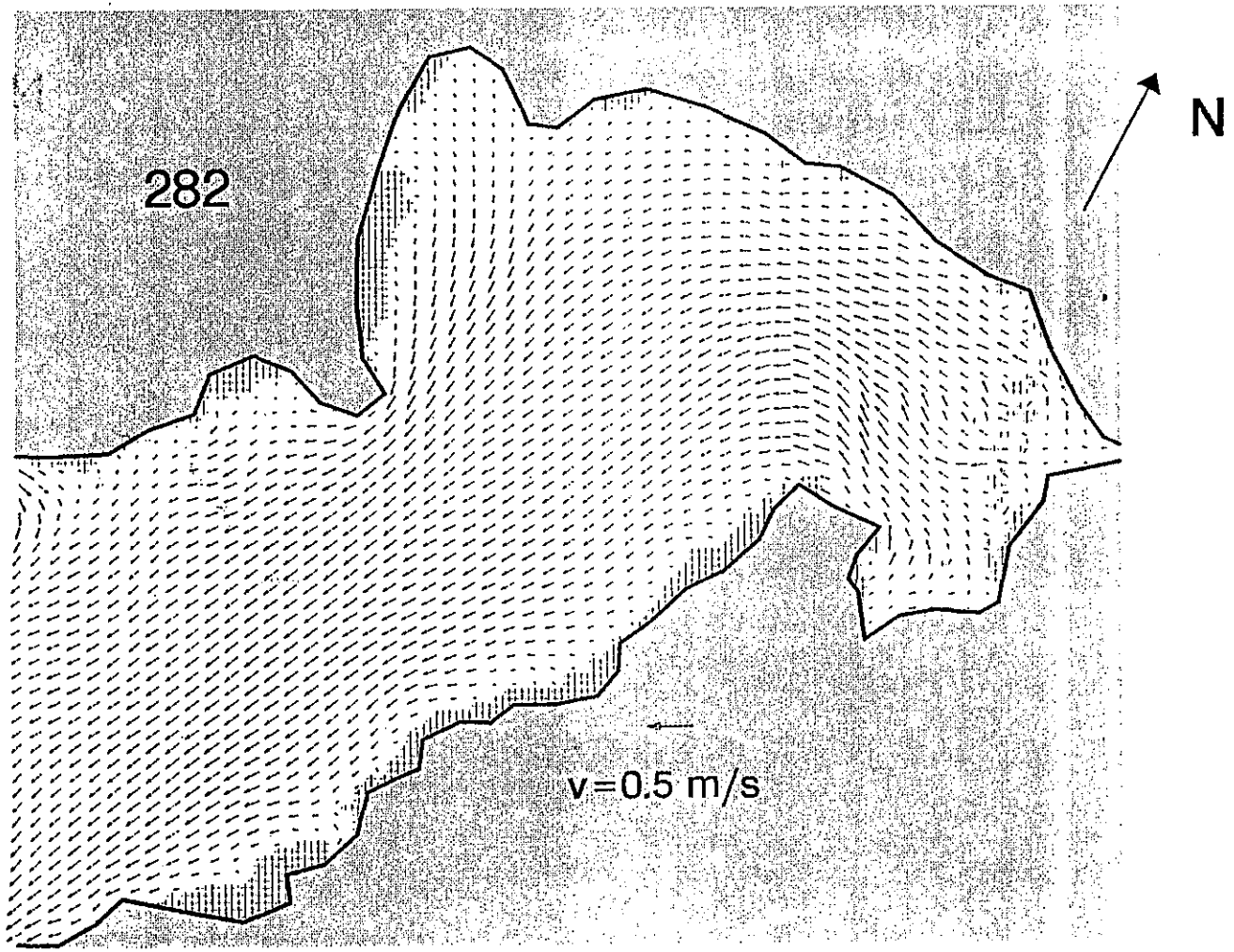

FIG. A7—12(e) Flow field in Deep Bay (Spring Tide)

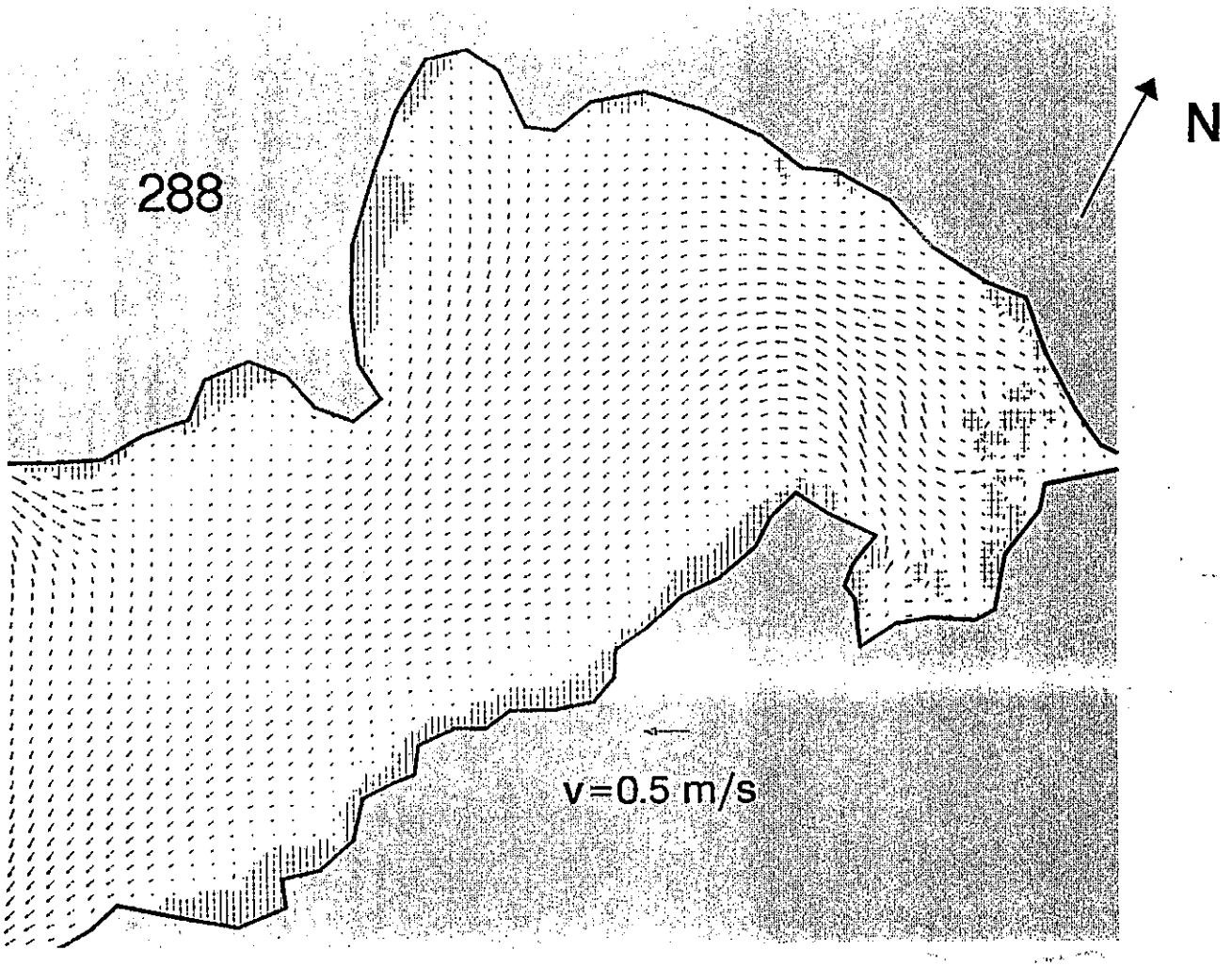

FIG. A7－12(f)　Flow field in Deep Bay (Spring Tide)

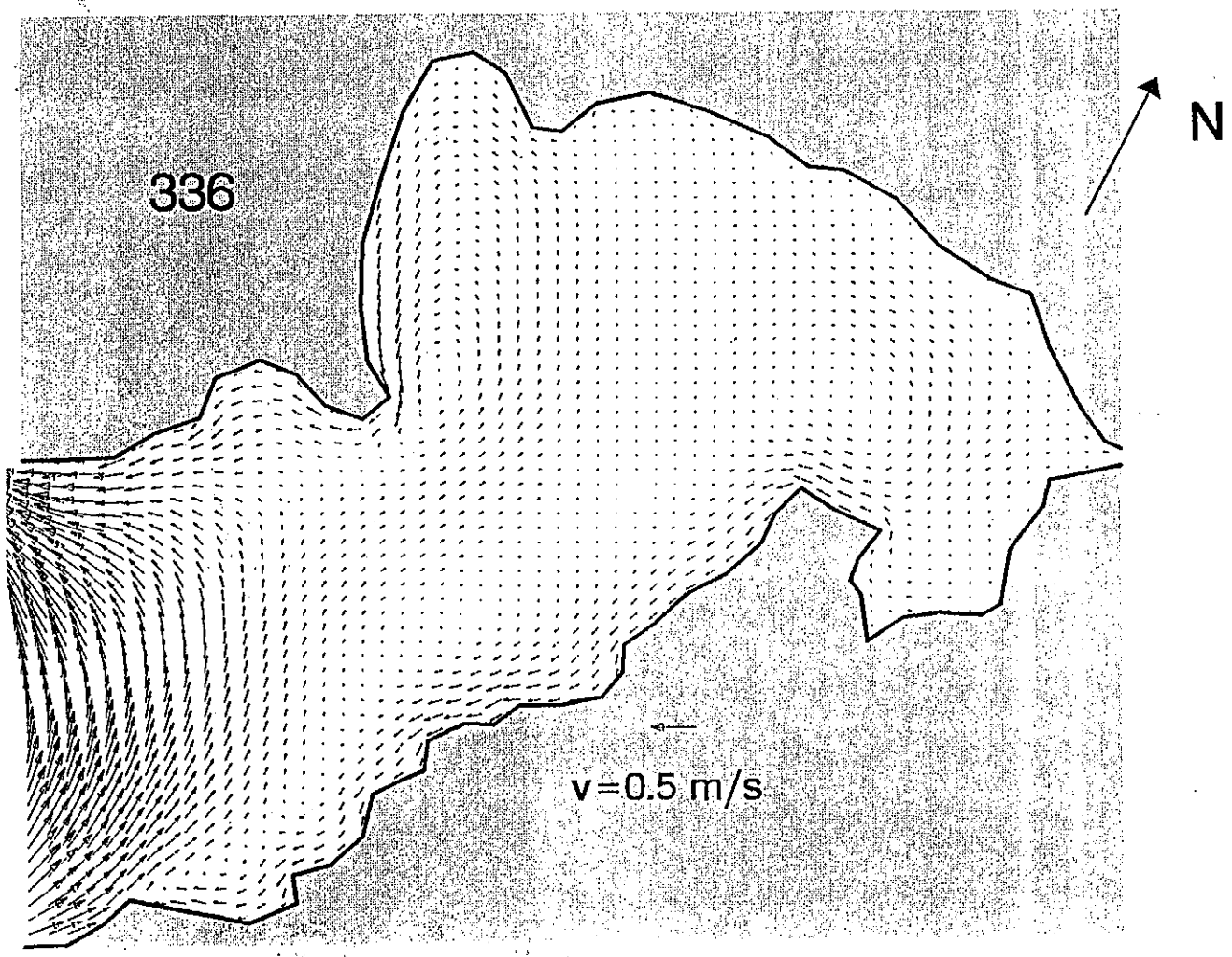

FIG. A7—12(g) Flow field in Deep Bay (Spring Tide)

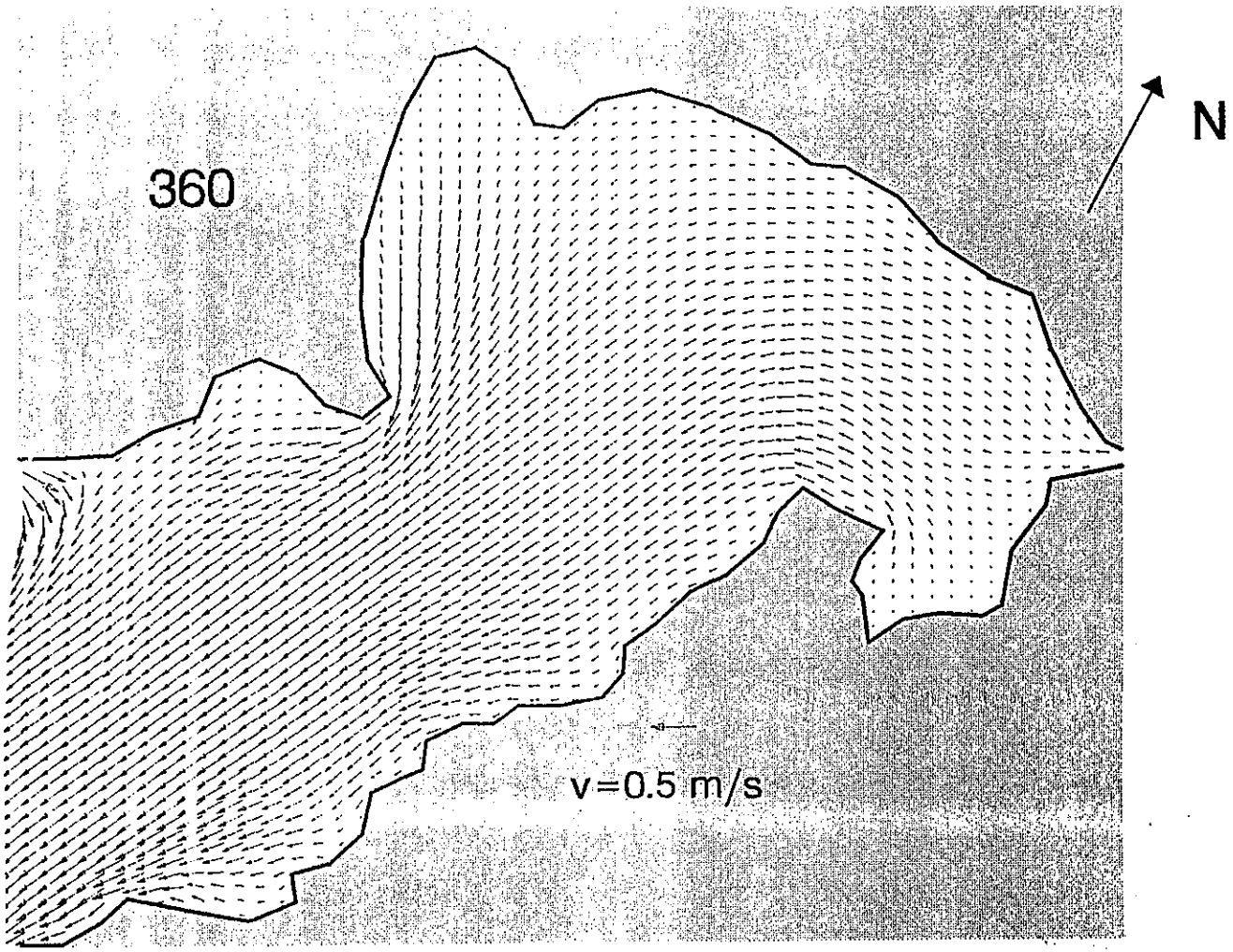

FIG. A7—12(h) Flow field in Deep Bay (Spring Tide)

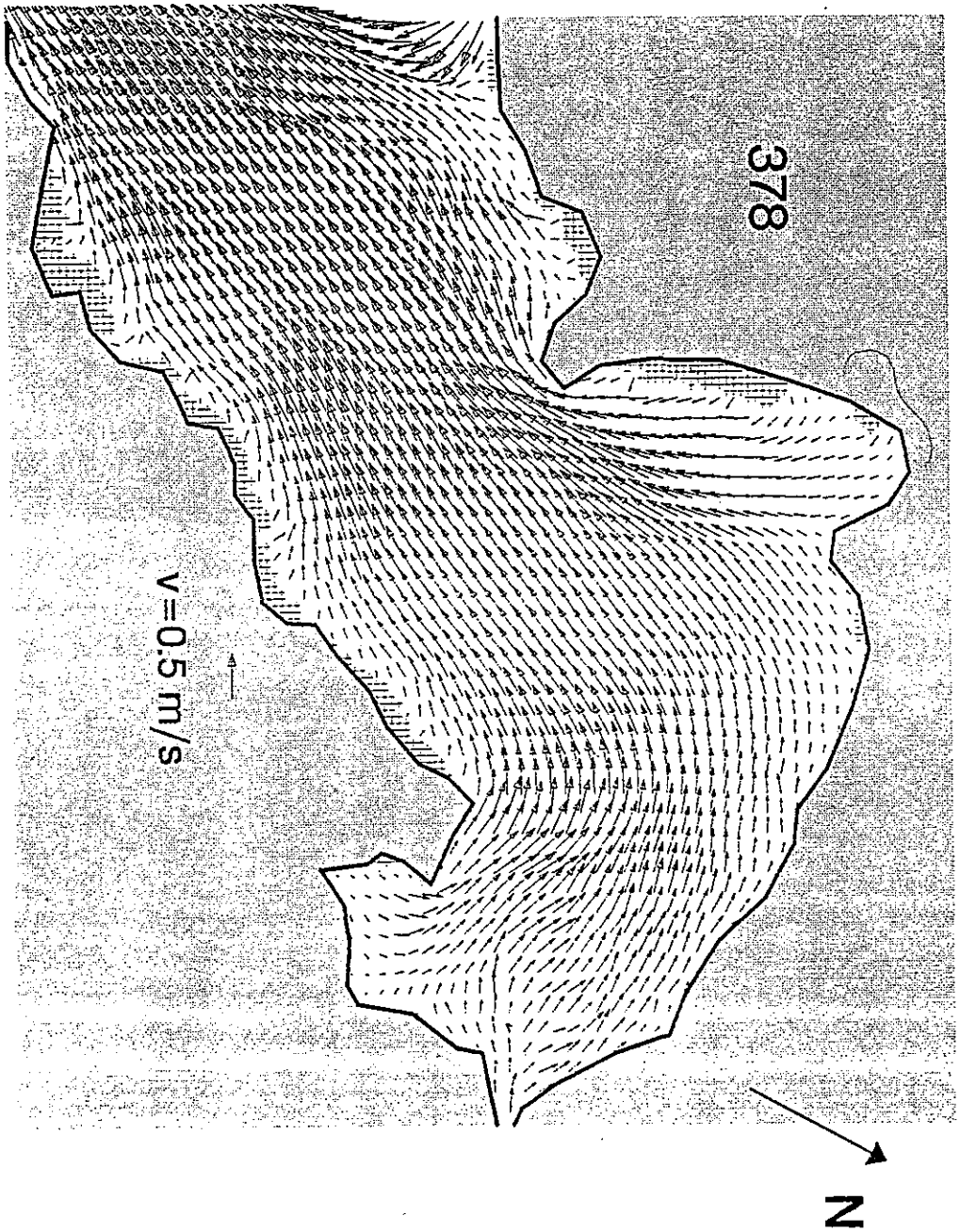

FIG. A7—12(i) Flow field in Deep Bay (Spring Tide)

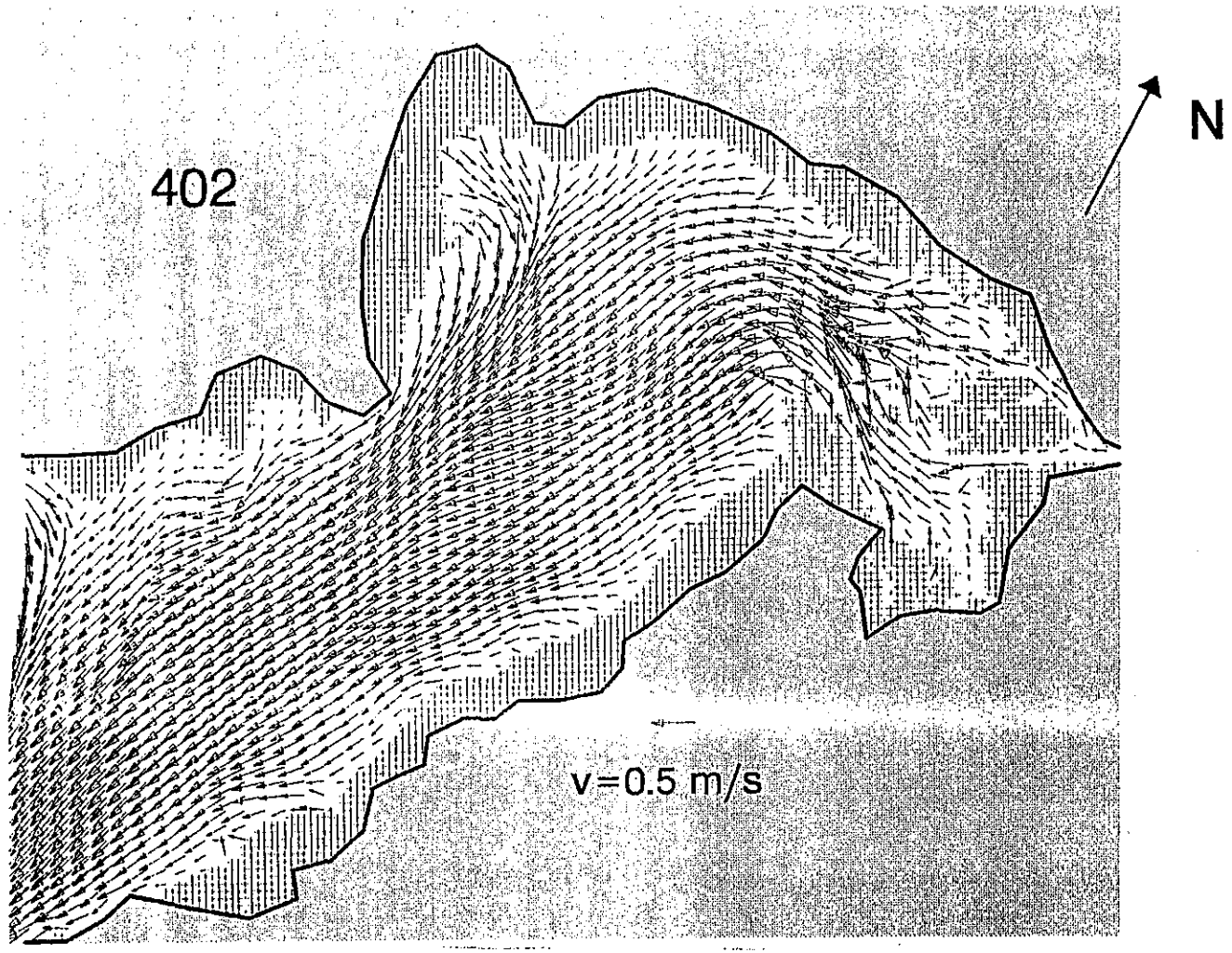

FIG. A7－12(j)　Flow field in Deep Bay (Spring Tide)

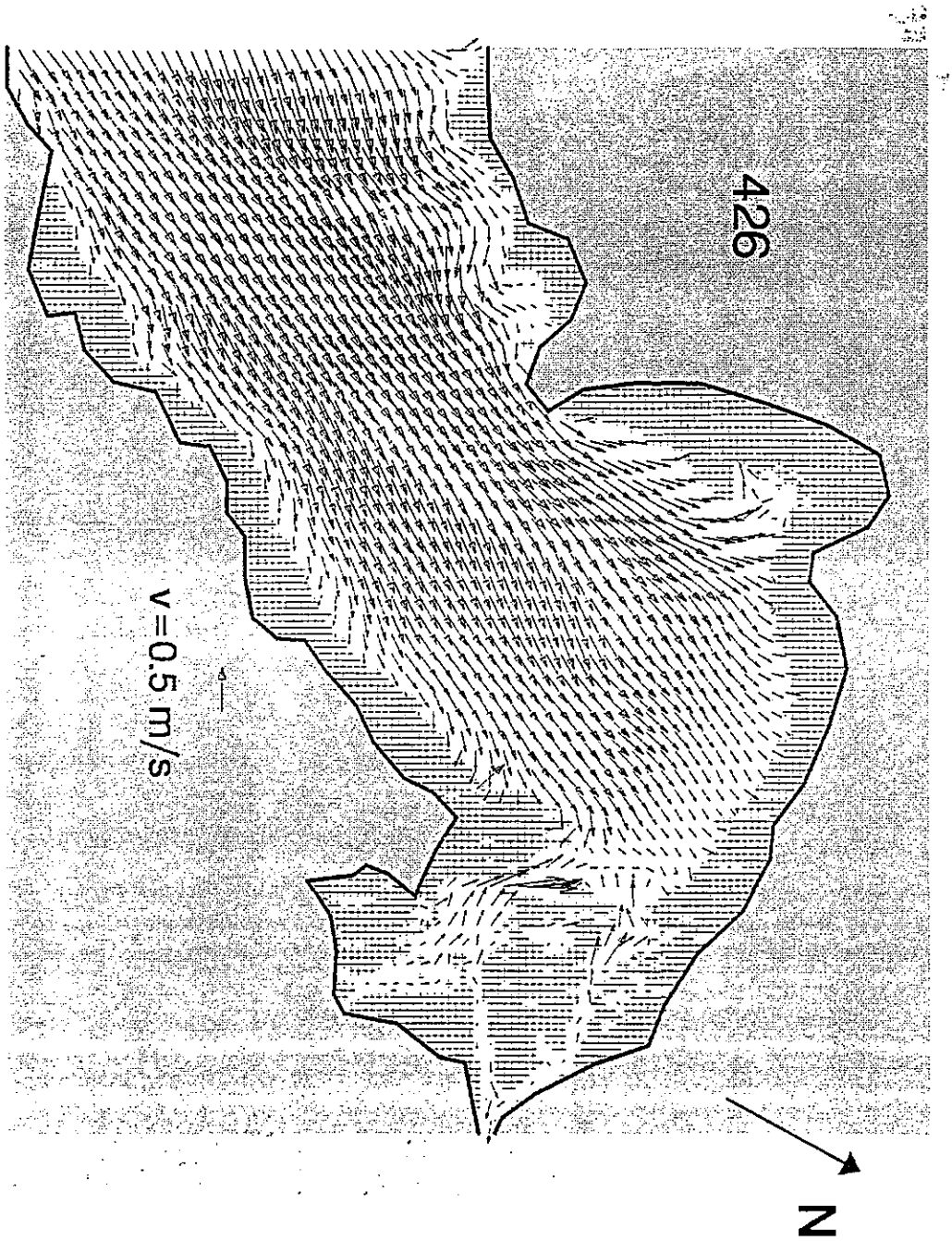

FIG. A7—12(k) Flow field in Deep Bay (Spring Tide)

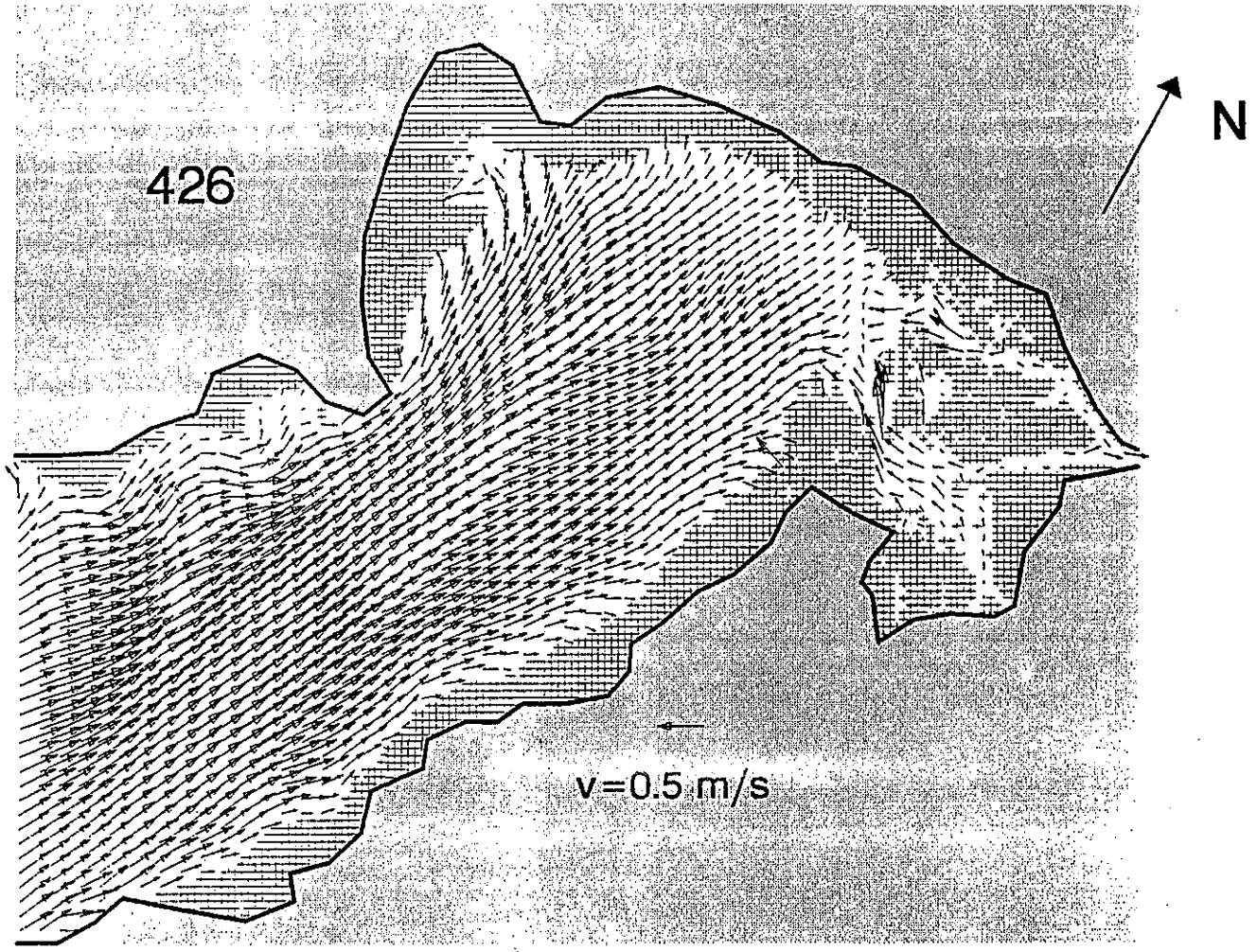

FIG. A7—12(1) Flow field in Deep Bay (Spring Tide)

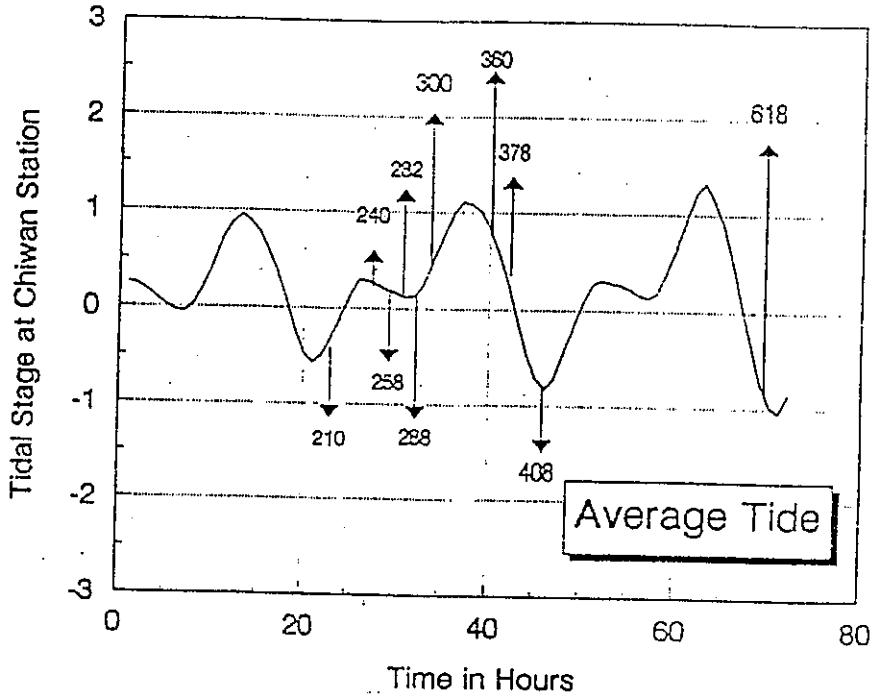

FIG. A7—13(a) Typical tide level process and time sequence (Average Tide)

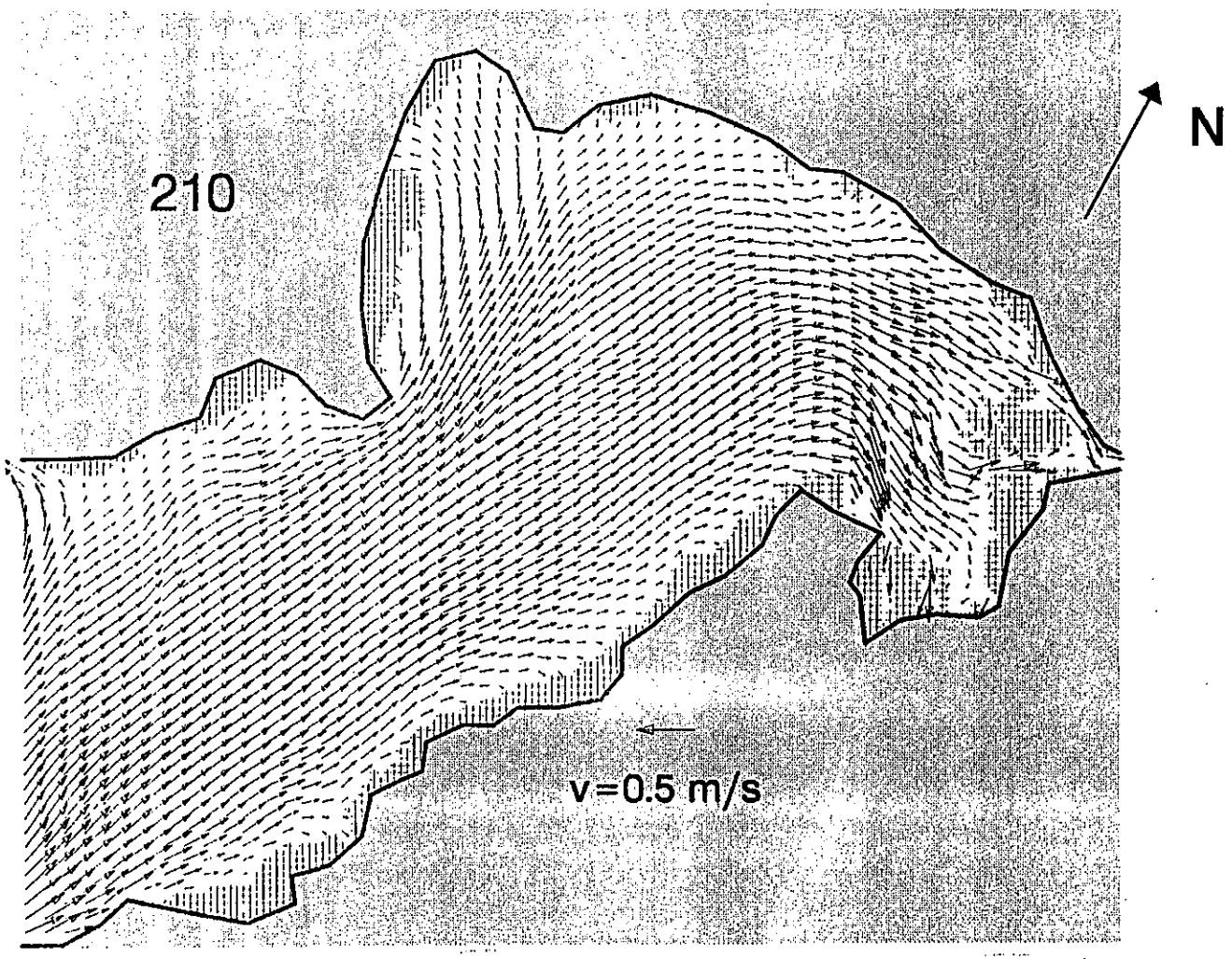

FIG. A7—13(b) **Flow field in Deep Bay (Average Tide)**

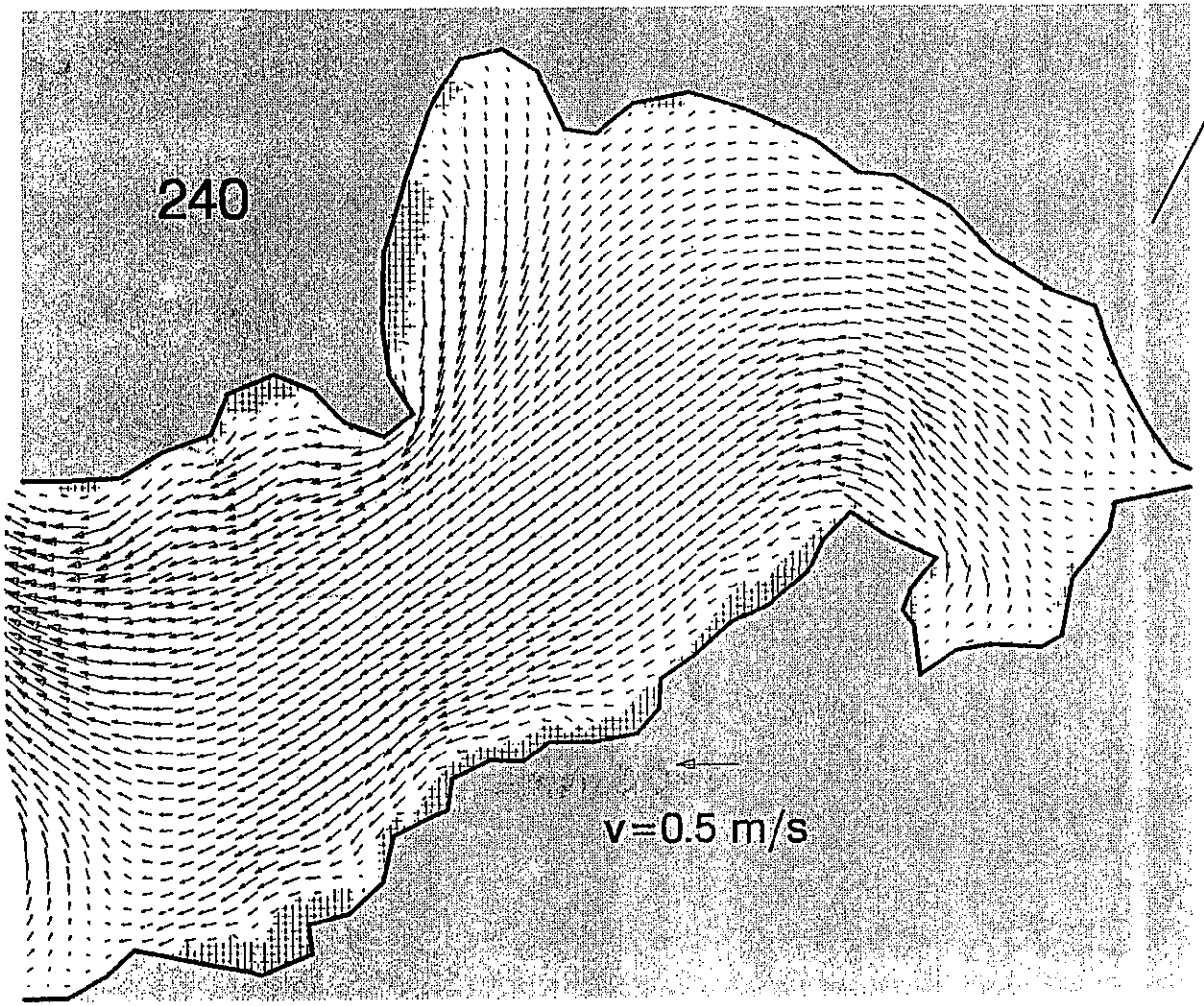

FIG. A7—13(c) Flow field in Deep Bay (Average Tide)

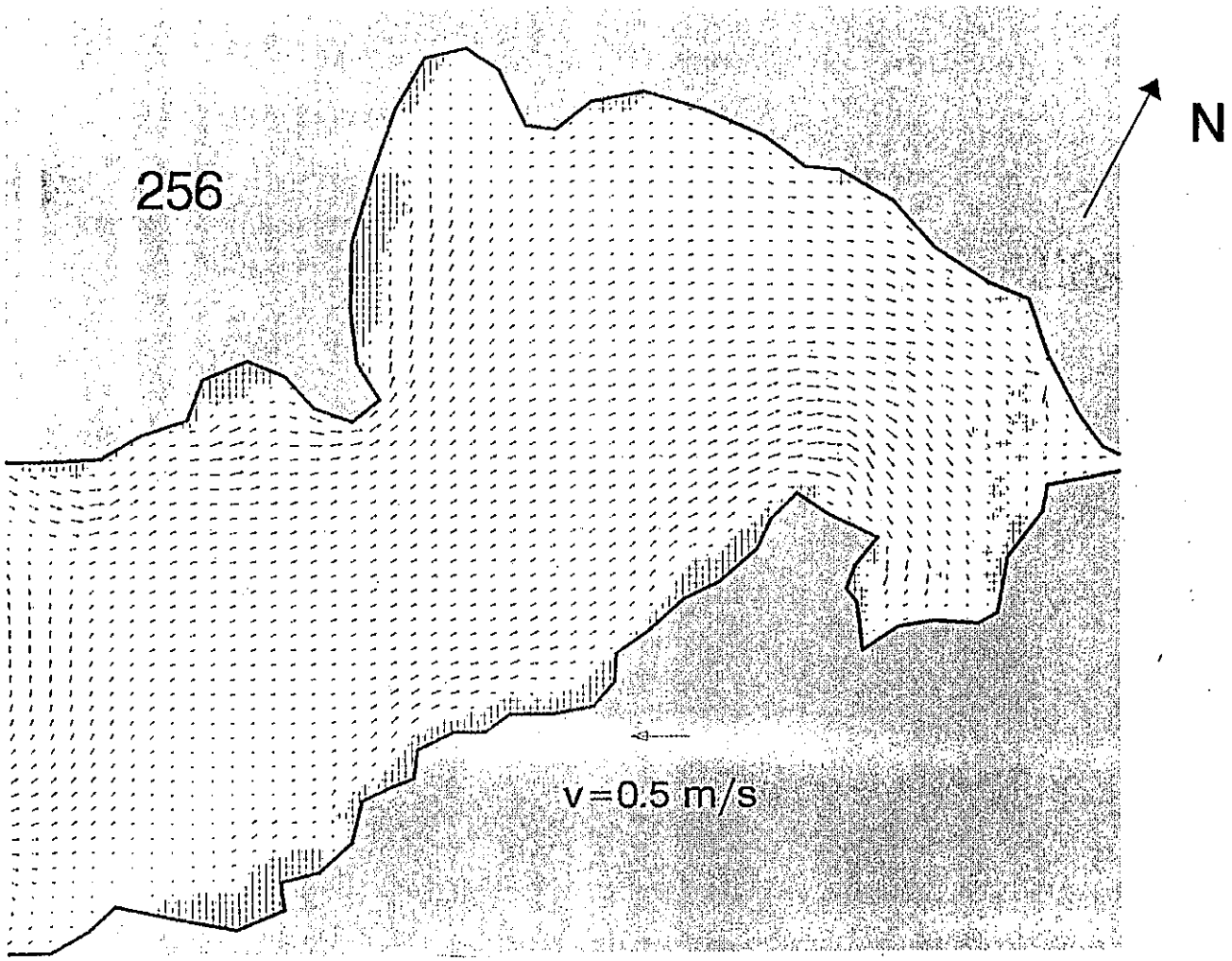

FIG. A7—13(d) Flow field in Deep Bay (Average Tide)

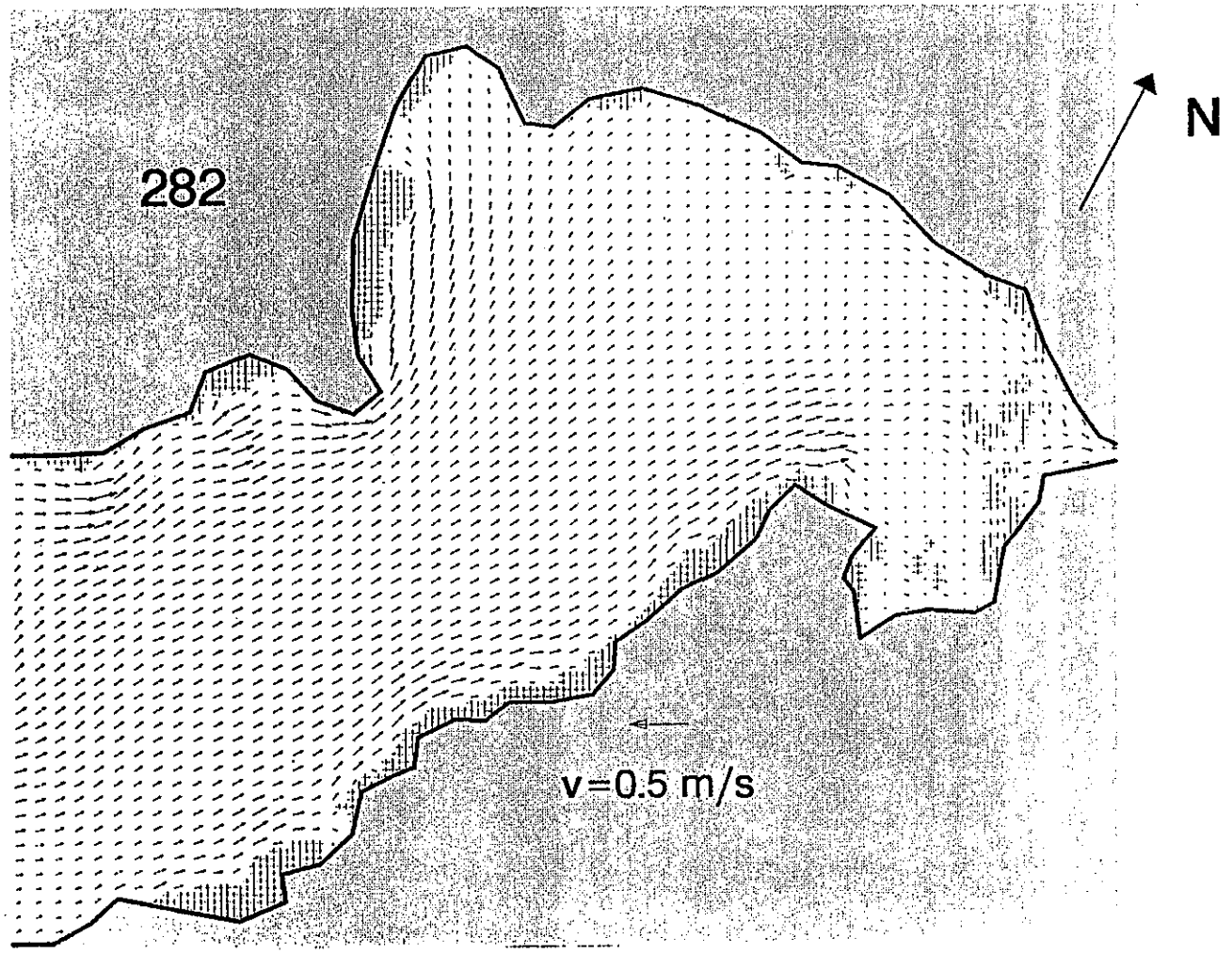

FIG. A7—13(e) Flow field in Deep Bay (Average Tide)

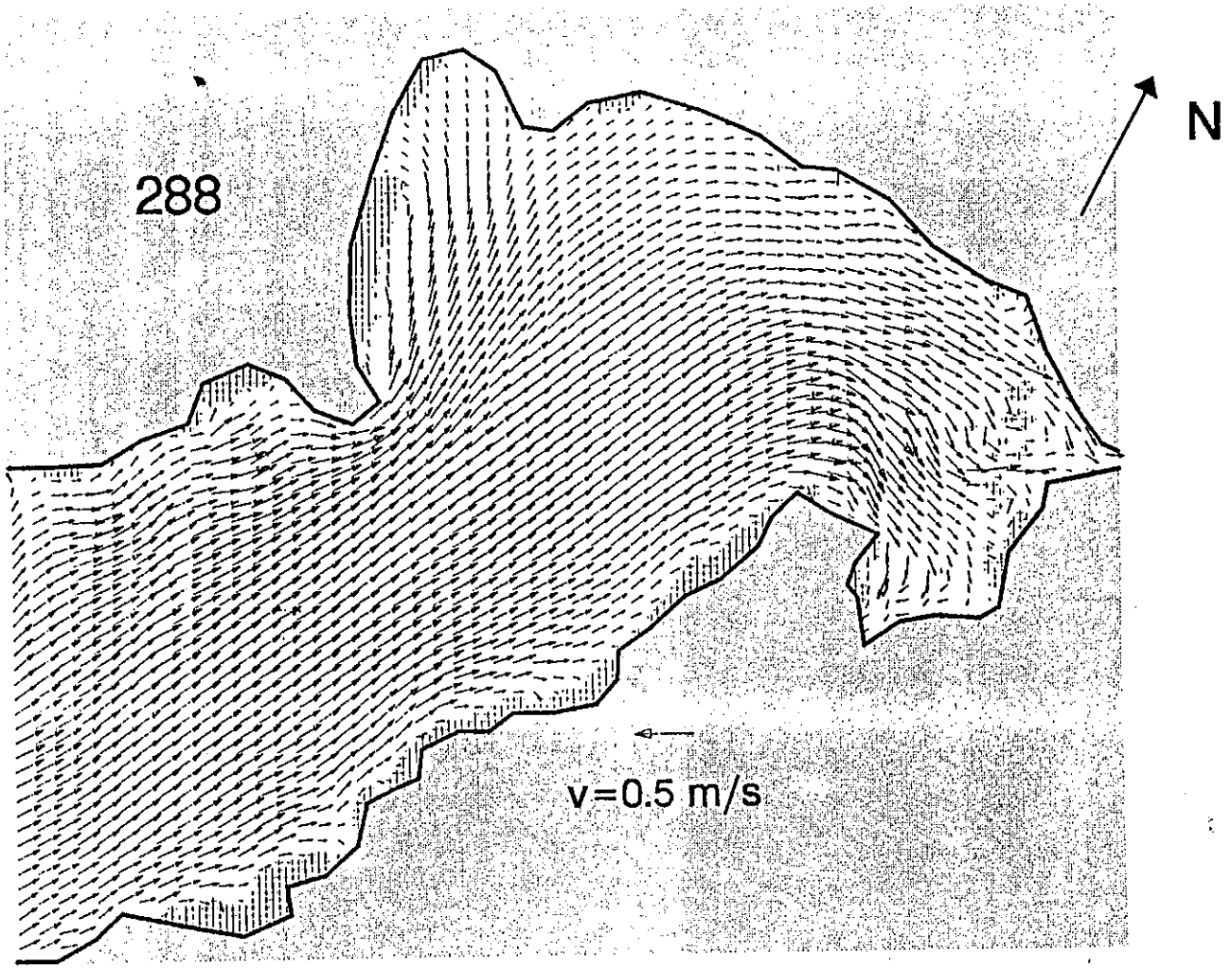

FIG. A7—13(f) Flow field in Deep Bay (Average Tide)

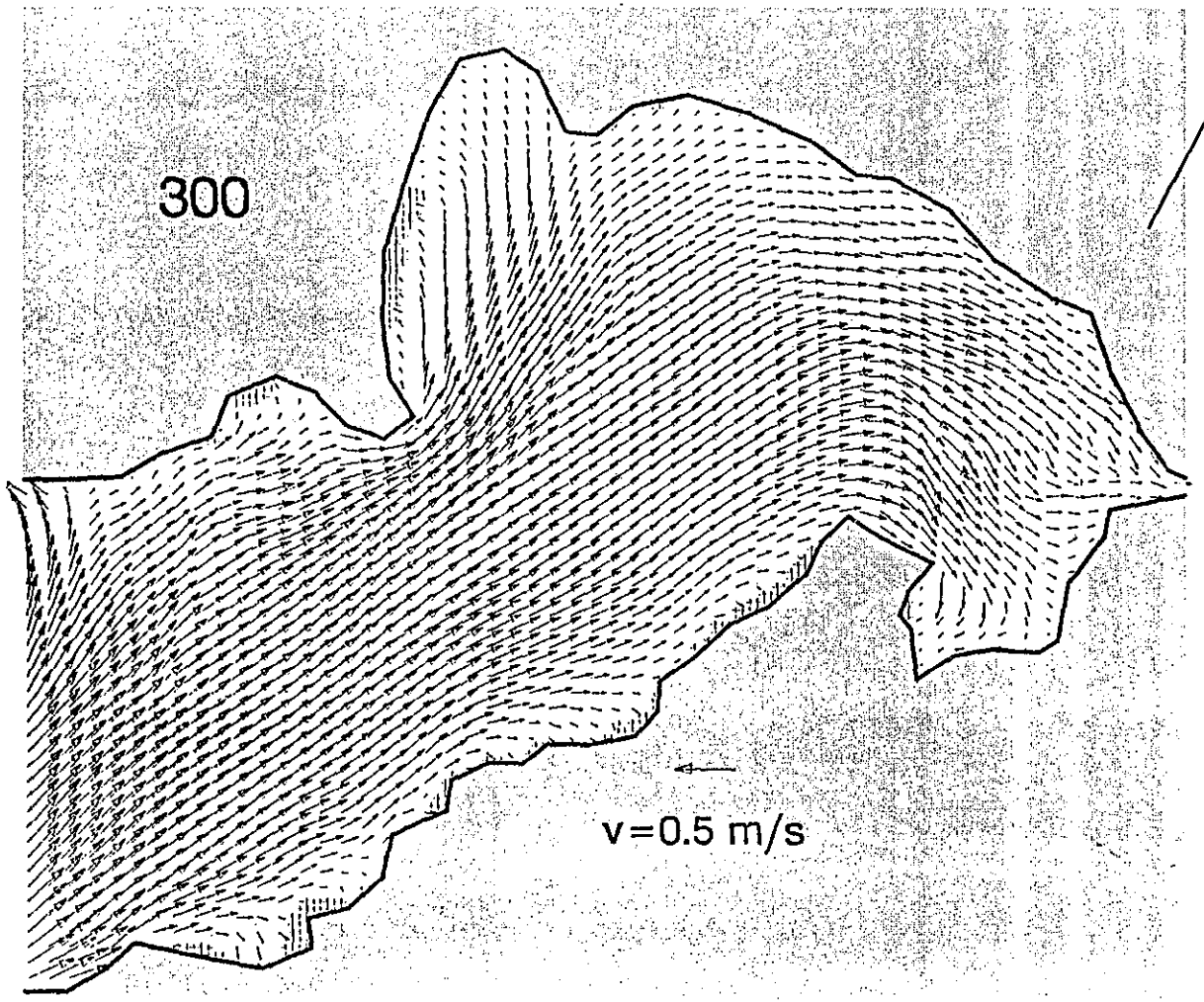

FIG. A7—13(g) Flow field in Deep Bay (Average Tide)

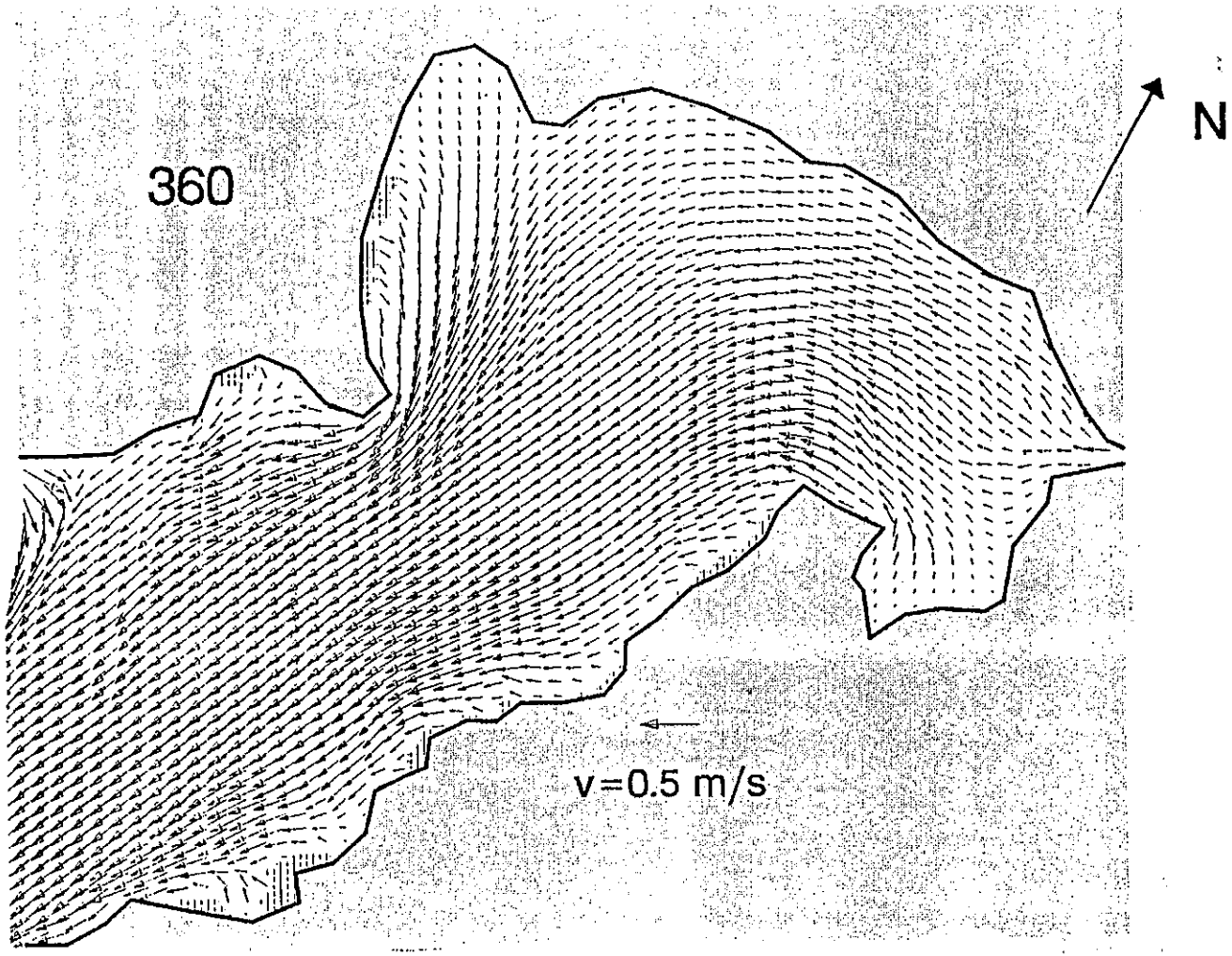

FIG. A7—13(h) Flow field in Deep Bay (Average Tide)

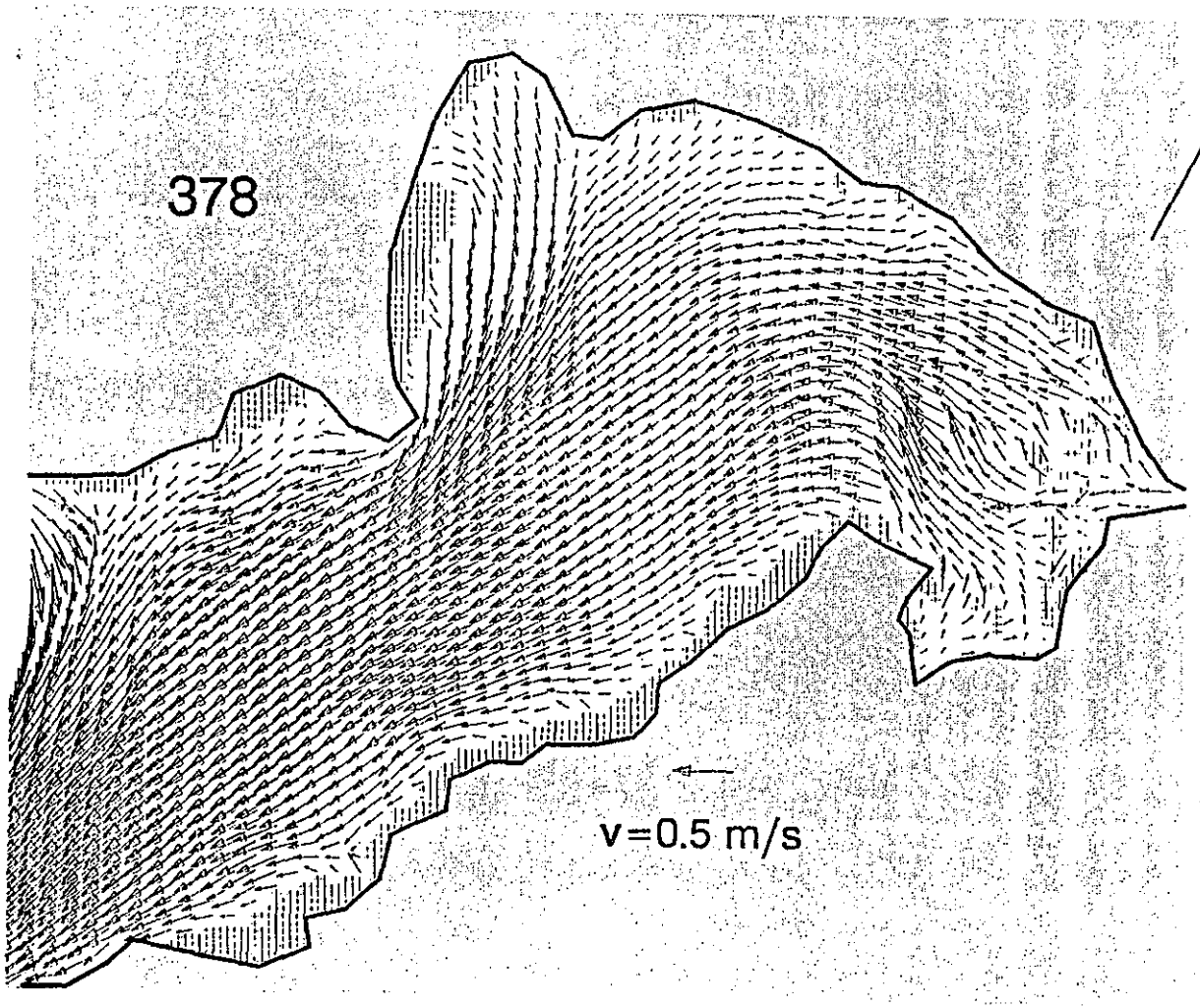

FIG. A7—13(i) Flow field in Deep Bay (Average Tide)

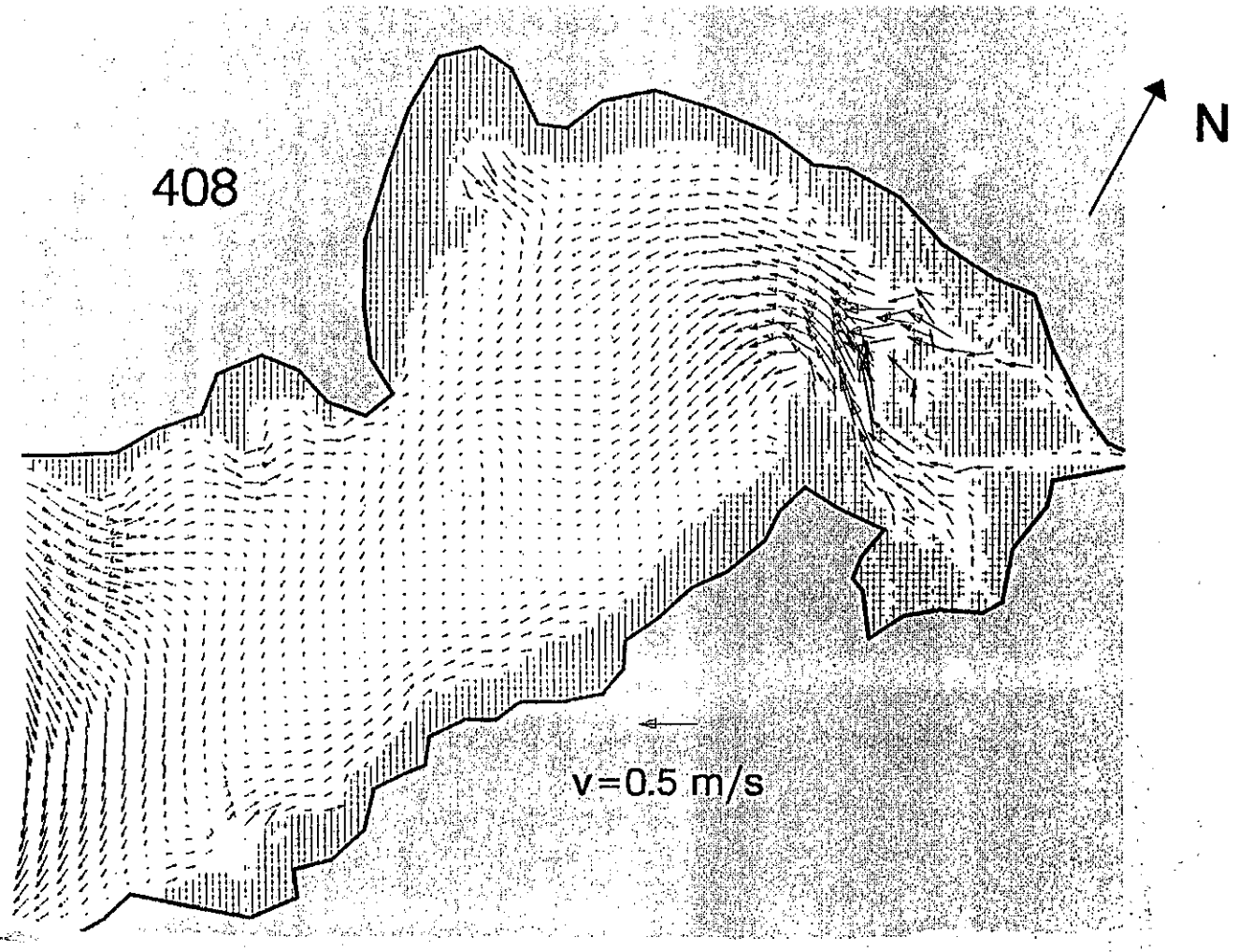

13(j) Flow field in Deep Bay (Average Tide)

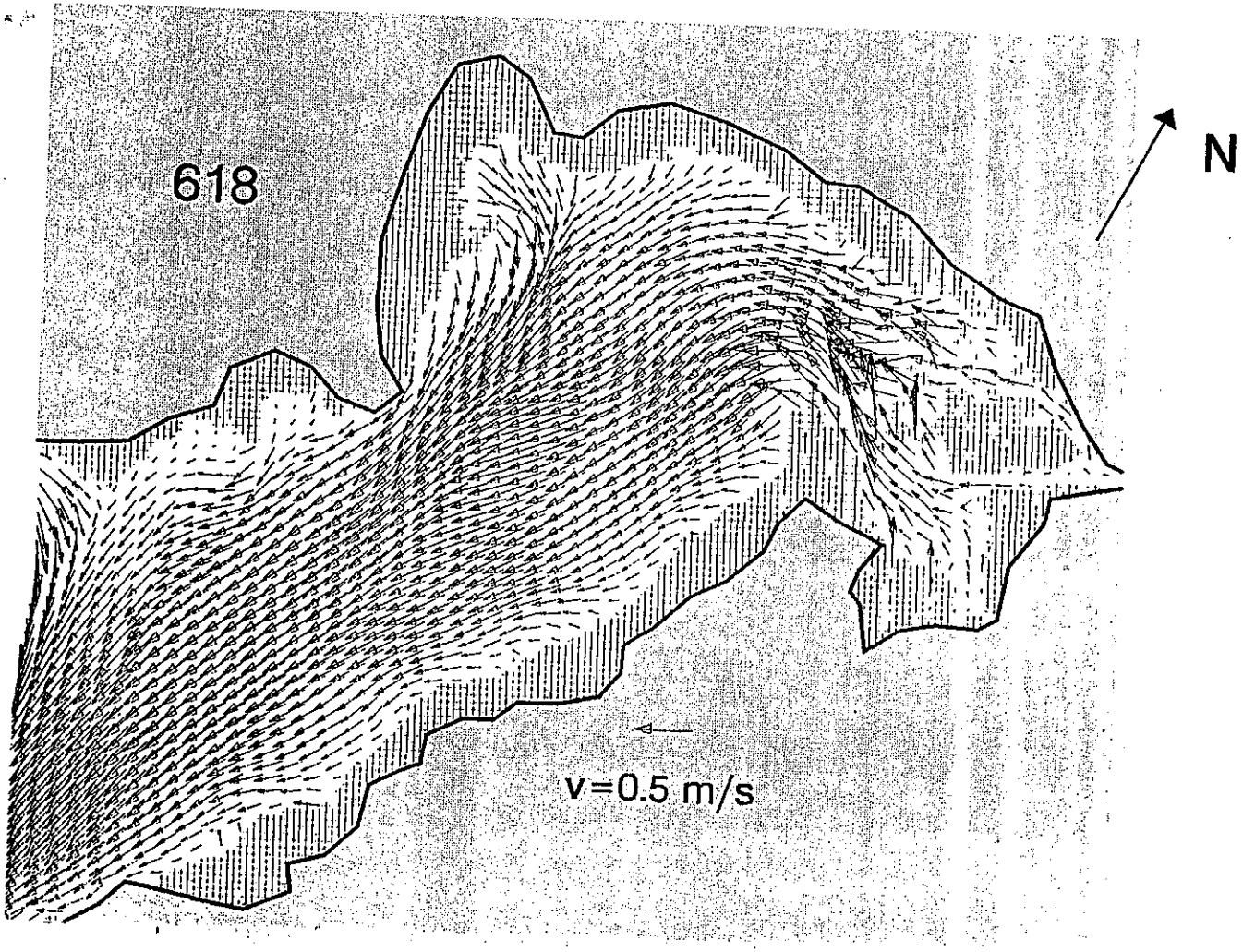

FIG. A7—13(k) Flow field in Deep Bay (Average Tide)

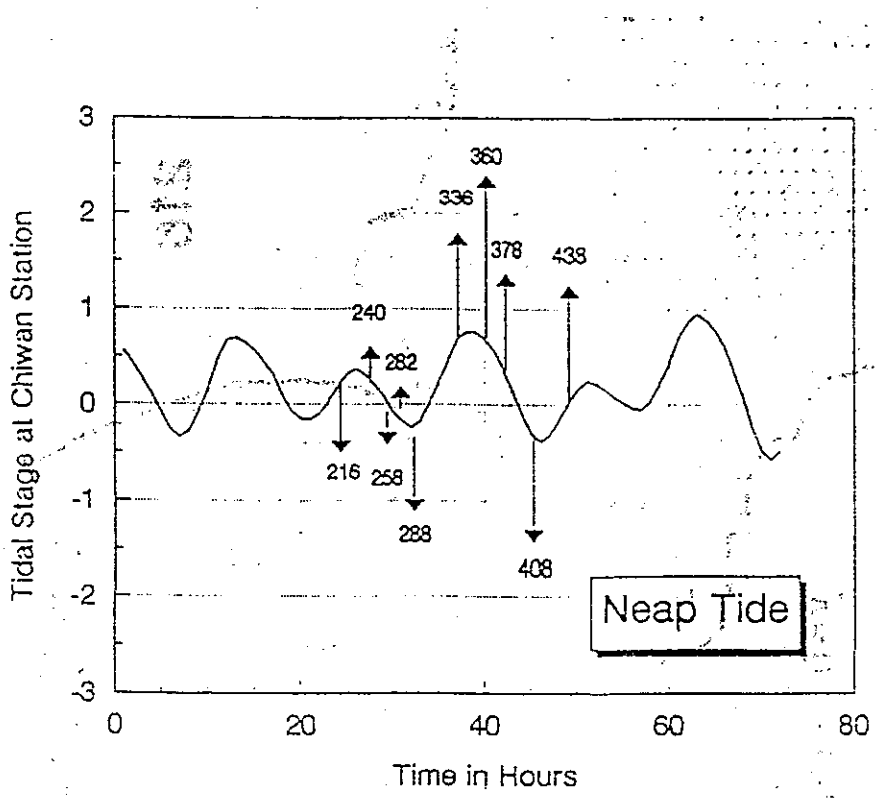

FIG. A7－14(a) **Typical tide level process and time sequence (Neap Tide)**

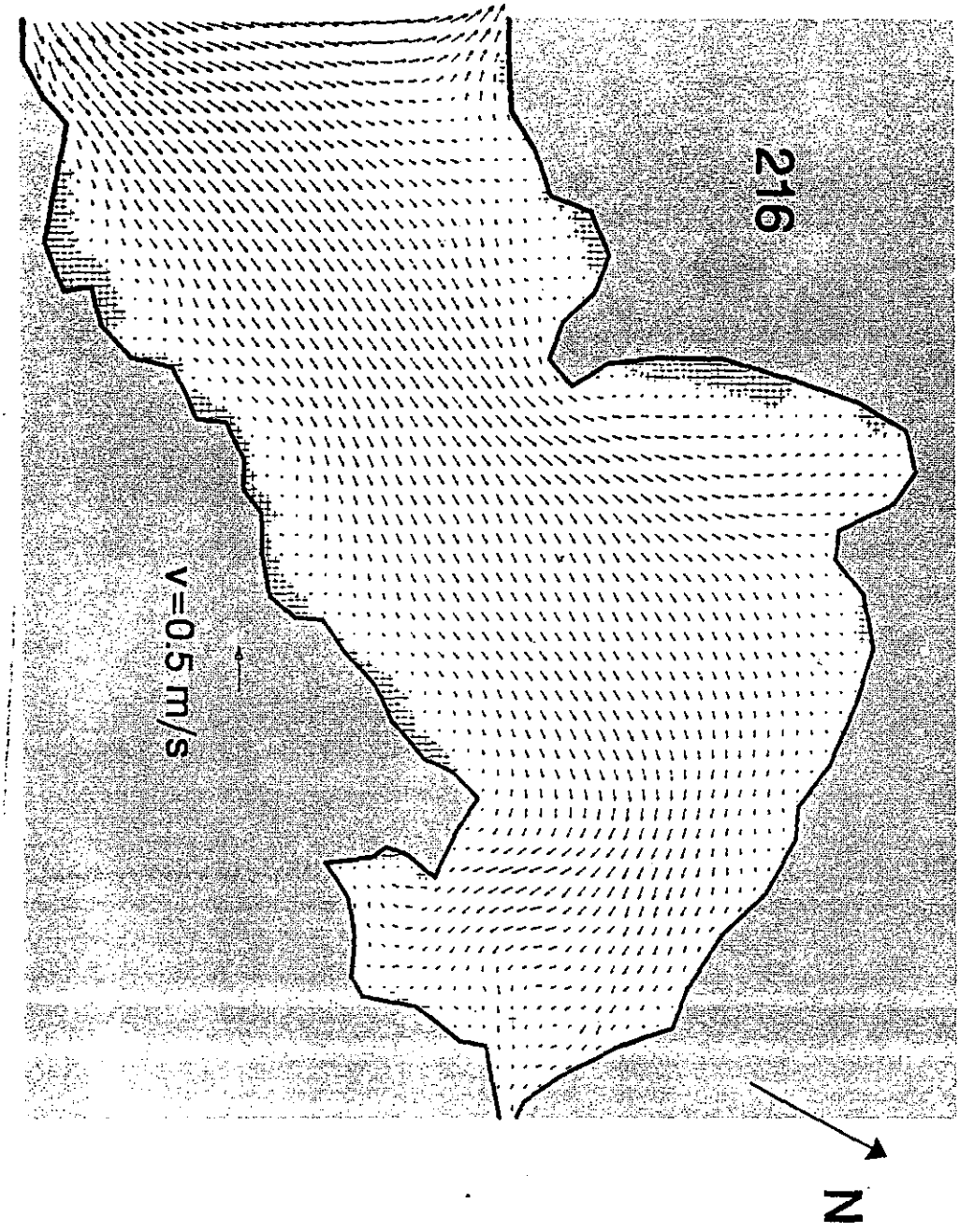

FIG. A7—14(b) Flow field in Deep Bay (Neap Tide)

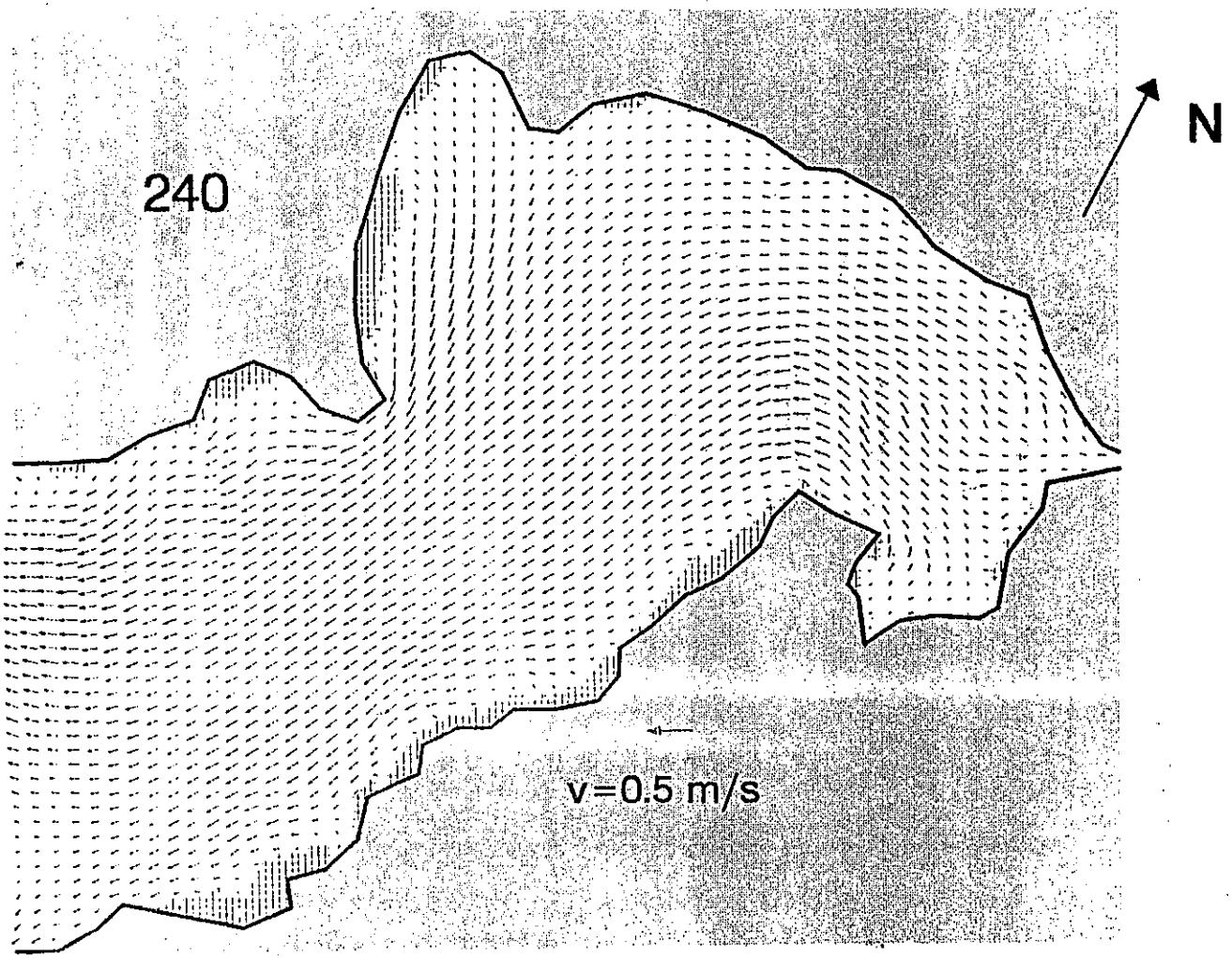

FIG. A7--14(c) Flow field in Deep Bay (Neap Tide)

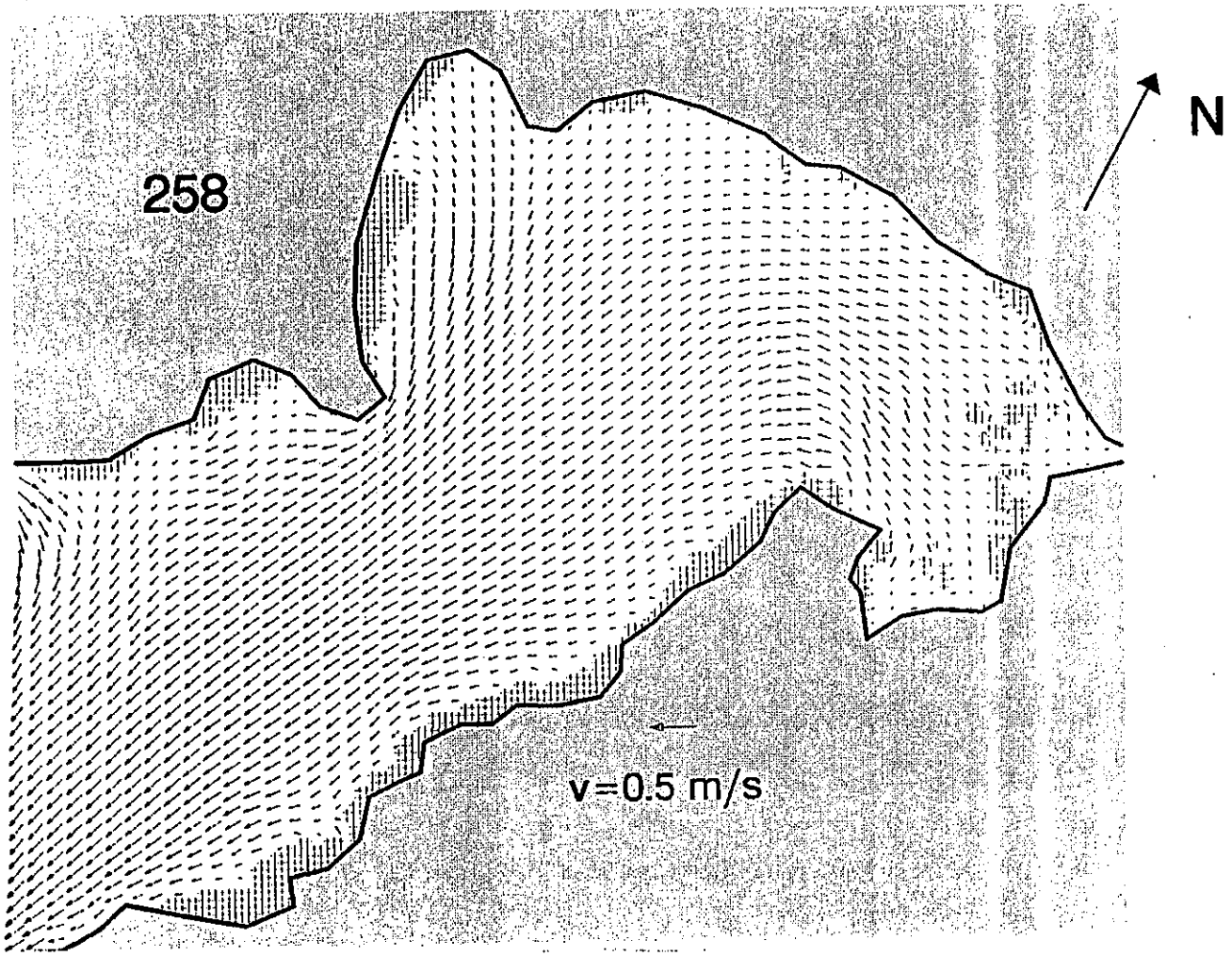

FIG. A7—14(d) Flow field in Deep Bay (Neap Tide)

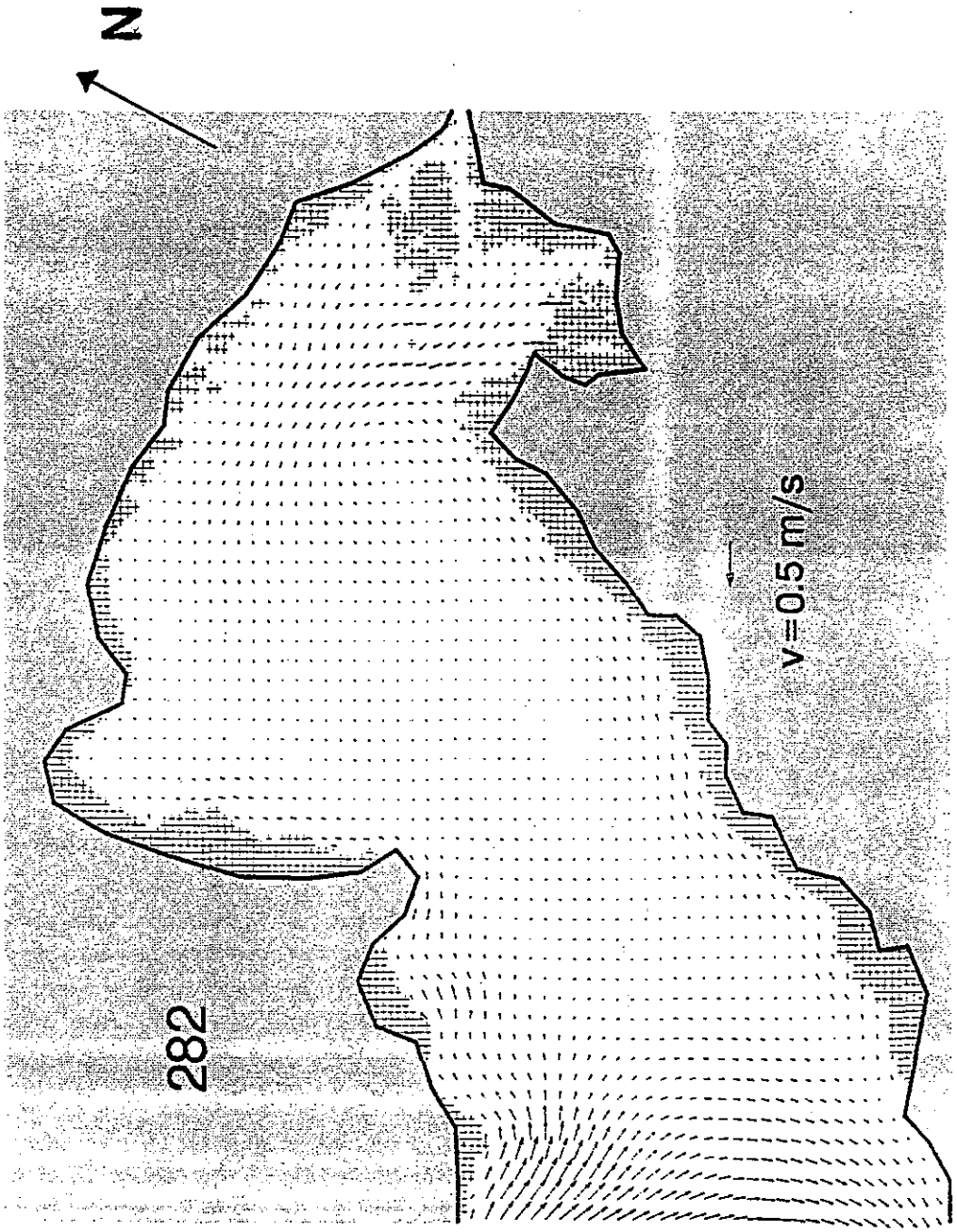

FIG. A7—14(e) Flow field in Deep Bay (Neap Tide)

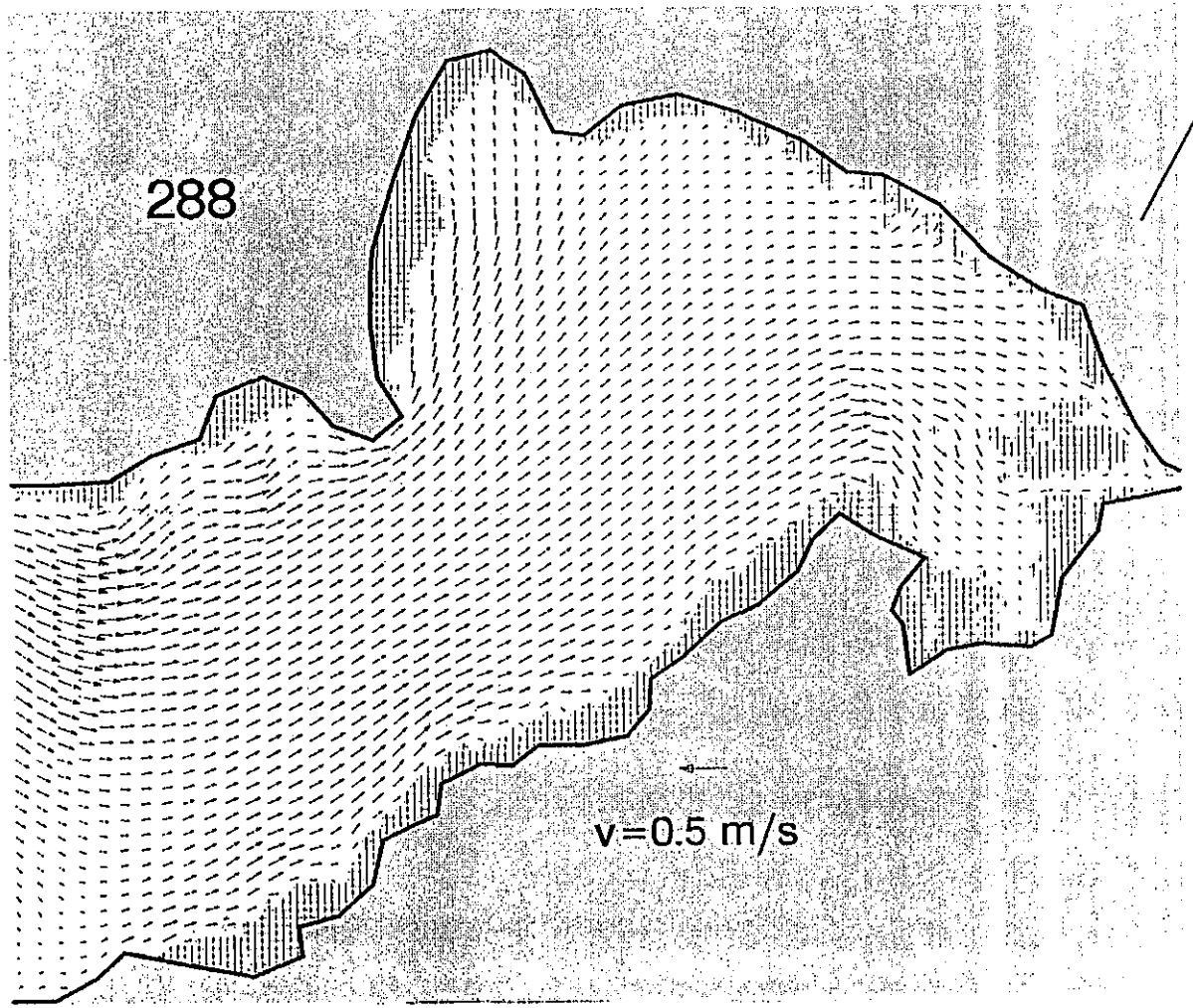

FIG. A7−14(f) Flow field in Deep Bay (Neap Tide)

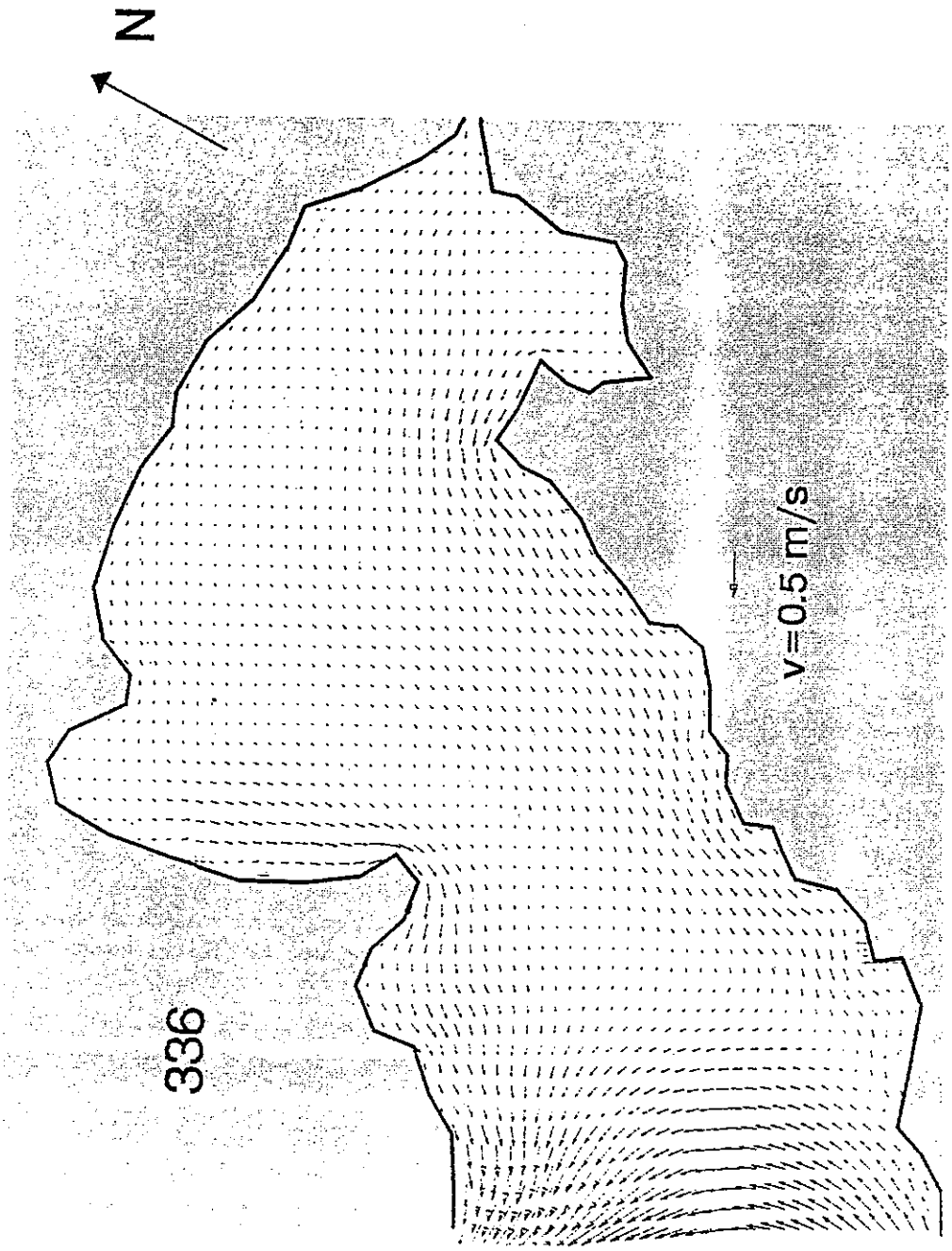

FIG. A7—14(g) Flow field in Deep Bay (Neap Tide)

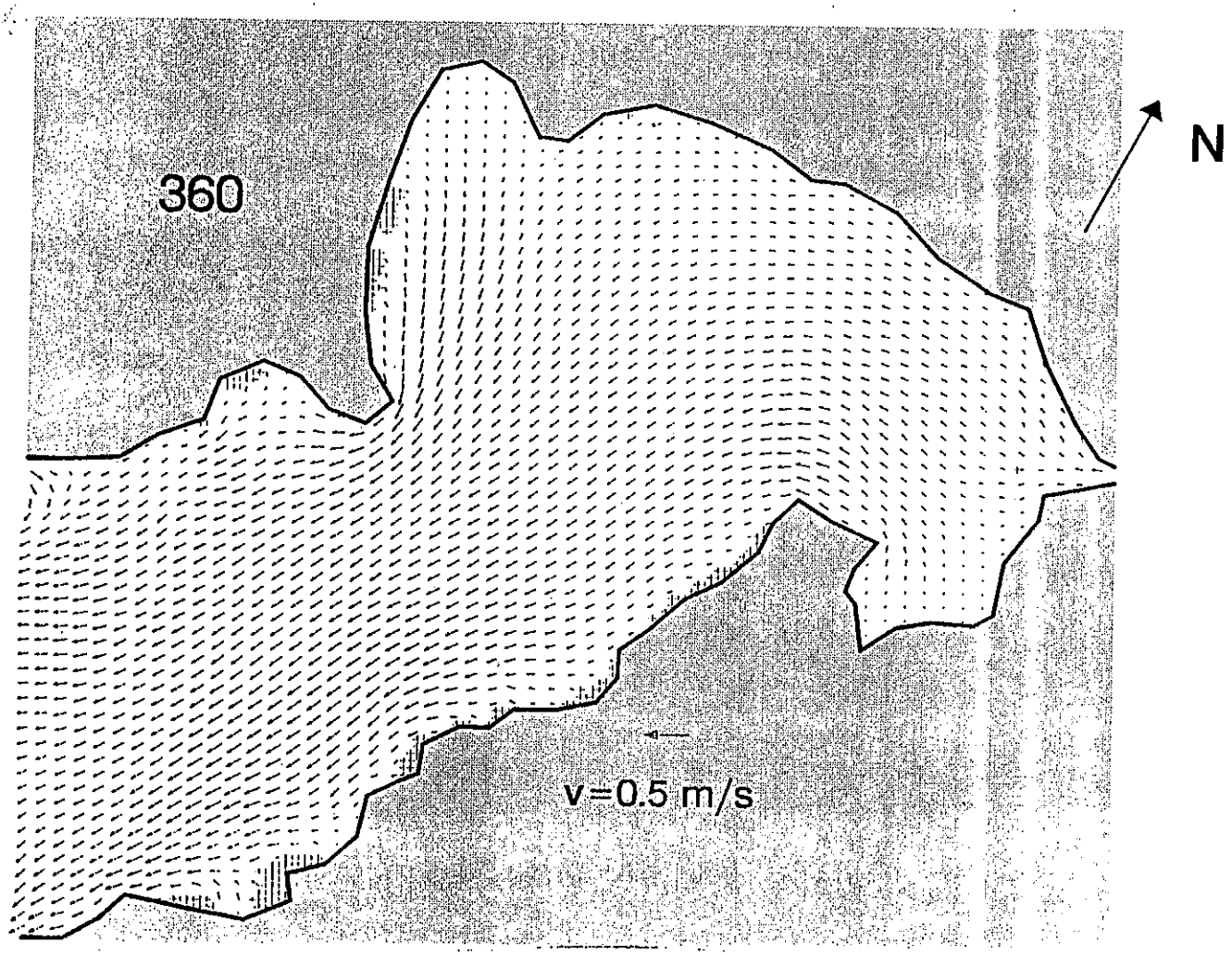

FIG. A7−14(h) Flow field in Deep Bay (Neap Tide)

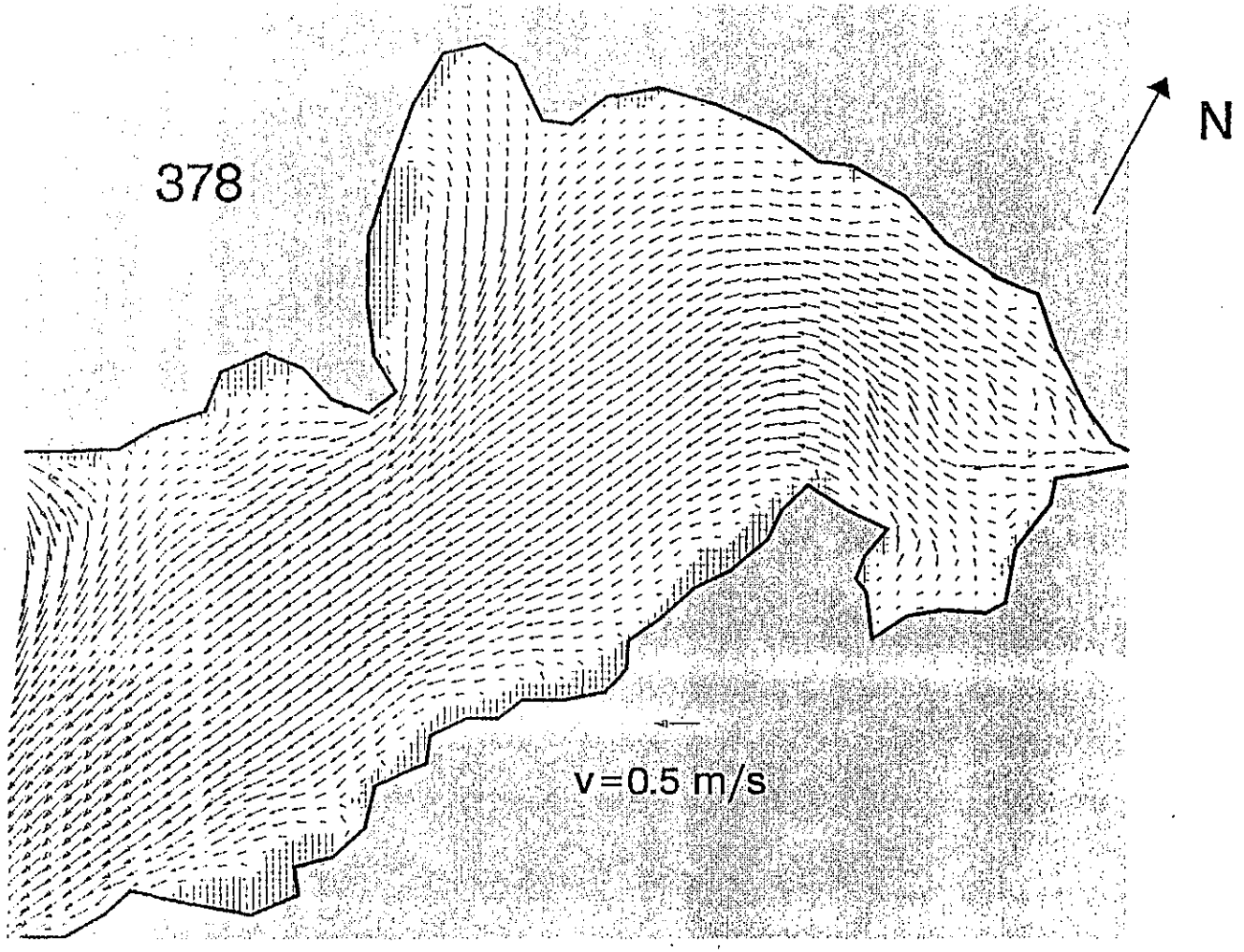

FIG. A7—14(i) Flow field in Deep Bay (Neap Tide)

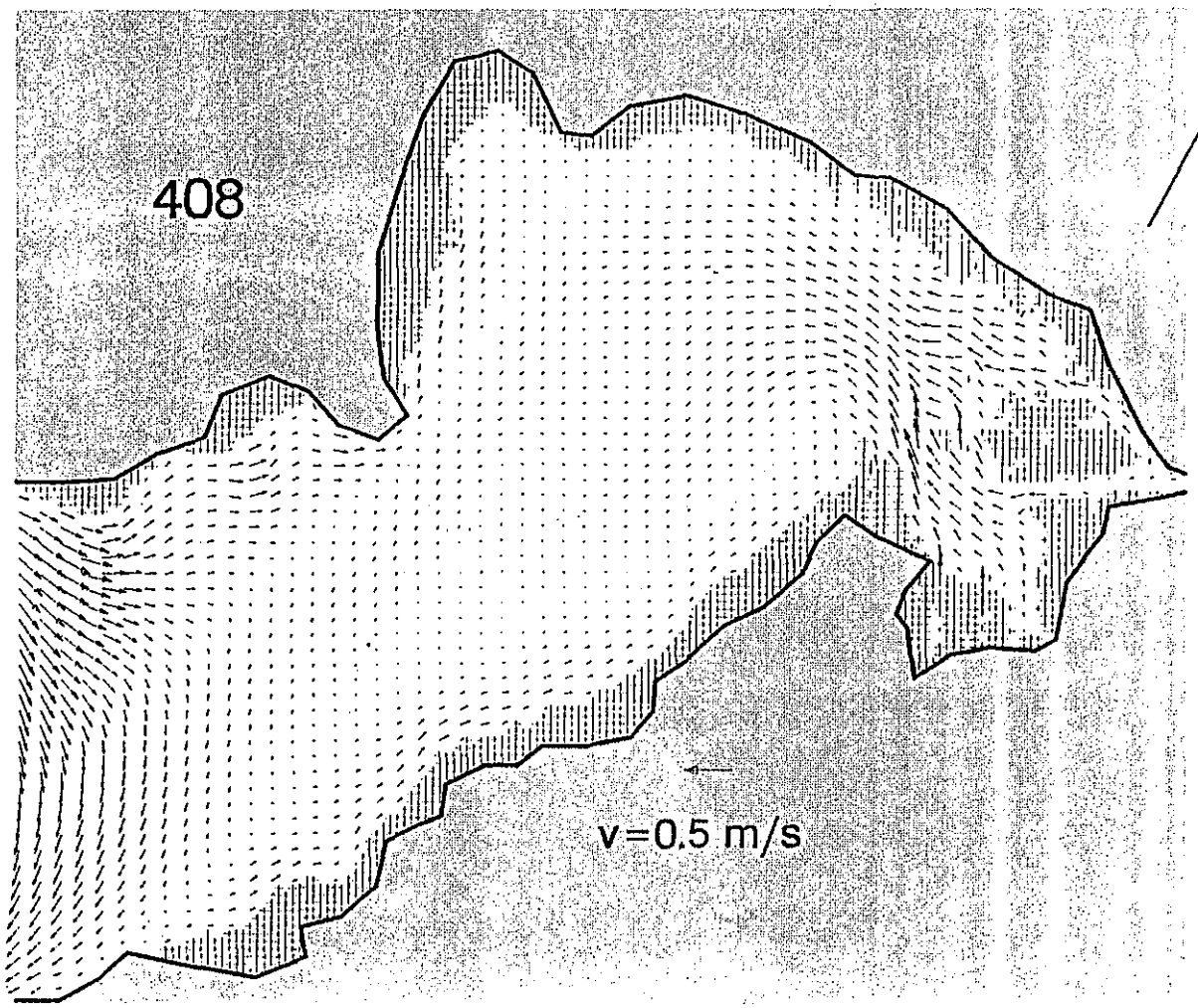

FIG. A7—14(j) Flow field in Deep Bay (Neap Tide)

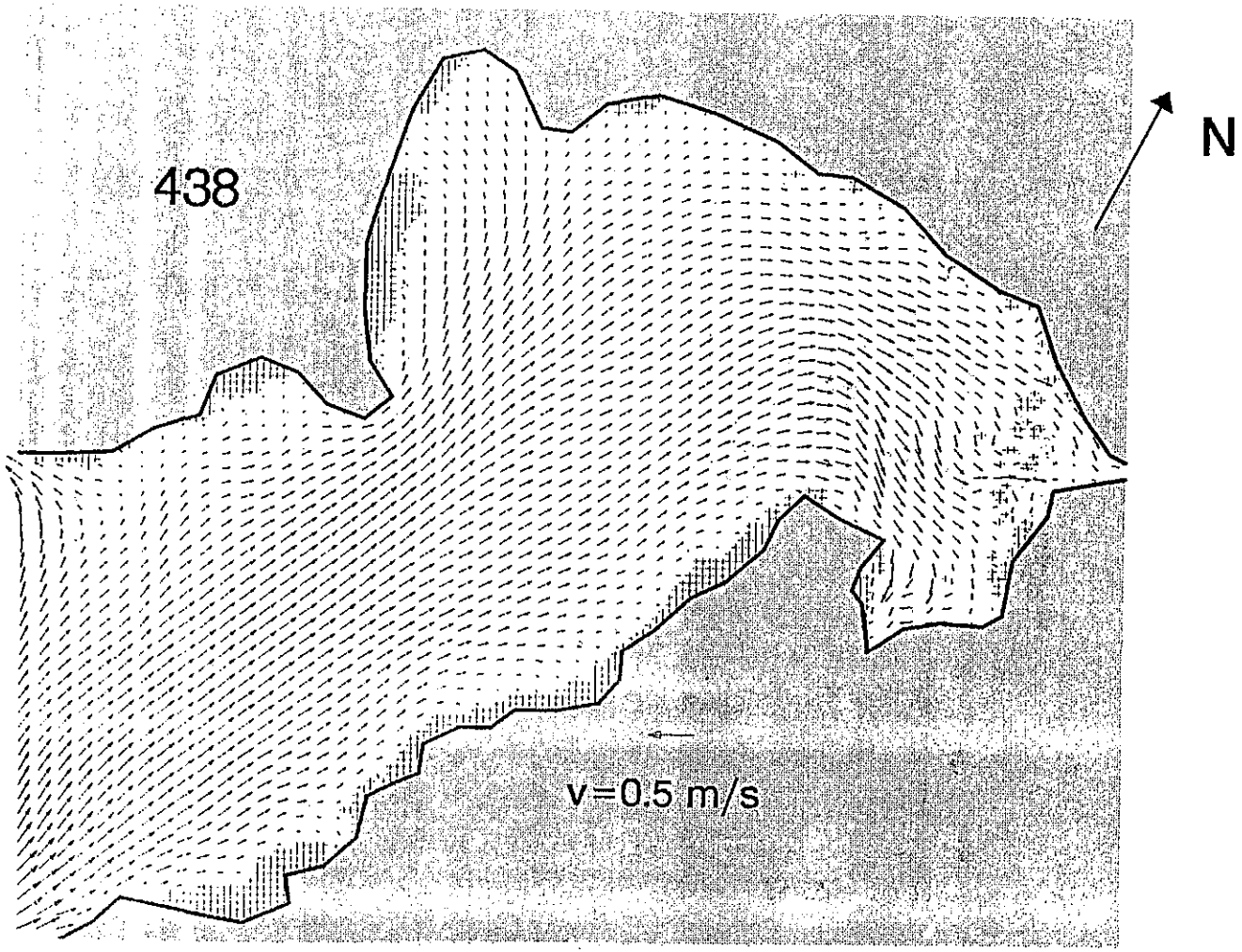

FIG. A7—14(k) Flow field in Deep Bay (Neap Tide)

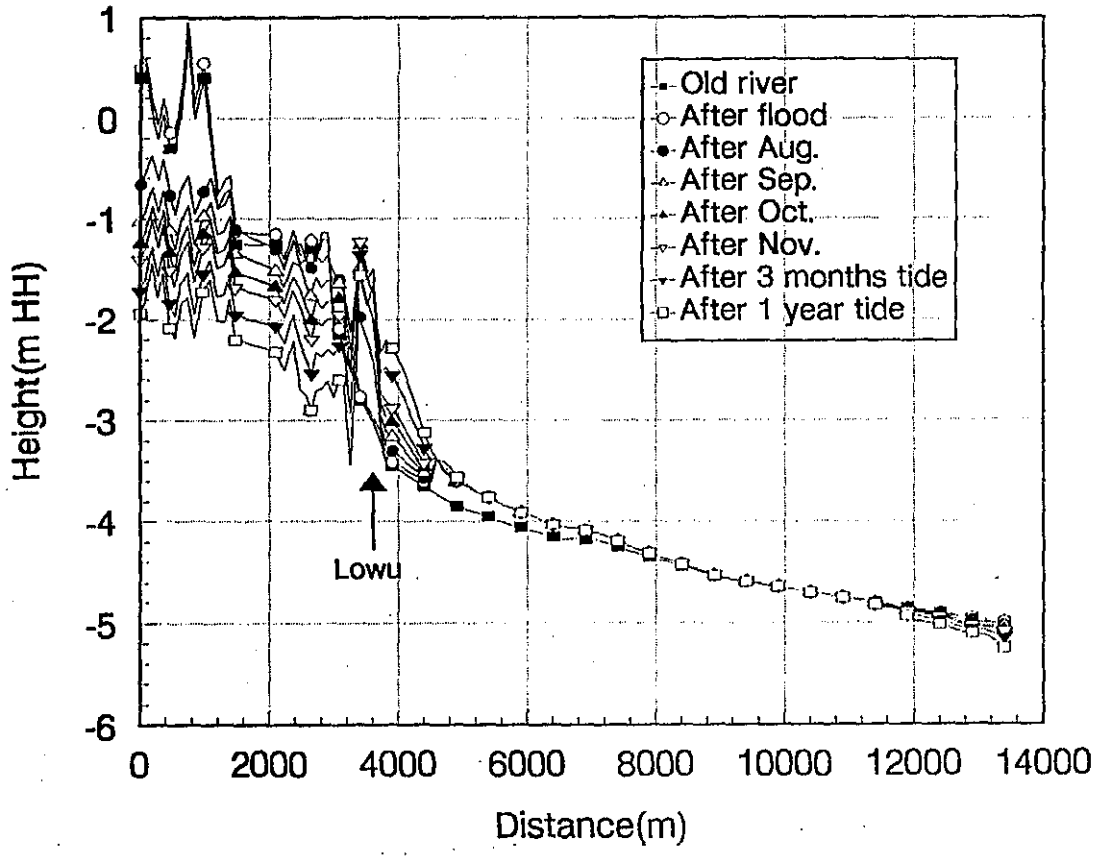

FIG. A7—16 Variation of bed elevation within a year after stage 2 works

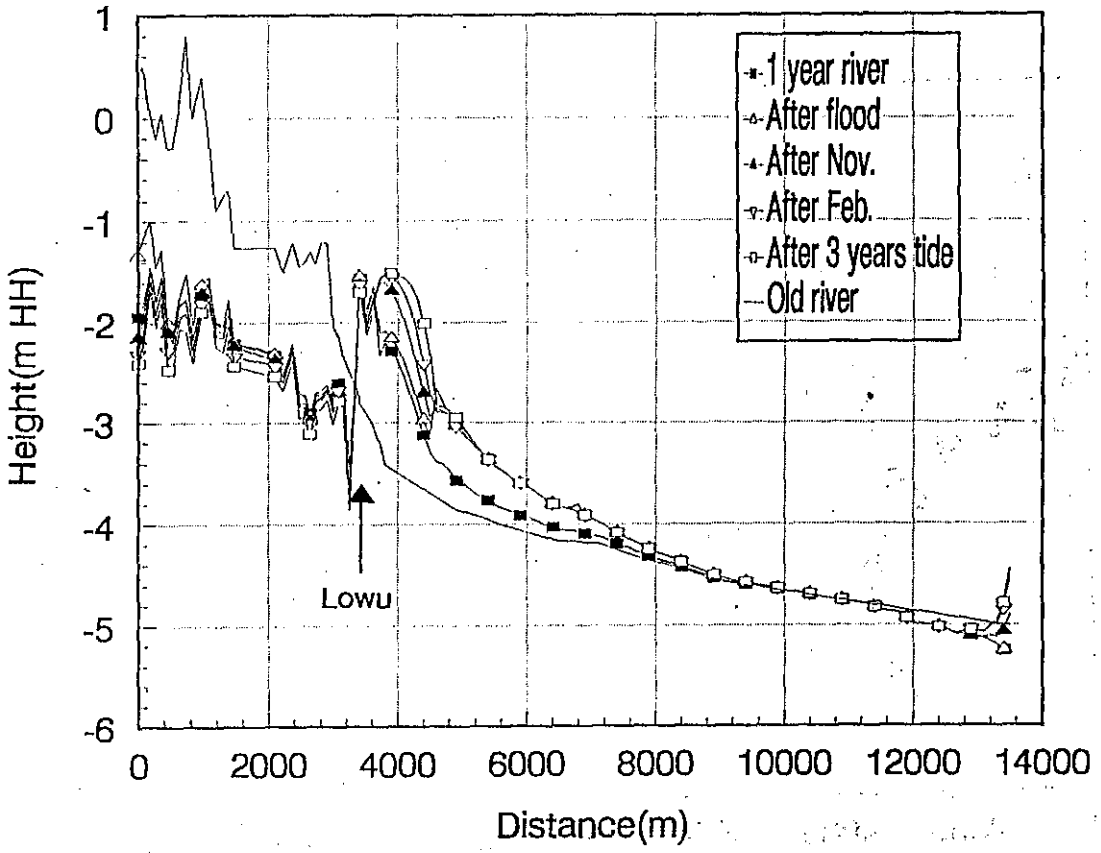

FIG. A7—17 Variation of bed elevation within 3 year after stage 2 works

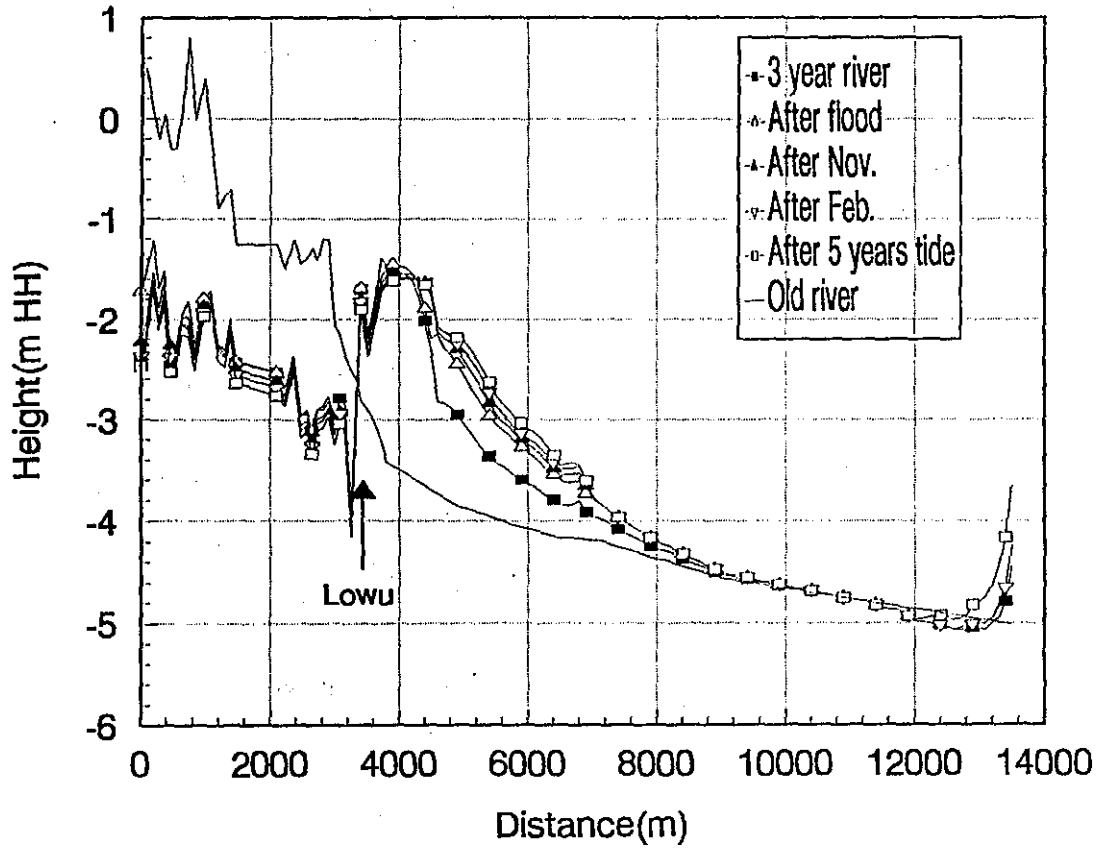

FIG. A7—18 **Variation of bed elevation within a year after stage 2 works**

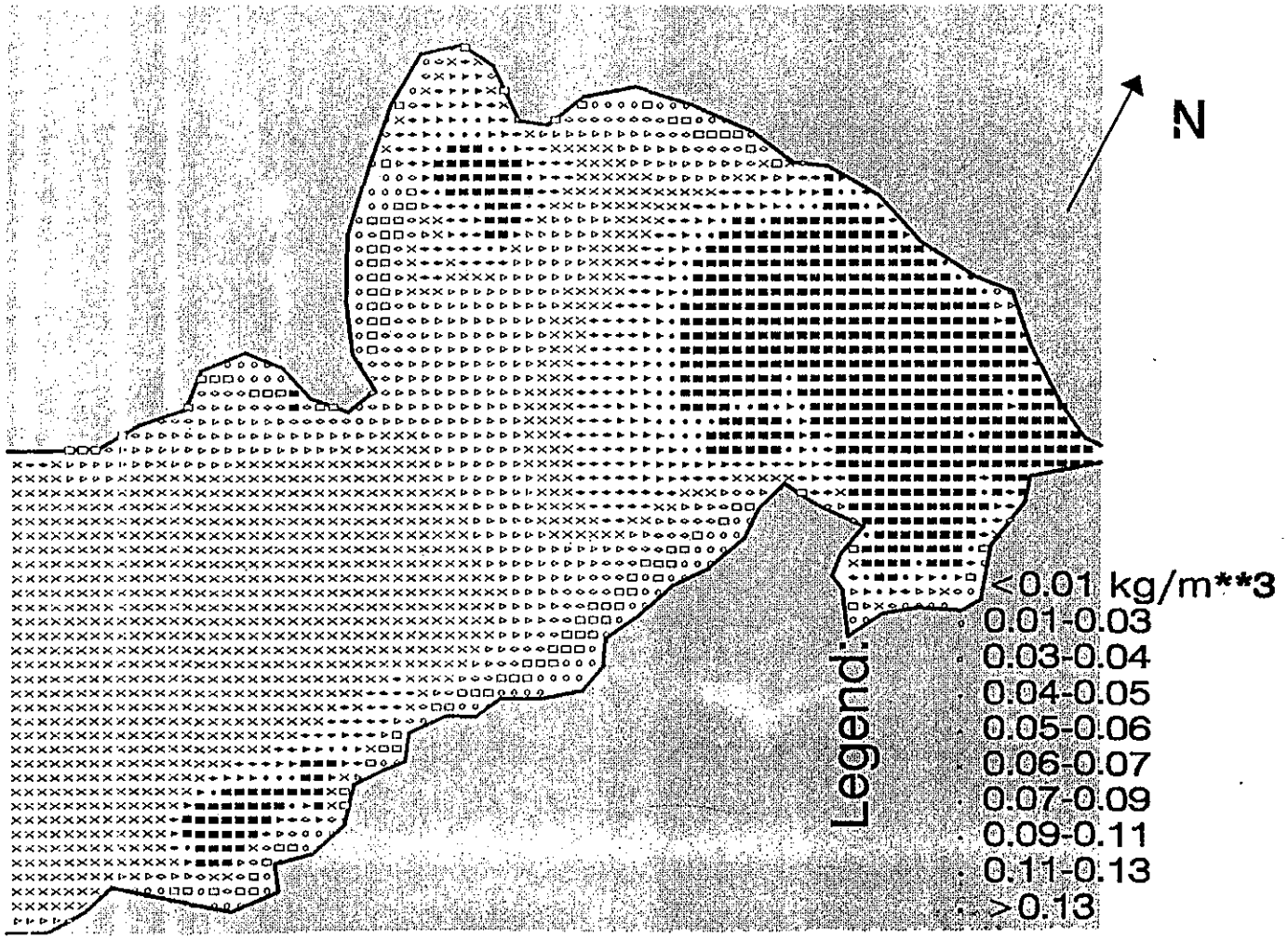

FIG. A7—20(a) Maximum sediment concentration within 2 days in Deep Bay during the construction of stage 2 works (Spring Tide)

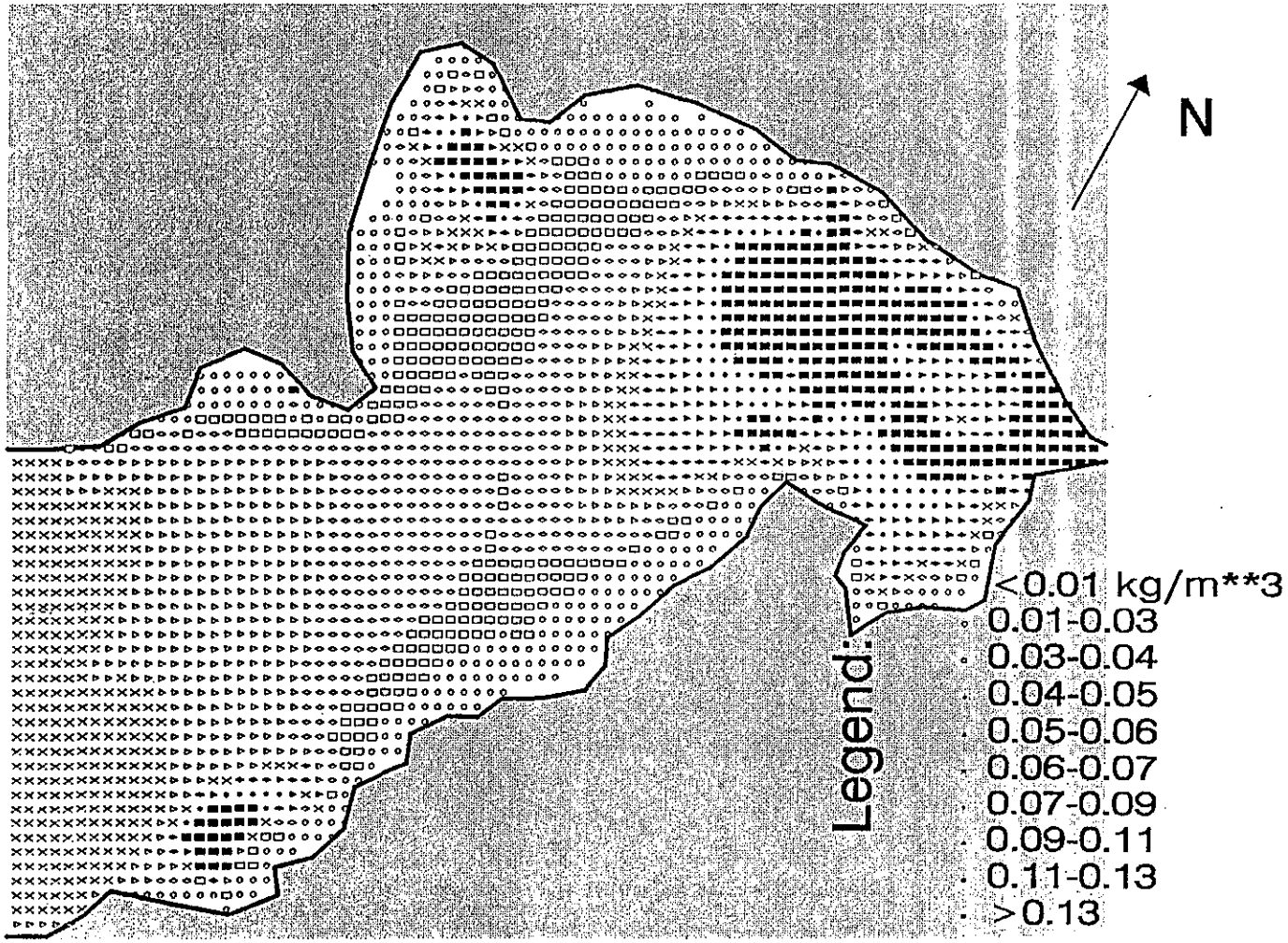

FIG. A7—20(b) Maximum sediment concentration within 2 days in Deep Bay during the construction of stage 2 works (Average Tide)

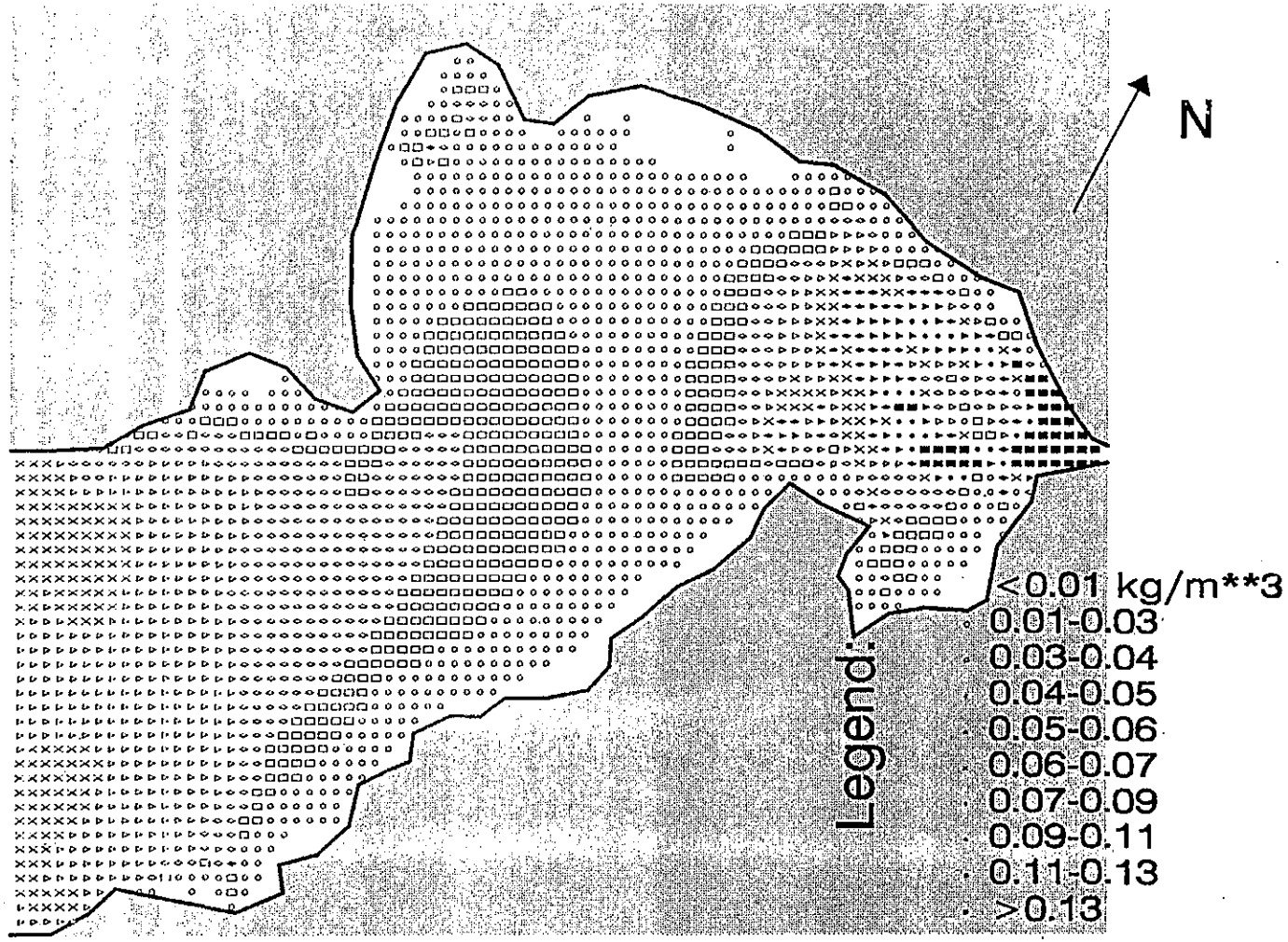

FIG. A7—20(c) Maximum sediment concentration within 2 days in Deep Bay during the construction of stage 2 works (Neap Tide)

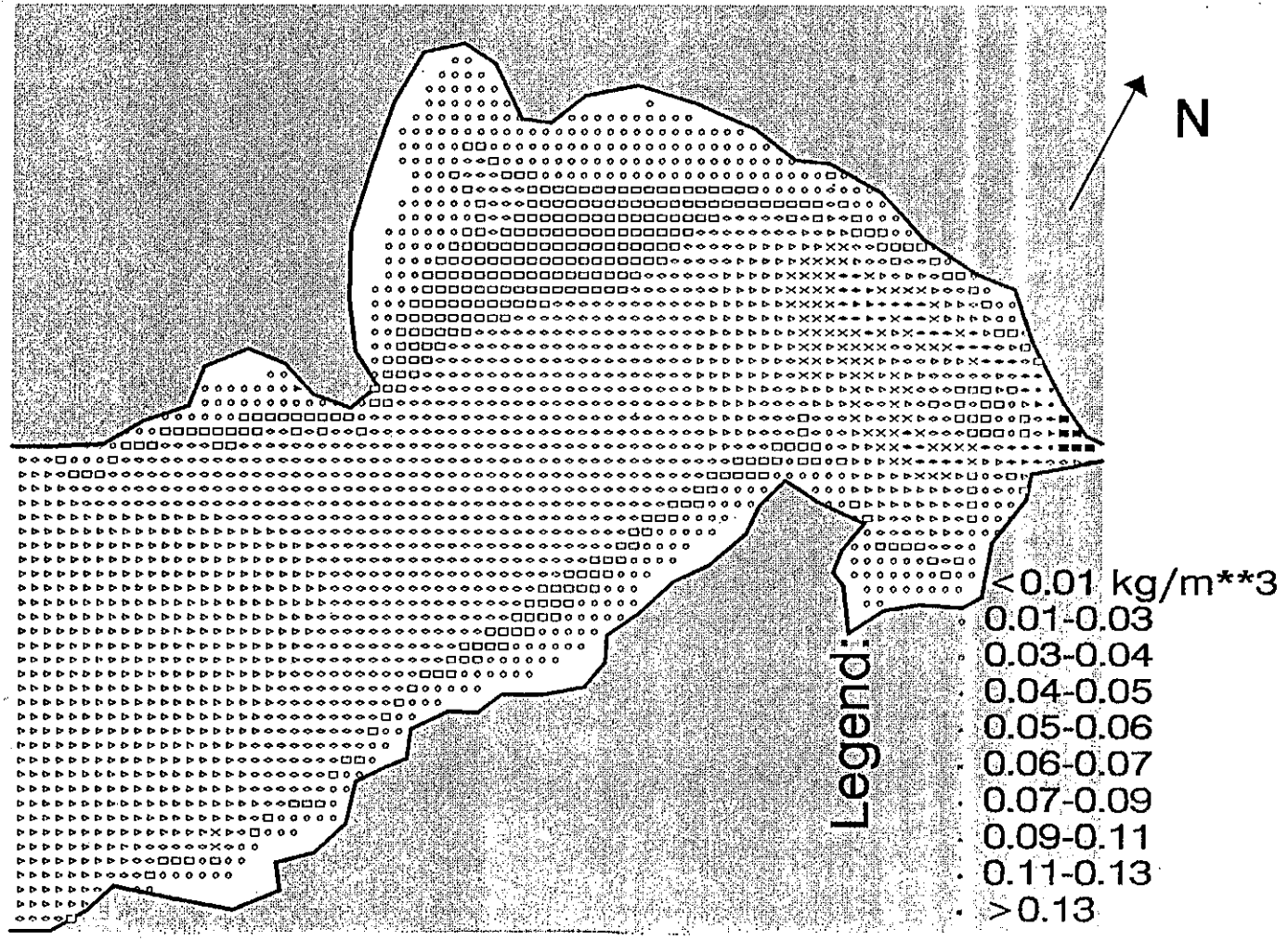

FIG. A7—21(a) Maximum sediment concentration over 2 days in Deep Bay during the construction of stage 2 works (Spring Tide)

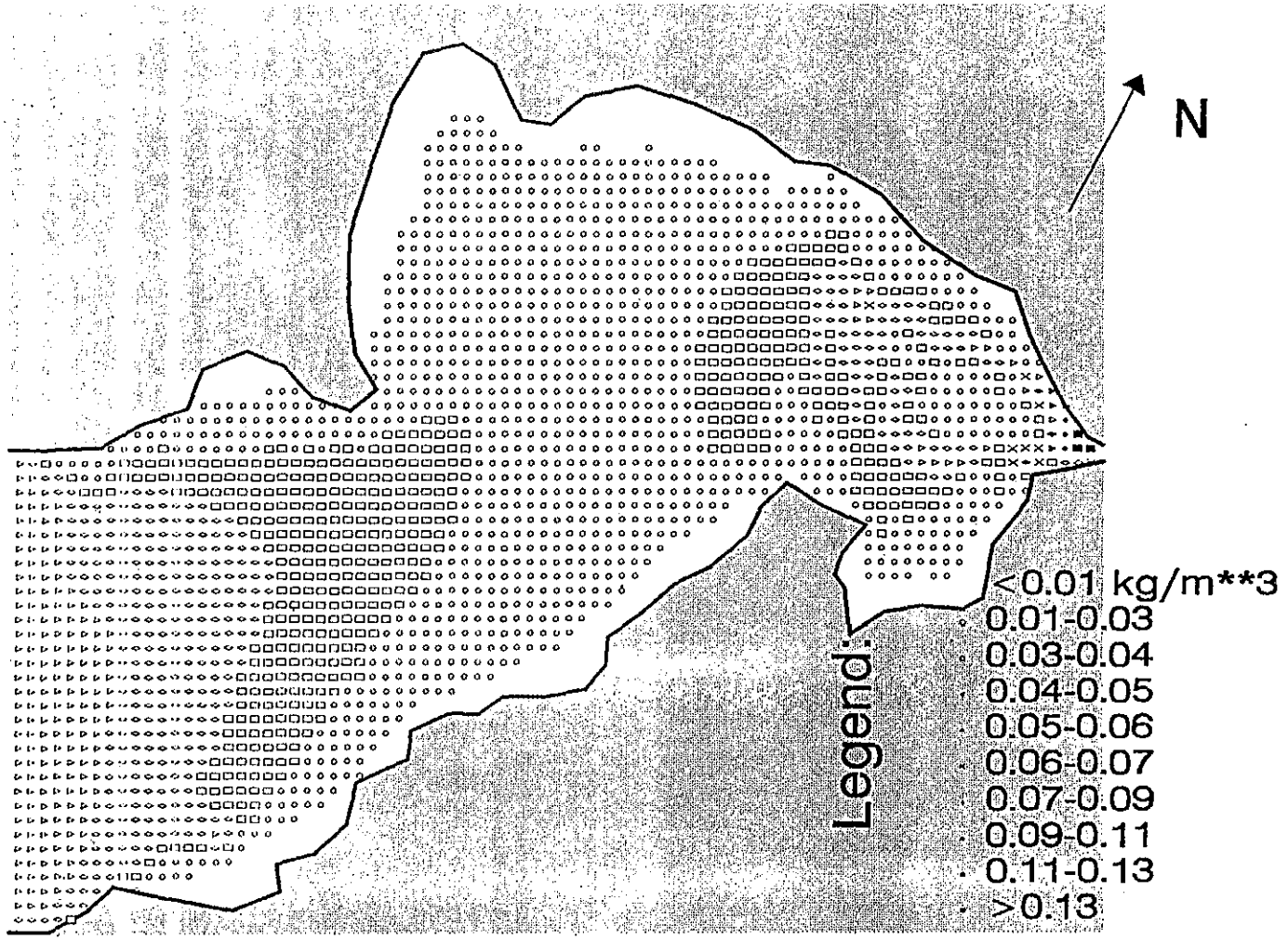

FIG. A7—21(b) Maximum sediment concentration over 2 days in Deep Bay during the construction of stage 2 works (Average Tide)

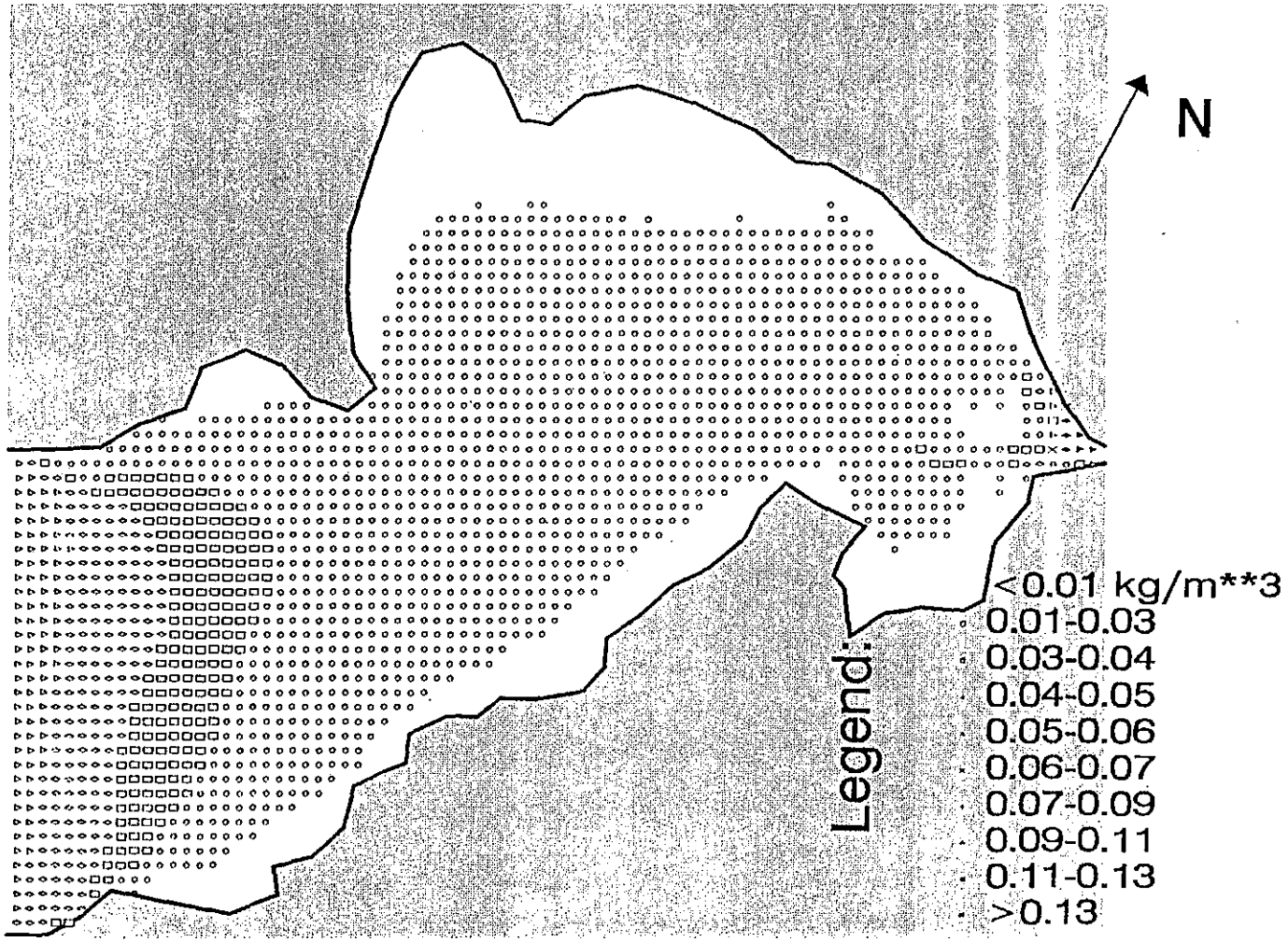

FIG. A7—21(c) Maximum sediment concentration over 2 days in Deep Bay during the construction of stage 2 works (Neap Tide)

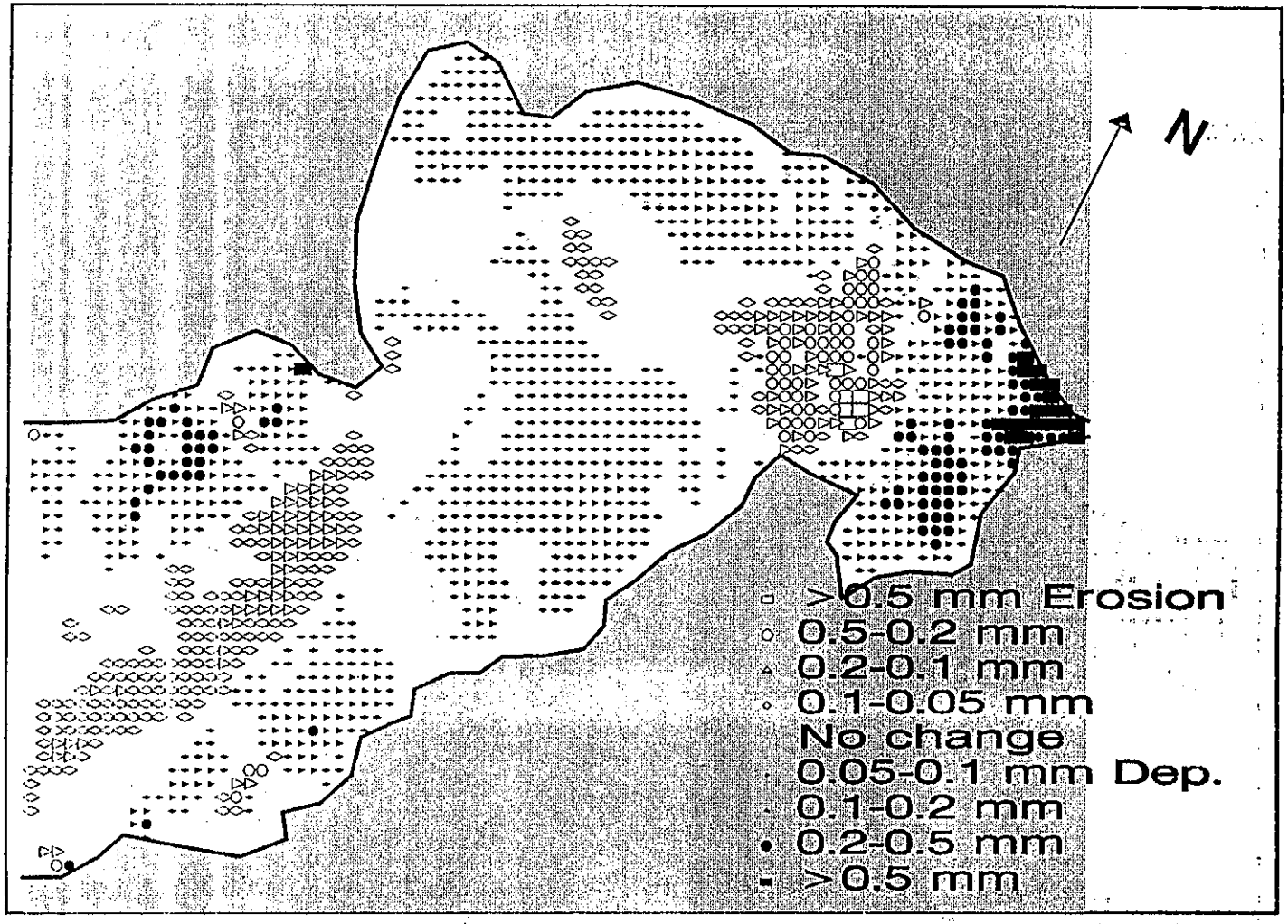

FIG. A7—22(a) Sediment erosion and deposition over 2 days in Deep Bay during the construction of stage 2 works (Spring Tide)

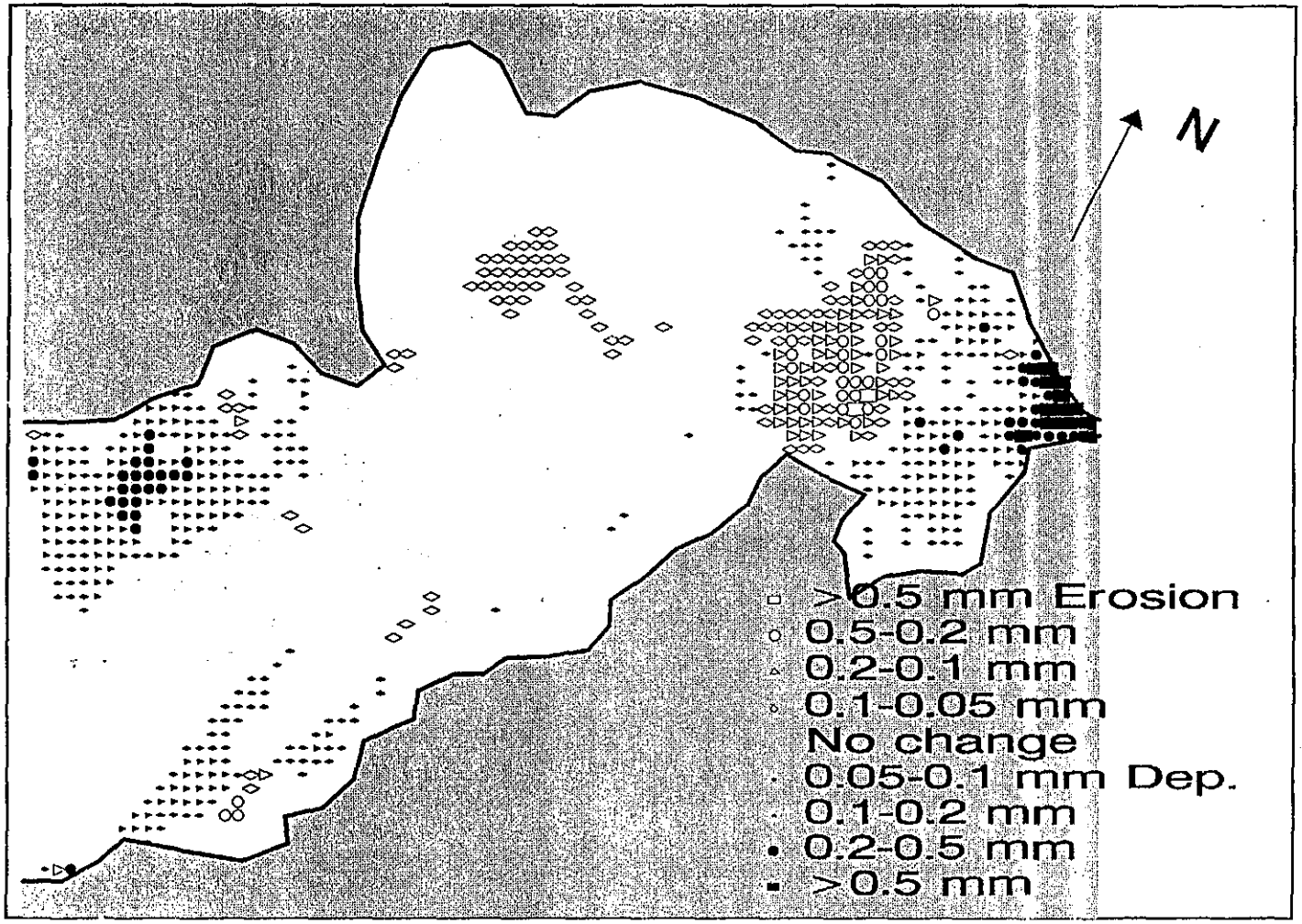

FIG. A7—22(b) Sediment erosion and deposition over 2 days in Deep Bay during the construction of stage 2 works (Average Tide)

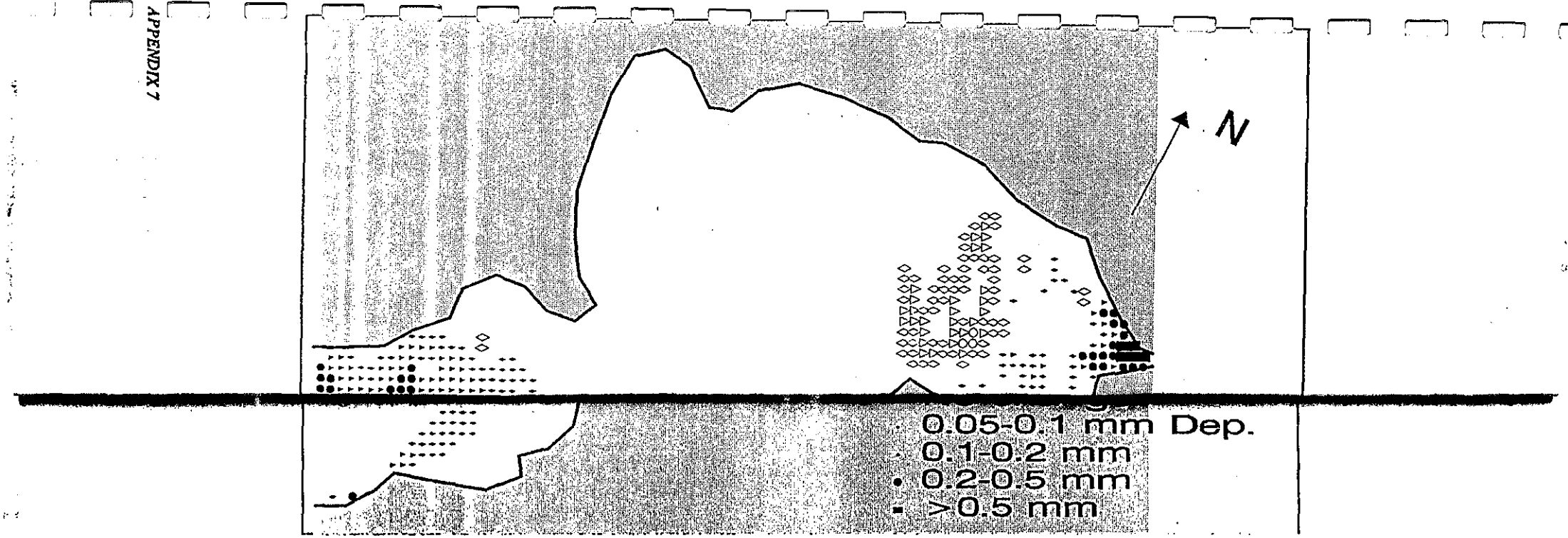

FIG. A7—22(c) Sediment erosion and deposition over 2 days in Deep Bay during the construction of stage 2 works (Neap Tide)

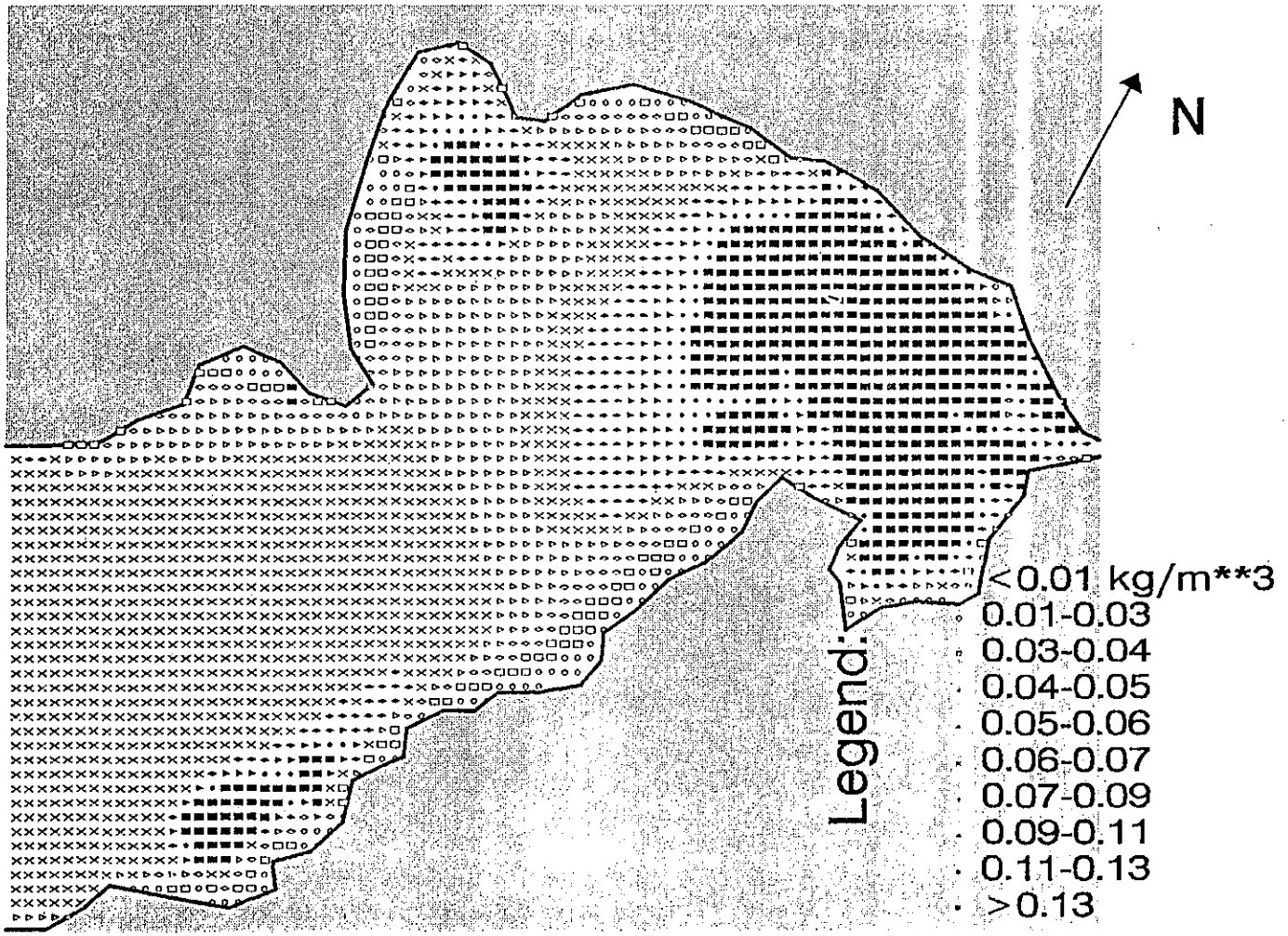

FIG. A7 — 23 (a) Maximum sediment concentration within 2 days in Deep Bay after stage 2 works (Spring Tide in Wet Season)

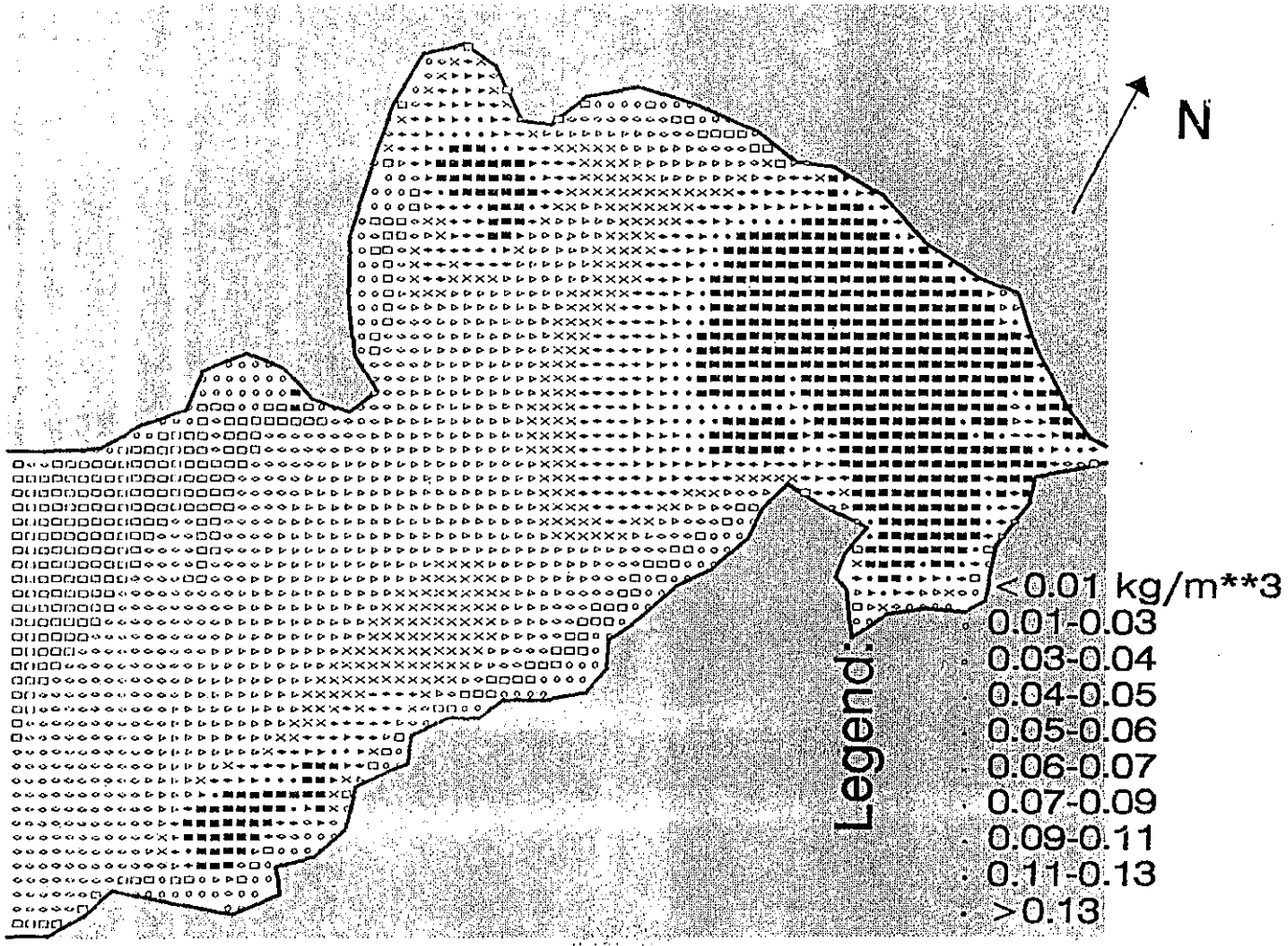

FIG. A7－23(b) Maximum sediment concentration within 2 days in Deep Bay after stage 2 works (Spring Tide in Dry Season)

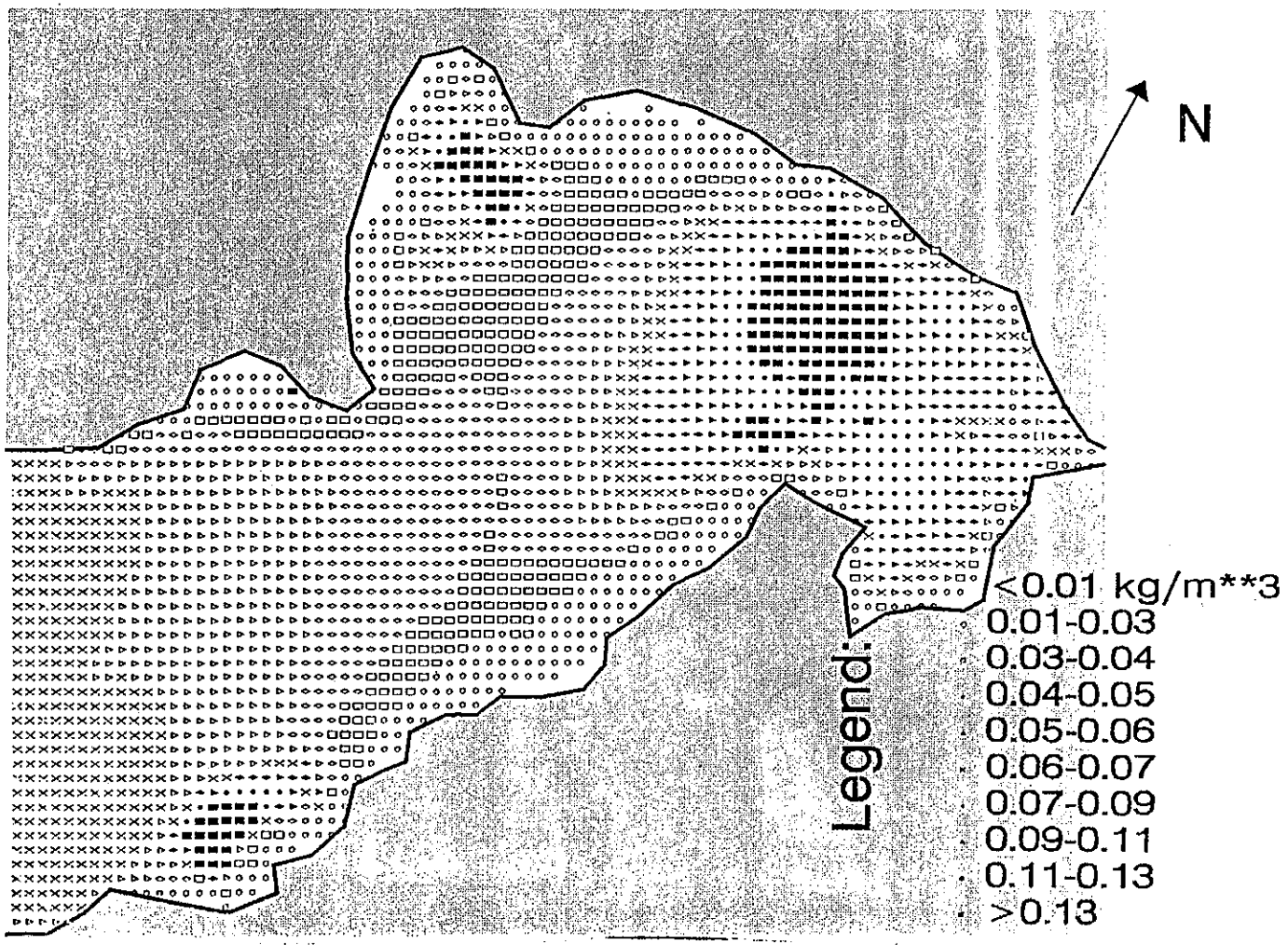

FIG. A7 — 23(c) Maximum sediment concentration within 2 days in Deep Bay after stage 2 works (Average Tide in Wet Season)

FIG. A7 — 23 (d) Maximum sediment concentration within 2 days in Deep Bay after stage 2 works (Average Tide in Dry Season)

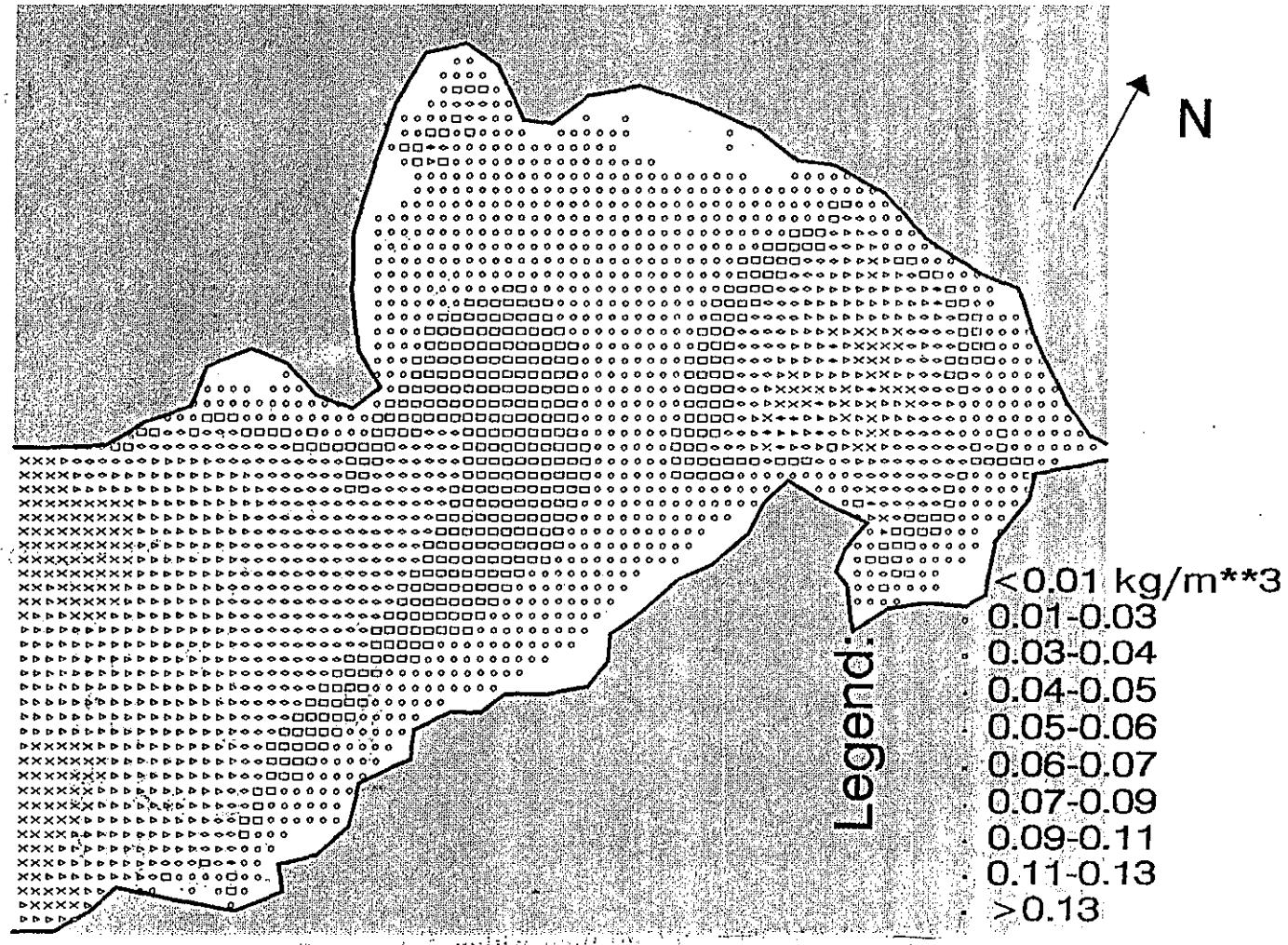

FIG. A7—23(e) Maximum sediment concentration within 2 days in Deep Bay after stage 2 works (Neap Tide in Wet Season)

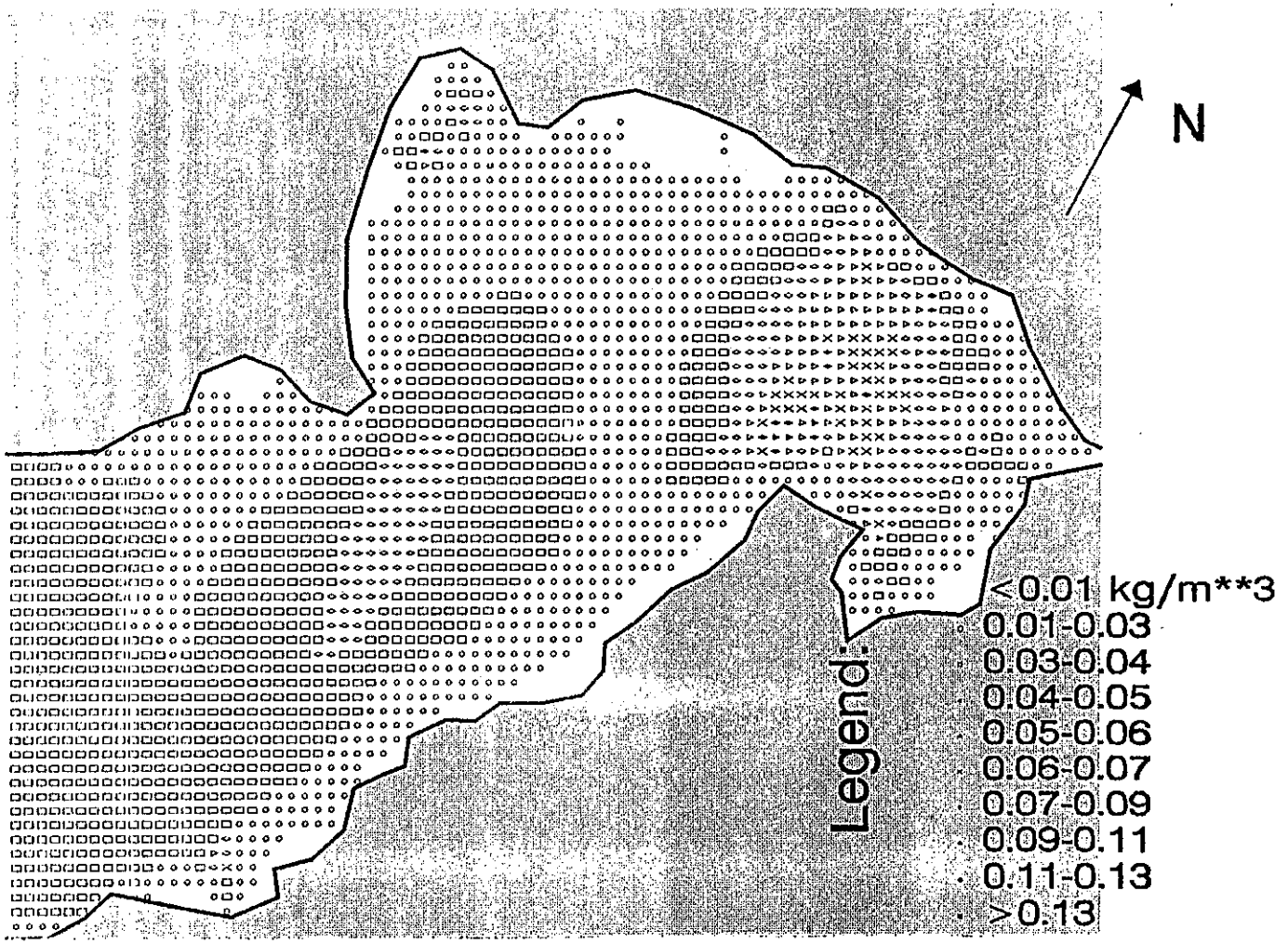

FIG. A7 — 23(f) Maximum sediment concentration within 2 days in Deep Bay after stage 2 works (Neap Tide in Dry Season)

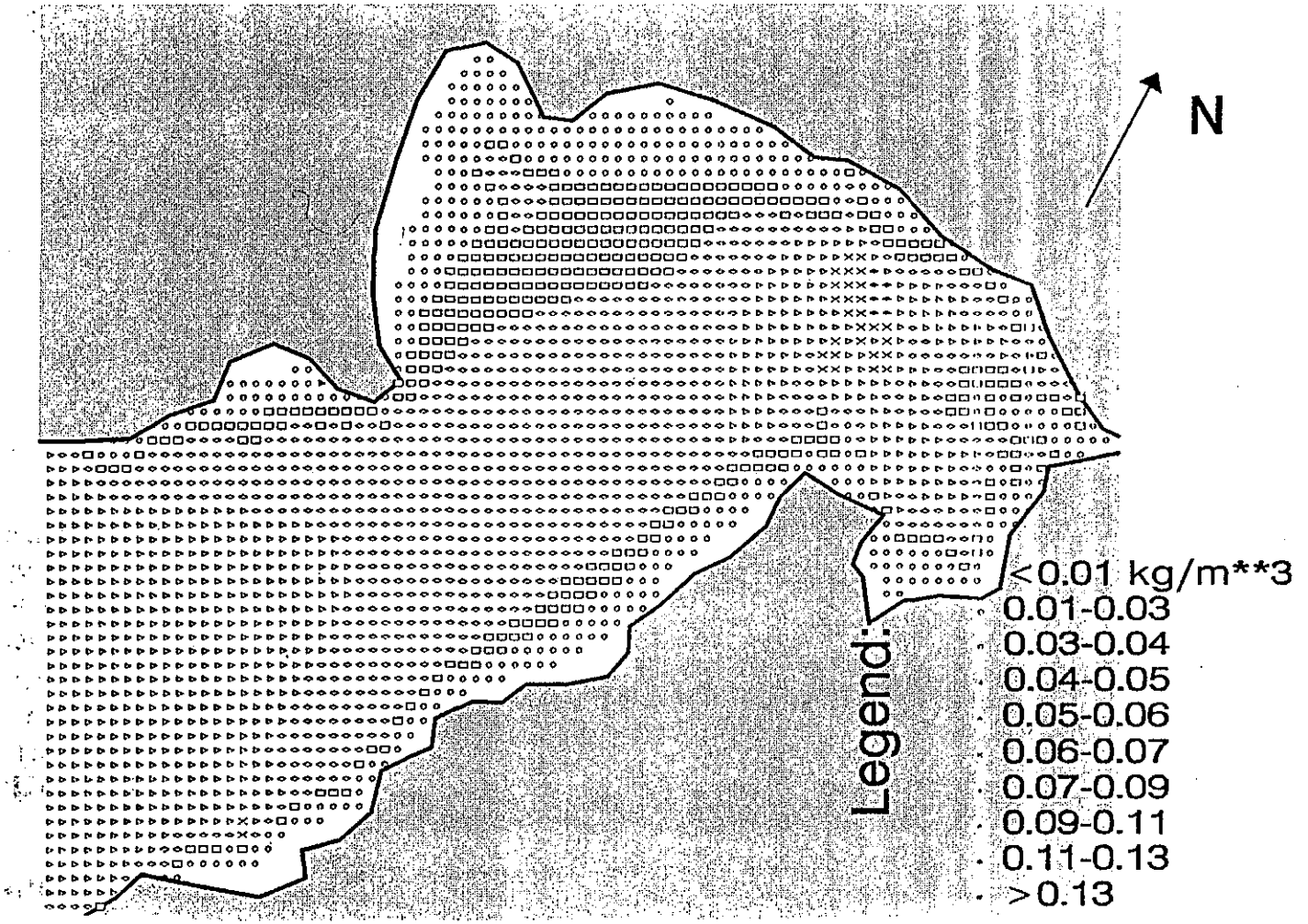

FIG. A7—24(a) **Average sediment concentration within 2 days in Deep Bay after stage 2 works (Spring Tide in Wet Season)**

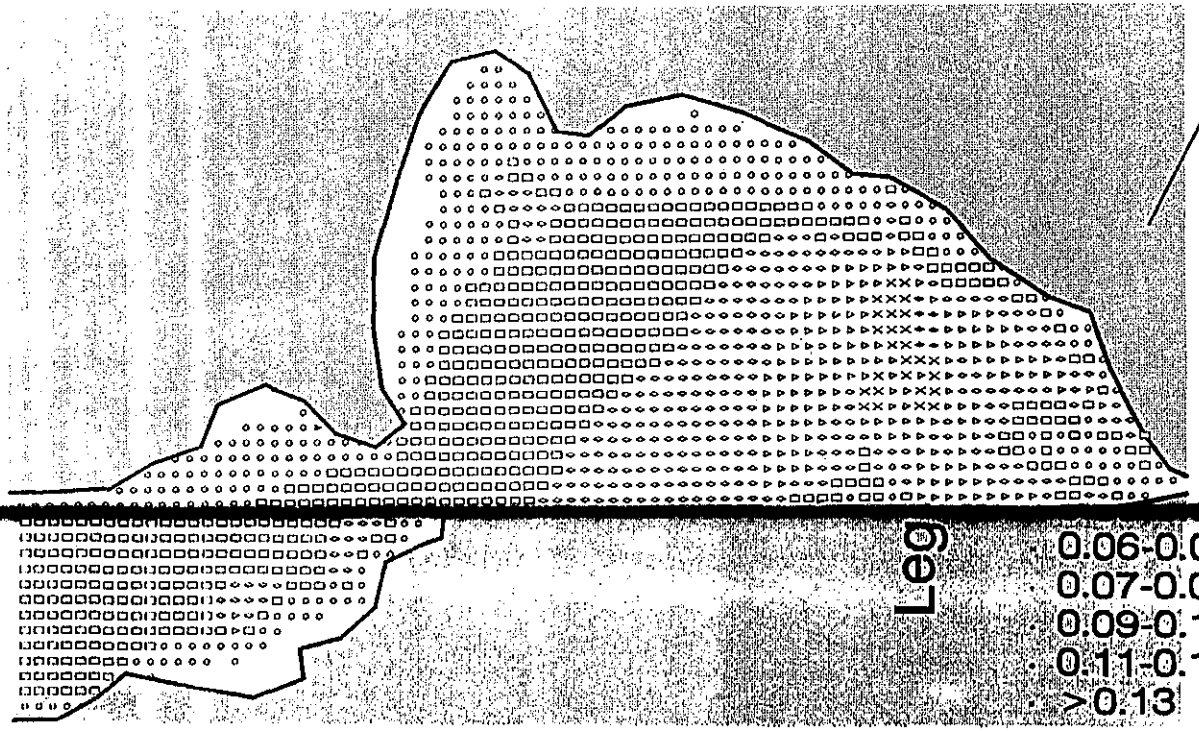

FIG. A7—24(b) Average sediment concentration within 2 days in De-
2 works (Spring Tide in Day Season)

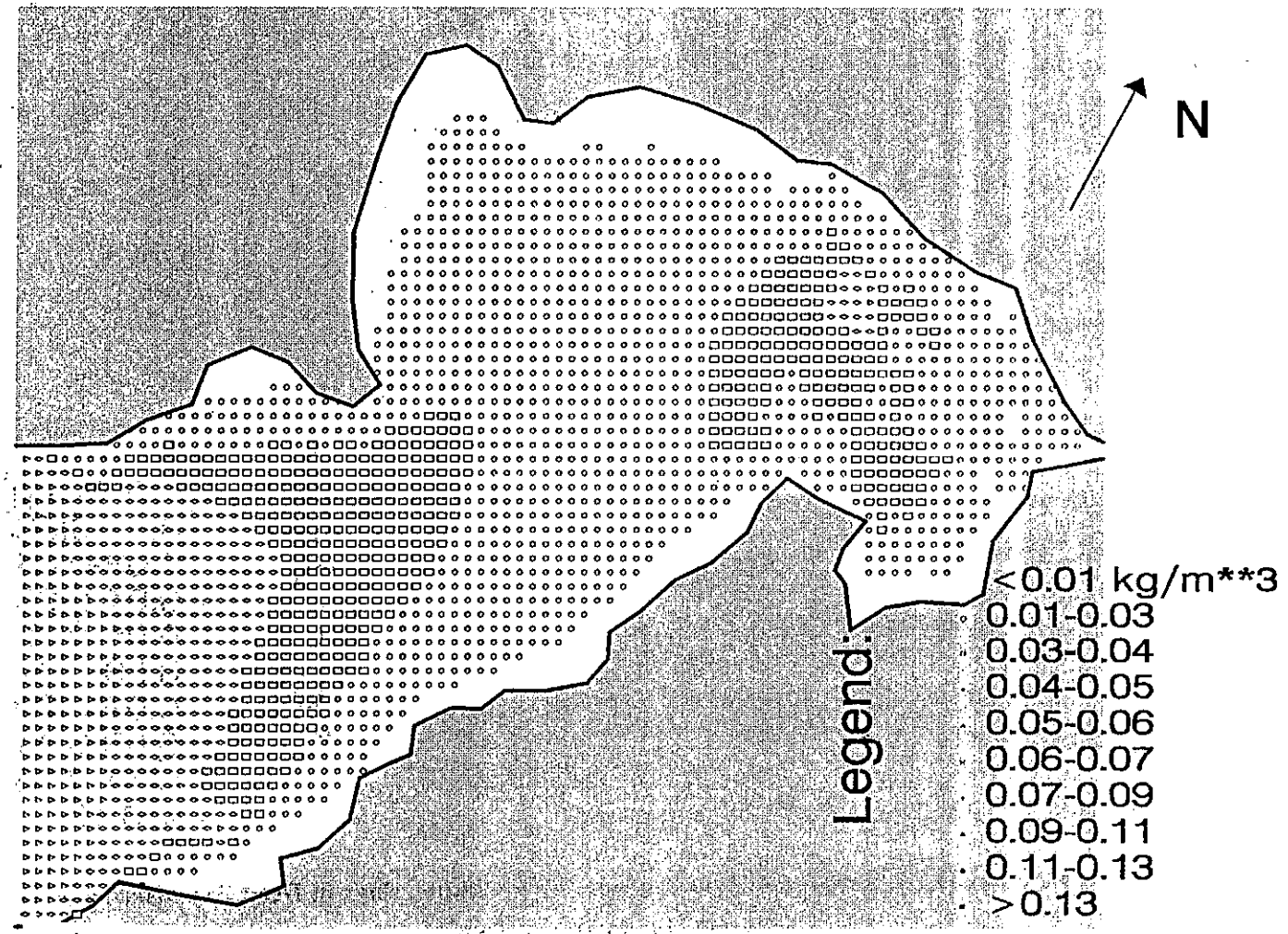

FIG. A7—24(c) Average sediment concentration within 2 days in Deep Bay after stage 2 works (Average Tide in Wet Season)

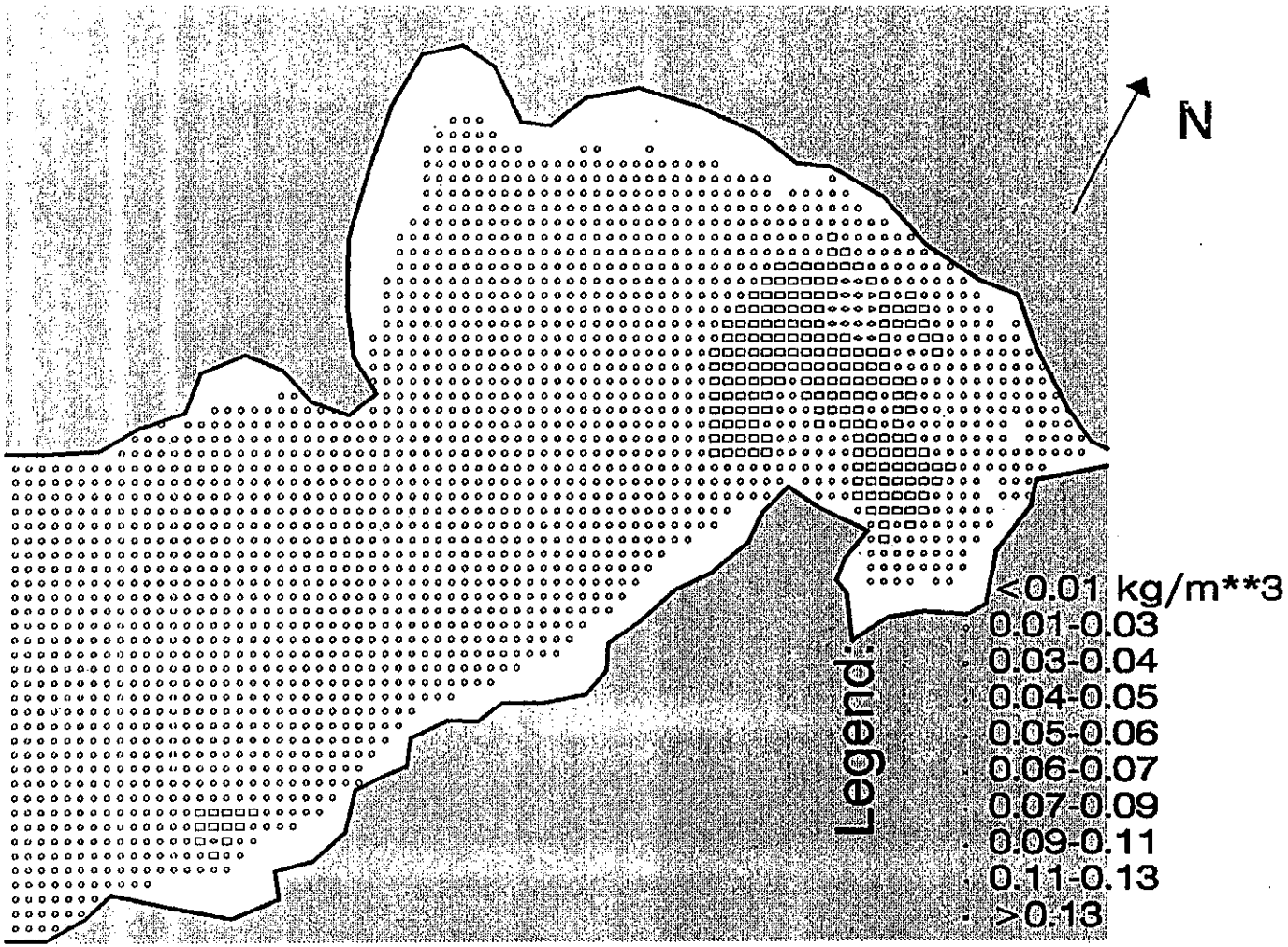

FIG. A7—24(d) Average sediment concentration within 2 days in Deep Bay after stage 2 works (Average Tide in Day Season)

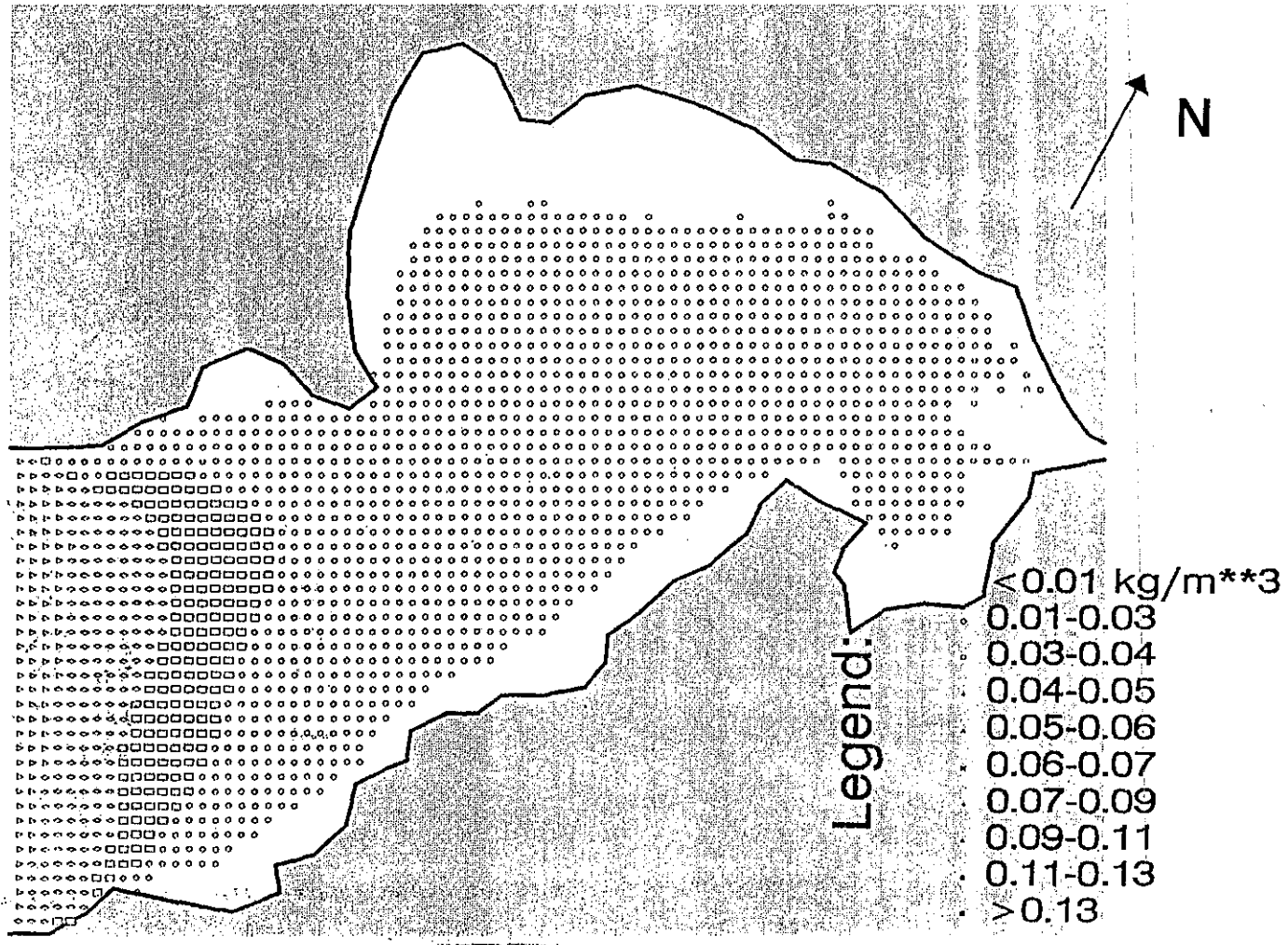

FIG. A7－24(e) Average sediment concentration within 2 days in Deep Bay after stage 2 works (Neap Tide in Wet Season)

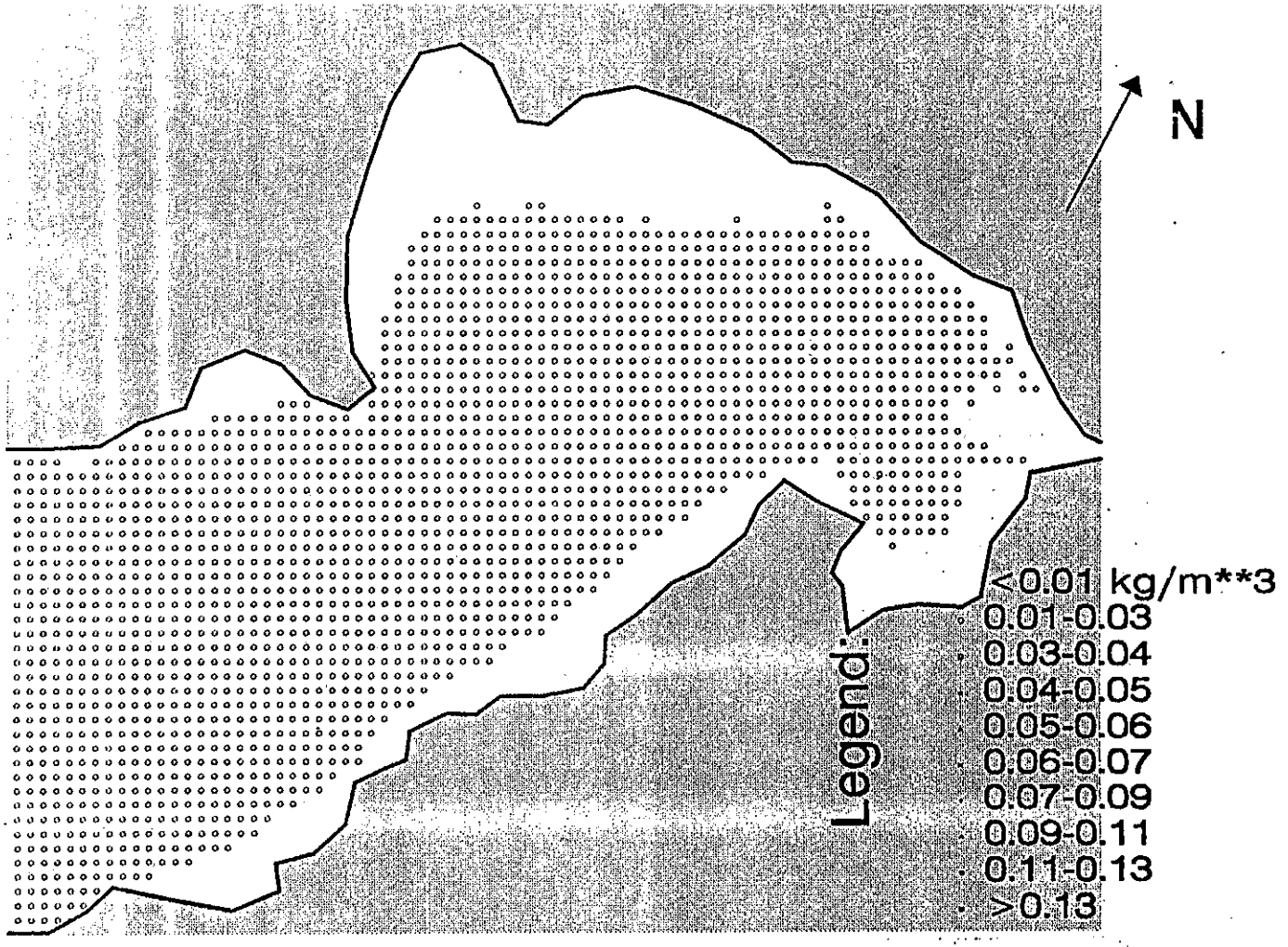

FIG. A7--24(f) Average sediment concentration within 2 days in Deep Bay after stage 2 works (Neap Tide in Dry Season)

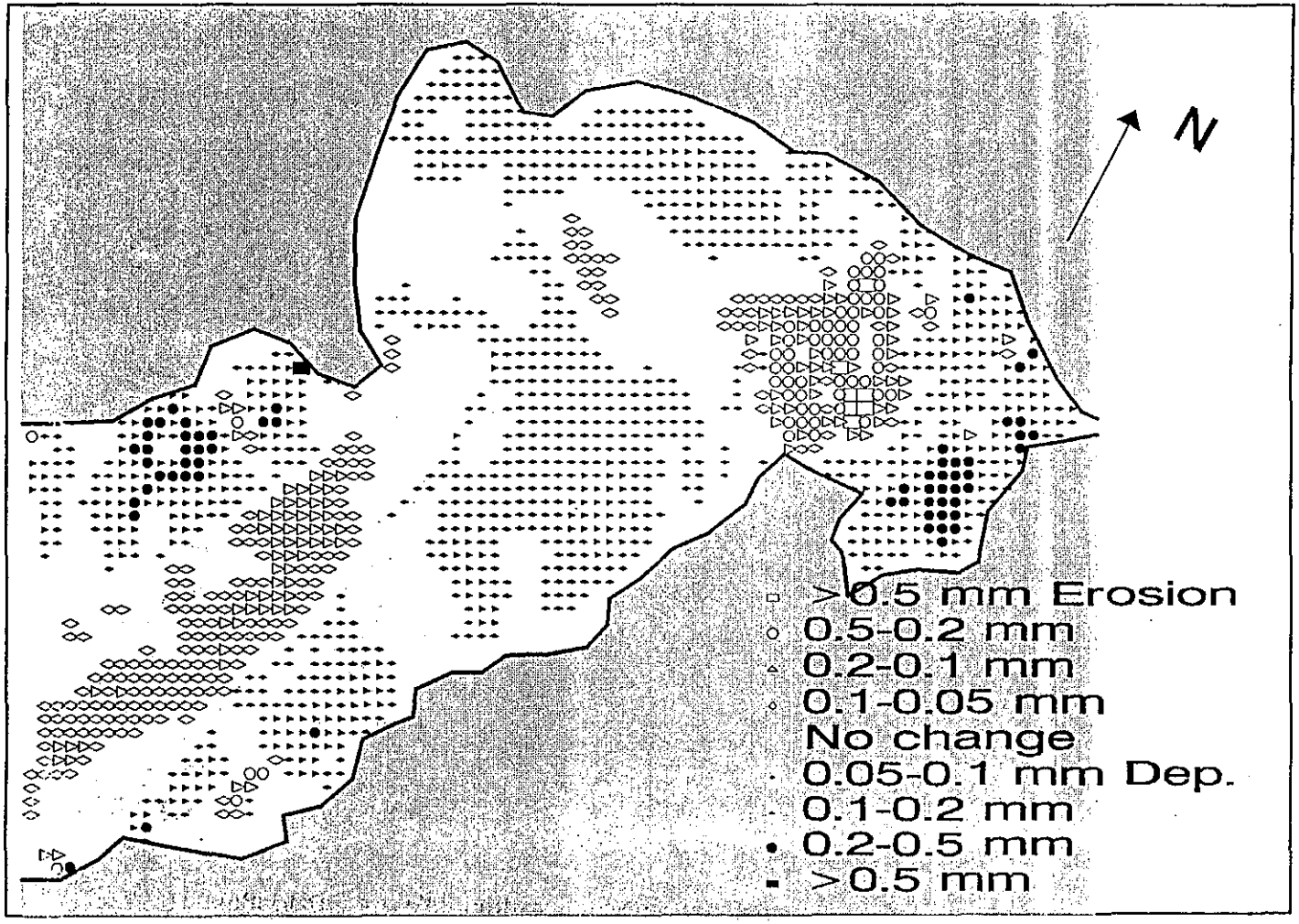

FIG. A7—25(a) Sediment erosion and deposition within 2 days in Deep Bay after stage 2 works (Spring Tide in Wet Season)

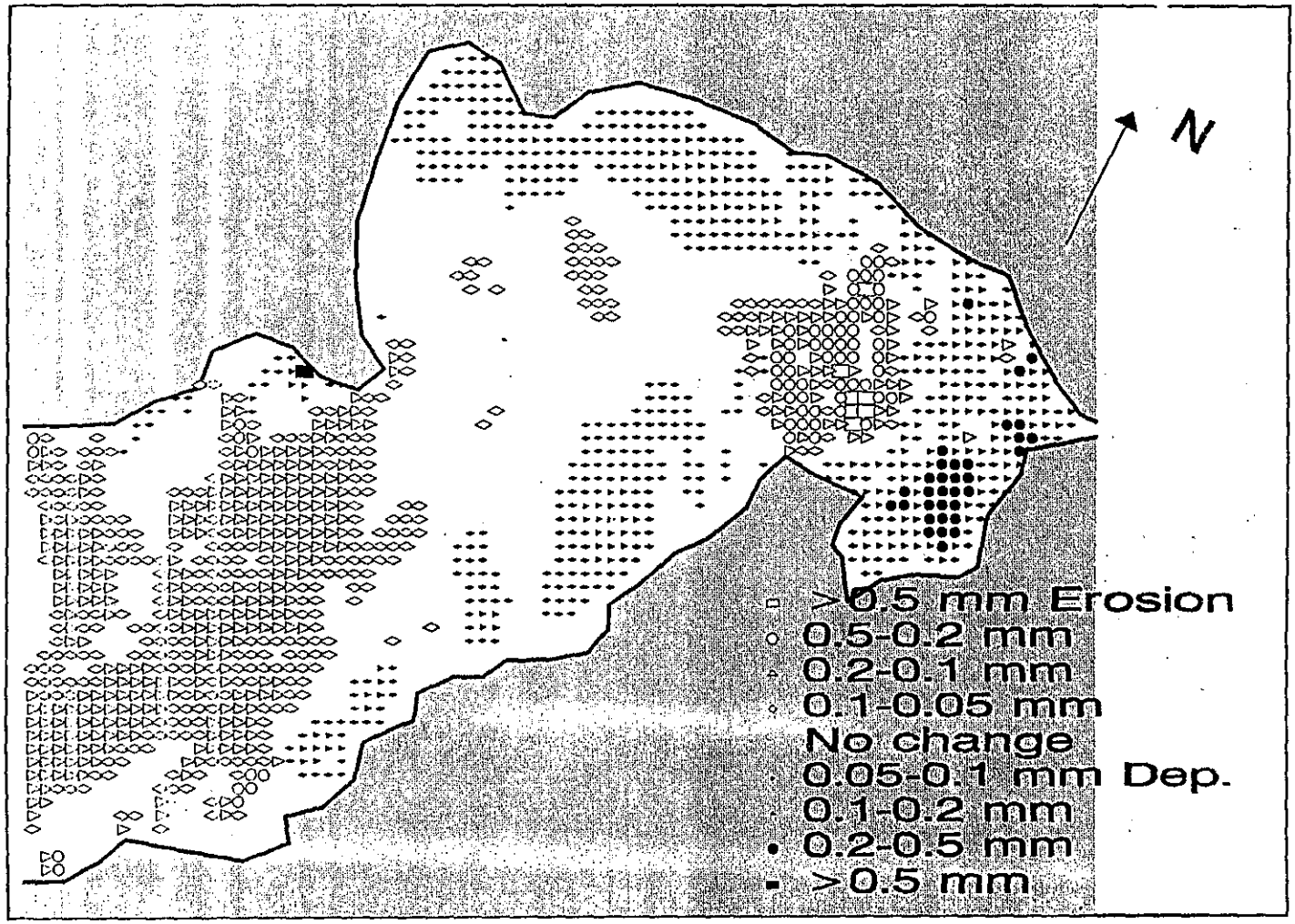

FIG. A7—25(b) Sediment erosion and deposition within 2 days in Deep Bay after stage 2 works (Spring Tide in Day Season)

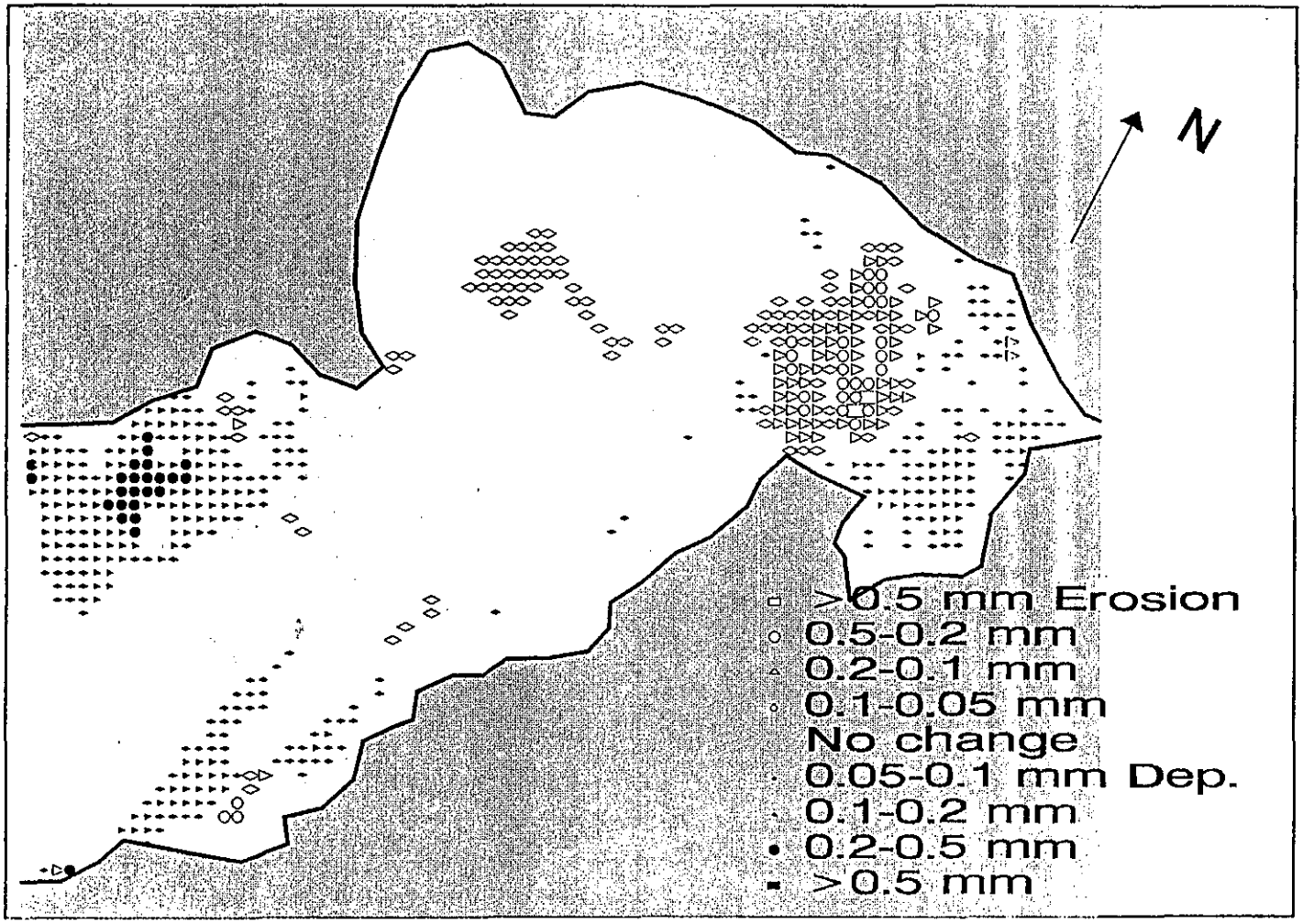

FIG. A7—25(c) Sediment erosion and deposition within 2 days in Deep Bay after stage 2 works (Average Tide in Wet Season)

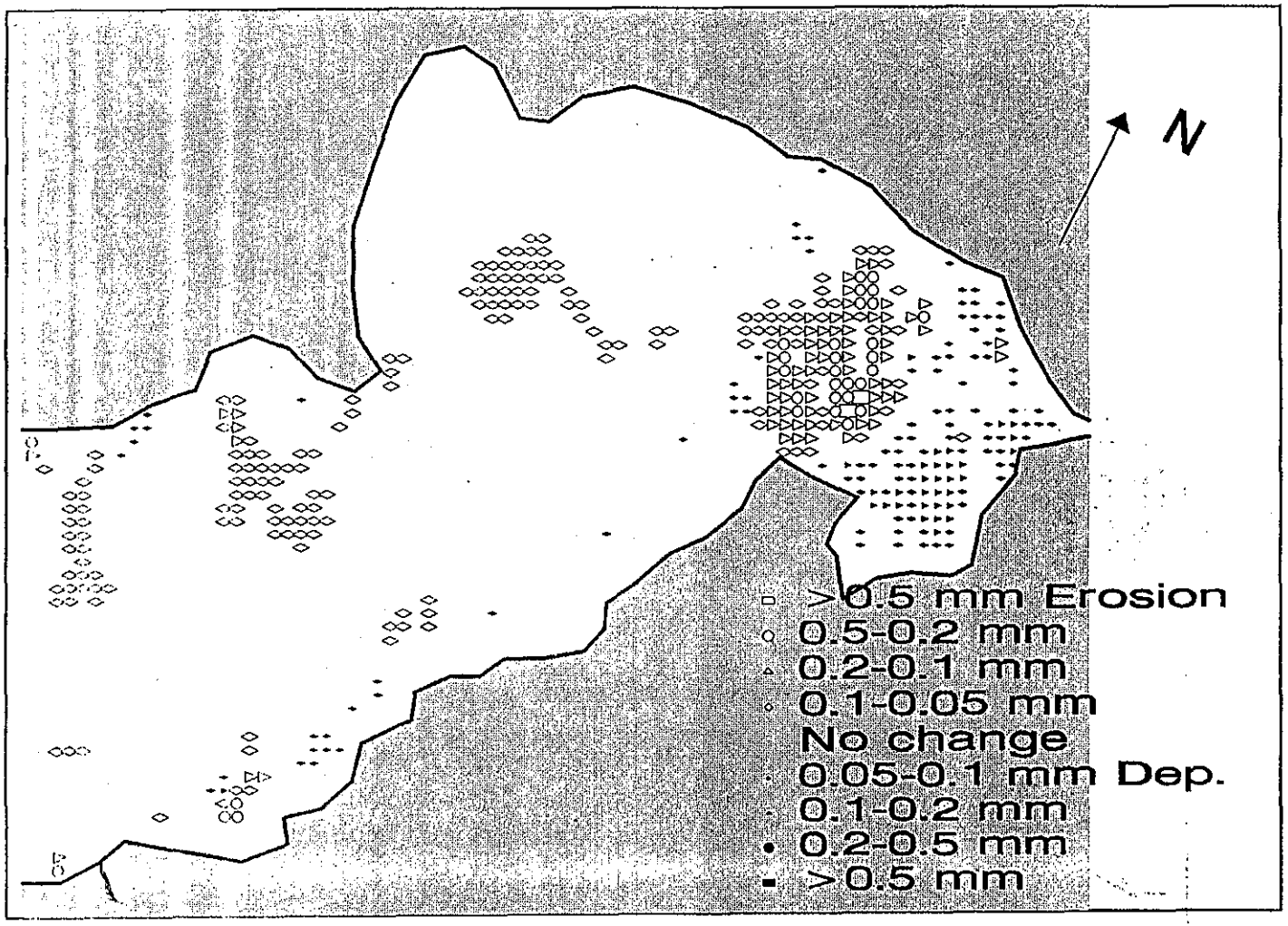

FIG. A7－25(d) Sediment erosion and deposition within 2 days in Deep Bay after stage 2 works (Average Tide in Day Season)

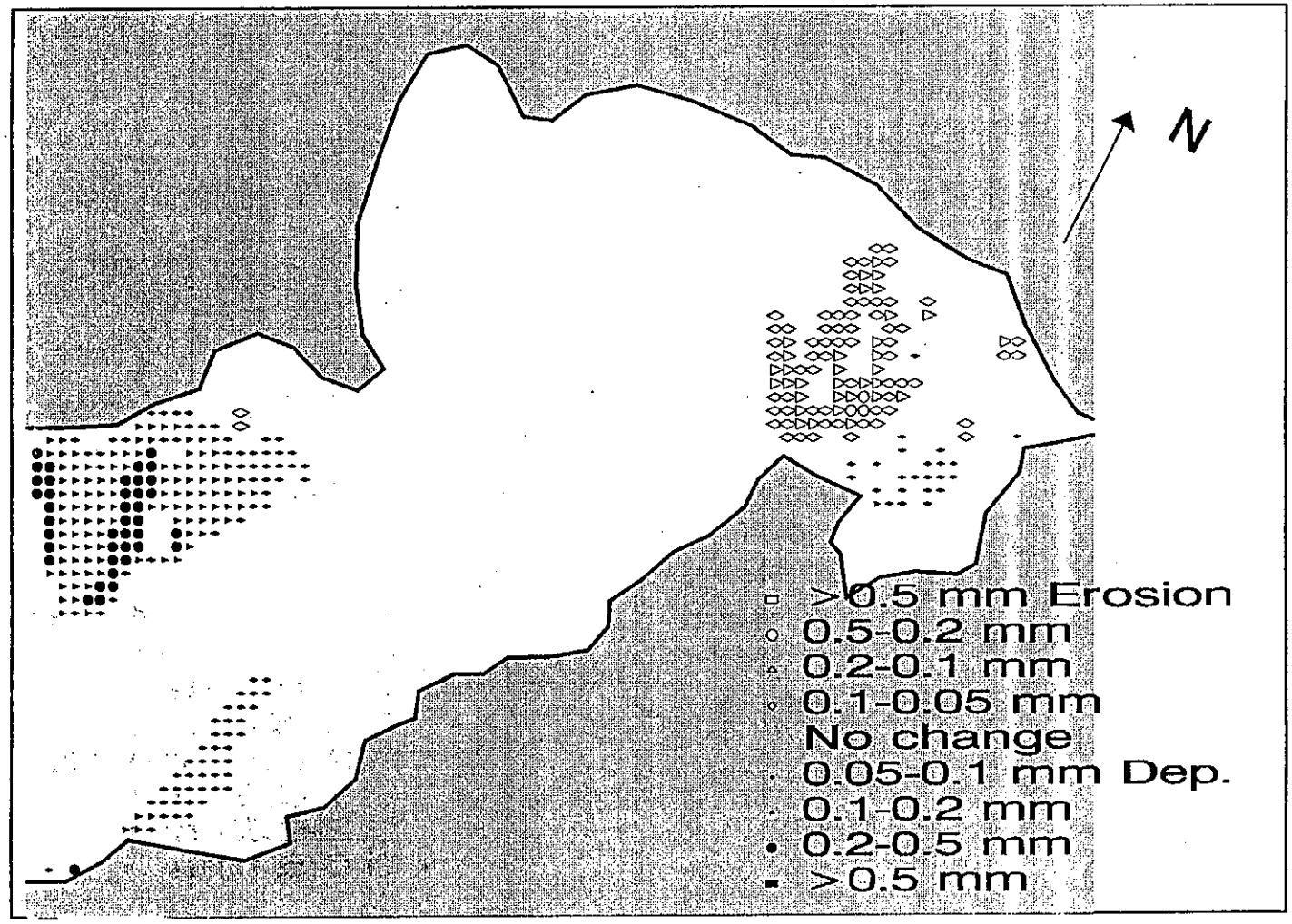

FIG. A7—25(e) Sediment erosion and deposition within 2 days in Deep Bay after stage 2 works (Neap Tide in Wet Season)

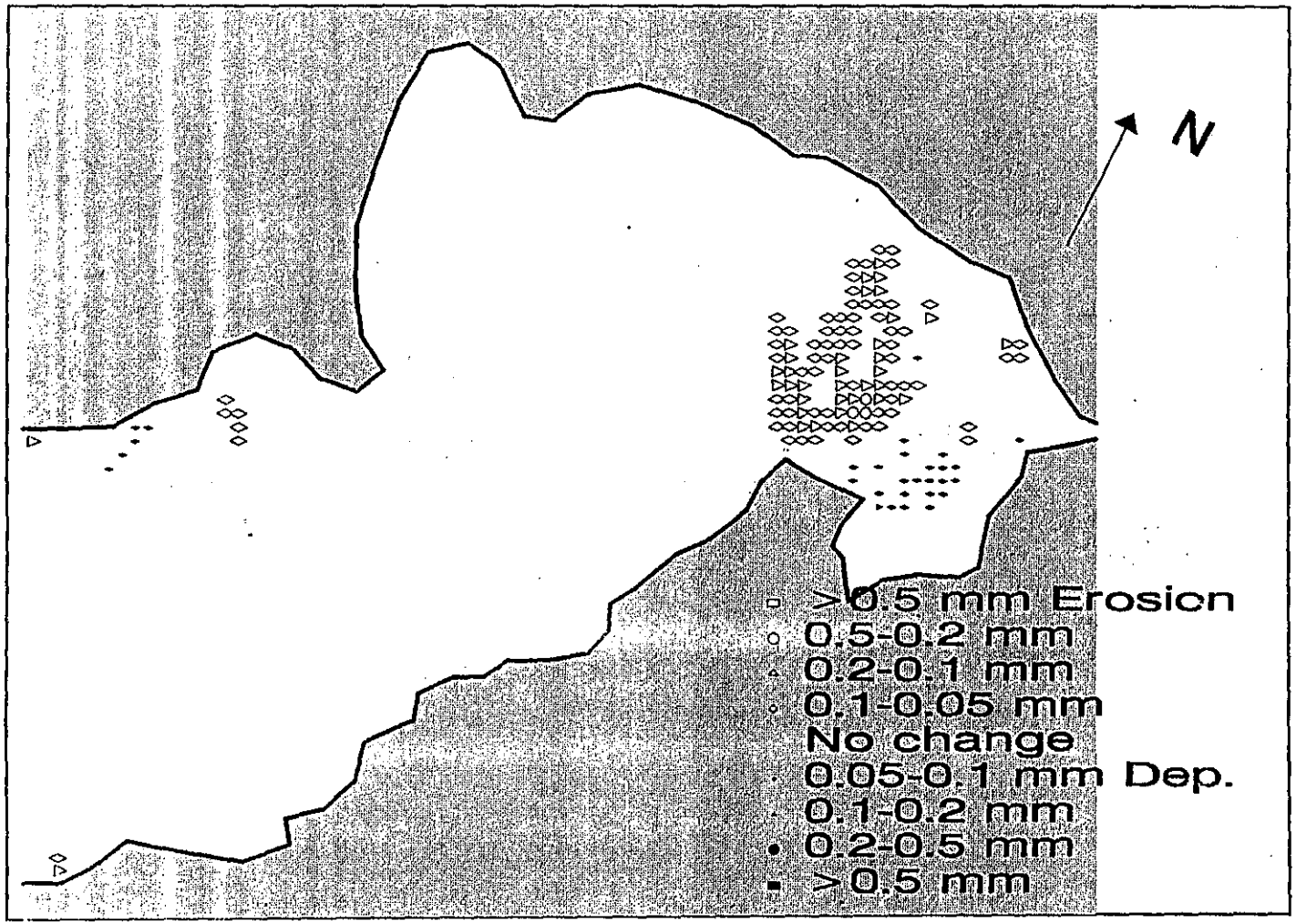

FIG. A7--25(f) **Sediment erosion and deposition within 2 days in Deep Bay after stage 2 works (Neap Tide in Day Season)**

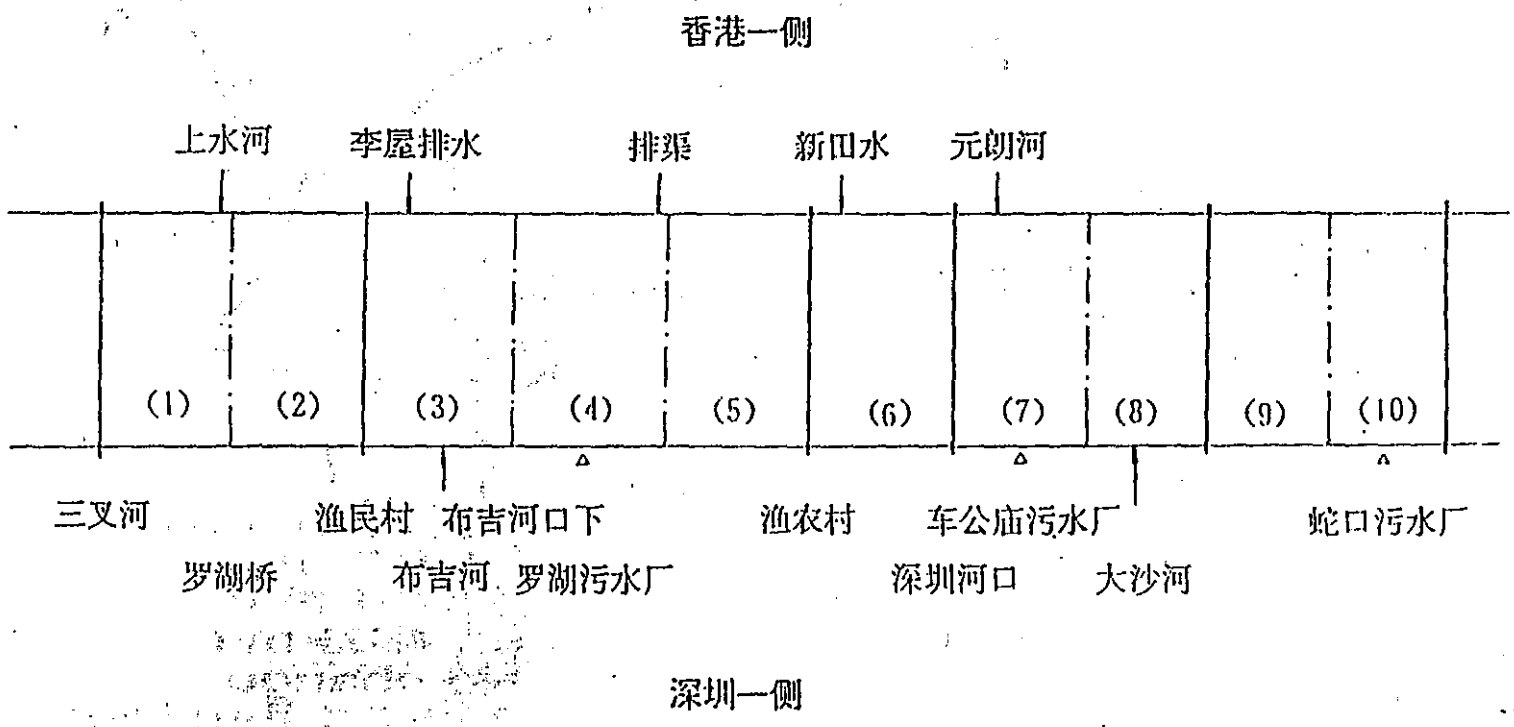

FIG. A7—26 General View of Drainage Area for Shenzhen River and Deep Bay

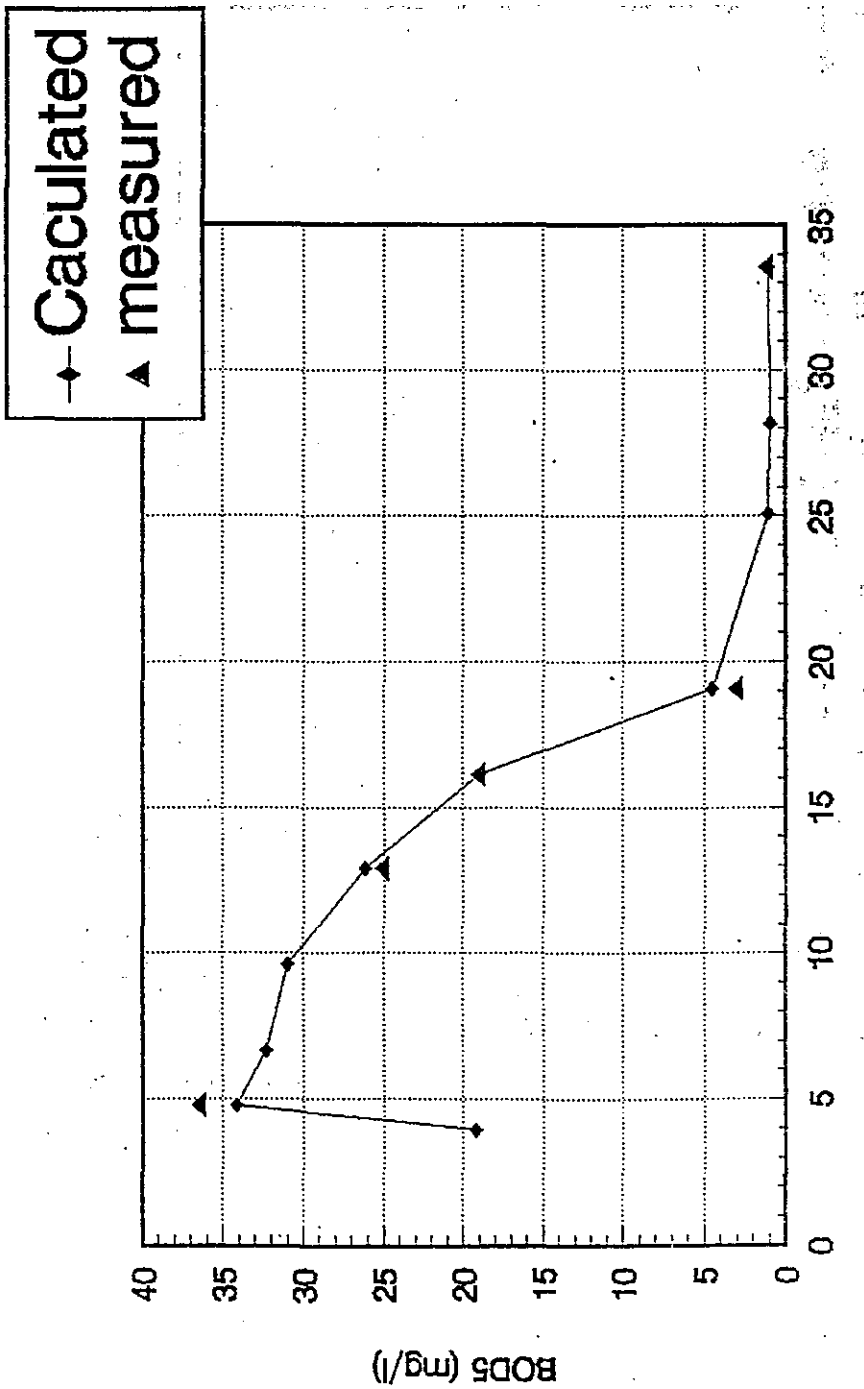

FIG. A7 – 27 Verification BOD_5 of model

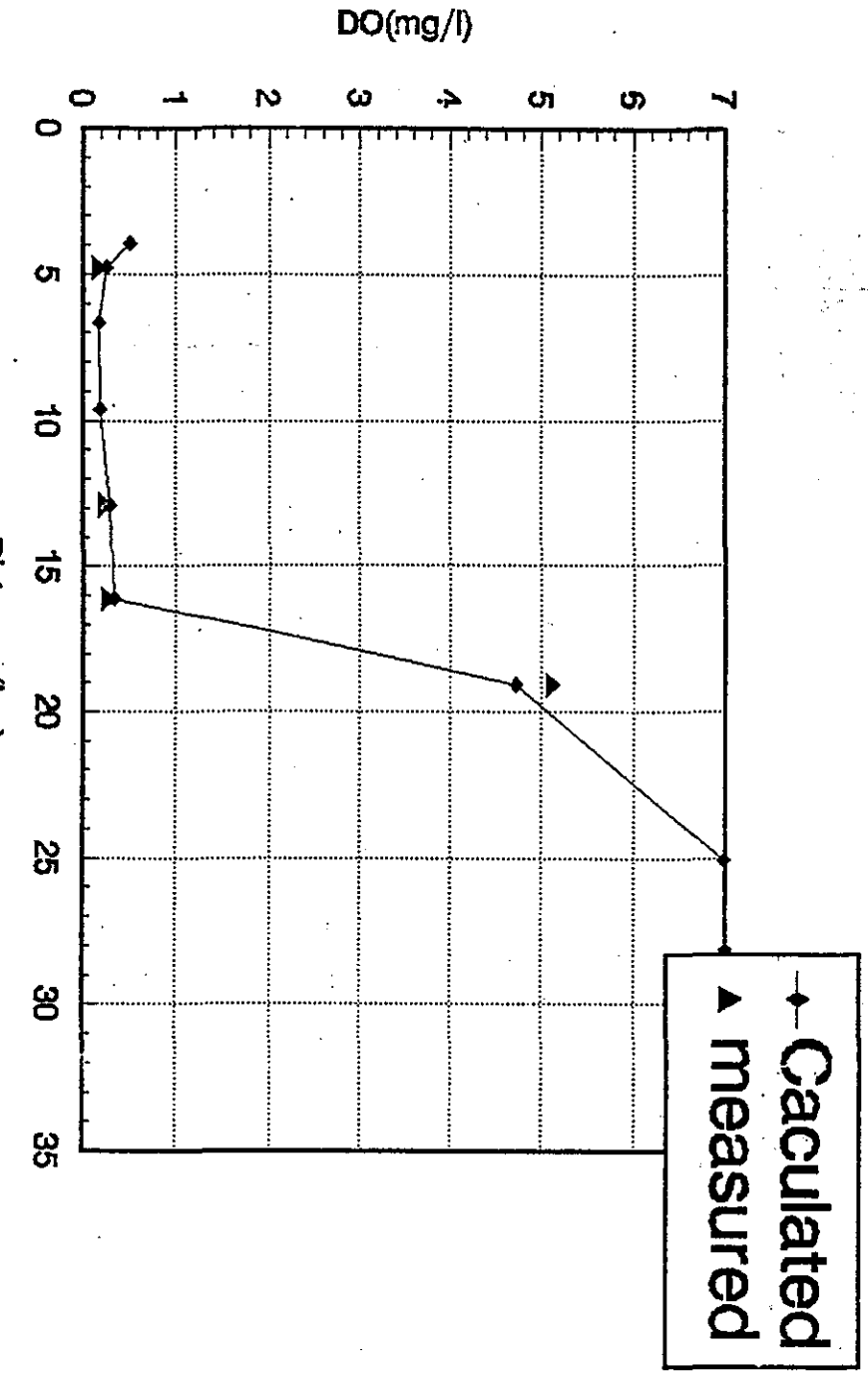

FIG. A7—28 Verification of DO model

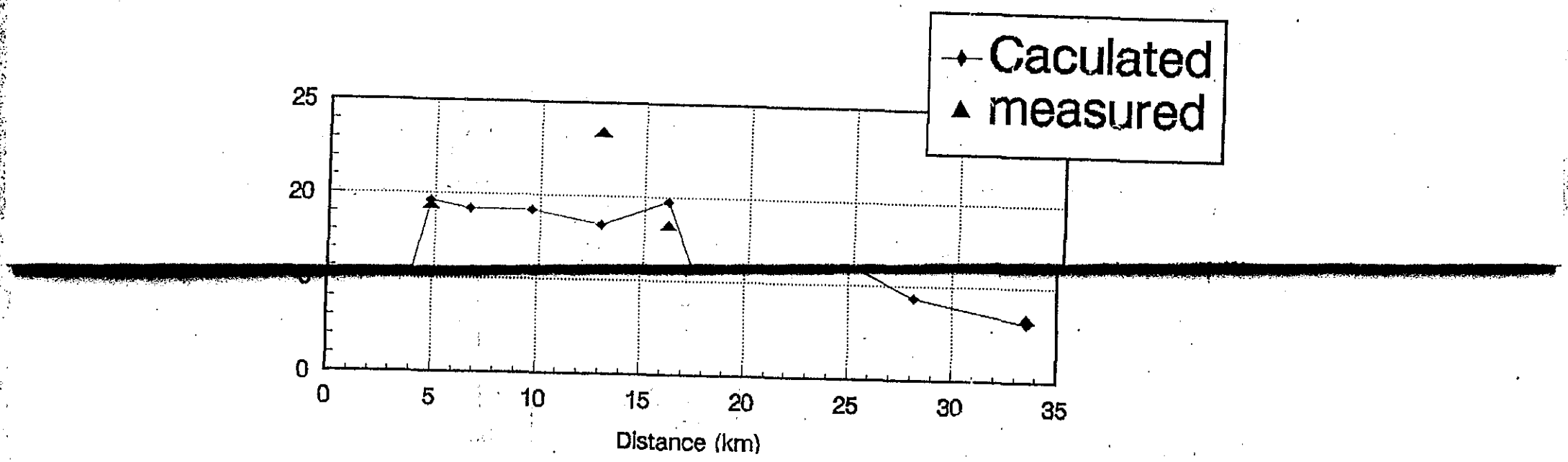

FIG. A7—29 Verification of COD model

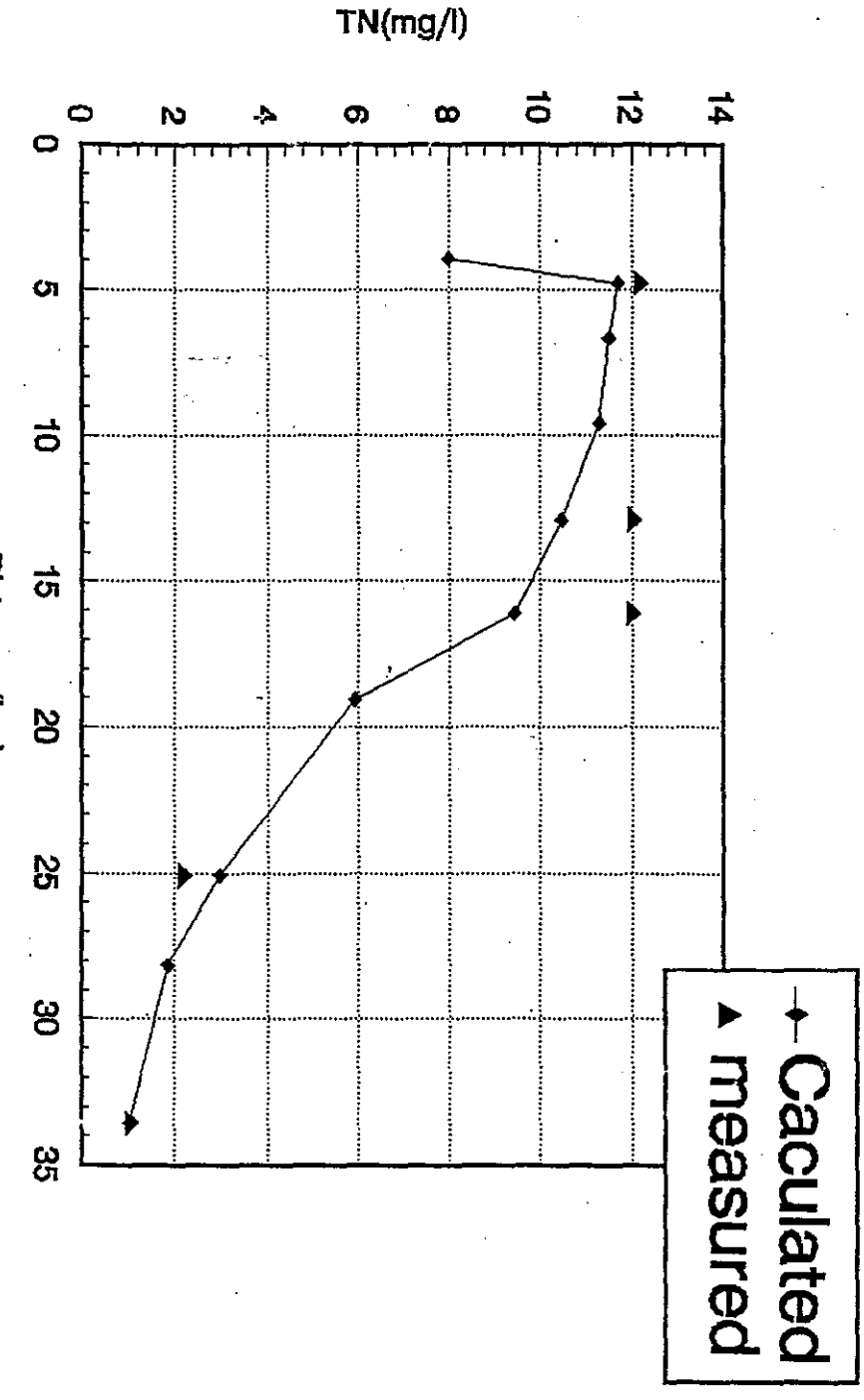

FIG. A7—30 Verification of T—N model

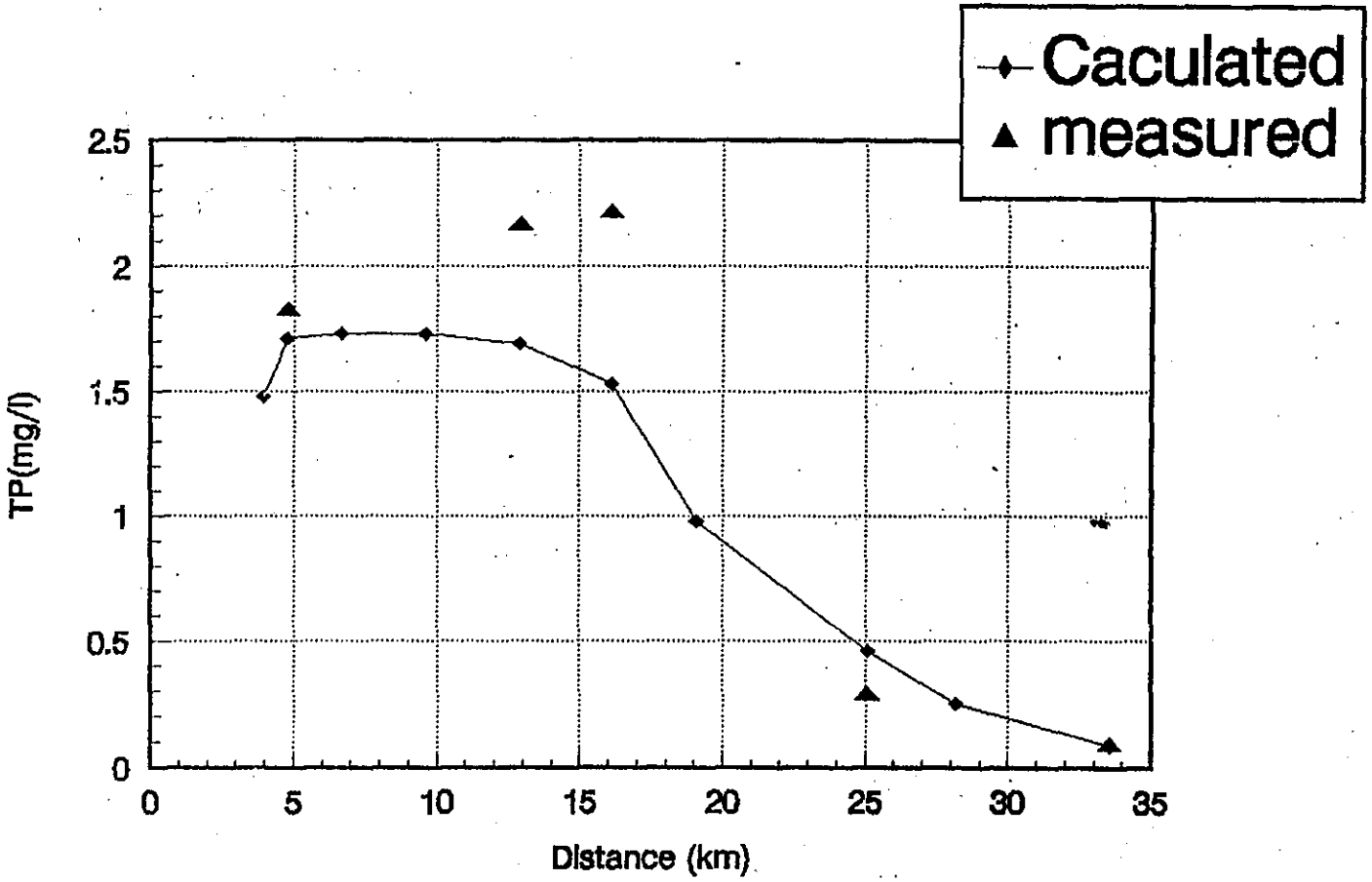

FIG. A7—31 Verification of T—P model

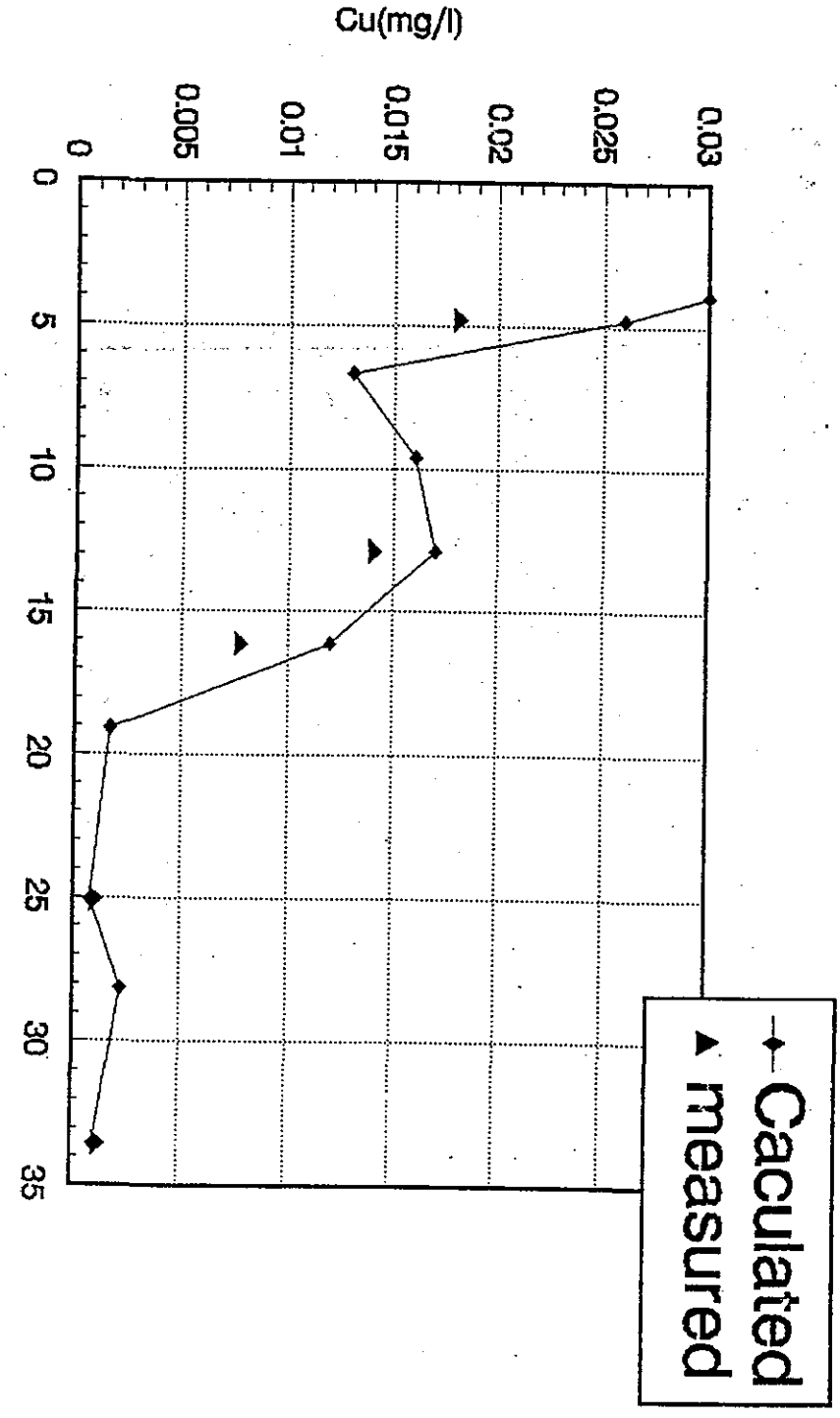

FIG. A7—32 Verification of Cu model

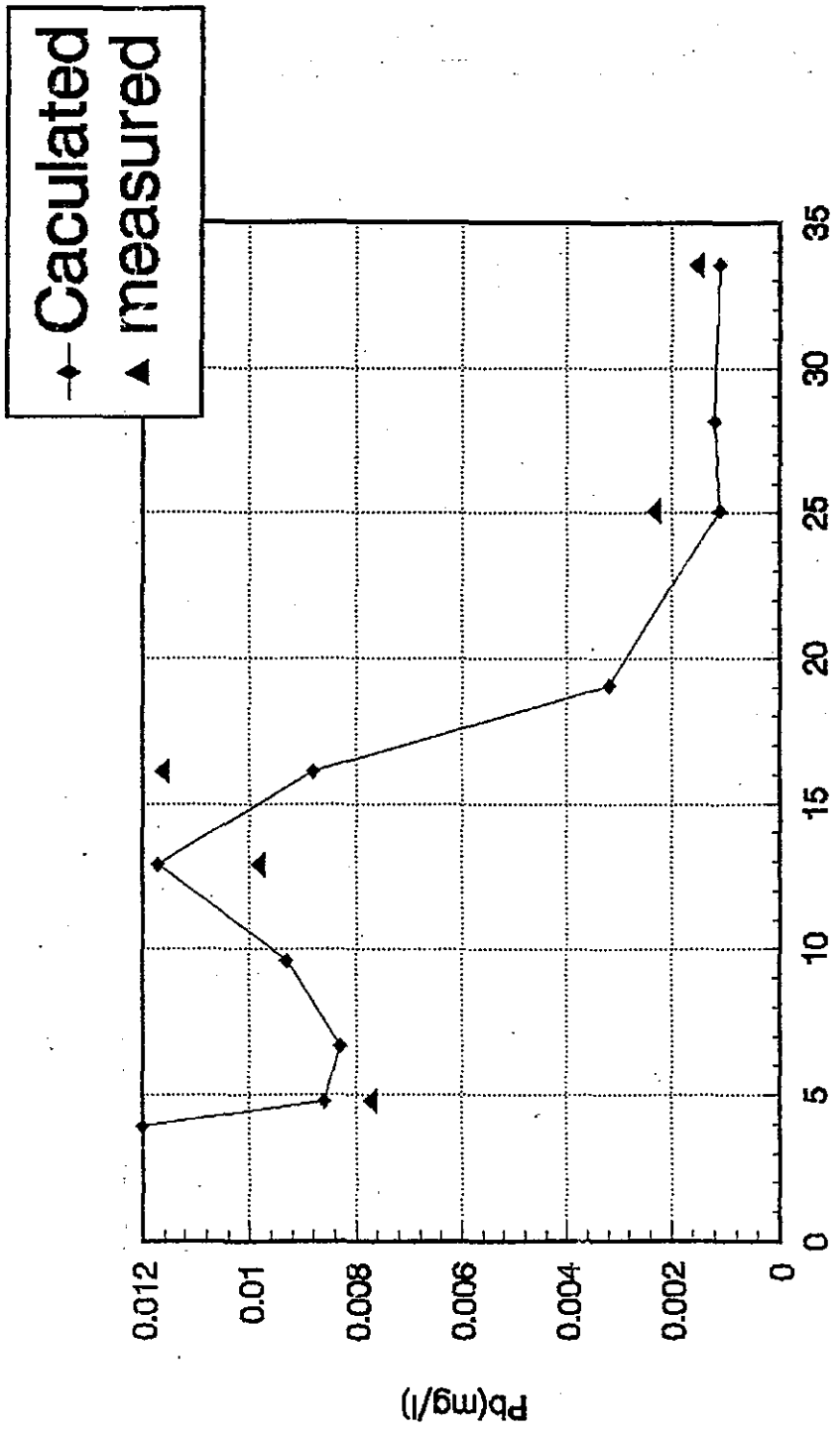

FIG. A7—33 Verification of Pb model

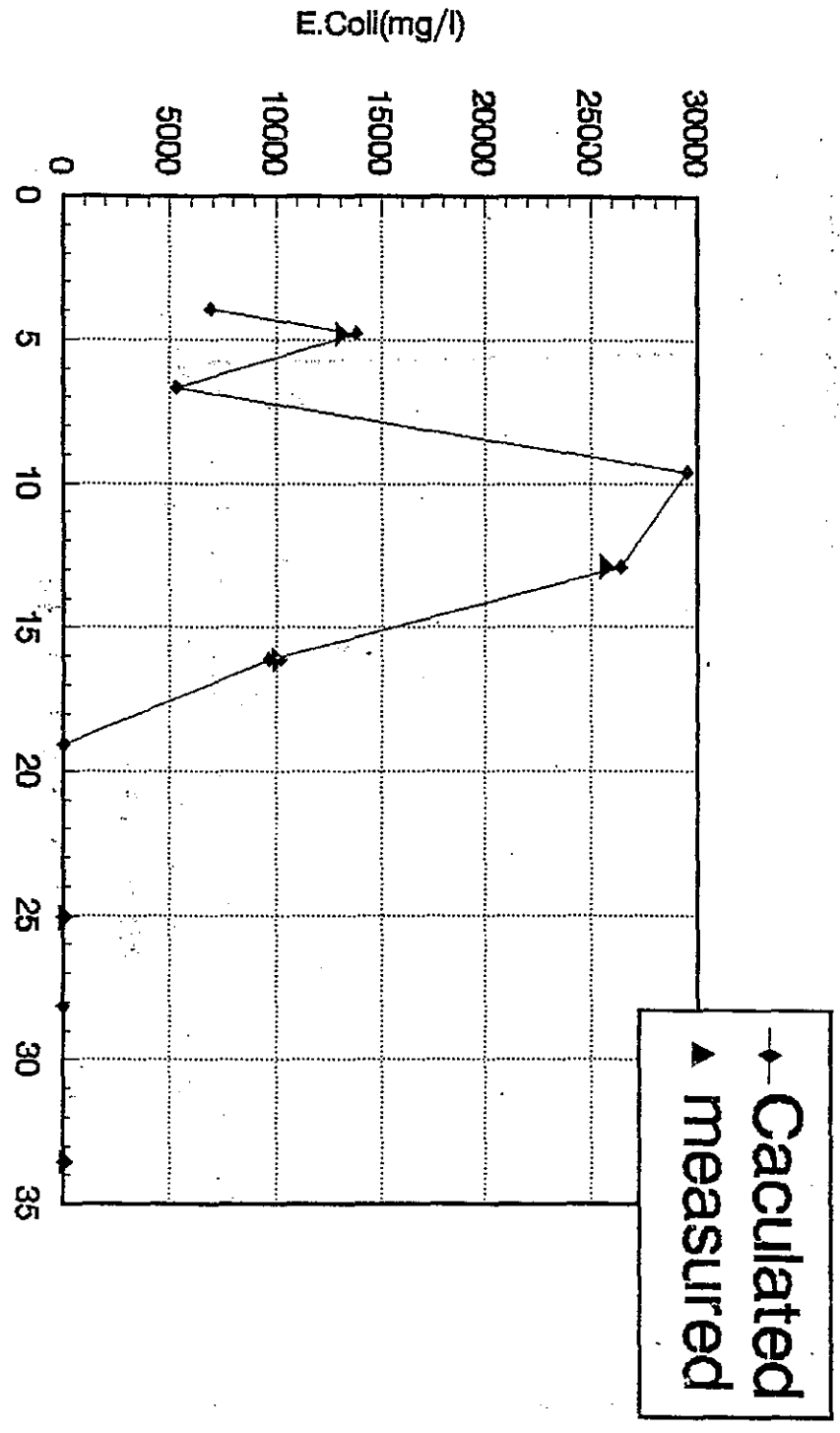

FIG. A7—34 Verification of Col. model

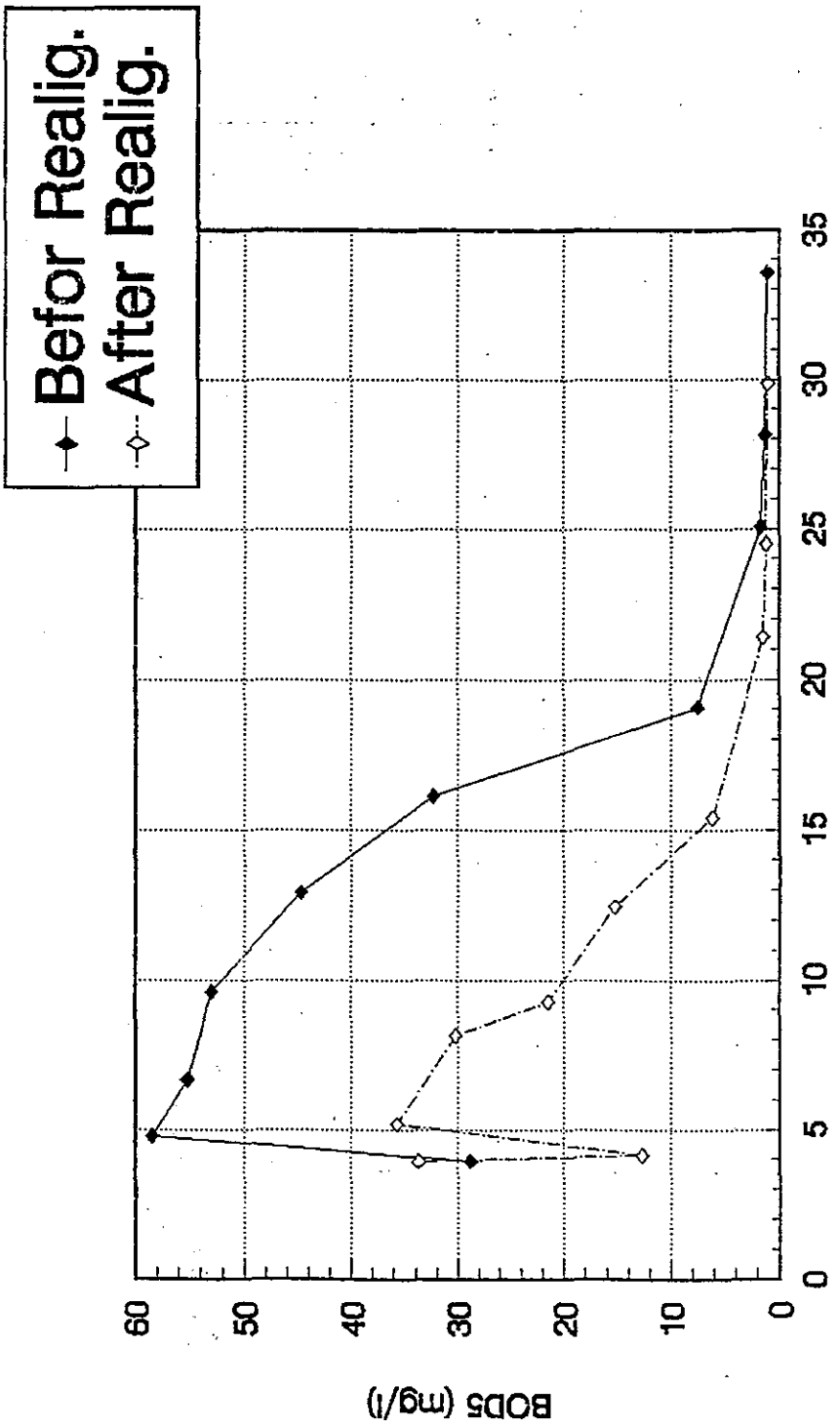

FIG. A7—35 BOD_5 variation in 2000

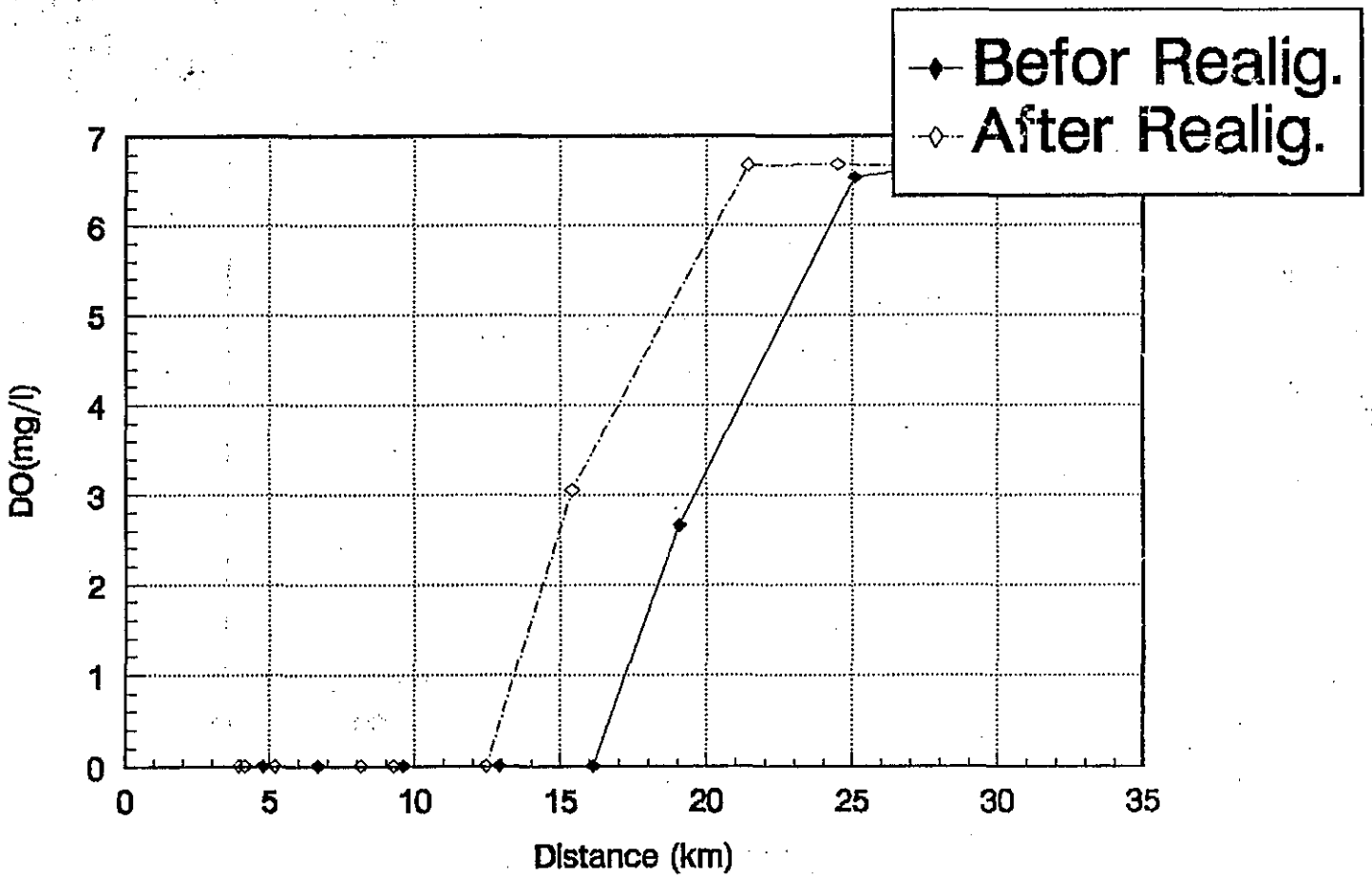

FIG. A7—36 **DO variation in** 2000

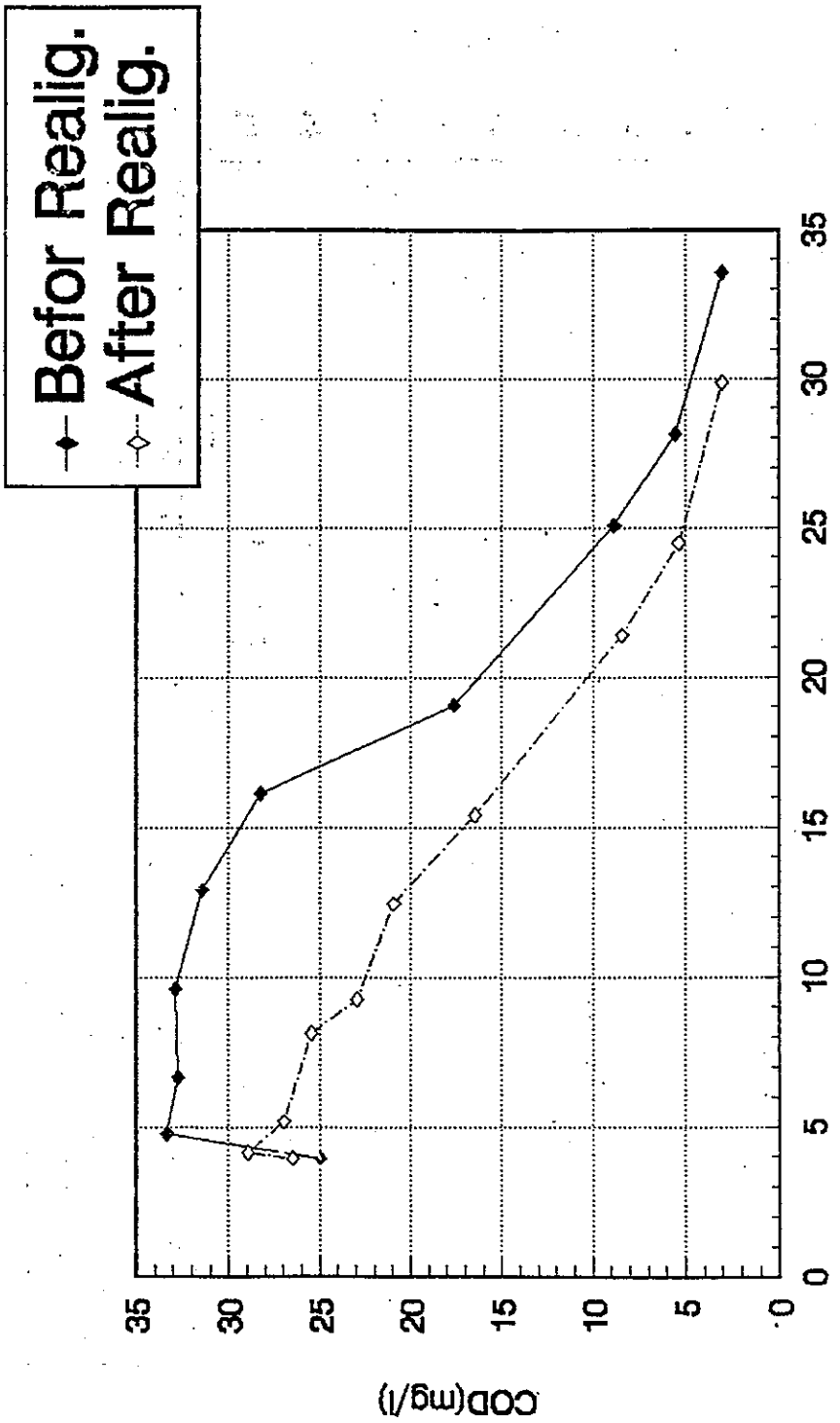

FIG. A7—37 COD variation in 2000

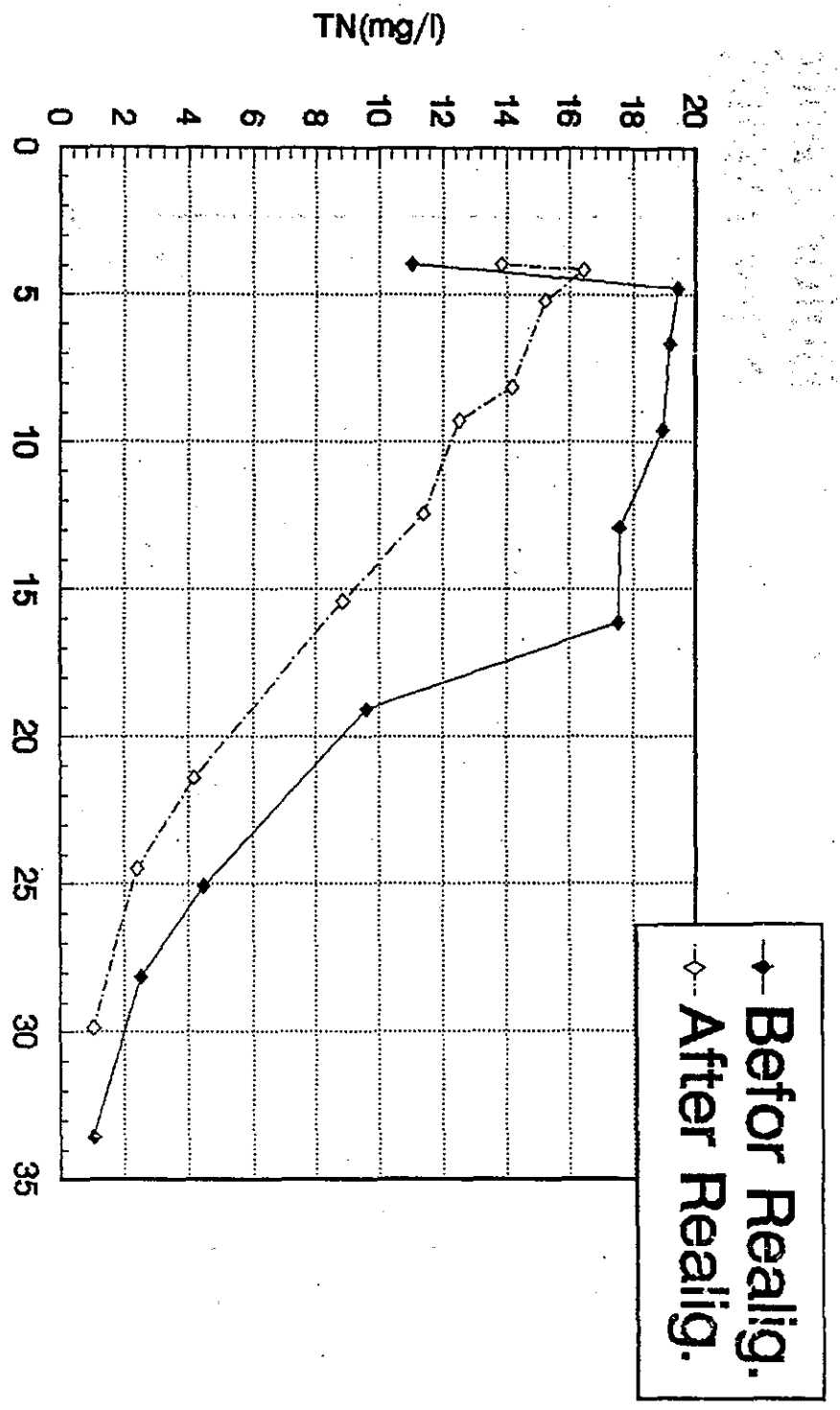

FIG. A7—38 T—N variation in 2000

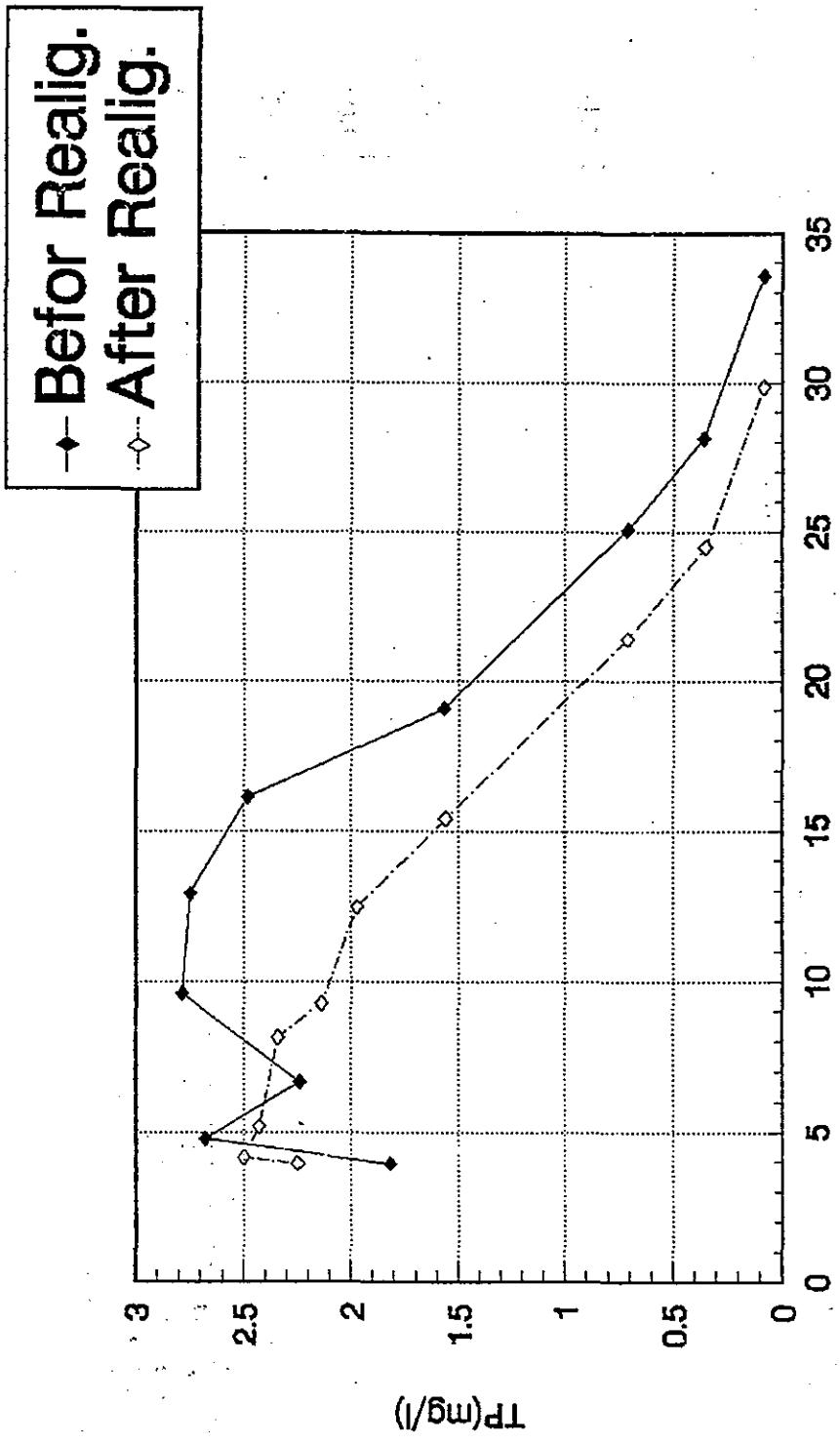

FIG. A7—39 T—P variation in 2000

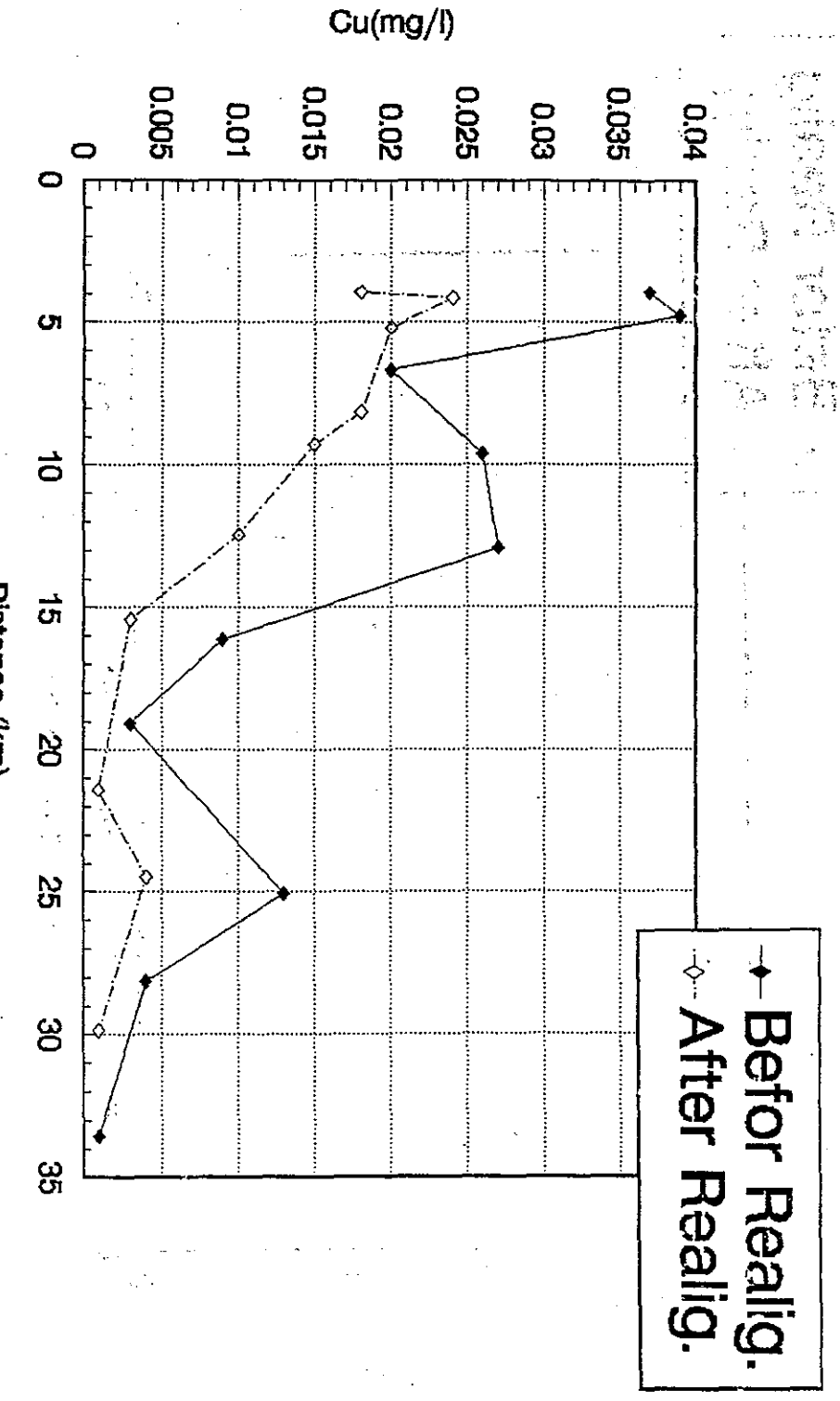

FIG. A7—40 Cu variation in 2000

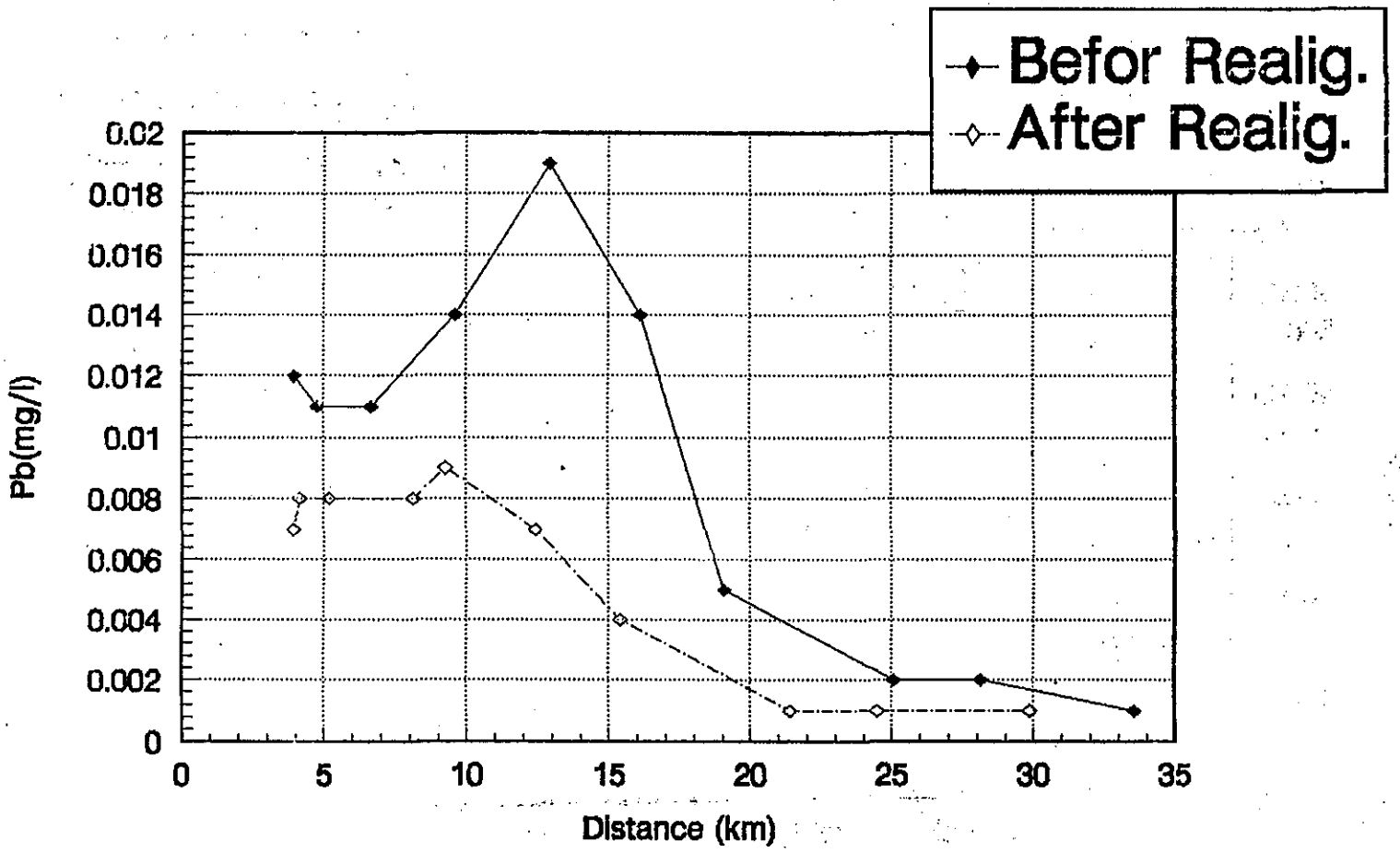

FIG. A7—41 **Pb variation in** 2000

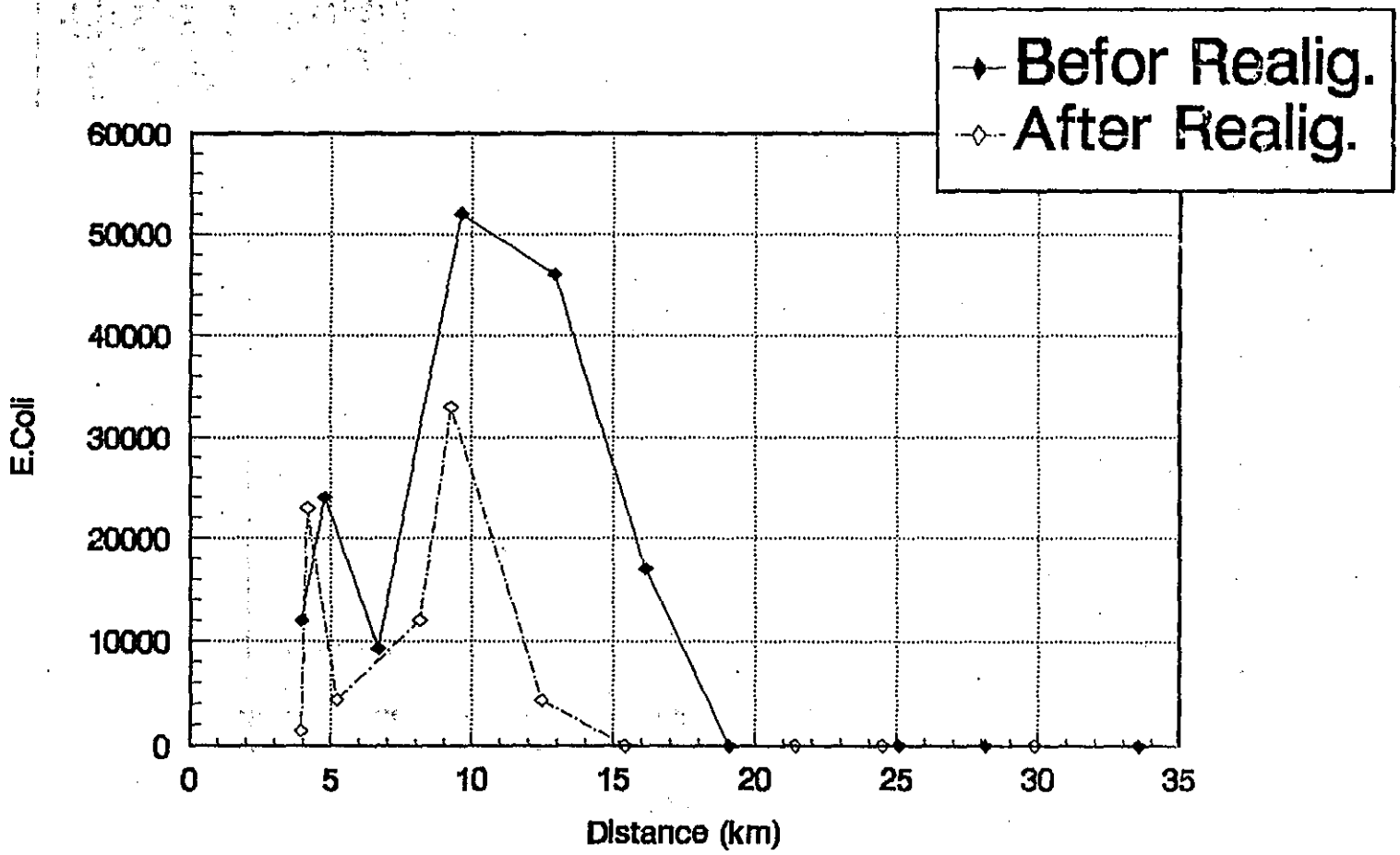

FIG. A7—42 Col. variation in 2000

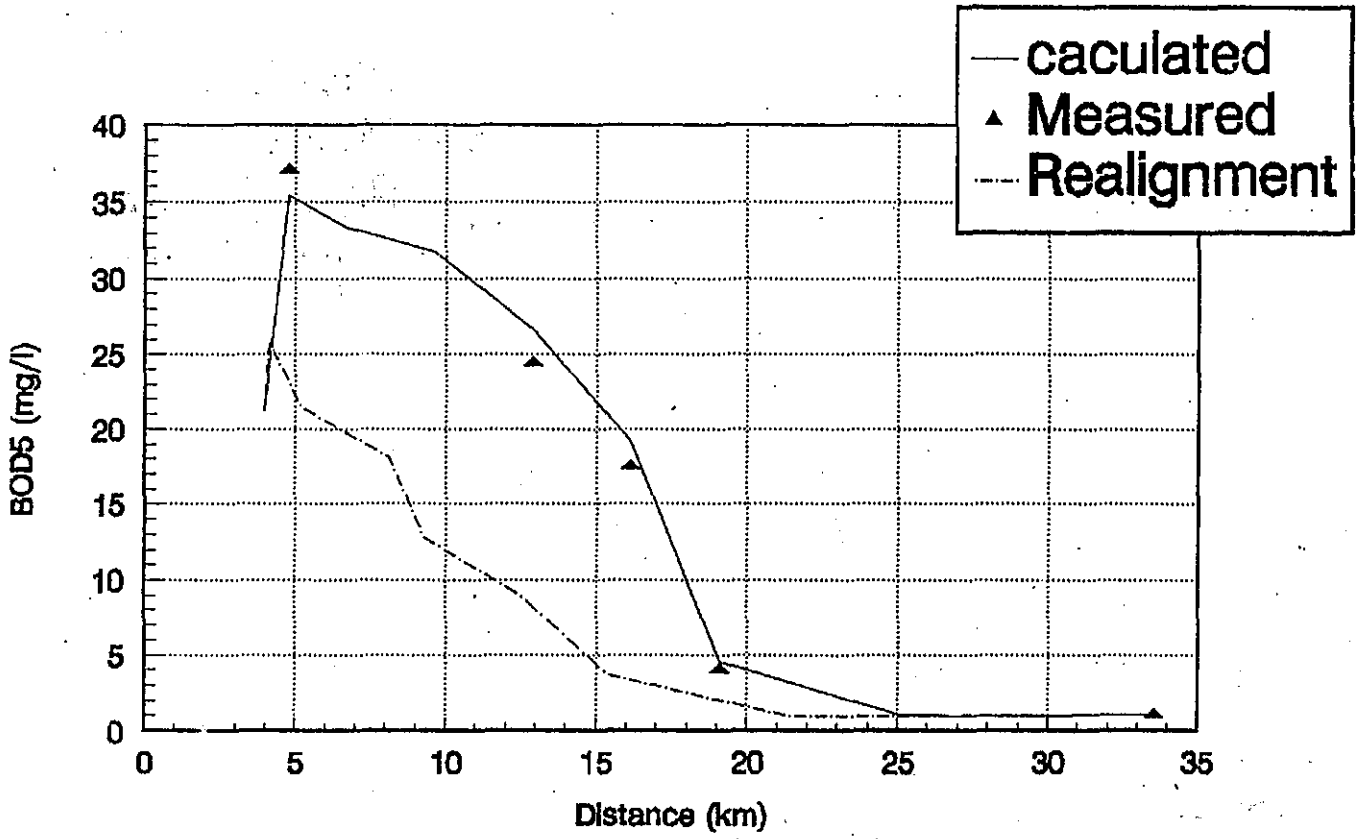

FIG. A7—43 BOD_5 variation before and after the works

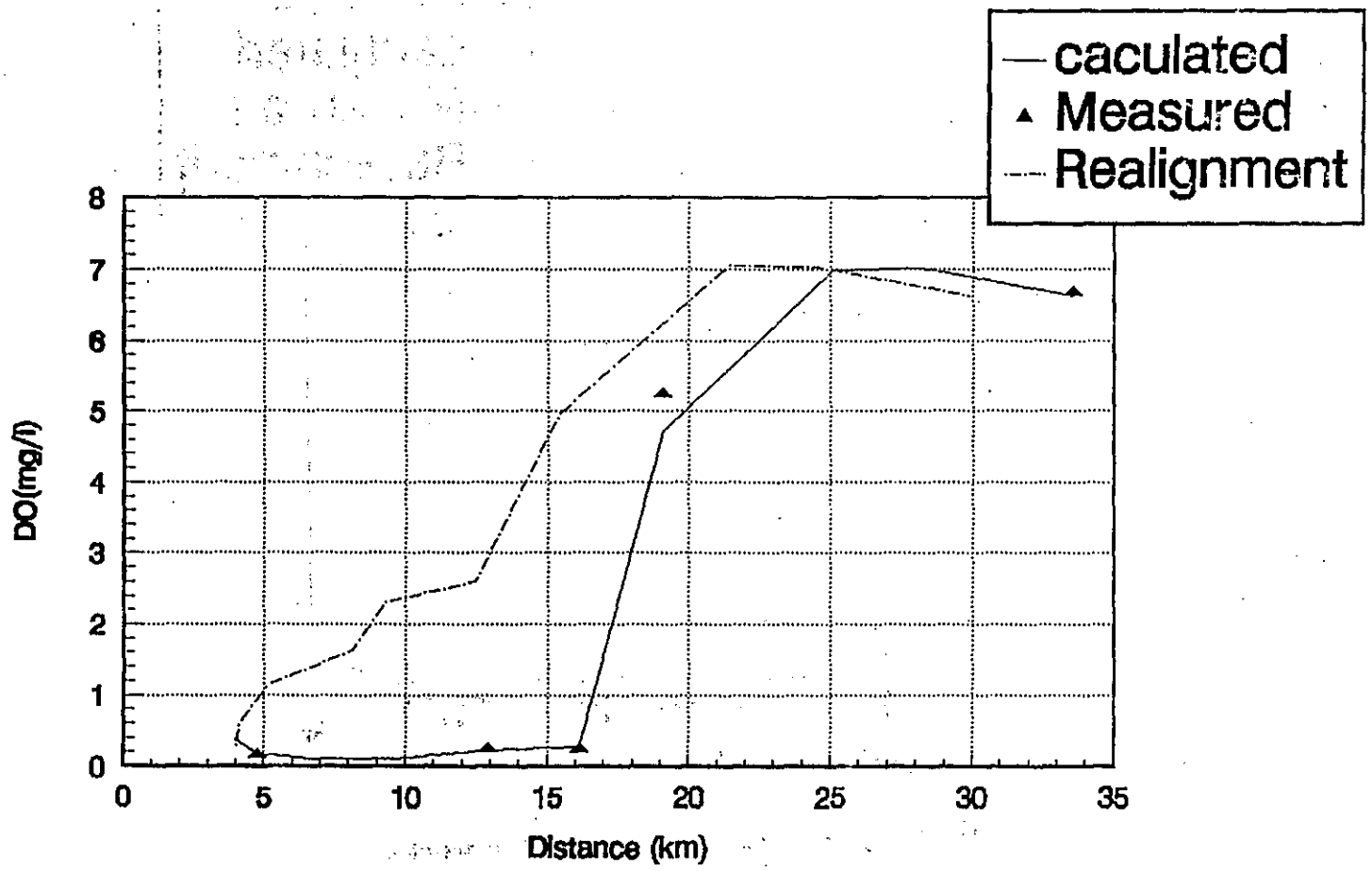

FIG. A7—44 DO variation before and after the works

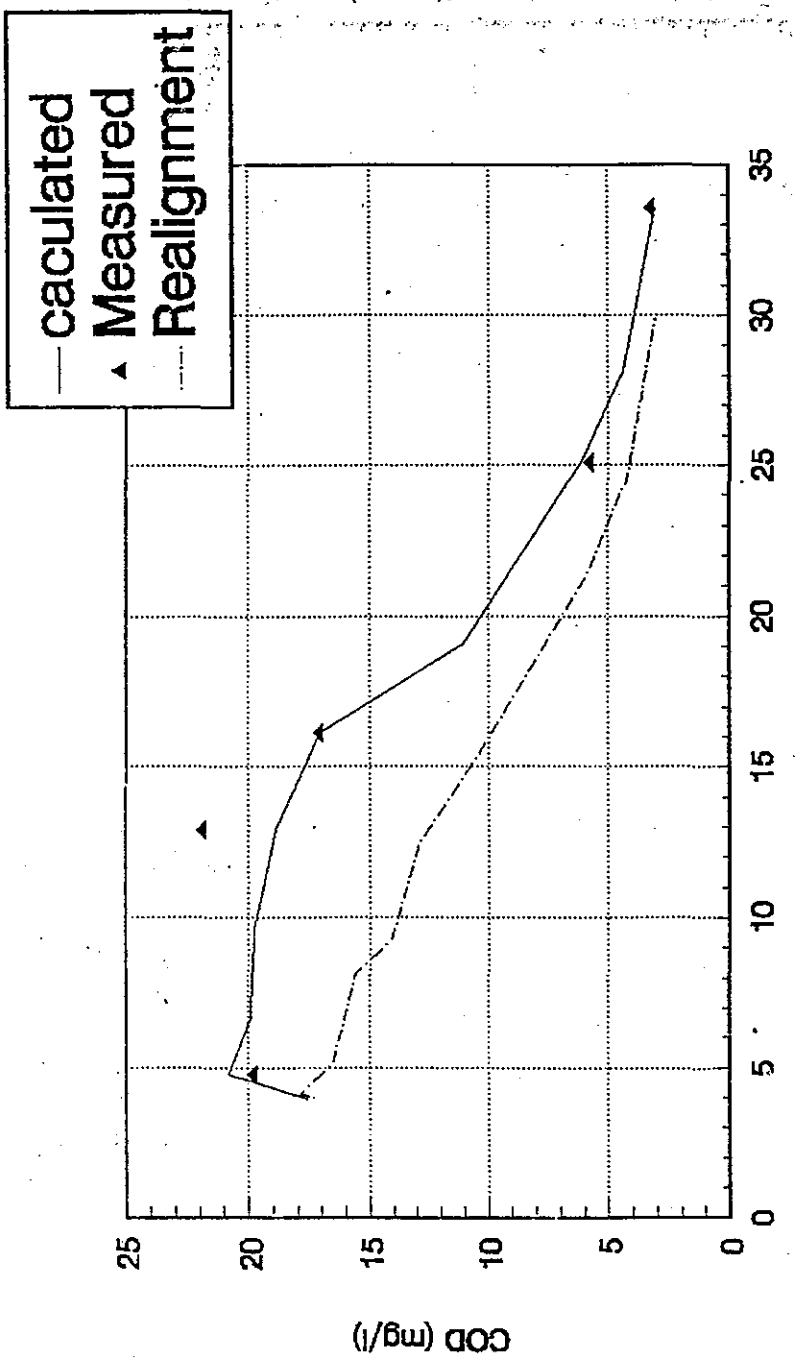

FIG. A7—45 COD variation before and after the works

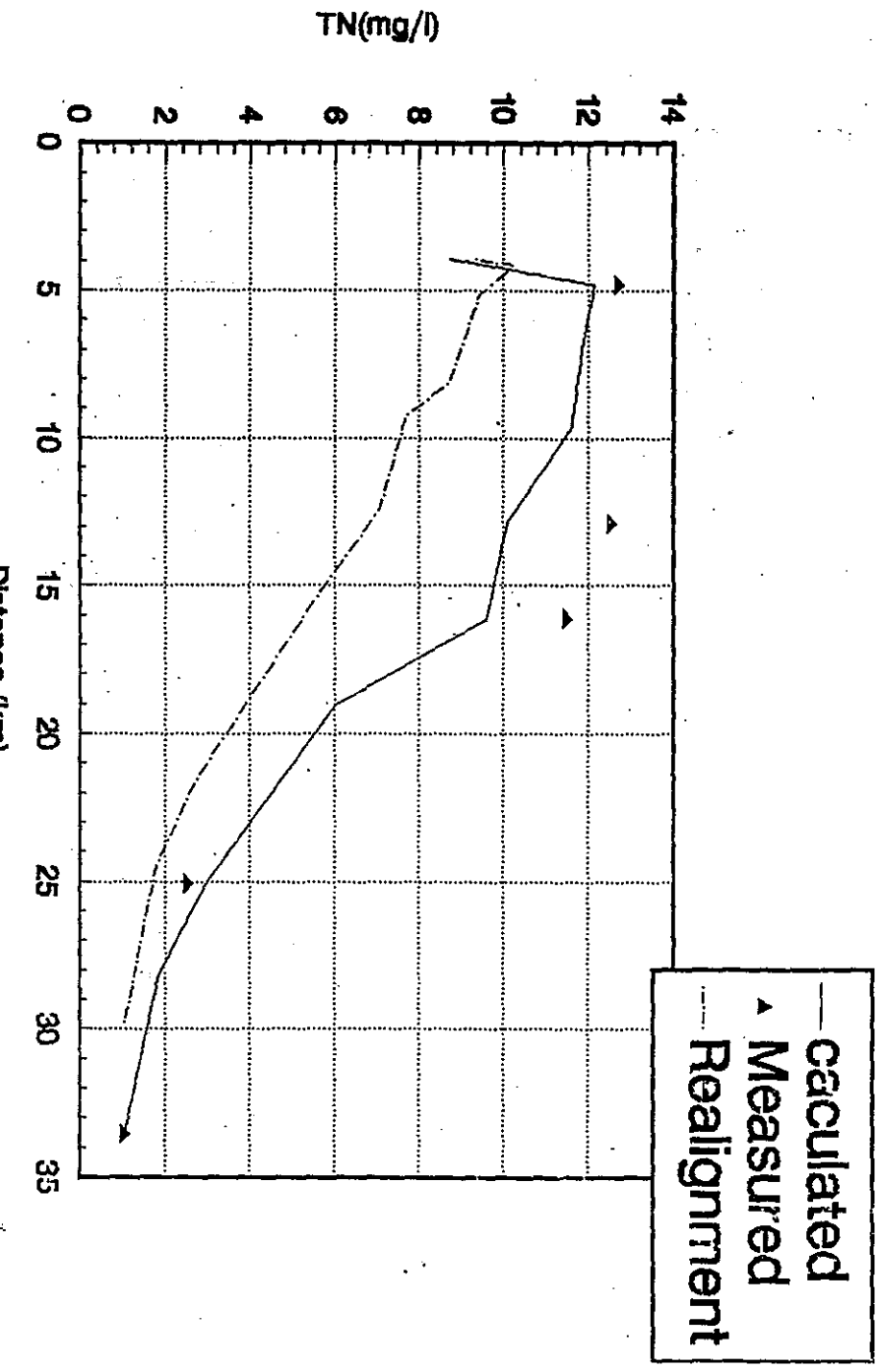

FIG. A7—46 T—N variation before and after the works

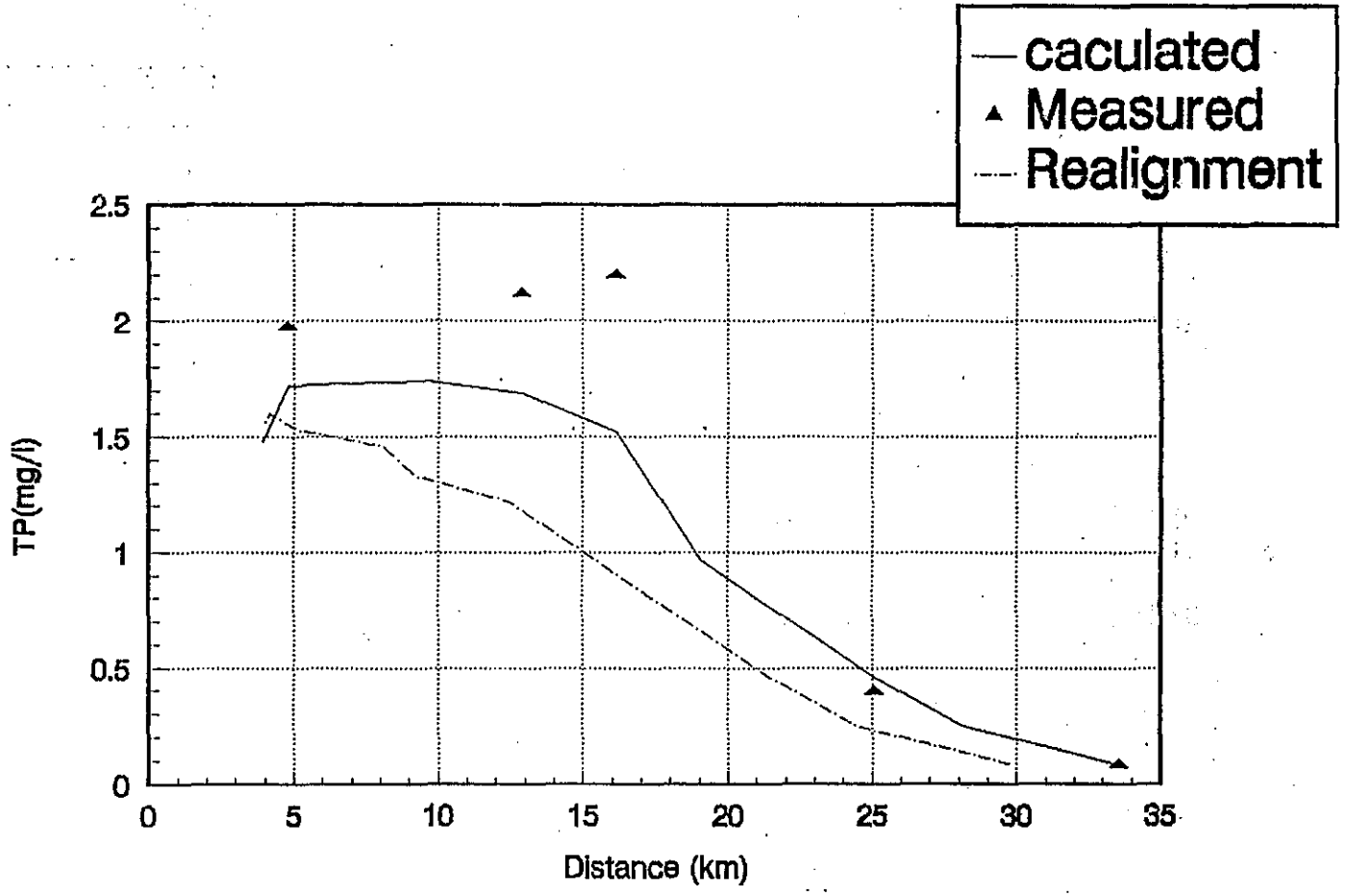

FIG. A7—47 T—P variation before and after the works

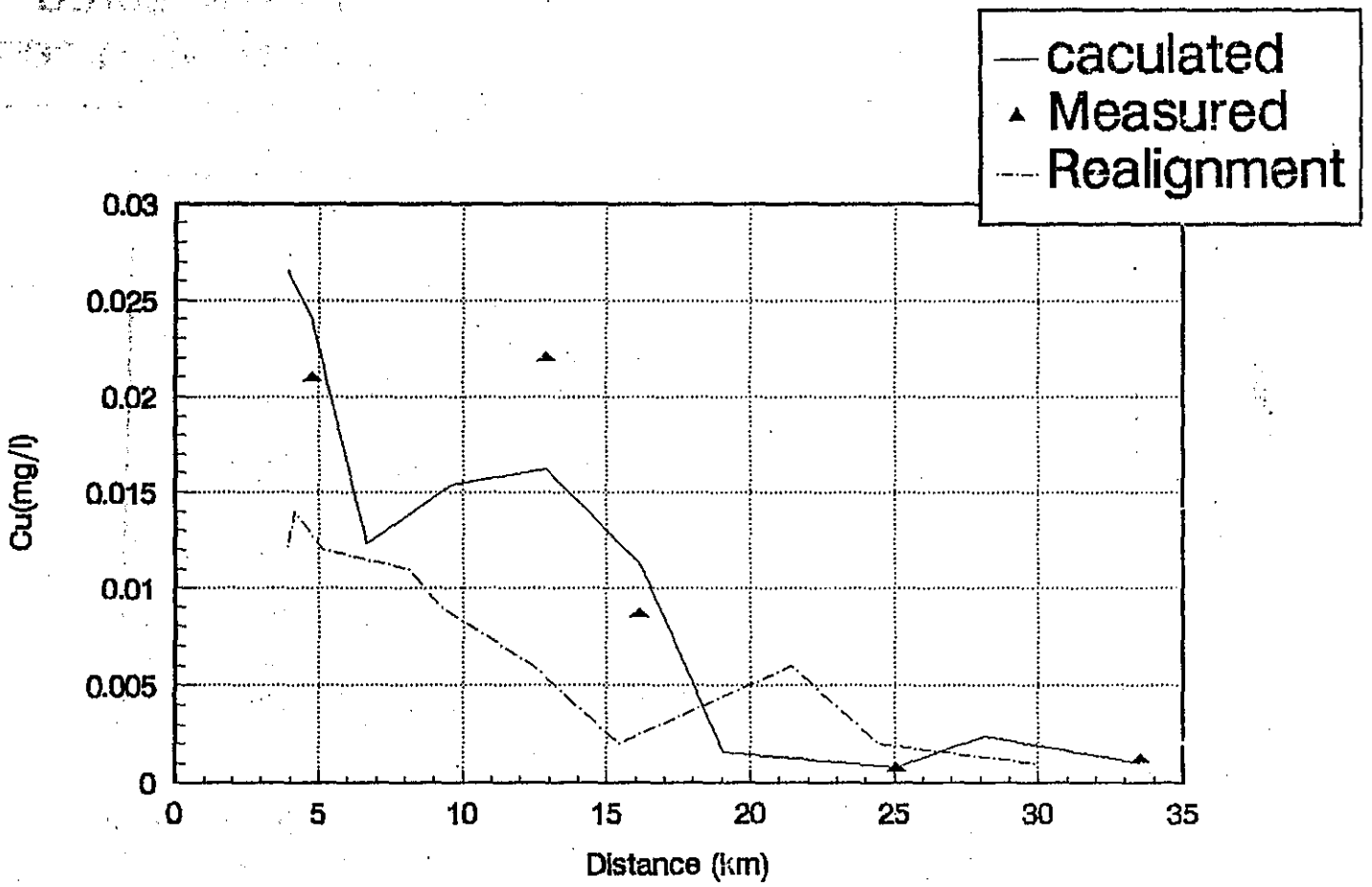

FIG. A7—48 Cu variation before and after the works

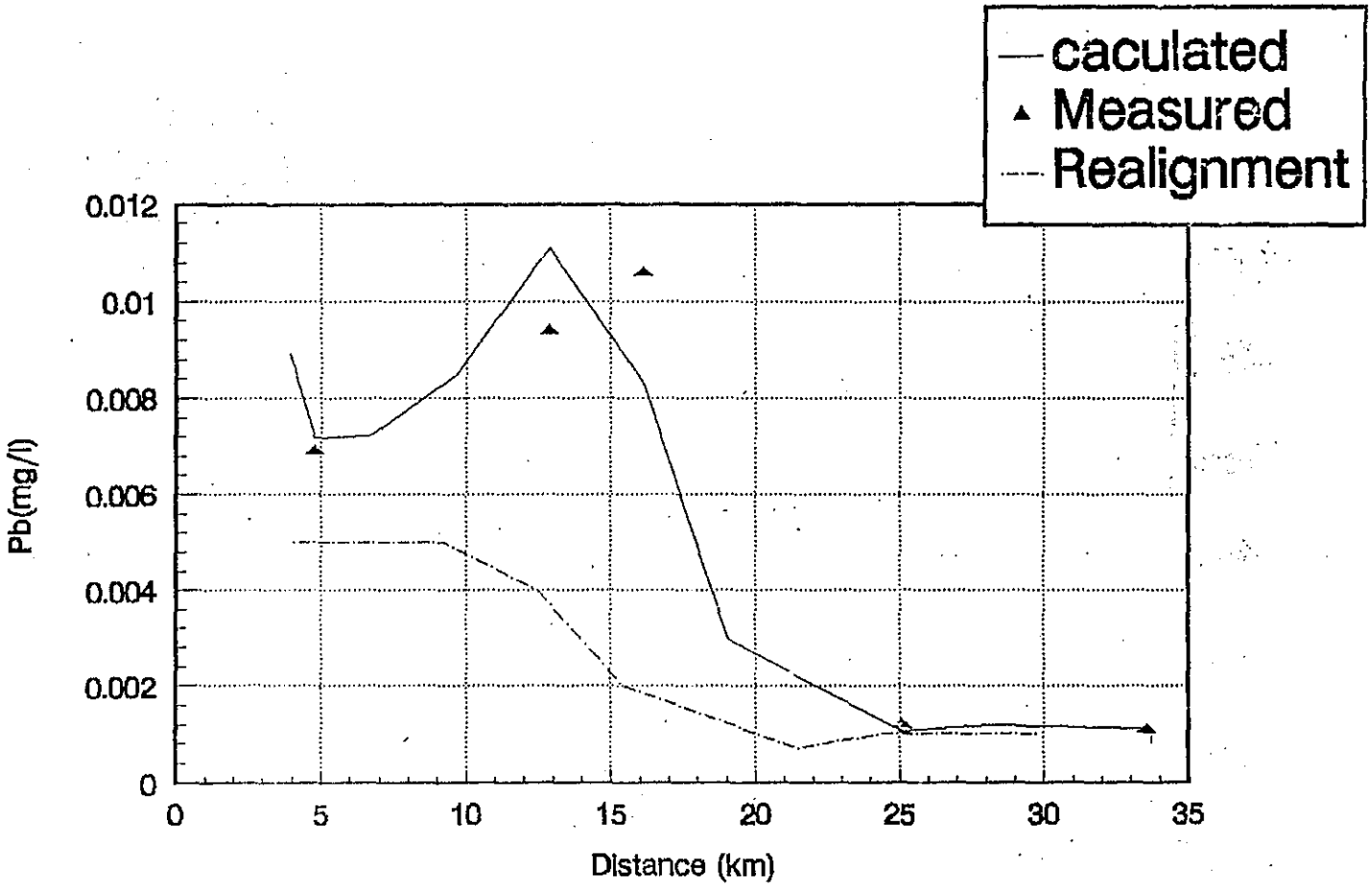

FIG. A7—49 Pb variation before and after the works

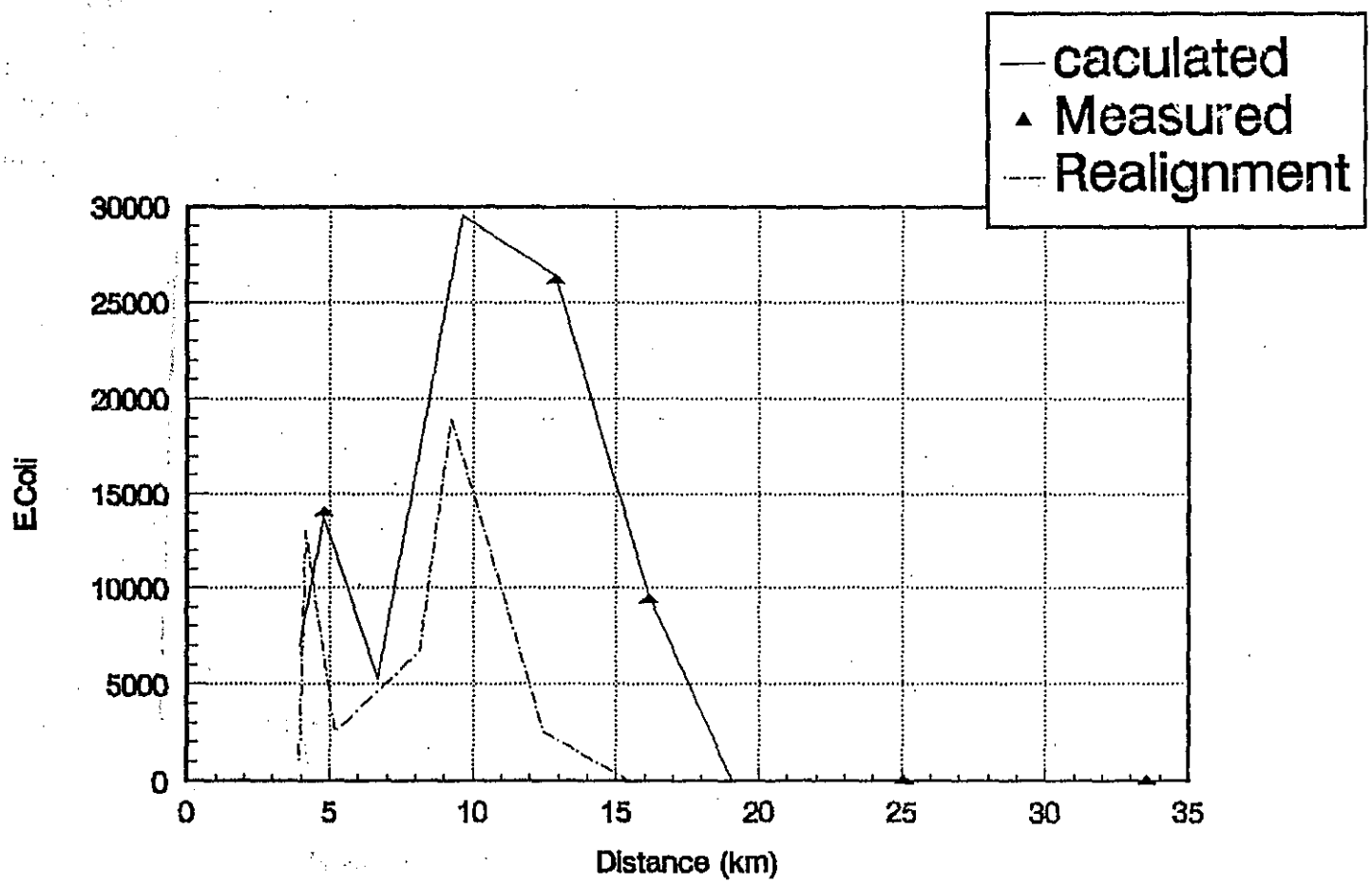

FIG. A7—50 Col. variation before and after the works

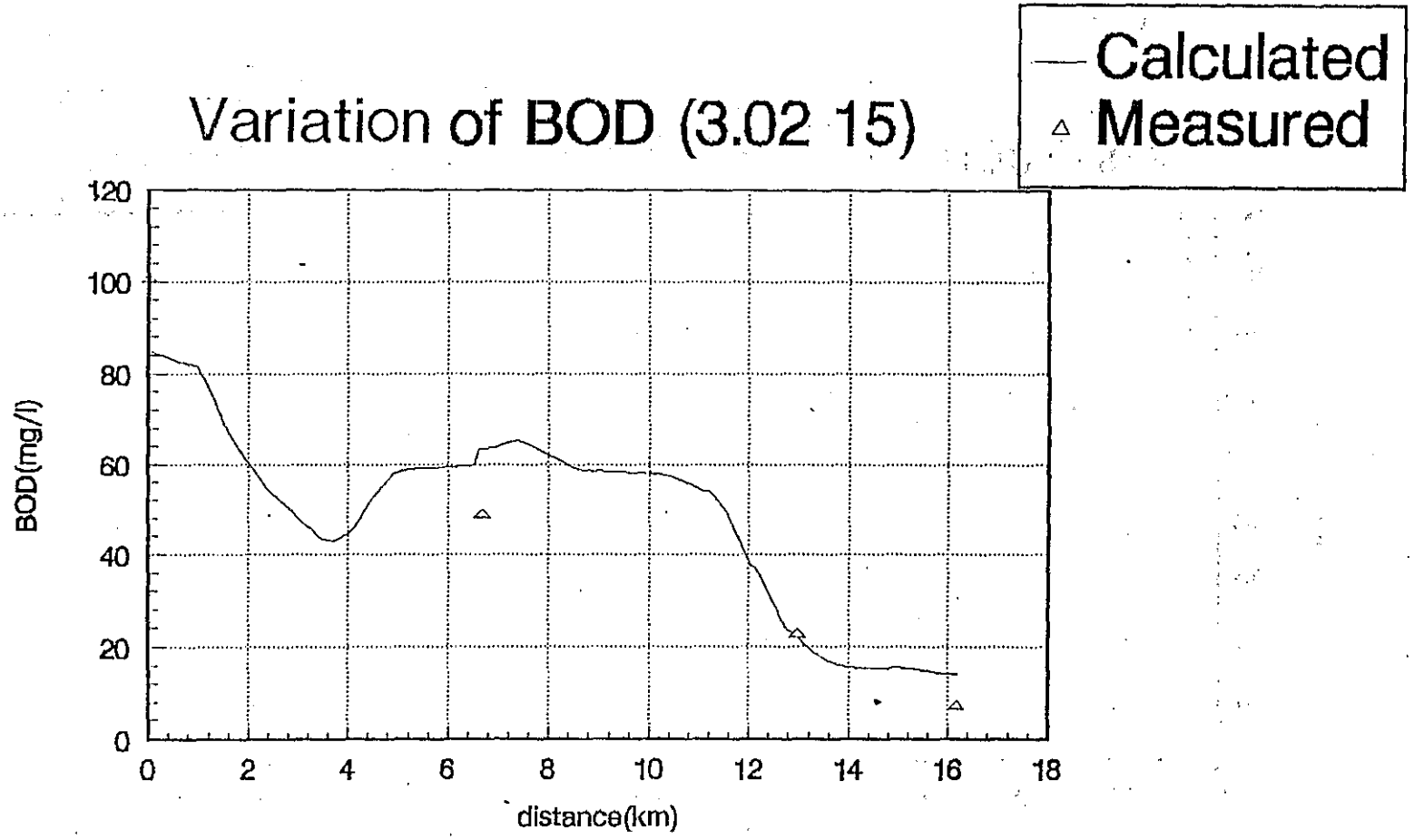

FIG. A7－51(a)　**BOD variation in dry season** (3. 02 15)

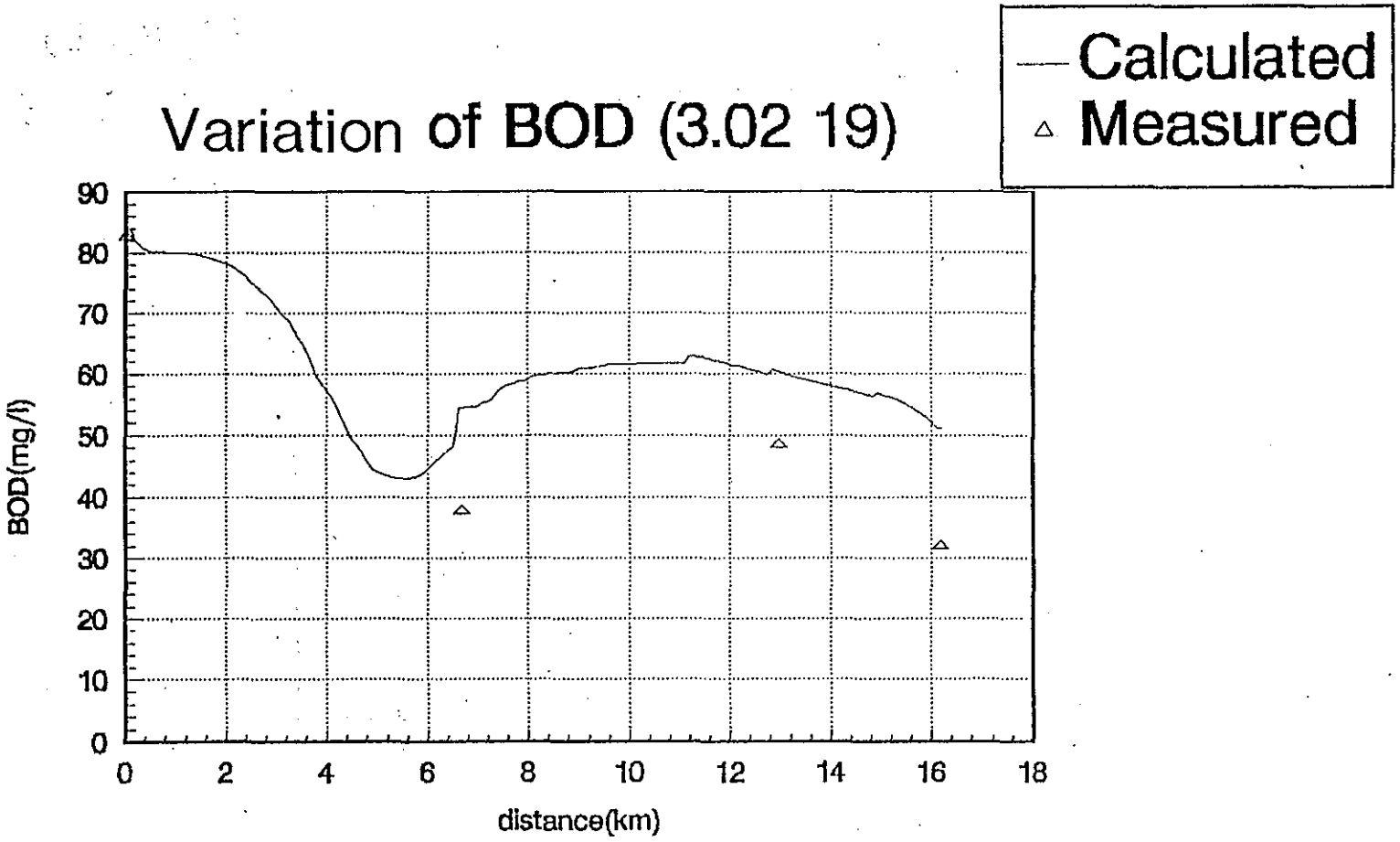

FIG. A7—51(b) **BOD variation in dry season** (3. 02 19)

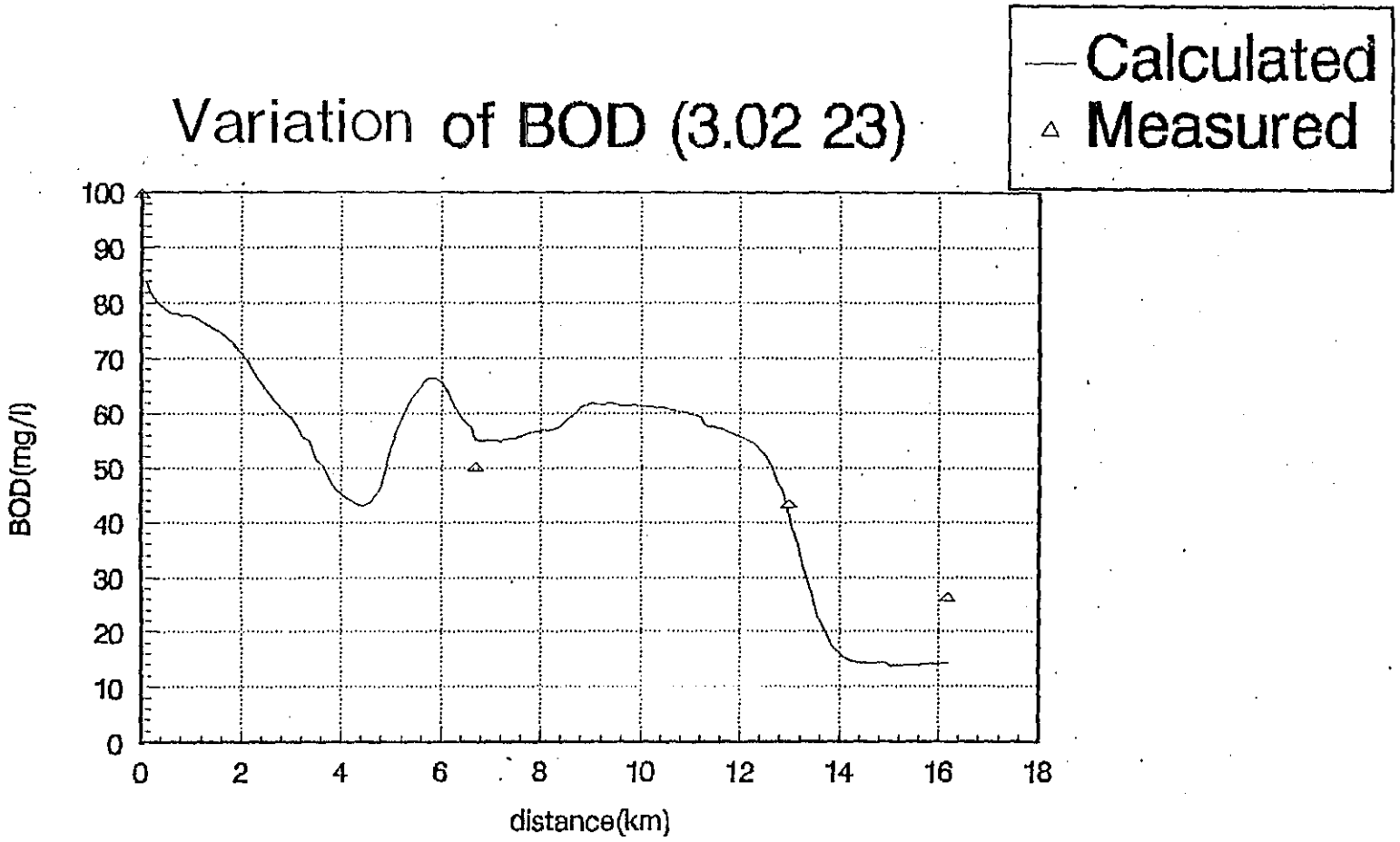

FIG. A7－51(c) **BOD variation in dry season** (3.02 23)

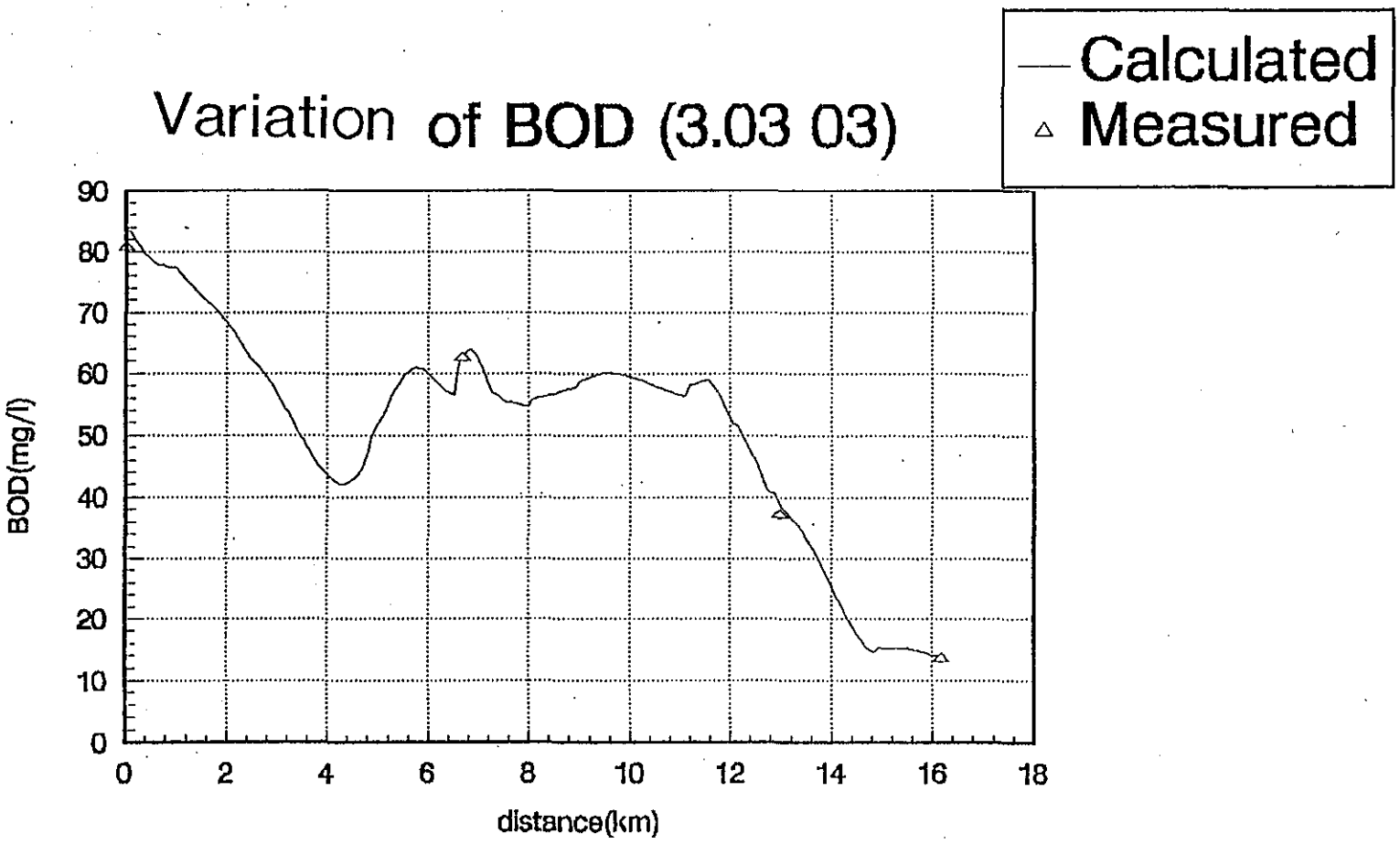

FIG. A7—51(d) BOD variation in dry season (3. 02 03)

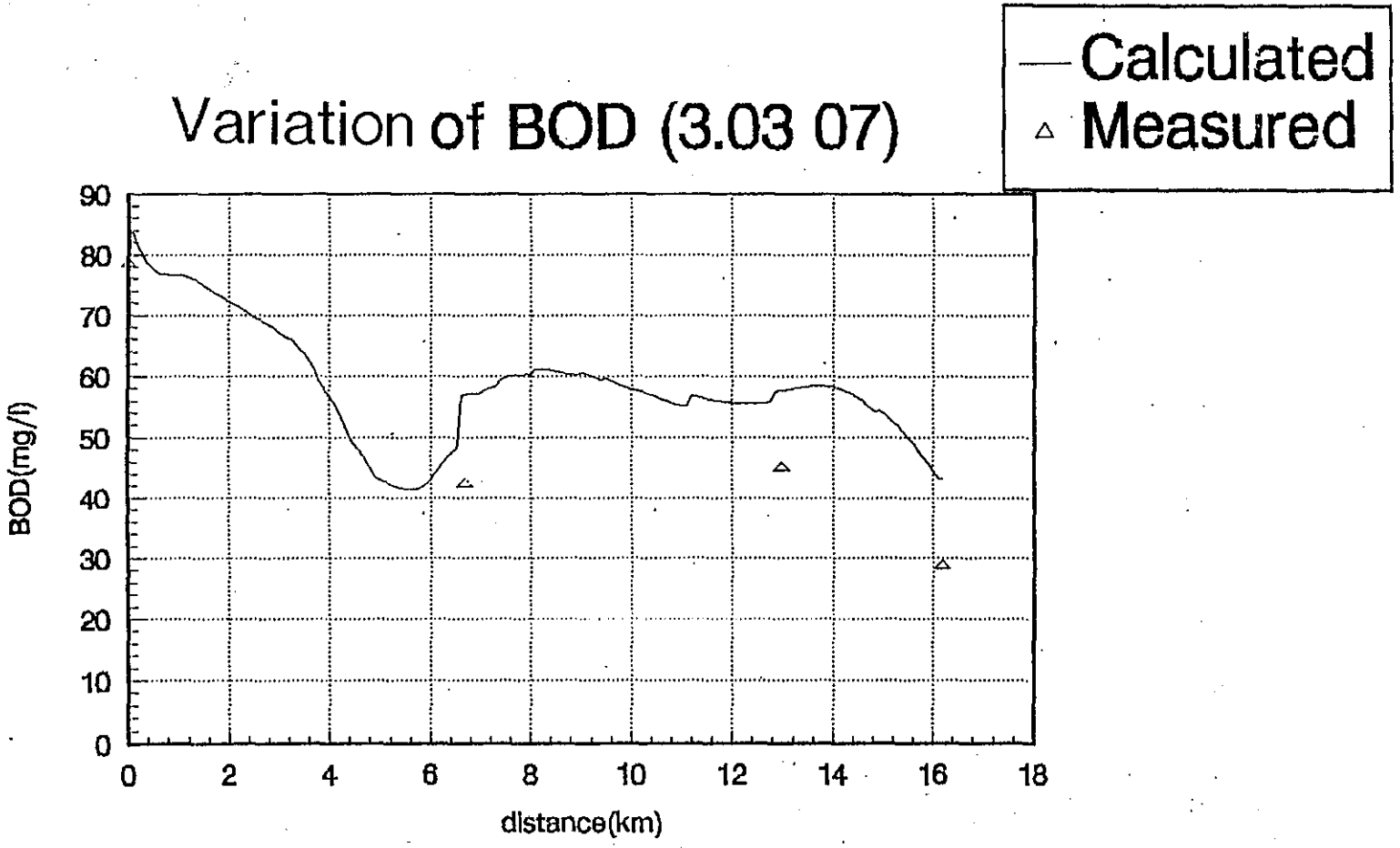

FIG. A7—51(e) **BOD variation in dry season** (3. 02 07)

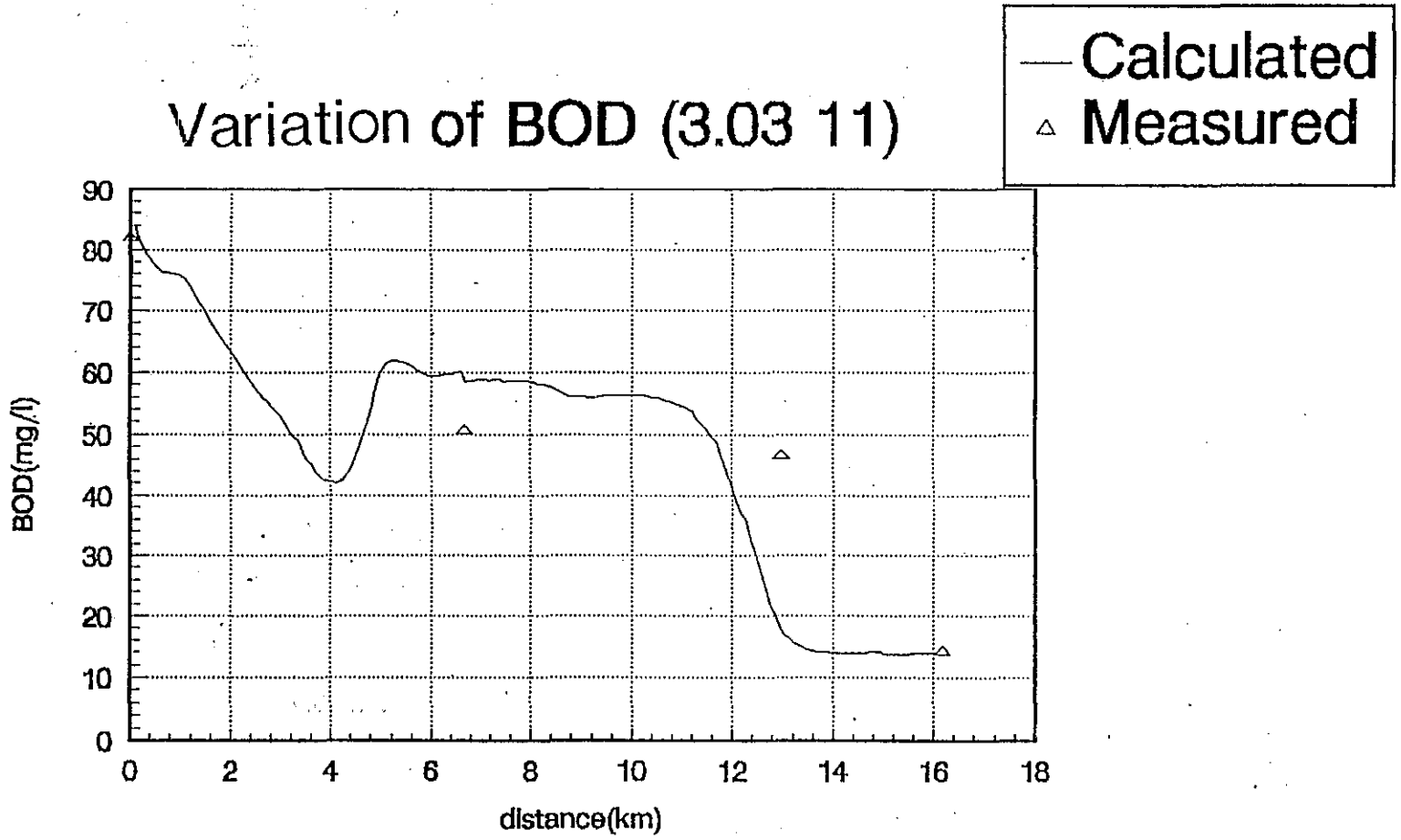

FIG. A7—51(f) **BOD variation in dry season** (3. 02 11)

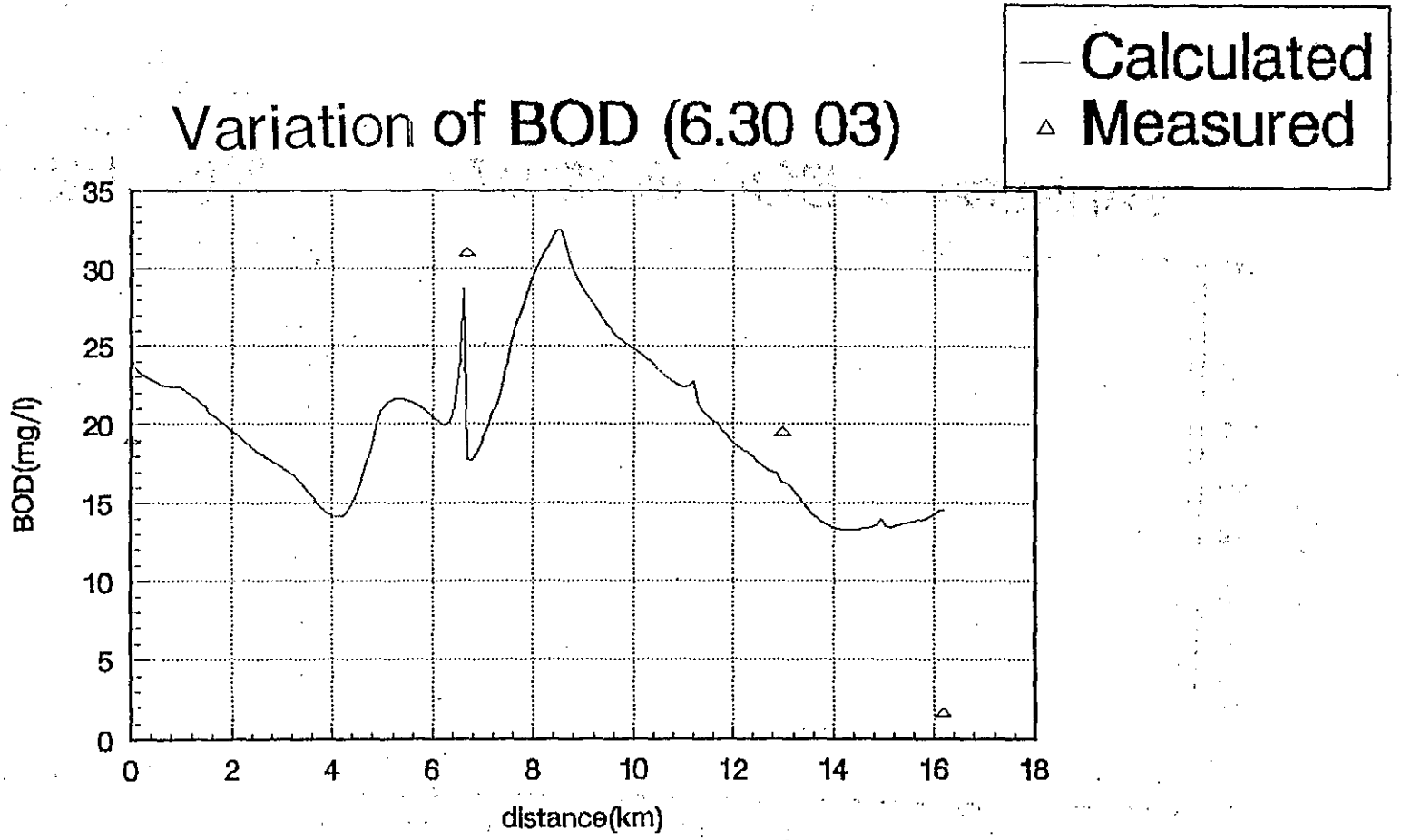

FIG. A7—51(g) **BOD variation in wet season** (6. 30 03)

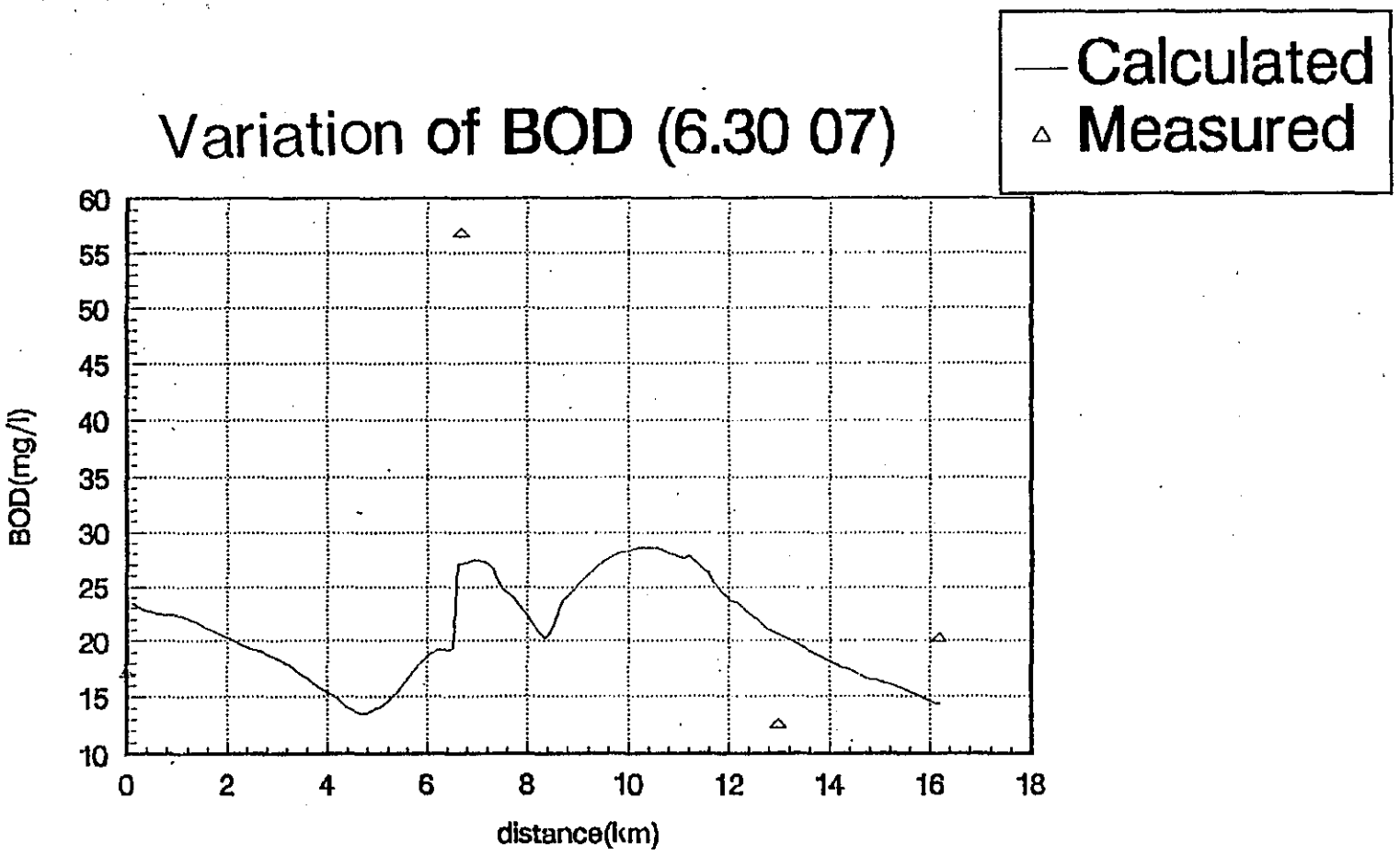

FIG. A7—51(h) **BOD variation in wet season** (6. 30 07)

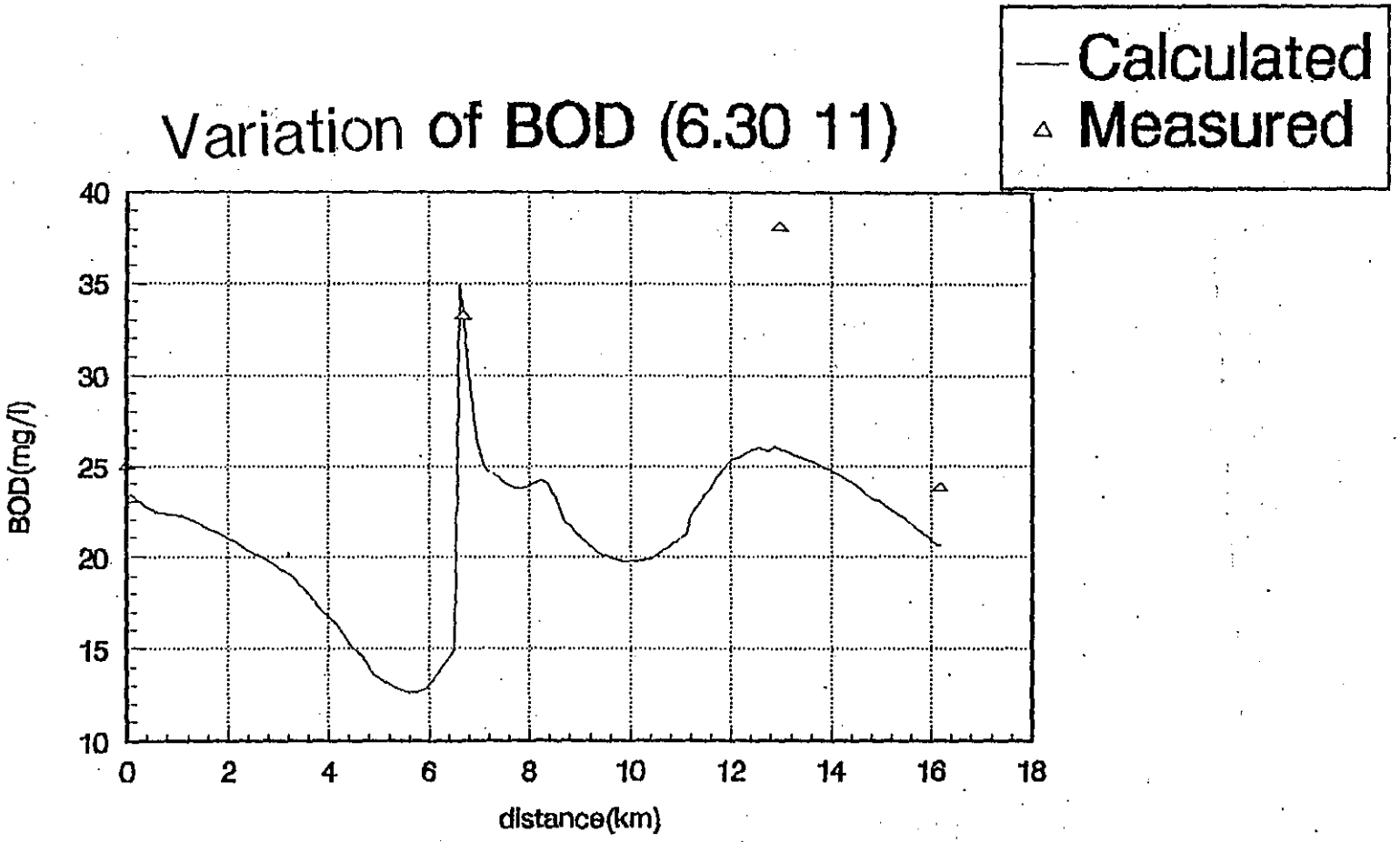

FIG. A7－51(i) **BOD variation in wet season** (6. 30 11)

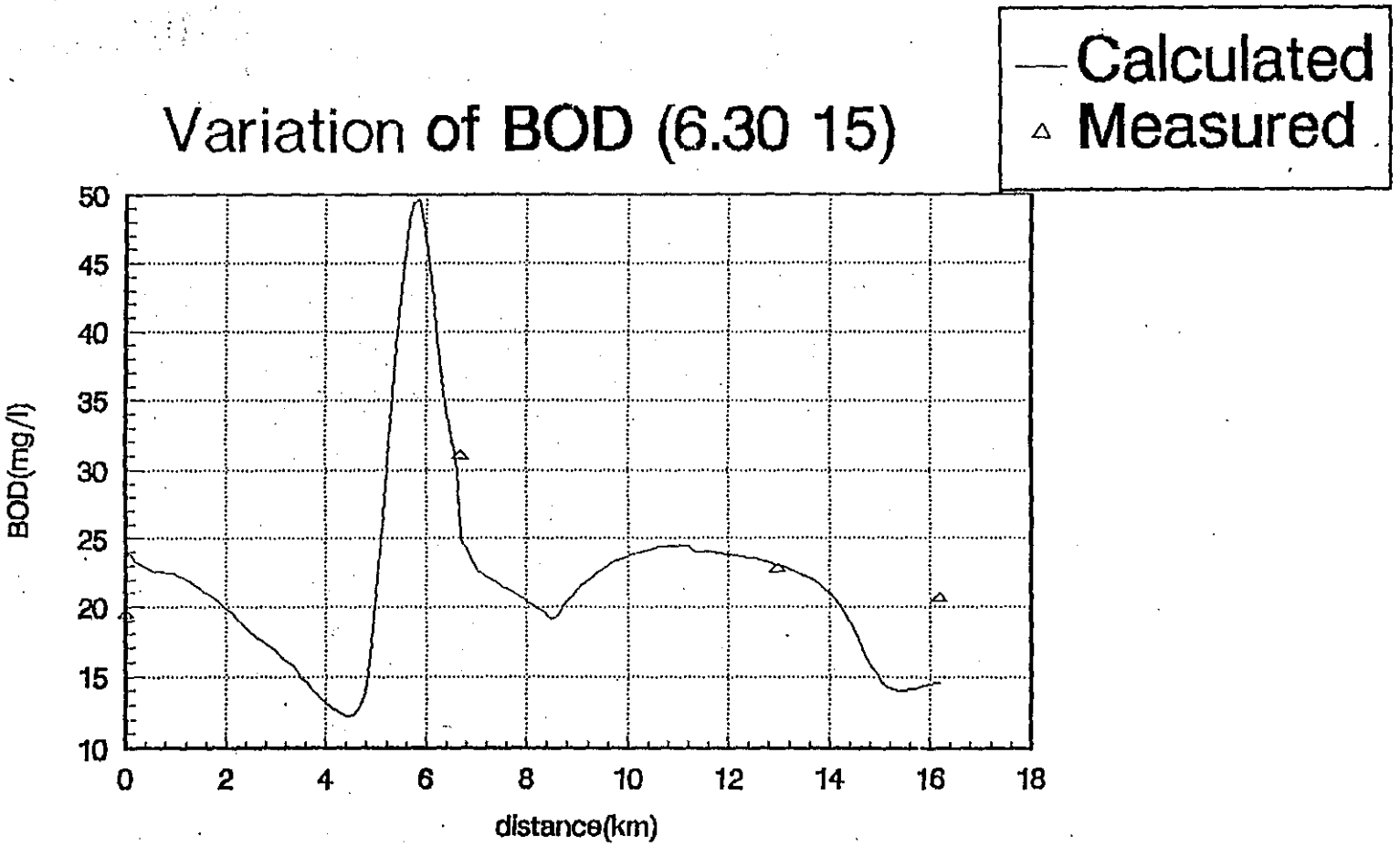

FIG. A7－51(j)　BOD variation in wet season (6. 30 15)

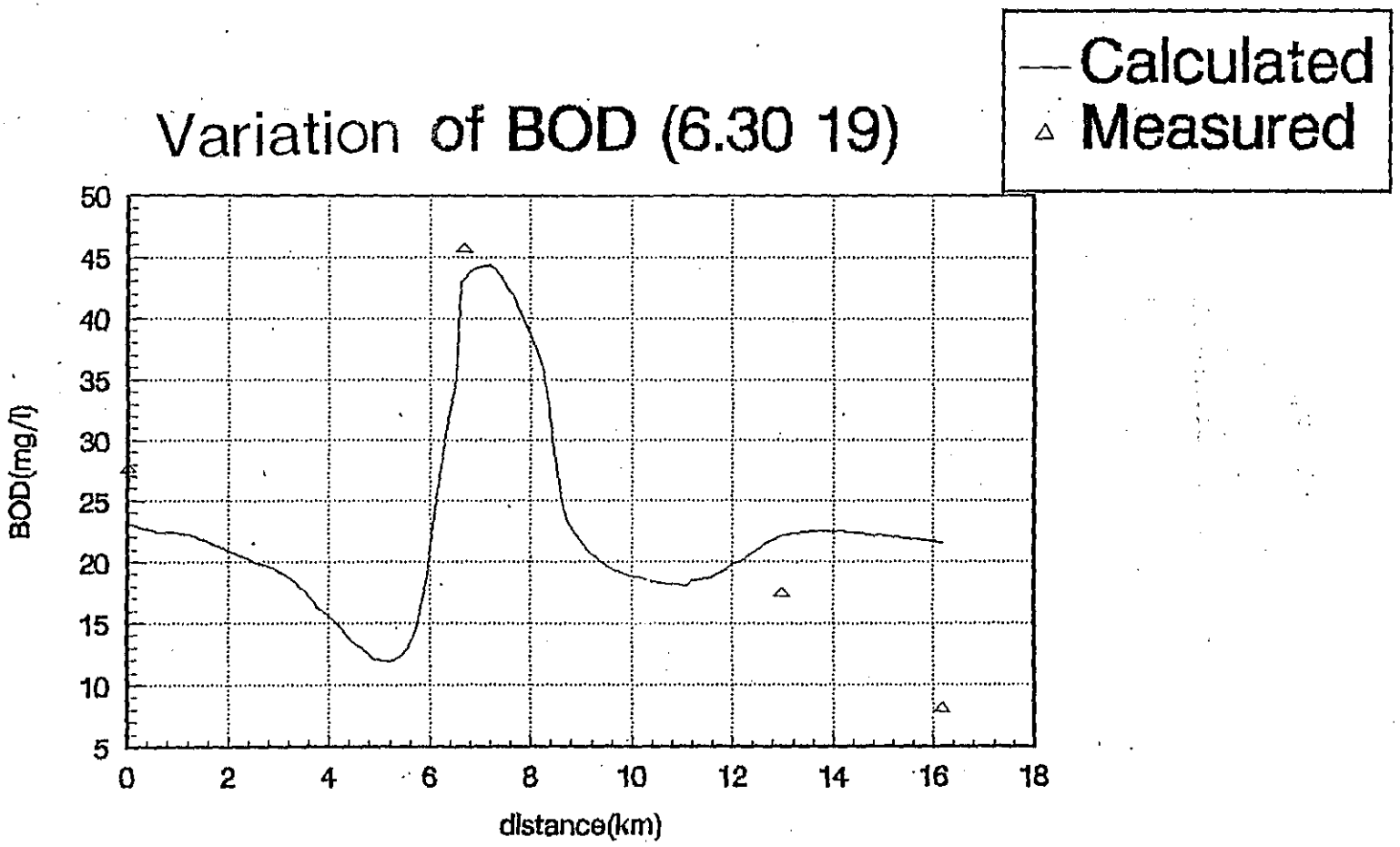

FIG. A7－51(k) **BOD variation in wet season** (6. 30 19)

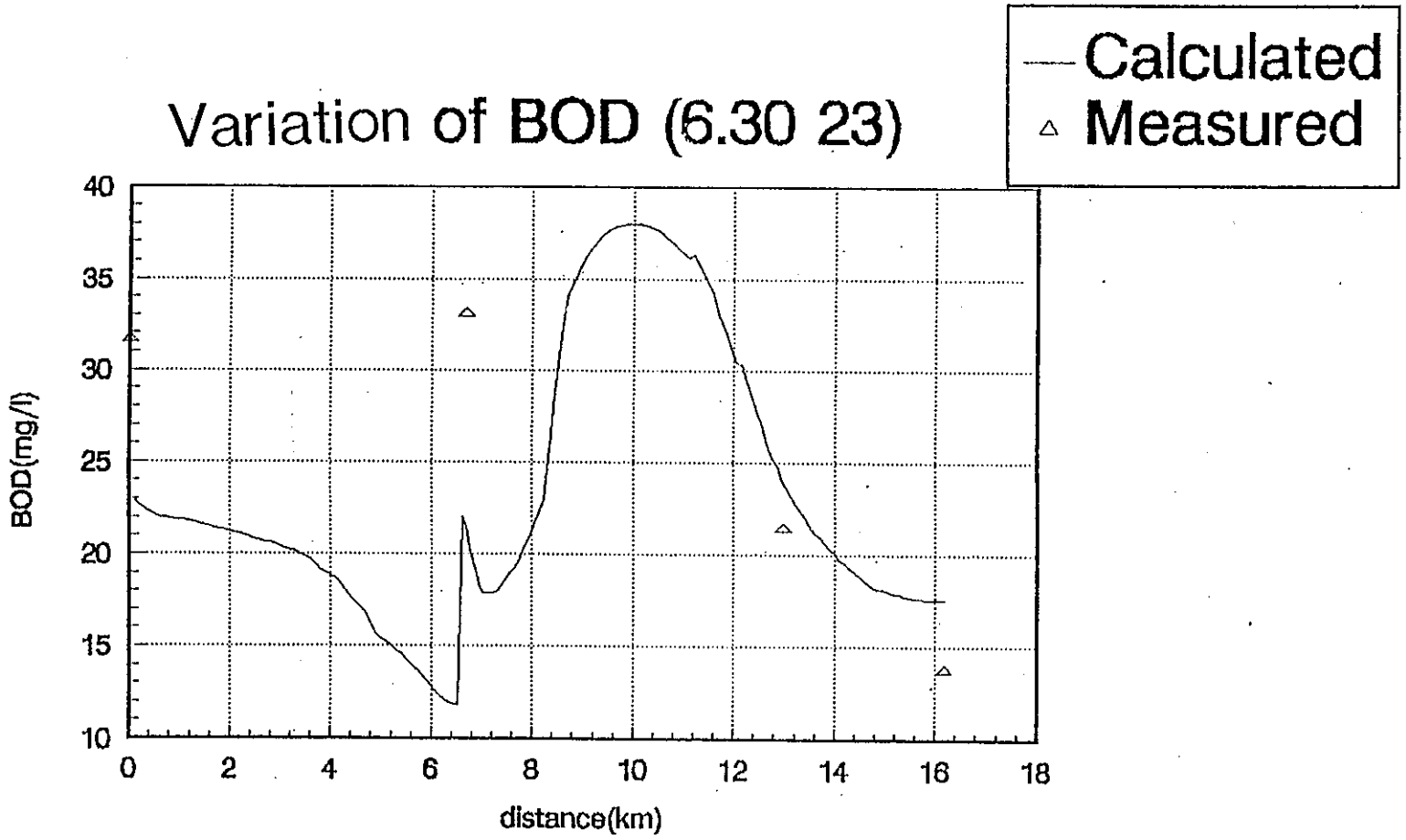

FIG. A7—51(1) BOD variation in wet season (6. 30 23)

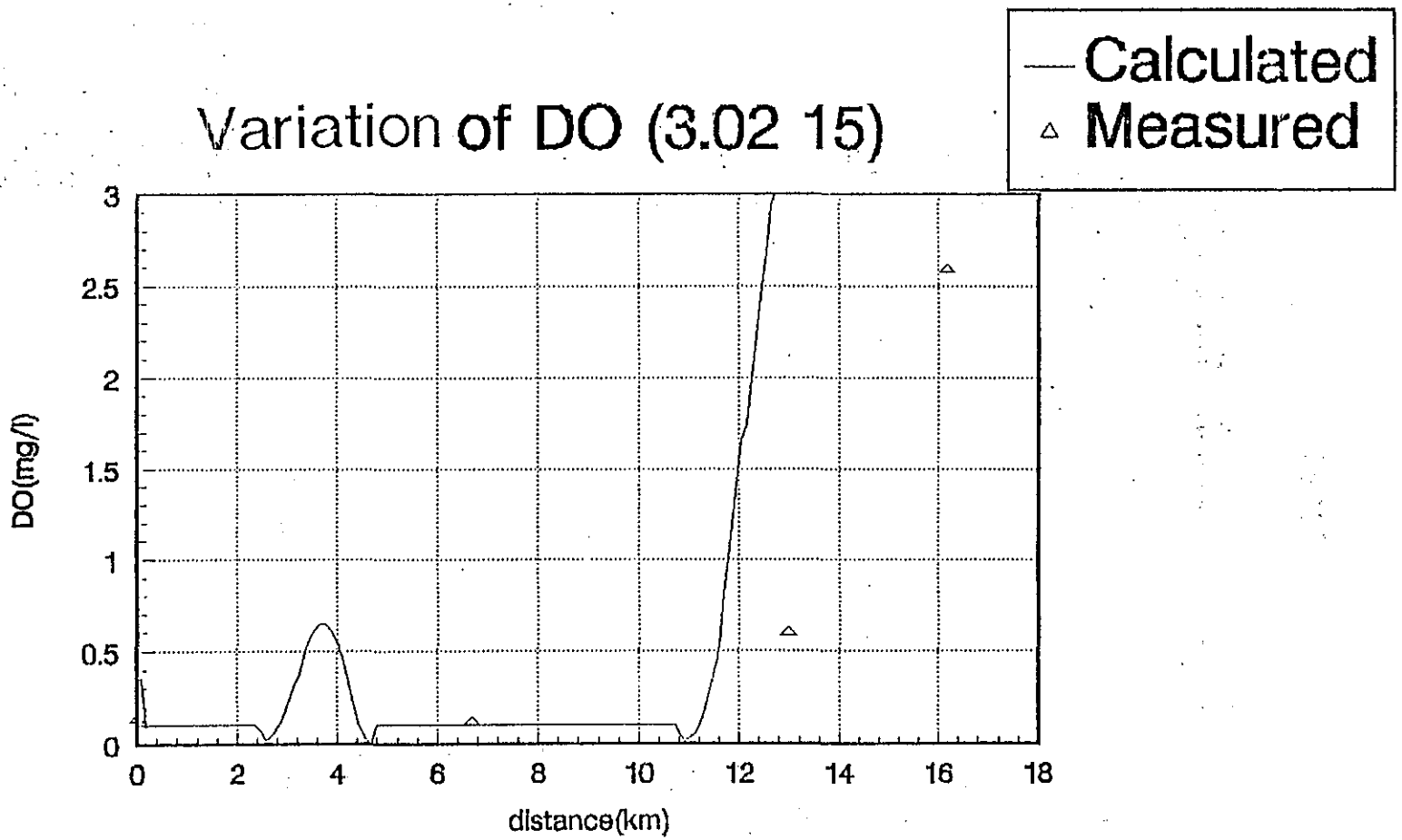

FIG. A7—52(a) **DO variation in dry season** (3. 02 15)

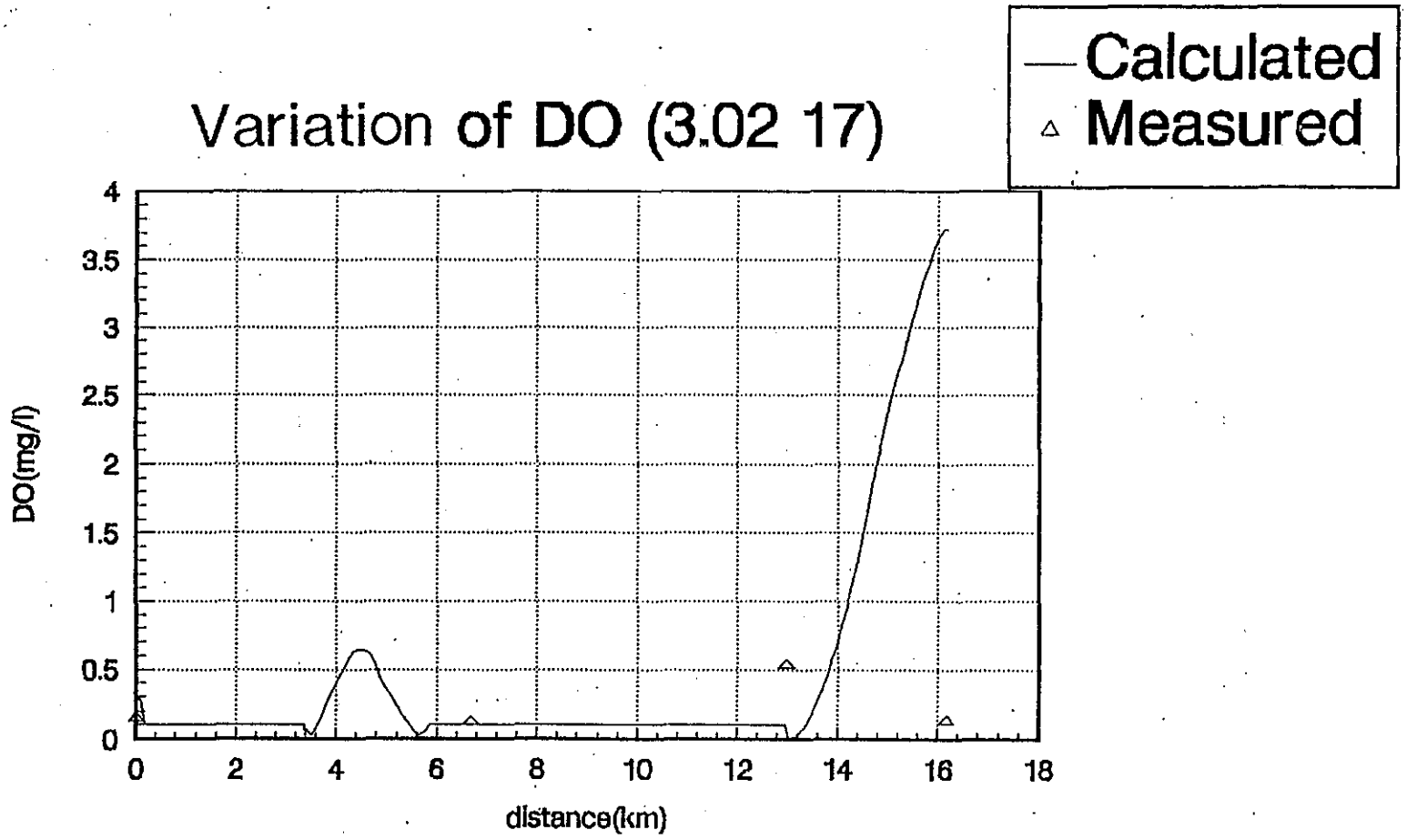

FIG. A7—52(b) DO variation in dry season (3. 02 17)

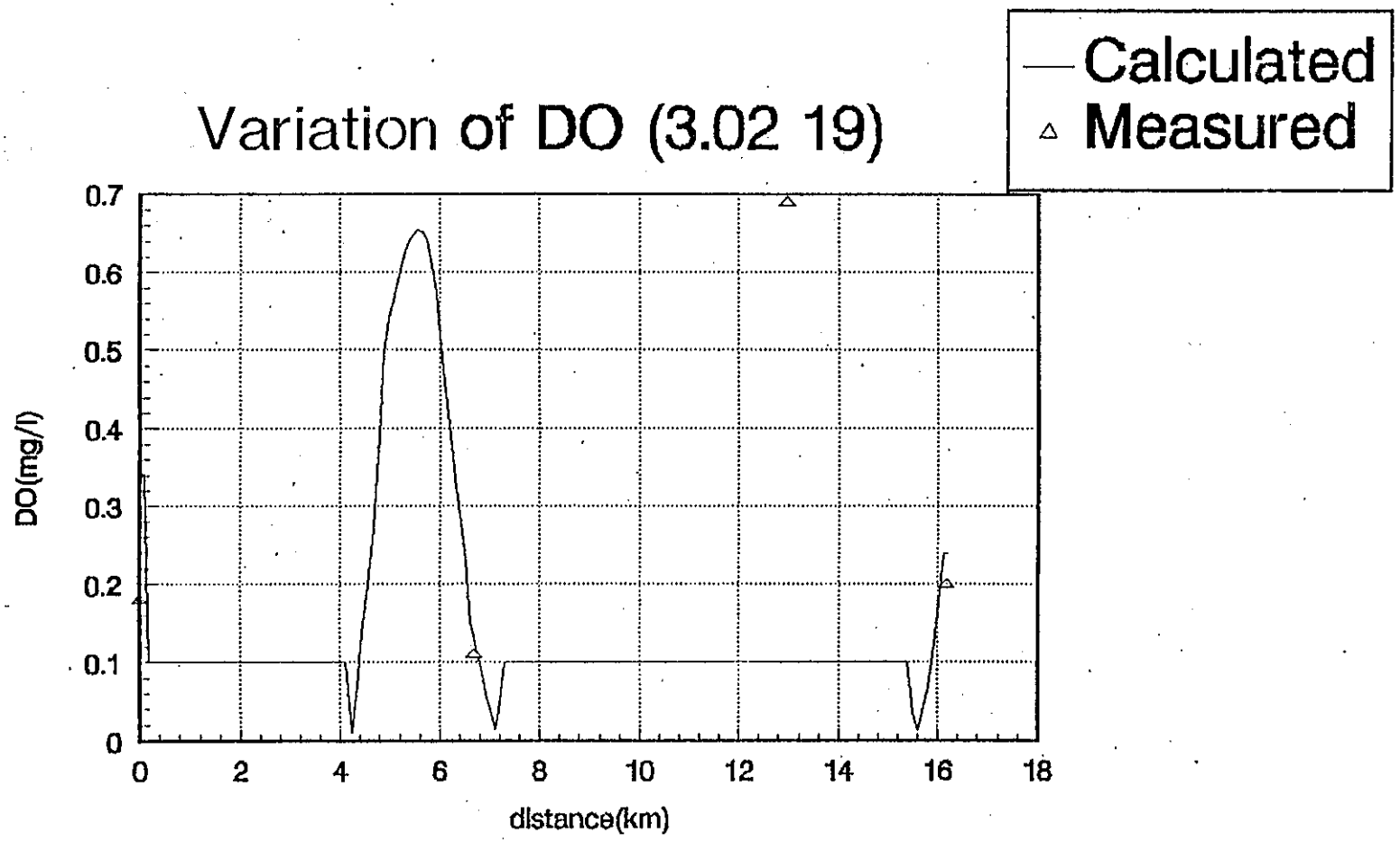

FIG. A7—52(c) **DO variation in dry season** (3.02 19)

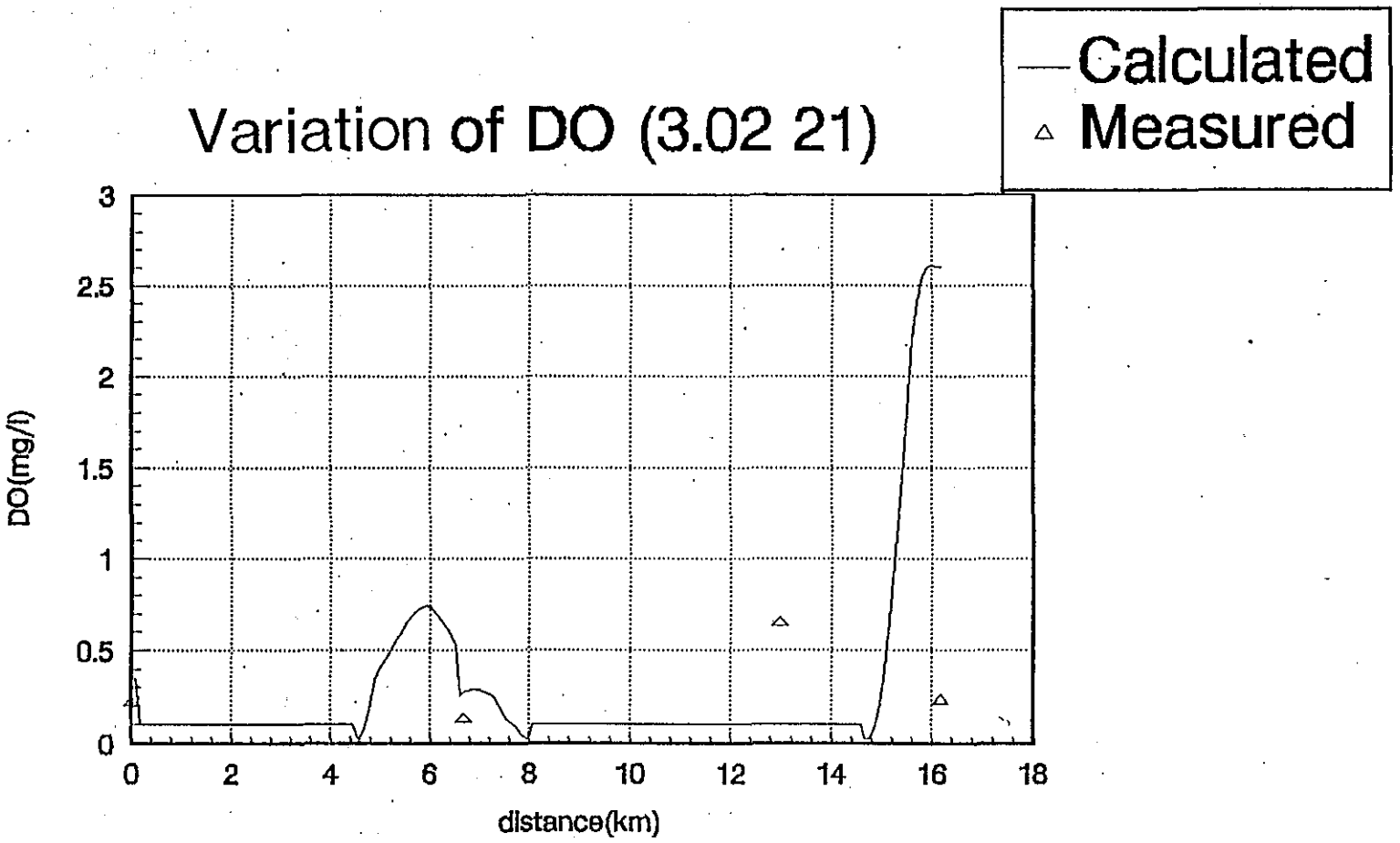

FIG. A7－52(d)　DO variation in dry season (3.02 21)

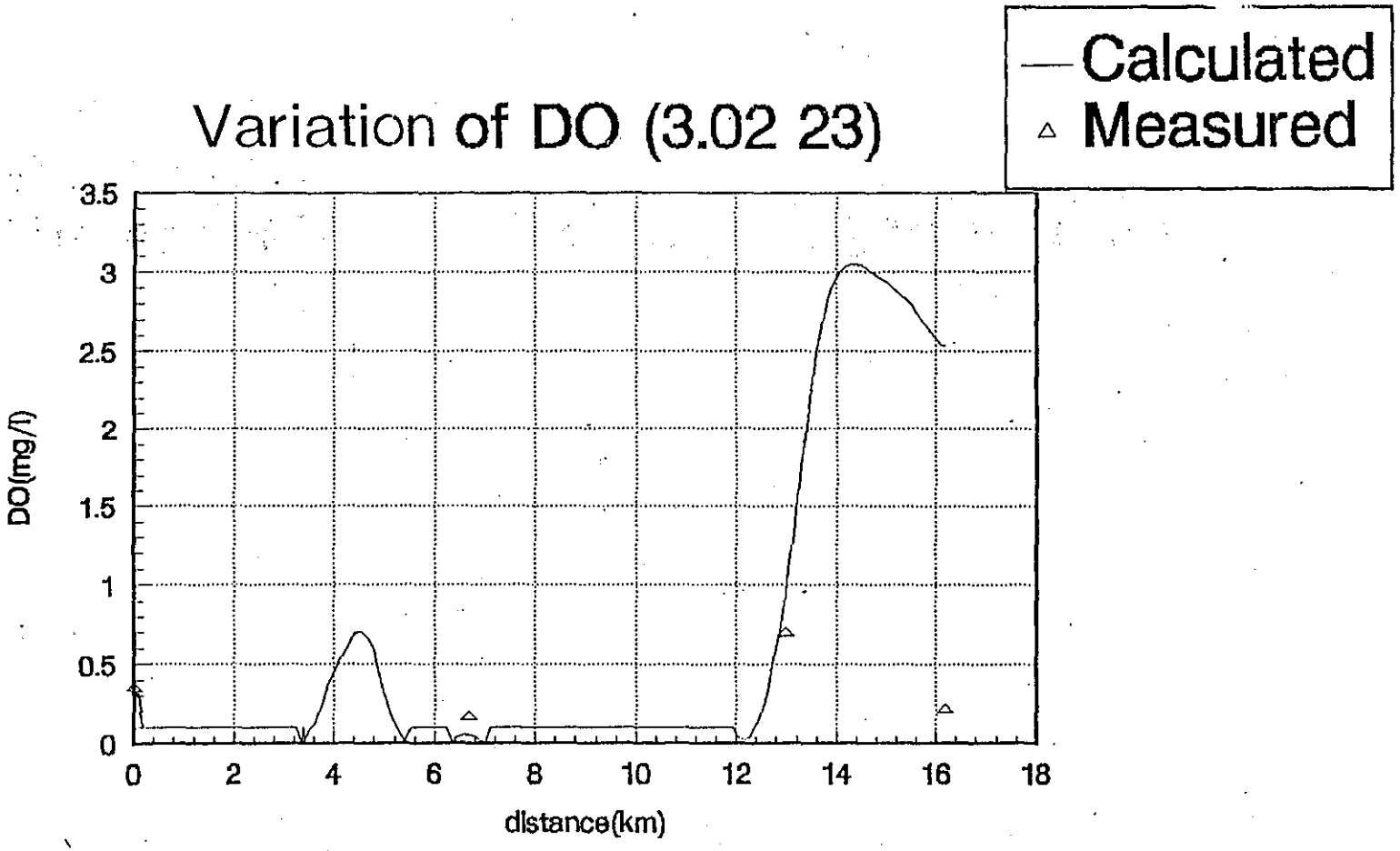

FIG. A7—52(e) DO variation in dry season (3. 02 23)

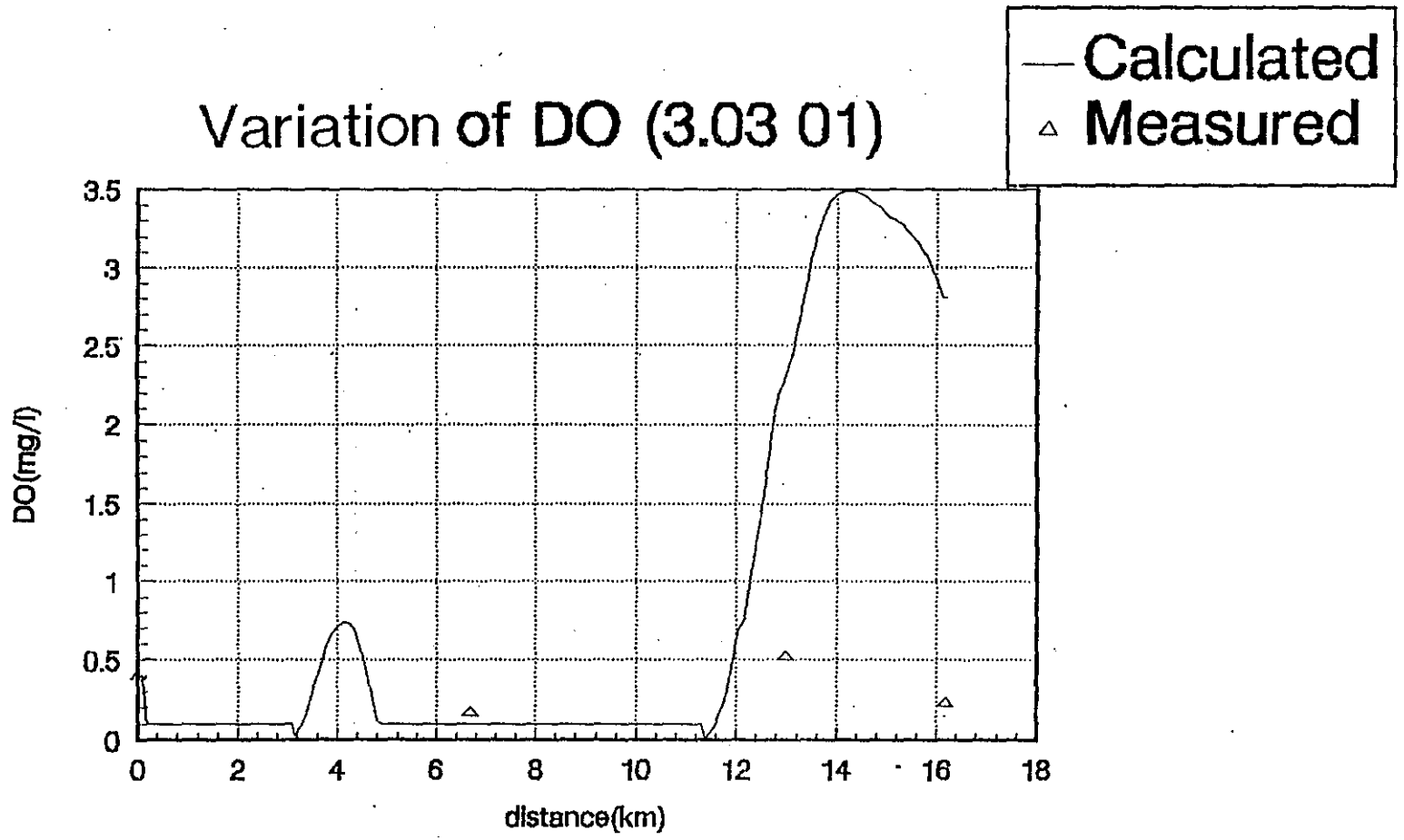

FIG. A7−52(f) **DO variation in dry season** (3. 03 01)

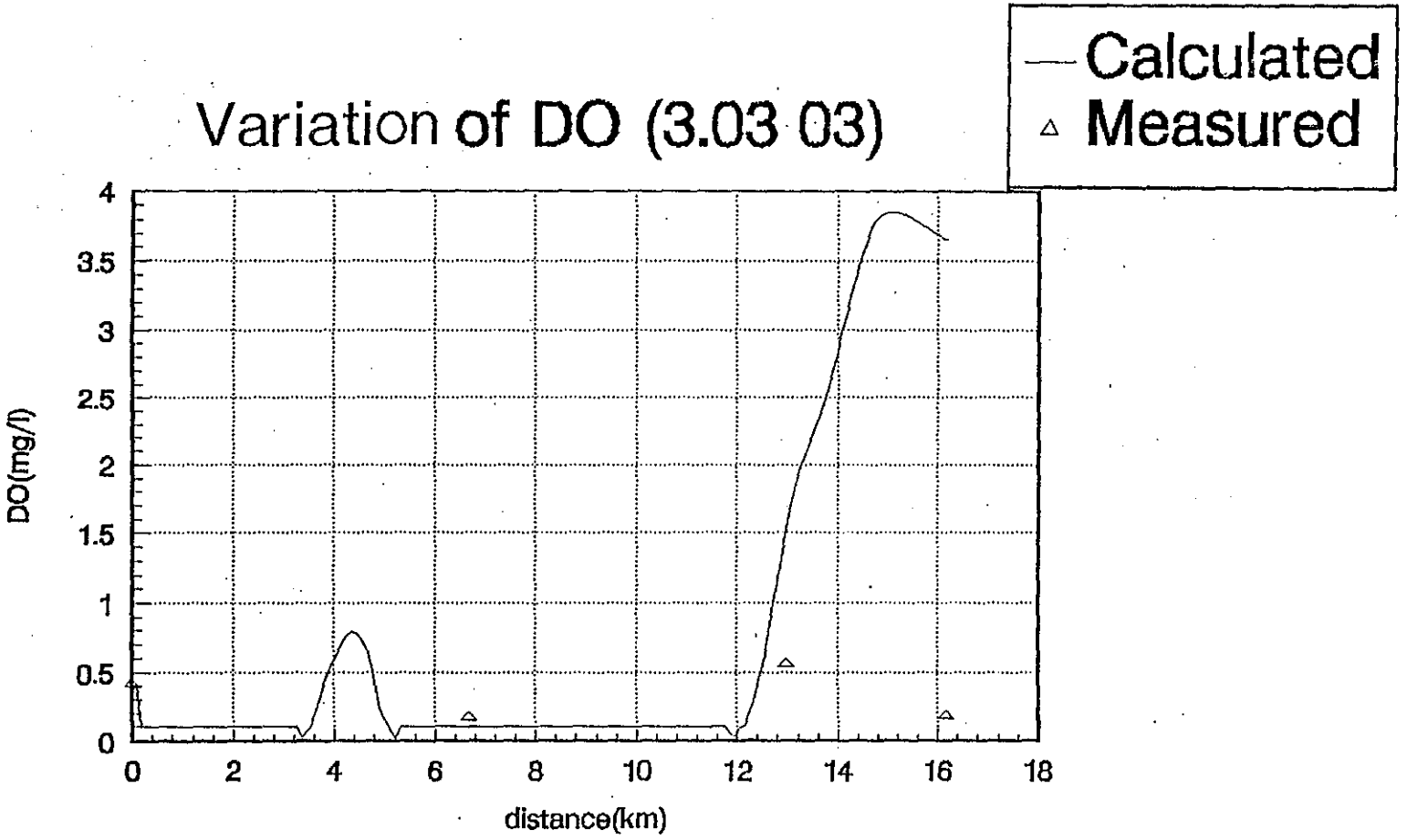

FIG. A7—52(g) **DO variation in dry season** (3. 03 03)

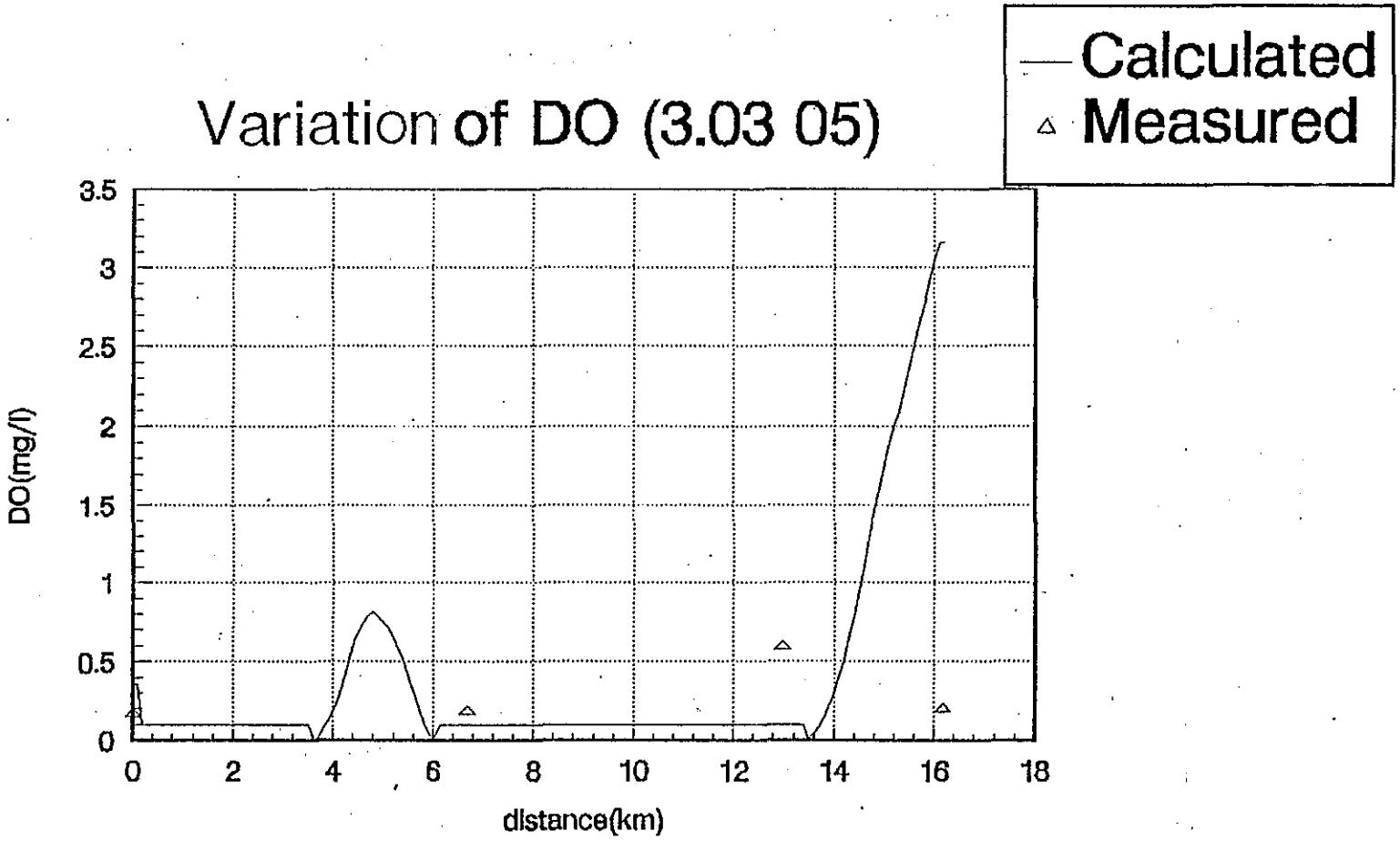

FIG. A7—52(h) **DO variation in dry season** (3. 03 05)

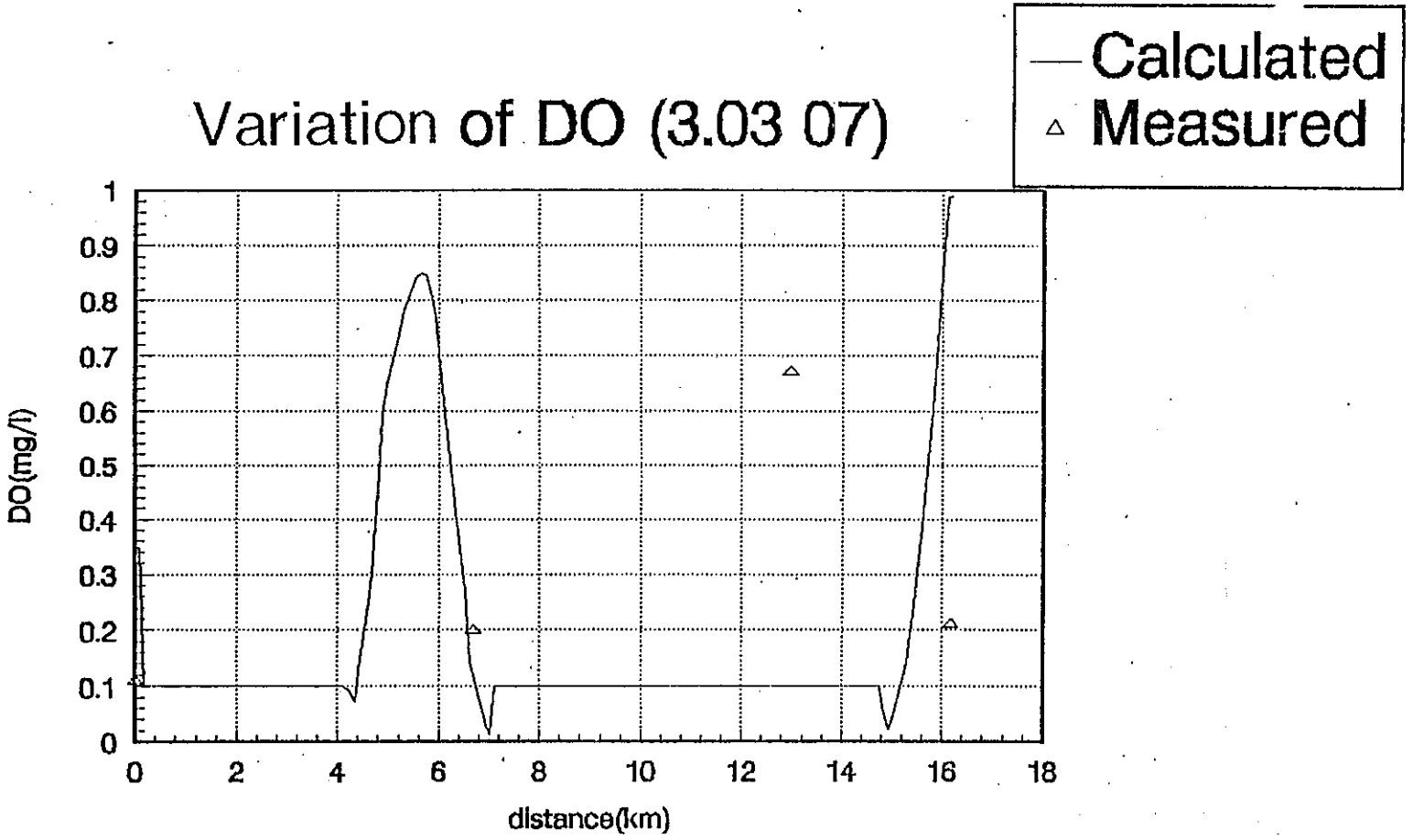

FIG. A7—52(i) **DO variation in dry season** (3. 03 07)

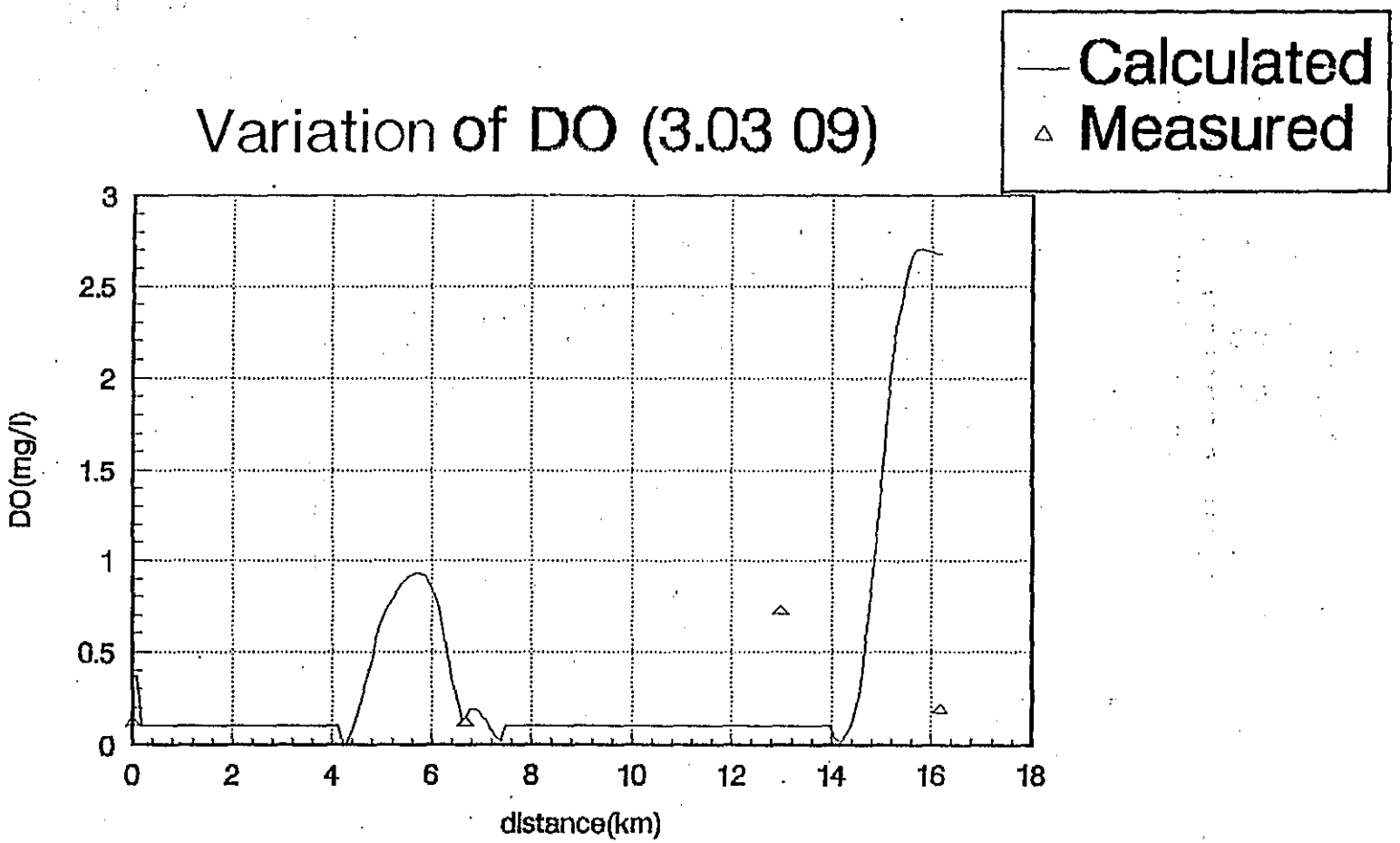

FIG. A7—52(j) DO variation in dry season (3. 03 09)

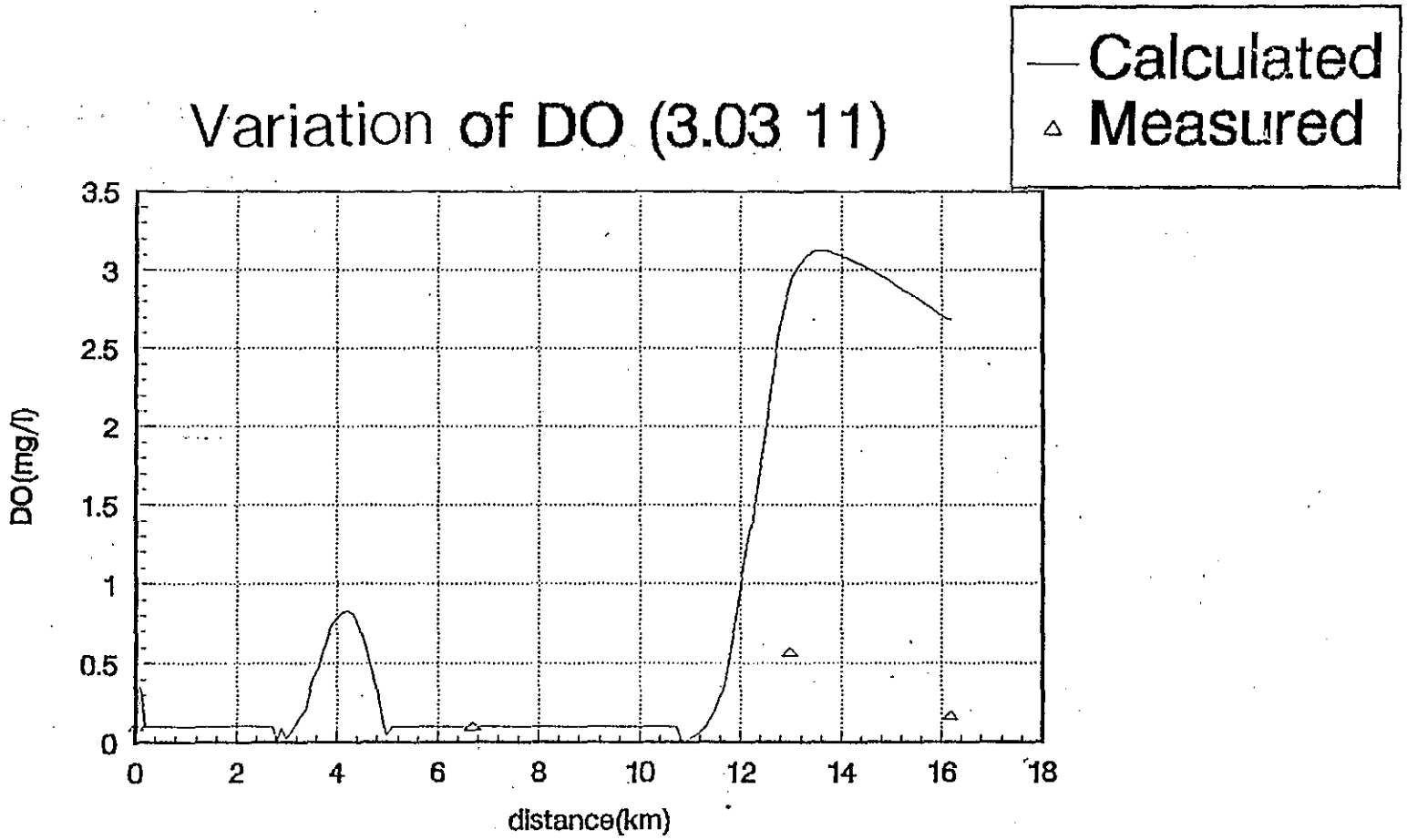

FIG. A7—52(k) **DO variation in dry season** (3.03 11)

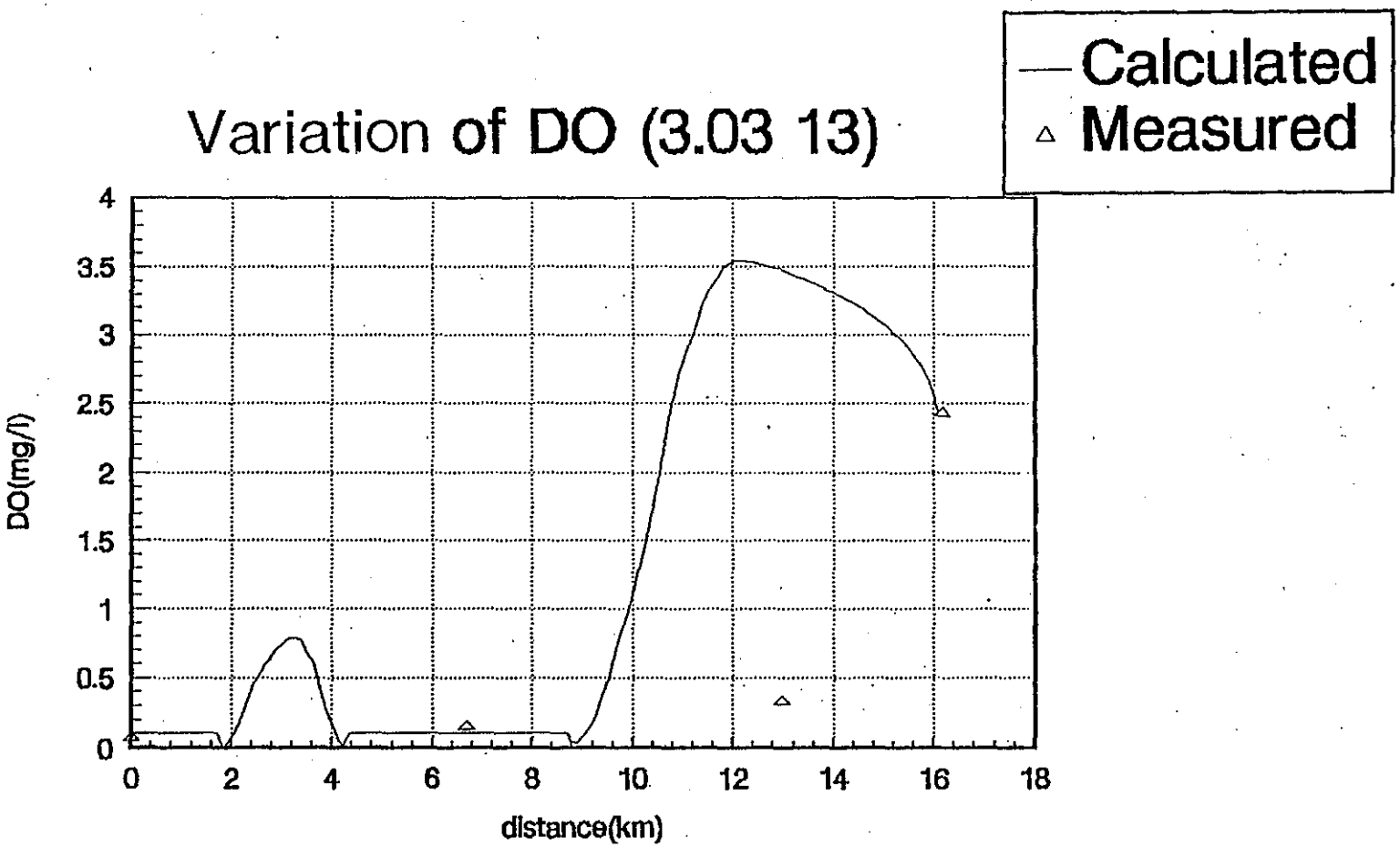

FIG. A7—52(1) **DO variation in dry season** (3. 03 13)

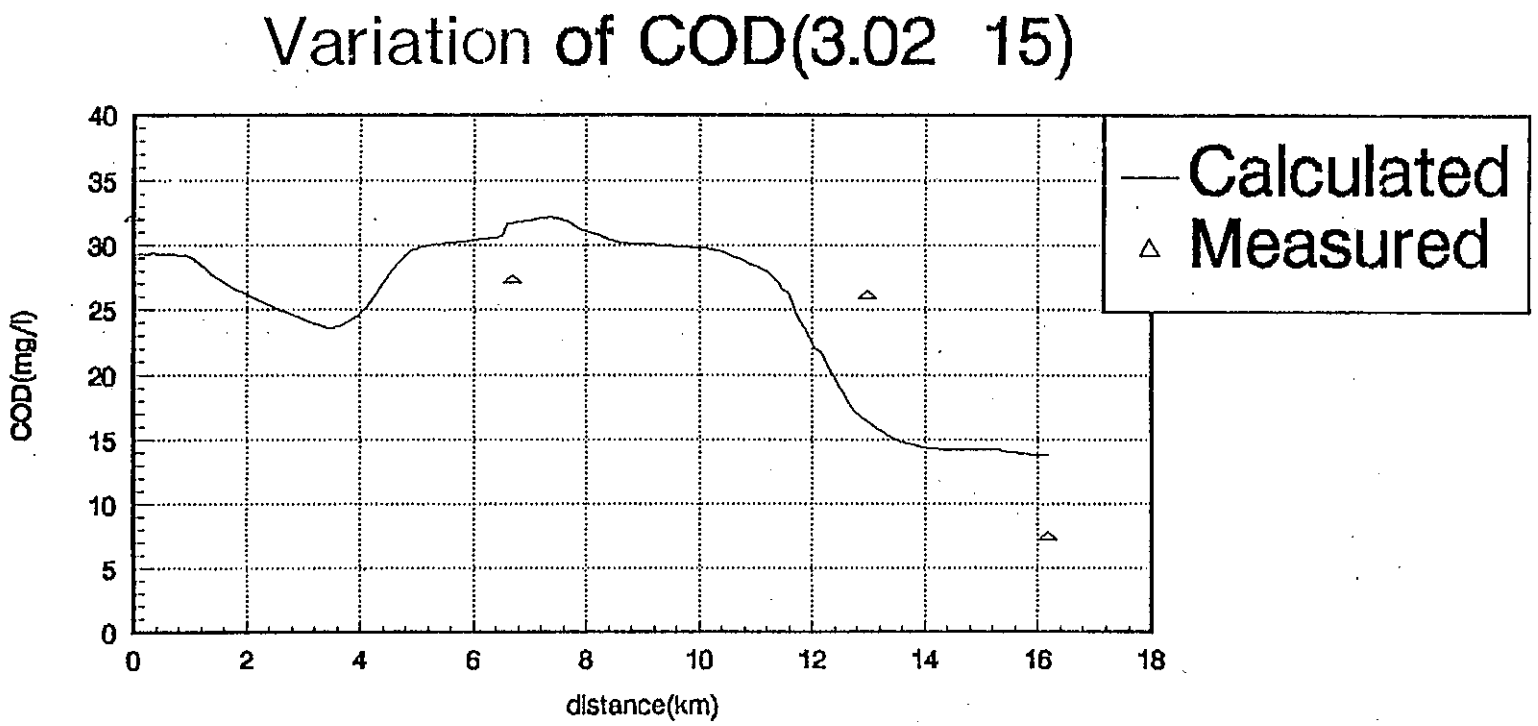

FIG. A7—53(a) COD variation in dry season (3.02 15)

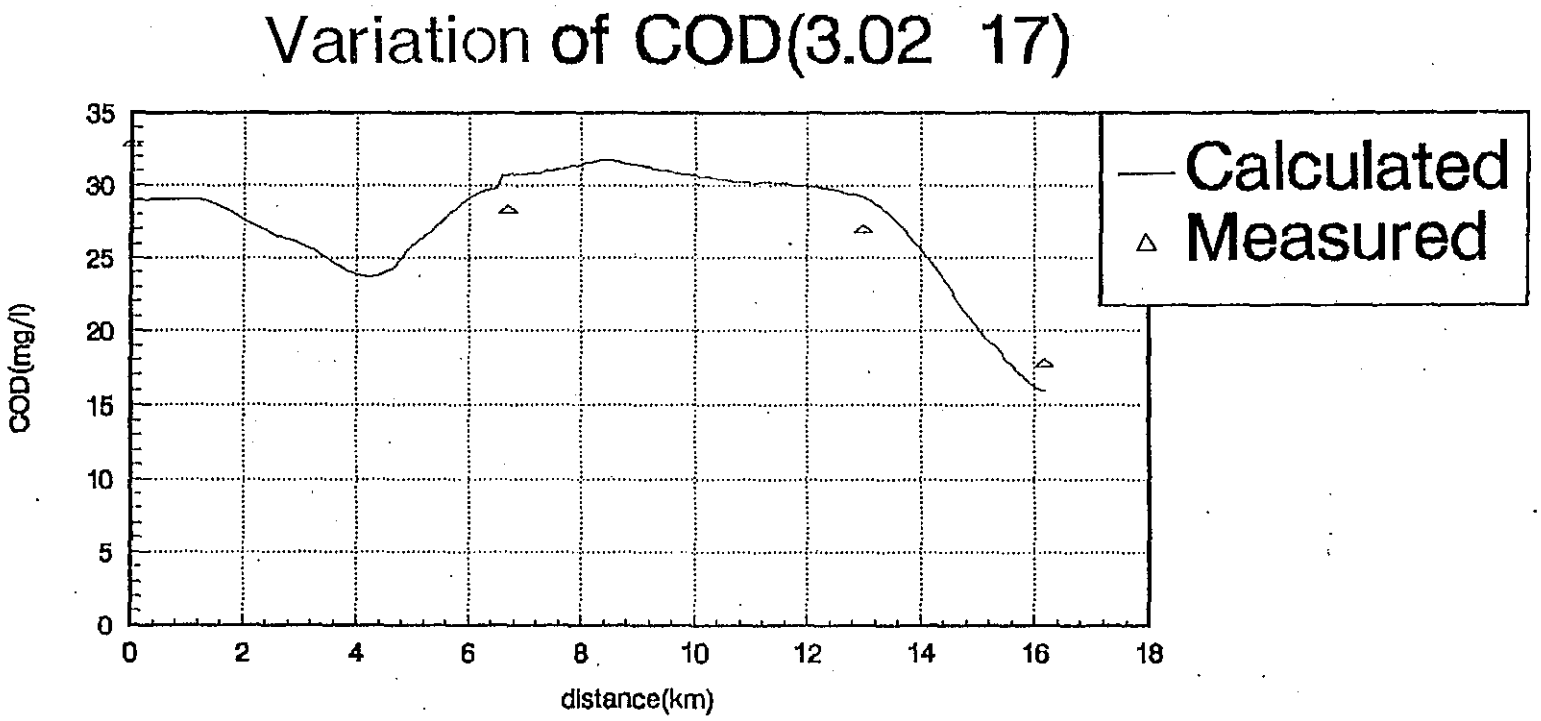

FIG. A7－53(b) COD variation in dry season (3. 02 17)

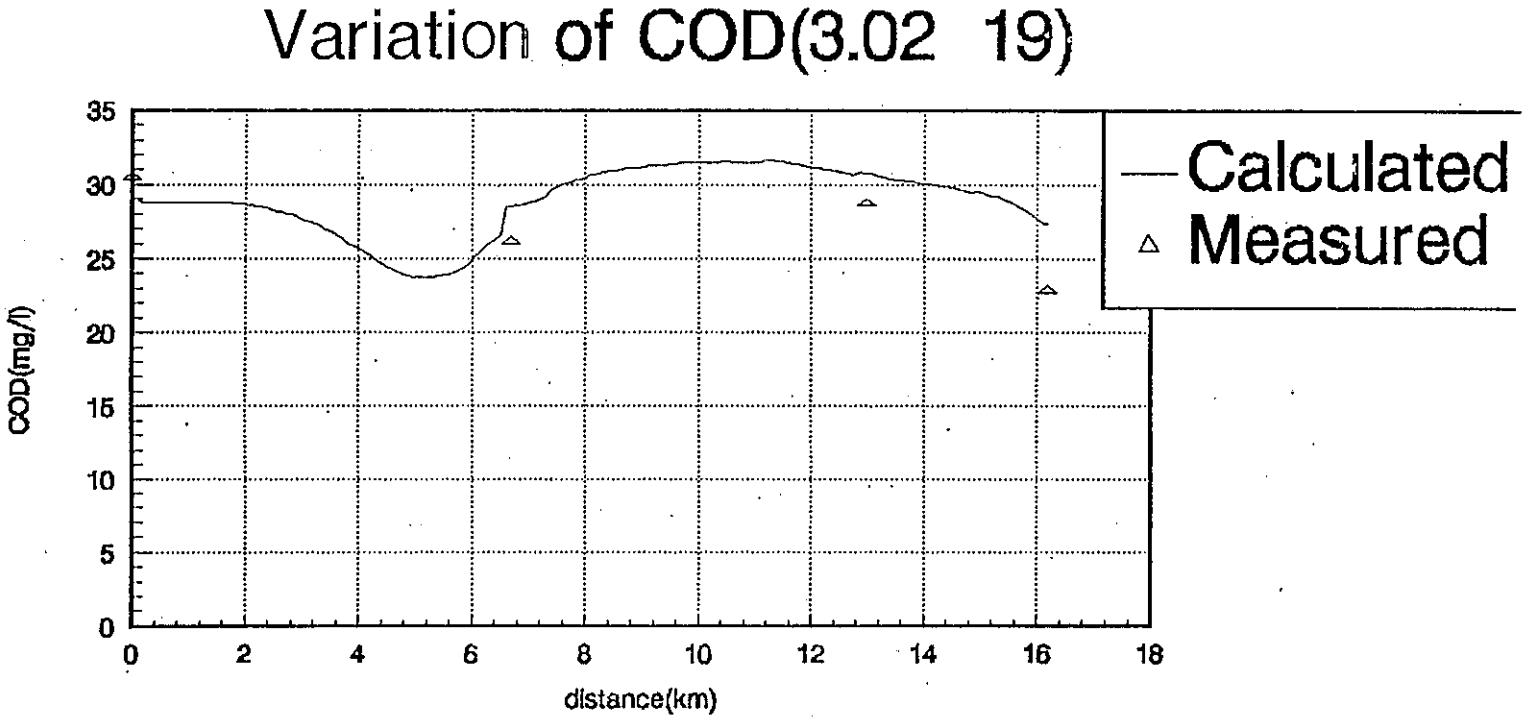

FIG. A7—53(c) COD variation in dry season (3. 02 19)

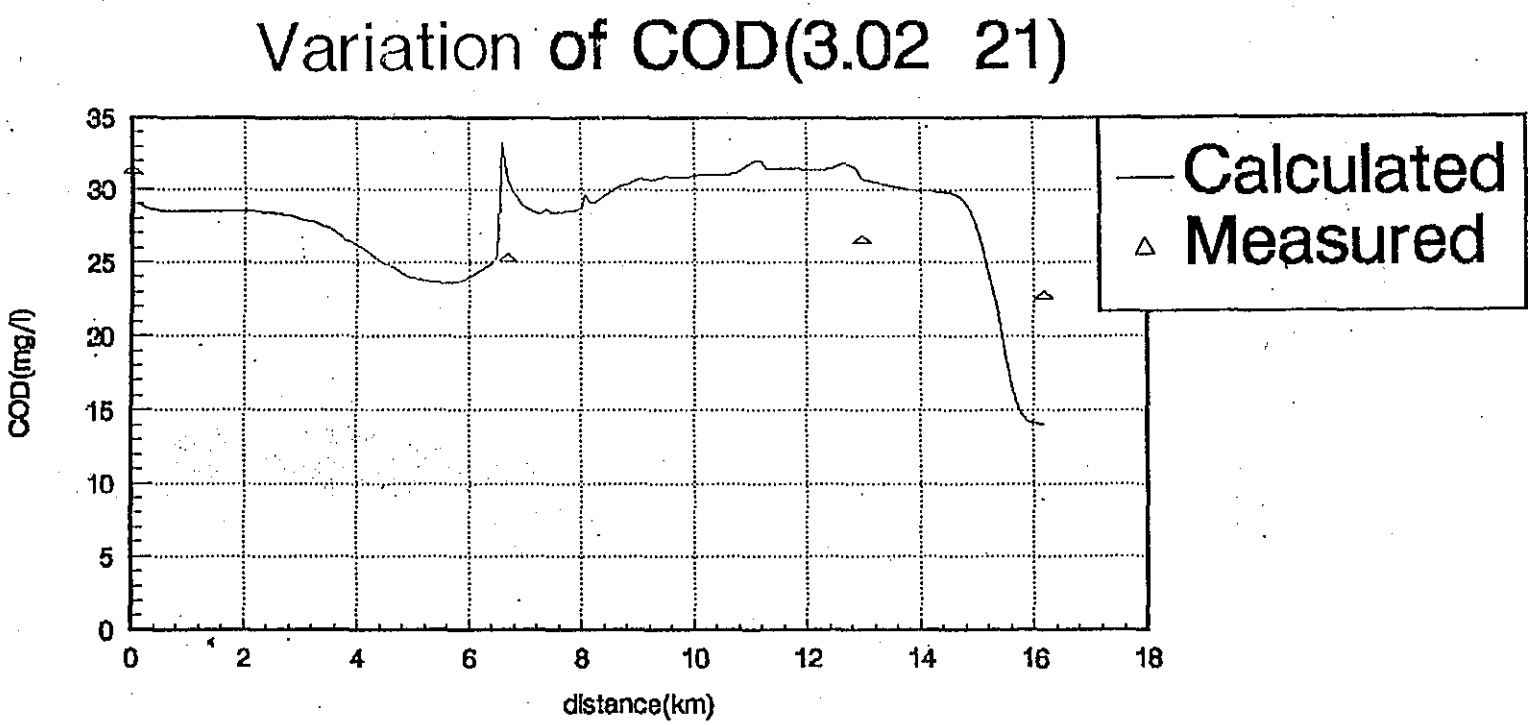

FIG. A7—53(d) COD variation in dry season (3. 02 21)

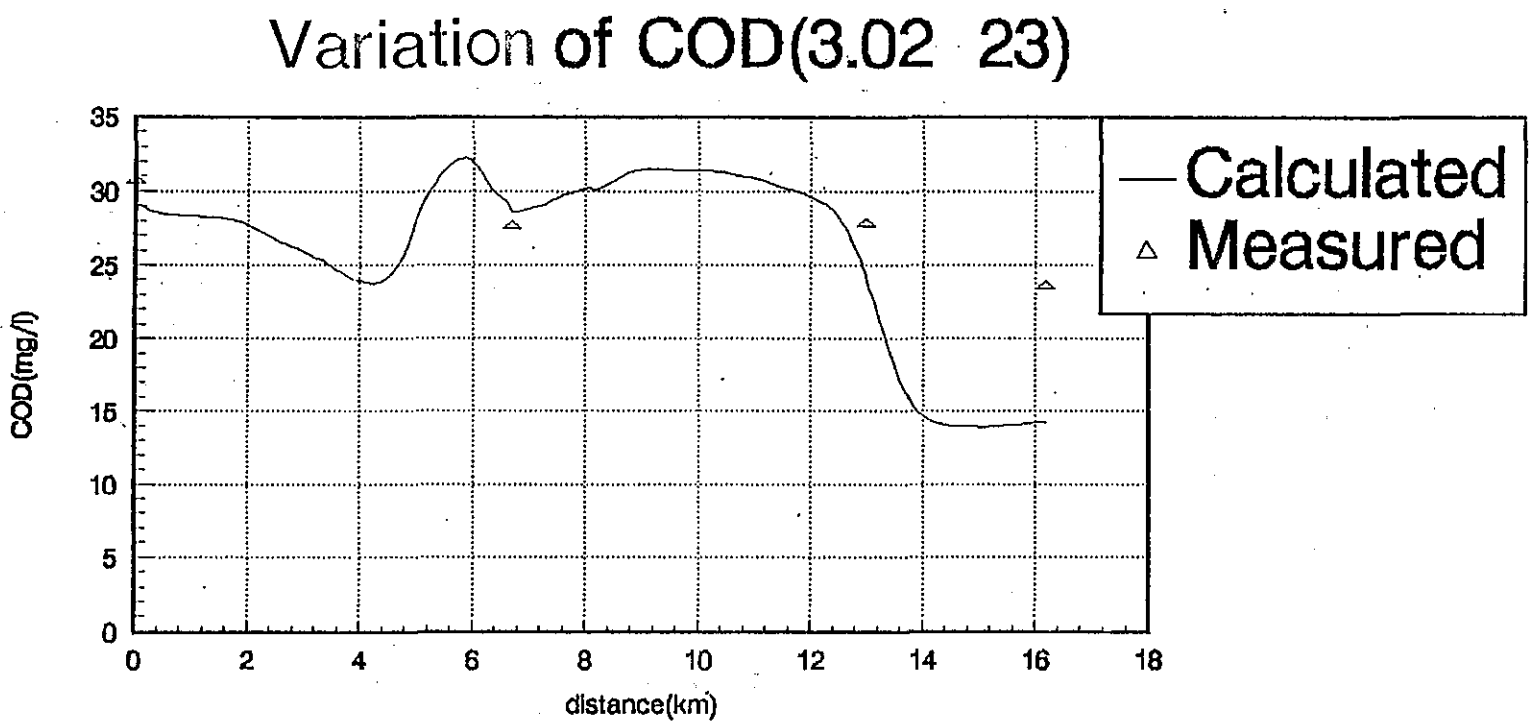

FIG. A7－53(e) **COD variation in dry season** (3. 02 23)

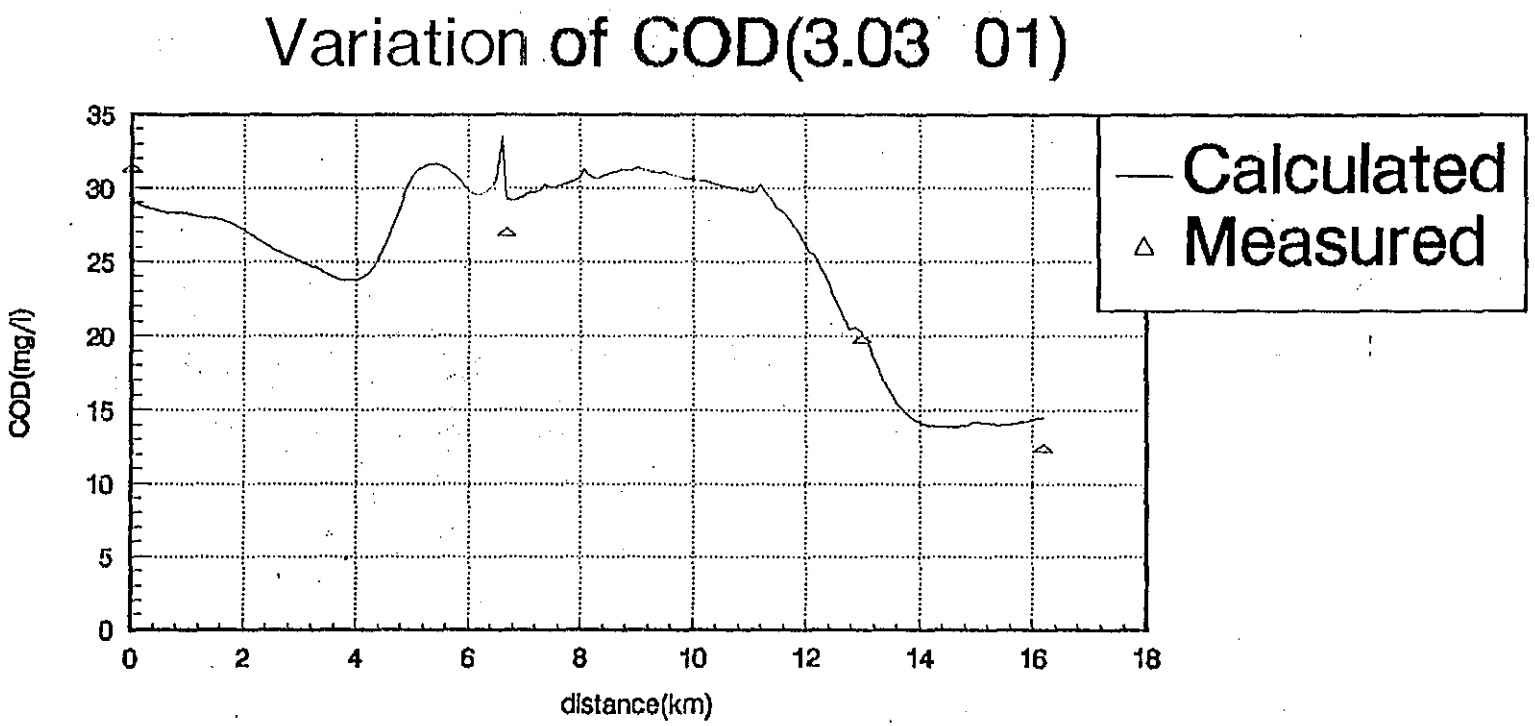

FIG. A7—53(f) COD variation in dry season (3.03 01)

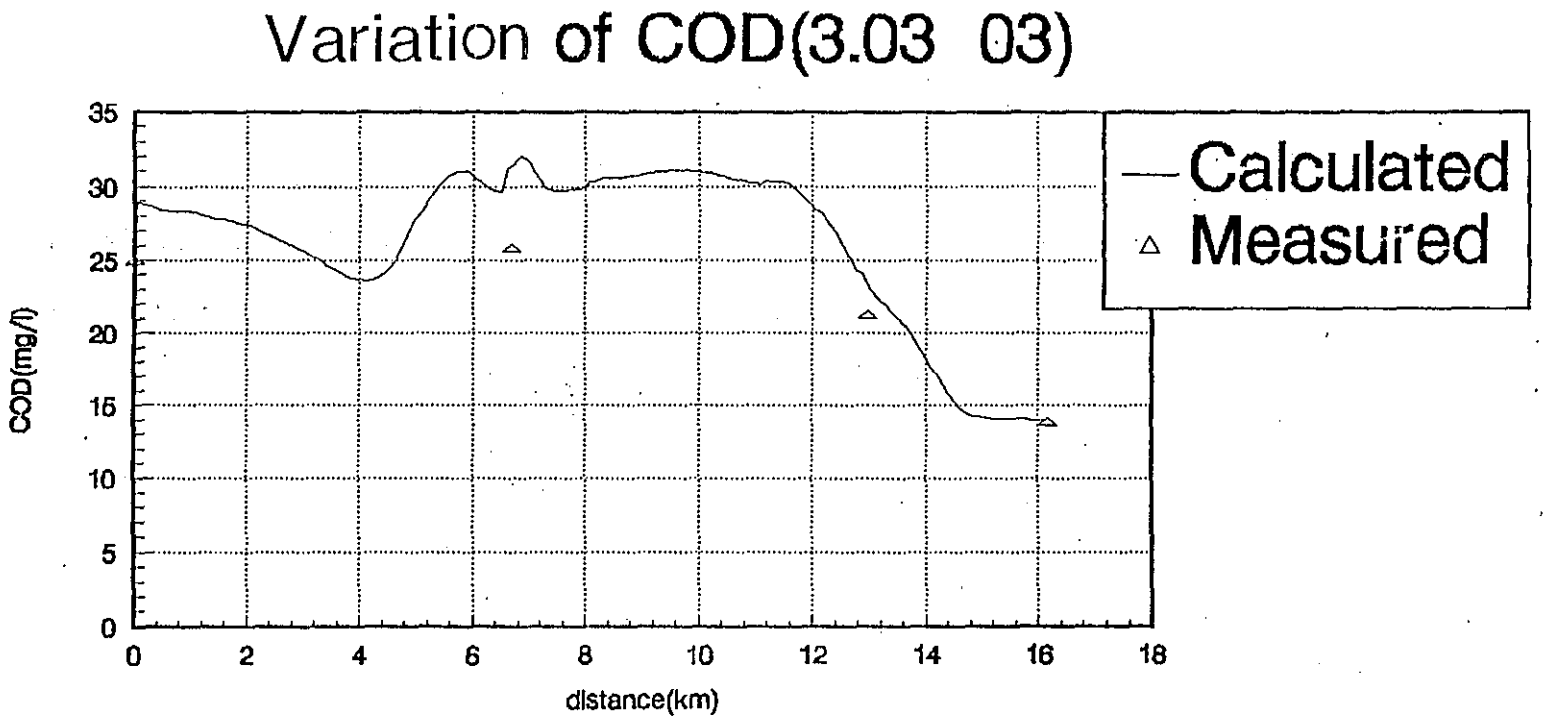

FIG. A7－53(g) COD variation in dry season (3. 03 03)

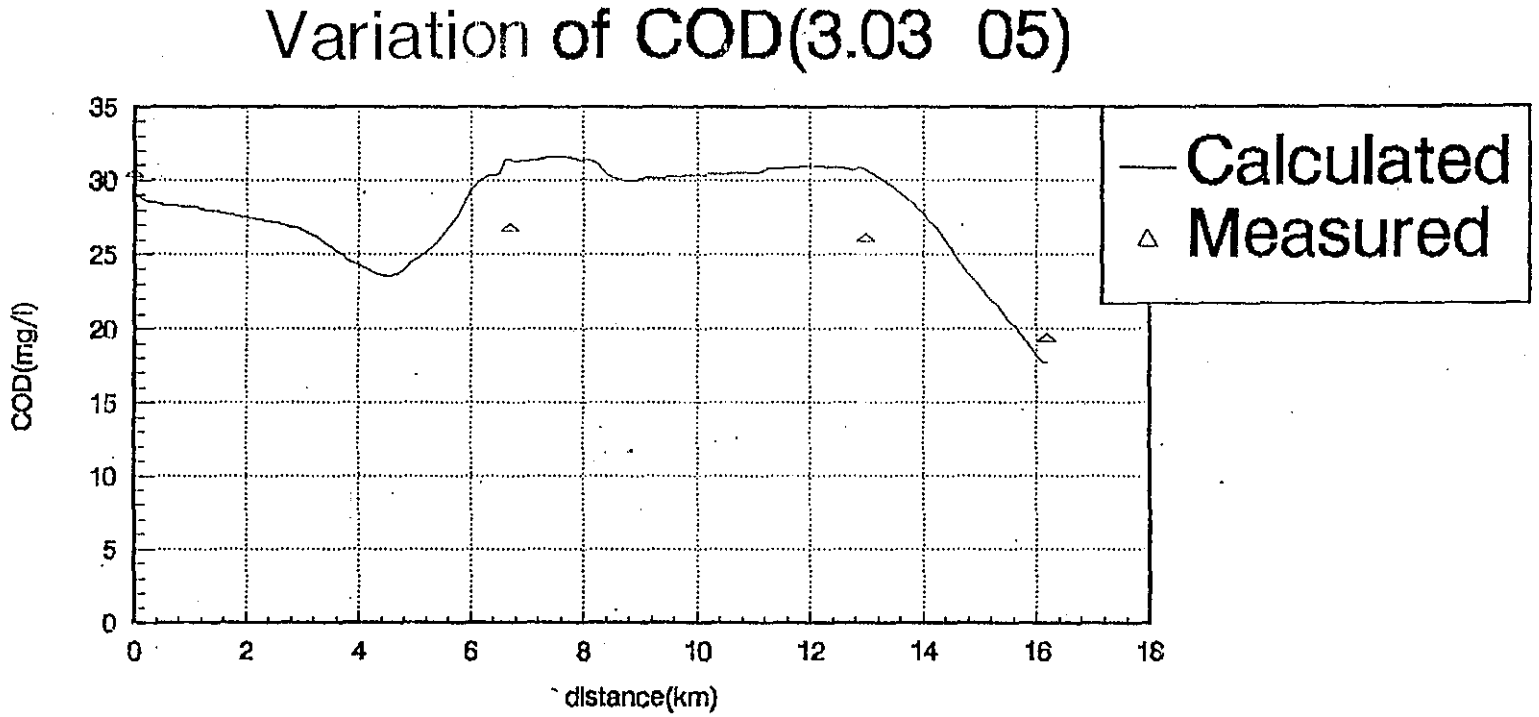

FIG. A7—53(h) **COD variation in dry season** (3. 03 05)

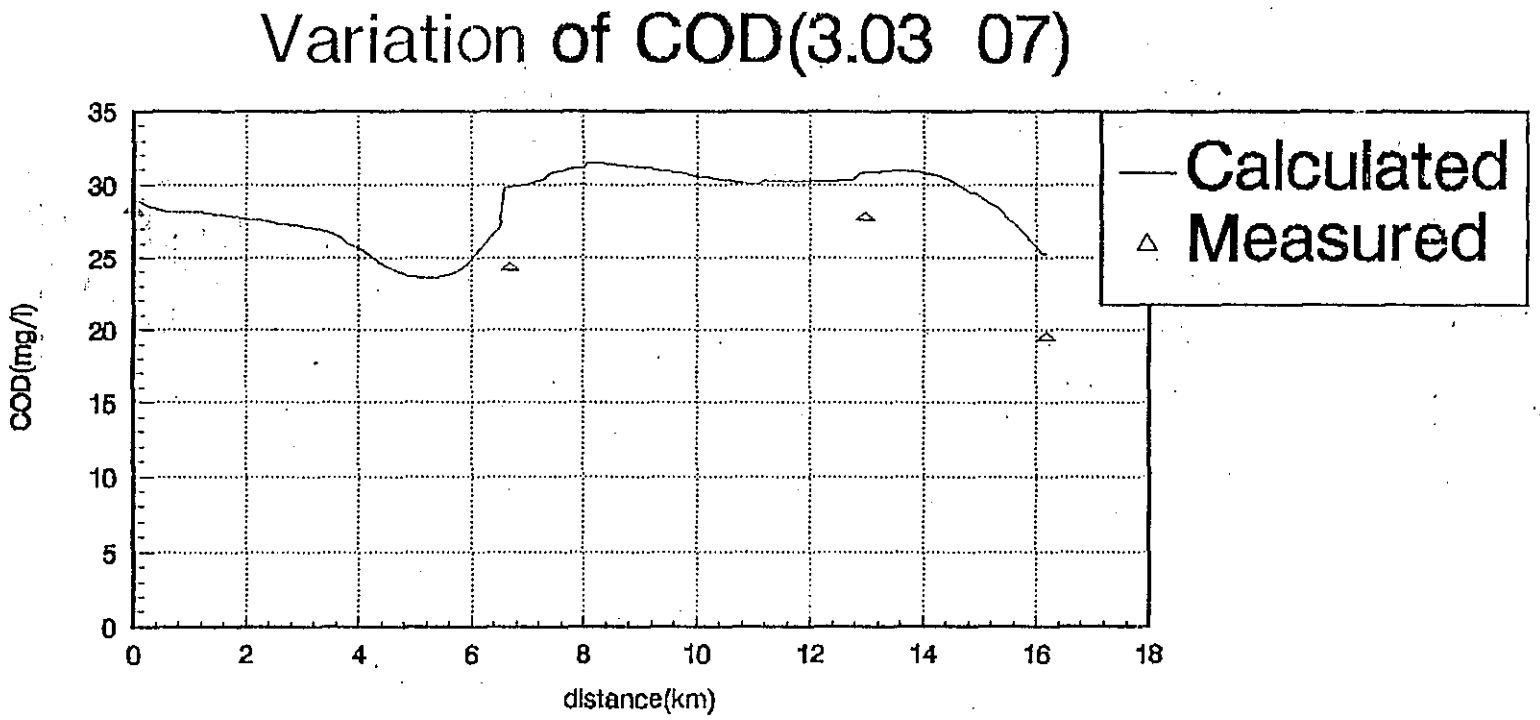

FIG. A7—53(i) COD variation in dry season (3. 03 07)

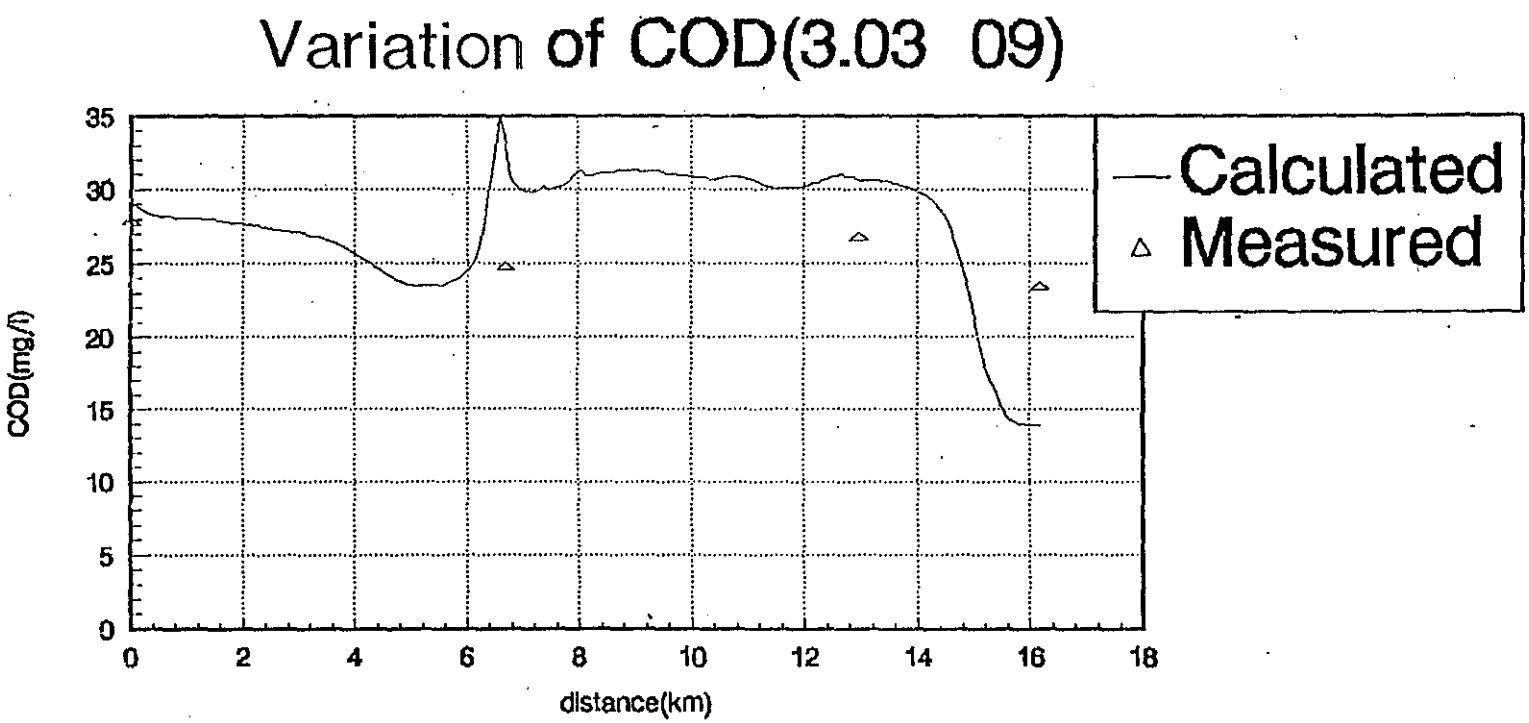

FIG. A7－53(j) COD variation in dry season (3. 03 09)

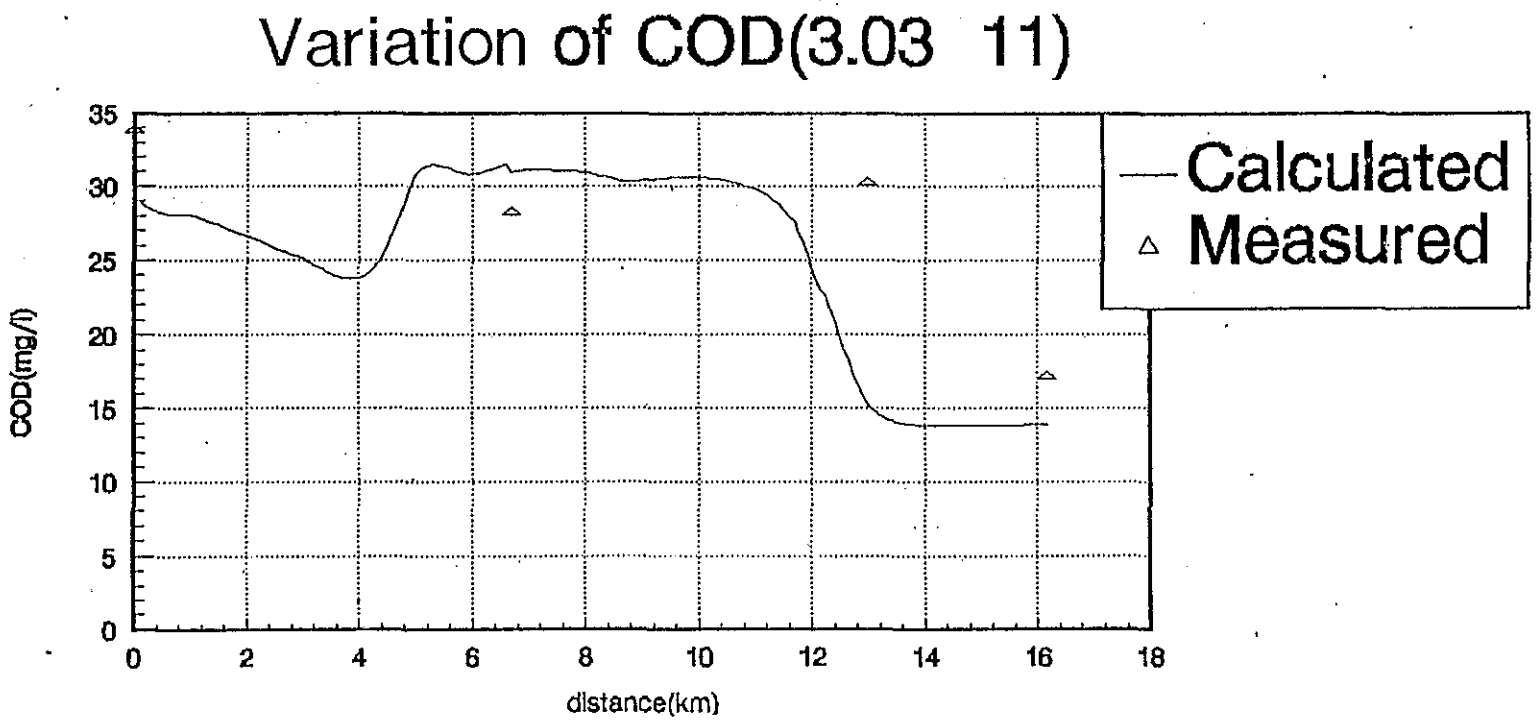

FIG. A7—53(k) COD variation in dry season (3. 03 11)

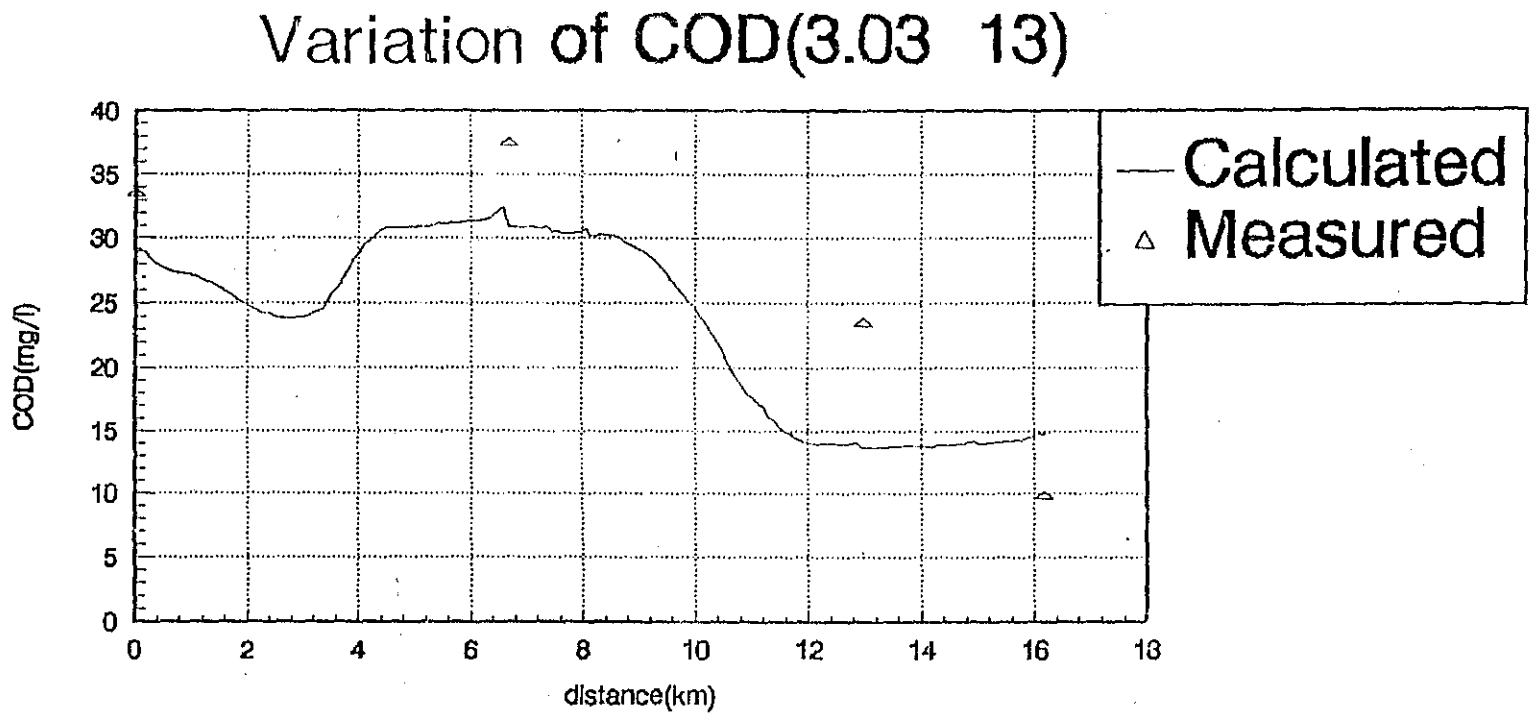

FIG. A7—53(I) COD variation in dry season (3. 03 13)

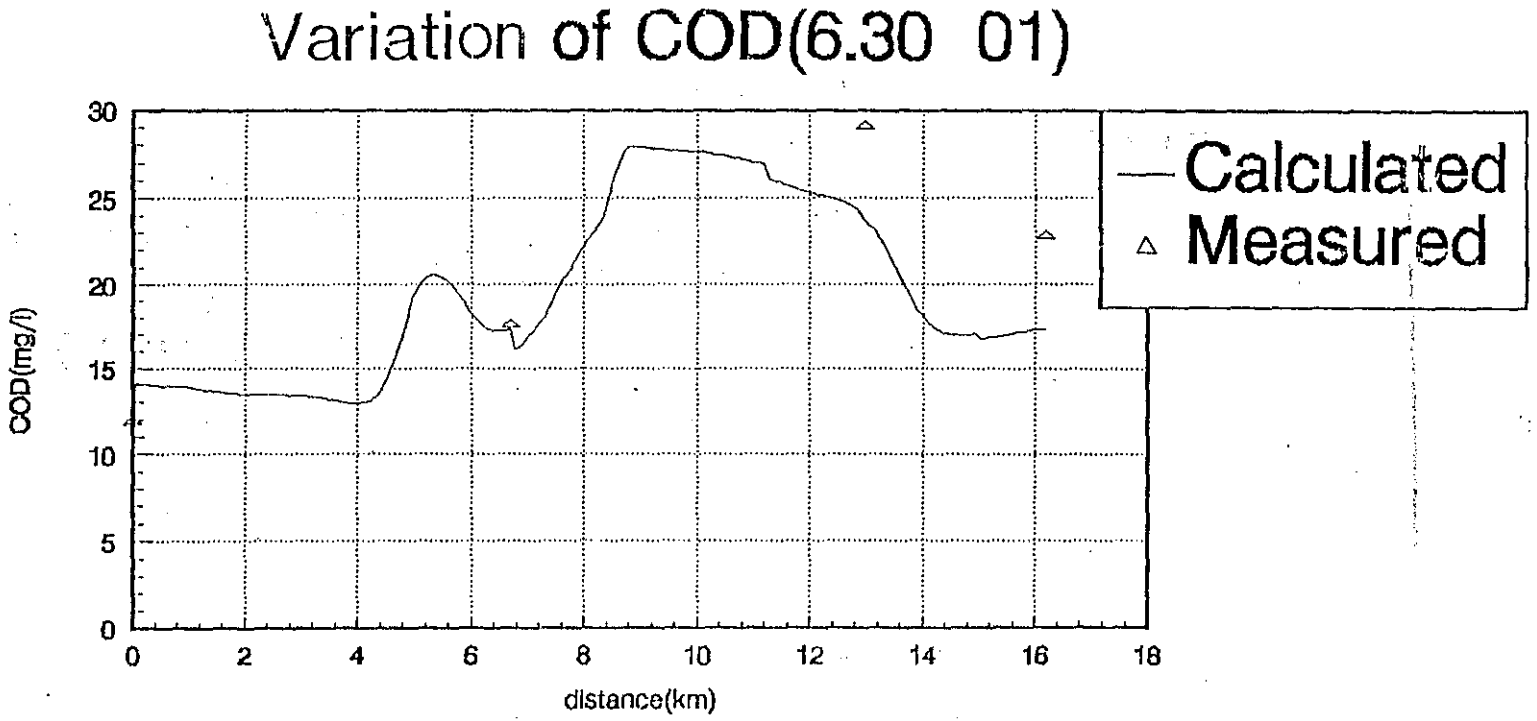

FIG. A7－53(m)　COD variation in wet season (6. 30 01)

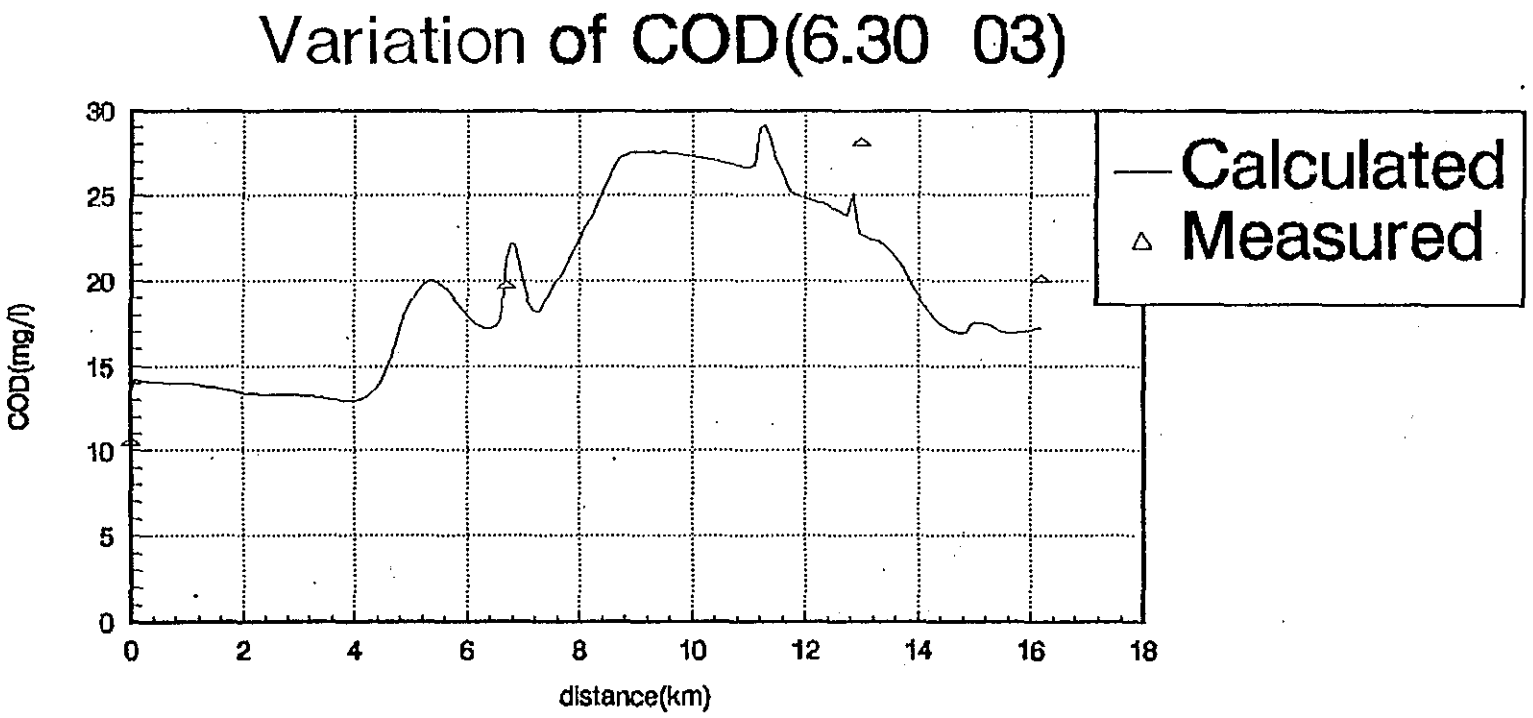

FIG. A7—53(n) COD variation in wet season (6. 30 03)

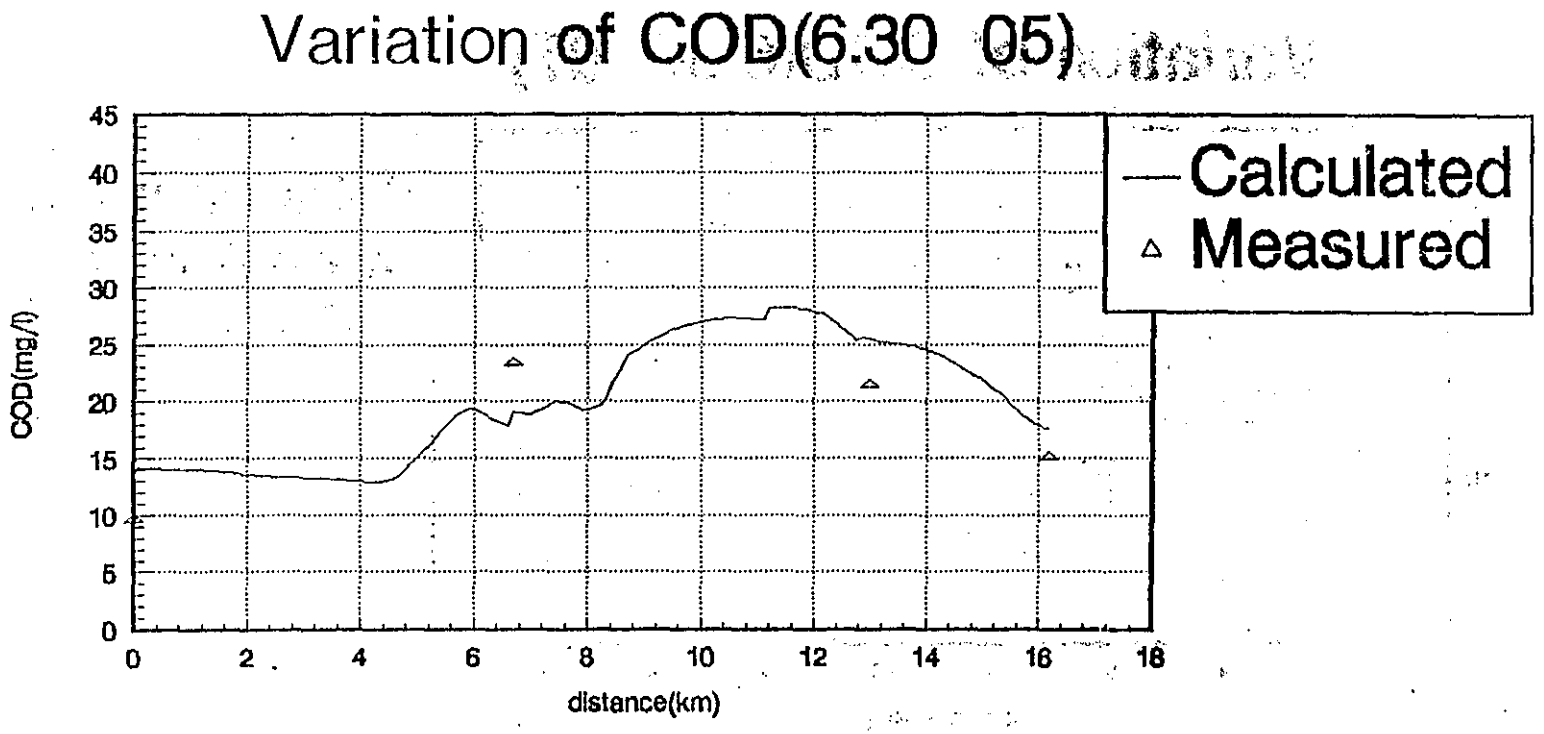

FIG. A7—53(o) **COD variation in wet season** (6.30'05)

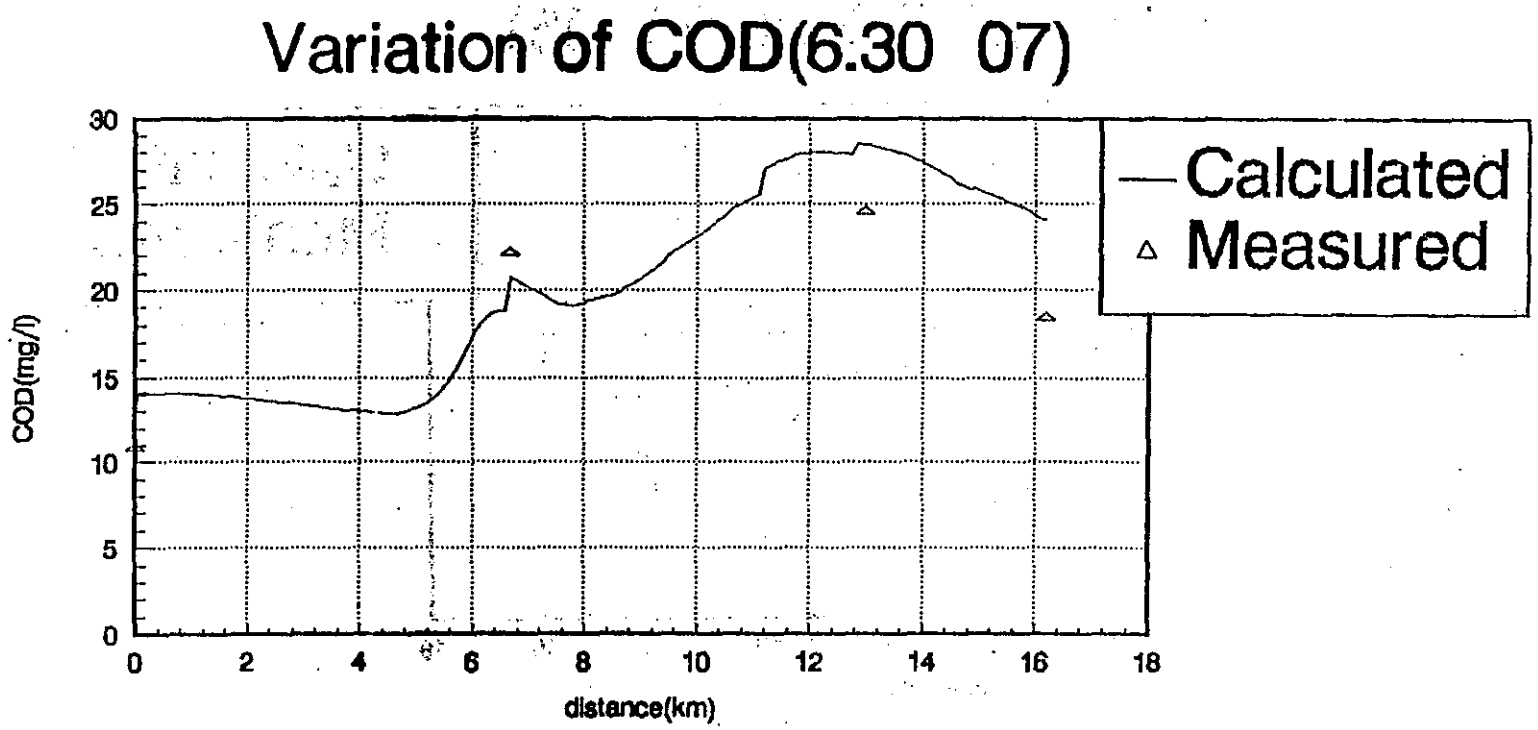

FIG. A7－53(p) **COD variation in wet season** (6. 30 07)

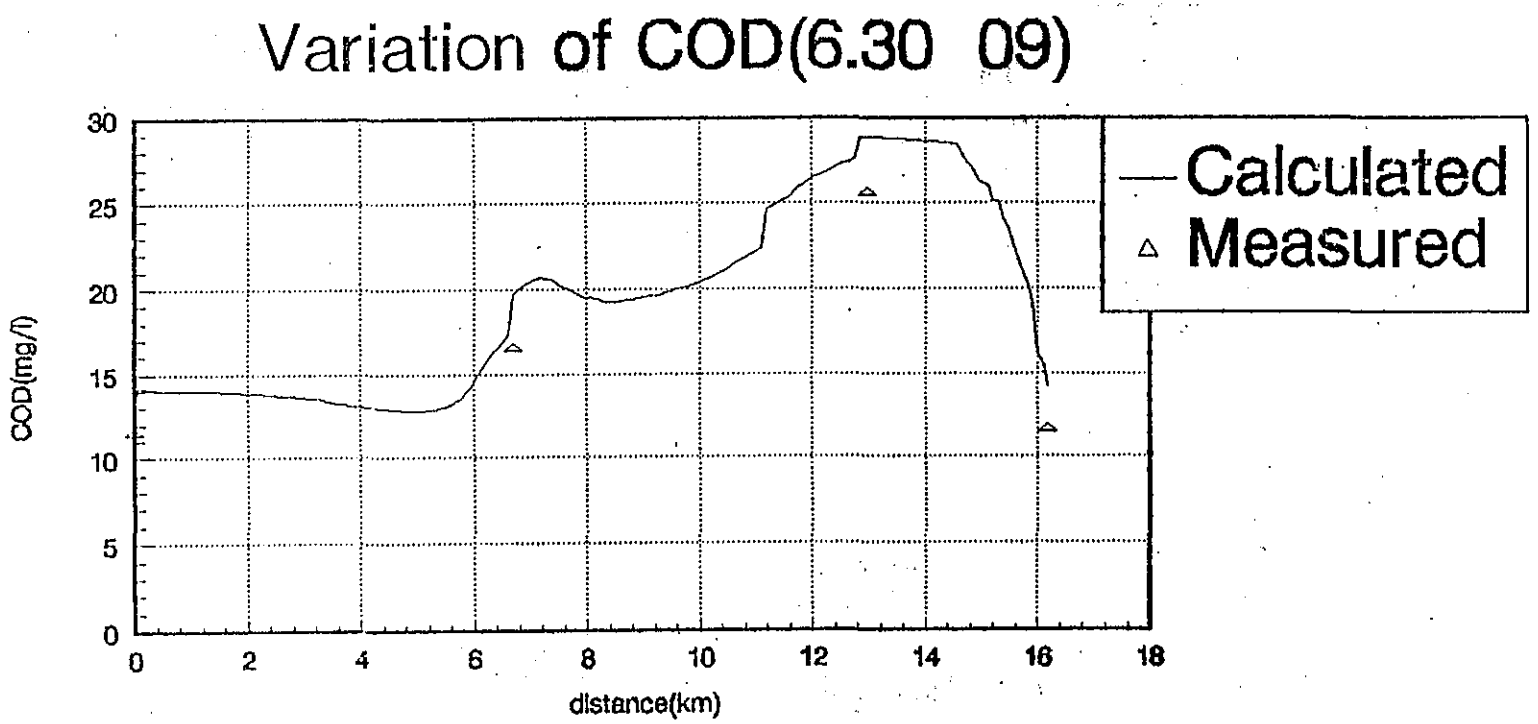

FIG. A7－53(q)　COD variation in wet season (6. 30 09)

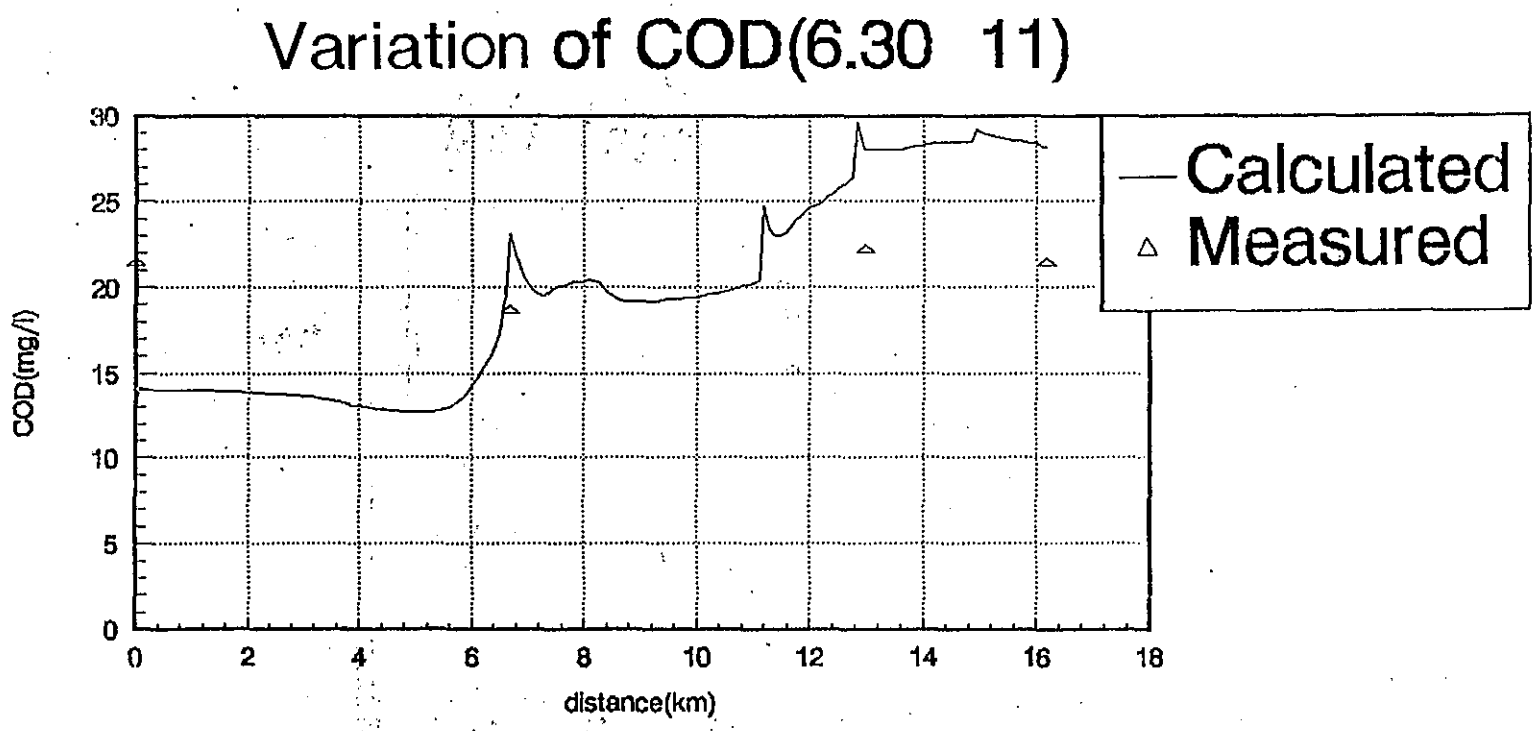

FIG. A7—53(r) COD variation in wet season (6. 30 11)

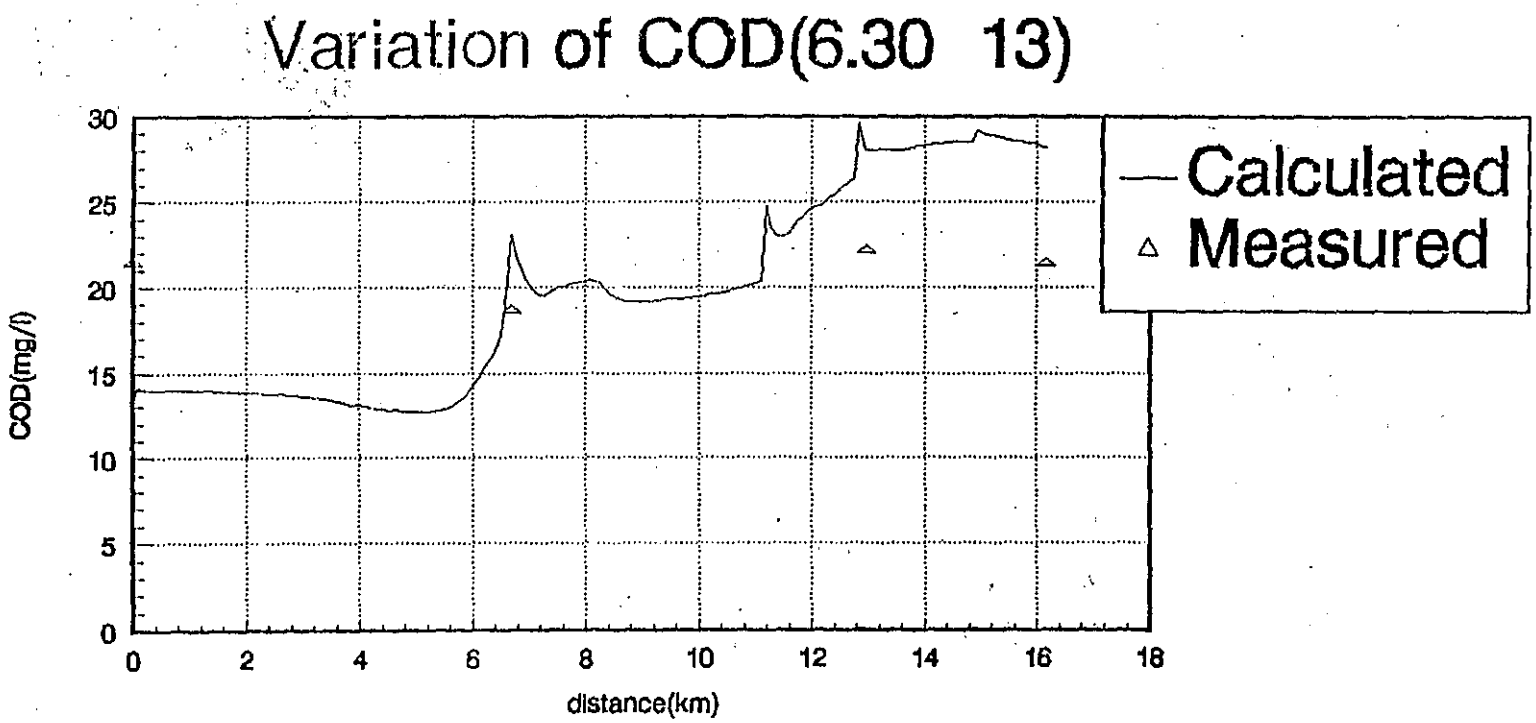

FIG. A7－53(s) COD variation in wet season (6. 30 13)

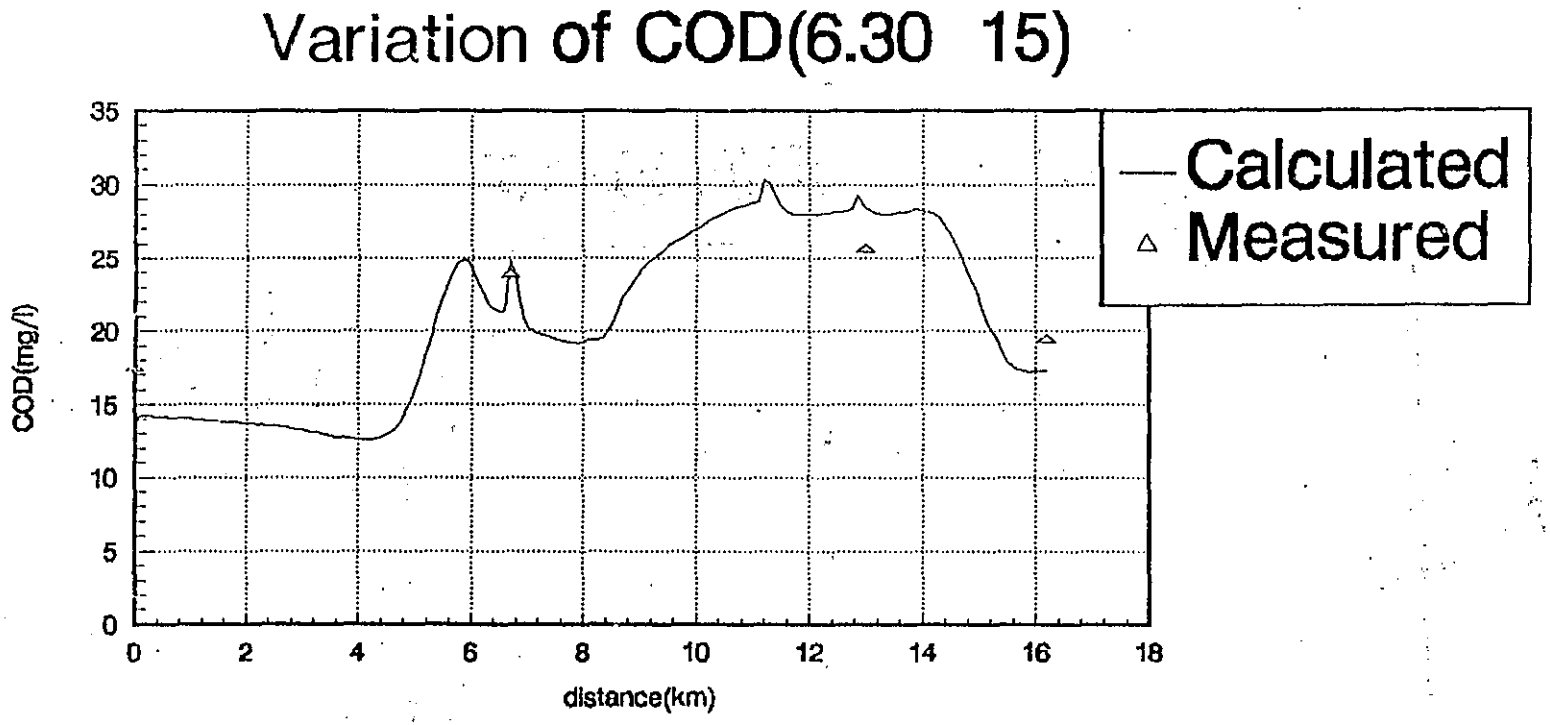

FIG. A7－53(t) COD variation in wet season (6. 30 15)

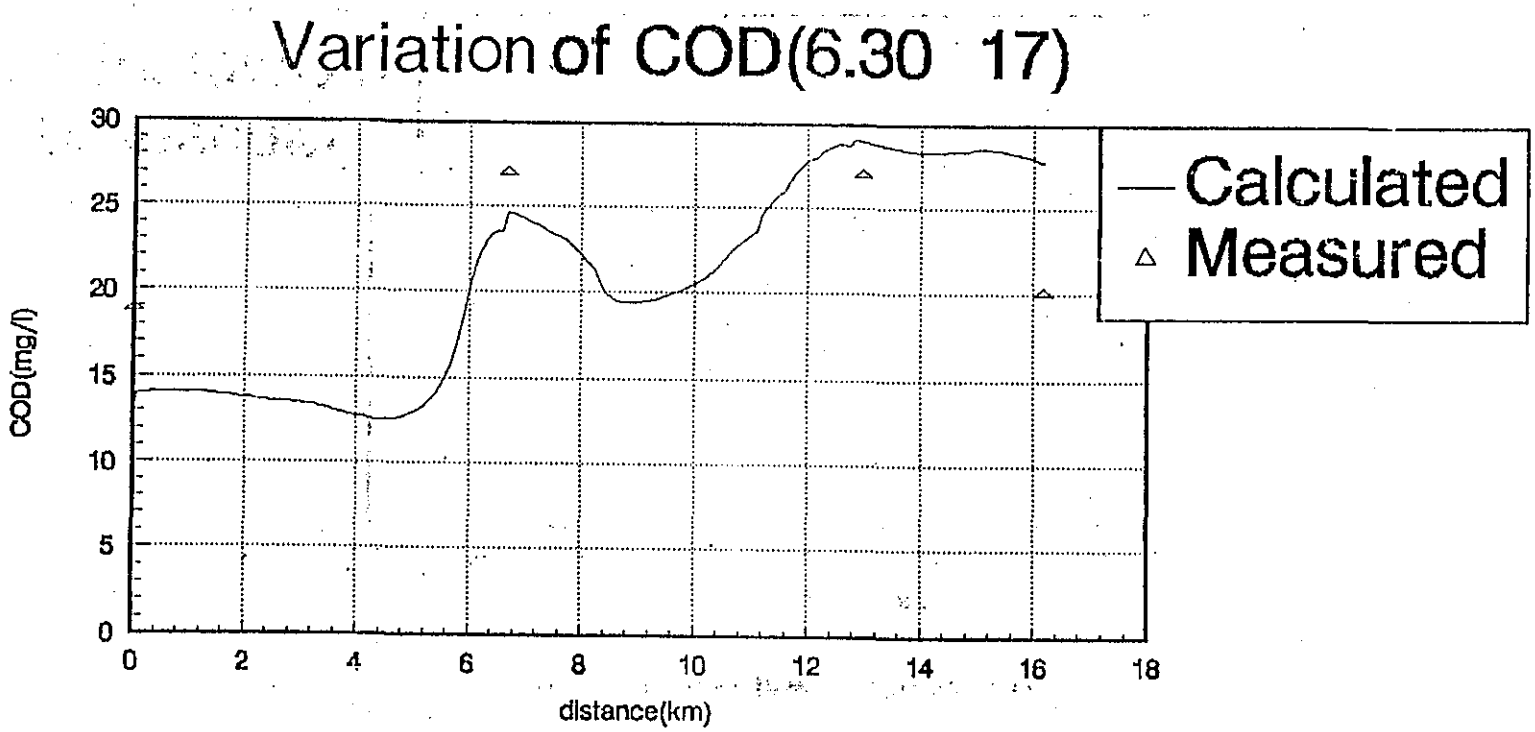

FIG. A7—53(u) **COD variation in wet season** (6. 30 17)

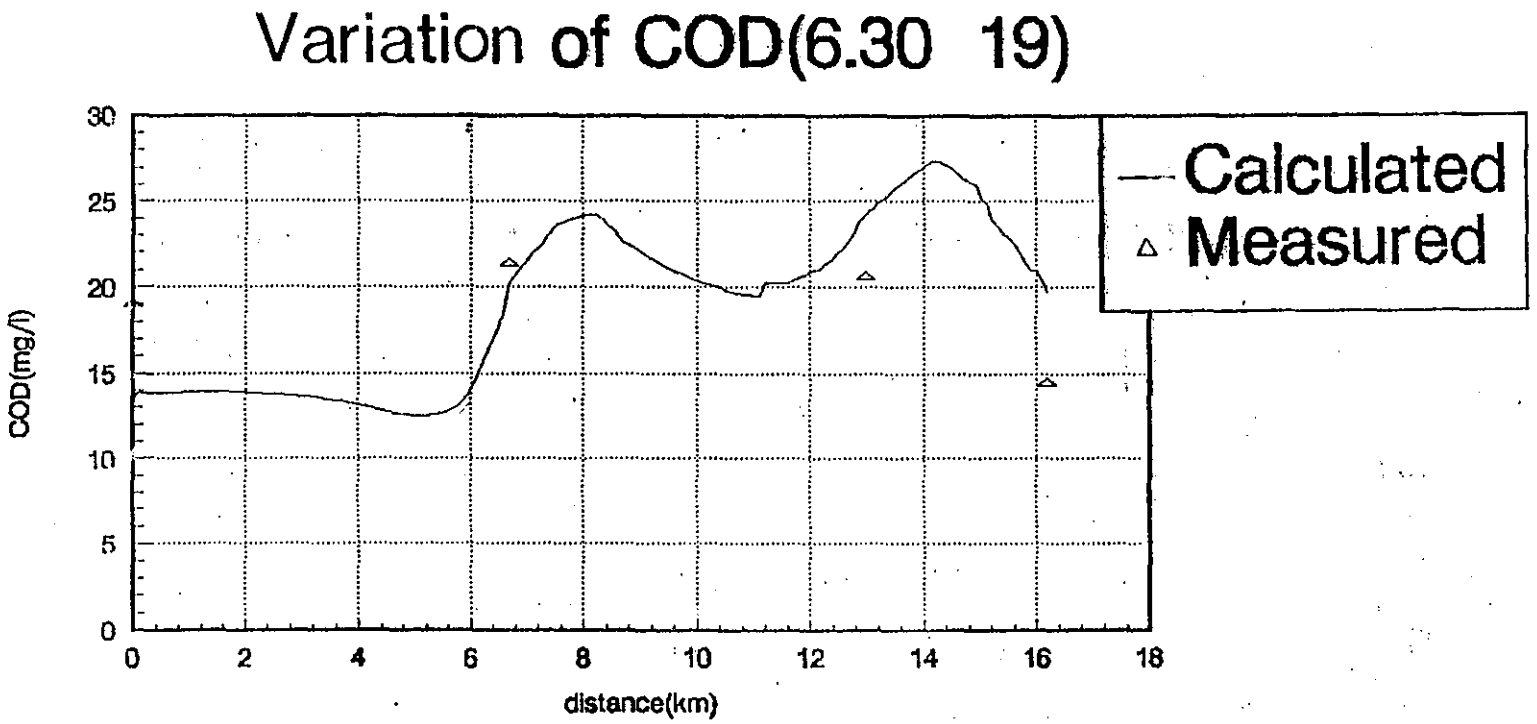

FIG. A7—53(v) COD variation in wet season (6. 30 19)

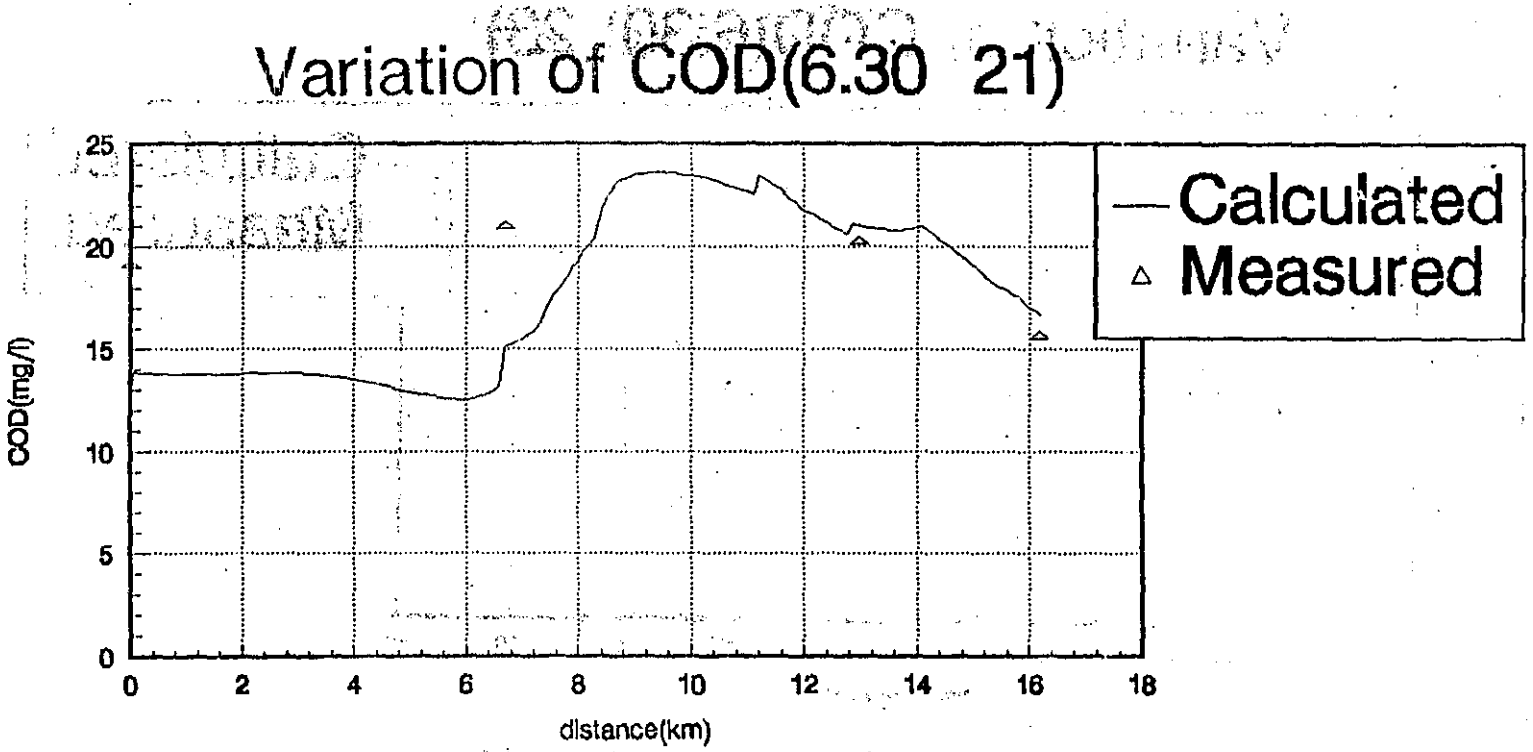

FIG. A7—53(w) COD variation in wet season (6. 30 21)

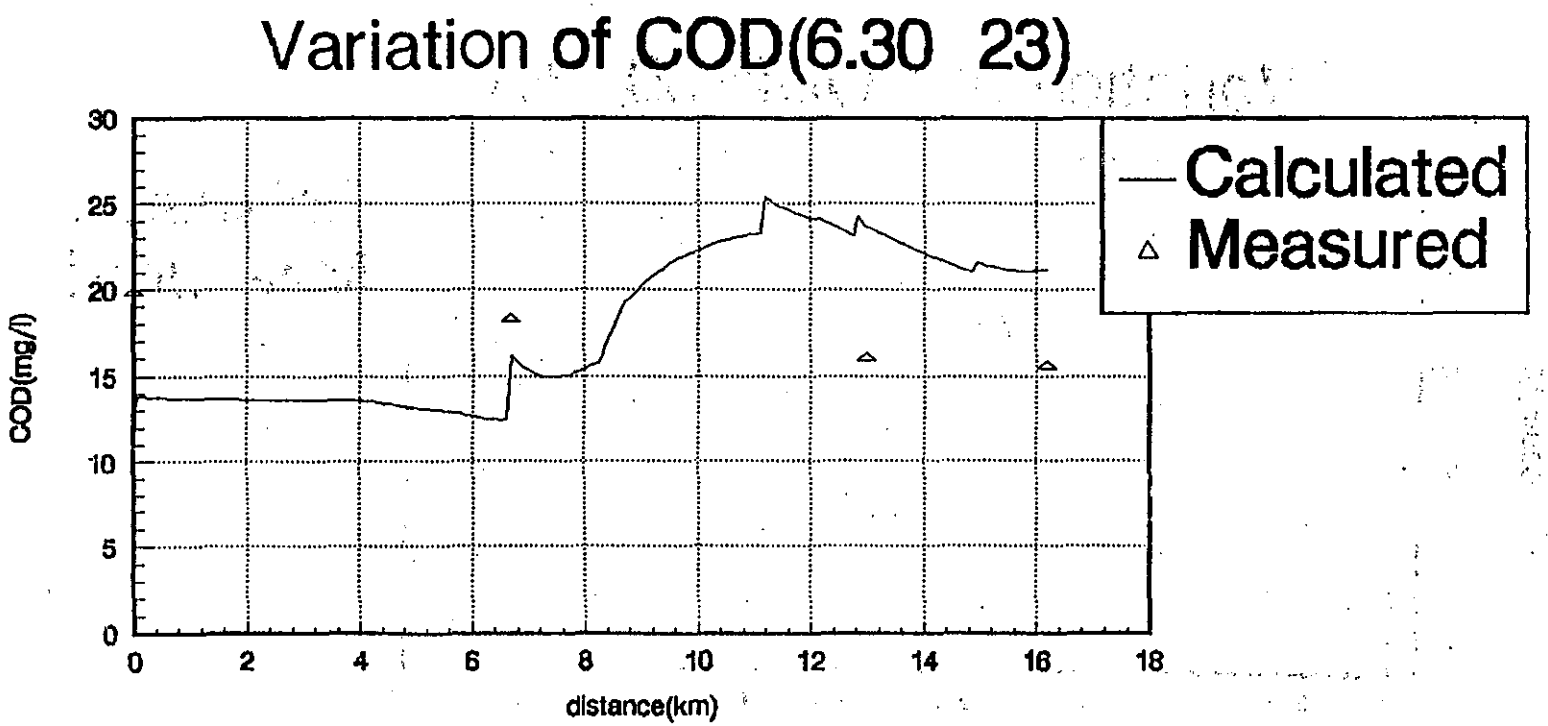

FIG. A7－53(x) COD variation in wet season (6. 30 23)

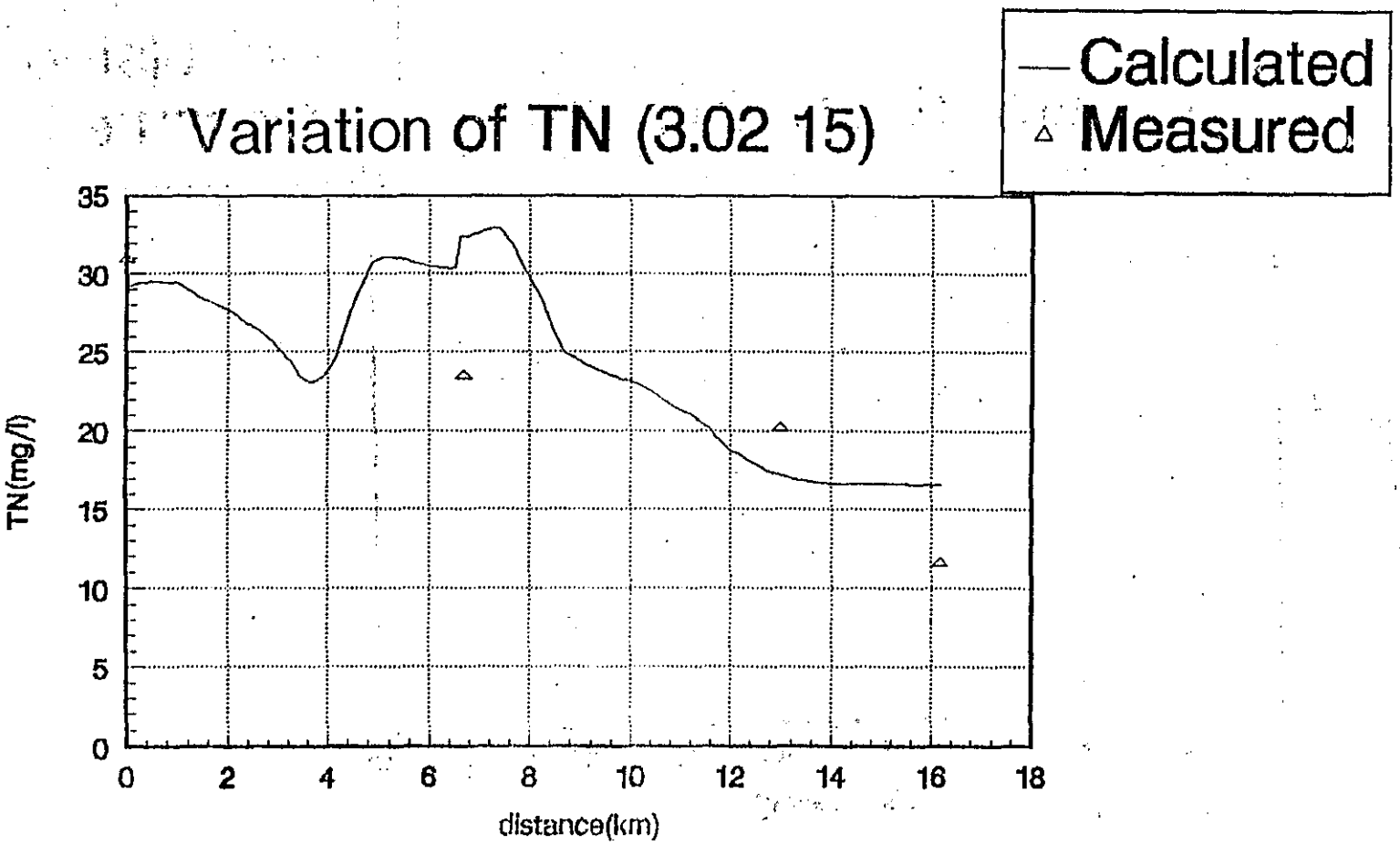

FIG. A7—54(a) TN variation in dry season (3.02 15)

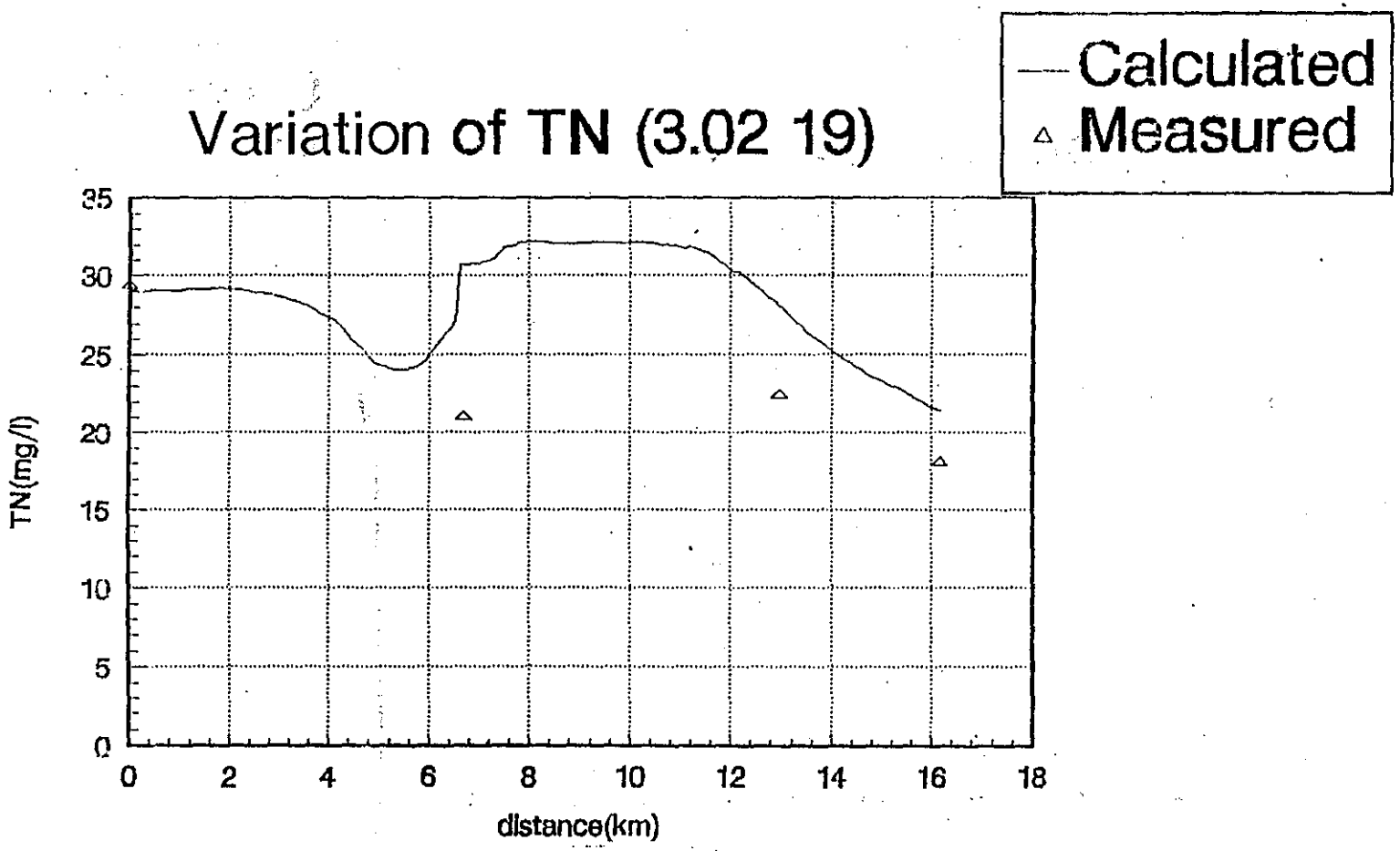

FIG. A7—54(b) TN variation in dry season (3.02 19)

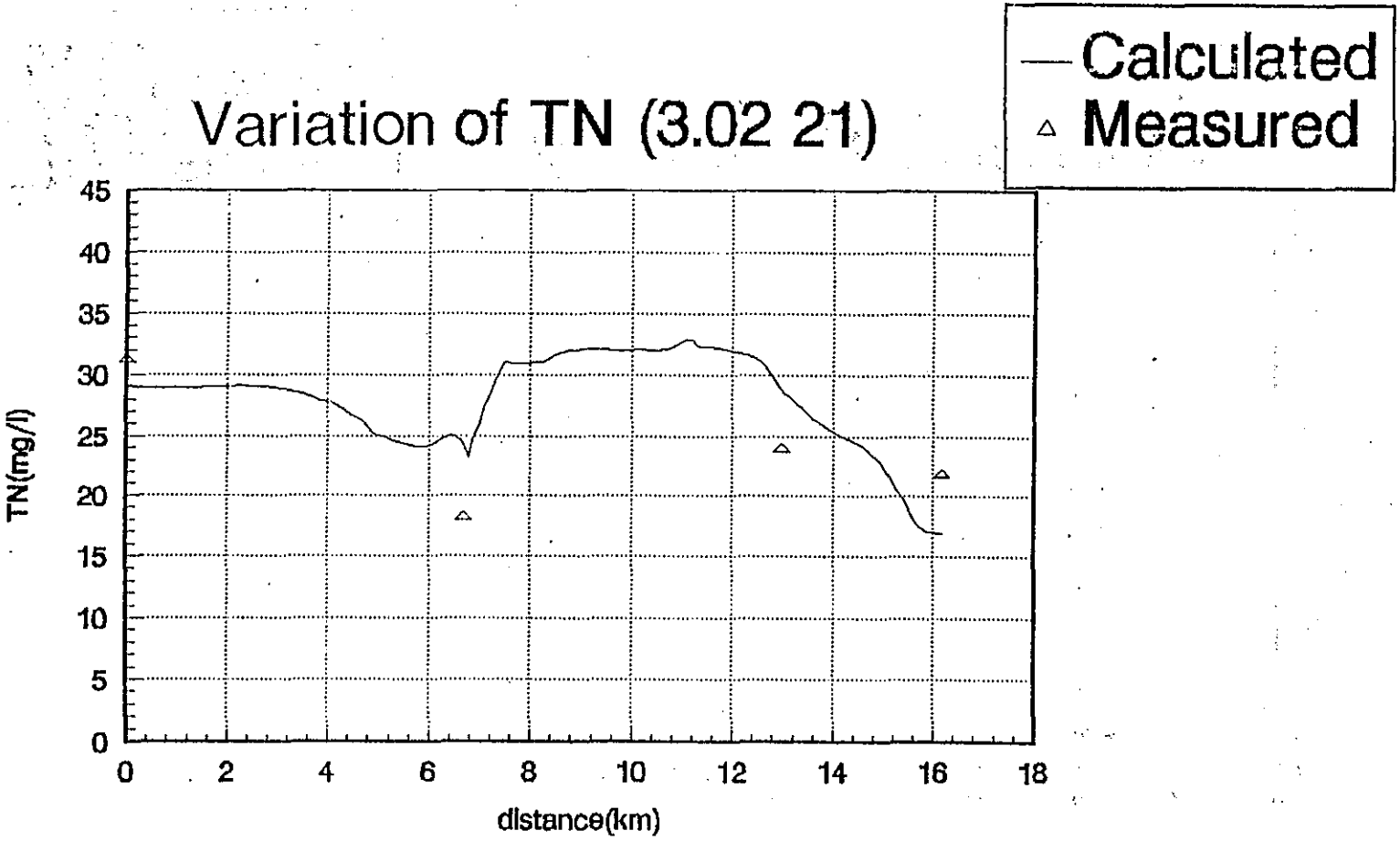

FIG. A7—54(c) TN variation in dry season (3. 02 21)

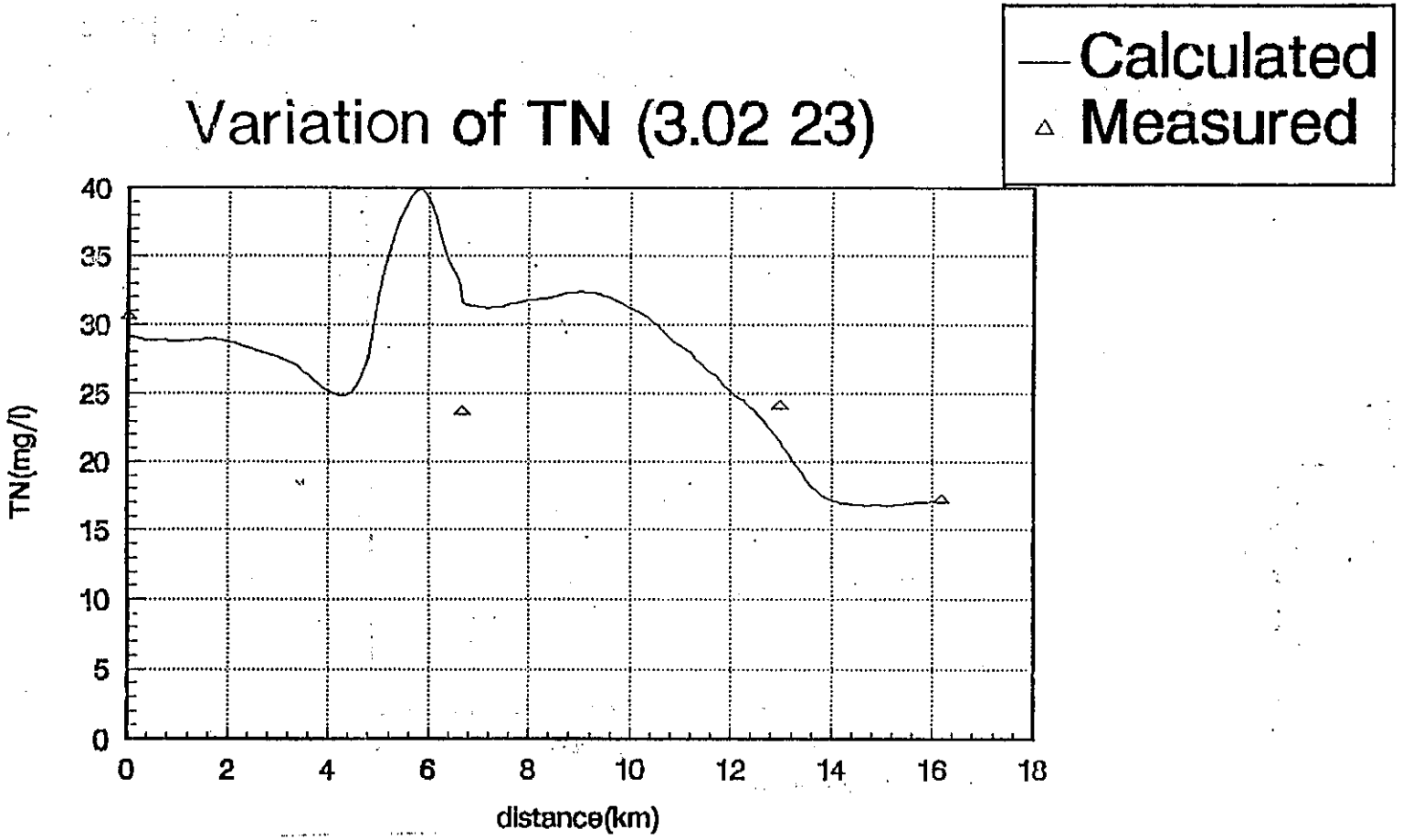

FIG. A7—54(d) TN variation in dry season (3. 02 23)

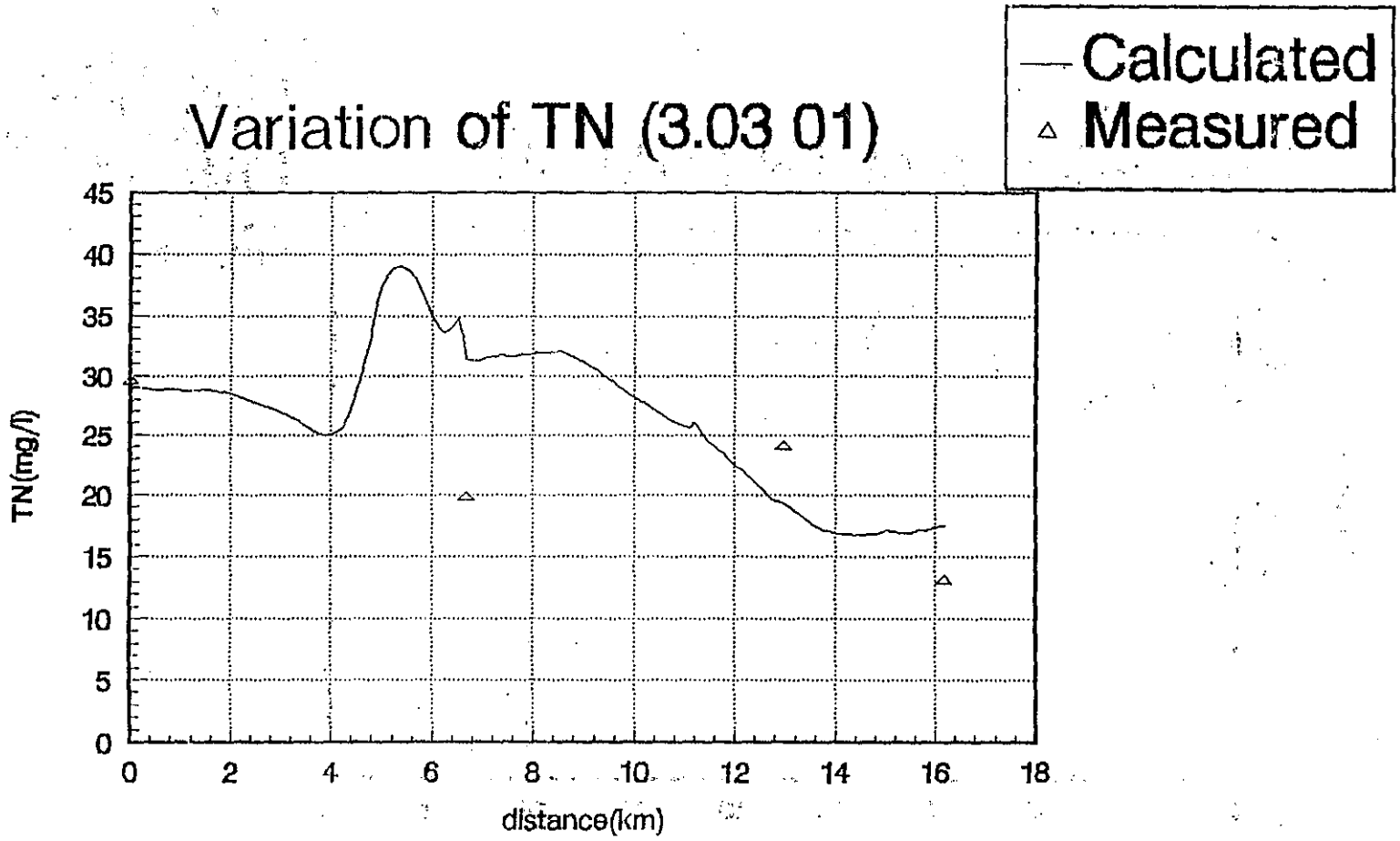

FIG. A7--54(e) TN variation in dry season (3.03 01)

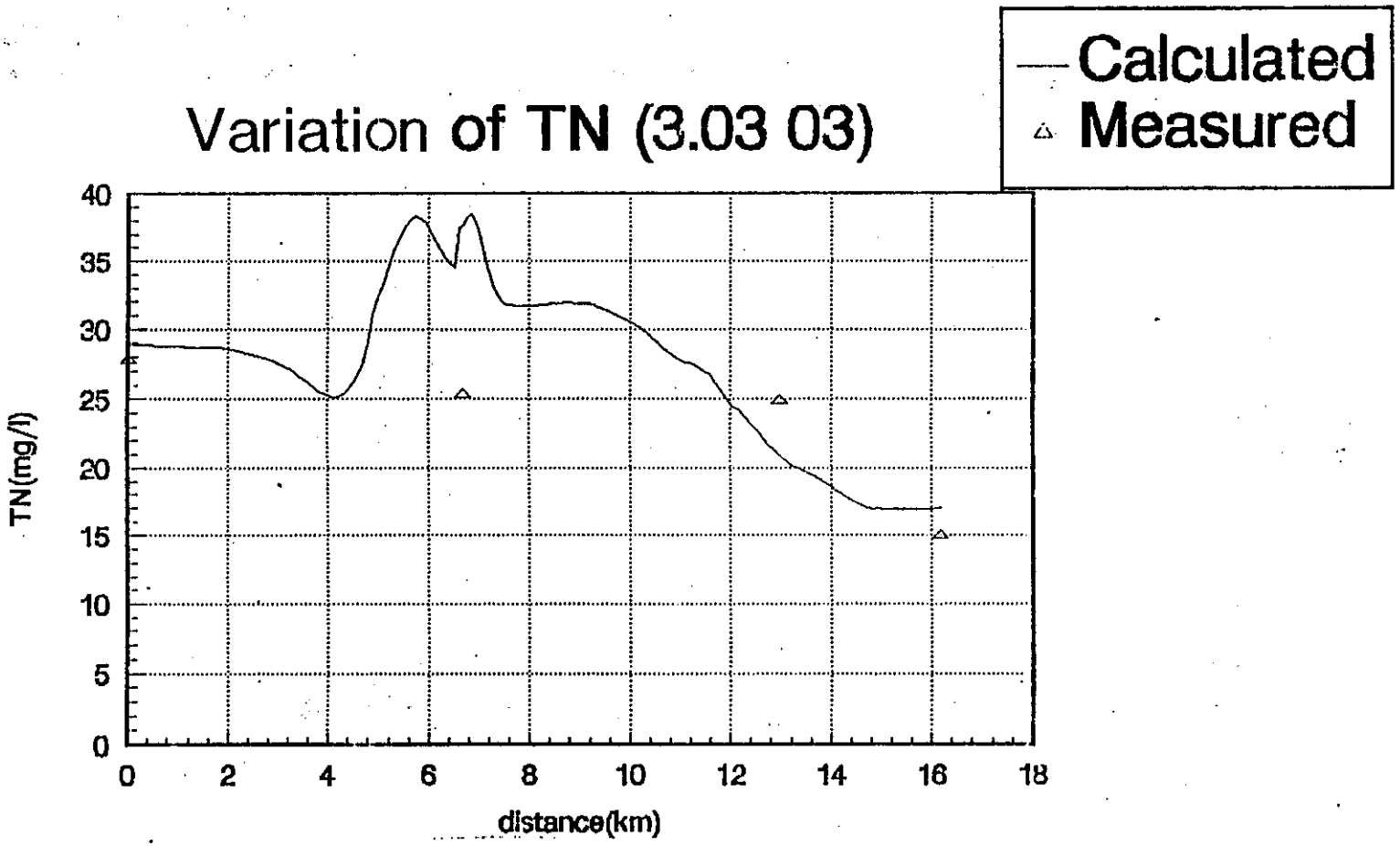

FIG. A7—54(f) TN variation in dry season (3. 03 03)

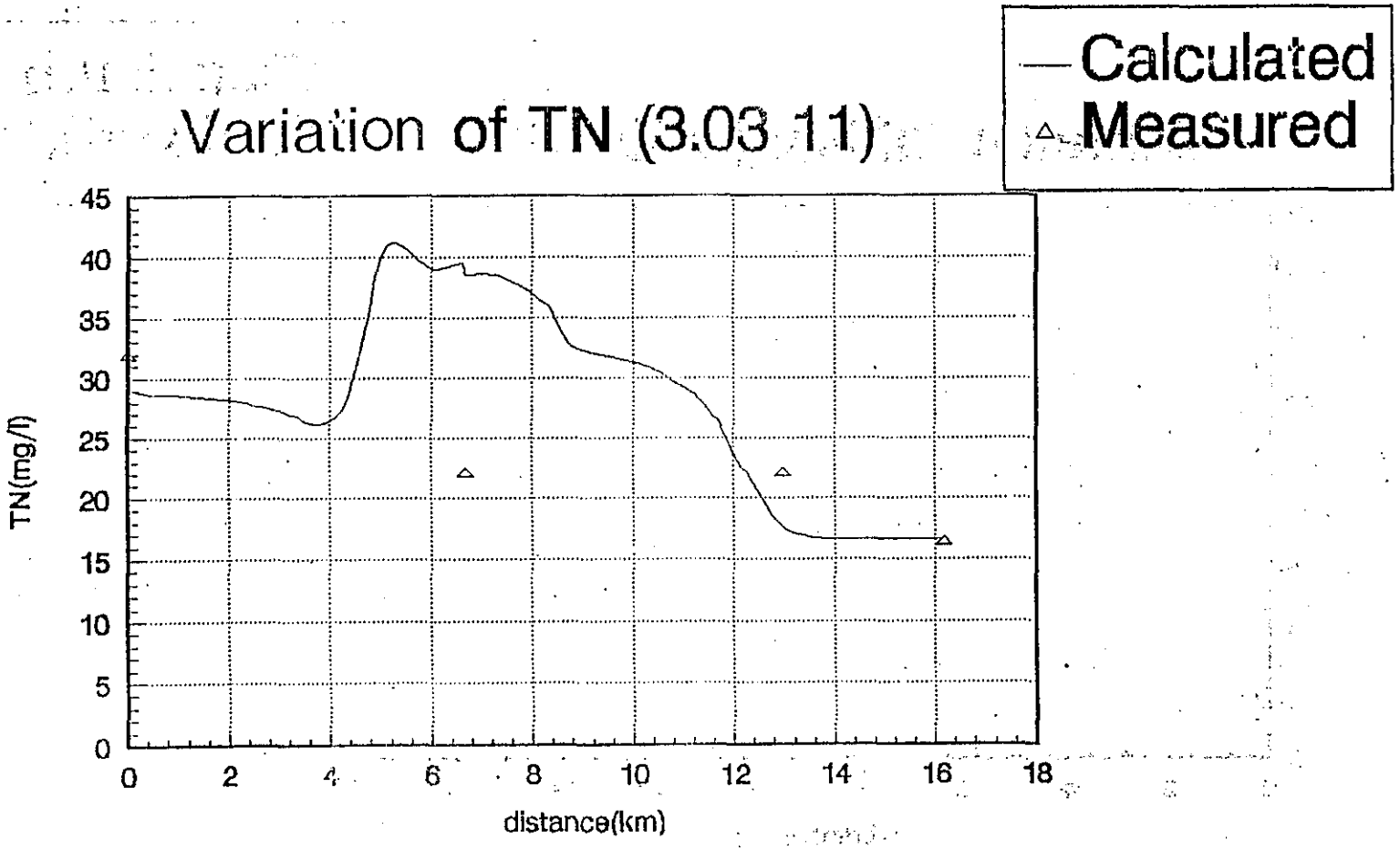

FIG. A7—54(g) TN variation in dry season (3. 03 11)

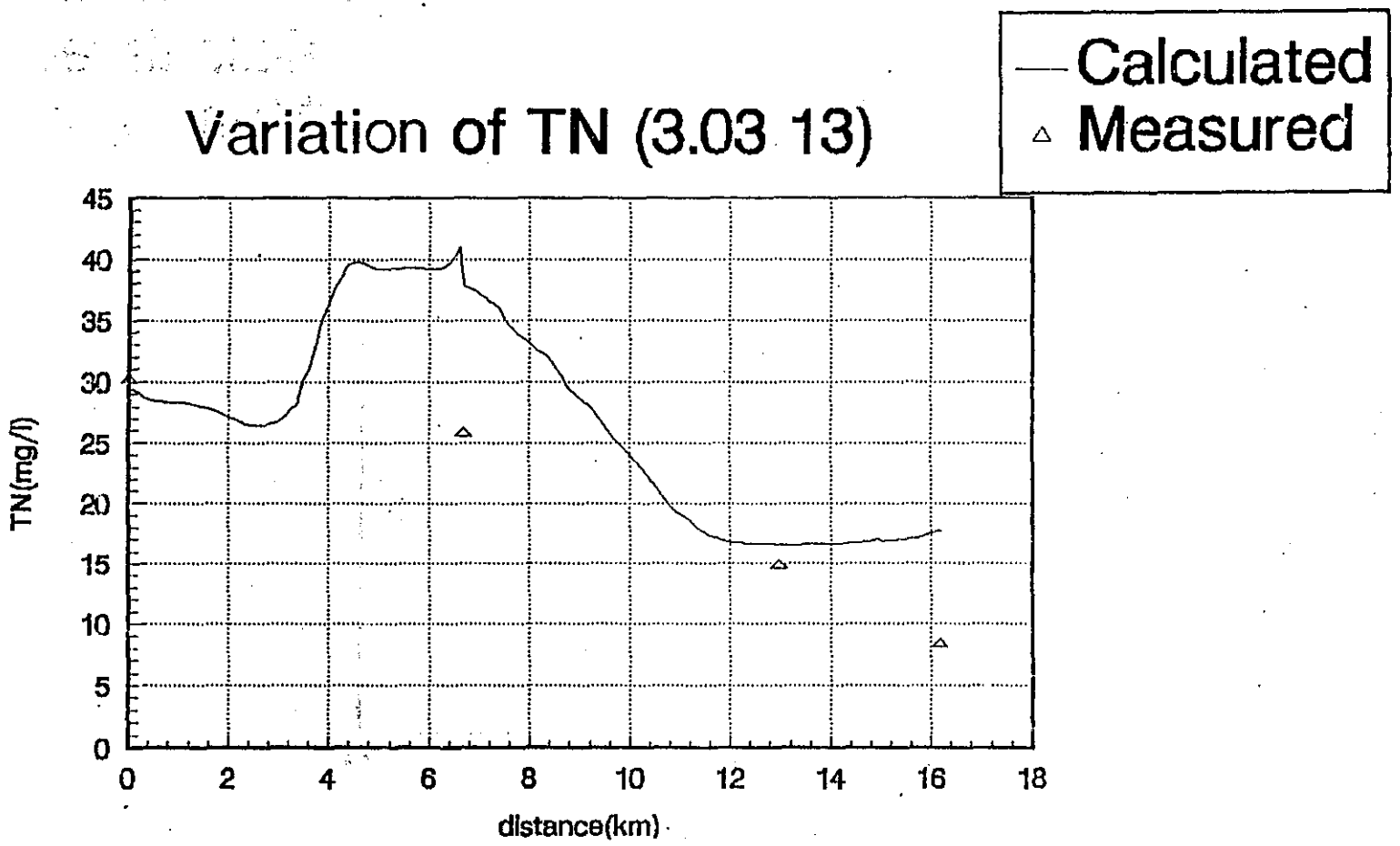

FIG. A7—54(h) TN variation in dry season (3. 03 13)

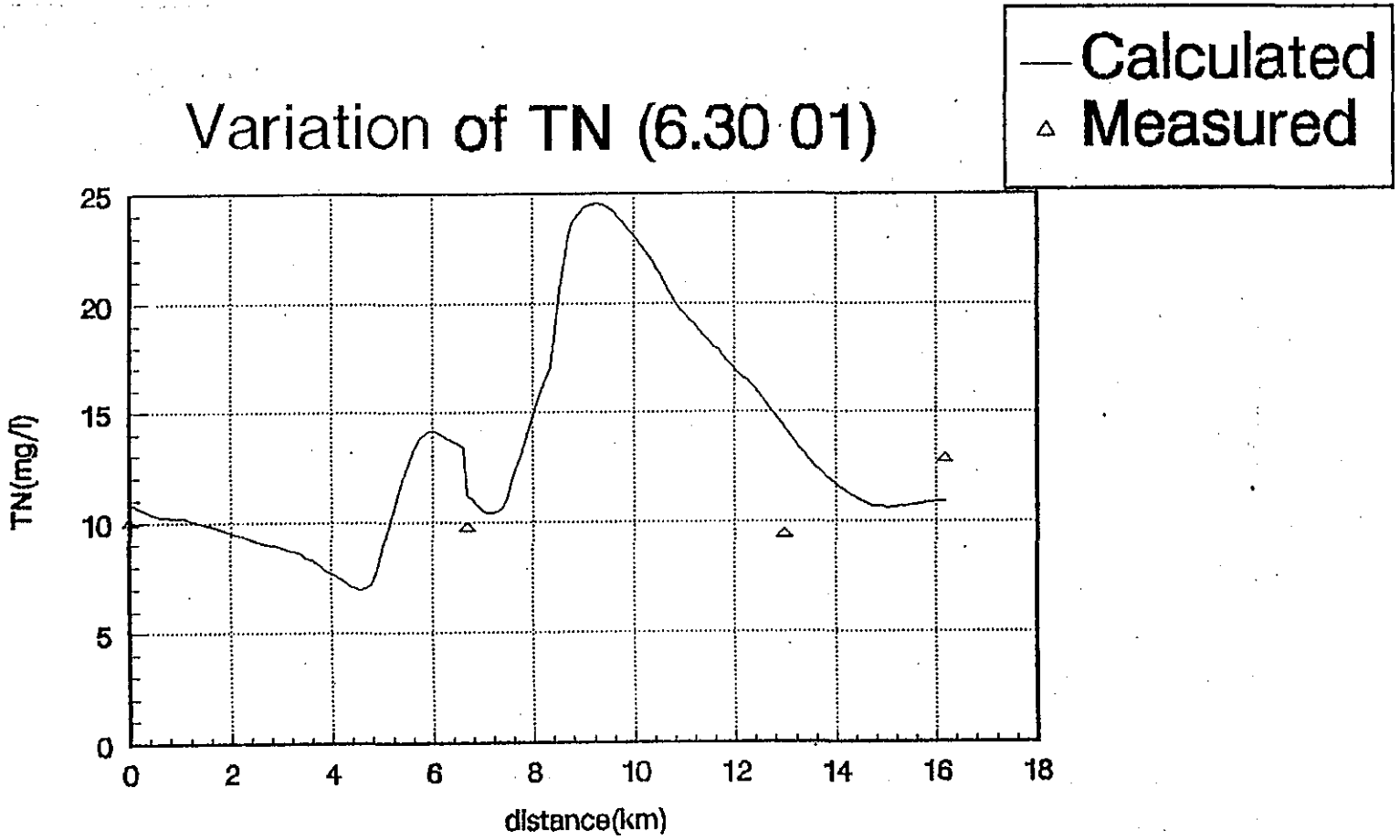

FIG. A7－54(i)　**TN variation in wet season** (6. 30 01)

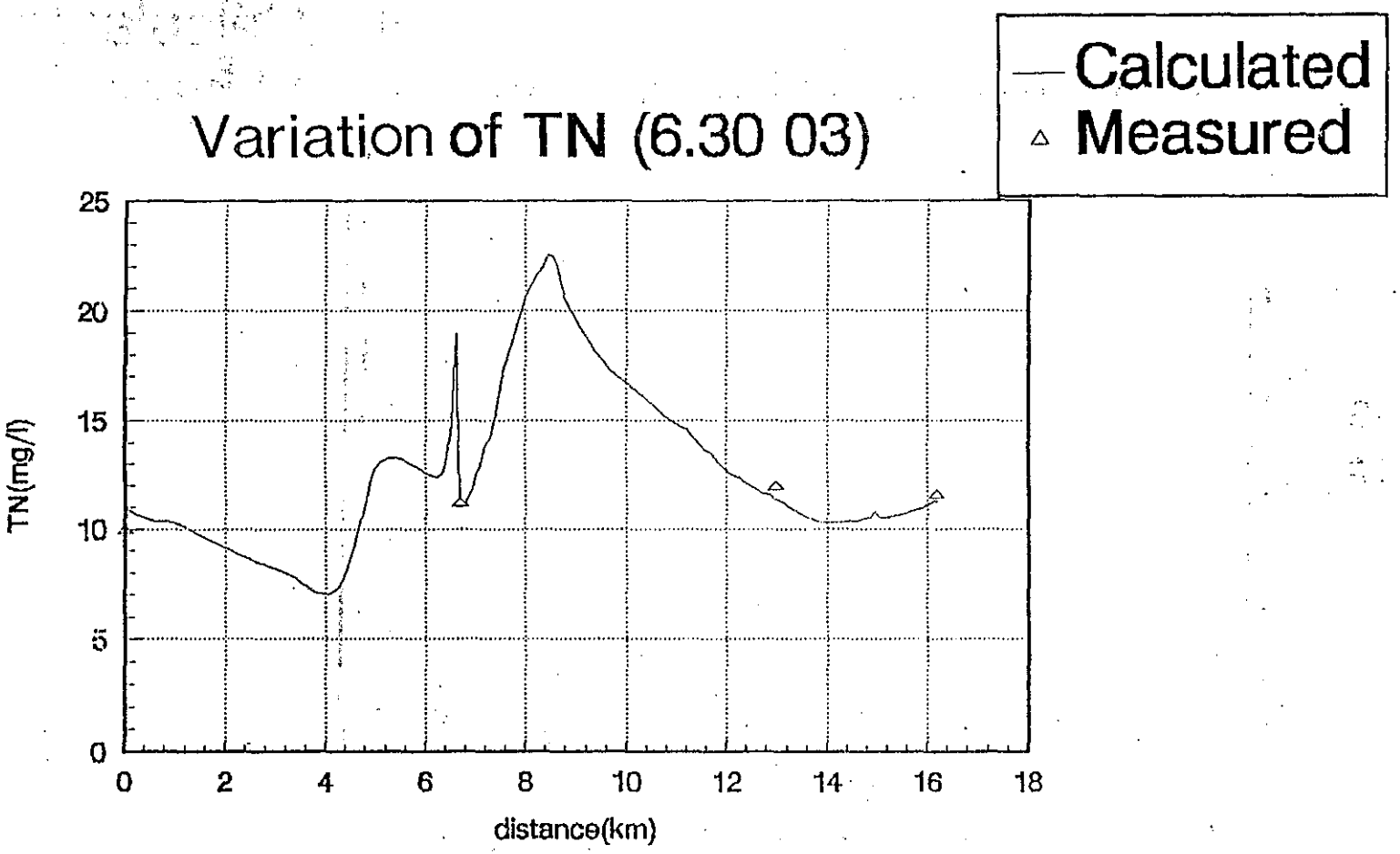

FIG. A7—54(j) TN variation in wet season (6. 30 03)

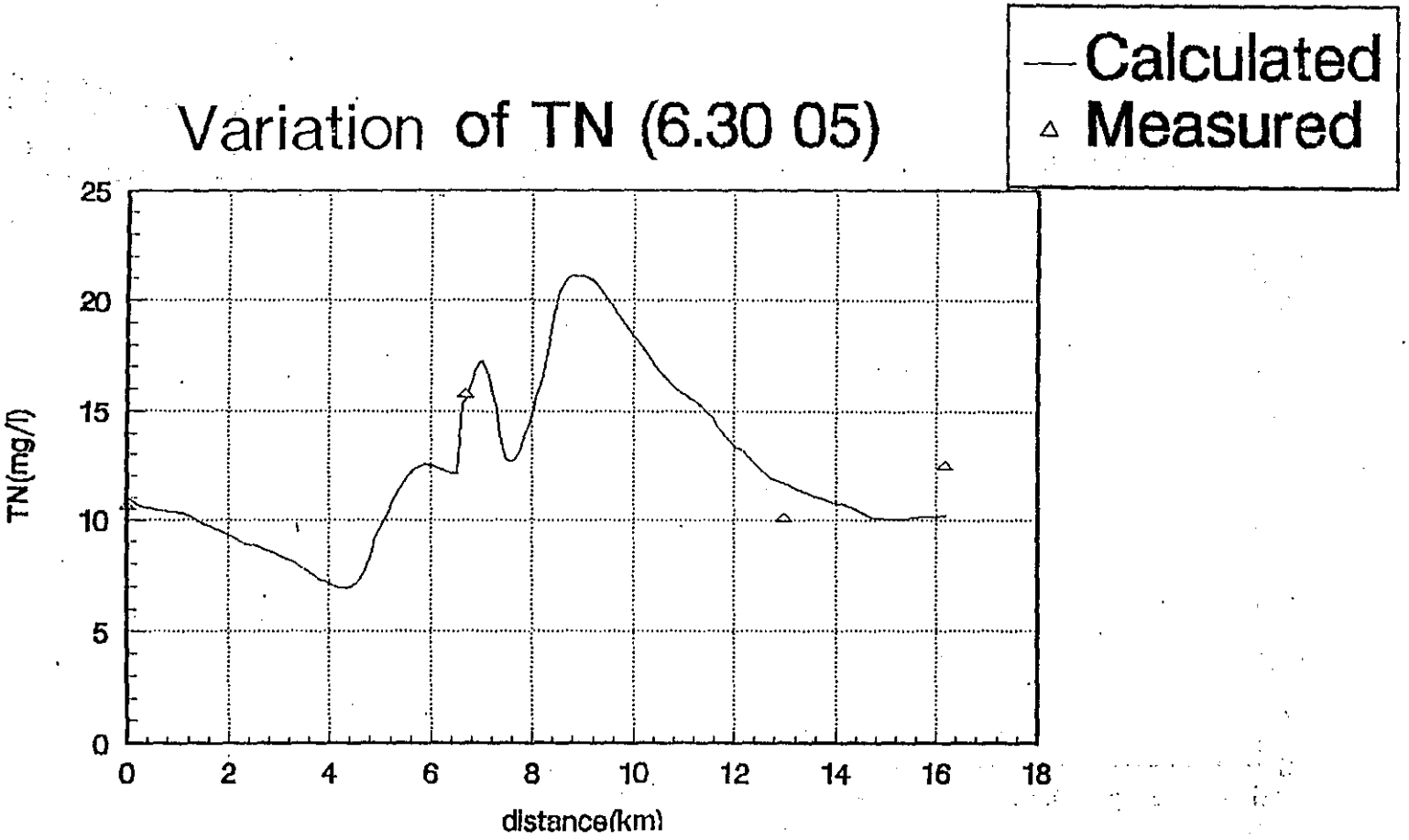

FIG. A7—54(k) TN variation in wet season (6. 30 05)

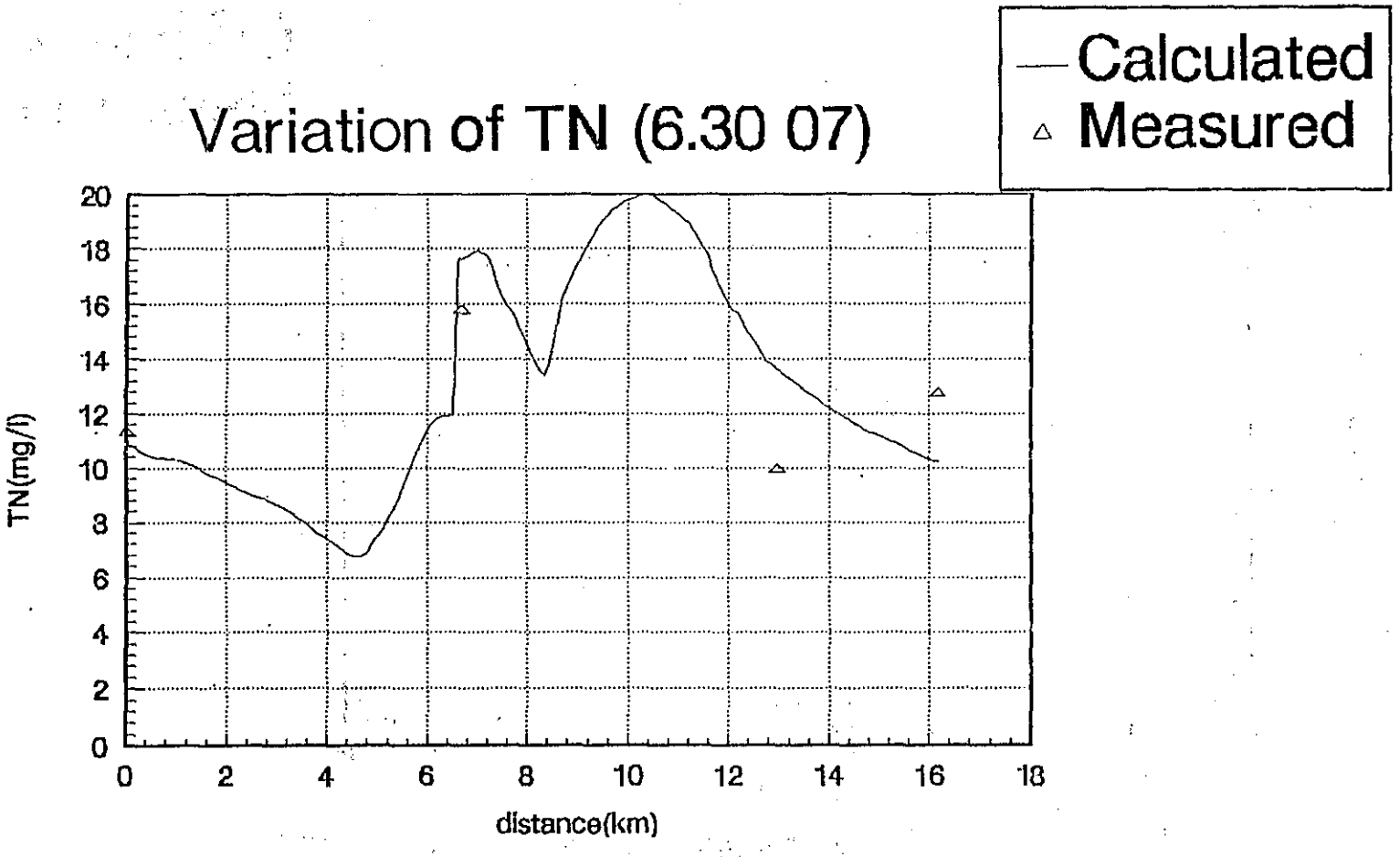

FIG. A7—54(1) TN variation in wet season (6. 30 07)

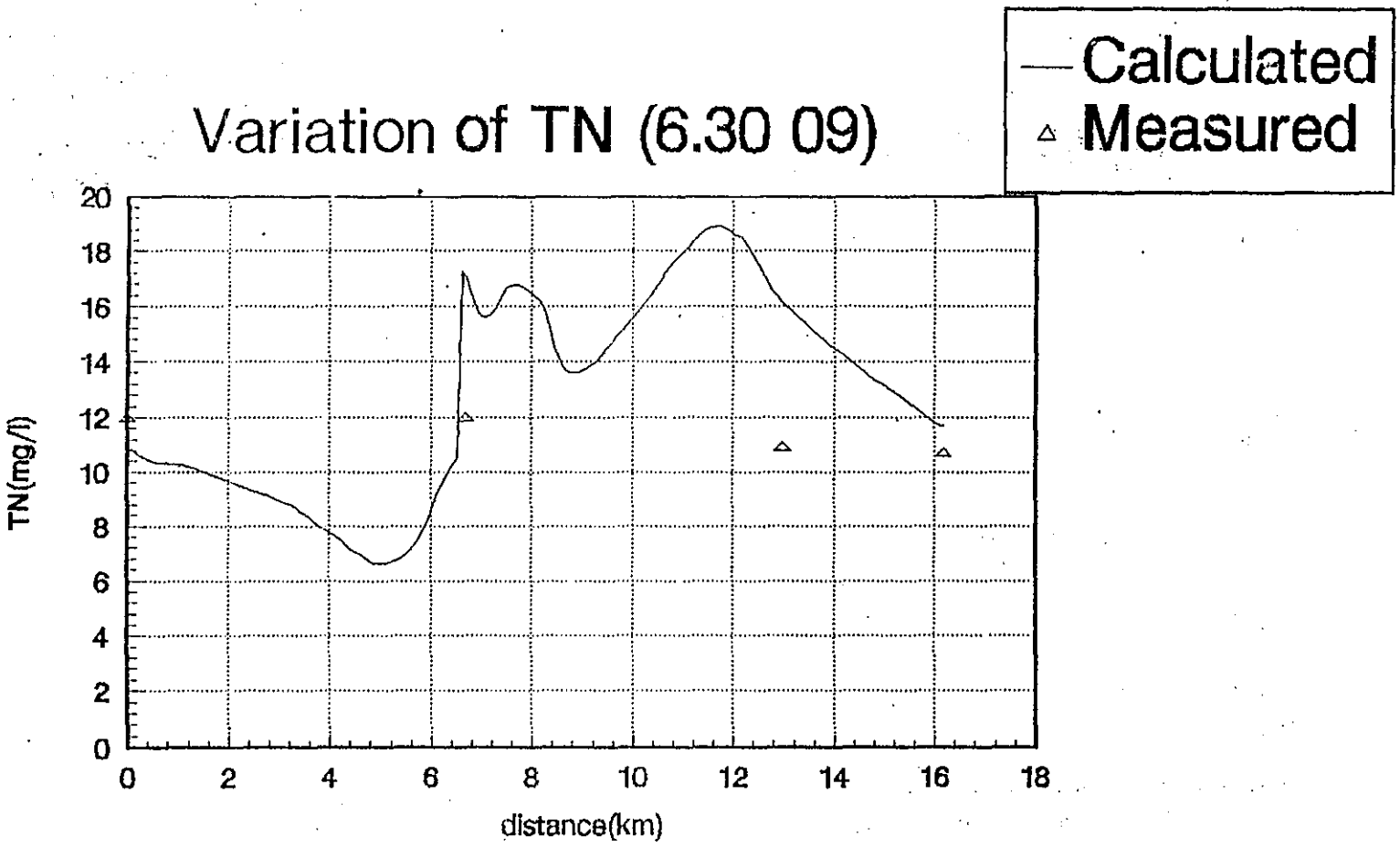

FIG. A7－54(m)　TN variation in wet season (6. 30 09)

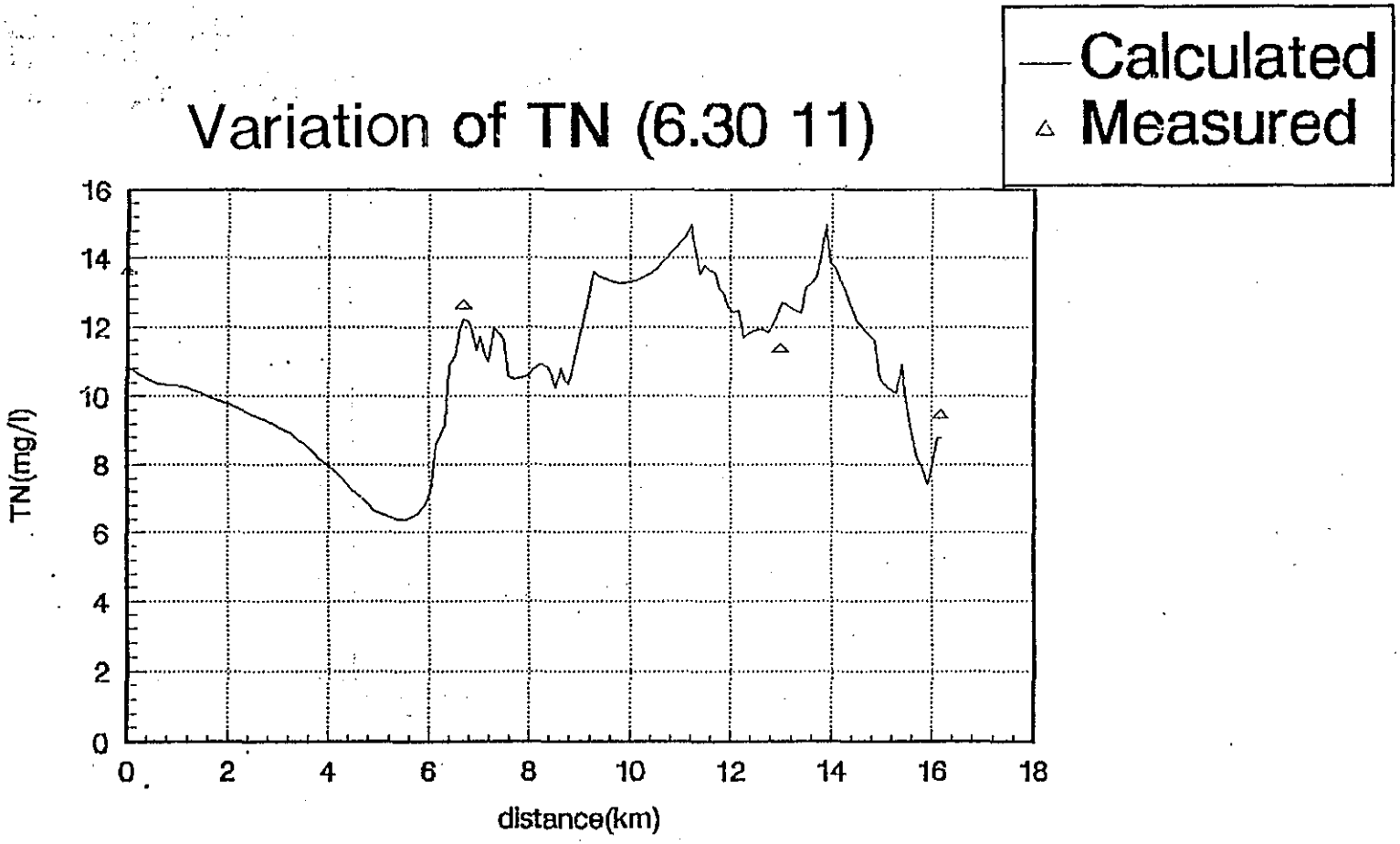

FIG. A7—54(n) TN variation in wet season (6. 30 11)

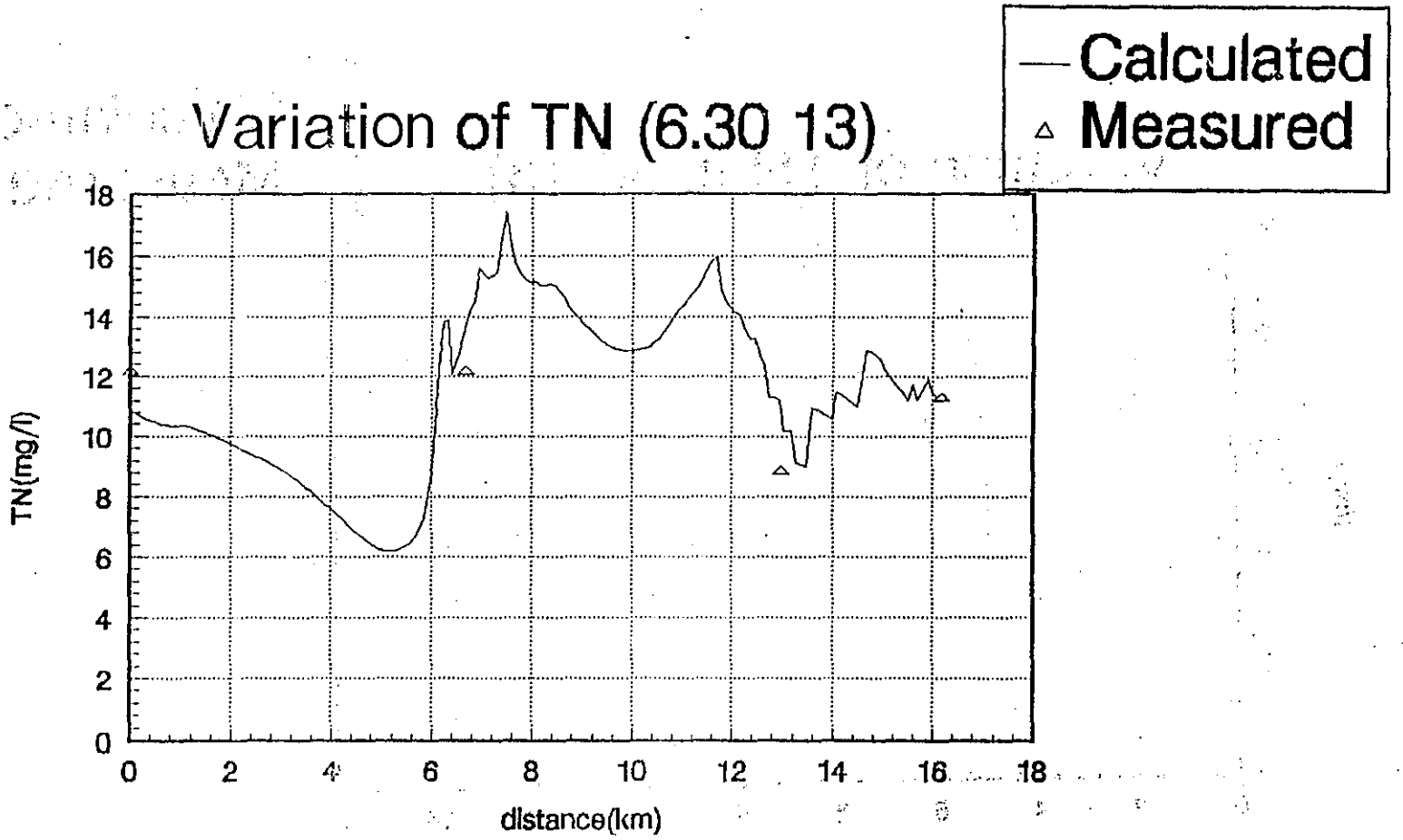

FIG. A7—54(o) TN variation in wet season (6. 30 13)

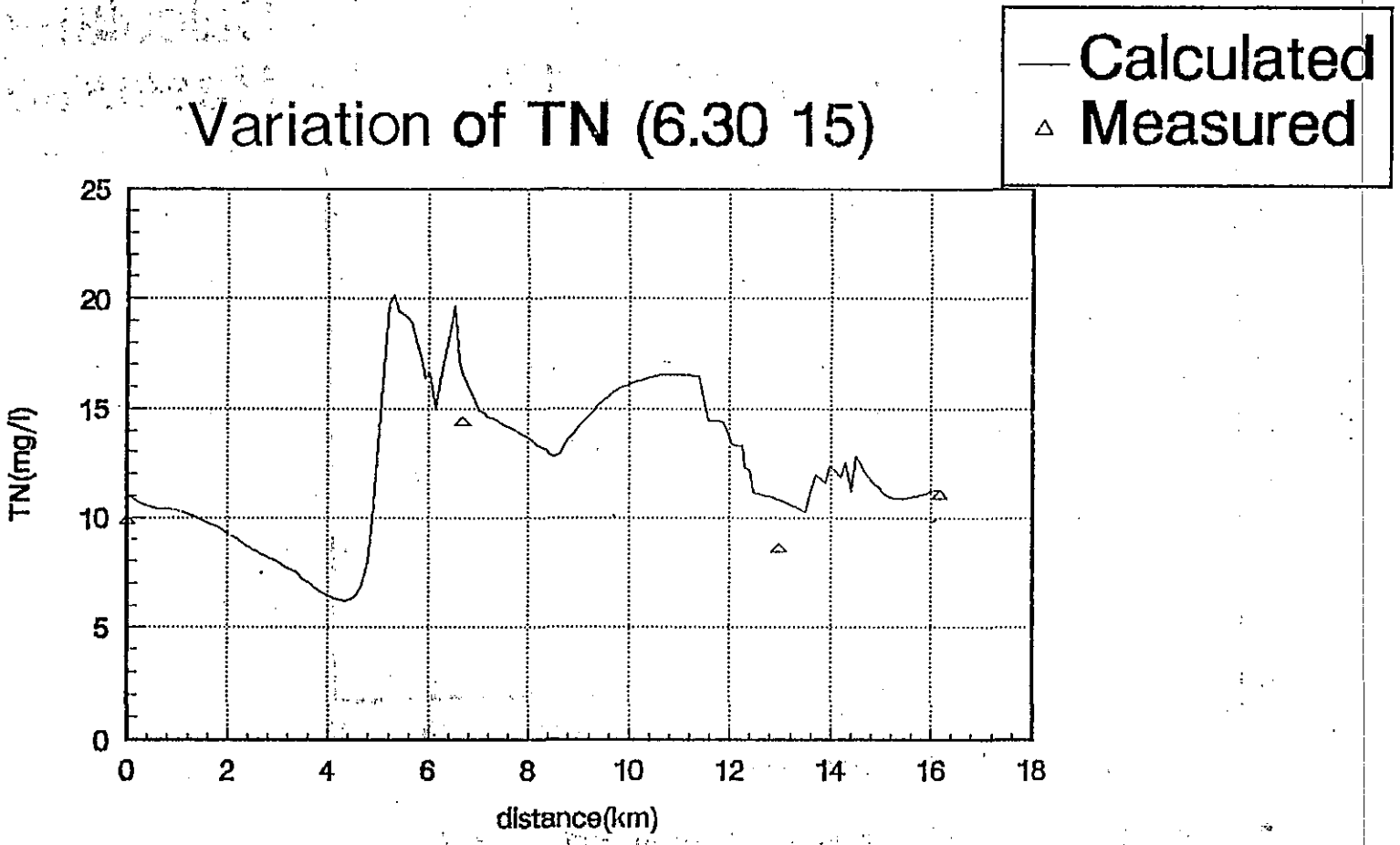

FIG. A7—54(p) TN variation in wet season (6. 30 15)

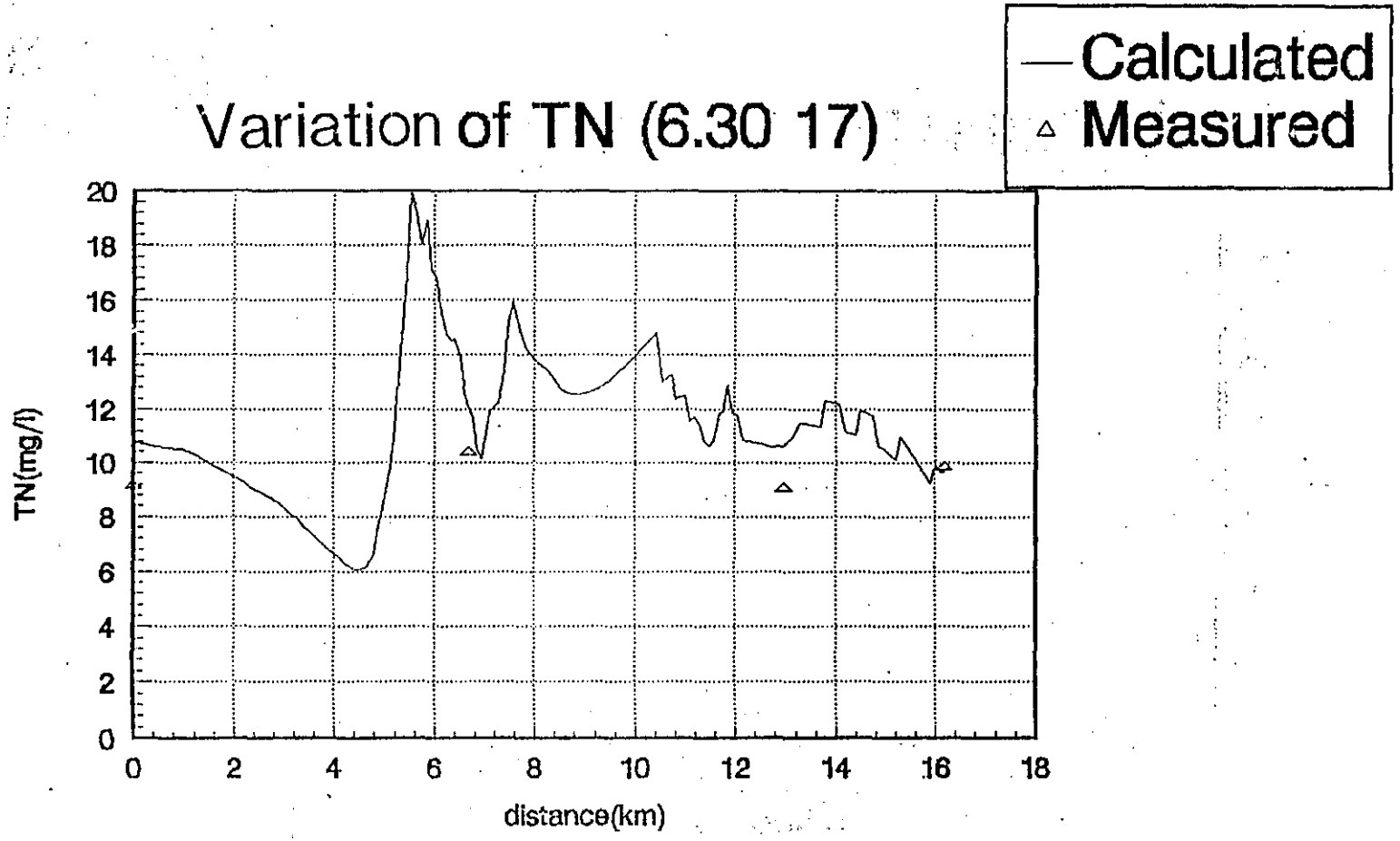

FIG. A7—54(q) TN variation in wet season (6. 30 17)

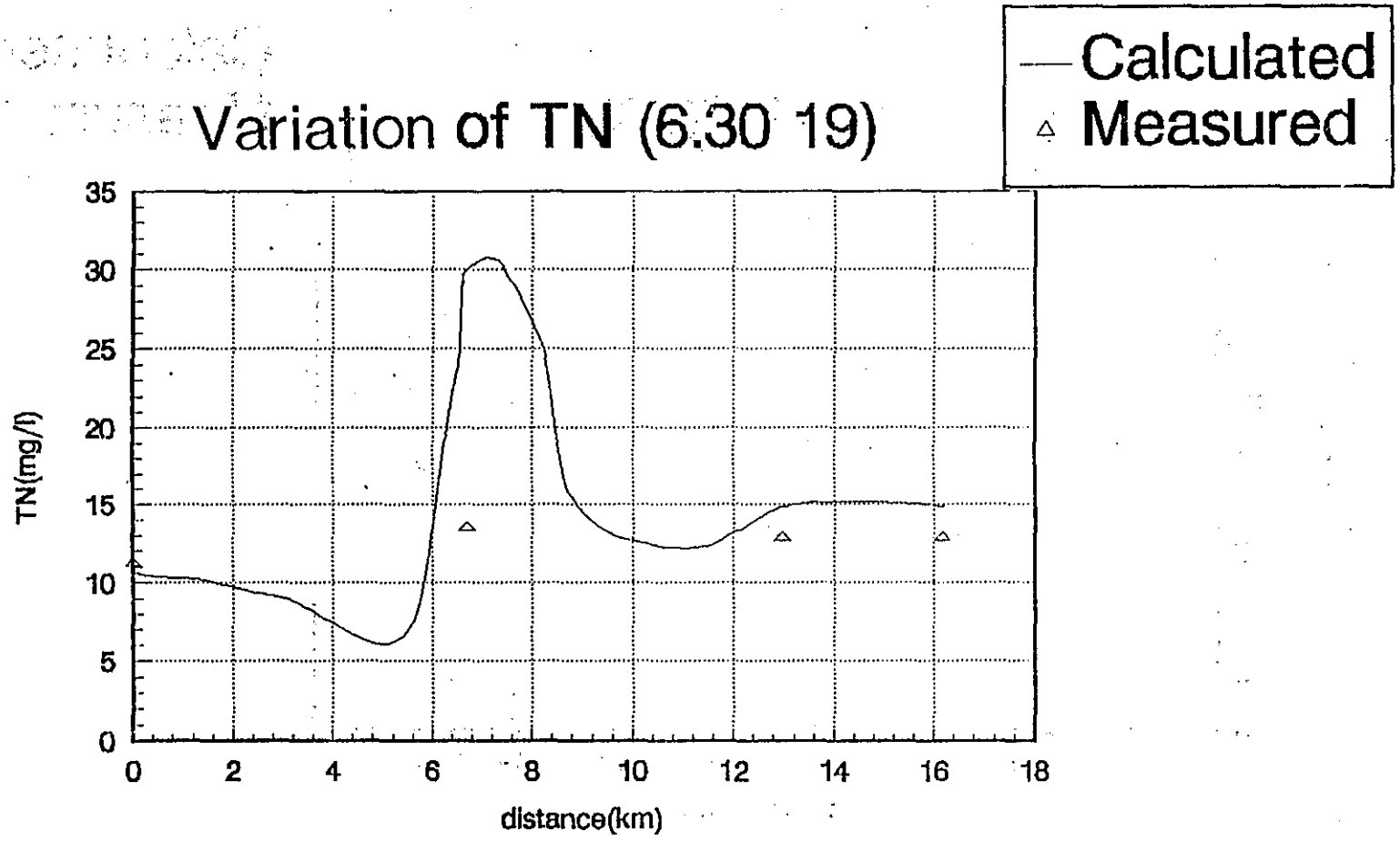

FIG. A7－54(r)　TN variation in wet season (6. 30 19)

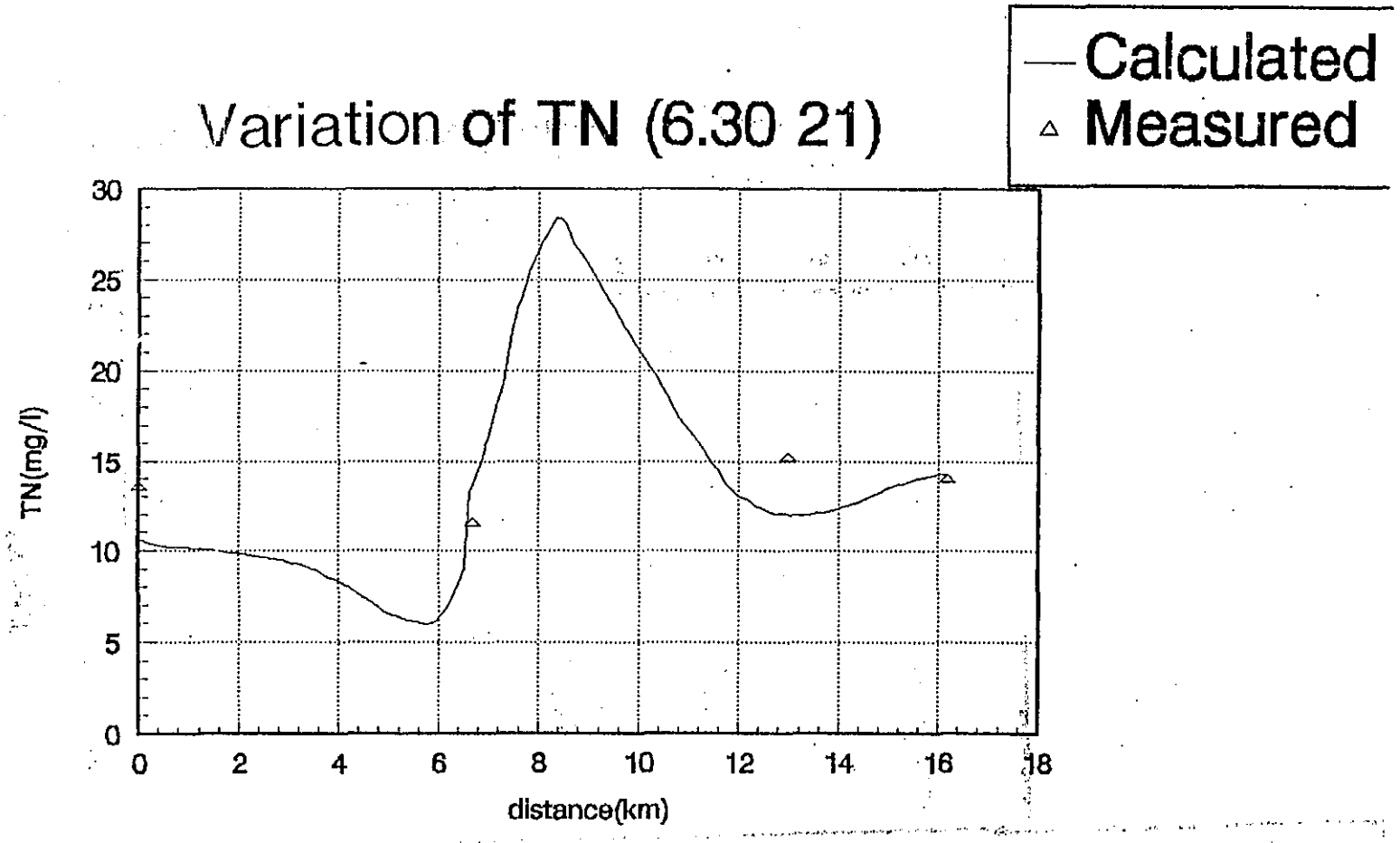

FIG. A7－54(s) TN variation in wet season (6.30 21)

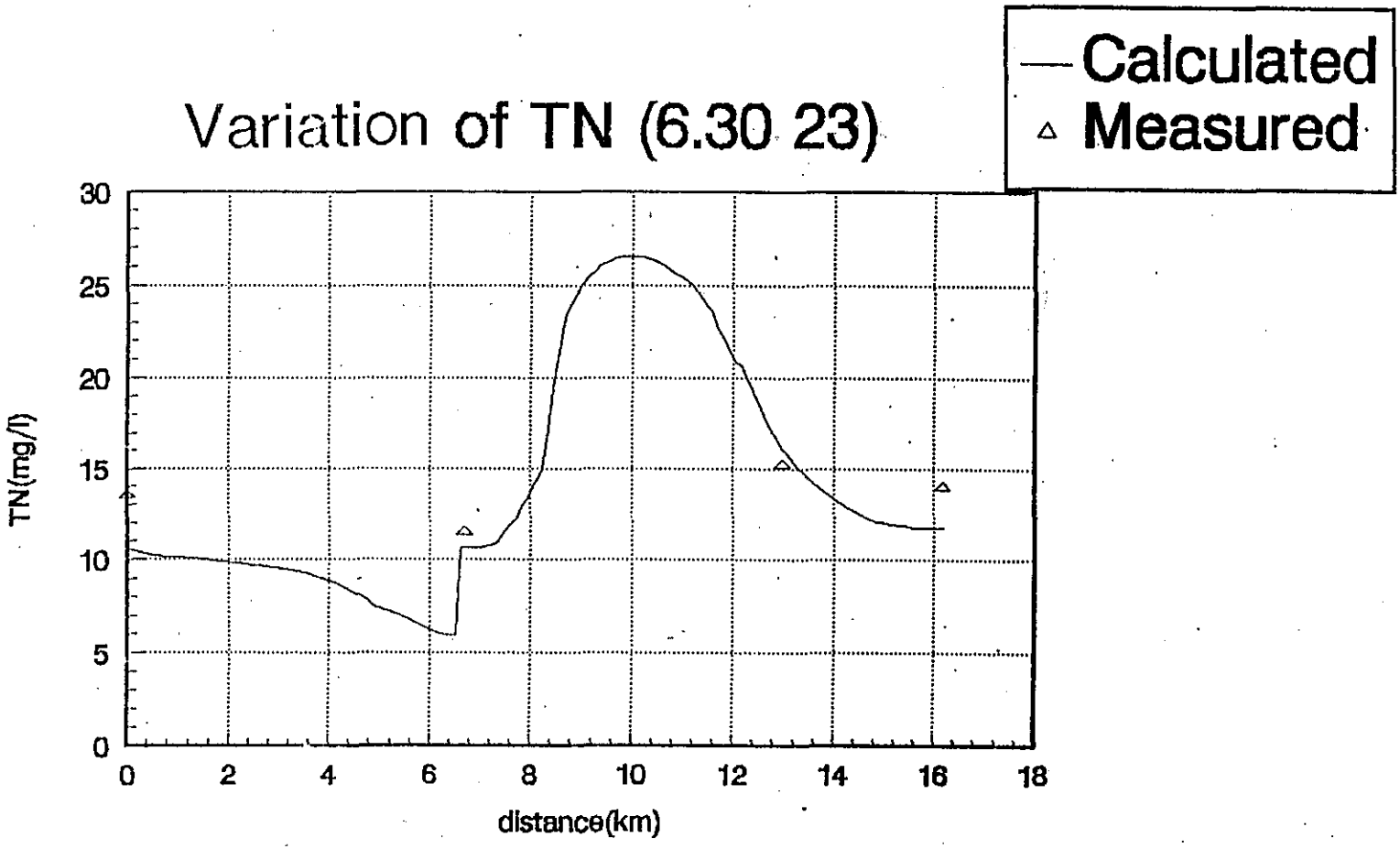

FIG. A7—54(t) TN variation in wet season (6. 30 23)

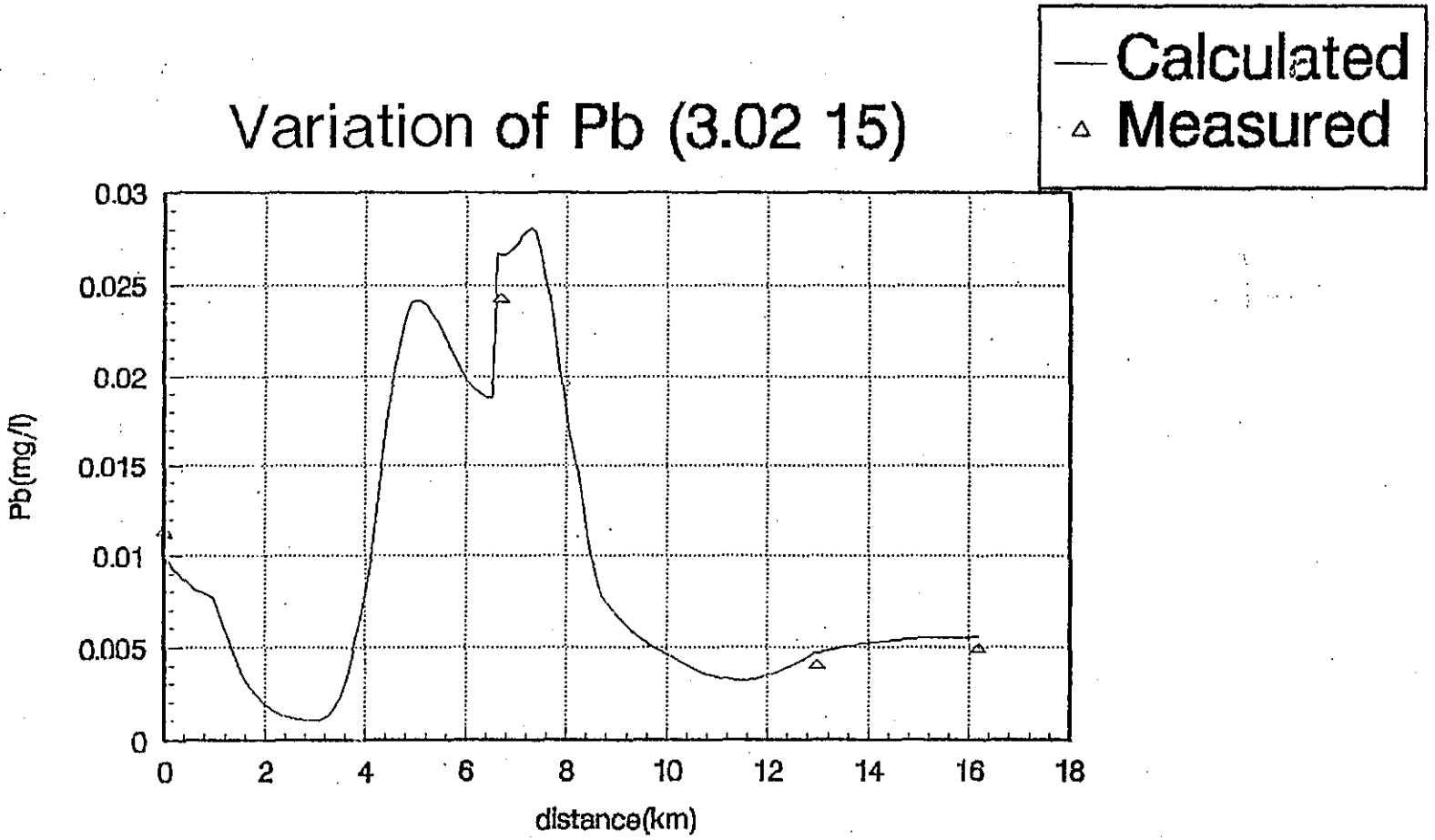

FIG. A7—55(a) **Pb variation in dry season** (3. 02 15)

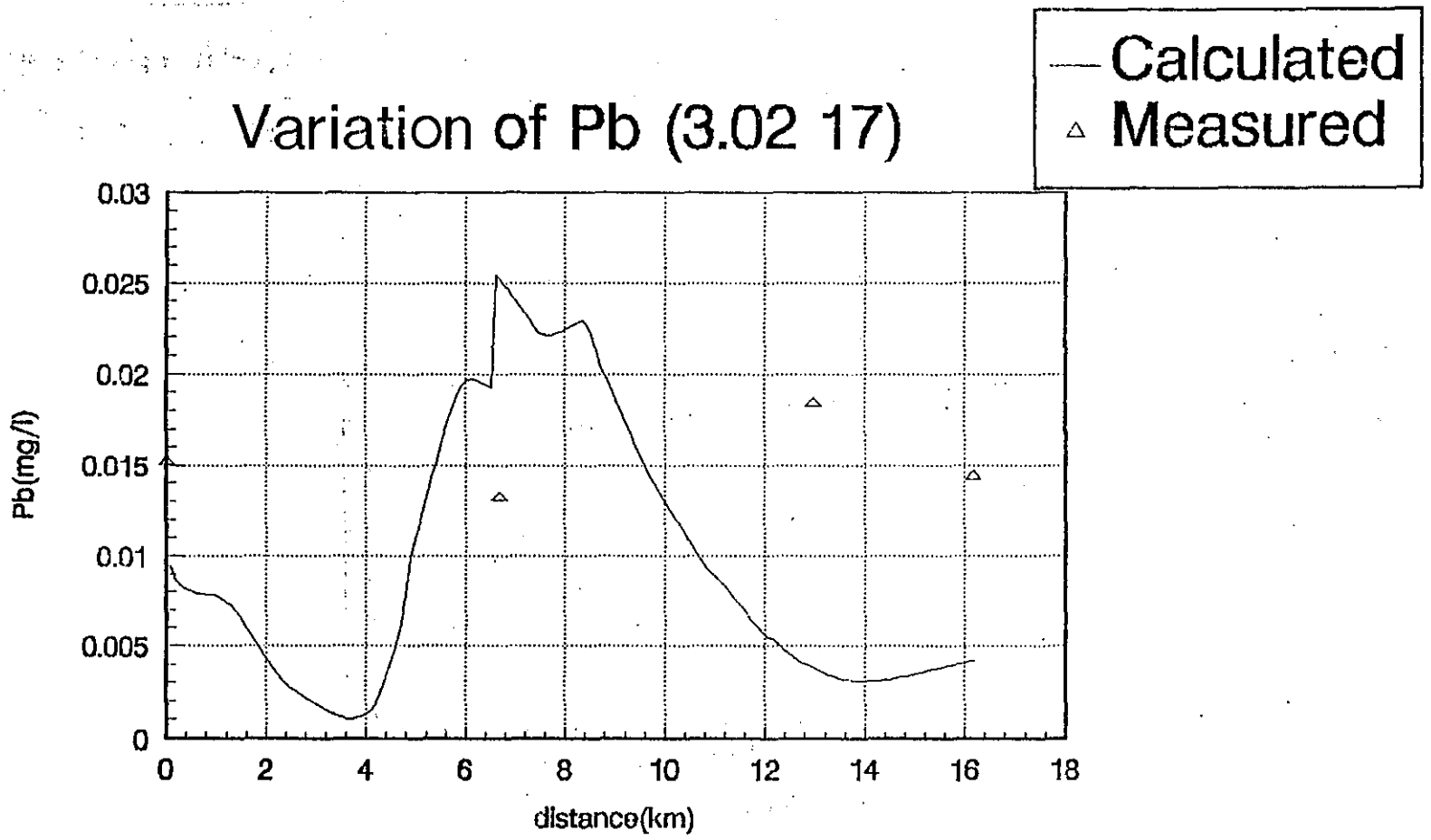

FIG. A7—55(b) Pb variation in dry season (3. 02 17)

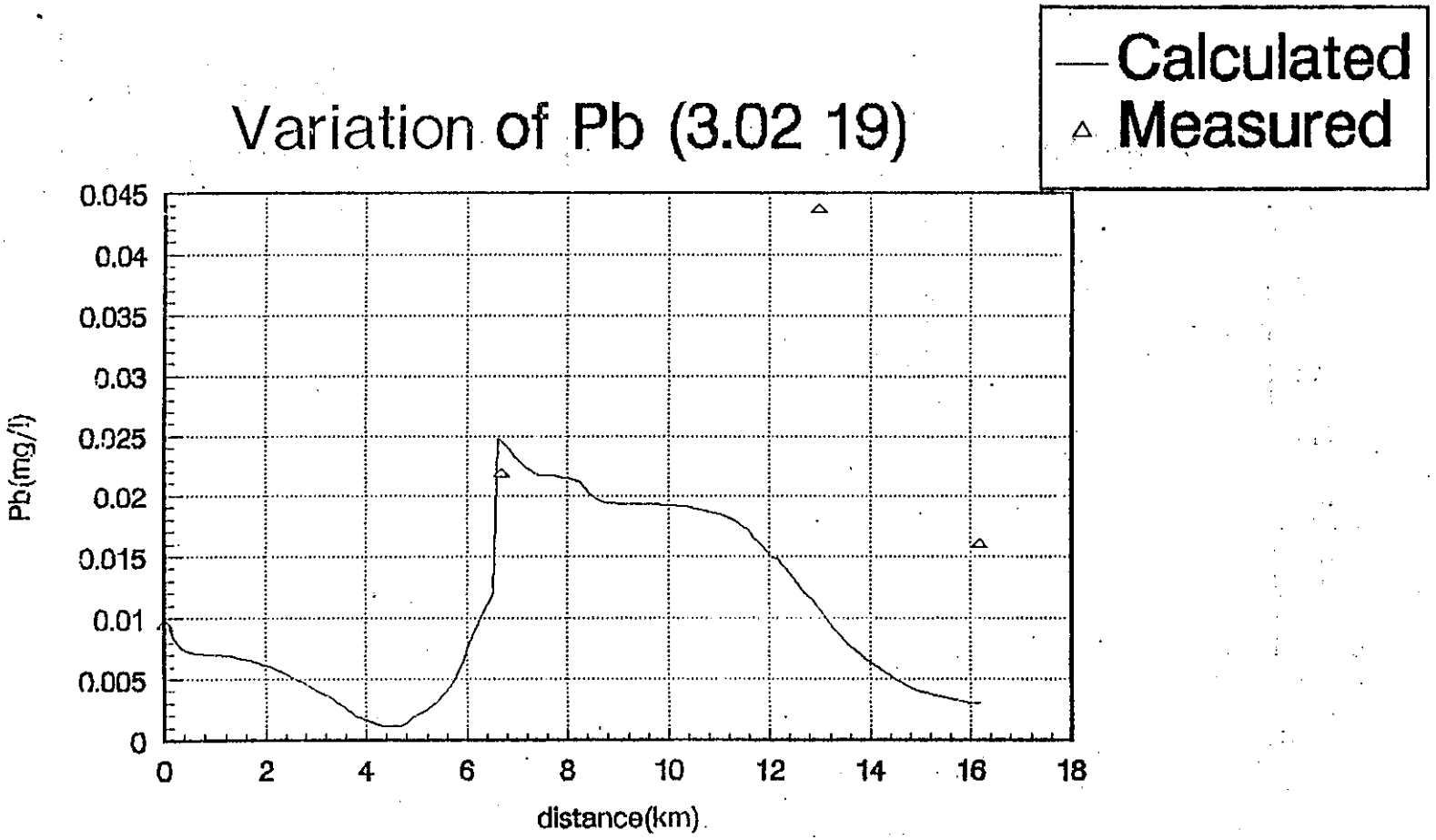

FIG. A7—55(c) **Pb variation in dry season** (3.02 19)

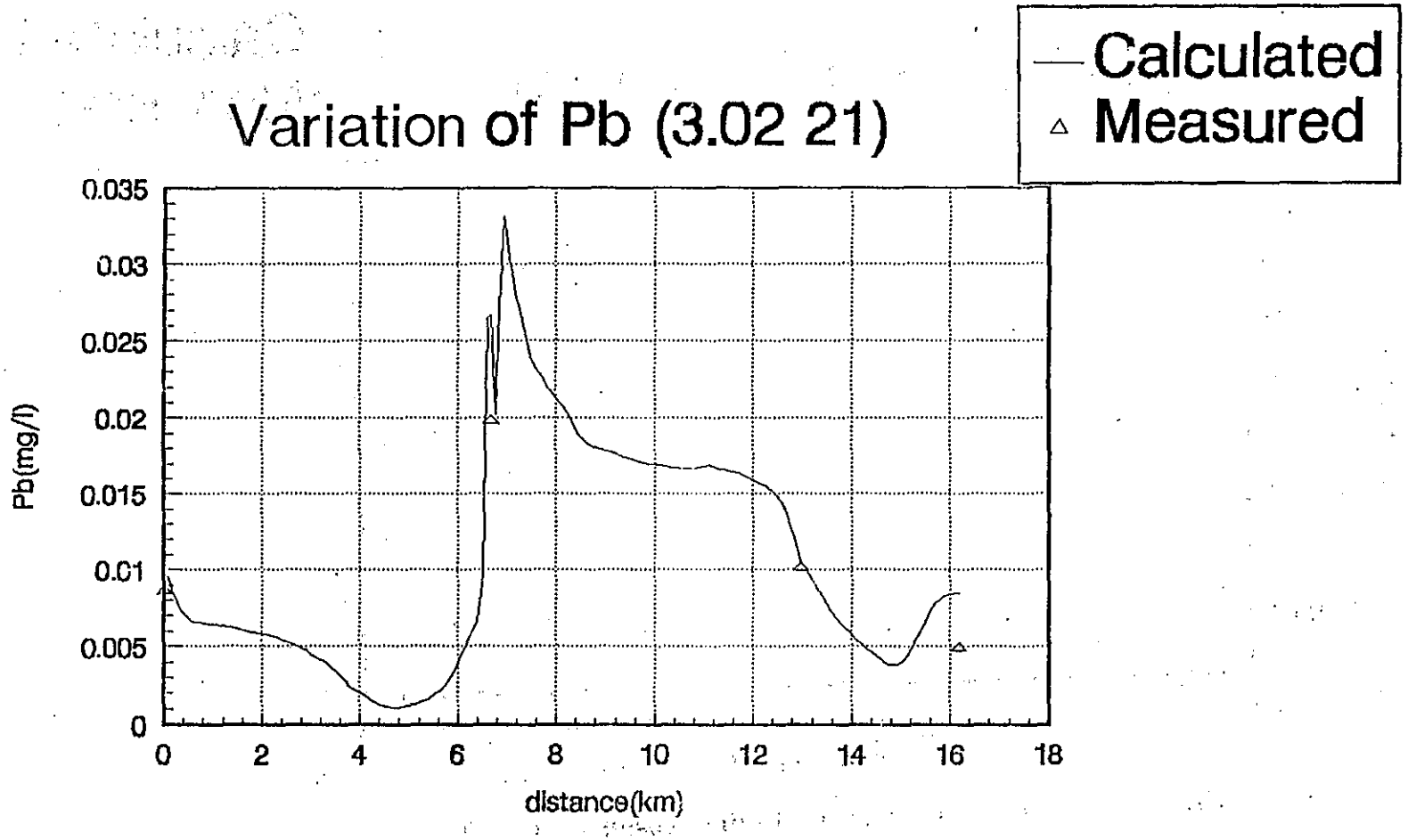

FIG. A7—55(d) Pb variation in dry season (3. 02 21)

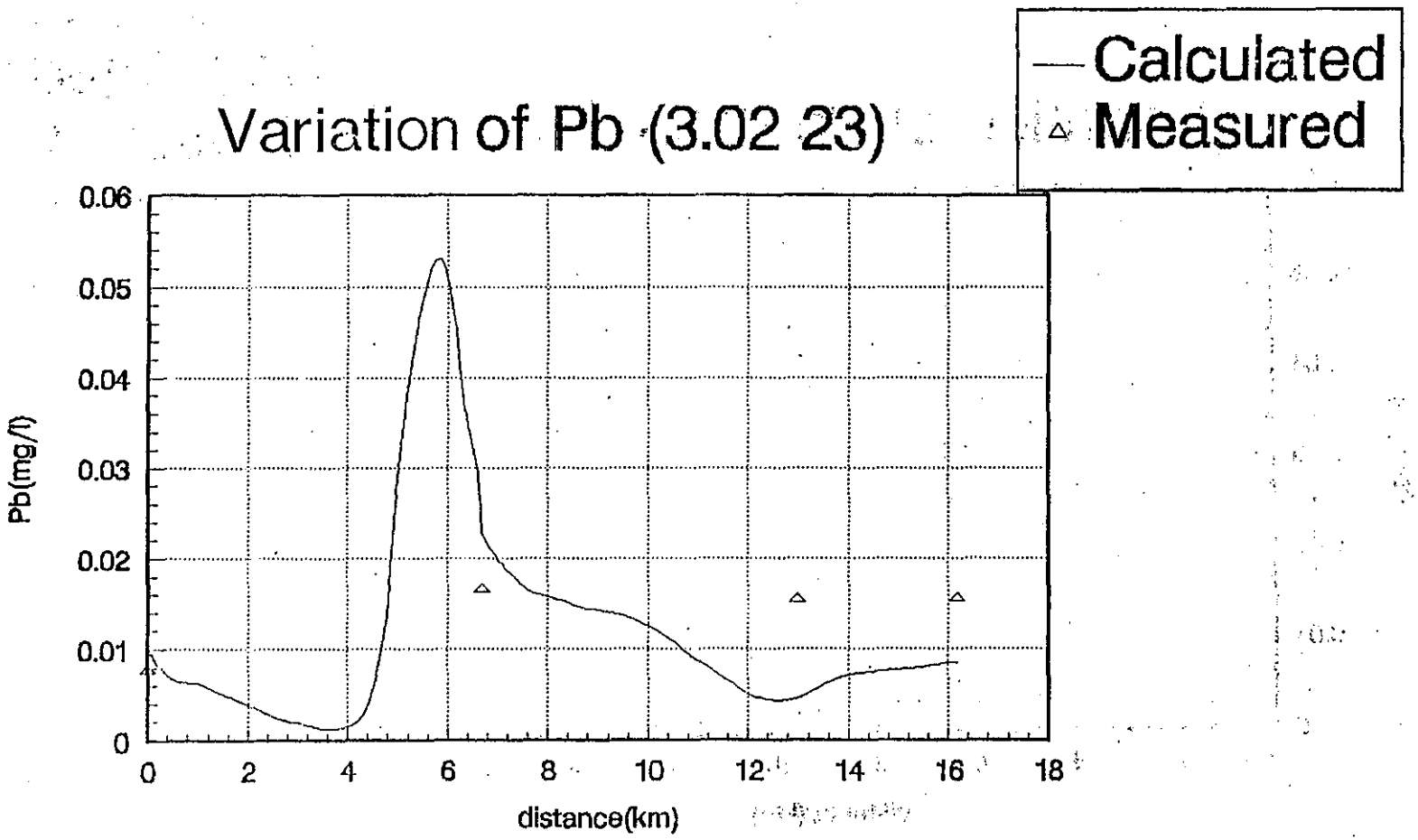

FIG. A7—55(e) Pb variation in dry season (3.02'23)

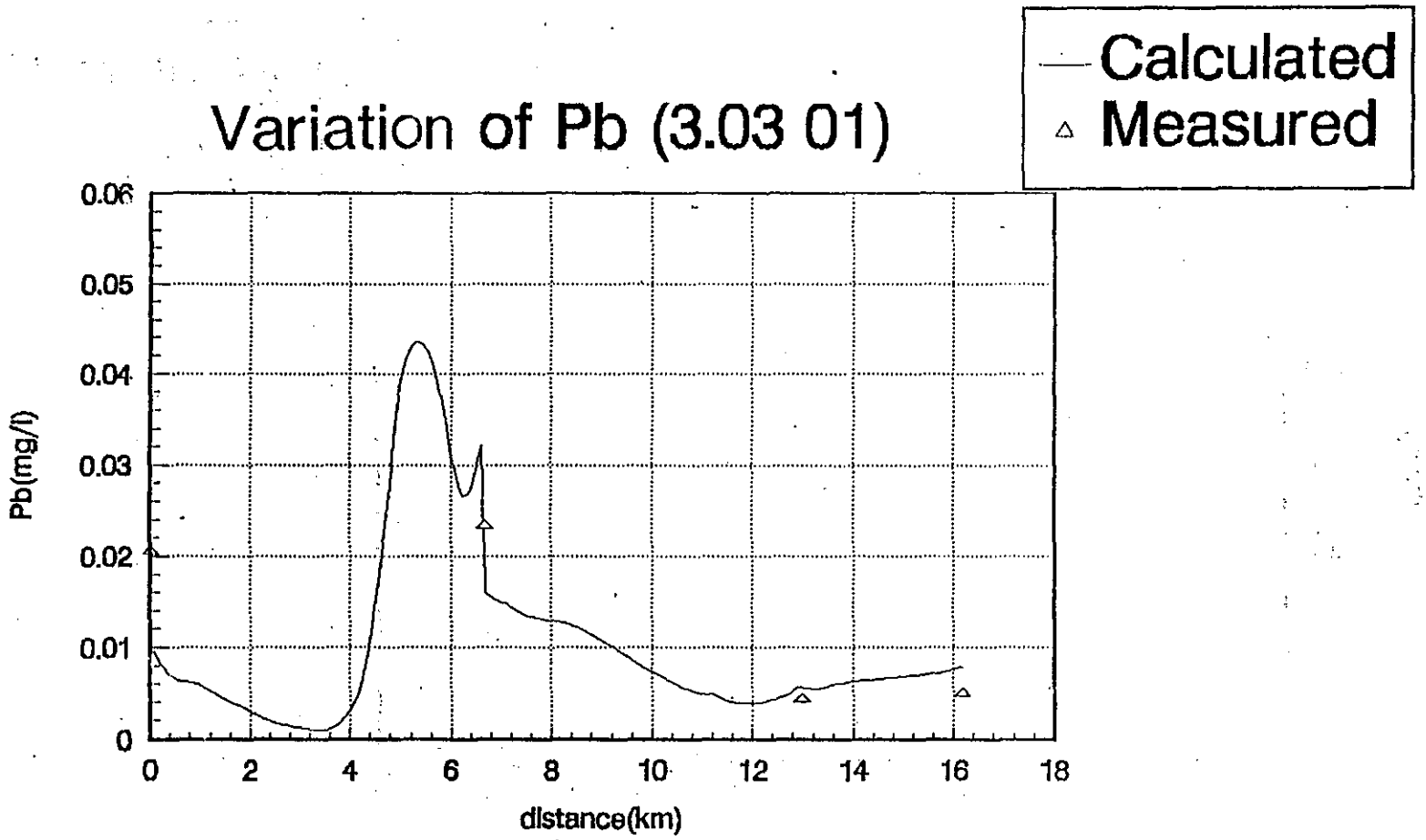

FIG. A7－55(f)　Pb variation in dry season (3. 03 01)

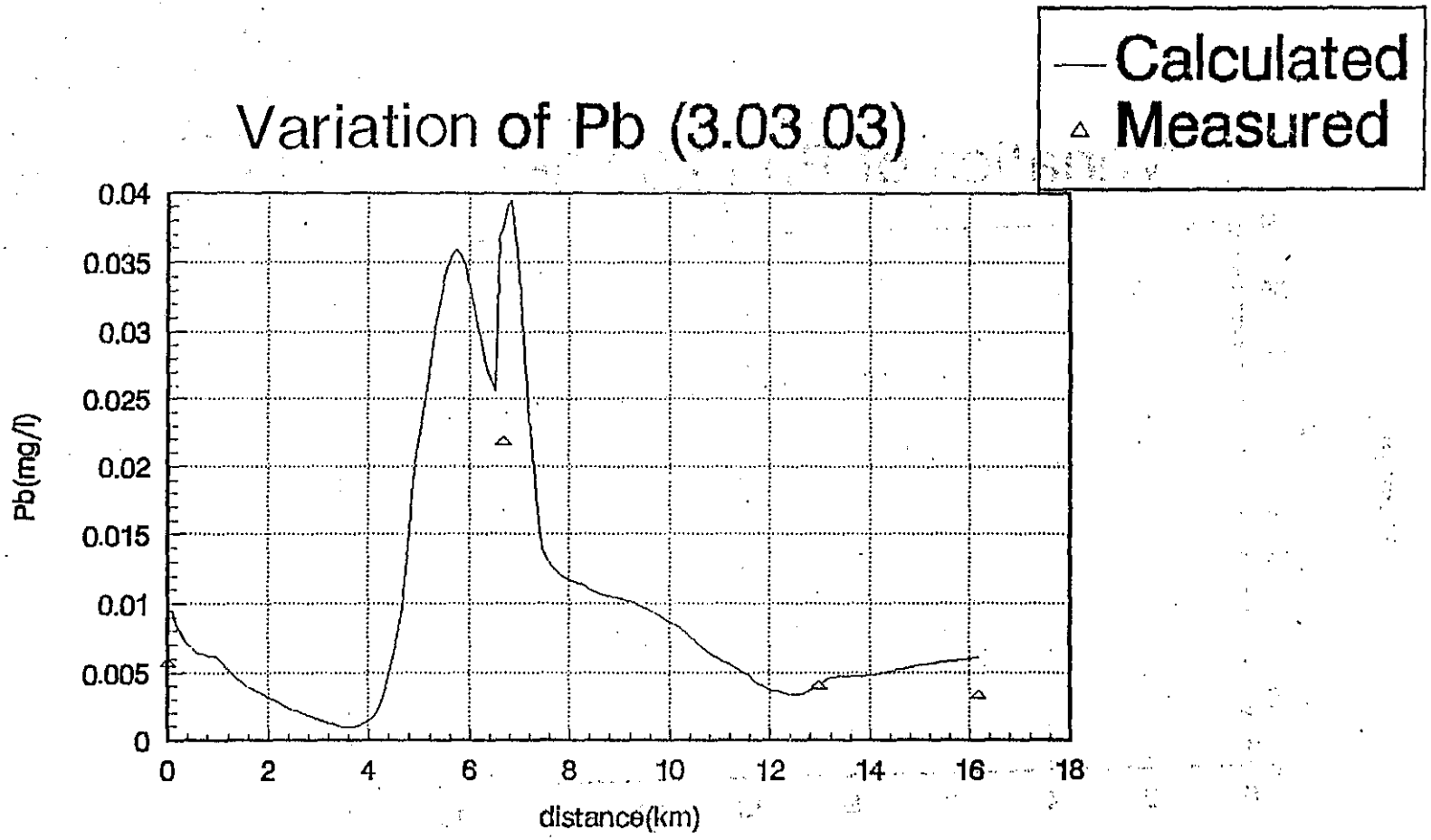

FIG. A7—55(g) Pb variation in dry season (3. 03 03)

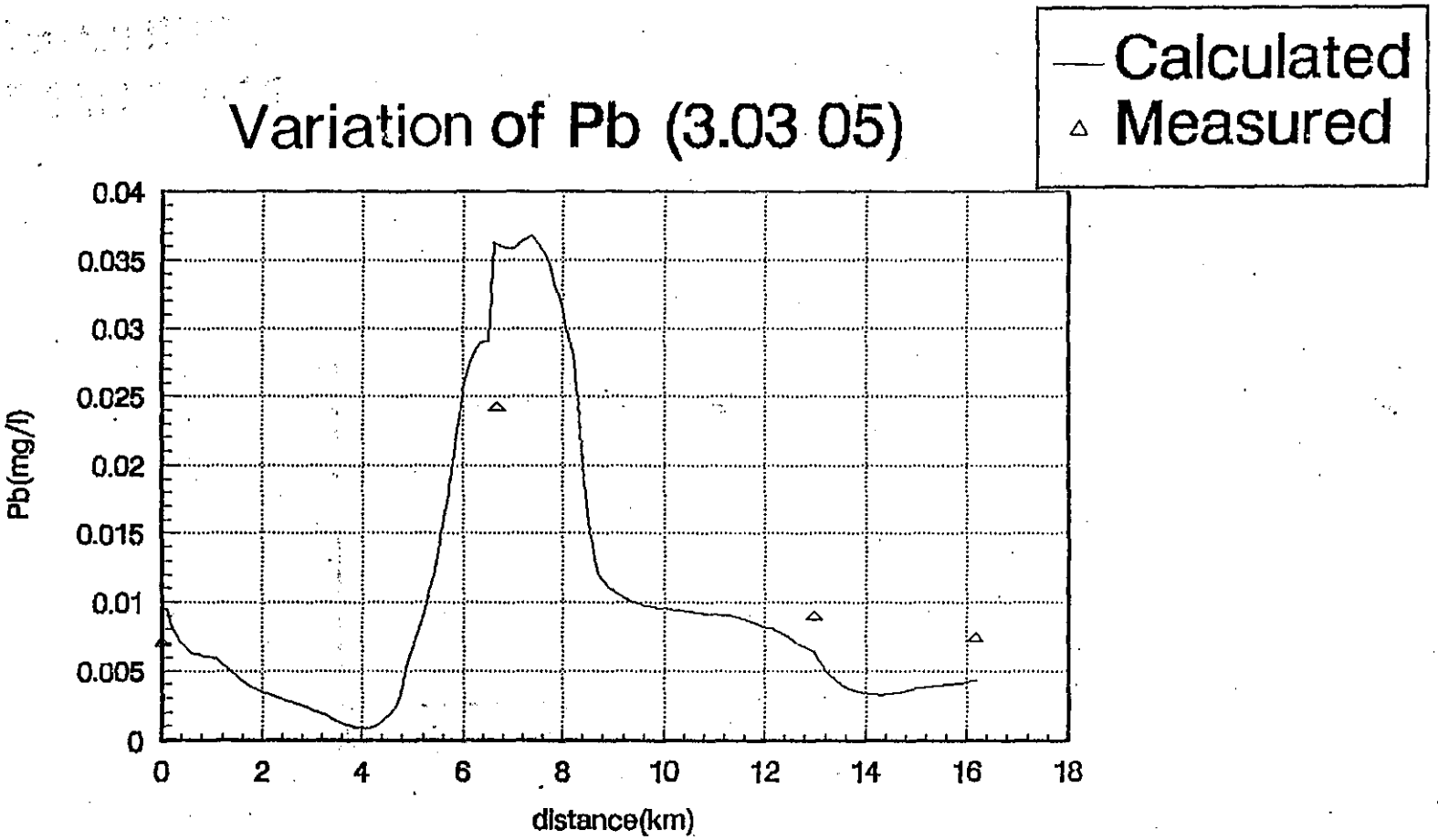

FIG. A7—55(h) Pb variation in dry season (3. 03 05)

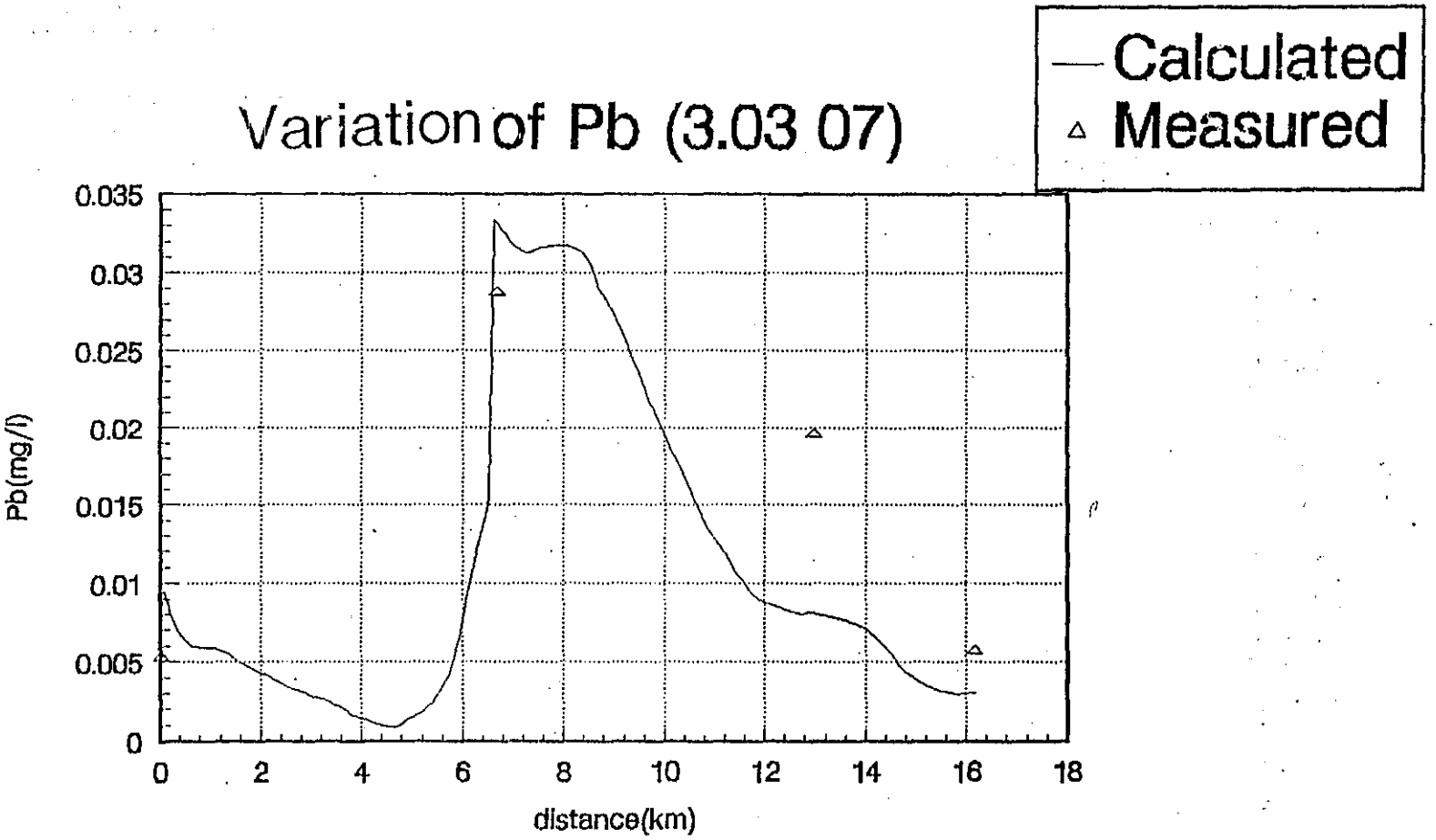

FIG. A7—55(i) Pb variation in dry season (3. 03 07)

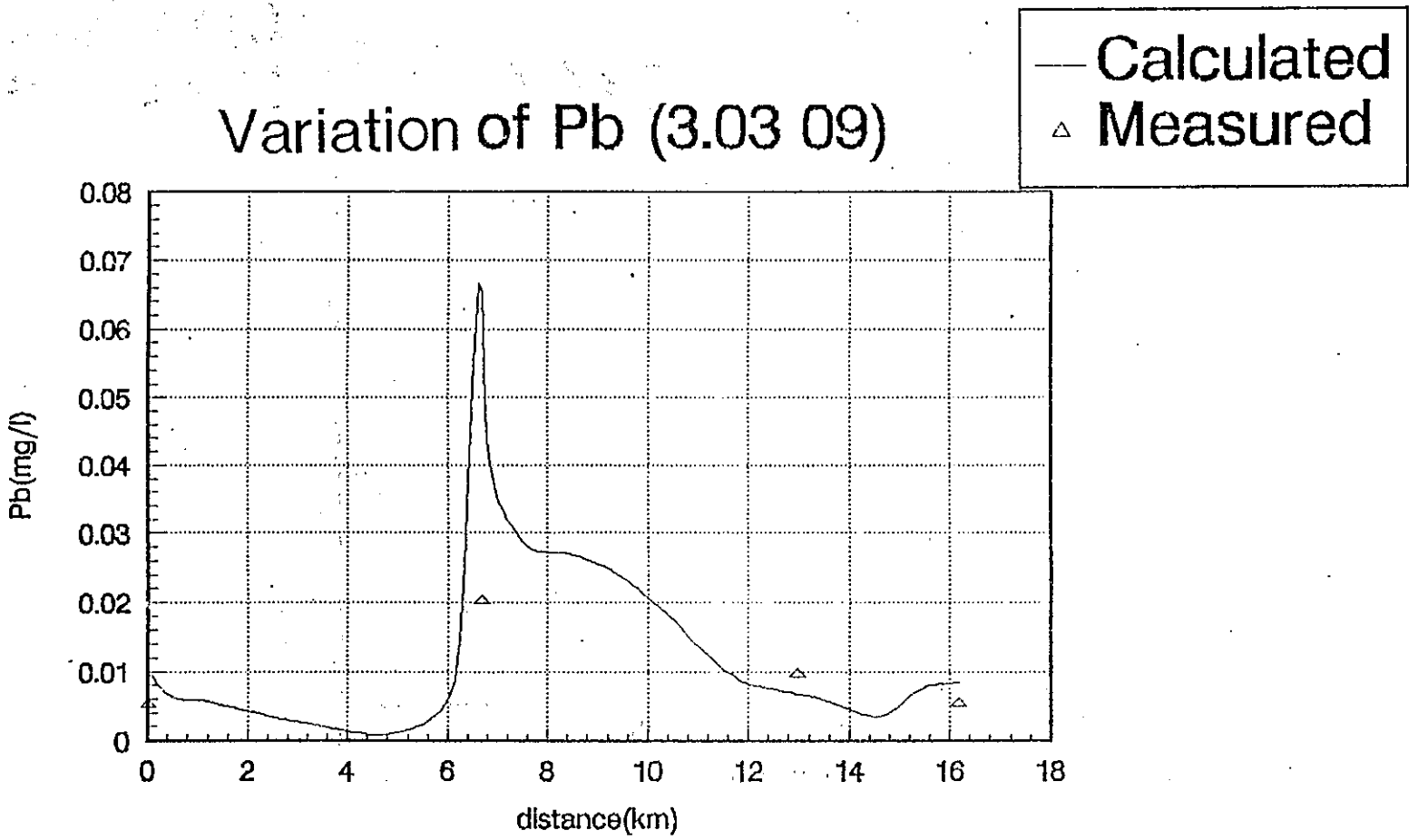

FIG. A7－55(j) Pb variation in dry season (3. 03 09)

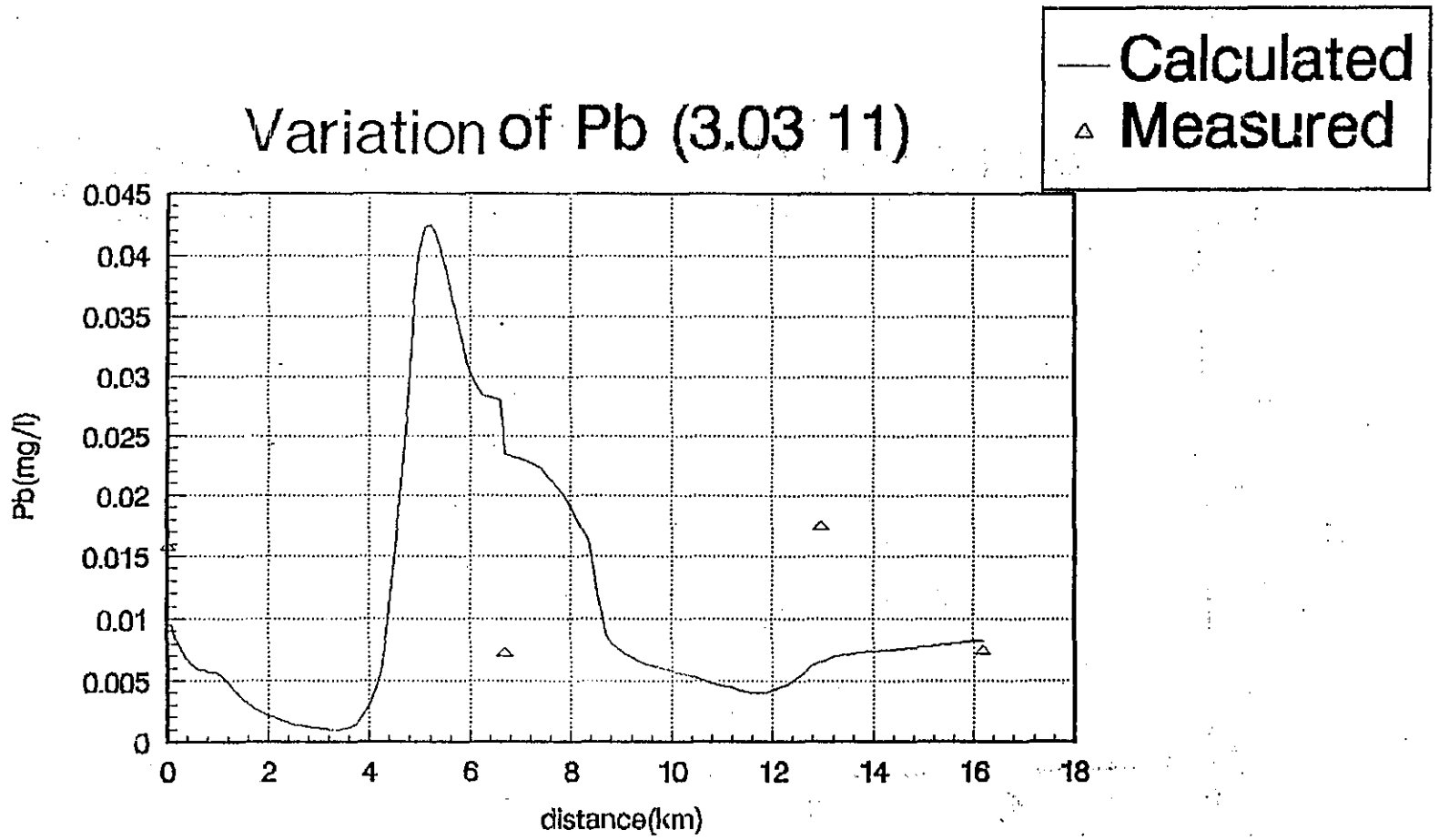

FIG. A7－55(k)　Pb variation in dry season (3.03 11)

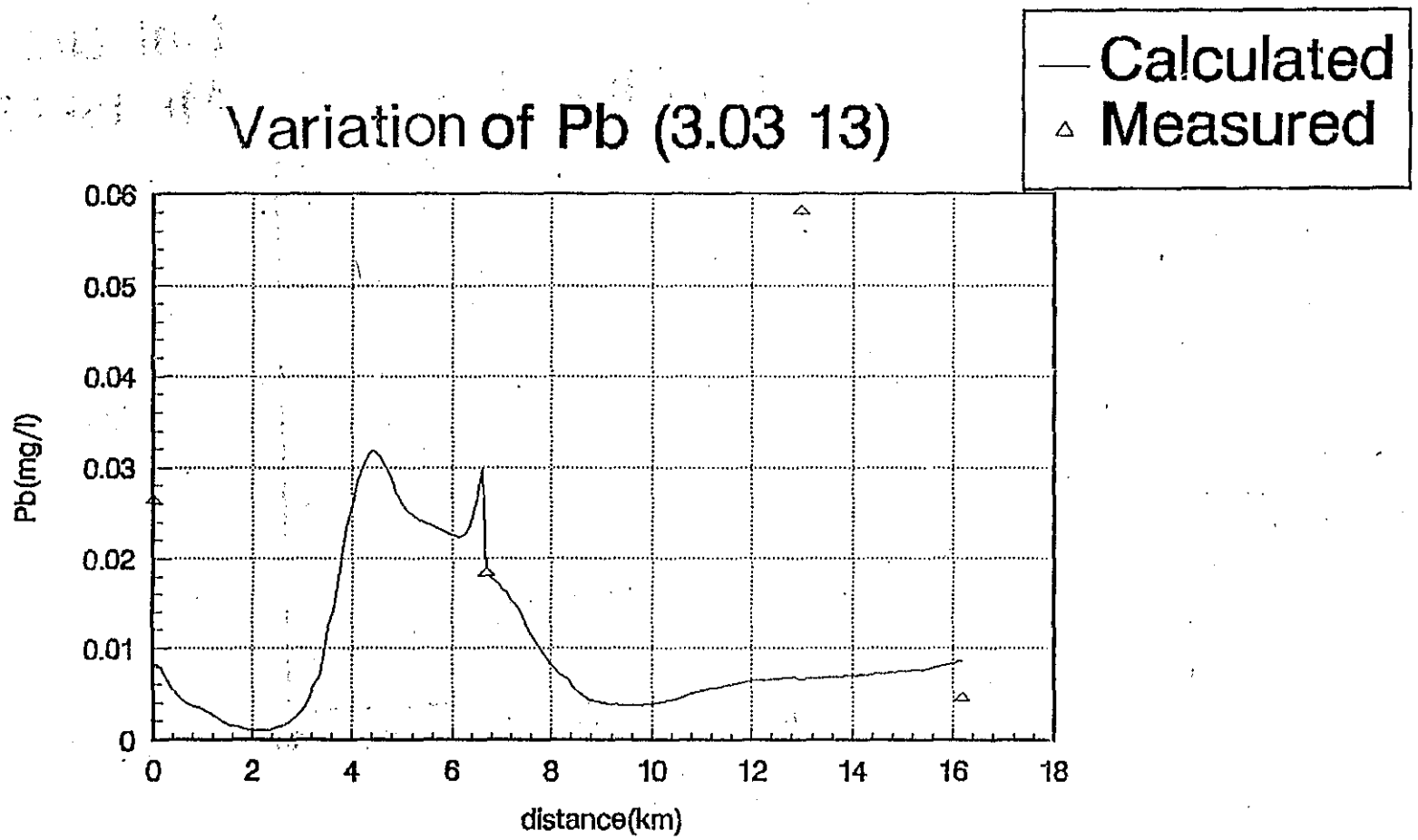

FIG. A7—55(1) Pb variation in dry season (3.03 13)

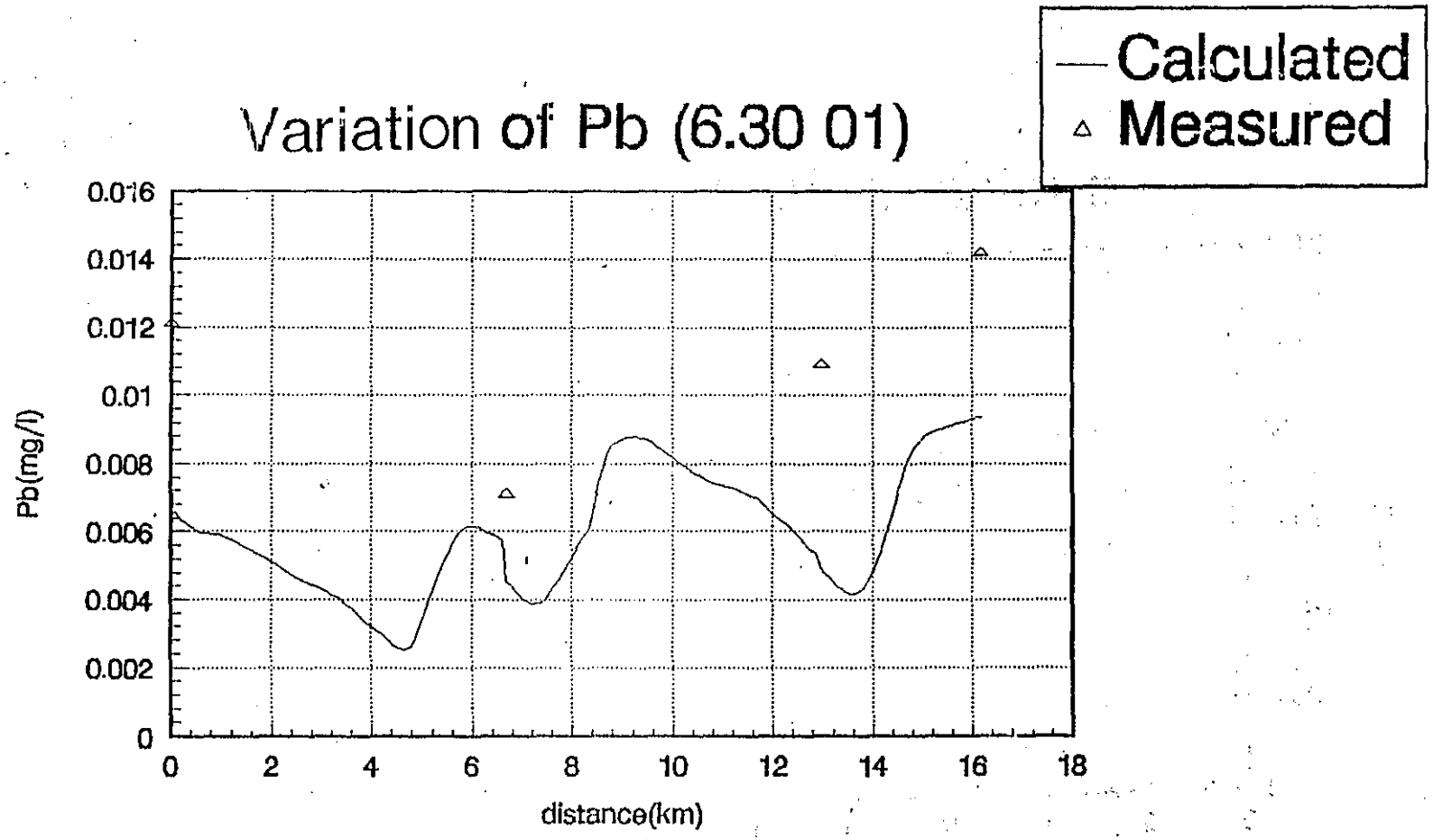

FIG. A7－55(m) Pb variation in wet season (6. 30 01)

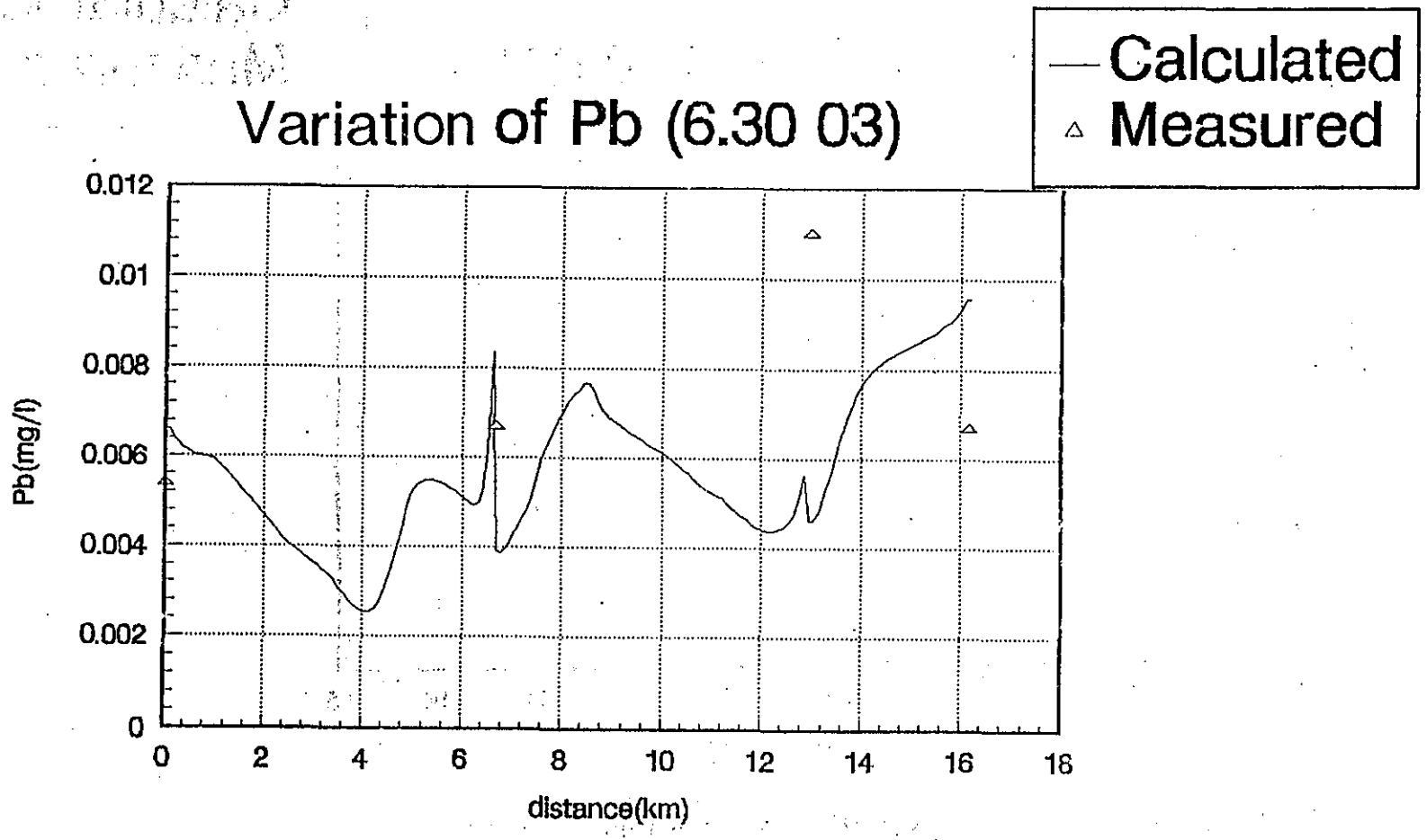

FIG. A7—55(n) Pb variation in wet season (6. 30 03)

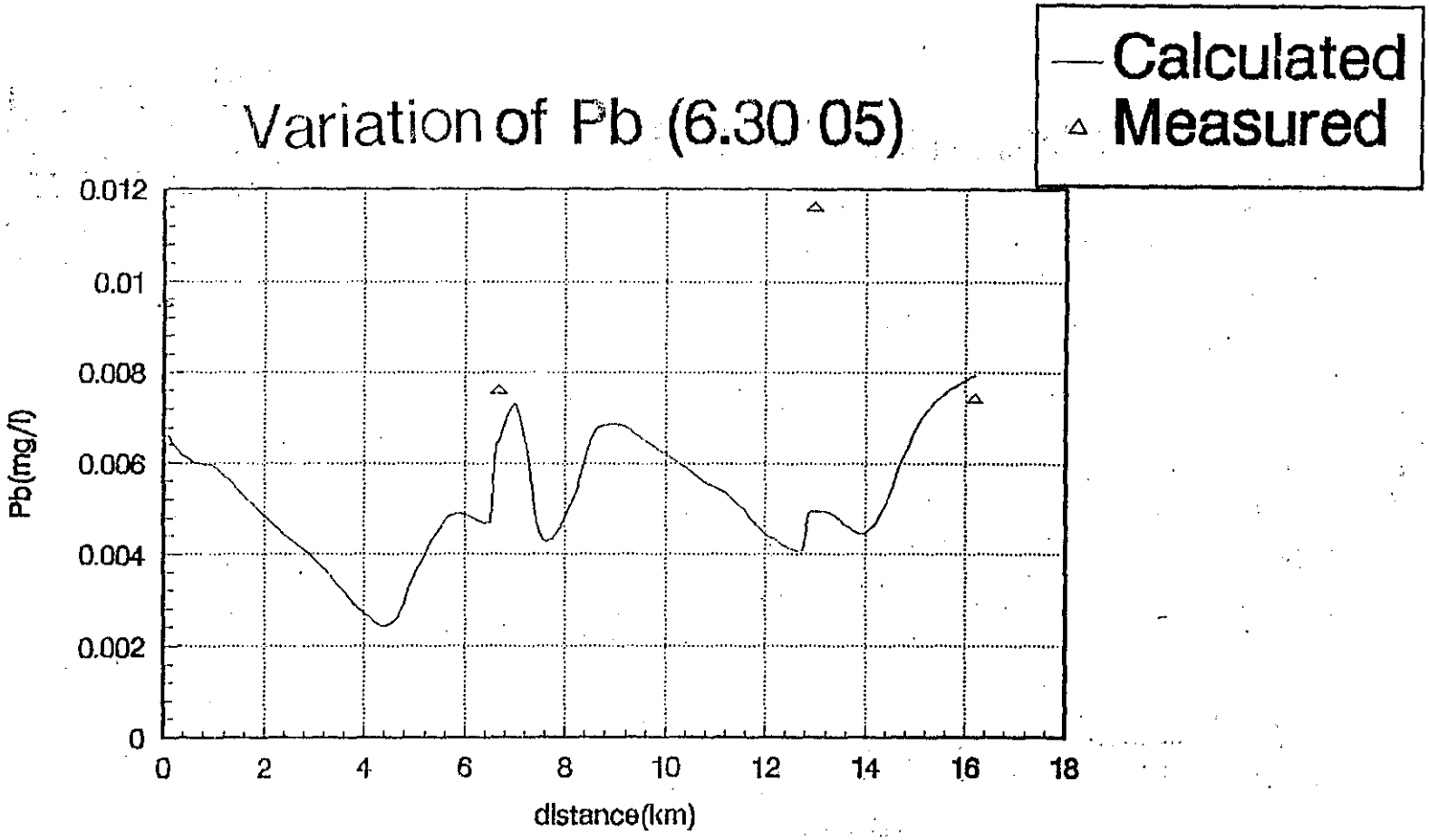

FIG. A7—55(o) Pb variation in wet season (6. 30 05)

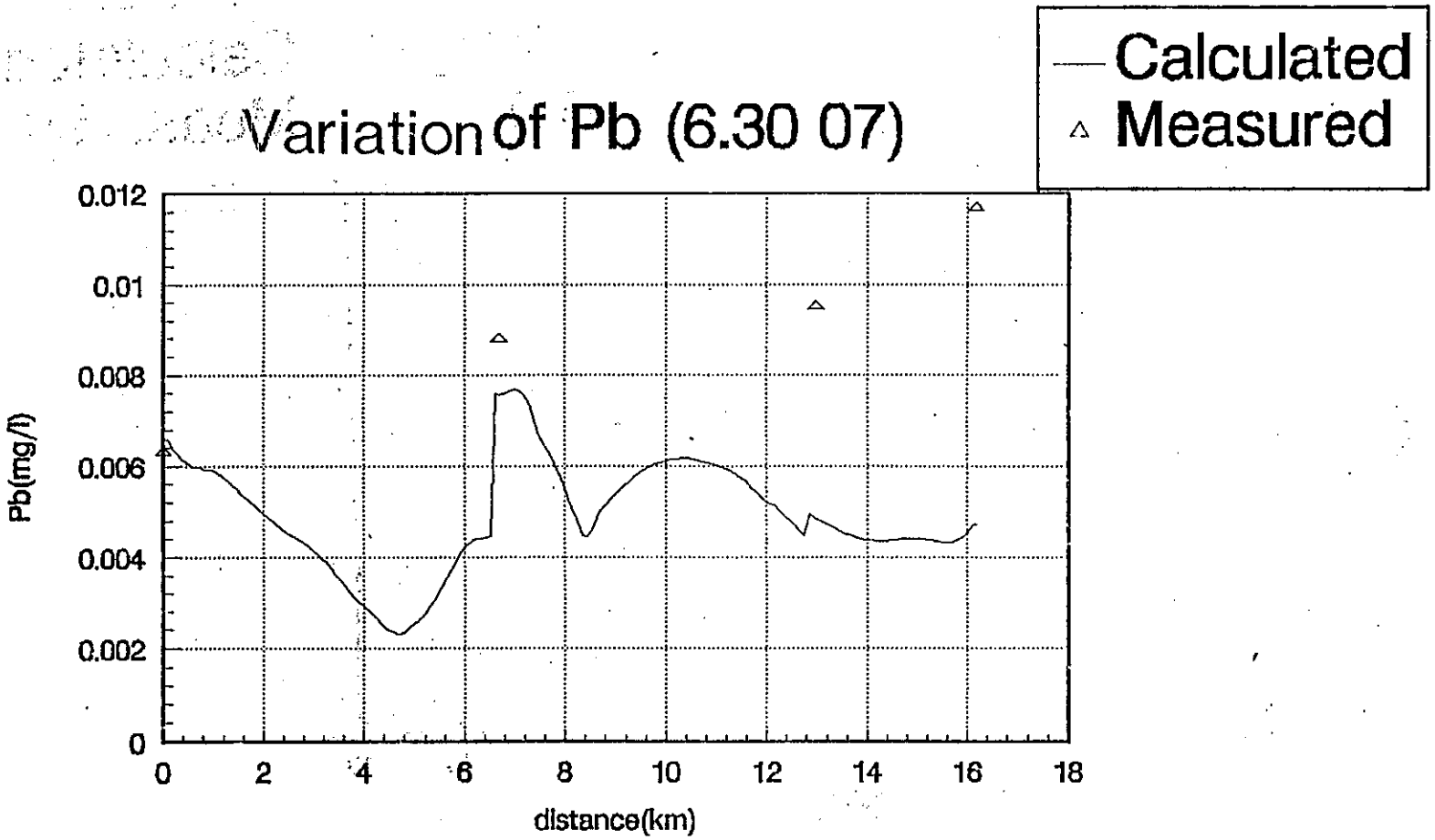

FIG. A7—55(p) Pb variation in wet season (6. 30 07)

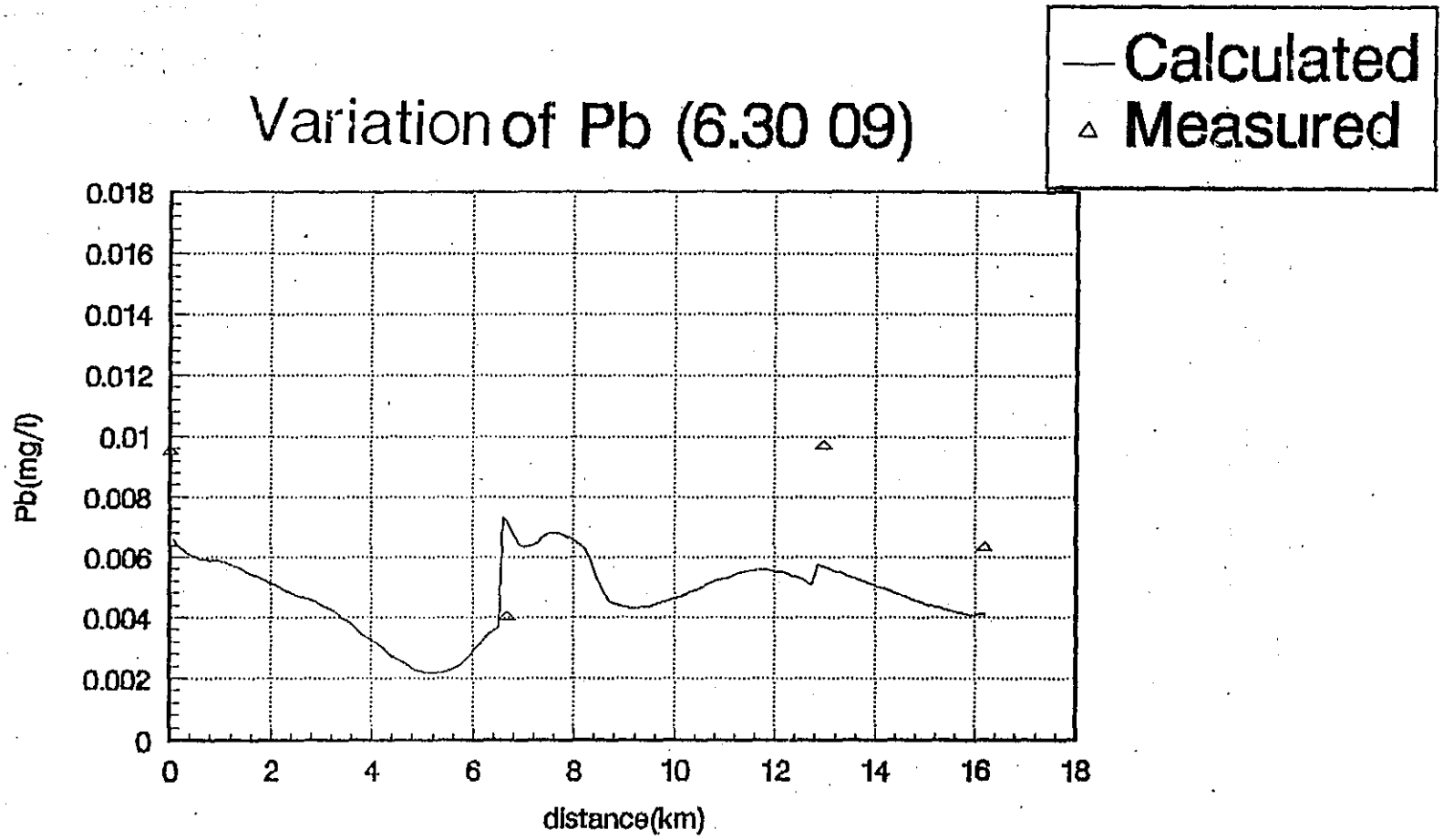

FIG. A7－55(q)　Pb variation in wet season (6. 30 09)

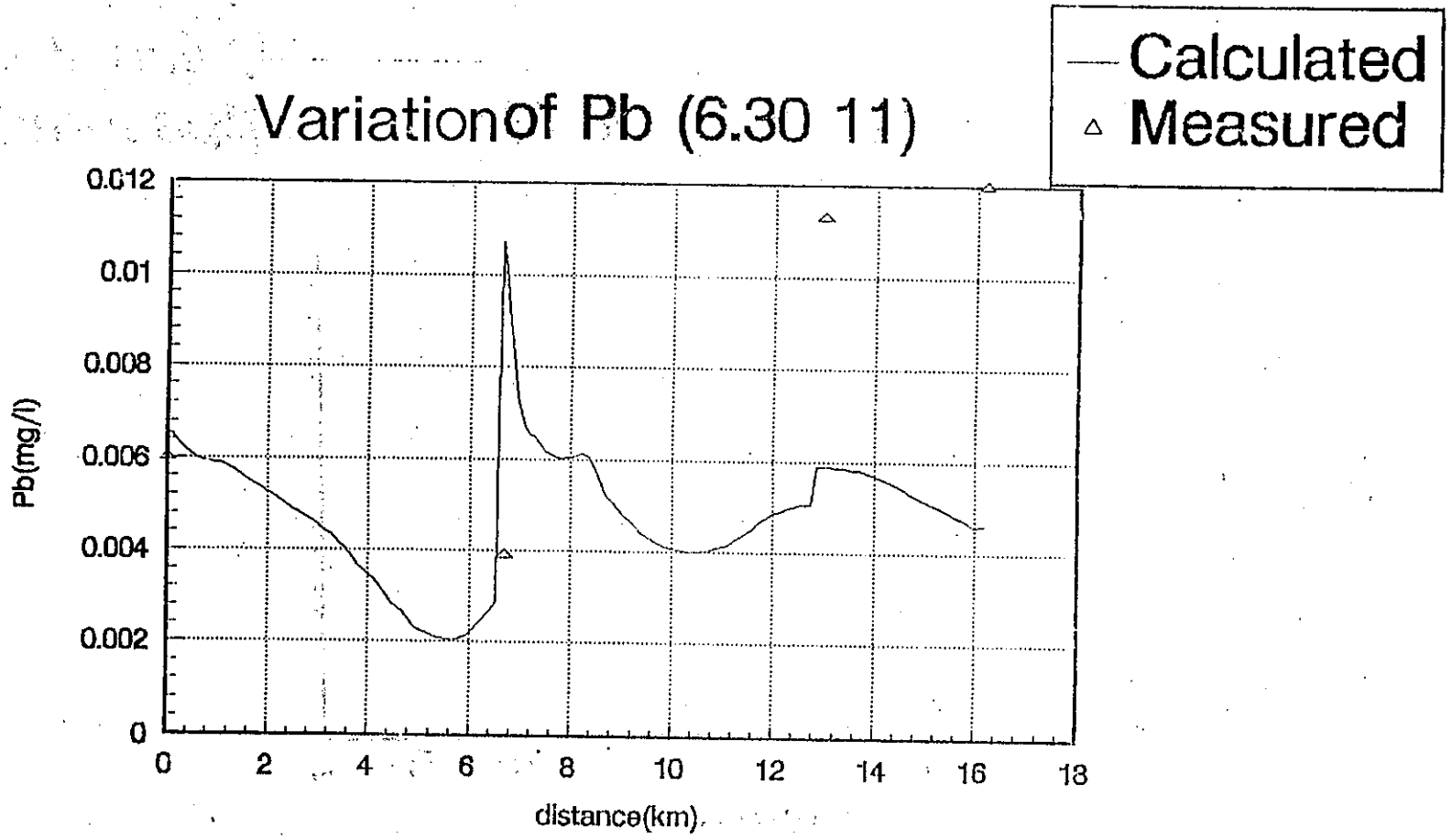

FIG. A7—55(r) Pb variation in wet season (6. 30 11)

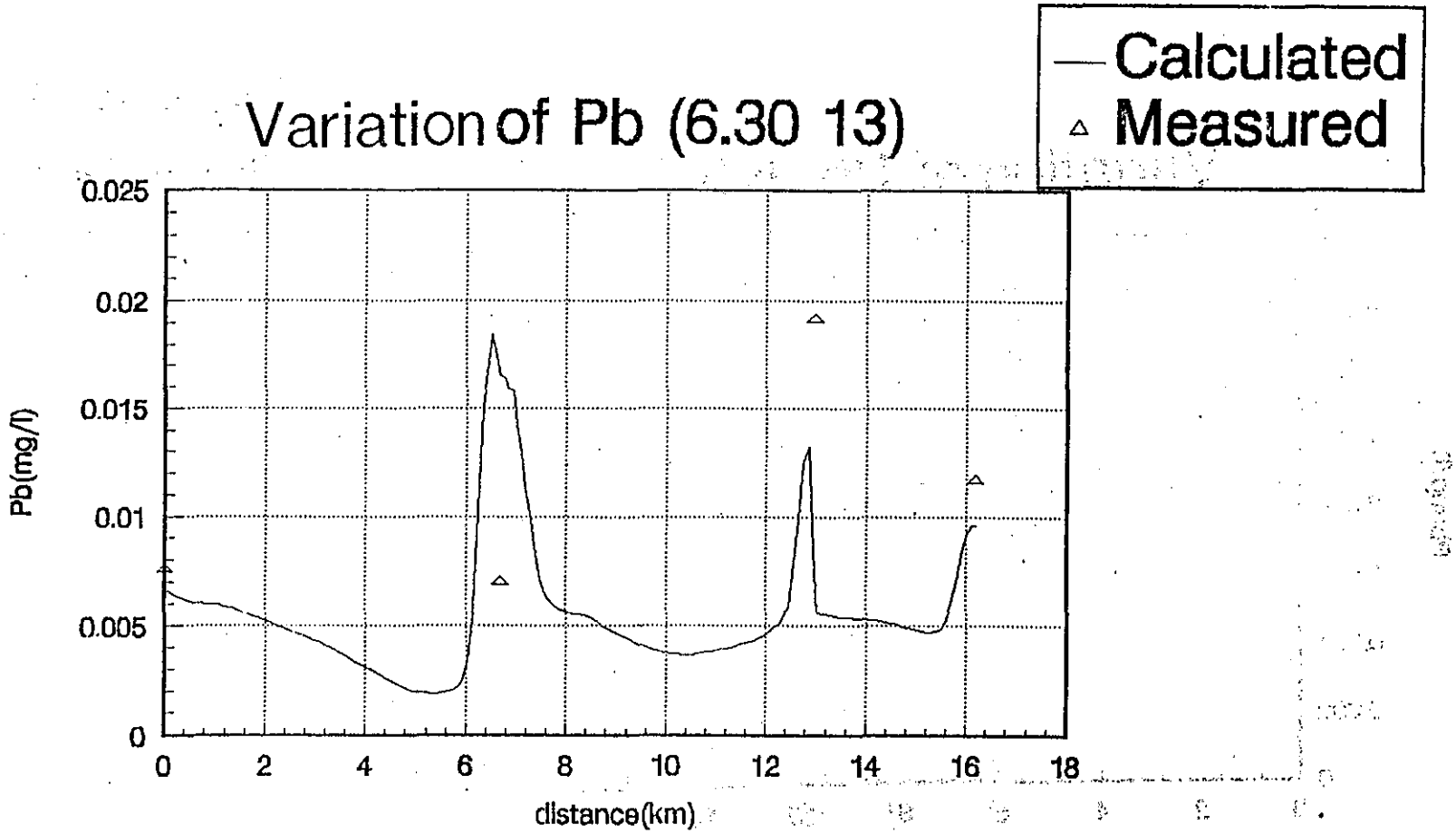

FIG. A7—55(s) Pb variation in wet season (6. 30 13)

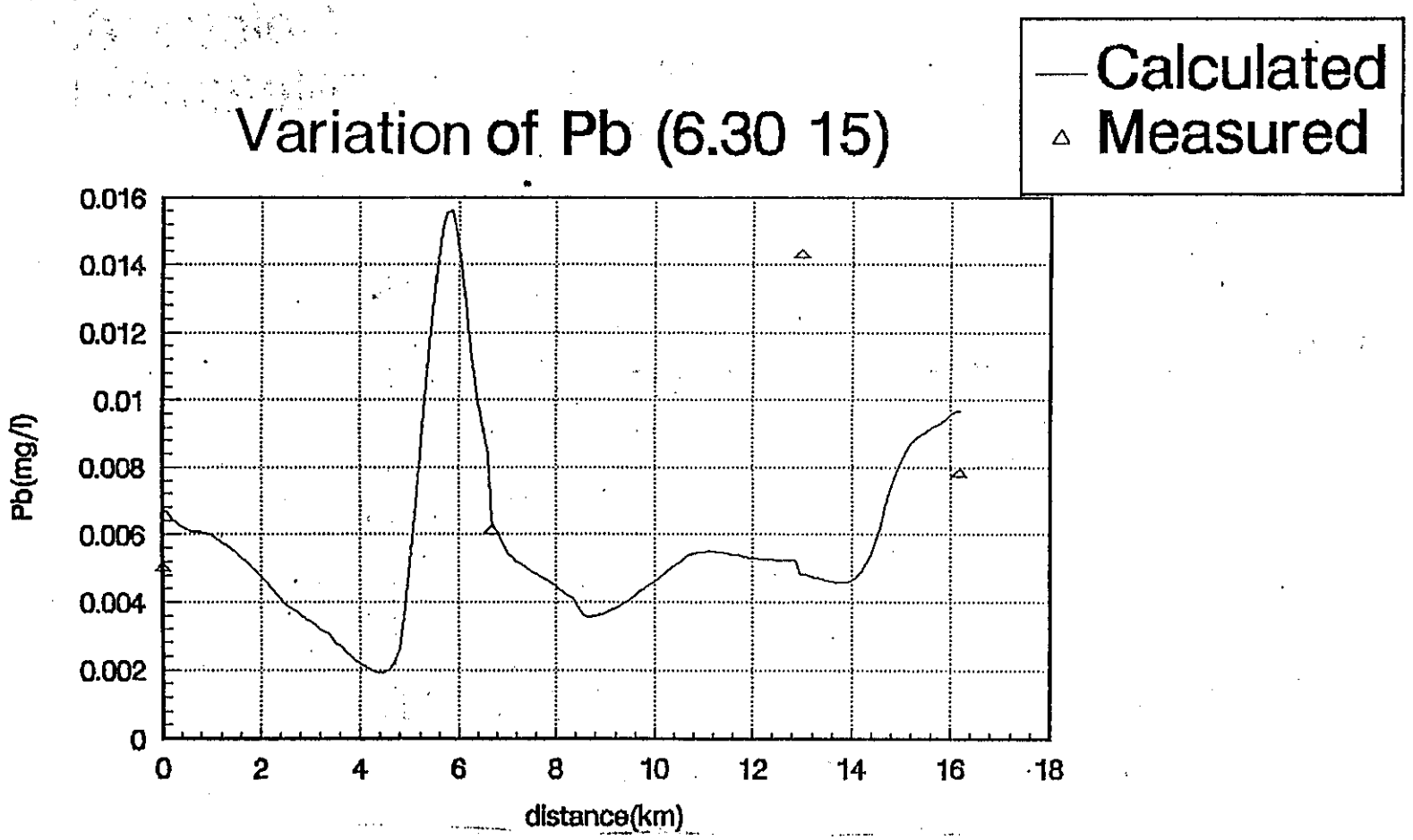

FIG. A7—55(t) Pb variation in wet season (6. 30 15)

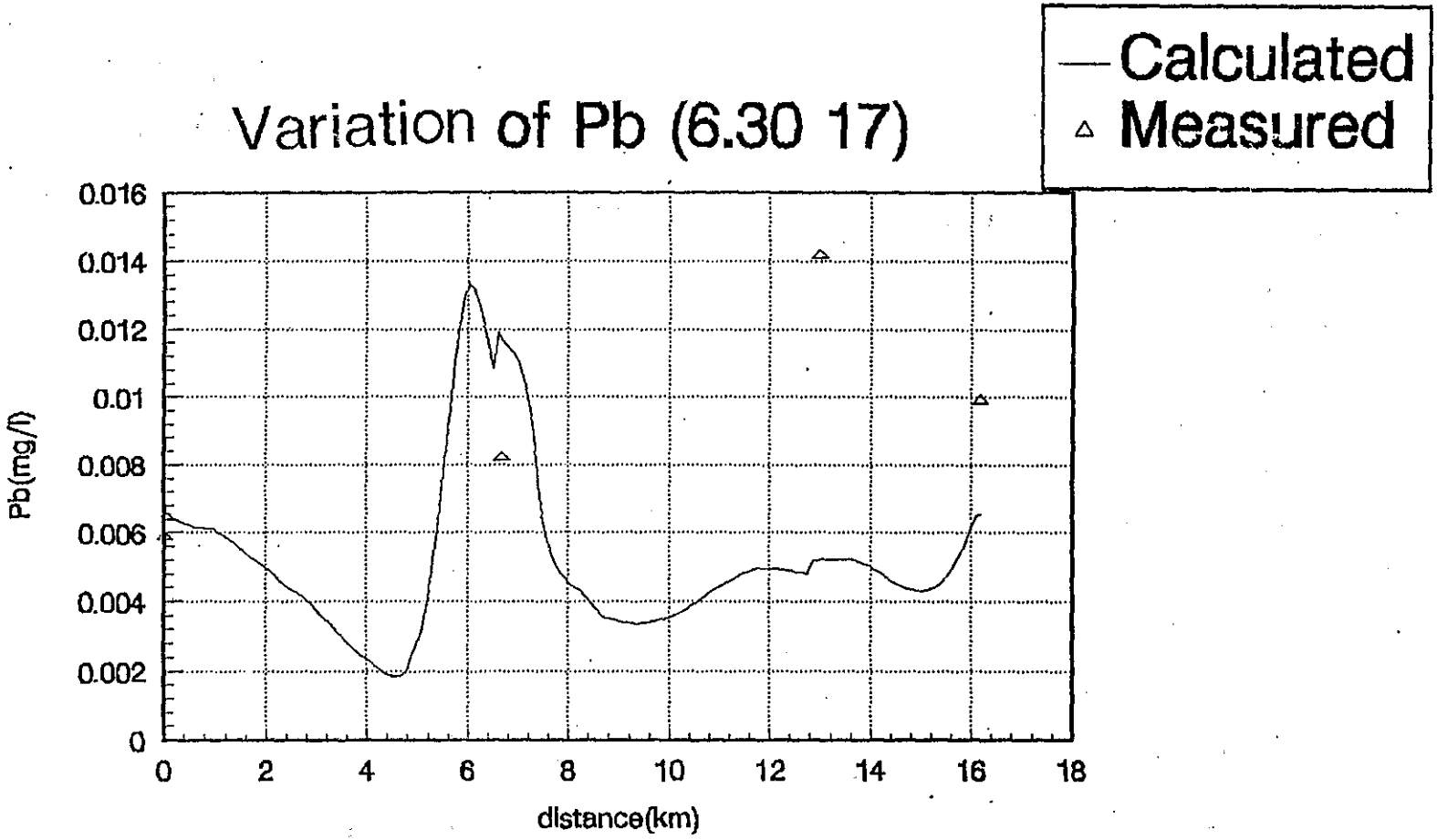

FIG. A7—55(u) Pb variation in wet season (6. 30 17)

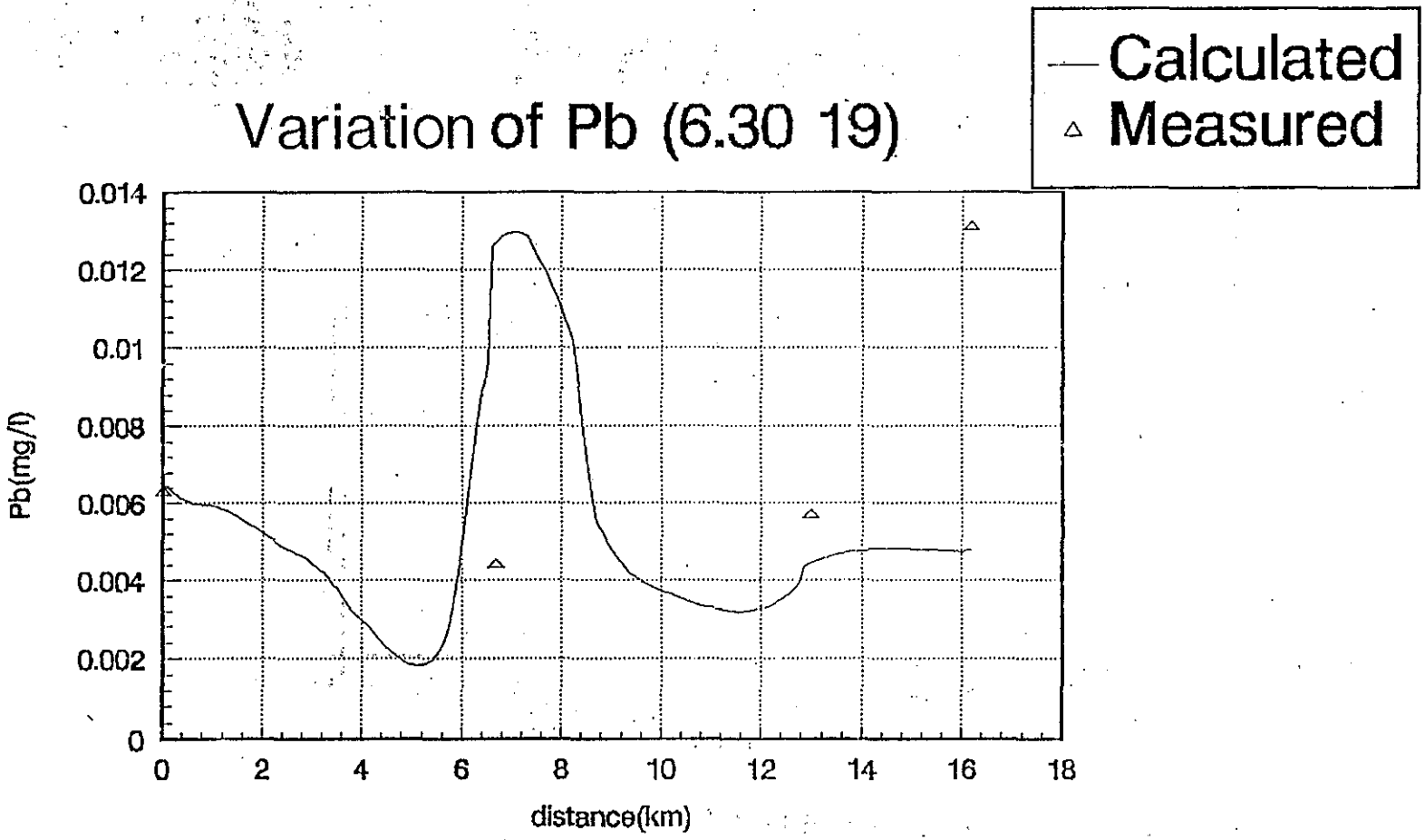

FIG. A7—55(v) Pb variation in wet season (6. 30 19)

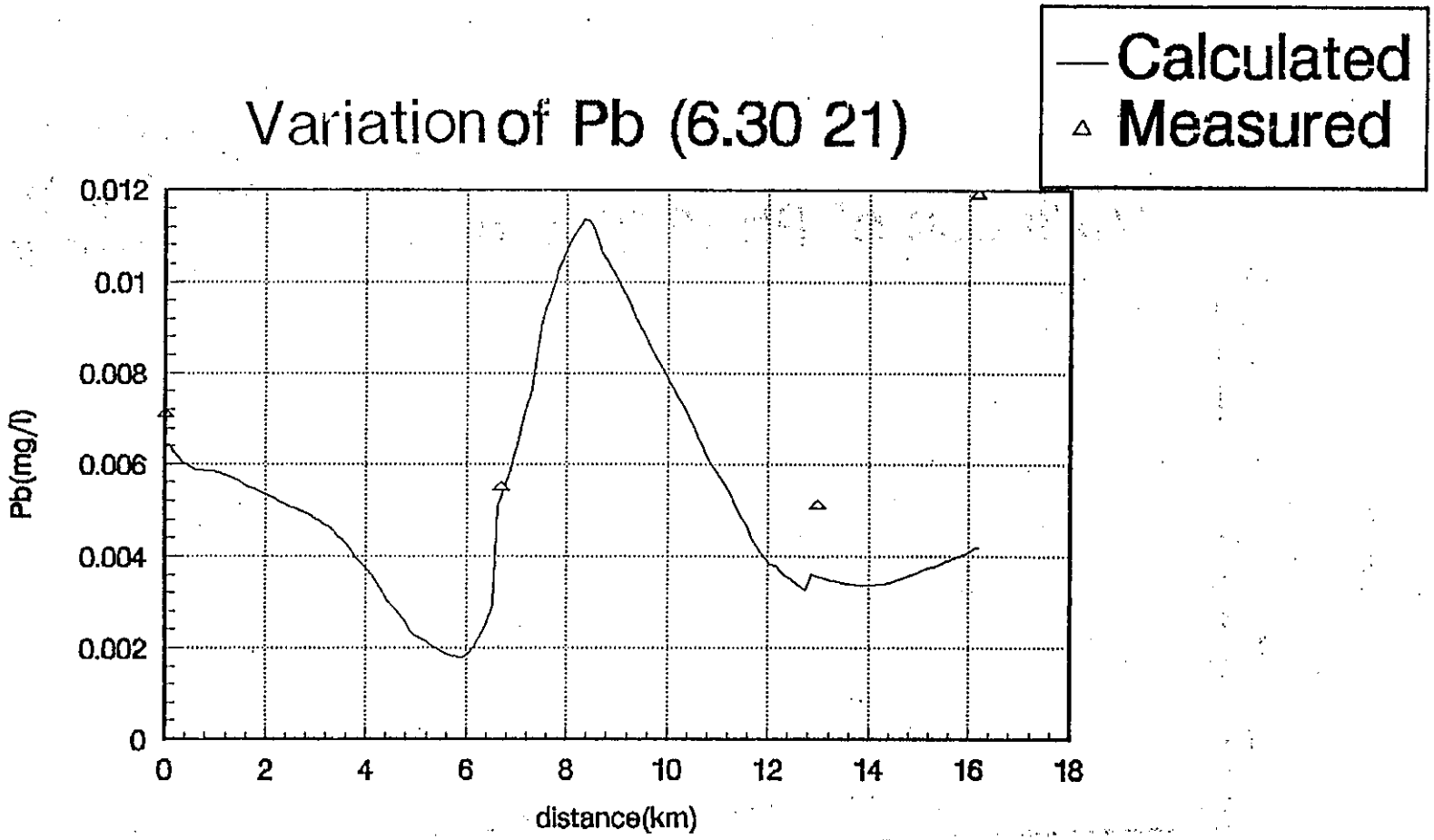

FIG. A7－55(w)　**Pb variation in wet season** (6. 30 21)

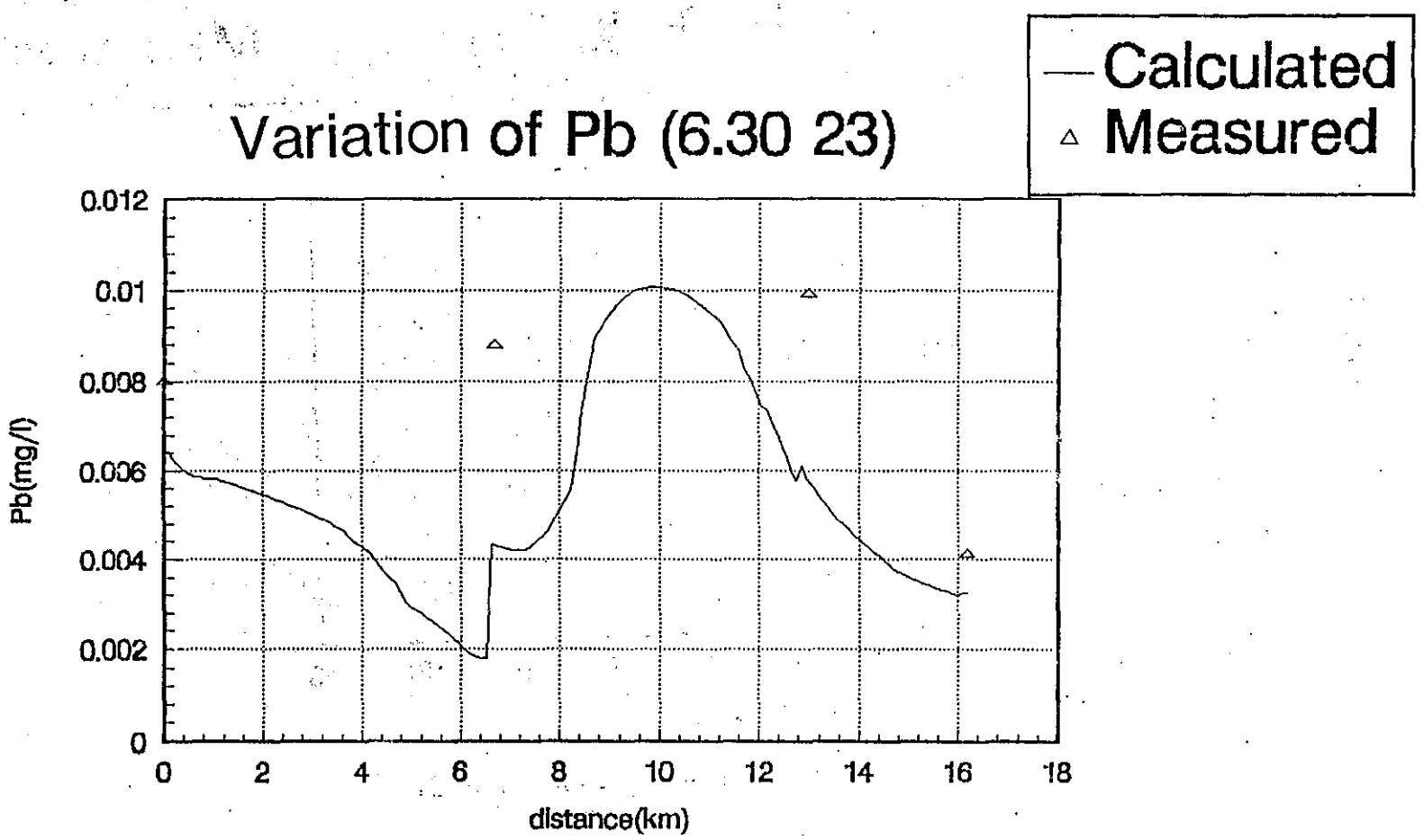

FIG. A7−55(x) Pb variation in wet season (6. 30 23)

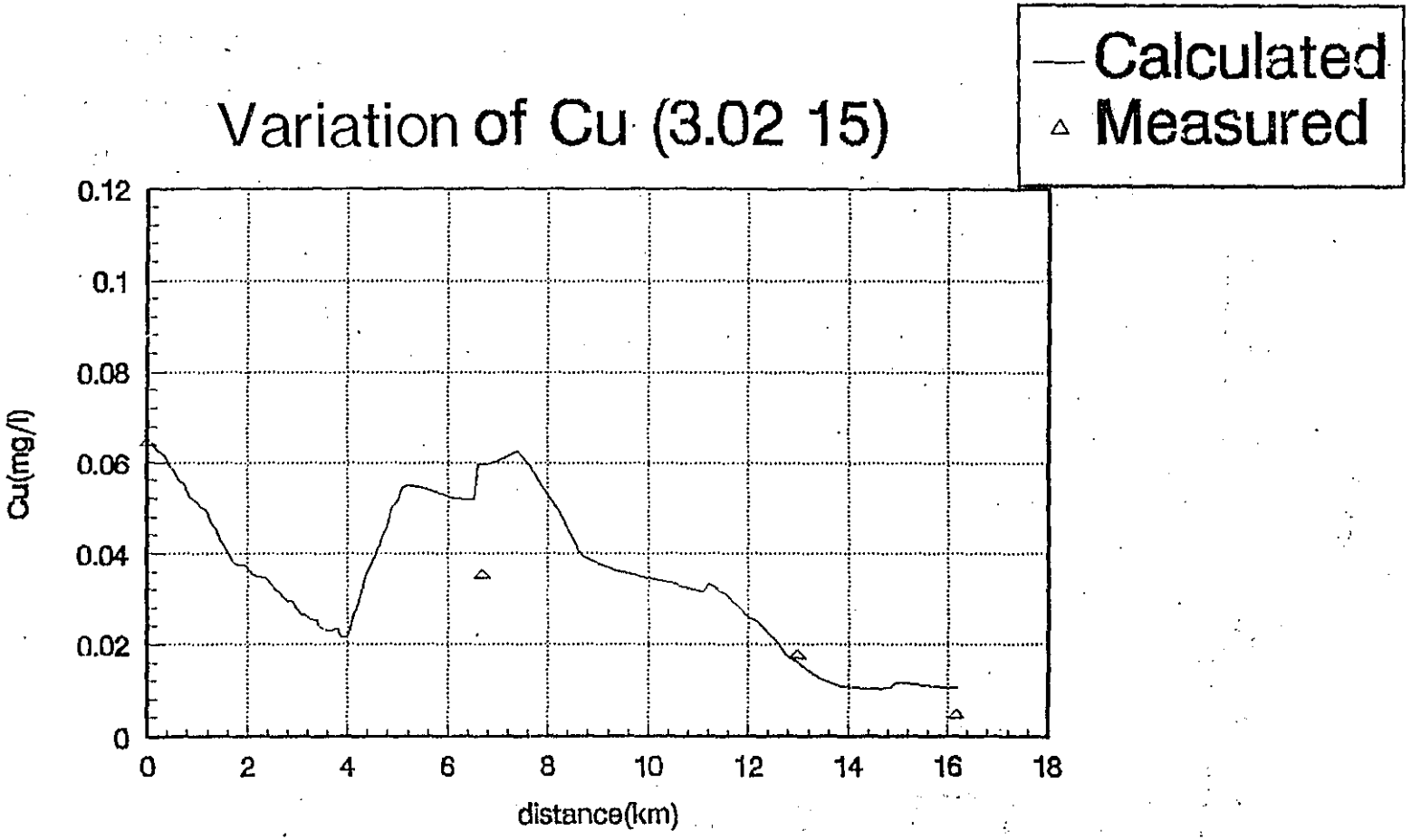

FIG. A7—56(a) Cu variation in dry season (3. 02 15)

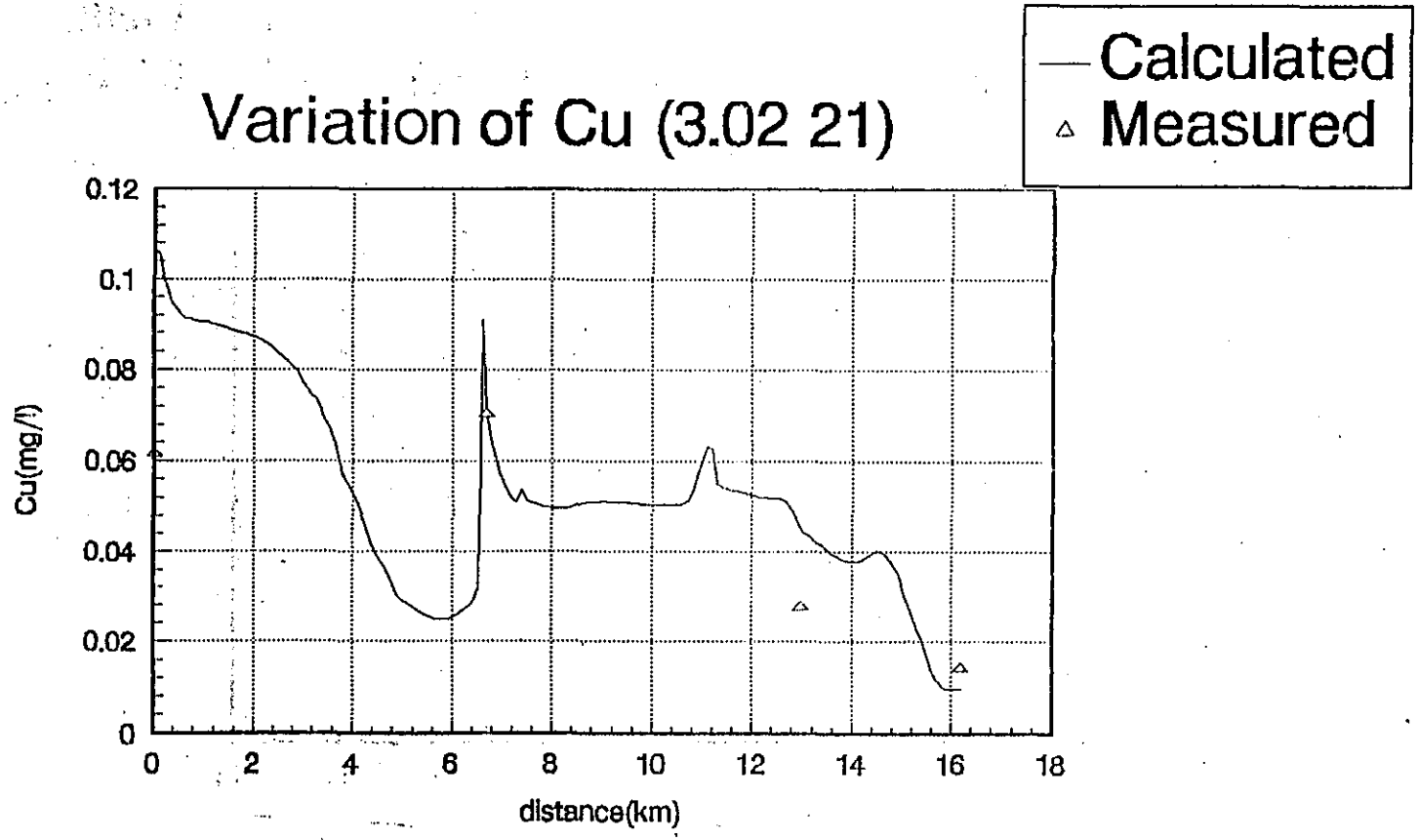

FIG. A7—56(d) Cu variation in dry season (3. 02 21)

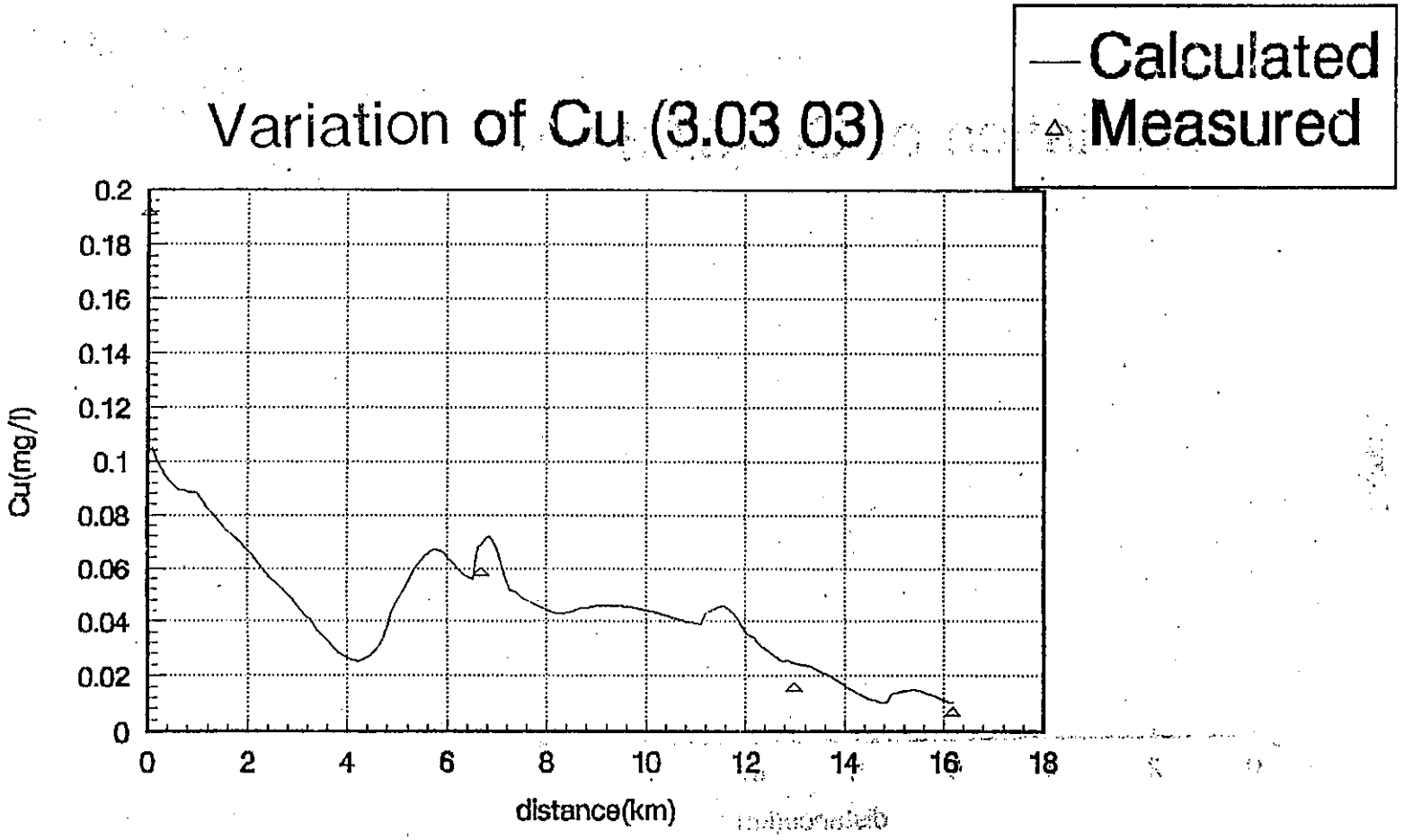

FIG. A7—56(g) Cu variation in dry season (3. 03 03)

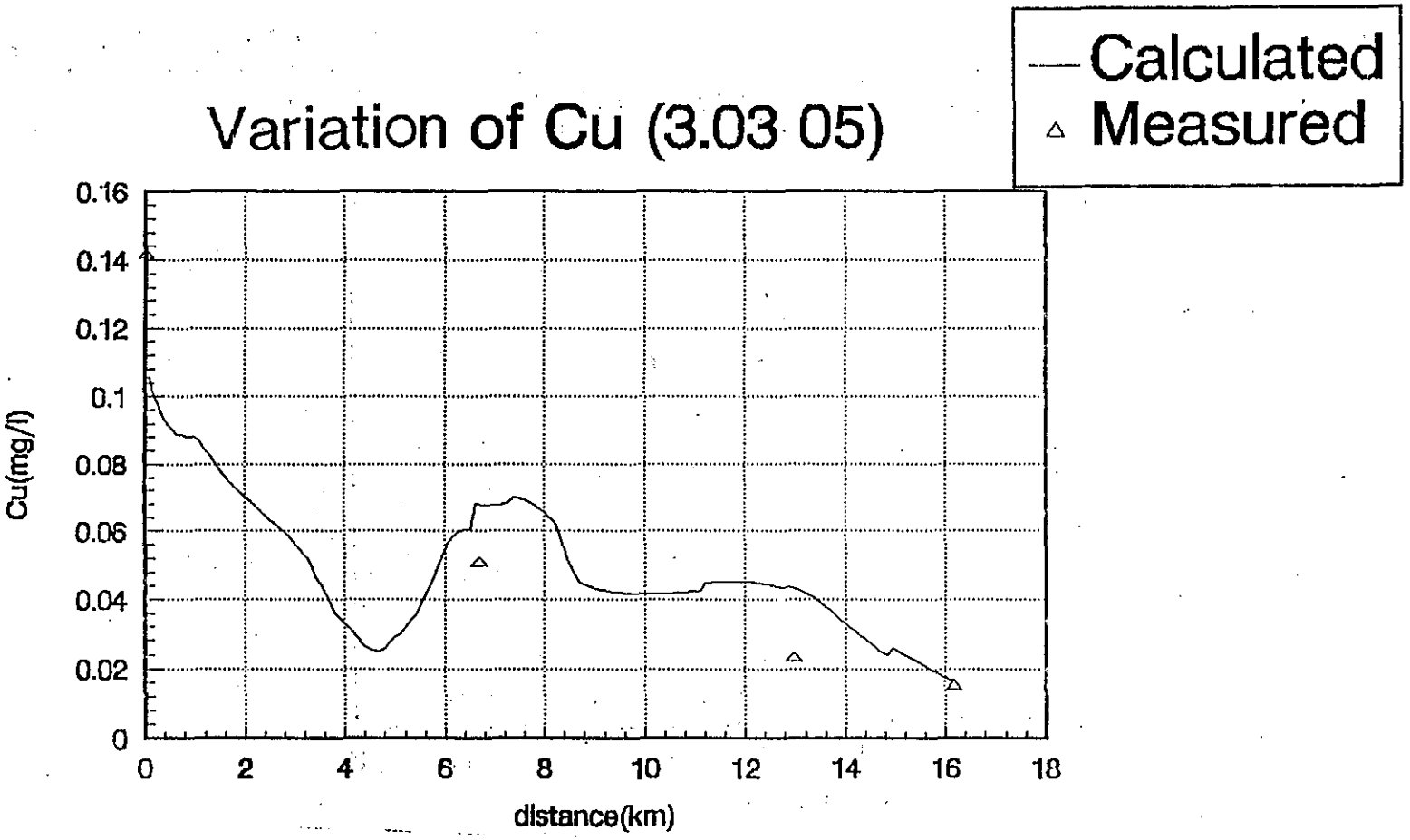

FIG. A7－56(h) Cu variation in dry season (3. 03 05)

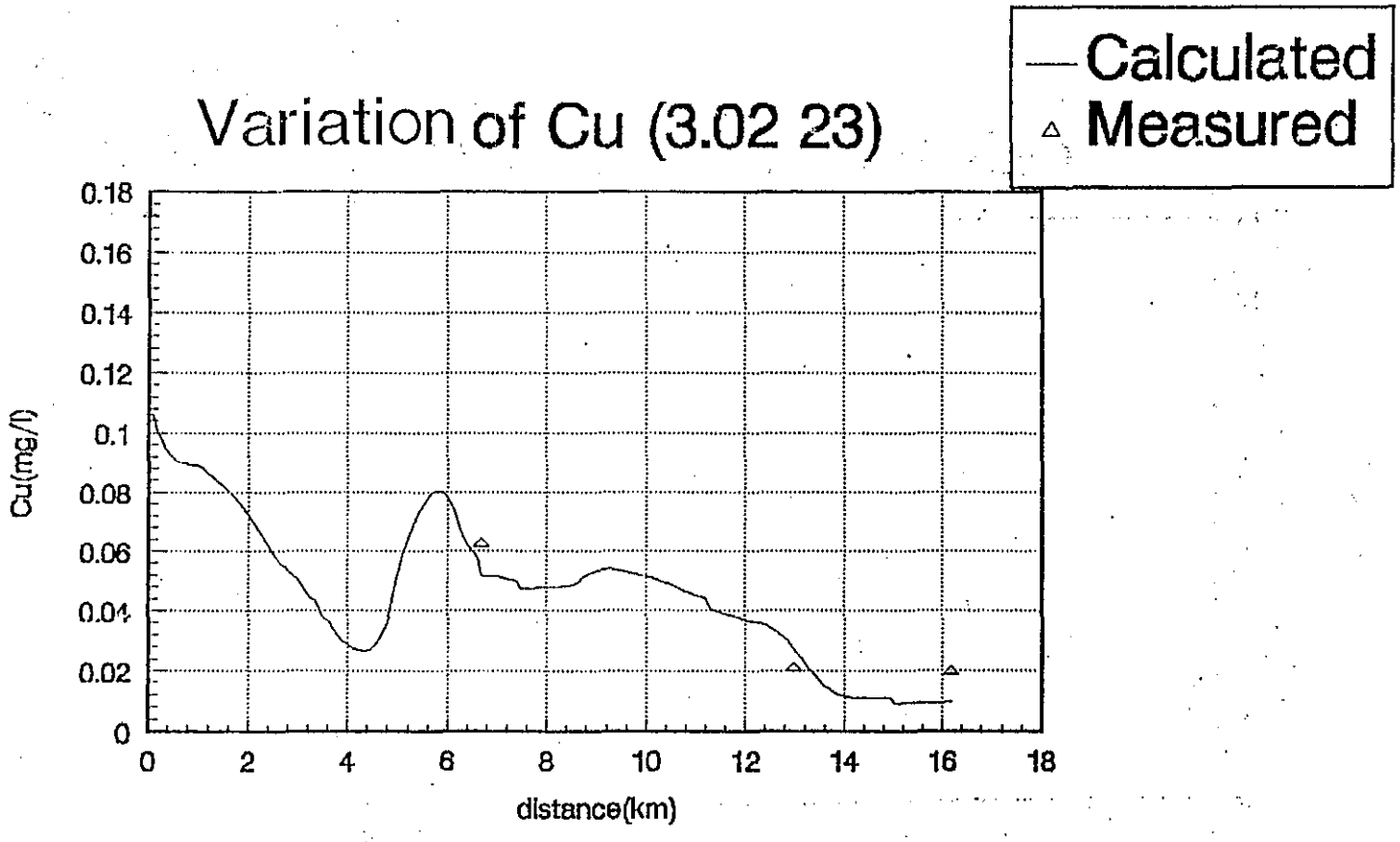

FIG. A7－56(e) Cu variation in dry season (3. 02 23)

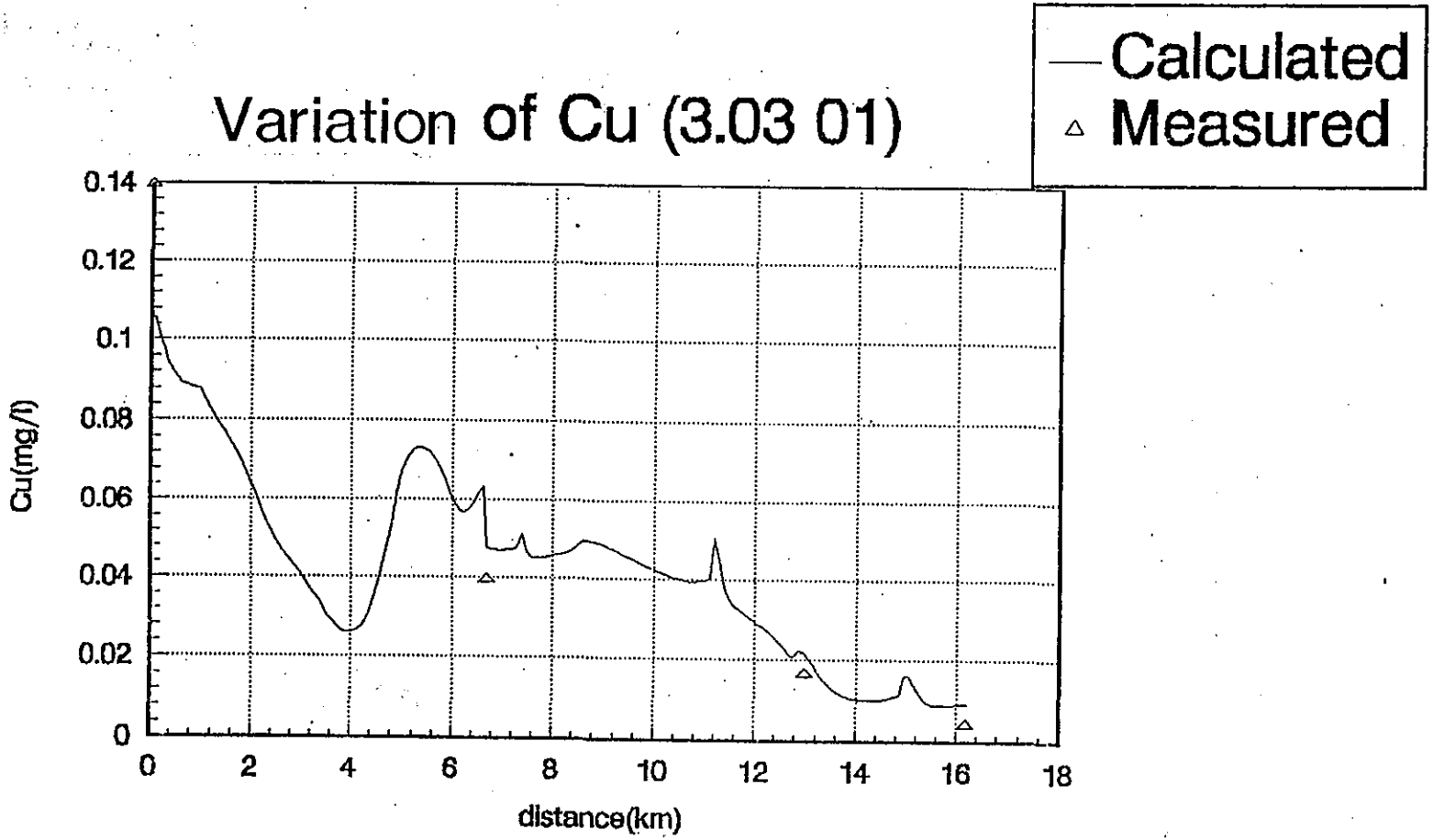

FIG. A7－56(f) **Cu variation in dry season** (3. 03 01)

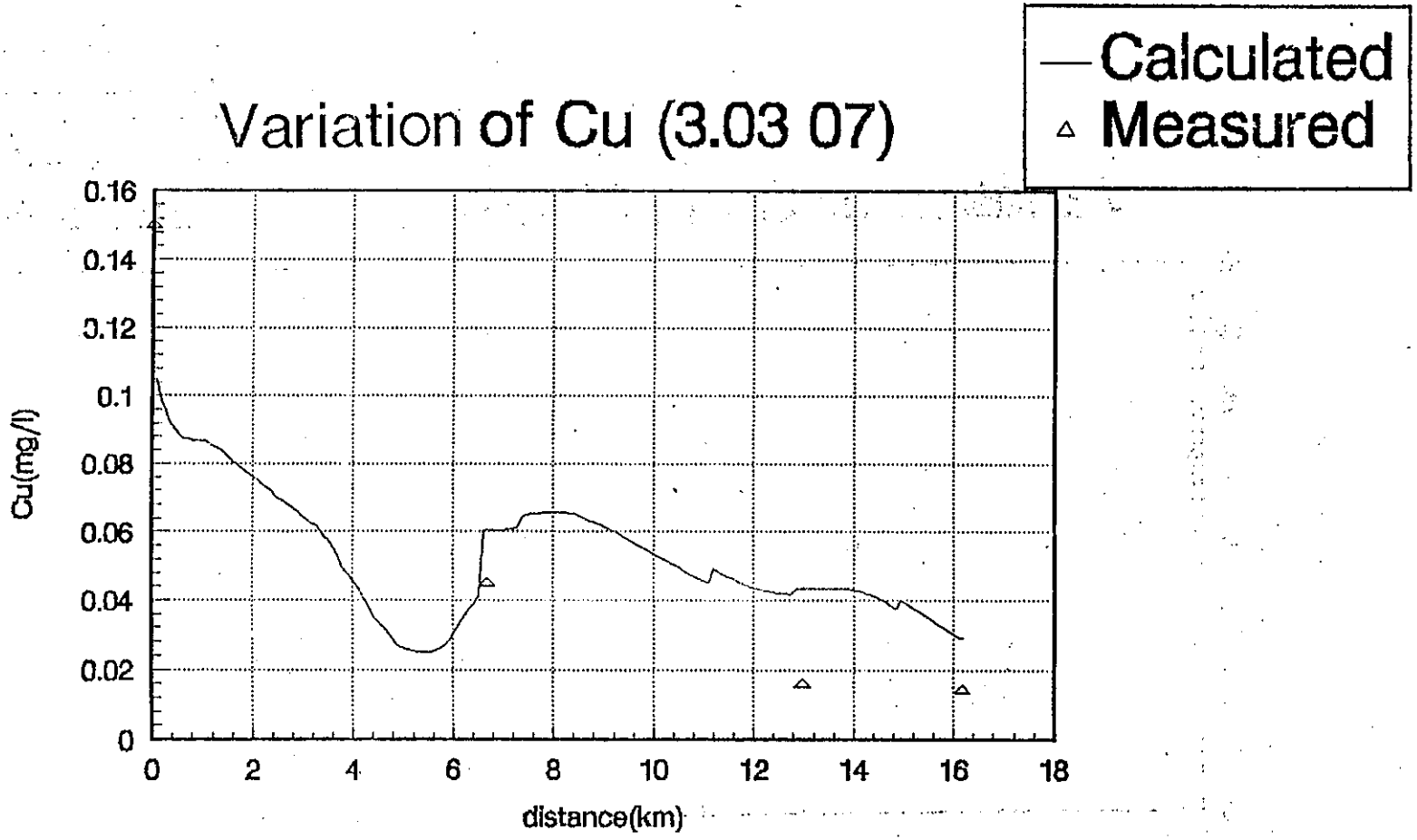

FIG. A7－56(i) Cu variation in dry season (3. 03 07)

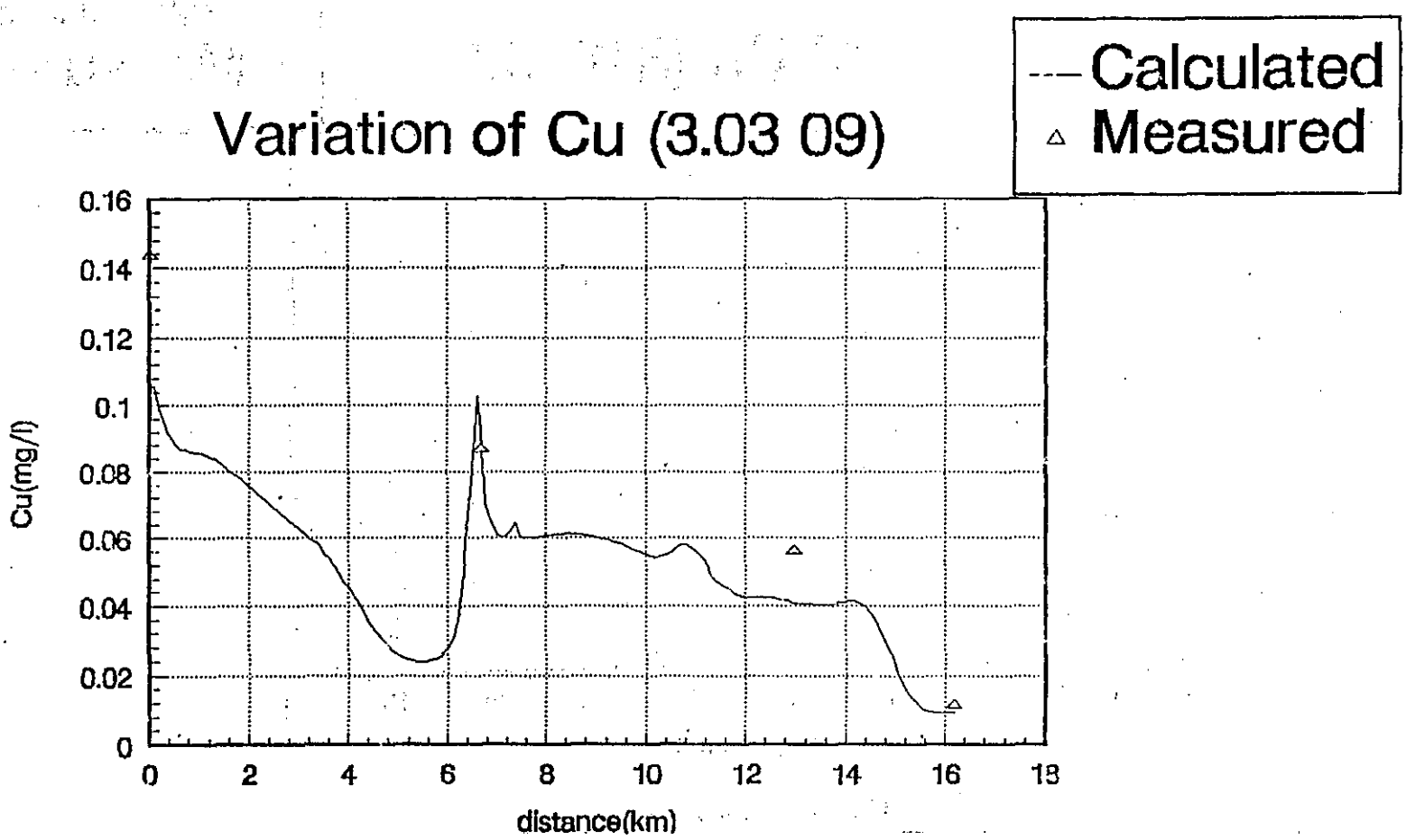

FIG. A7—56(j) Cu variation in dry season (3. 03 09)

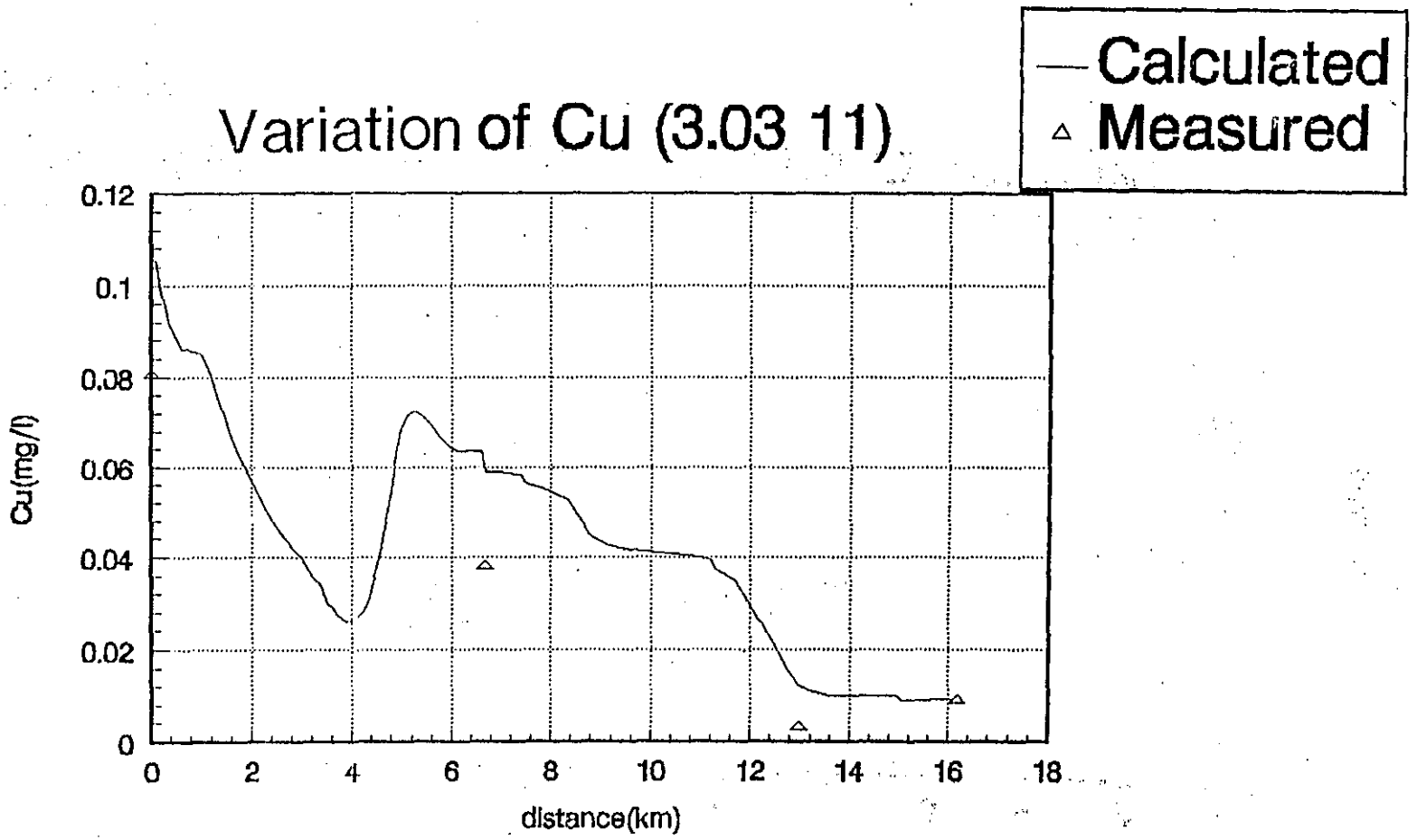

FIG. A7—56(k) Cu variation in dry season (3. 03 11)

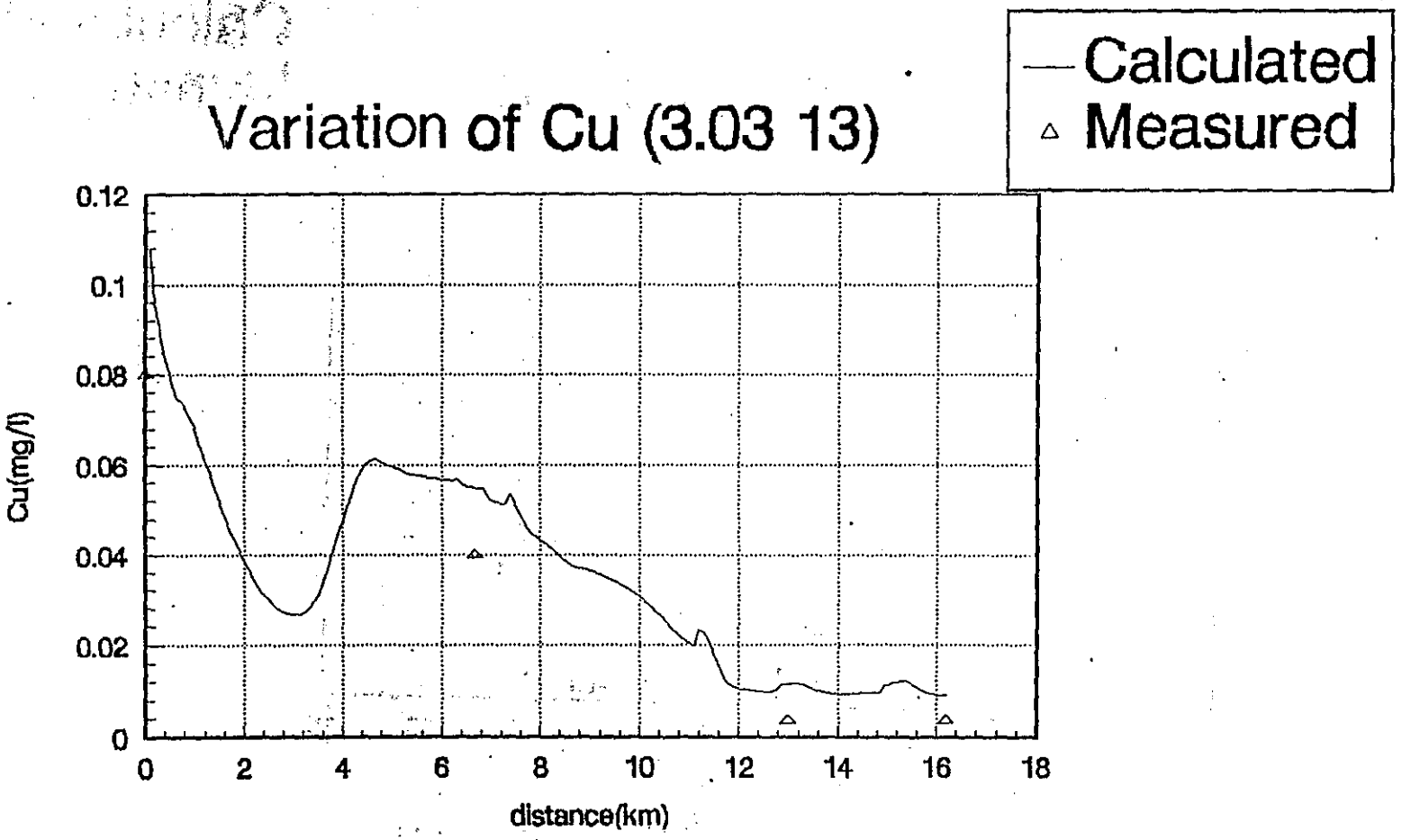

FIG. A7—56(1) Cu variation in dry season (3. 03 13)

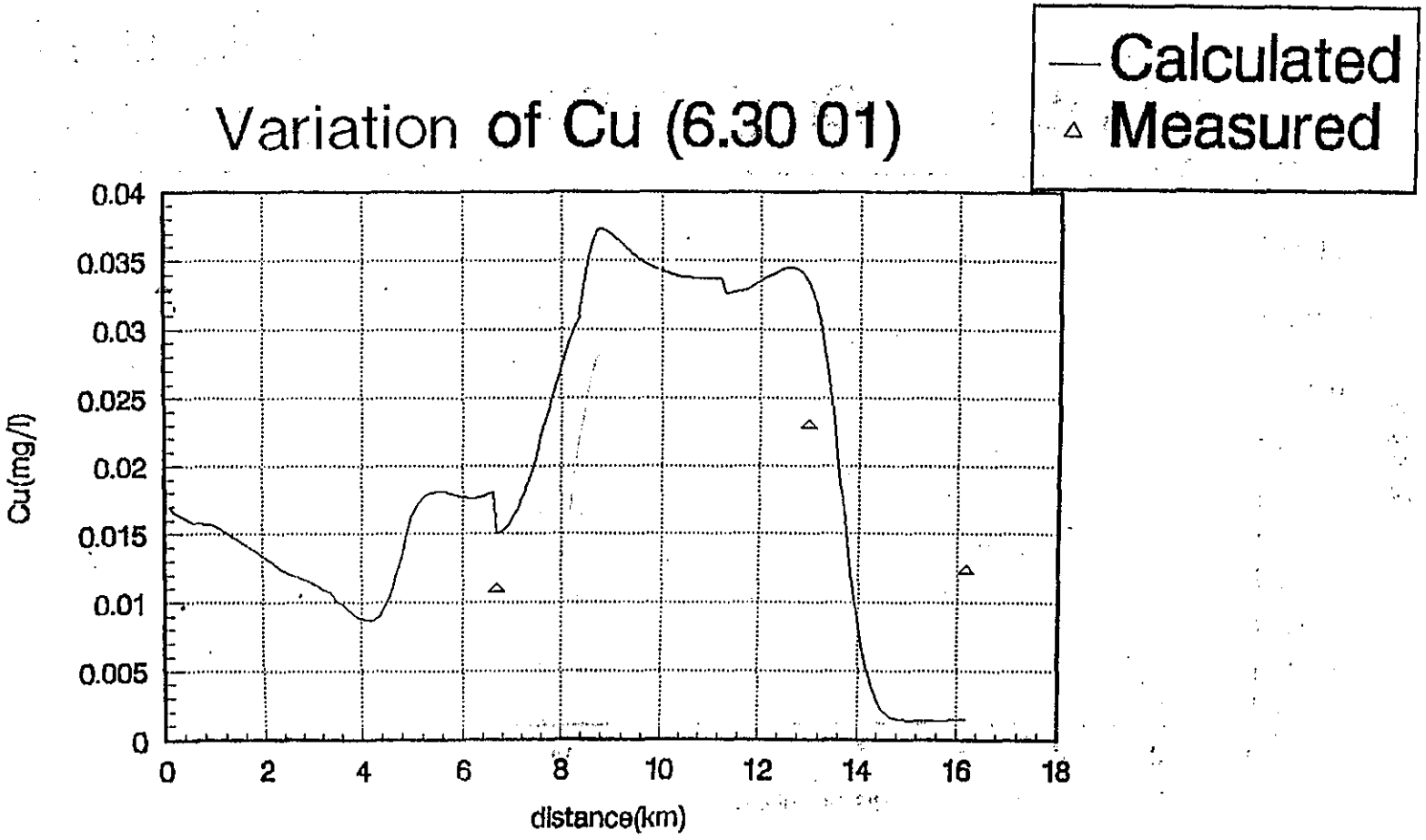

FIG. A7—56(m) Cu variation in wet season (6. 30 01)

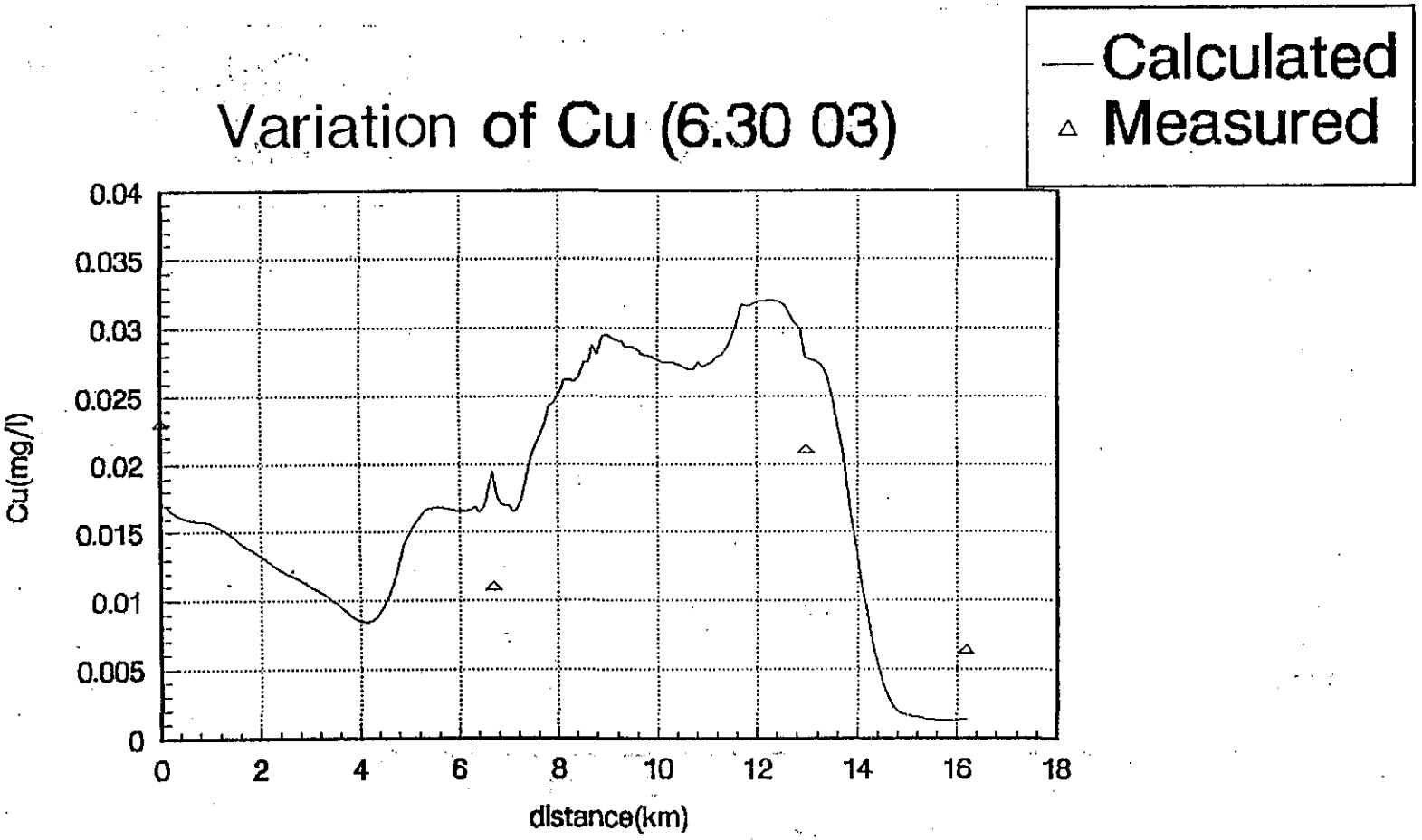

FIG. A7—56(n) Cu variation in wet season (6. 30 03)

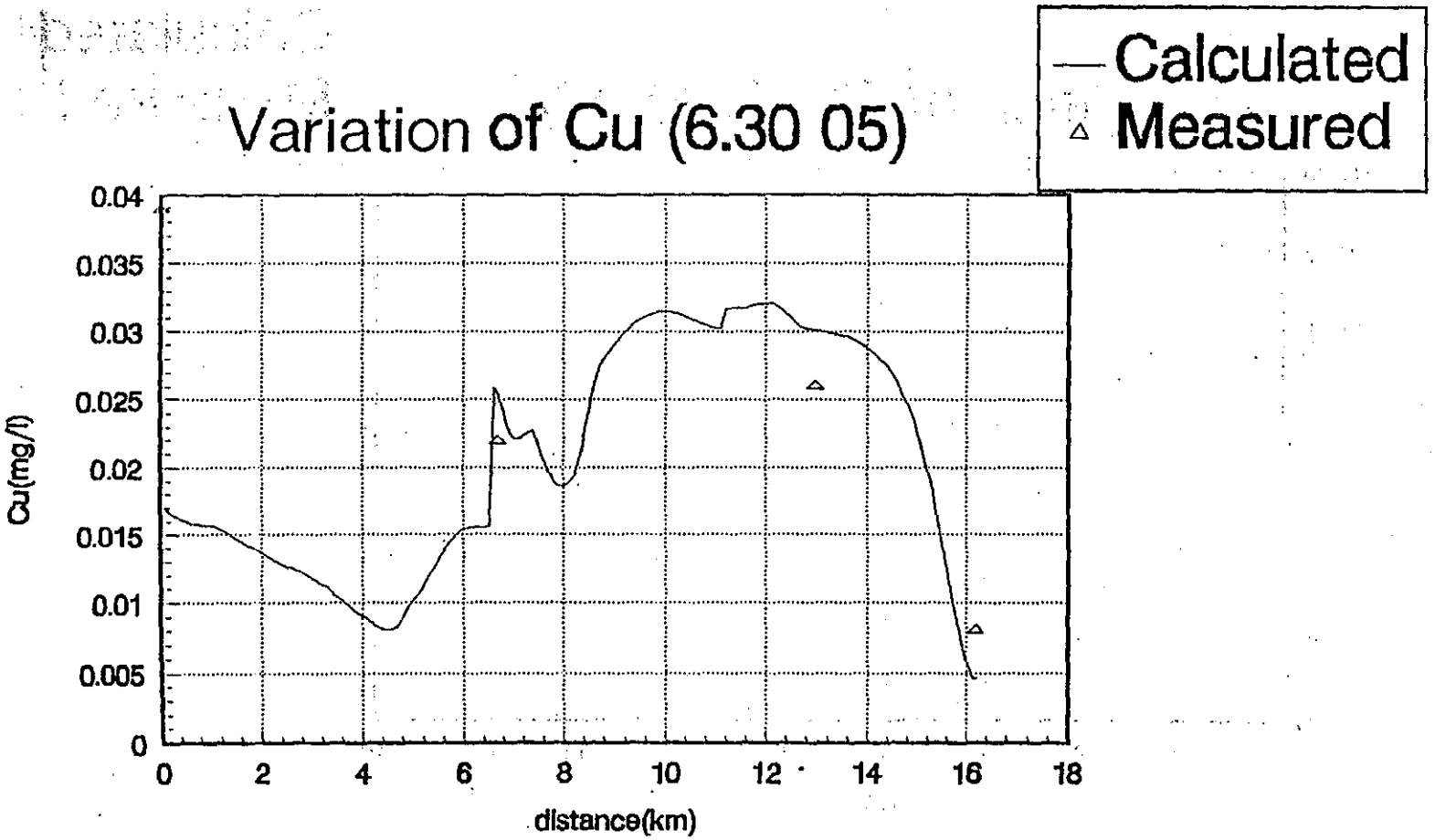

FIG. A7—56(o) Cu variation in wet season (6. 30 05)

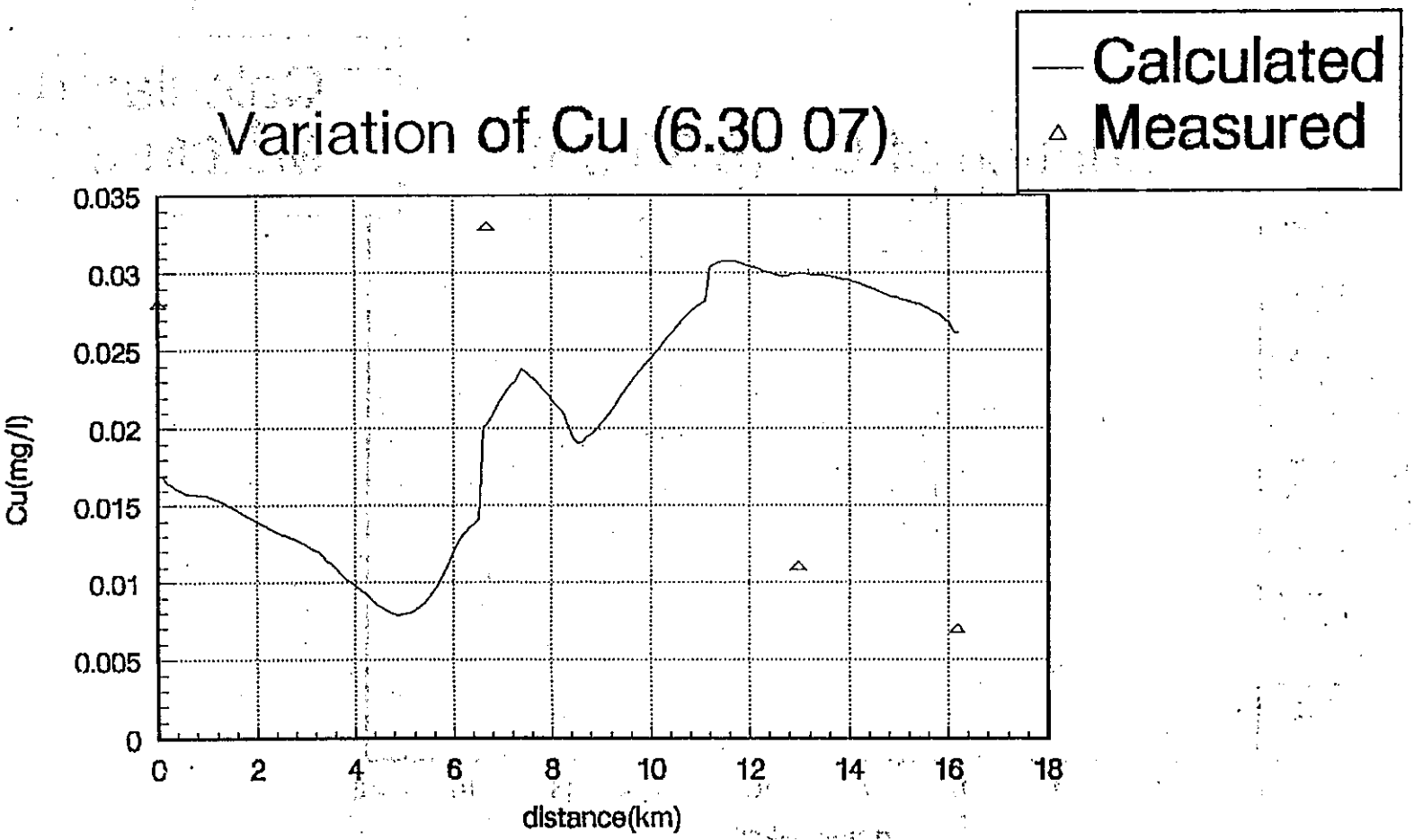

FIG. A7—56(p) Cu variation in wet season (6. 30 07)

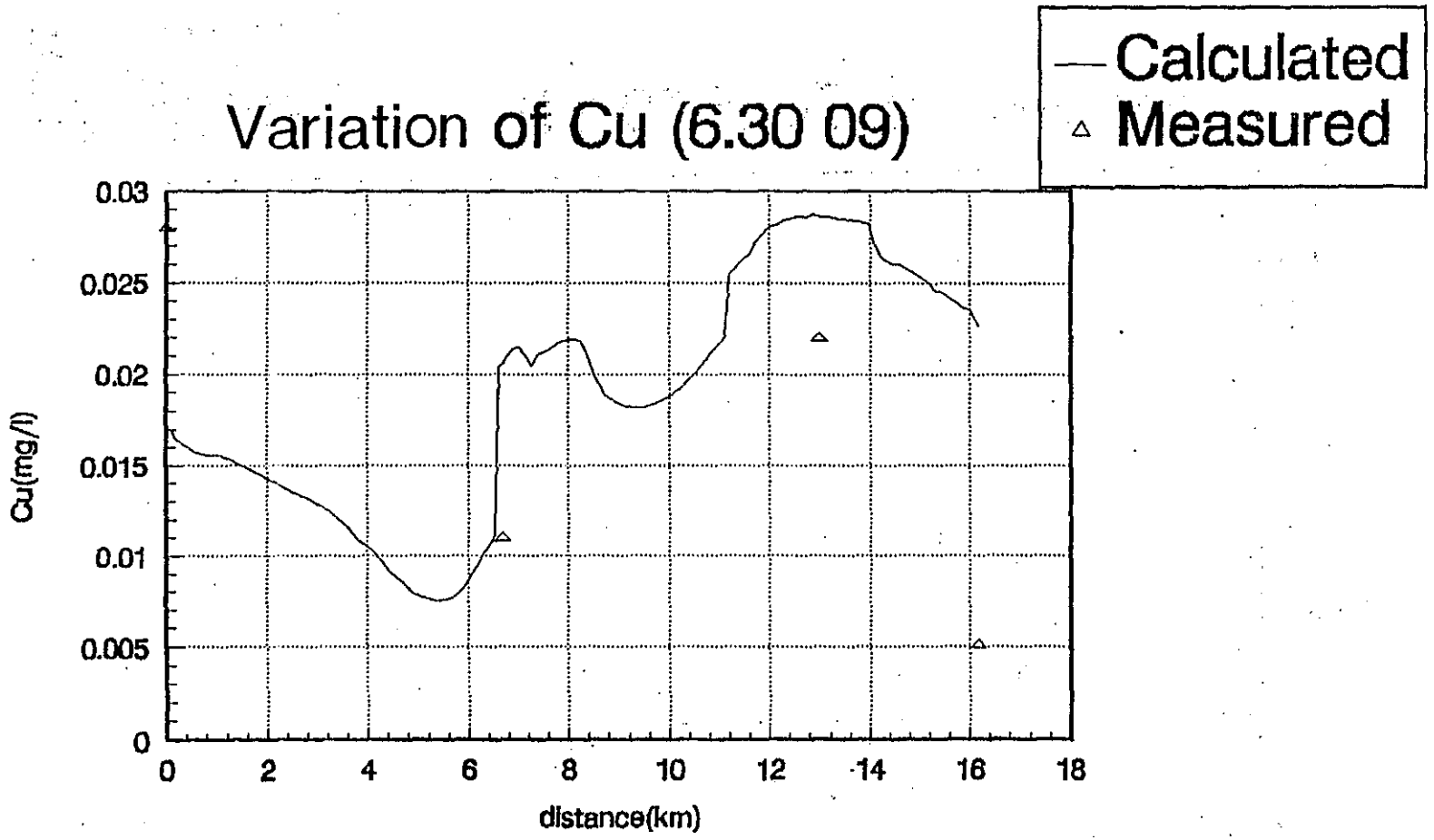

FIG. A7－56(q) **Cu variation in wet season** (6. 30 09)

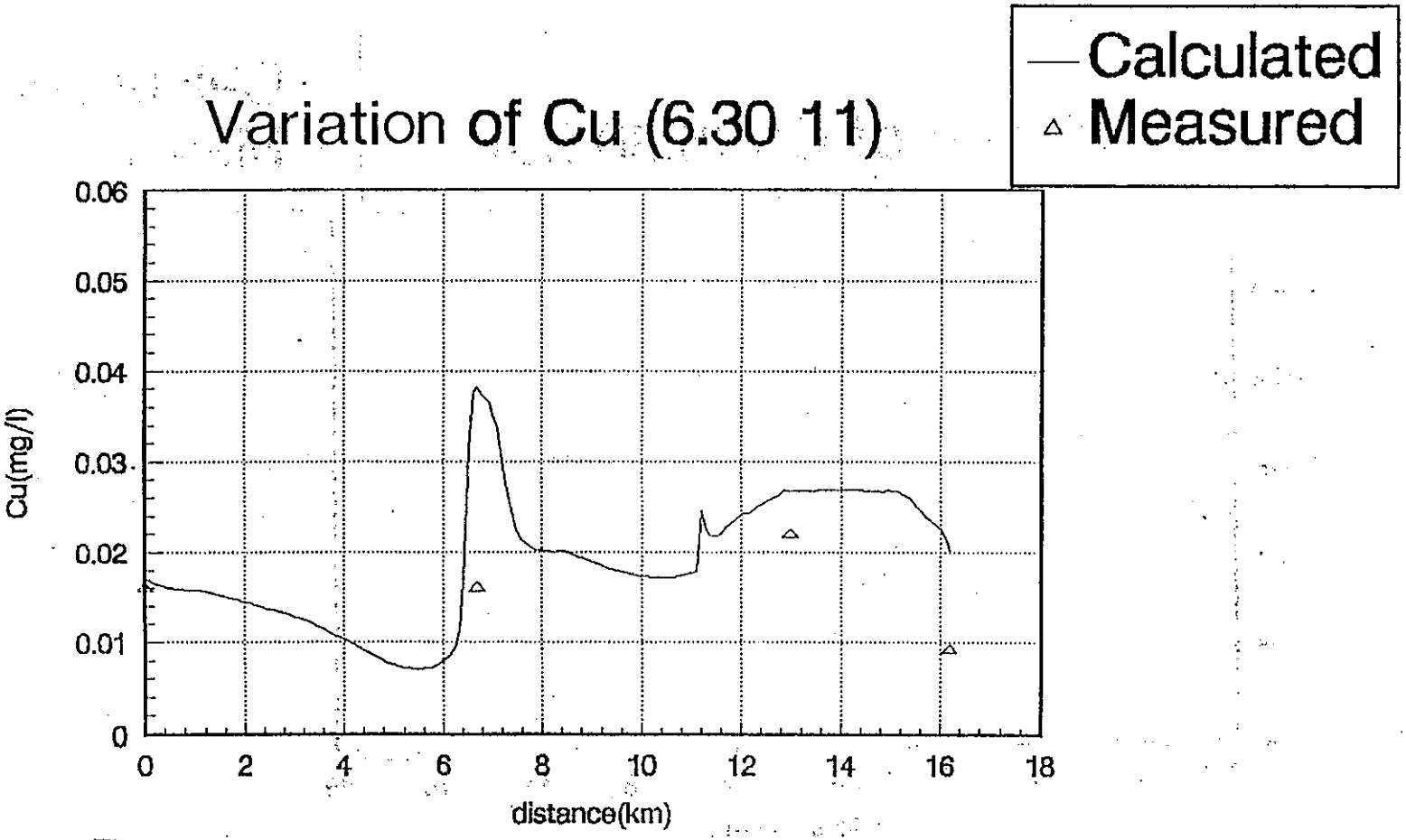

FIG. A7—56(r) Cu variation in wet season (6. 30 11)

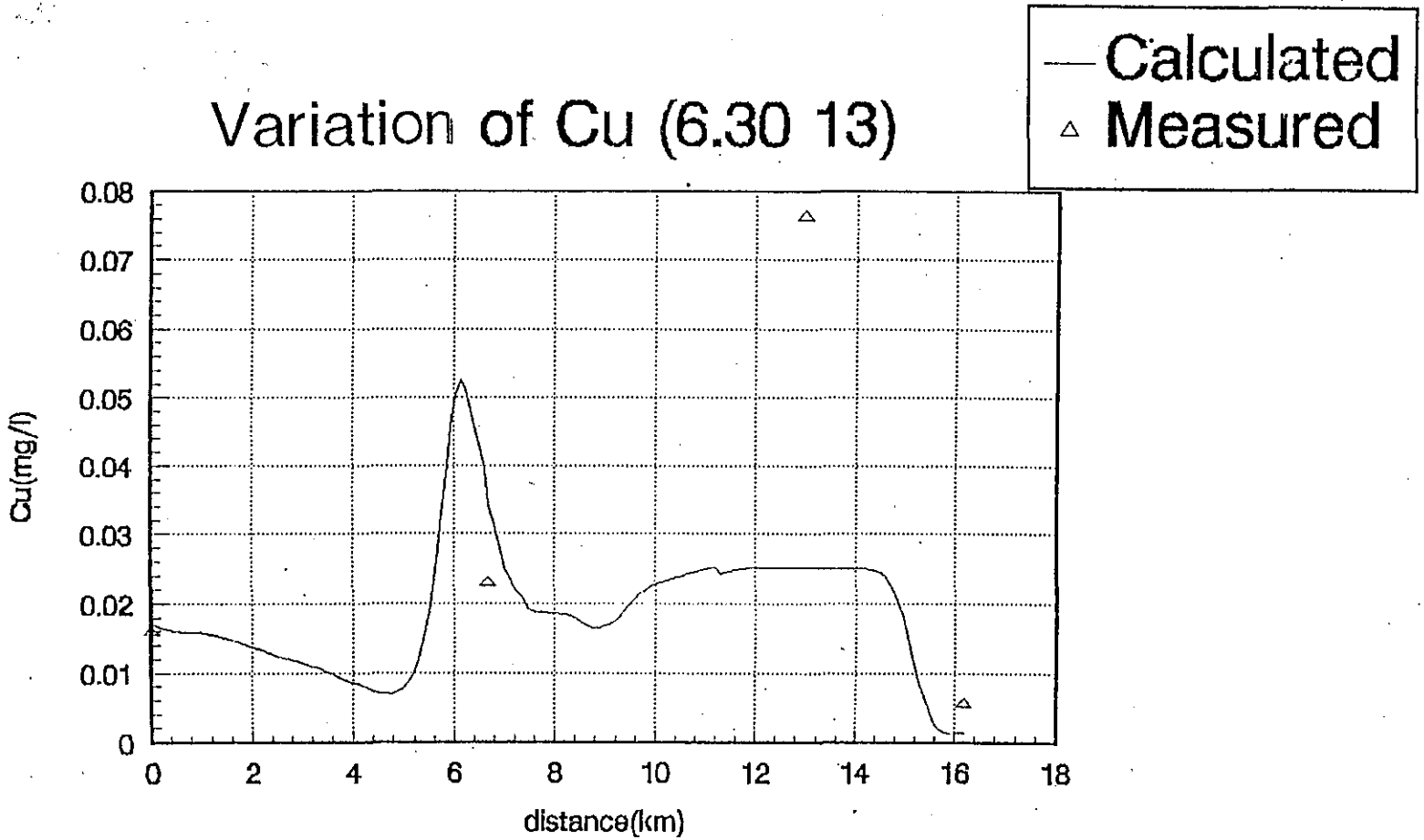

FIG. A7－56(s) Cu variation in wet season (6.30 13)

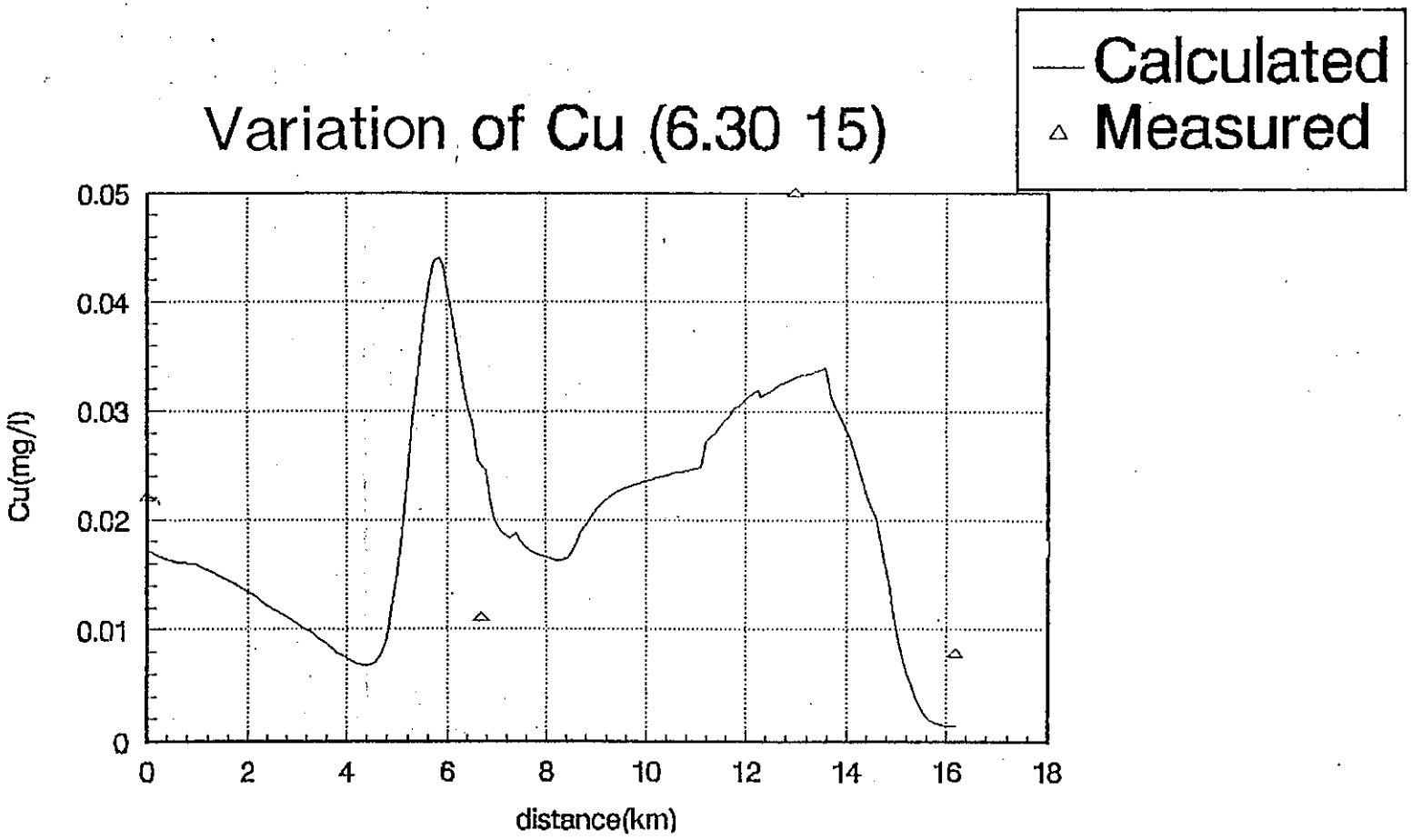

FIG. A7−56(t) Cu variation in wet season (6. 30 15)

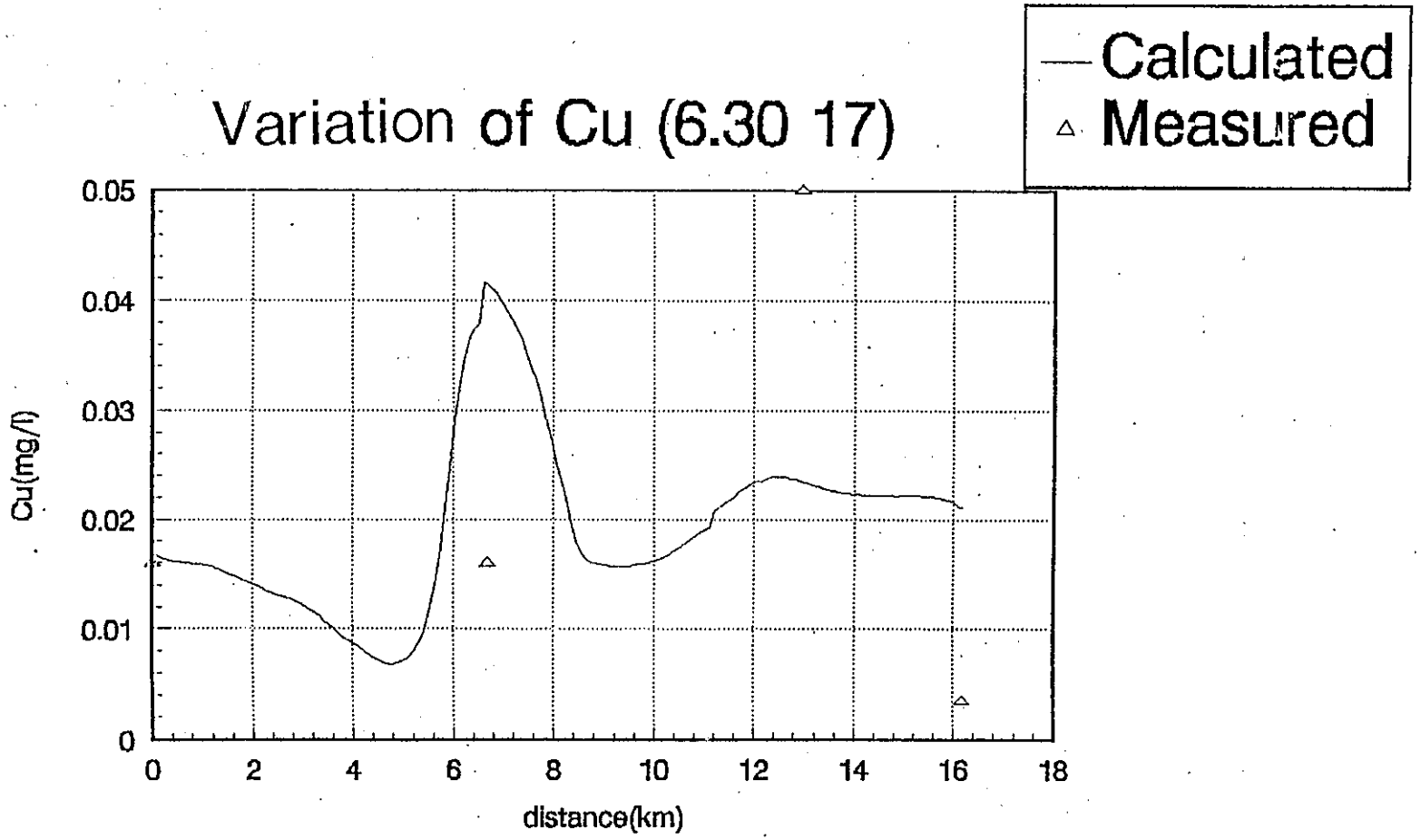

FIG. A7－56(u) Cu variation in wet season (6. 30 17)

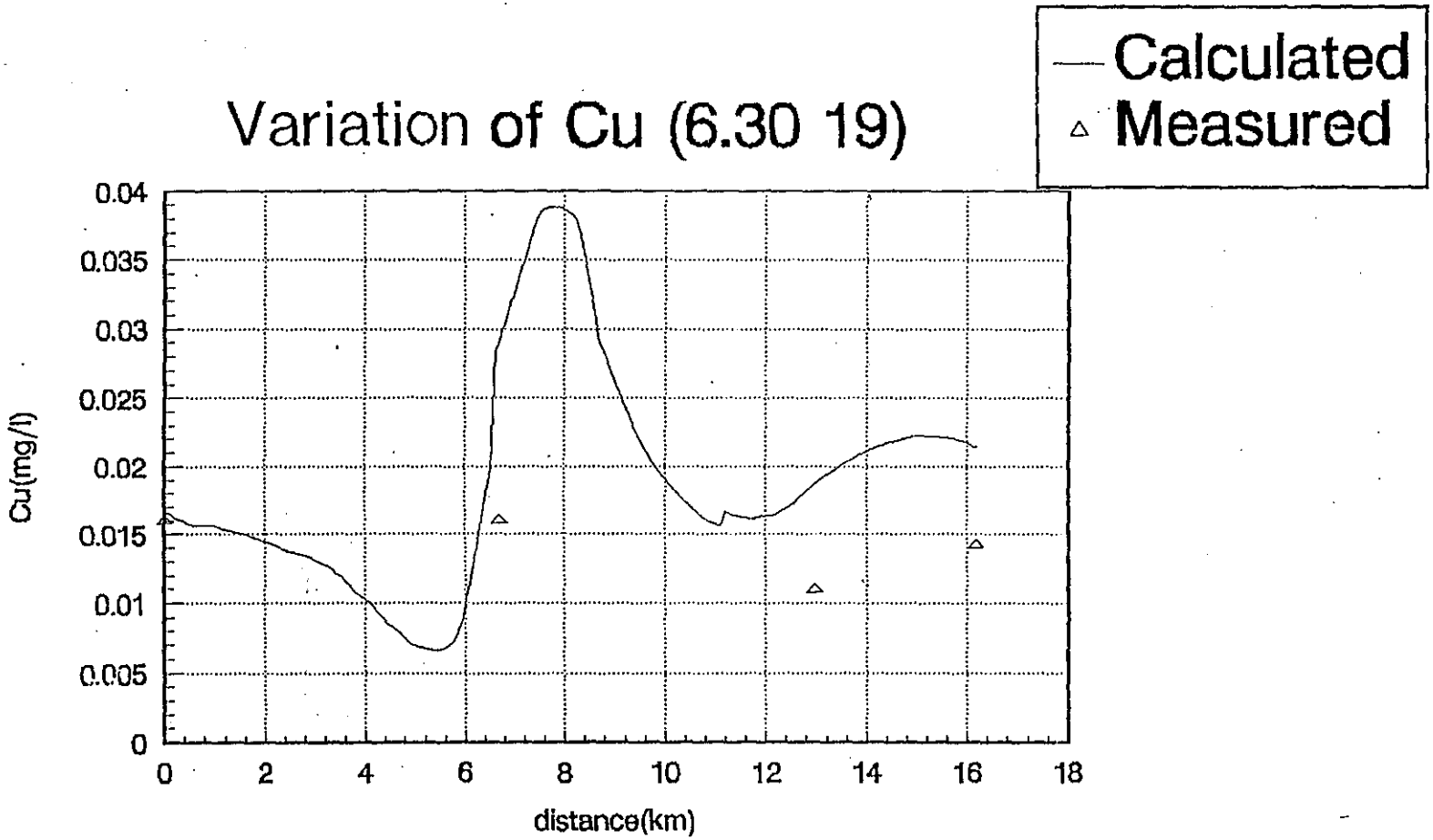

FIG. A7—56(v) **Cu variation in wet season** (6. 30 19)

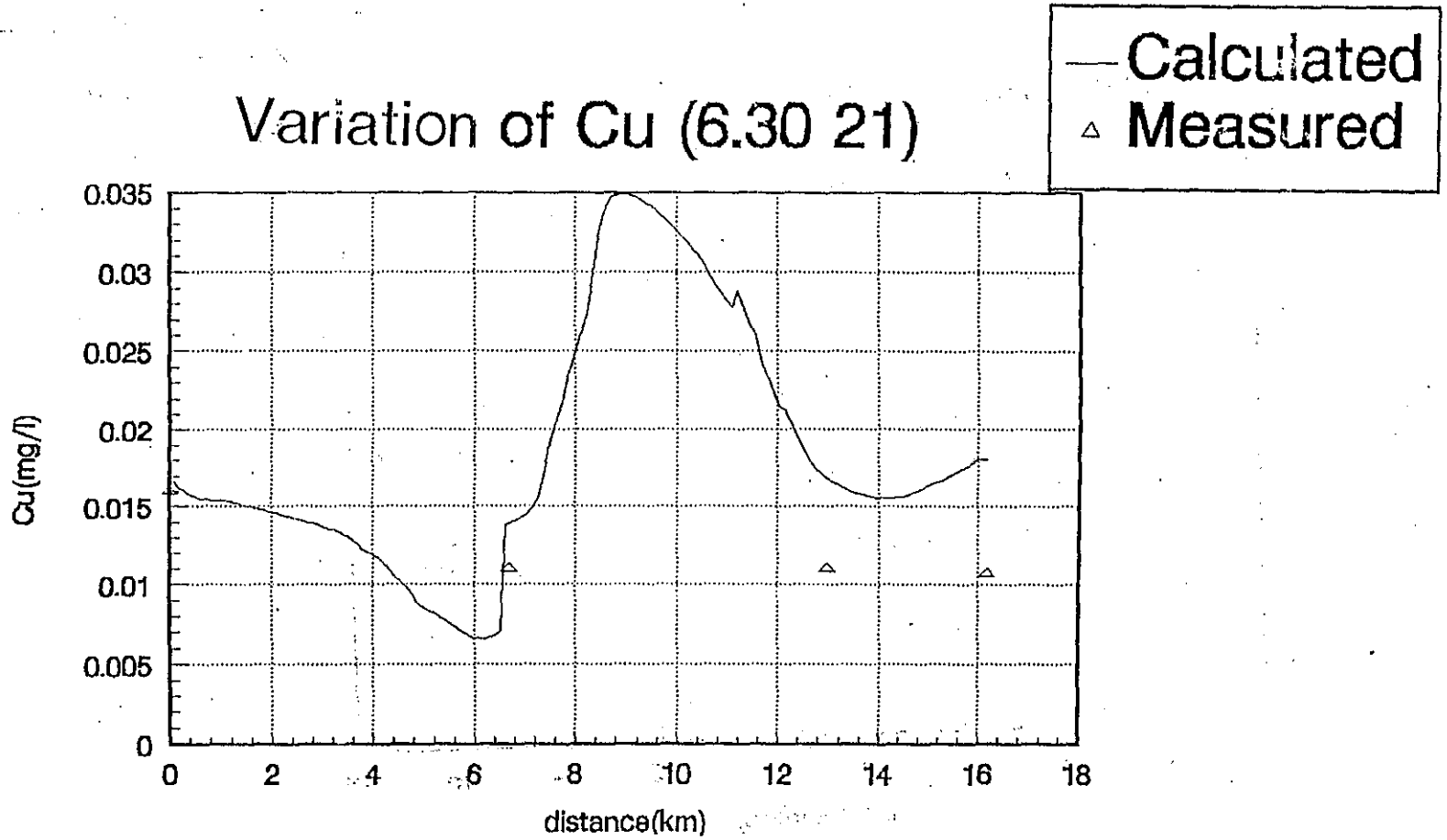

FIG. A7—56(w) Cu variation in wet season (6. 30 21)

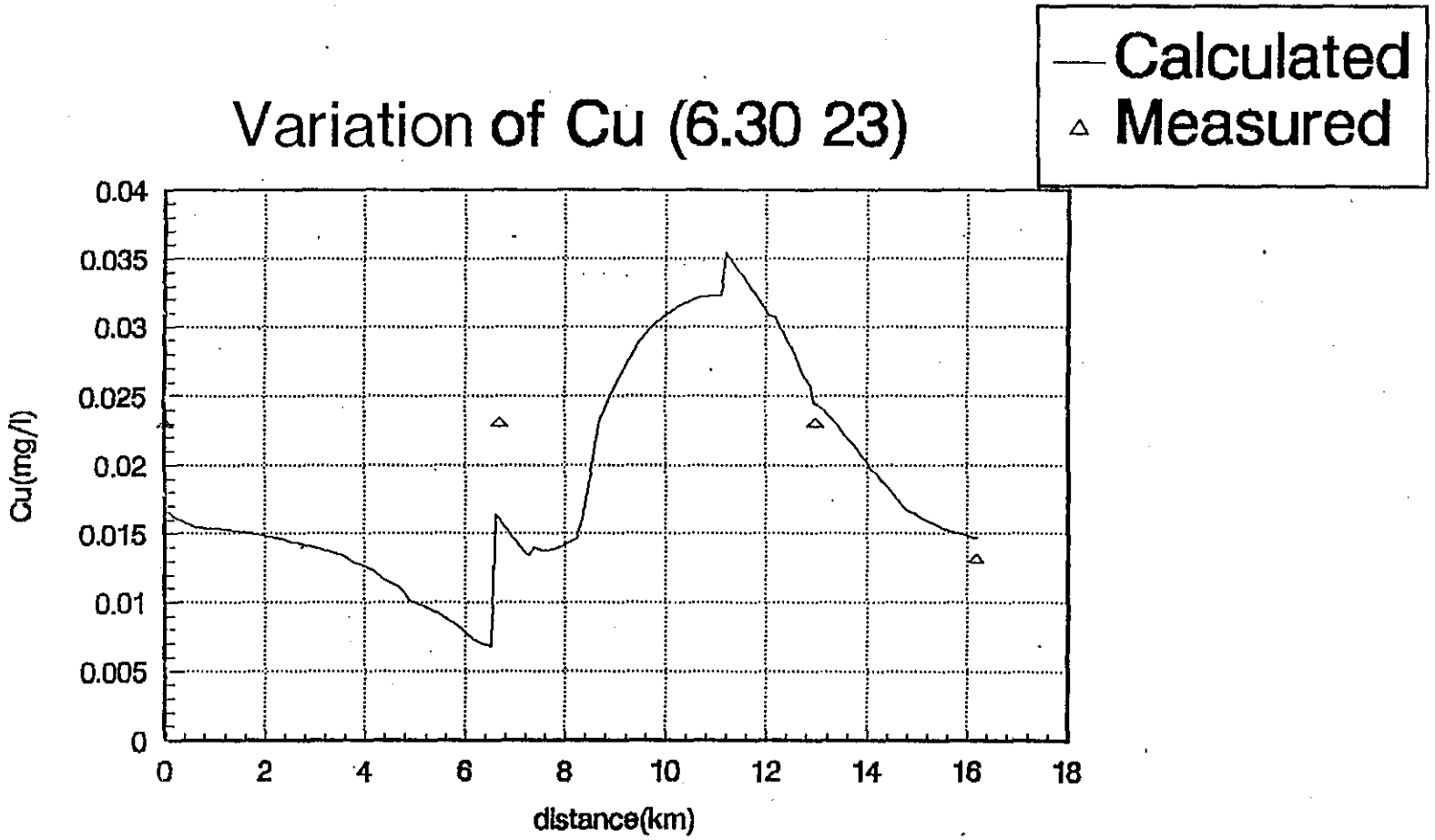

FIG. A7−56(x) **Cu variation in wet season** (6. 30 23)

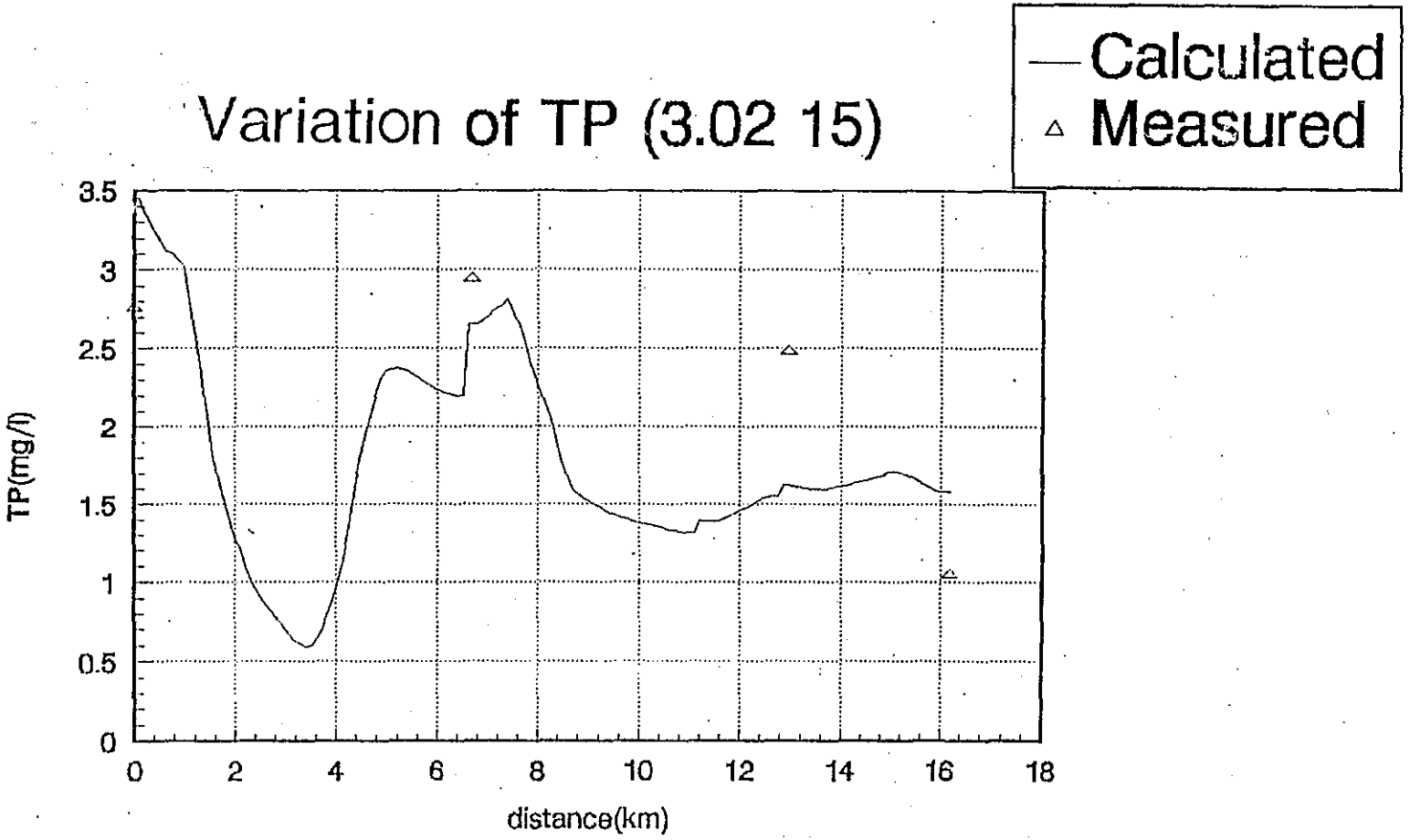

FIG. A7—57(a) TP variation in dry season (3. 02 15)

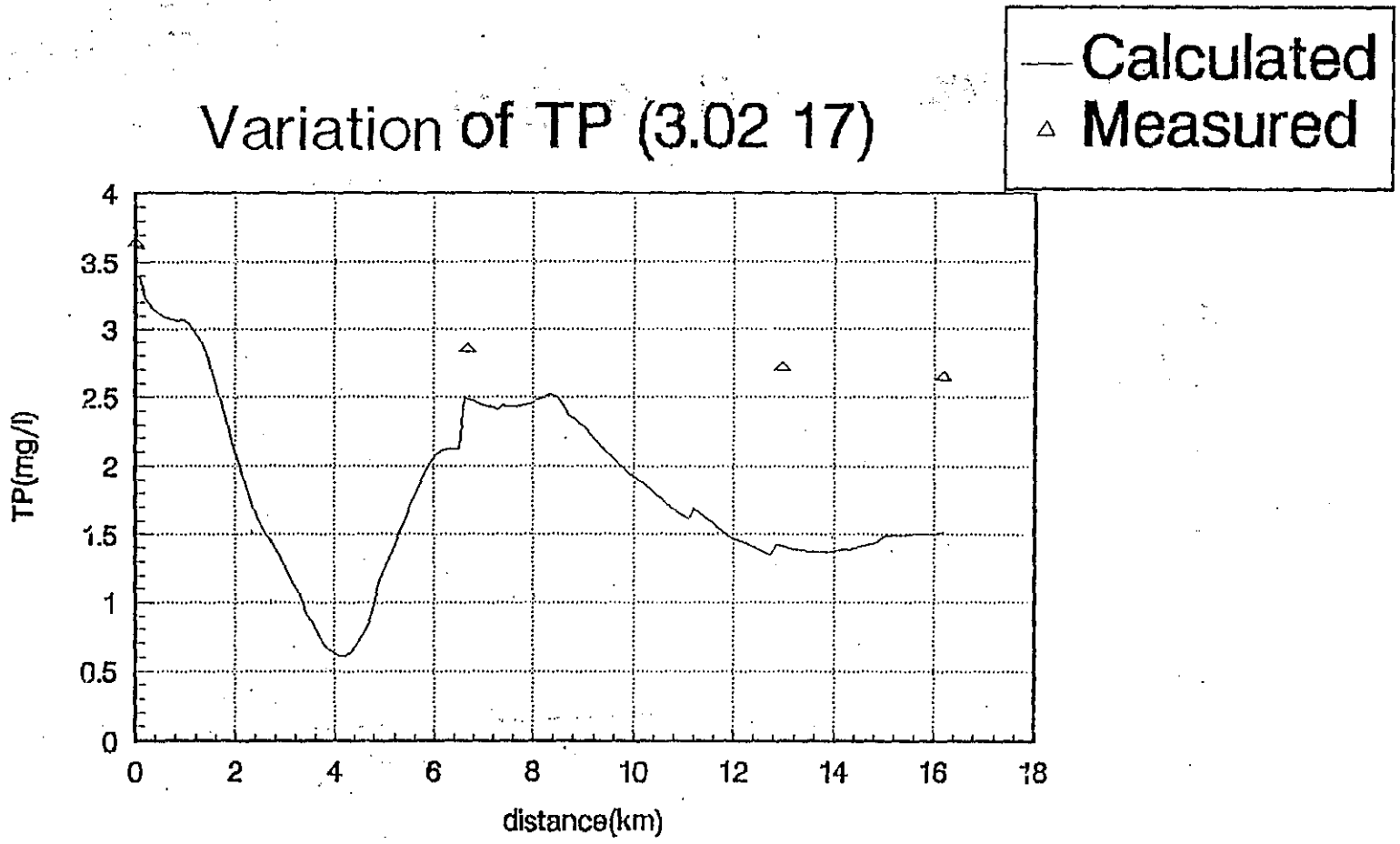

FIG. A7—57(b) **TP variation in dry season** (3. 02 17)

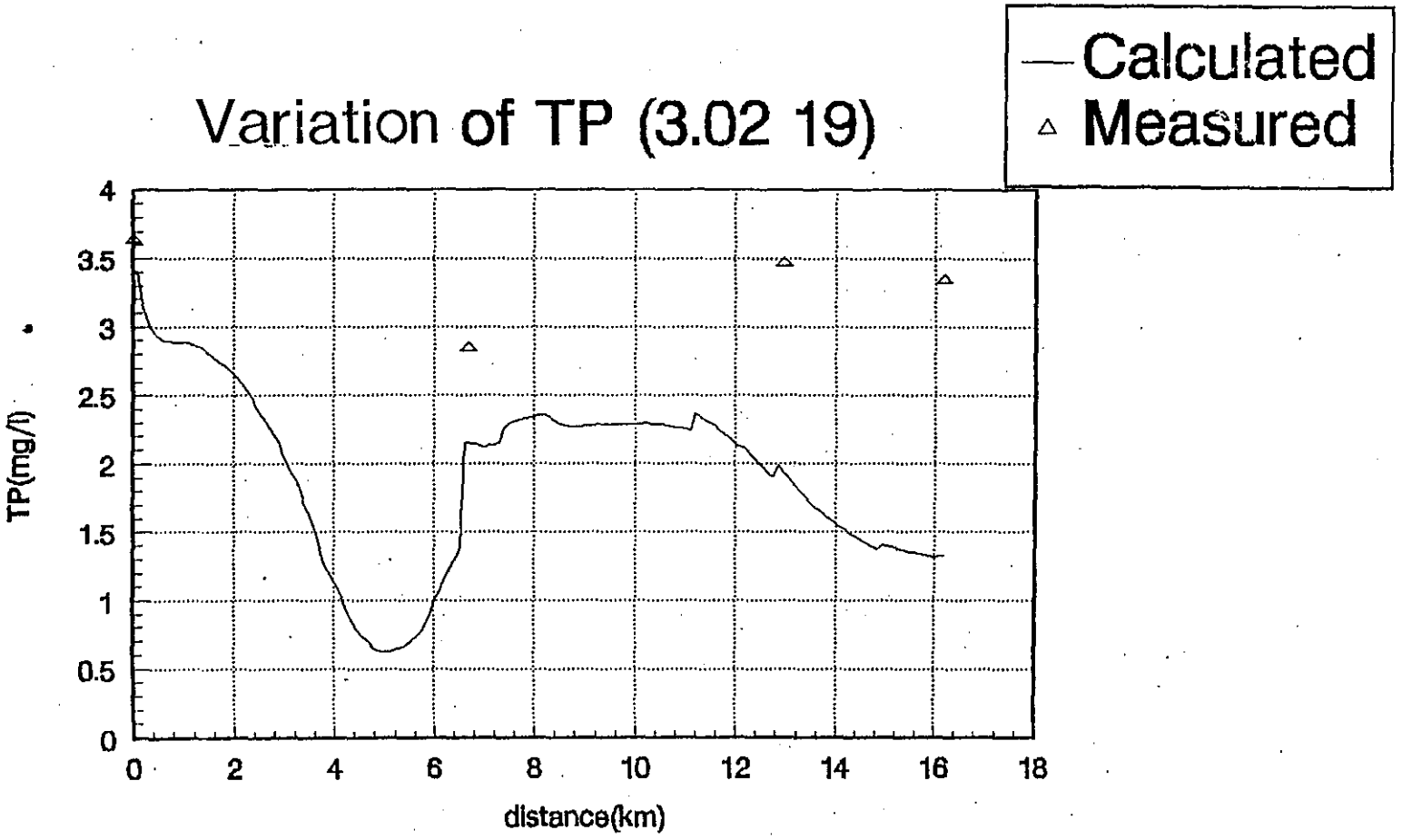

FIG. A7—57(c) **TP variation in dry season** (3.02 19)

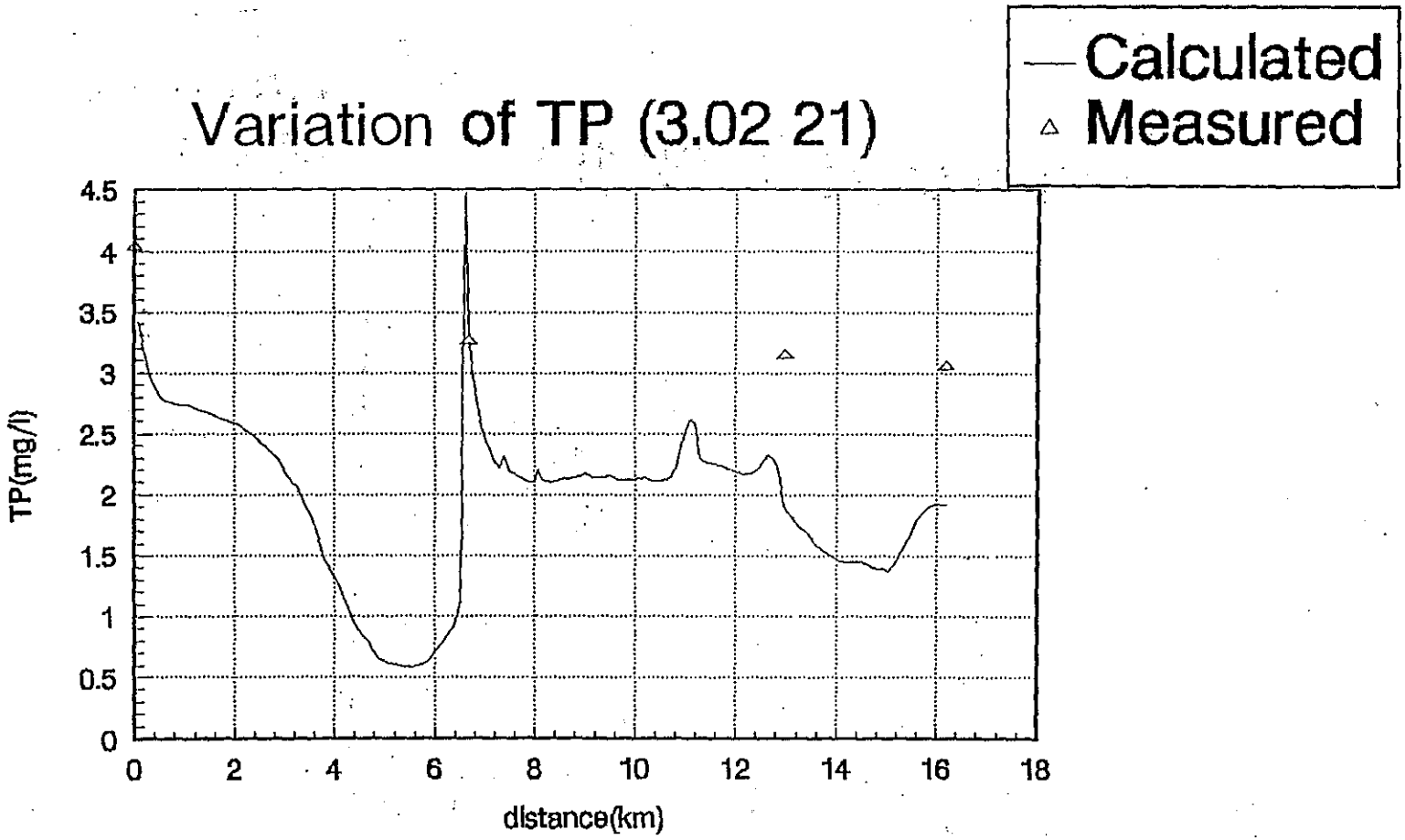

FIG. A7－57(d) **TP variation in dry season** (3. 02 21)

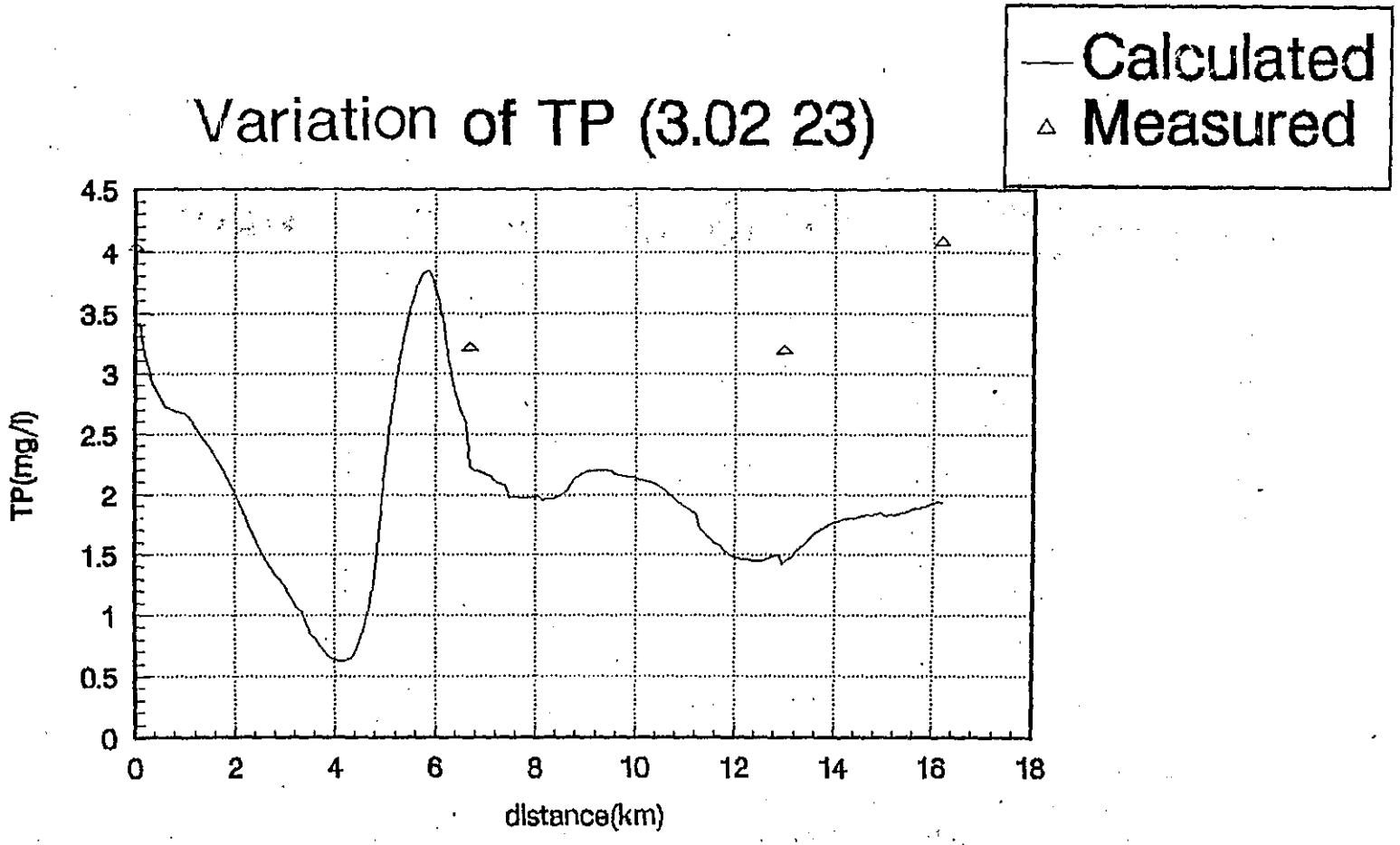

FIG. A7—57(e) **TP variation in dry season** (3. 02 23)

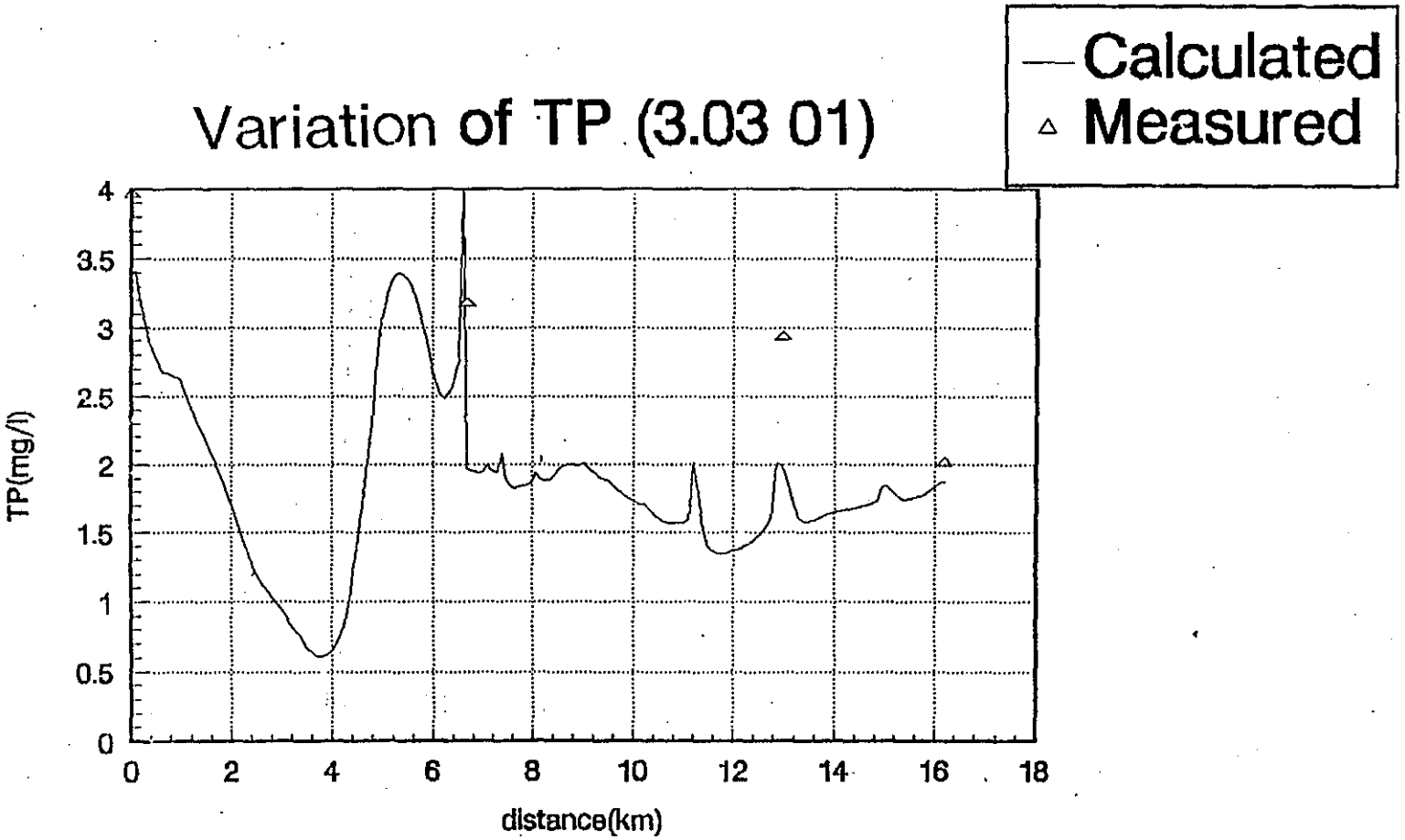

FIG. A7—57(f) **TP variation in dry season** (3. 03 01)

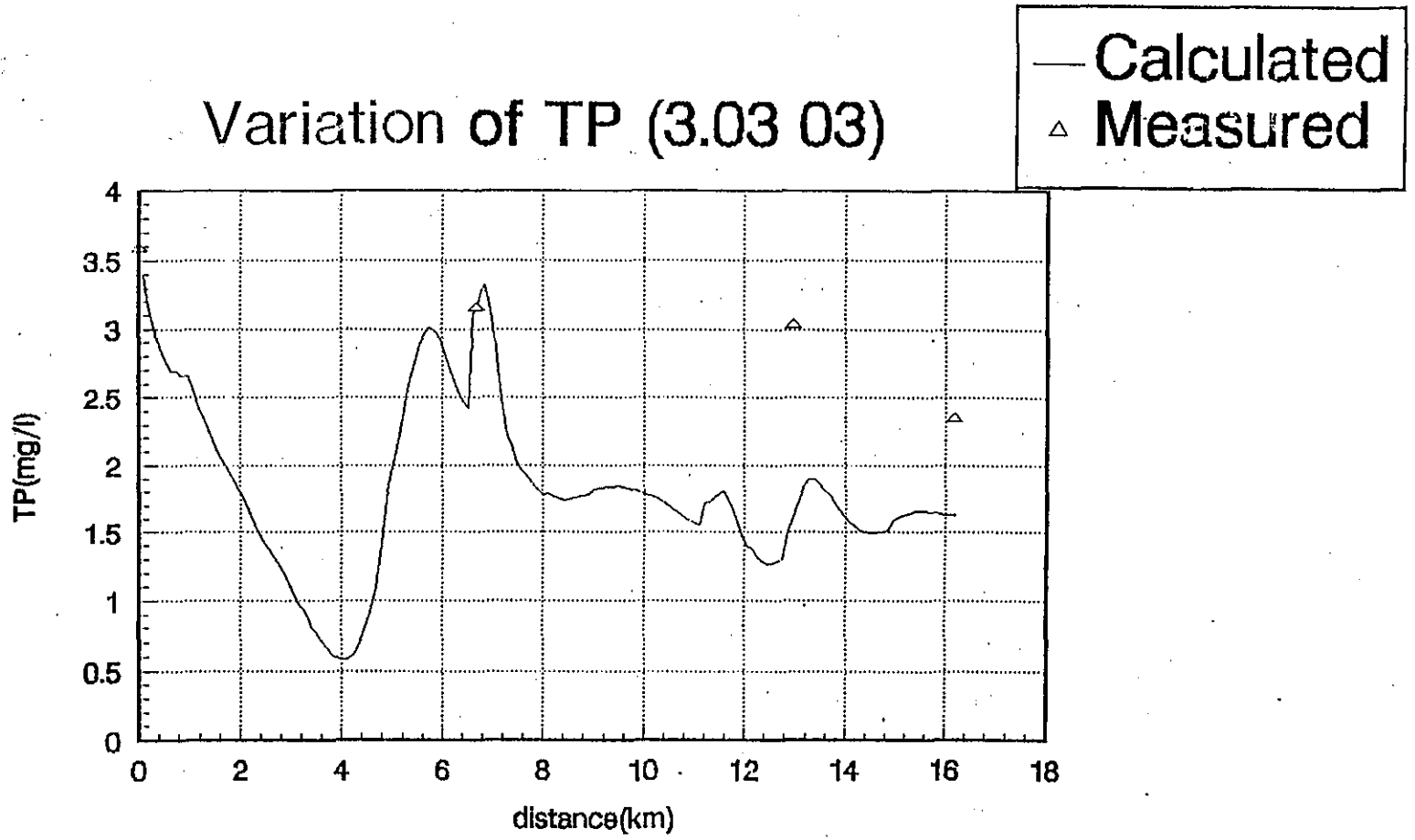

FIG. A7－57(g)　TP variation in dry season (3. 03 03)

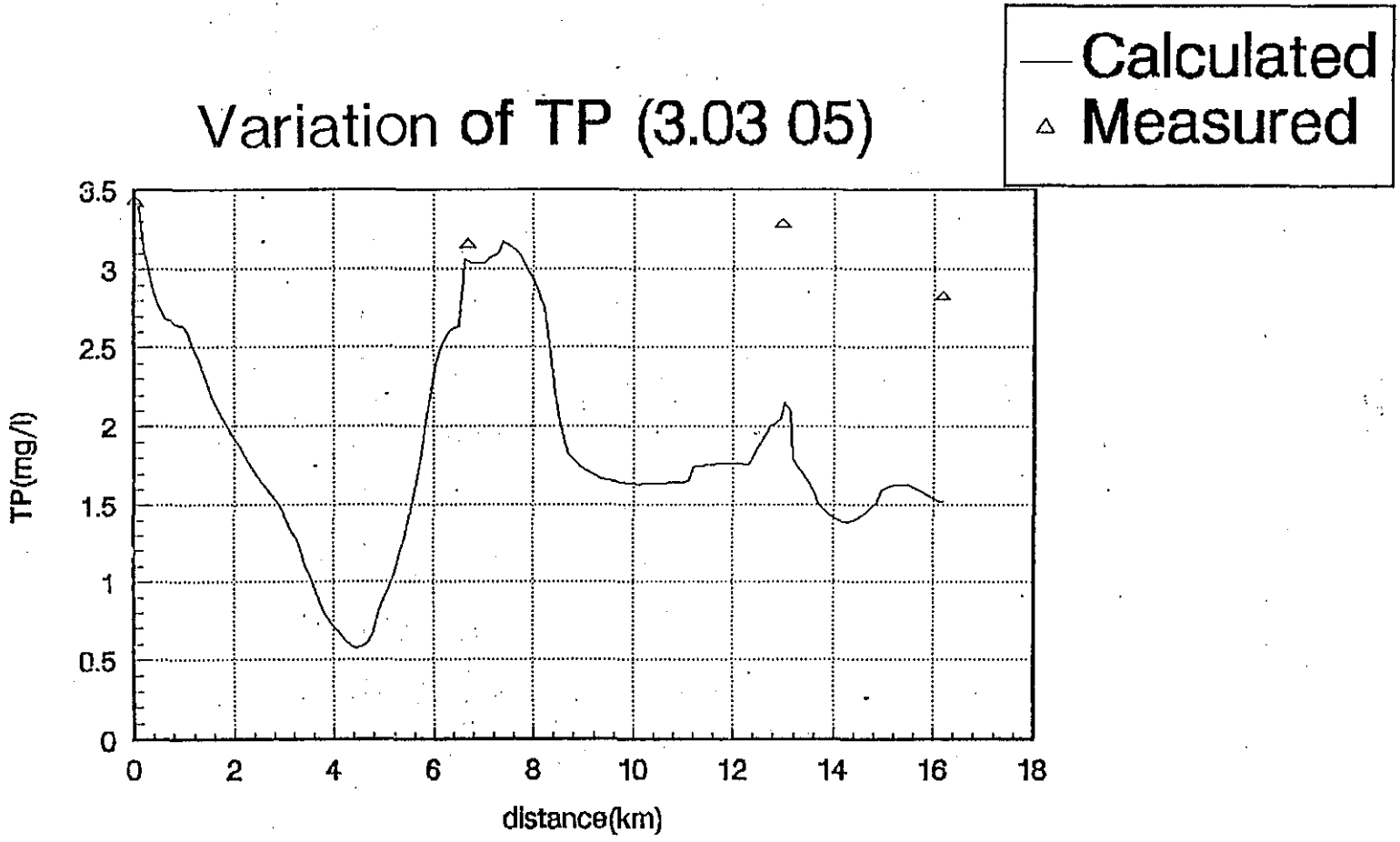

FIG. A7—57(h) **TP variation in dry season** (3. 03 05)

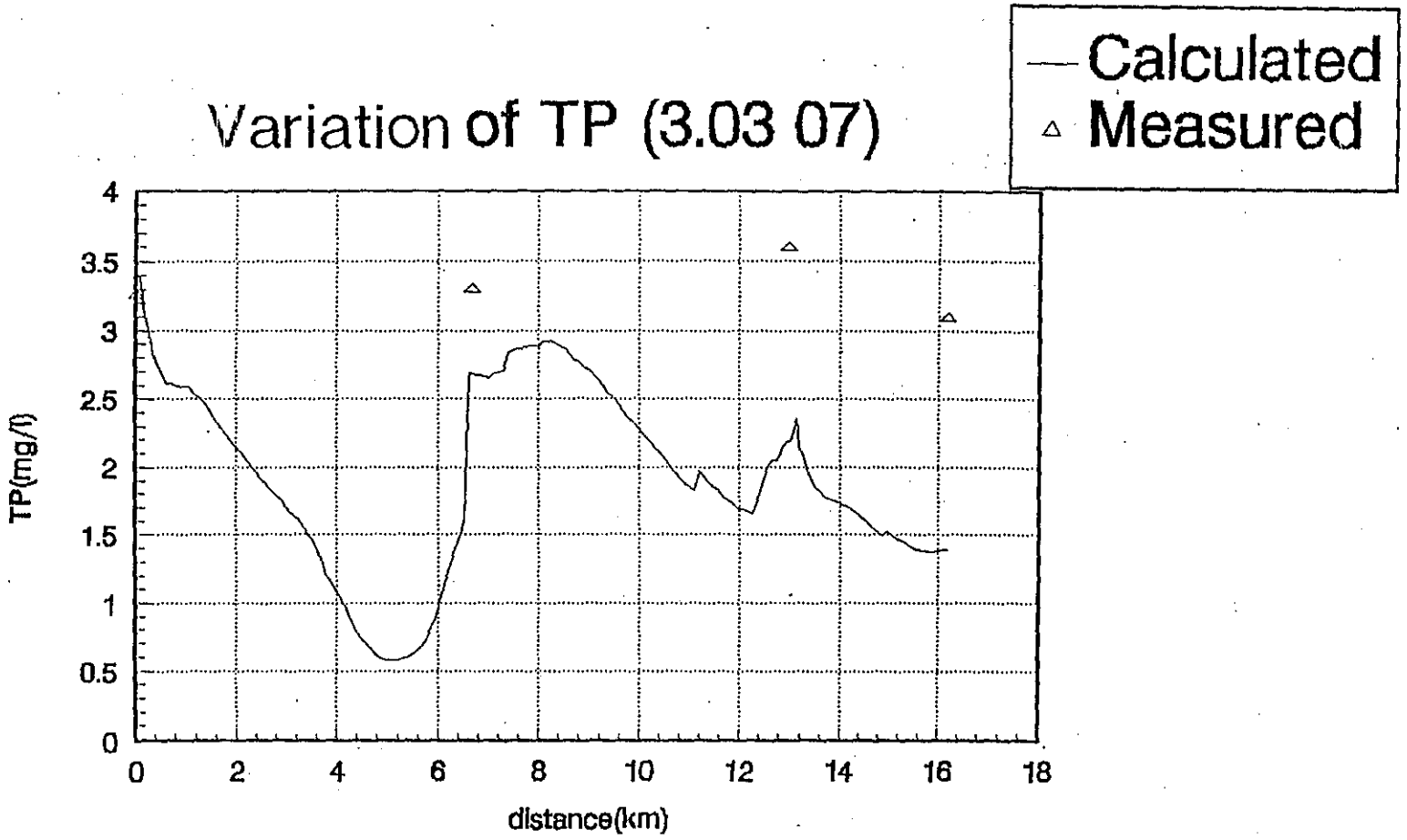

FIG. A7—57(i) TP variation in dry season (3. 03 07)

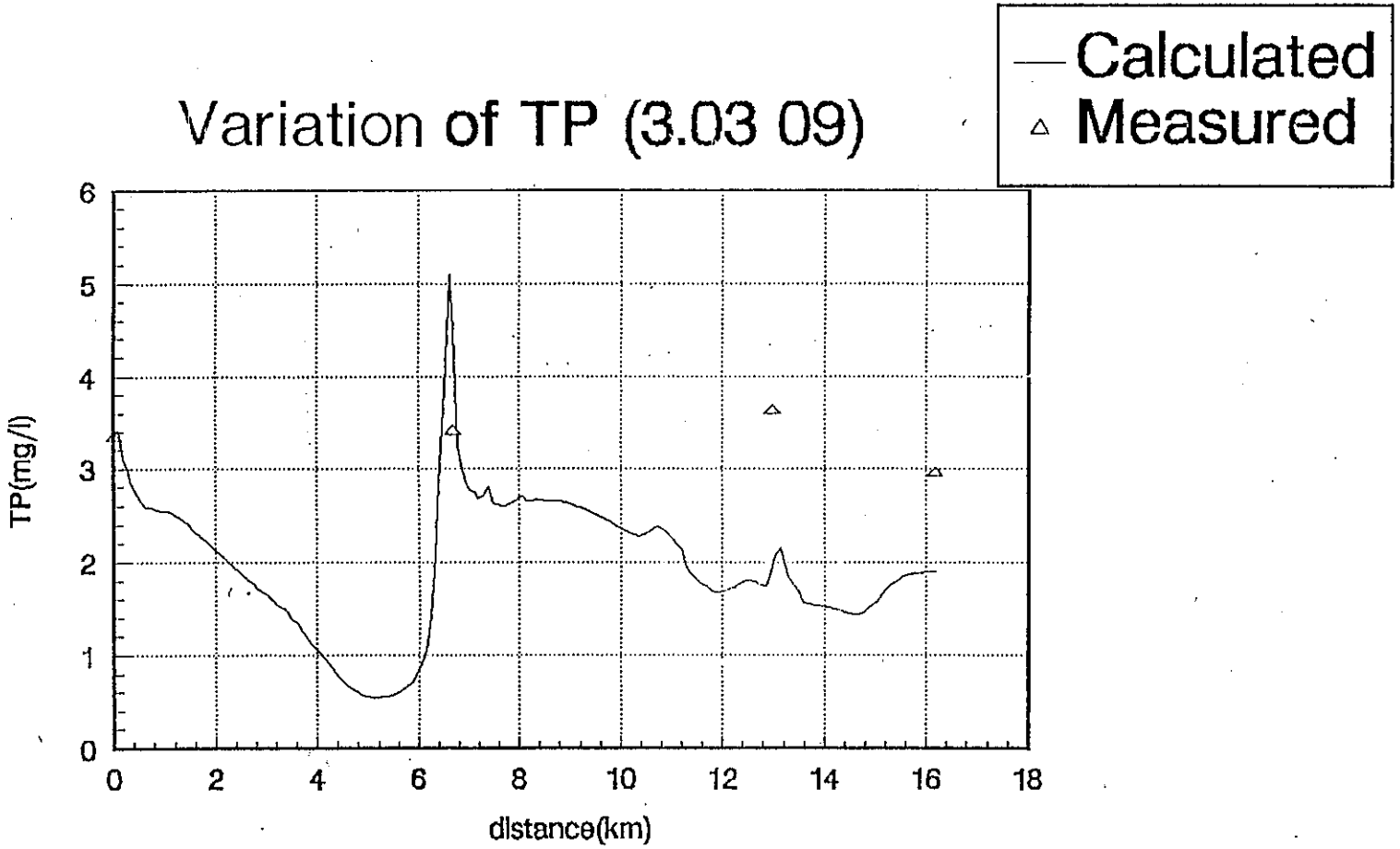

FIG. A7—57(j) **TP variation in dry season** (3. 03 09)

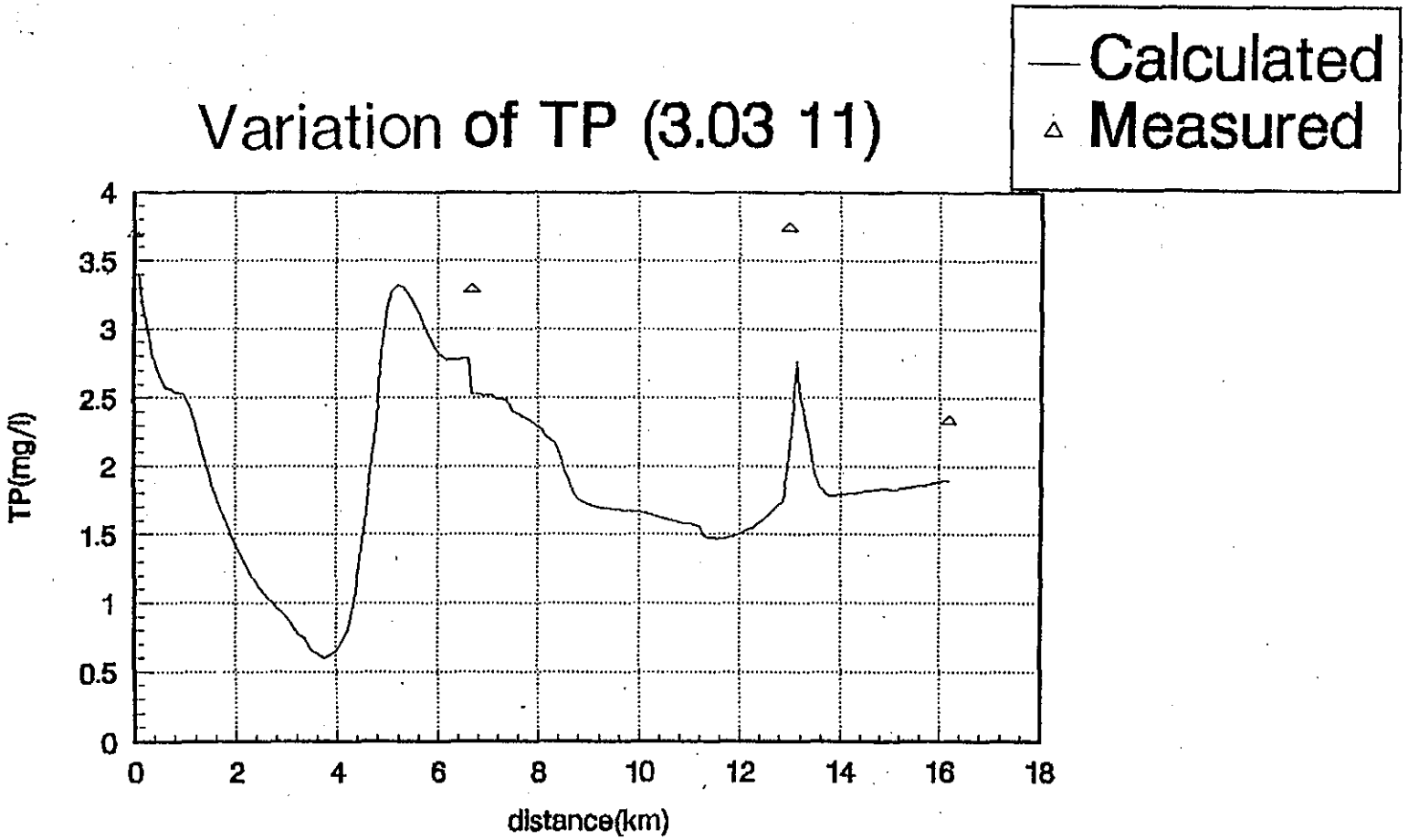

FIG. A7—57(k) **TP variation in dry season** (3. 03 11)

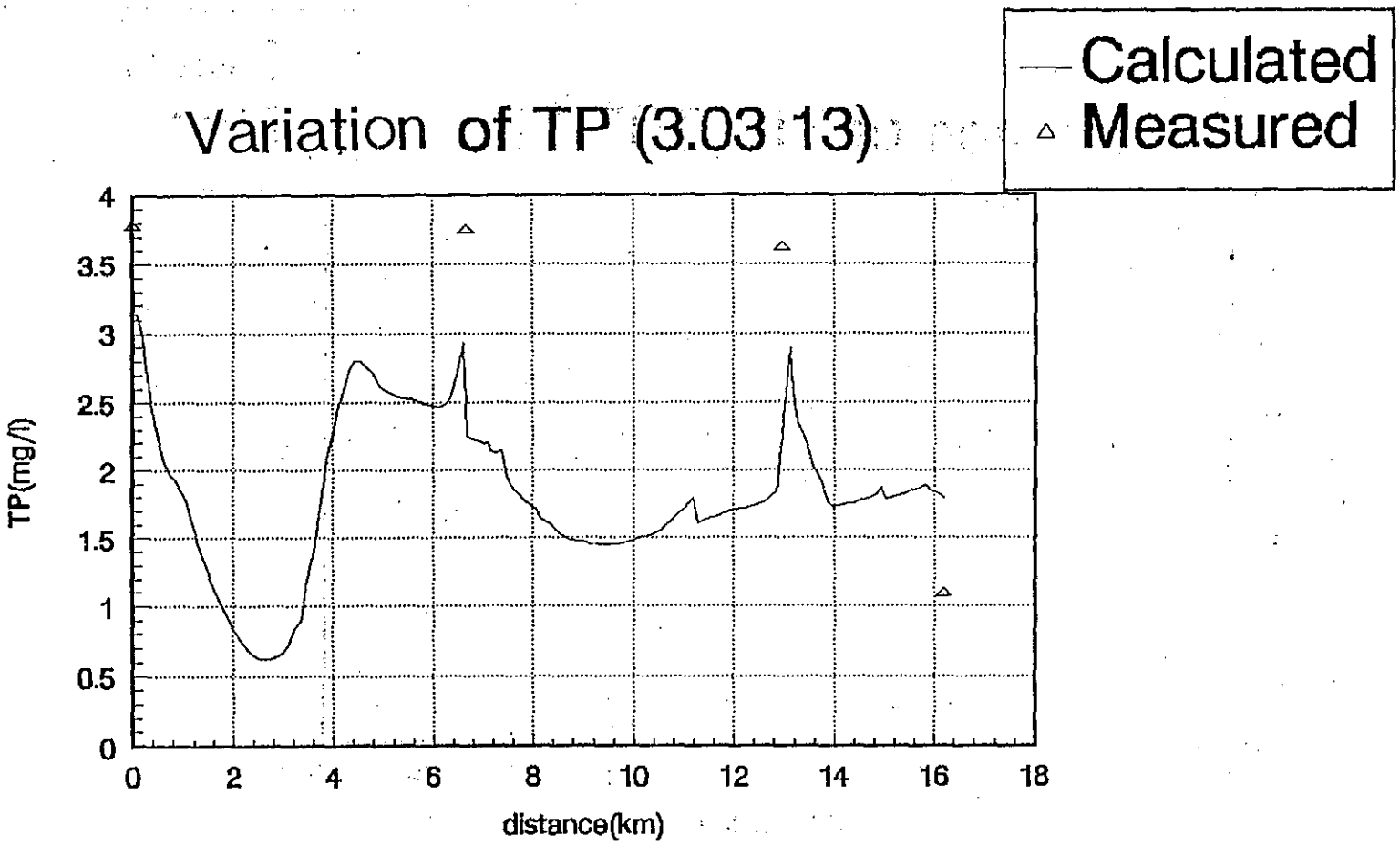

FIG. A7—57(1) TP variation in dry season (3. 03 13)

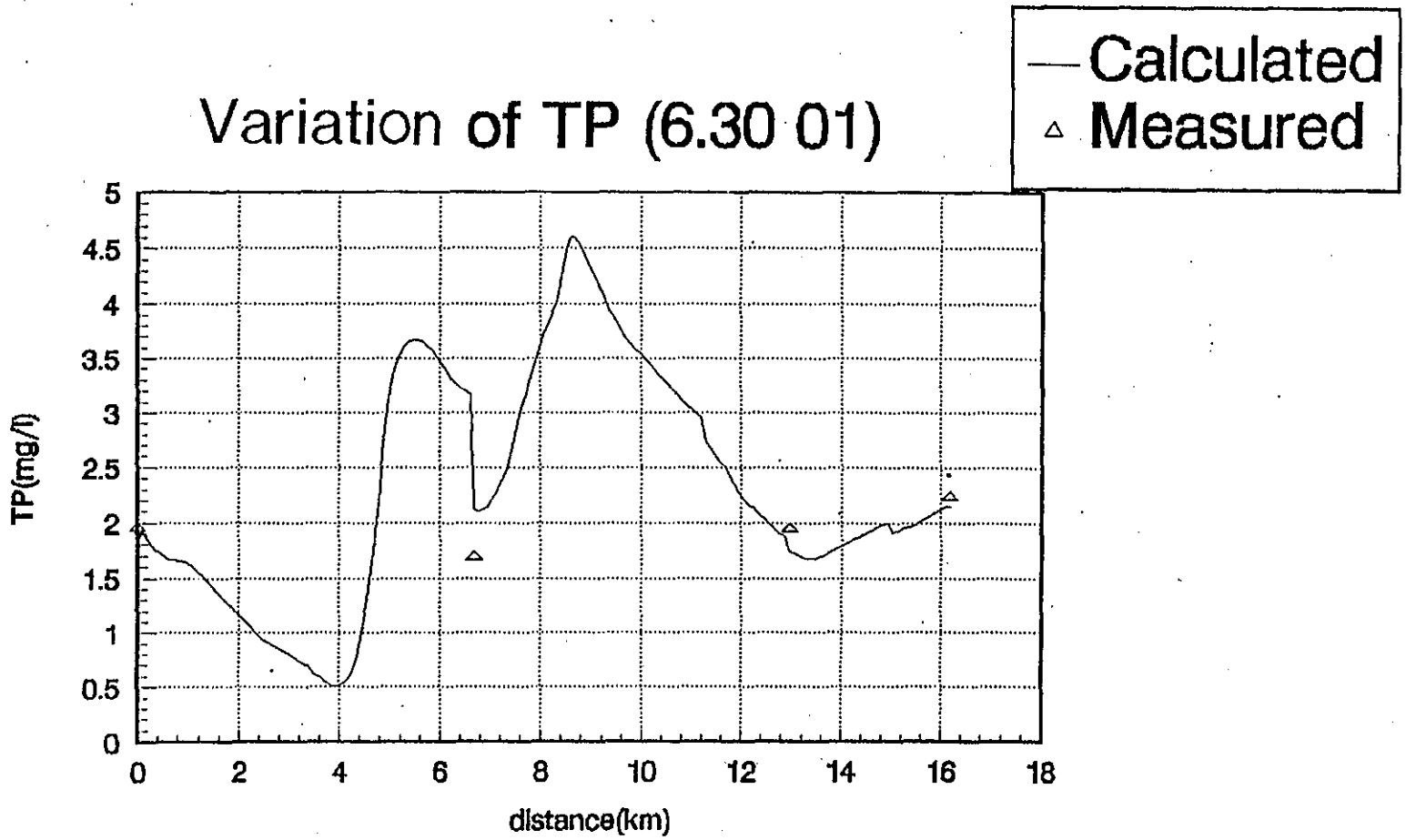

FIG. A7—57(m) TP variation in wet season (6. 30 01)

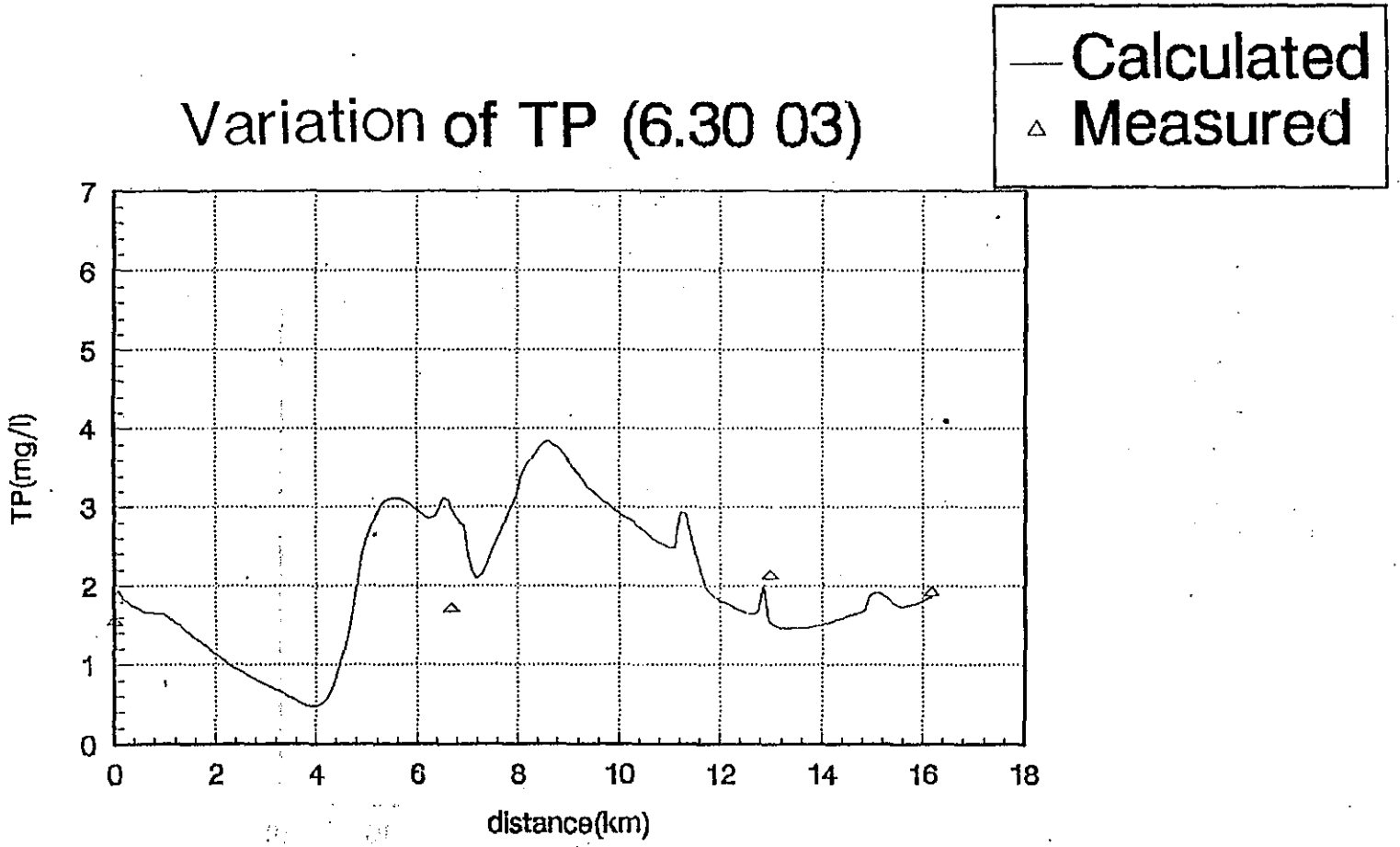

FIG. A7—57(n) **TP variation in wet season** (6. 30 03)

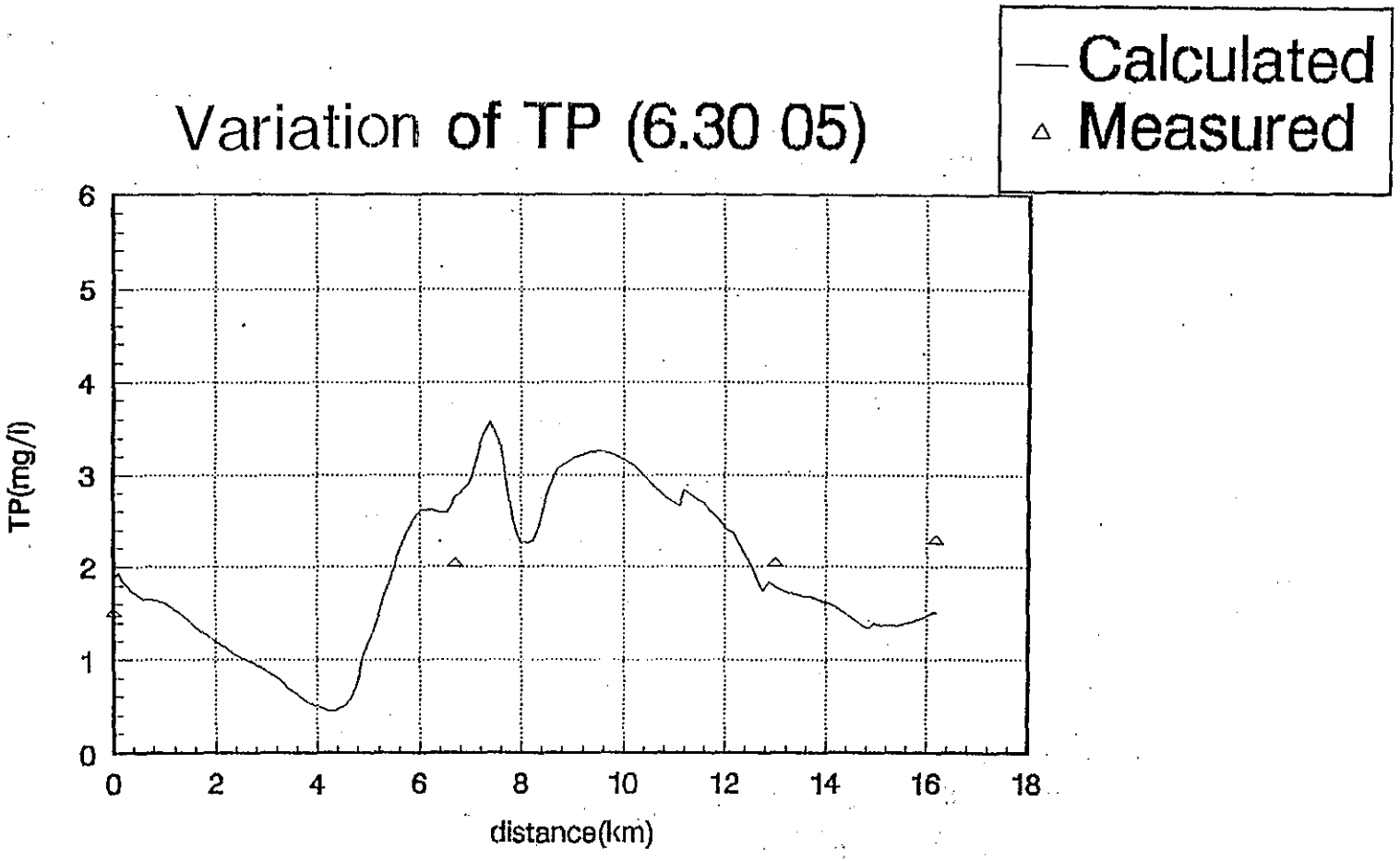

FIG. A7—57(o) TP variation in wet season (6. 30 05)

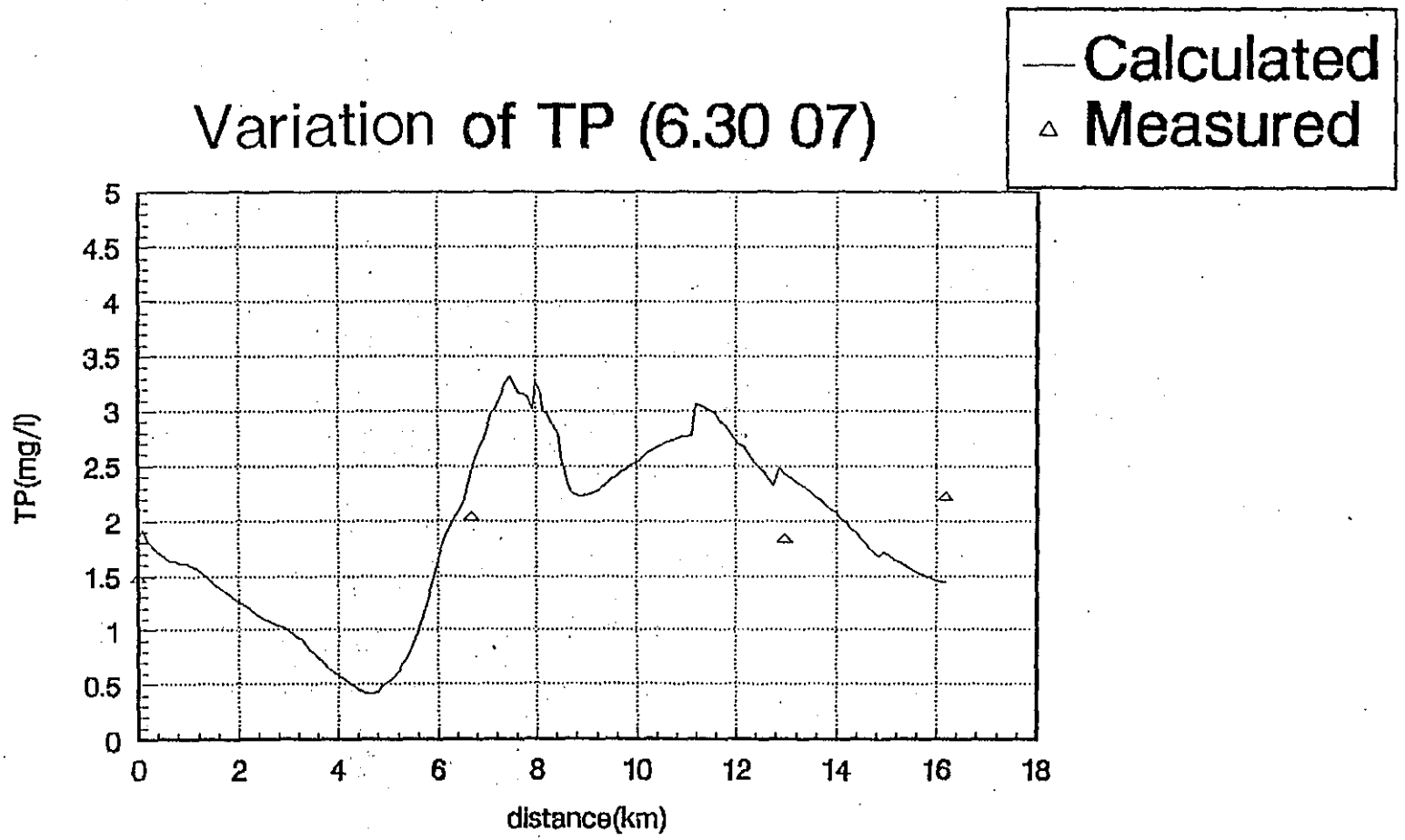

FIG. A7—57(p) **TP variation in wet season** (6. 30 07)

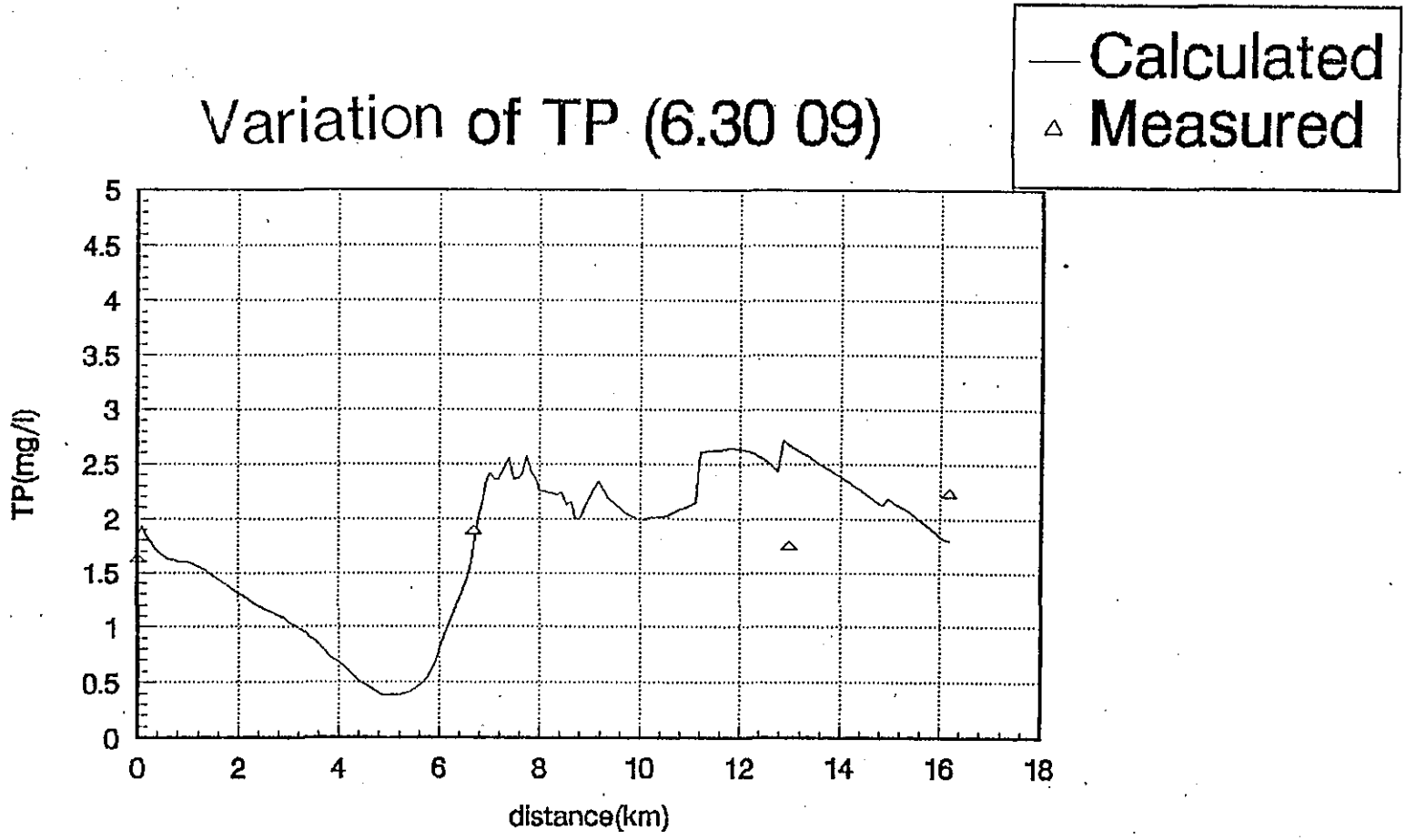

FIG. A7—57(q) **TP variation in wet season** (6. 30 09)

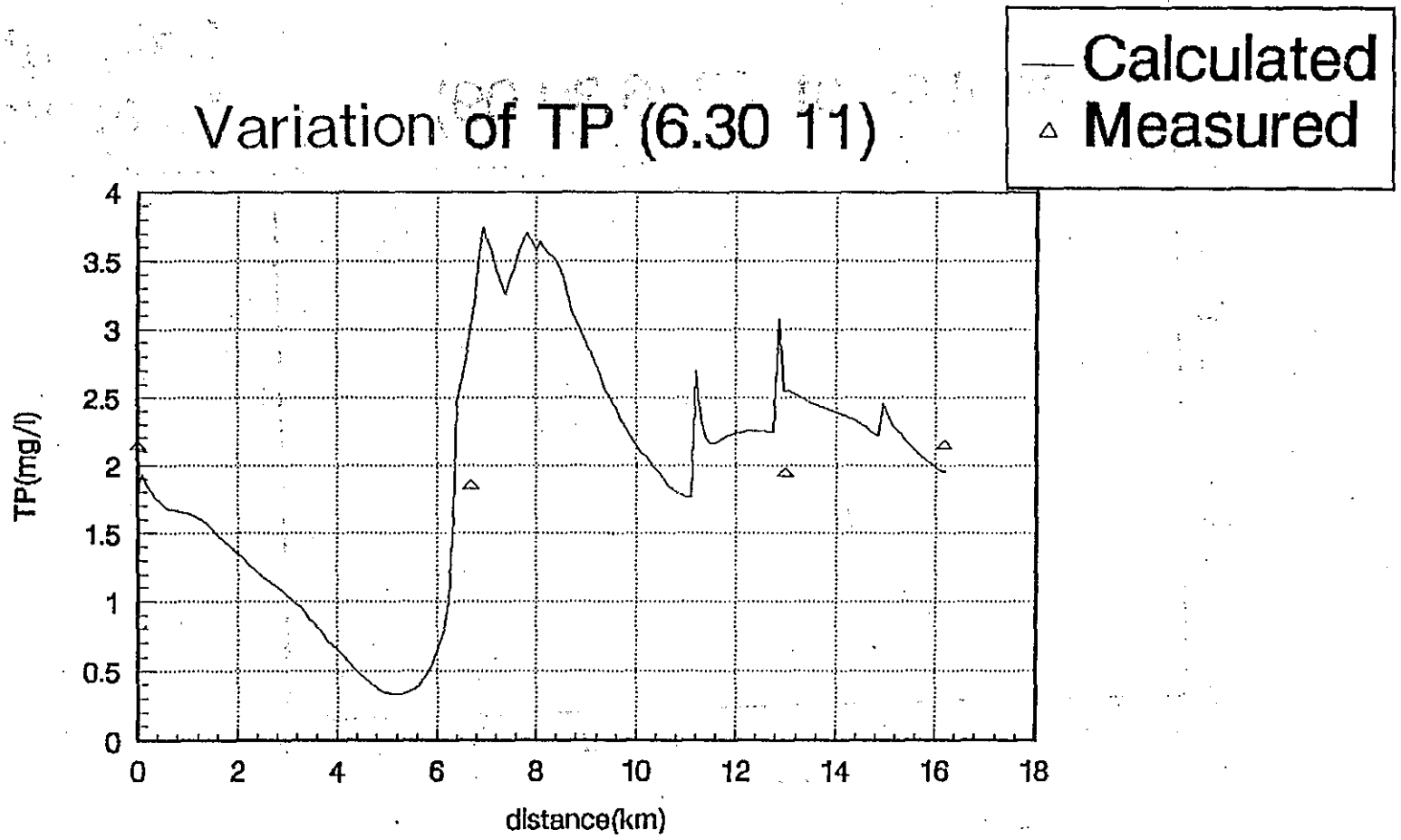

FIG. A7—57(r) TP variation in wet season (6. 30 11)

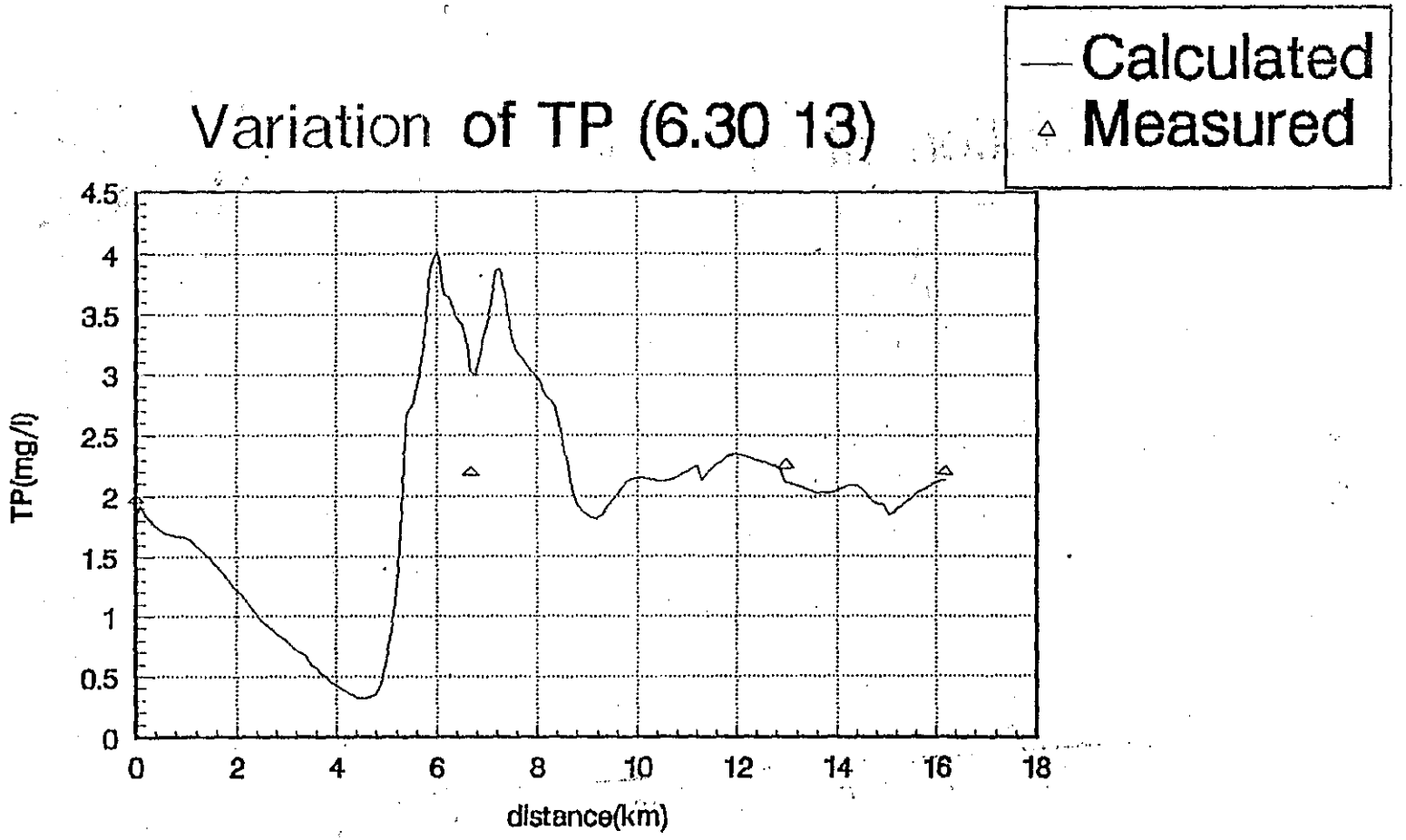

FIG. A7—57(s) **TP variation in wet season** (6.30.13)

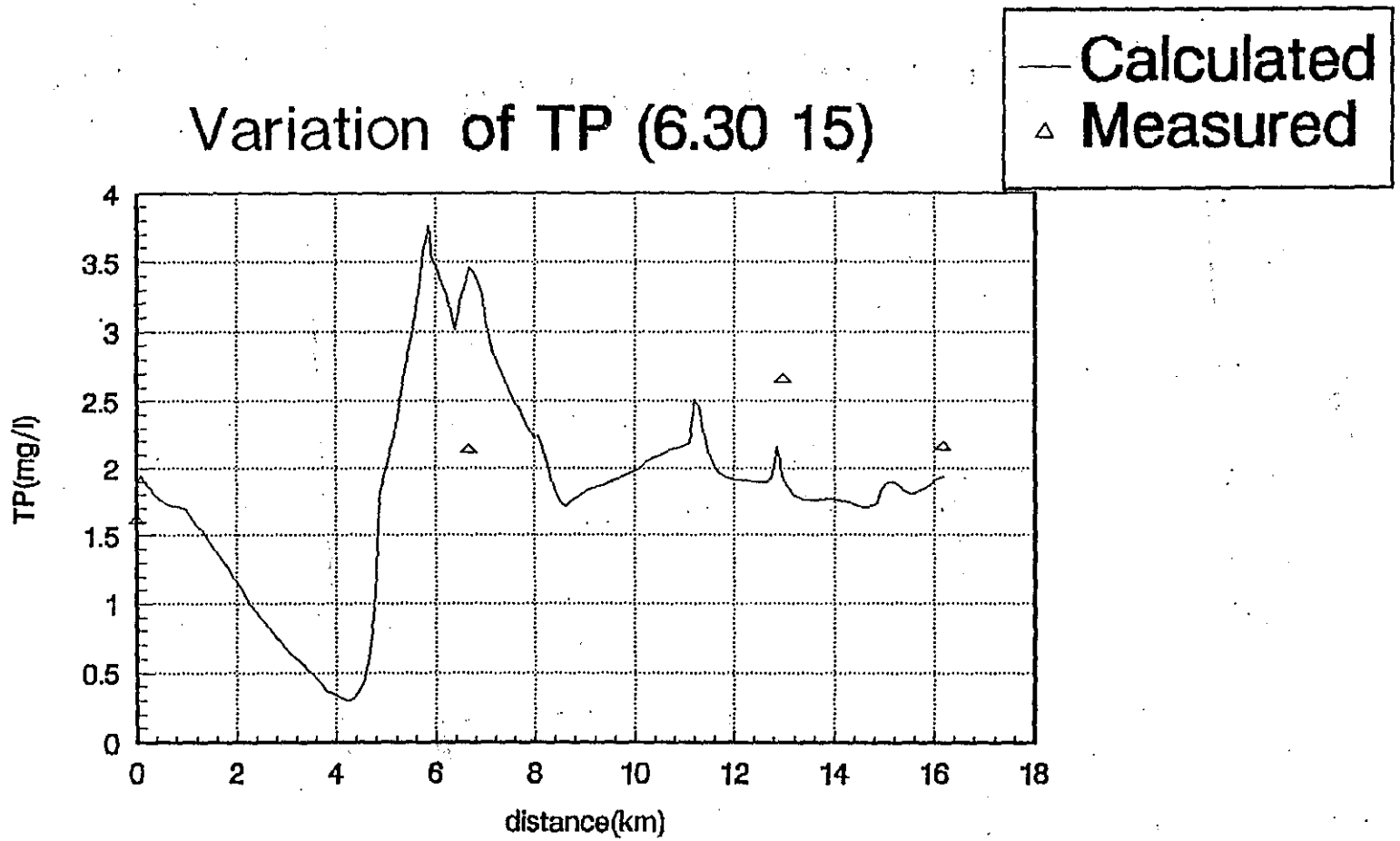

FIG. A7—57(t) TP variation in wet season (6. 30 15)

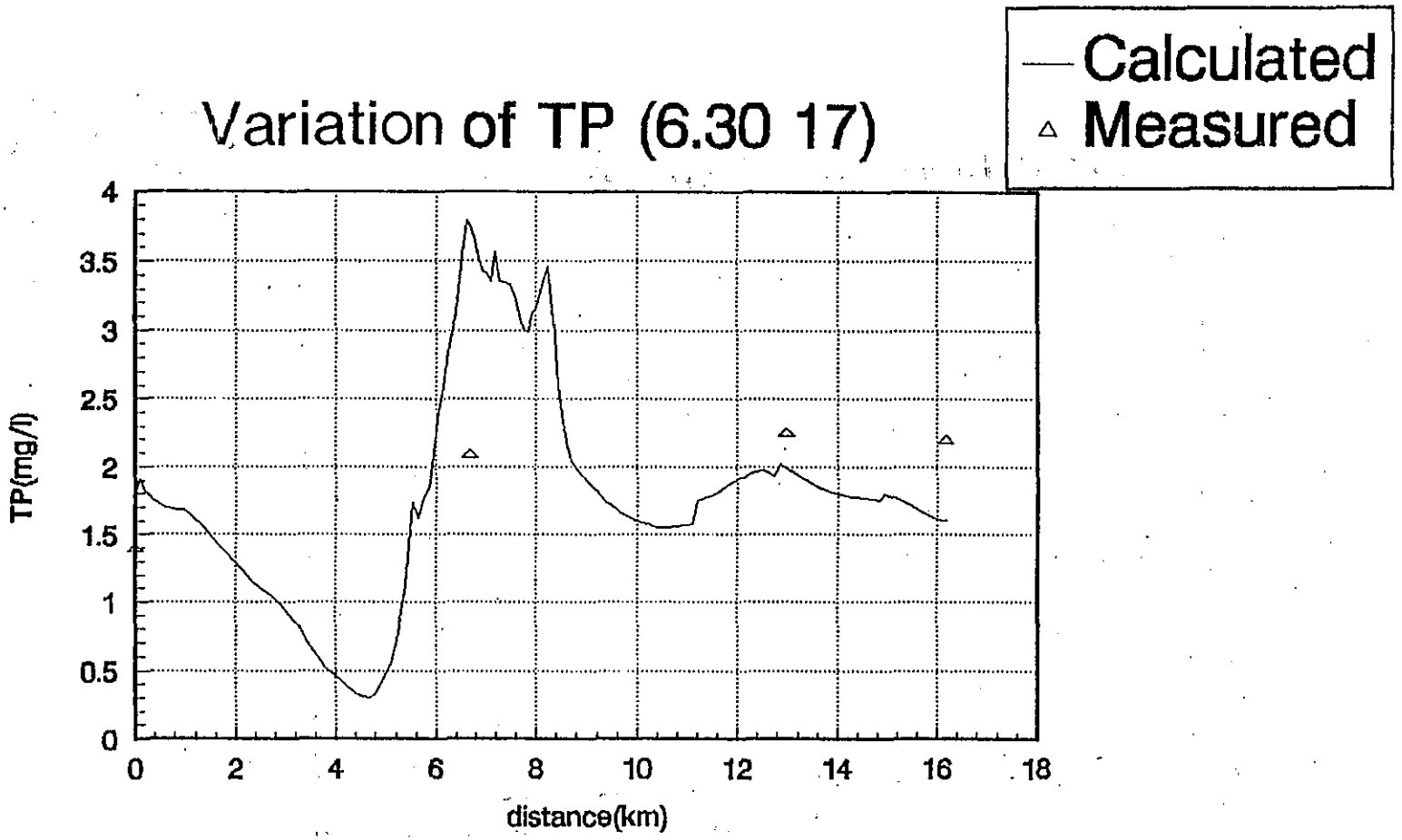

FIG. A7—57(u) **TP variation in wet season** (6. 30 17)

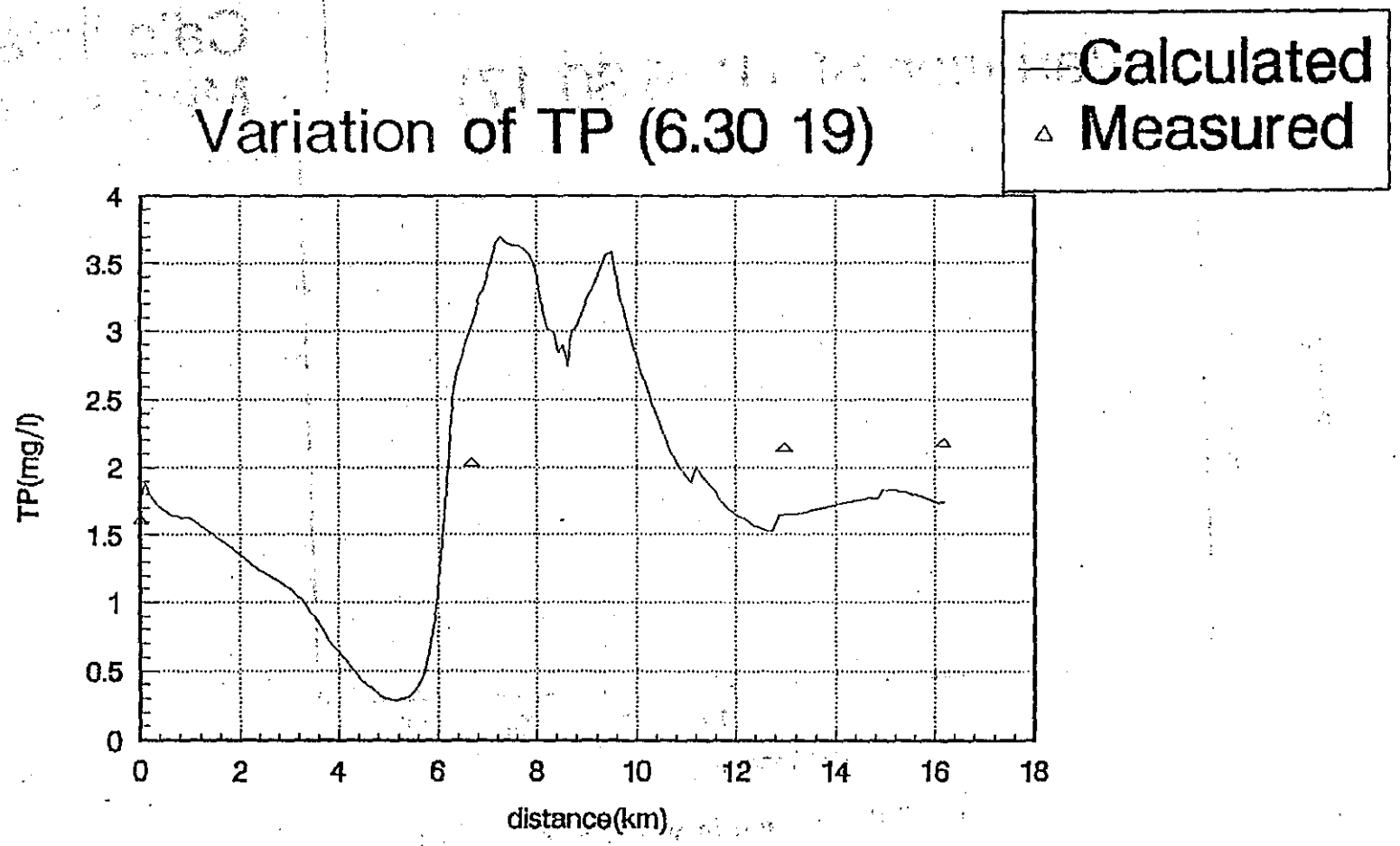

FIG. A7—57(v) **TP variation in wet season** (6. 30 19)

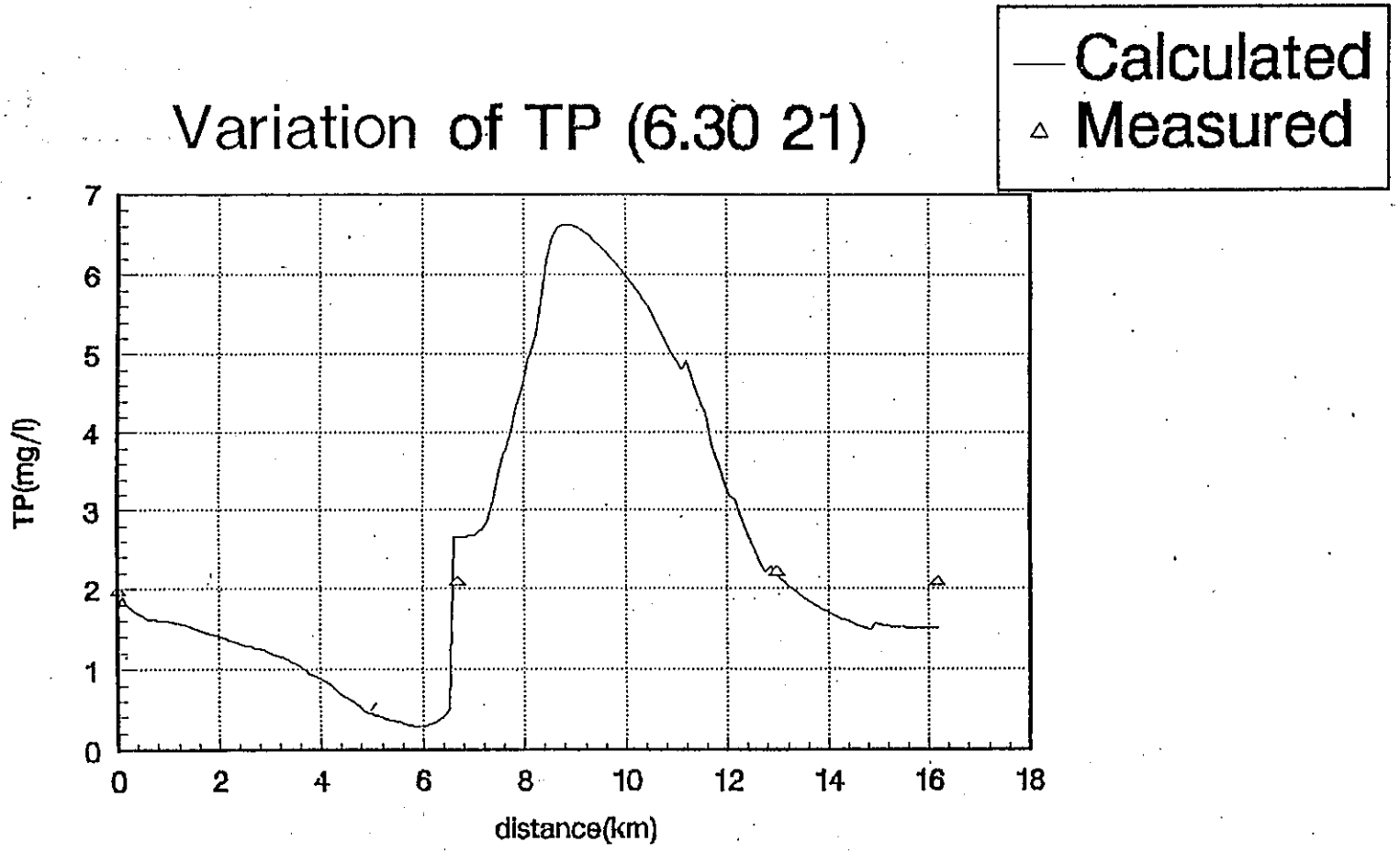

FIG. A7—57(w) TP variation in wet season (6. 30 21)

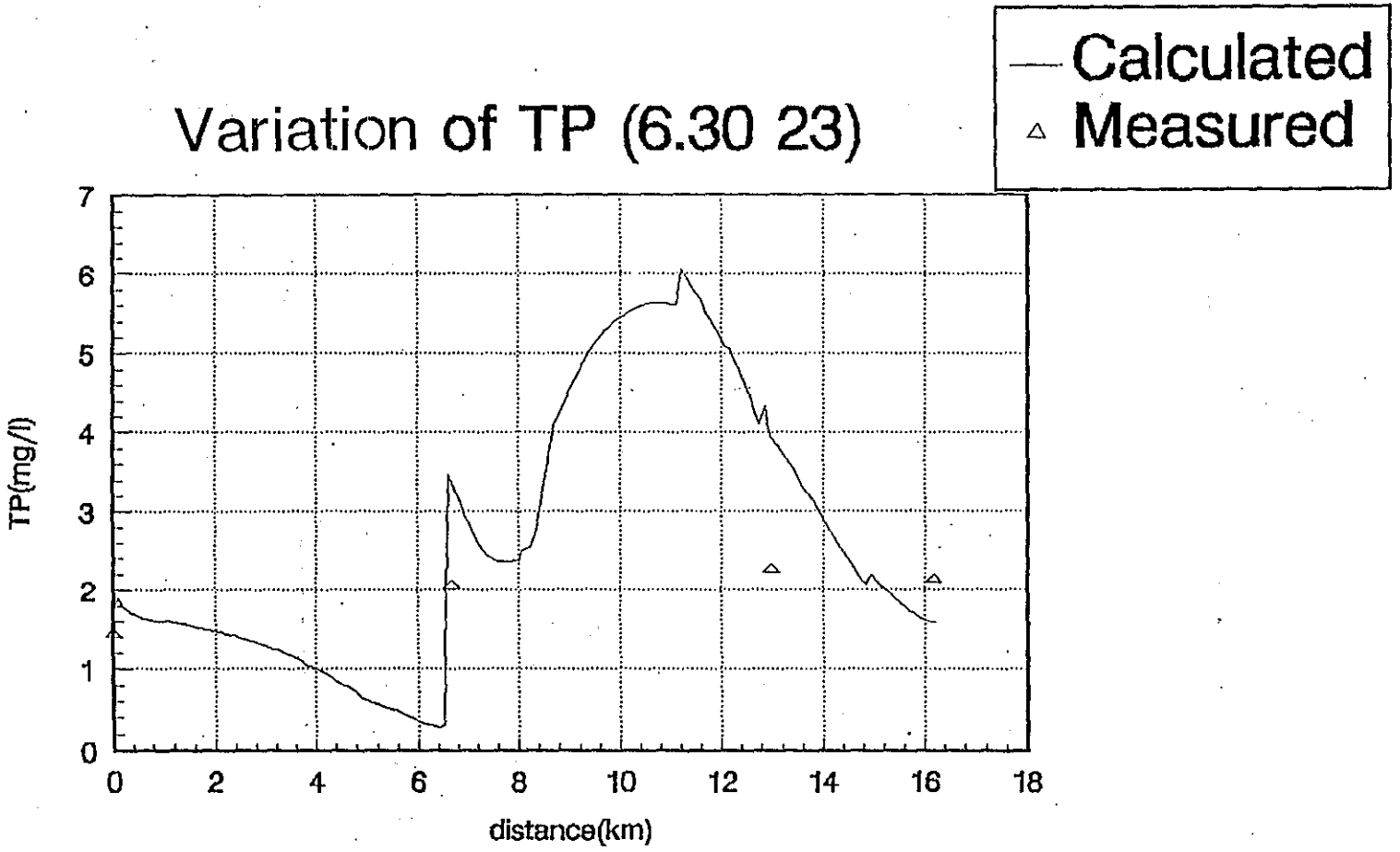

FIG. A7—57(x) **TP variation in wet season** (6. 30 23)

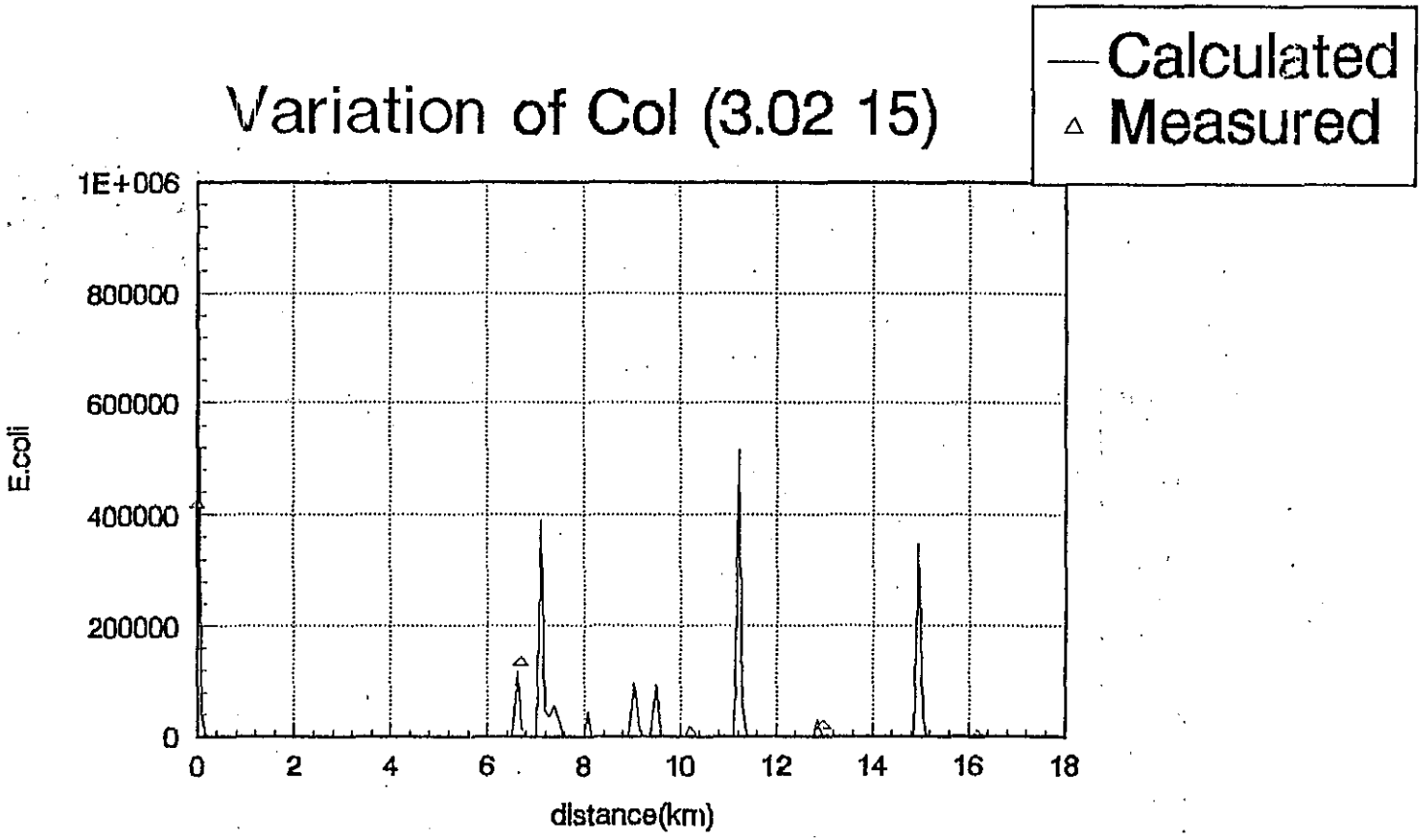

FIG. A7－58(a) **Col. variation in dry season** (3.02 15)

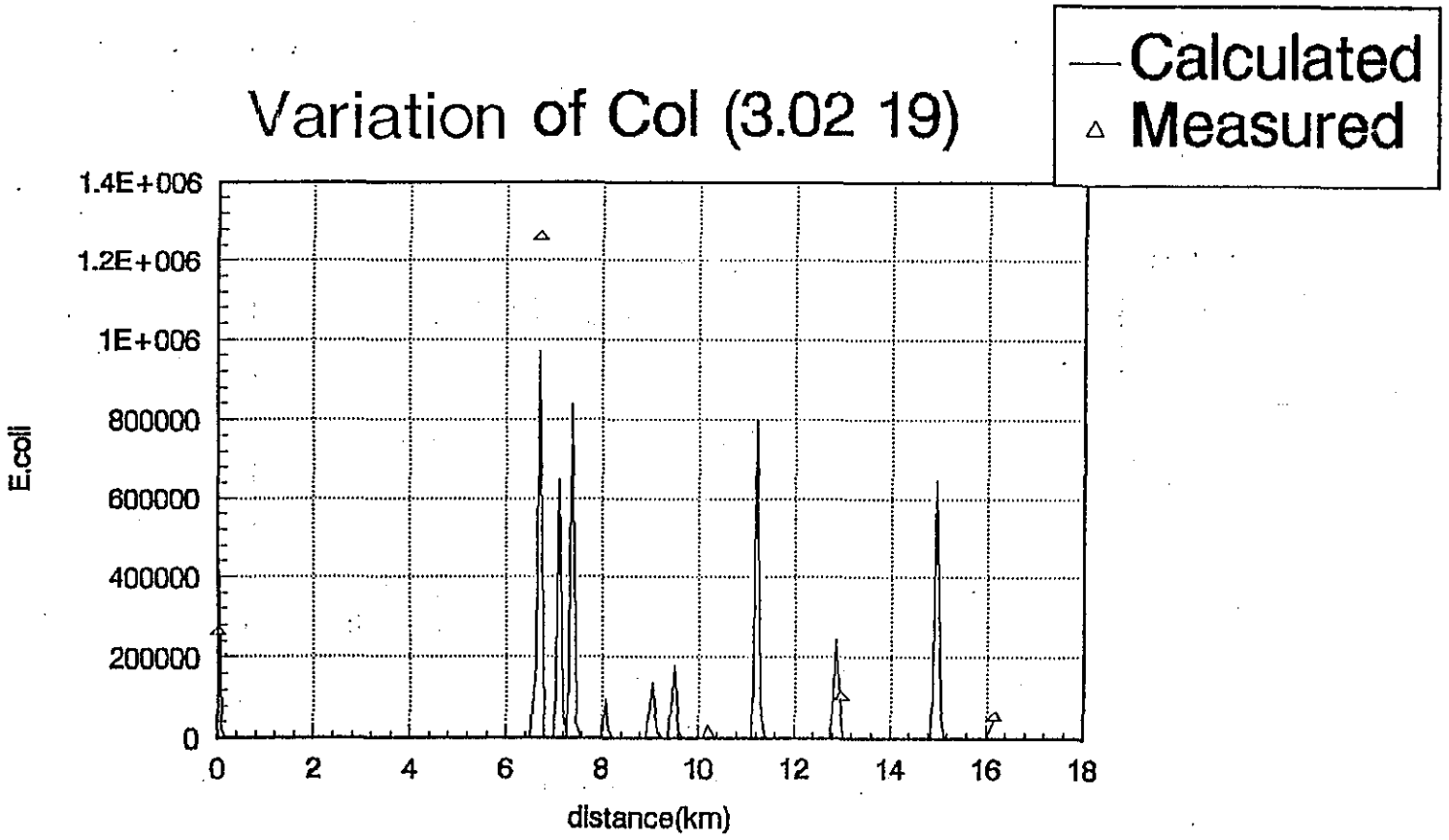

FIG. A7−58(b) Col. variation in dry season (3. 02 19)

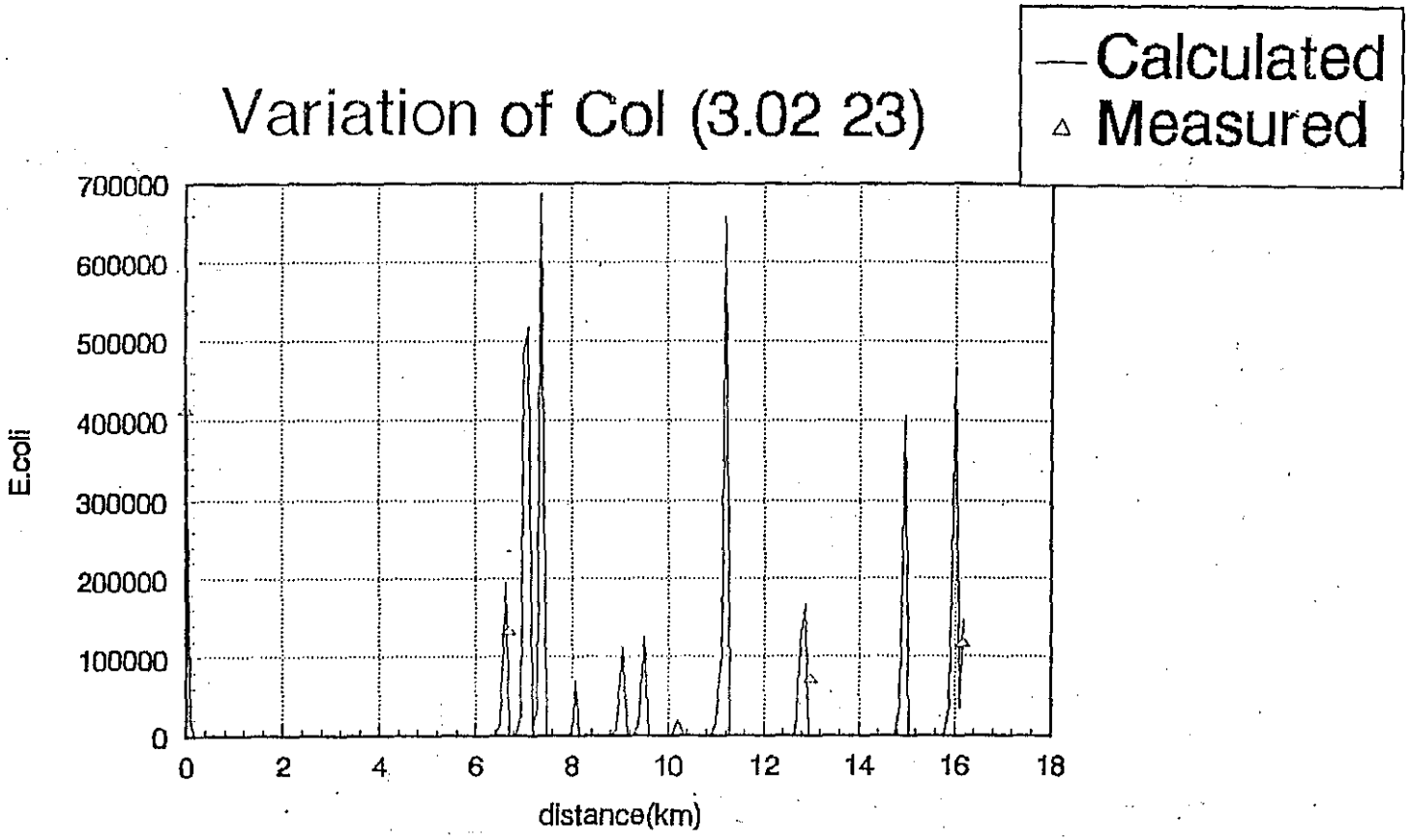

FIG. A7－58(c) Col. variation in dry season (3. 02 23)

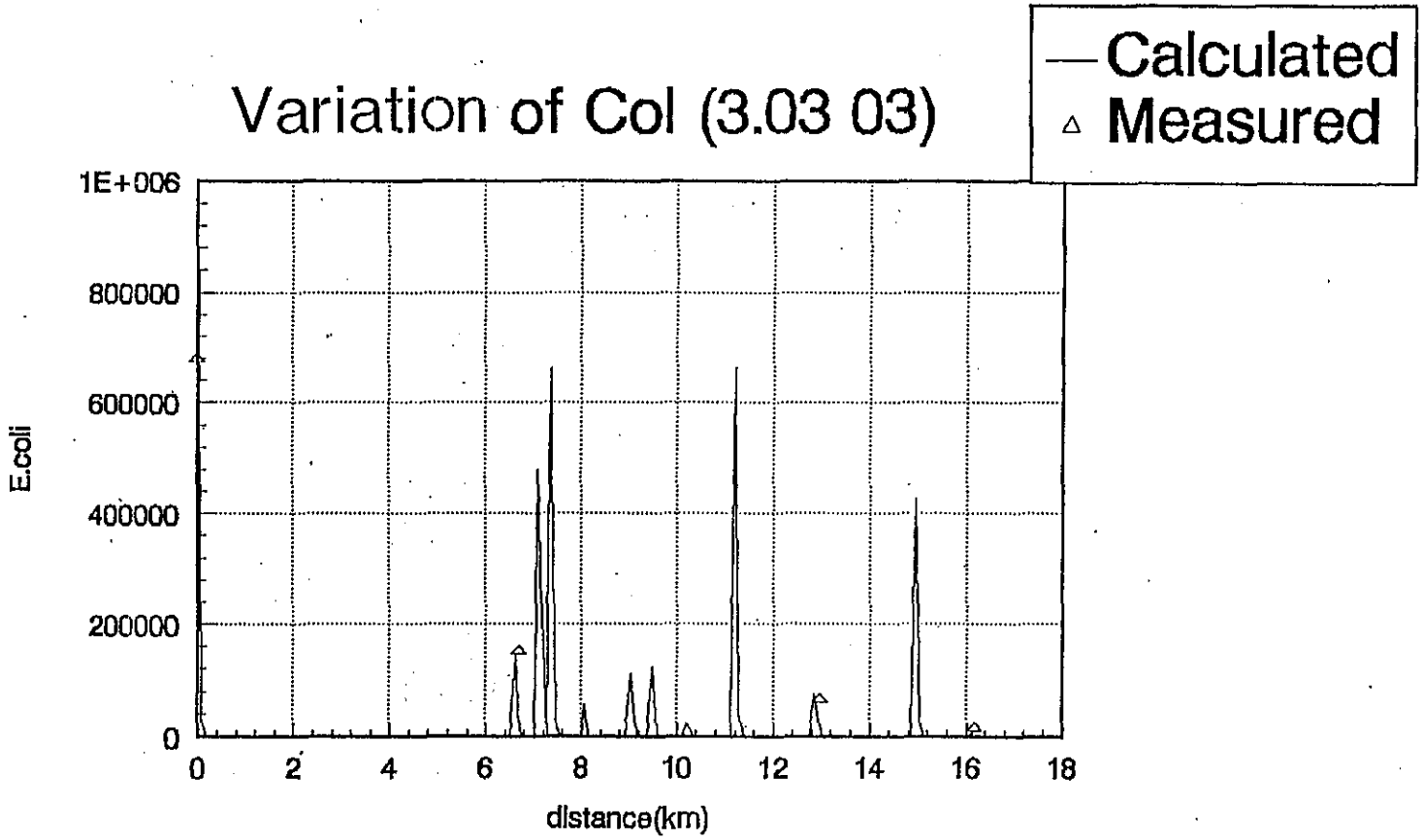

FIG. A7−58(d) Col. variation in dry season (3. 03 03)

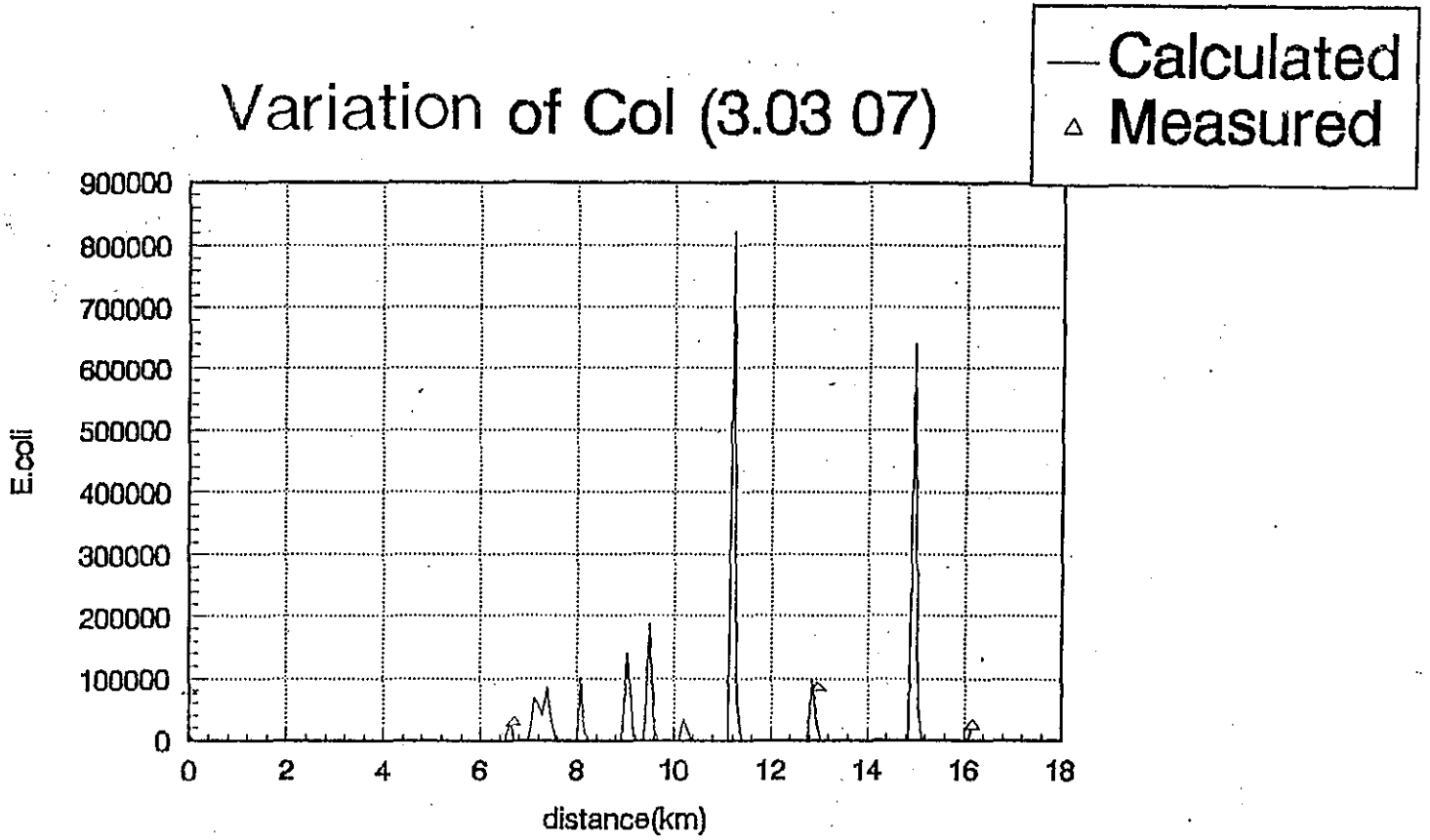

FIG. A7—58(e) **Col. variation in dry season** (3.03 07)

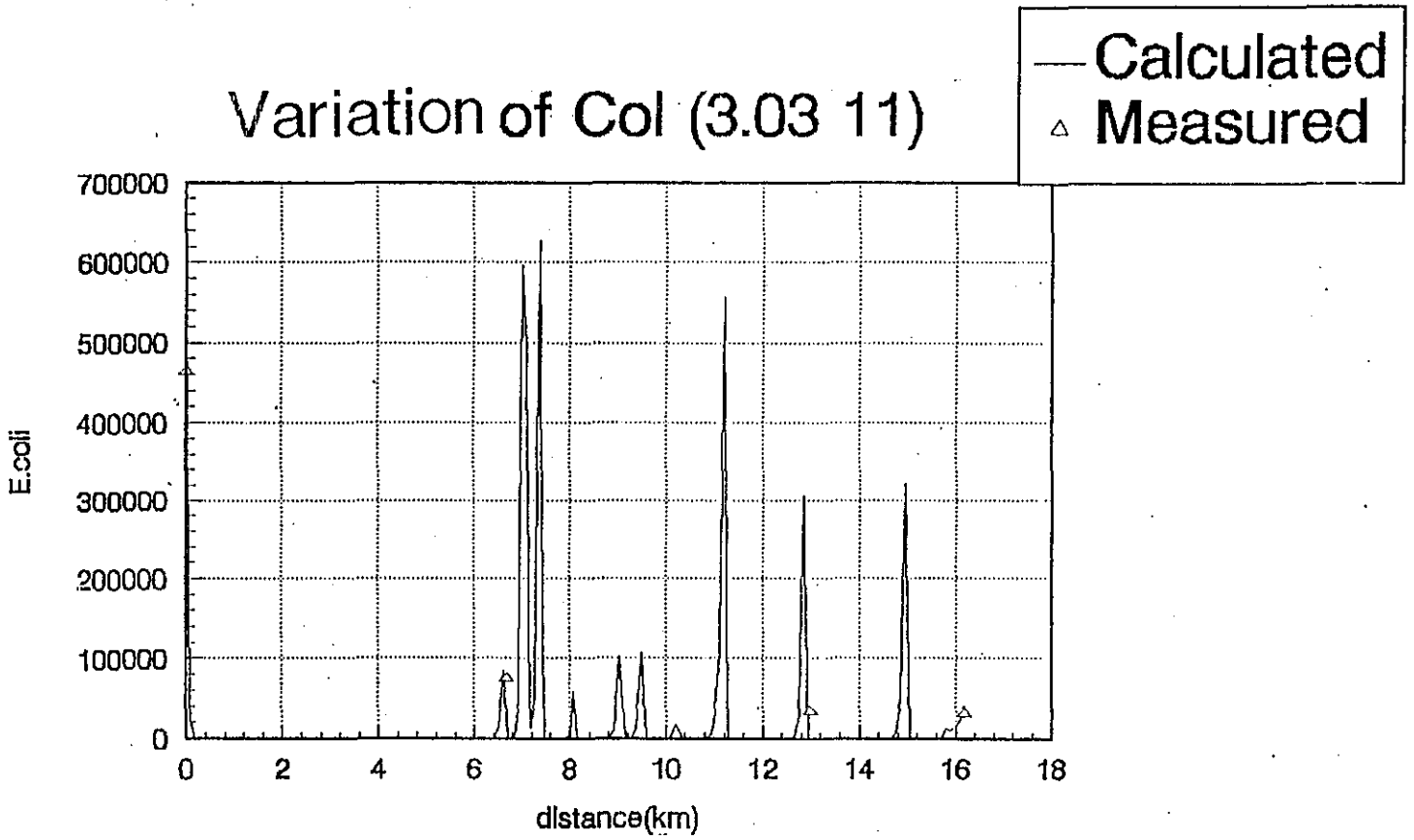

FIG. A7—58(f) Col. variation in dry season (3. 03 11)

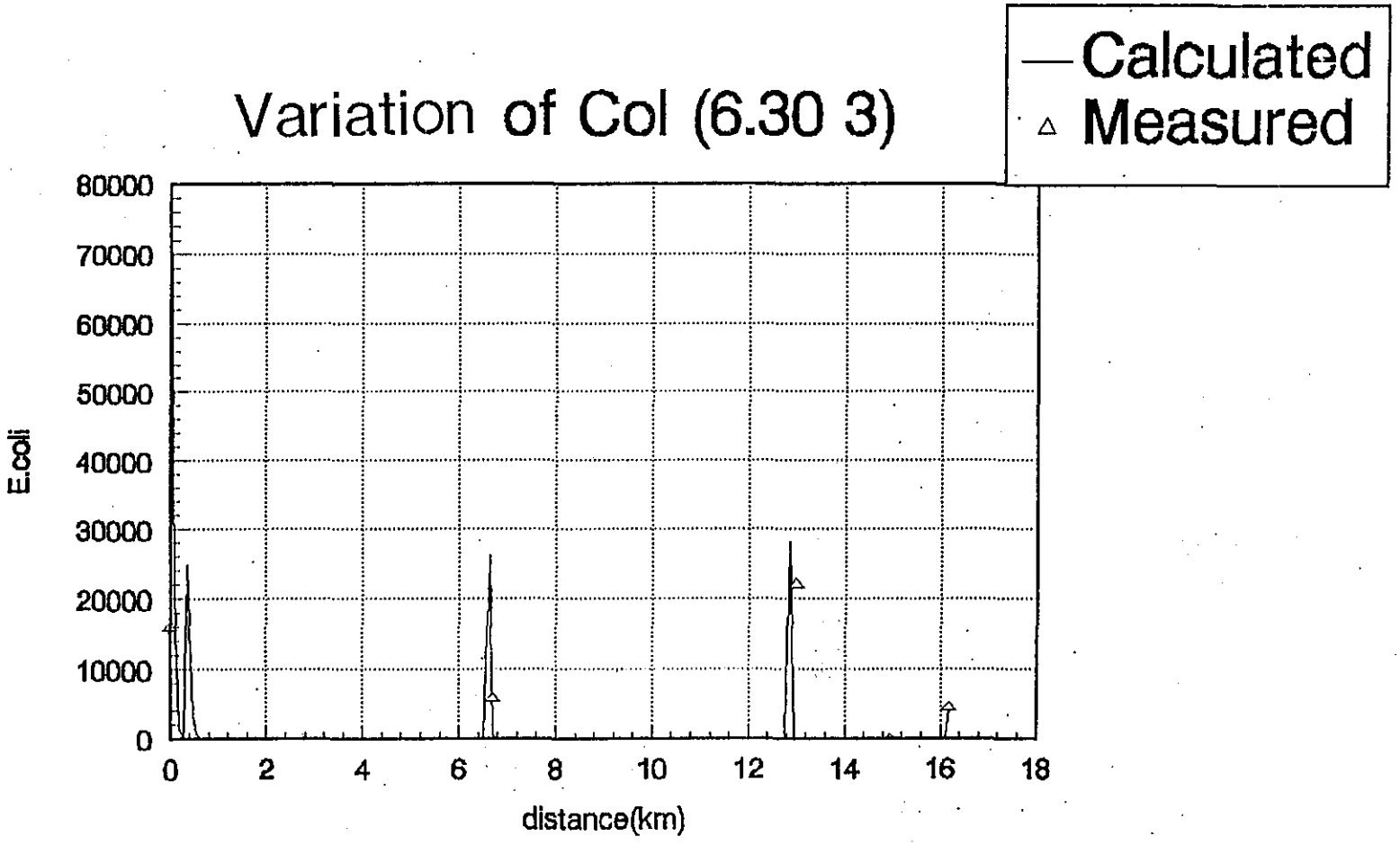

FIG. A7—58(g) Col. variation in wet season (6. 30 03)

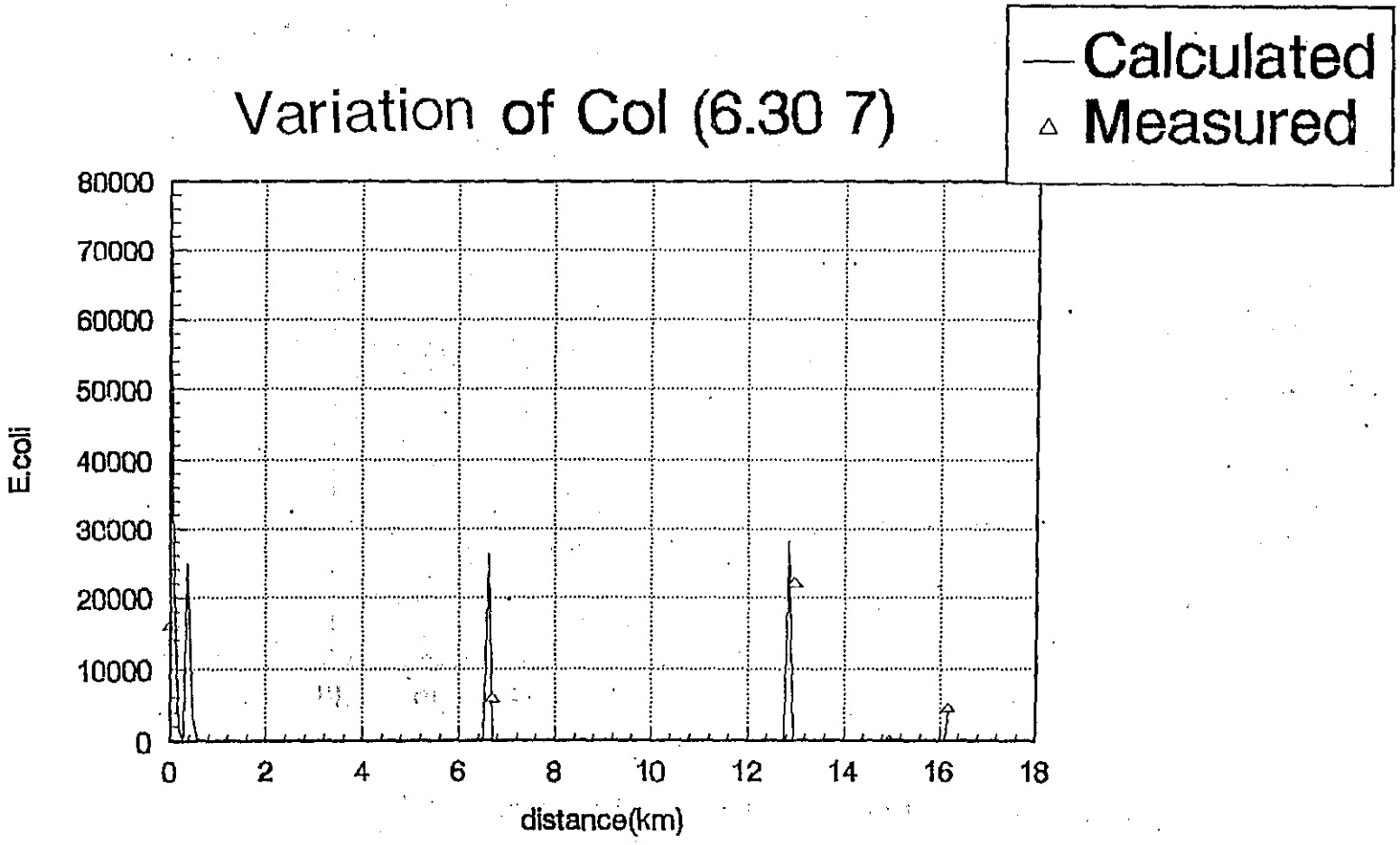

FIG. A7—58(h) Col. variation in wet season (6. 30 07)

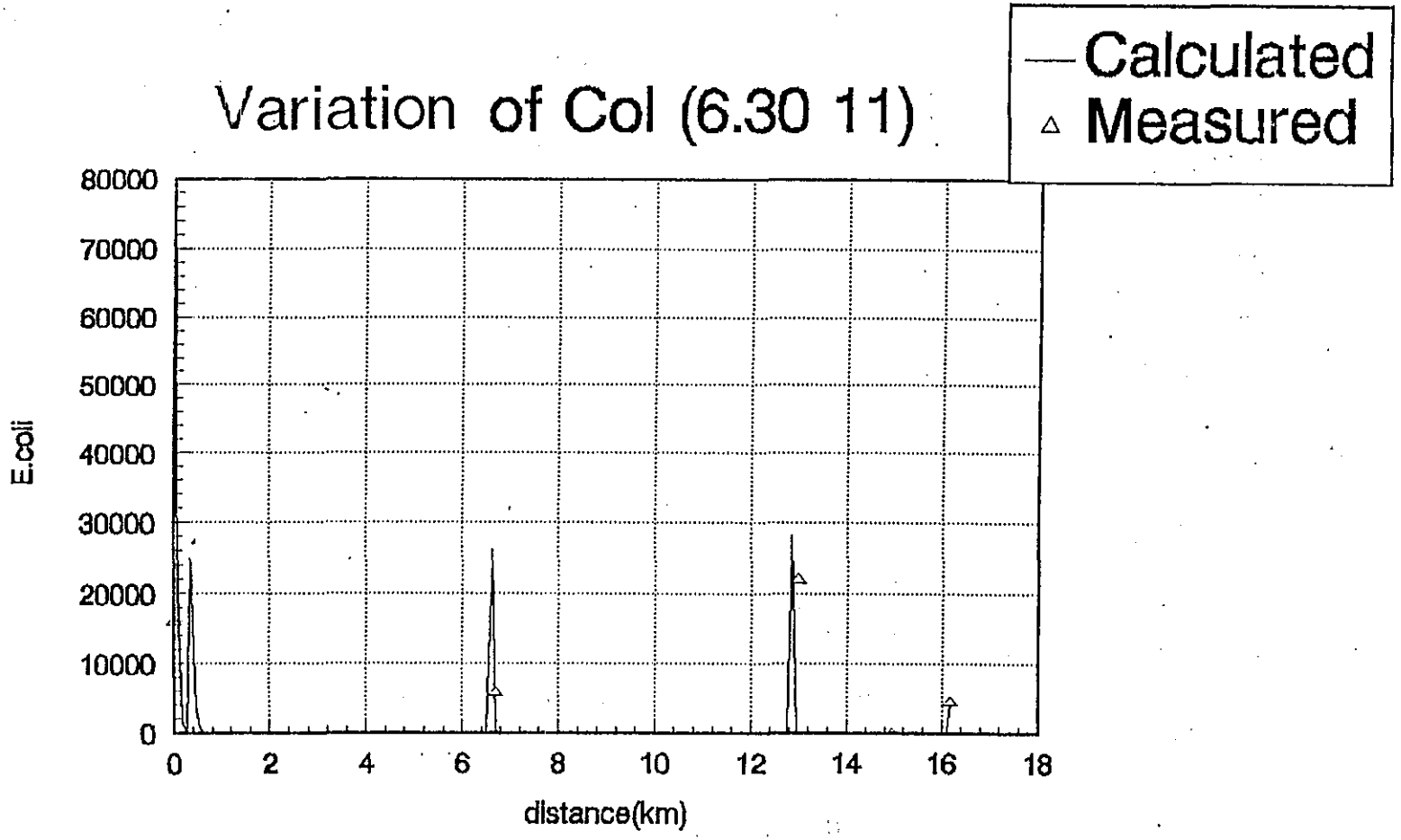

FIG. A7—58(i) Col. variation in wet season (6.30 11)

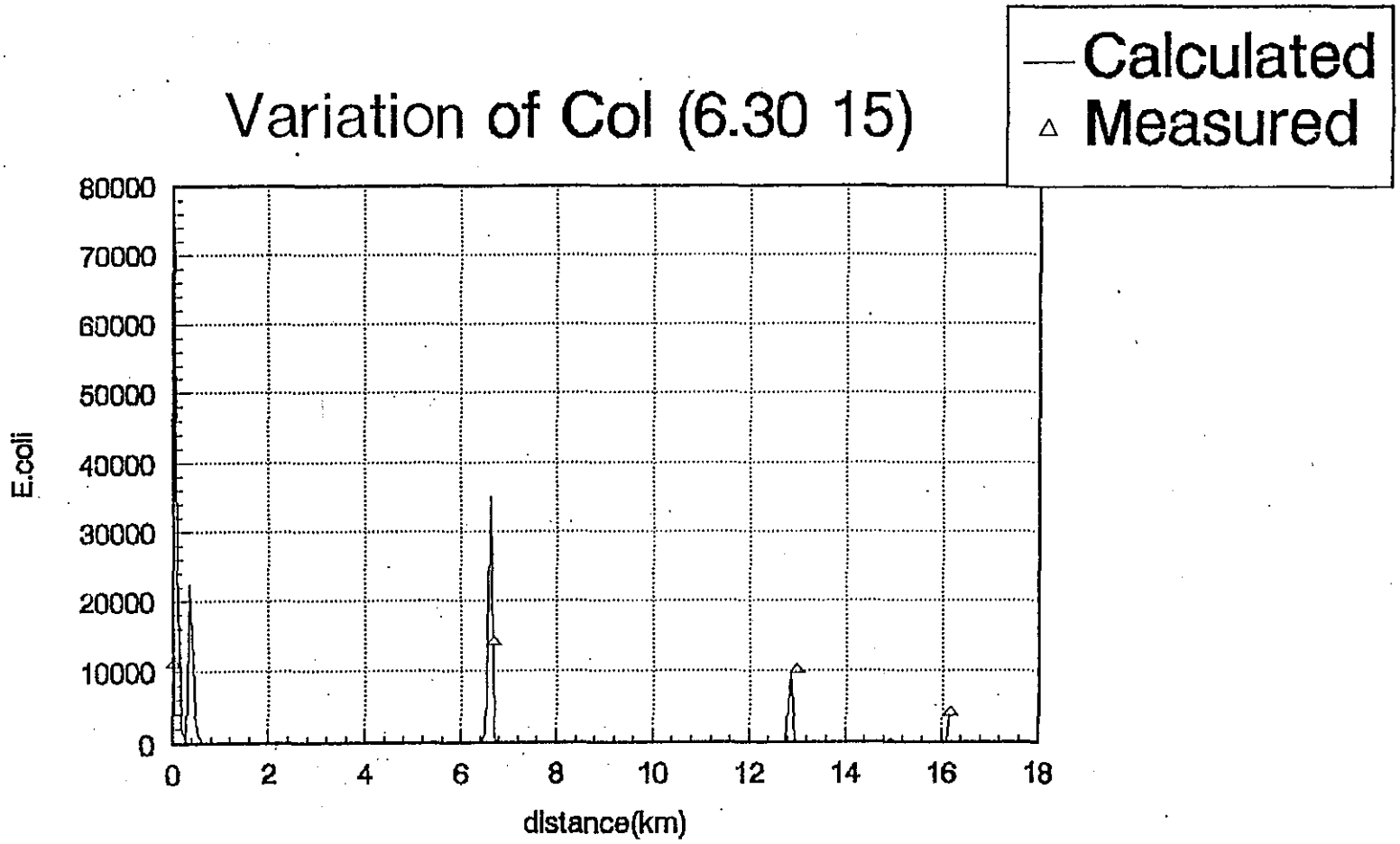

FIG. A7－58(j) Col. variation in wet season (6. 30 15)

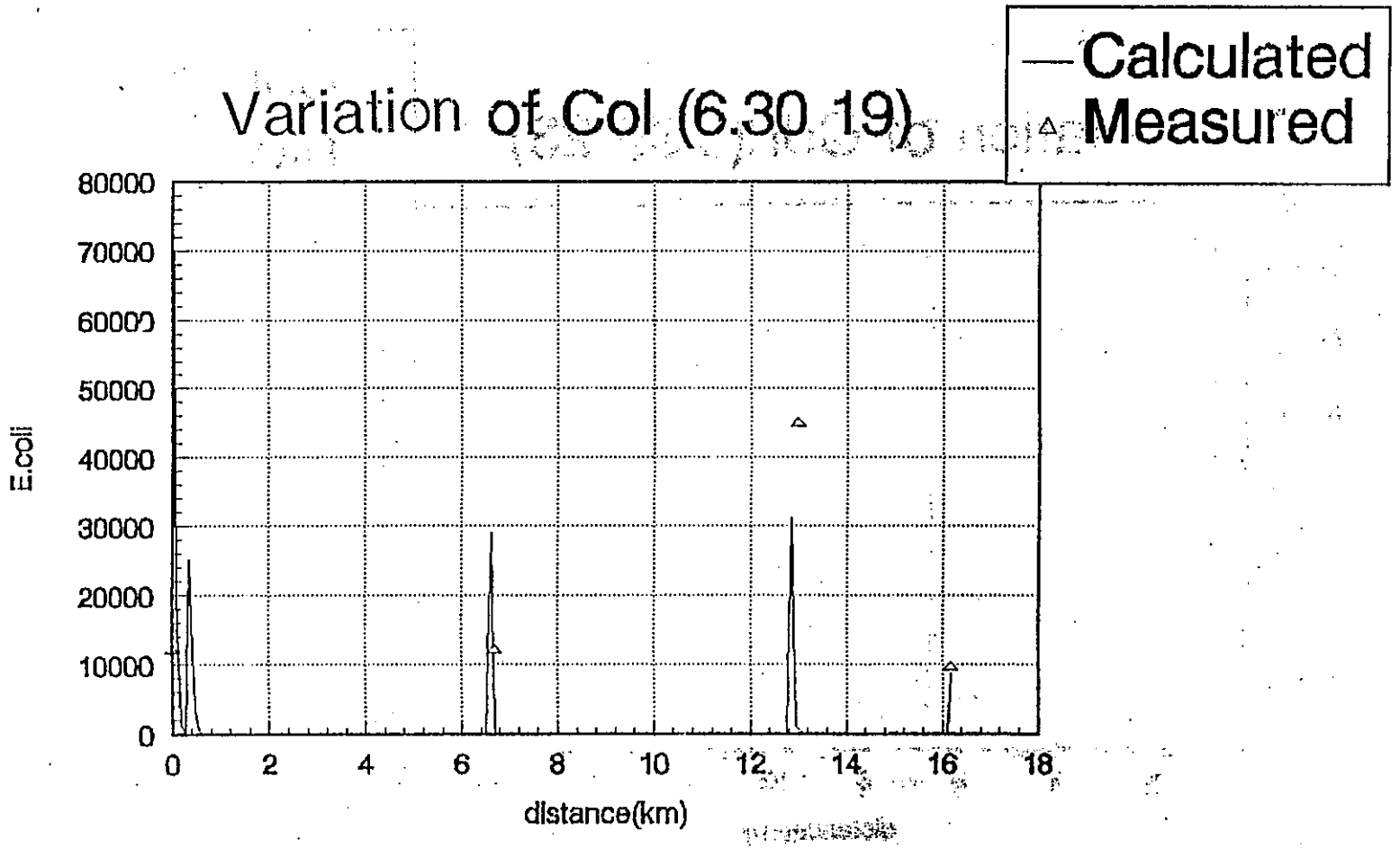

FIG. A7—58(k) Col. variation in wet season (6. 30. 19)

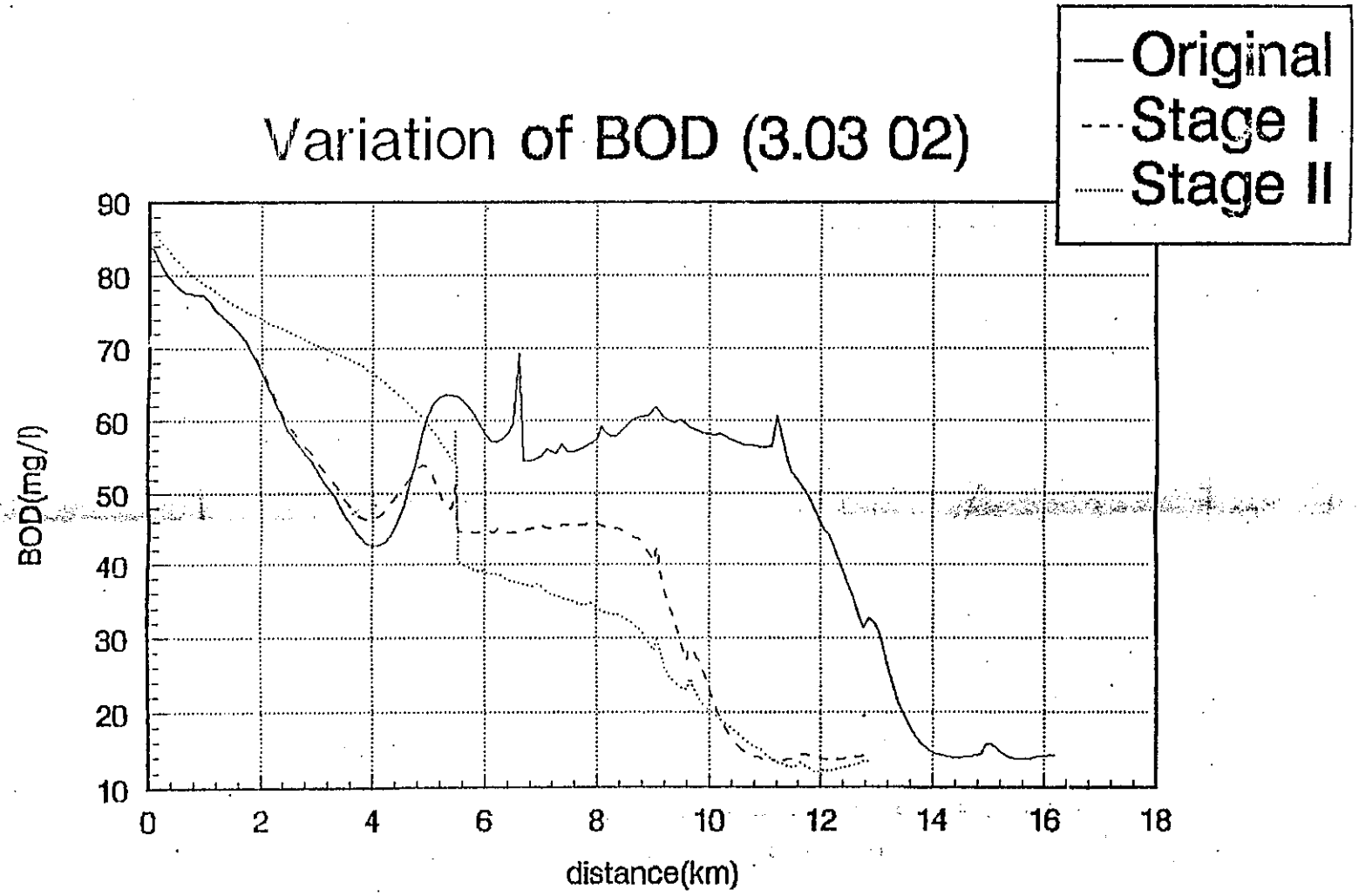

FIG. A7- 59(a) BOD variation before and after the works (3. 03 02)

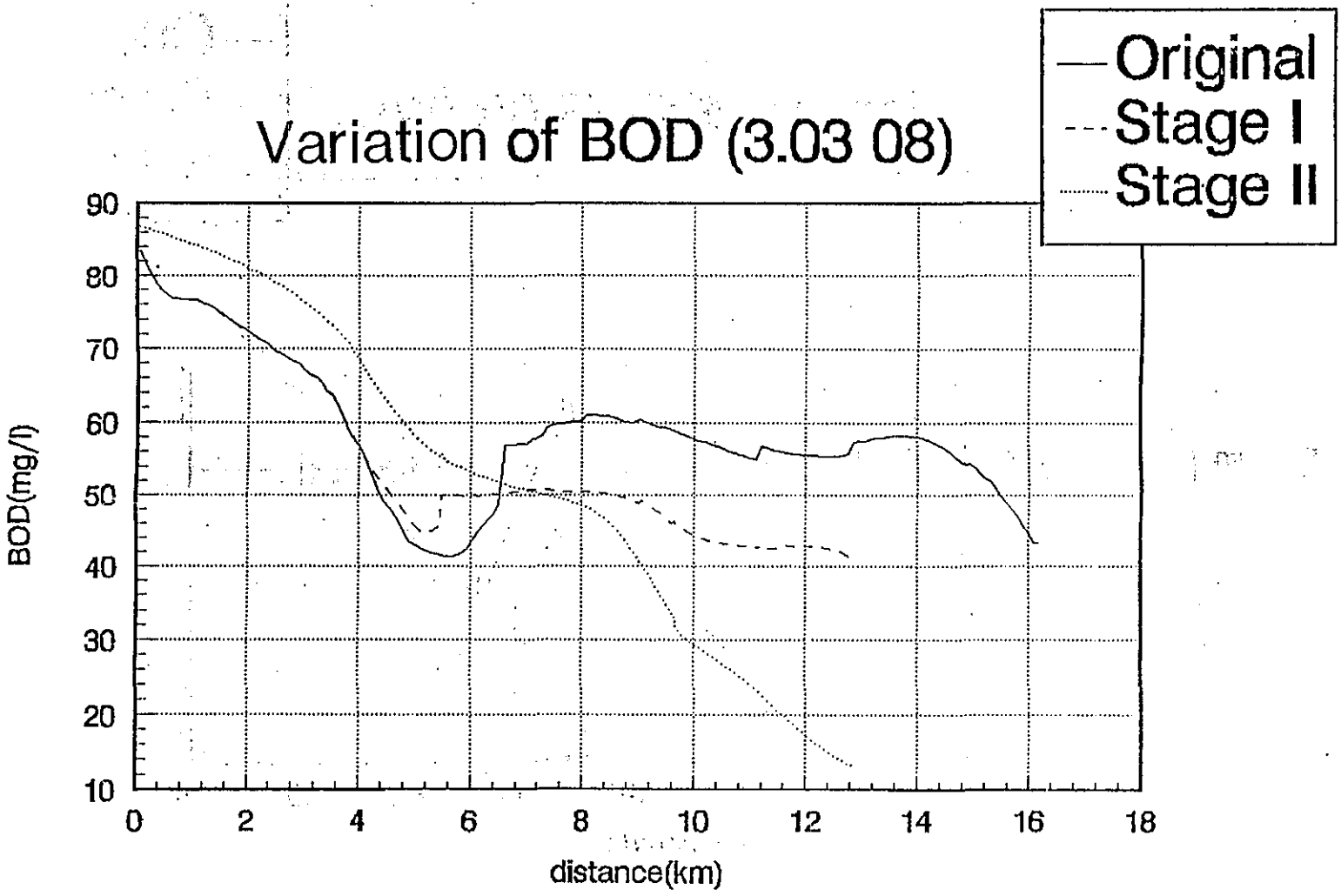

FIG. A7—59(b) BOD variation before and after the works (3. 03 08)

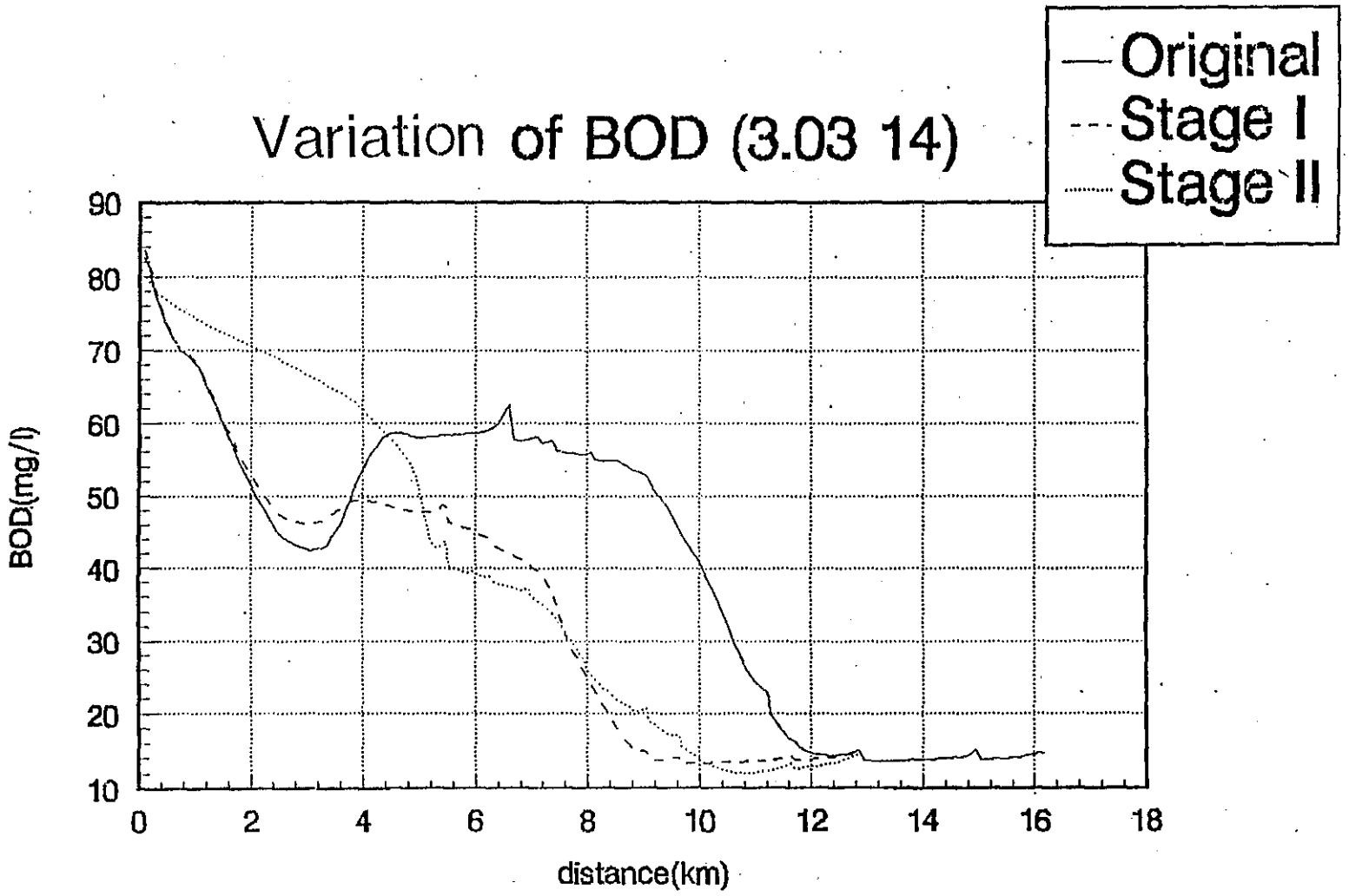

FIG. A7－59(c) **BOD variation before and after the works** (3. 03 14)

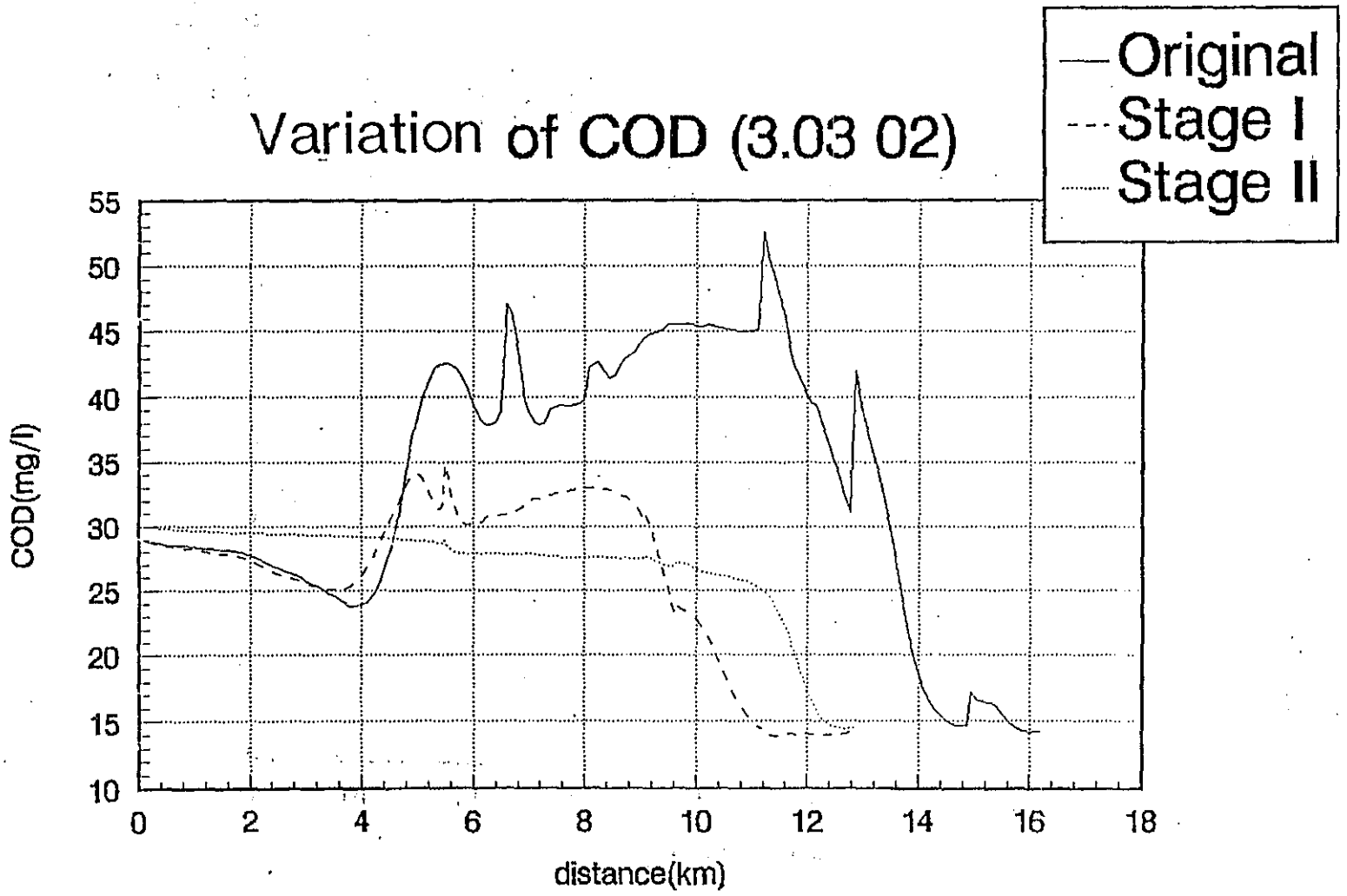

FIG. A7—60(a) **COD variation before and after the works** (3. 03 02)

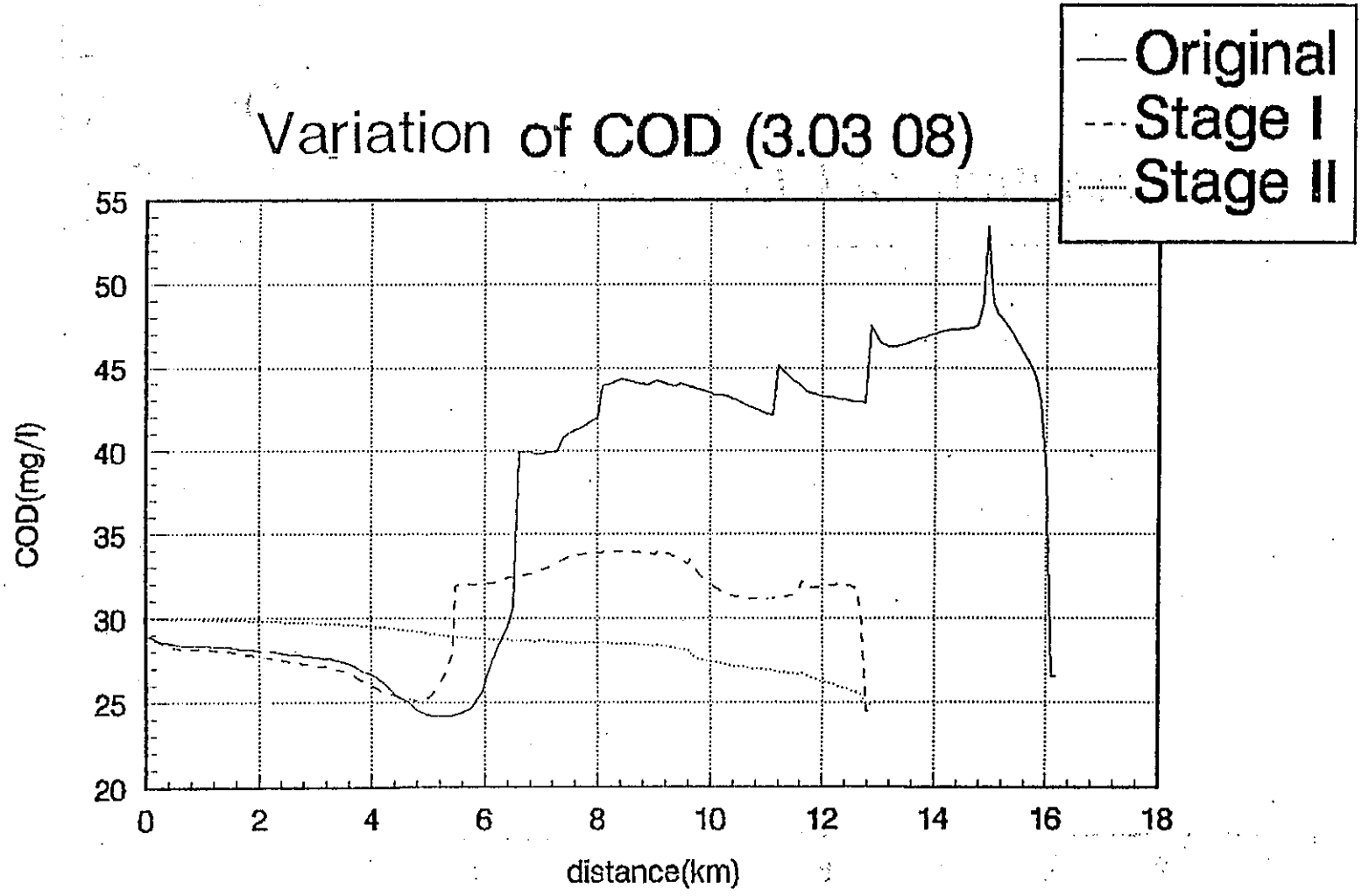

FIG. A7—60(b) **COD variation before and after the works** (3. 03 08)

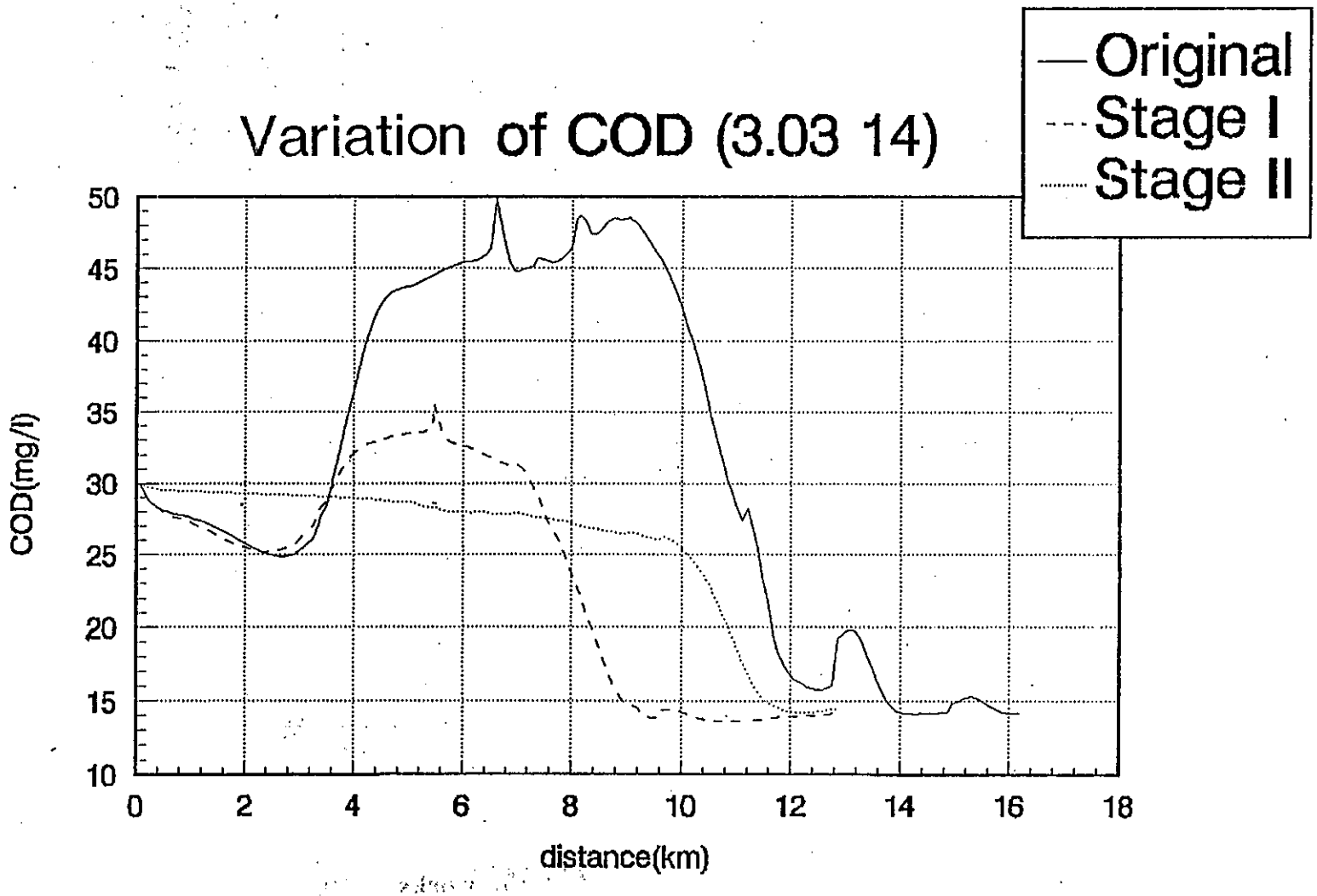

FIG. A7—60(c) COD variation before and after the works (3. 03 14)

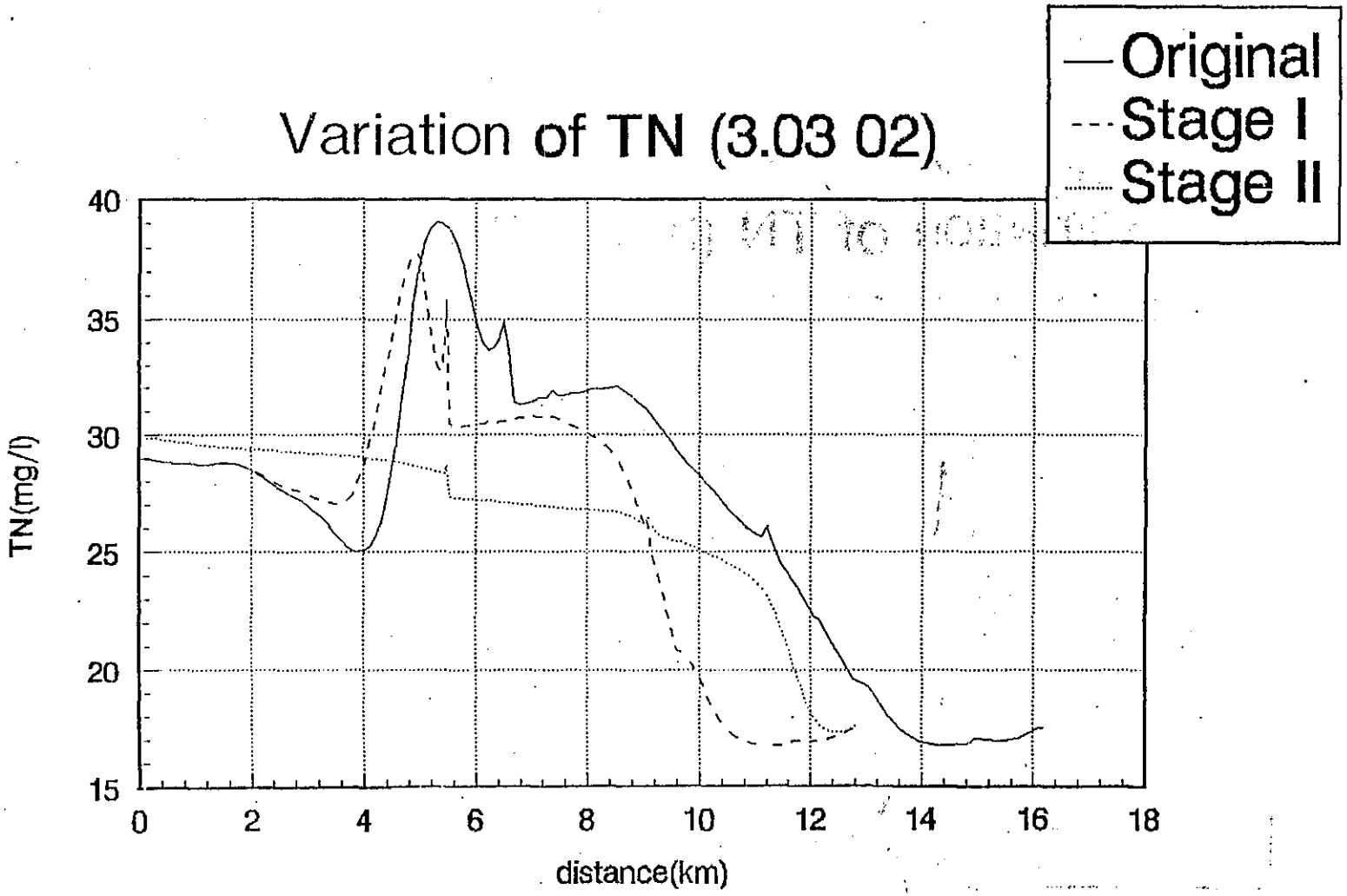

FIG. A7－61(a) **TN variation before and after the works** (3. 03 02)

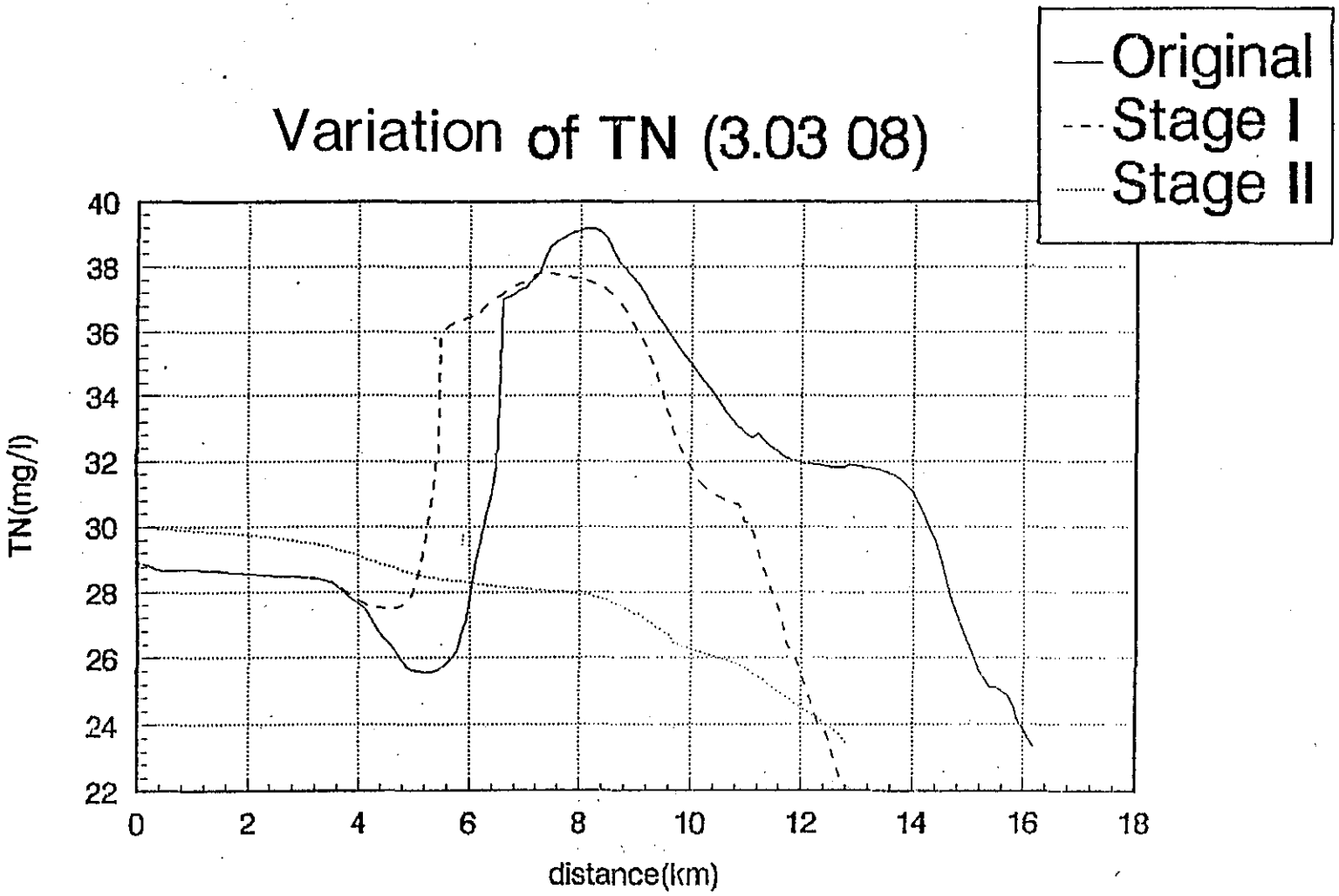

FIG. A7—61(b) **TN variation before and after the works** (3. 03 08)

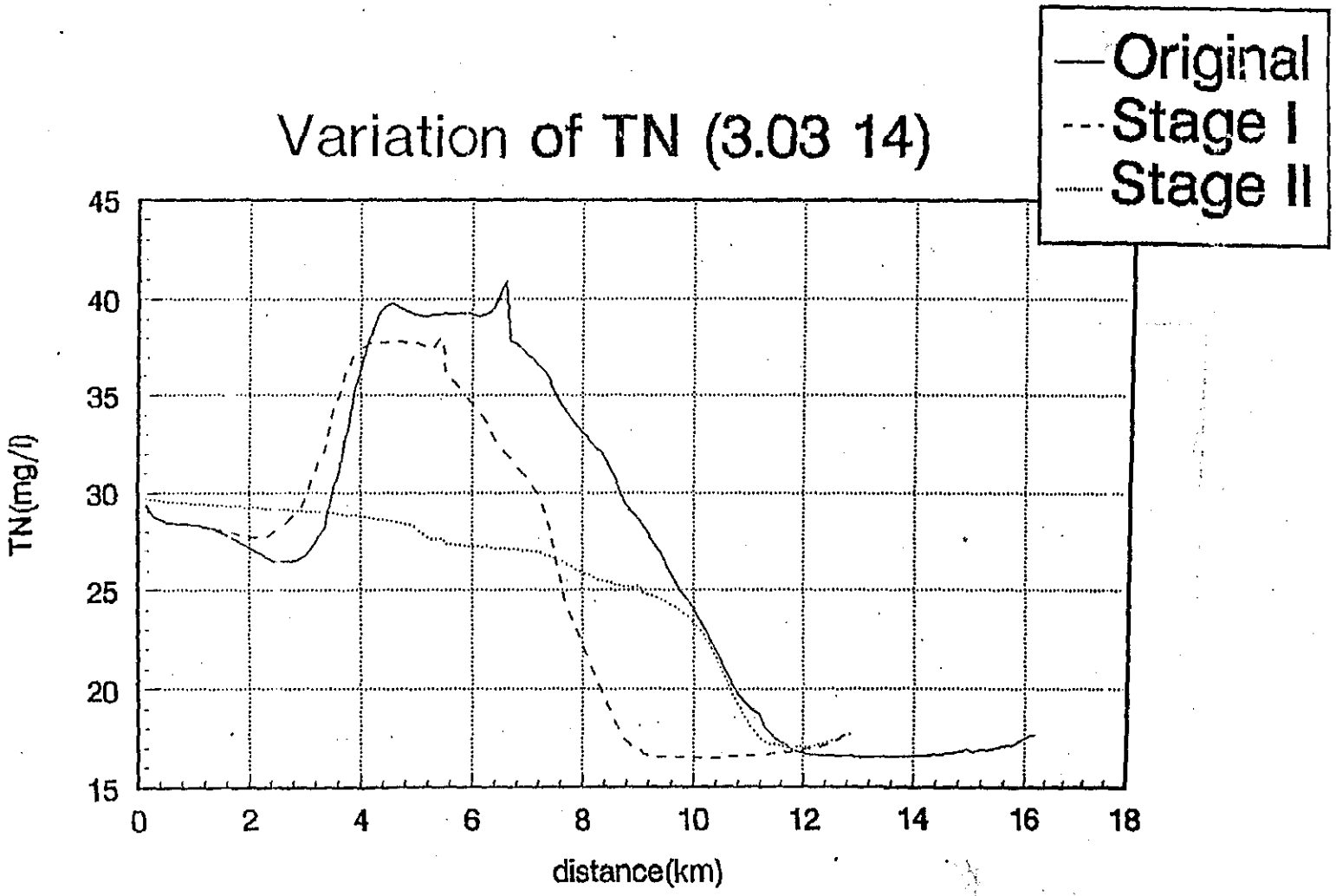

FIG. A7—61(c) TN variation before and after the works (3.03 14)

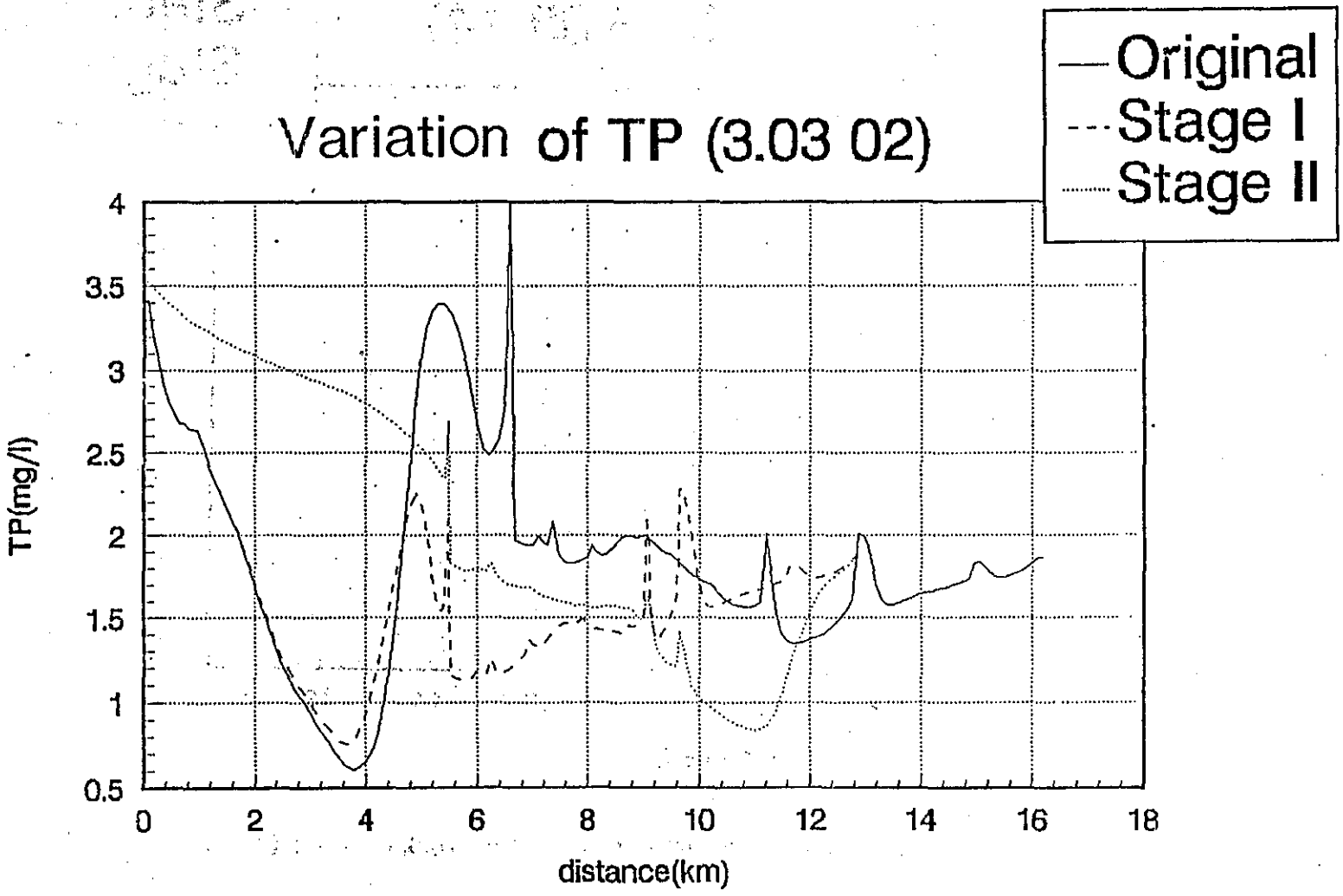

FIG. A7－62(a) **TP variation before and after the works** (3. 03 02)

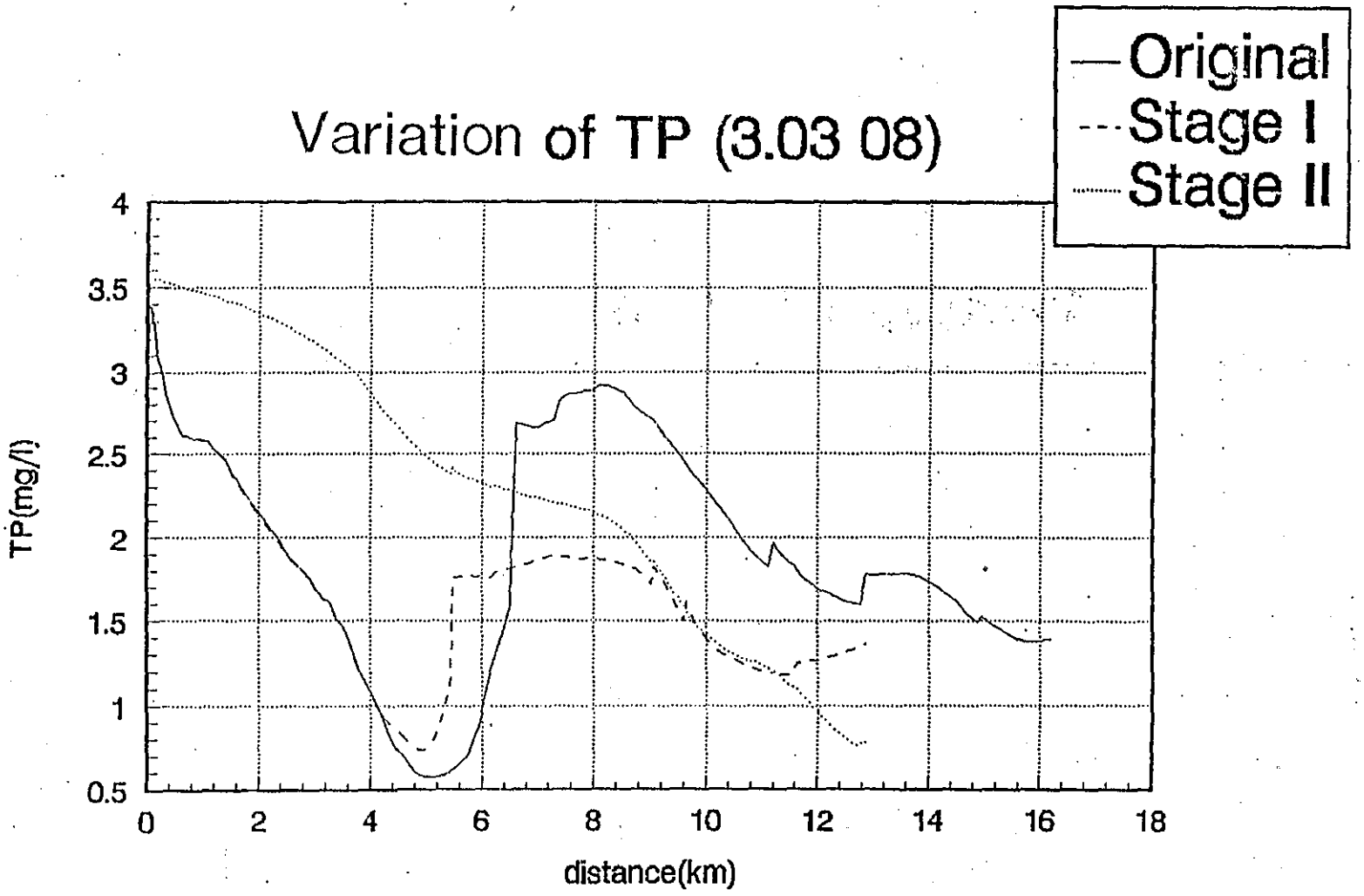

FIG. A7－62(b)　TP variation before and after the works (3. 03 08)

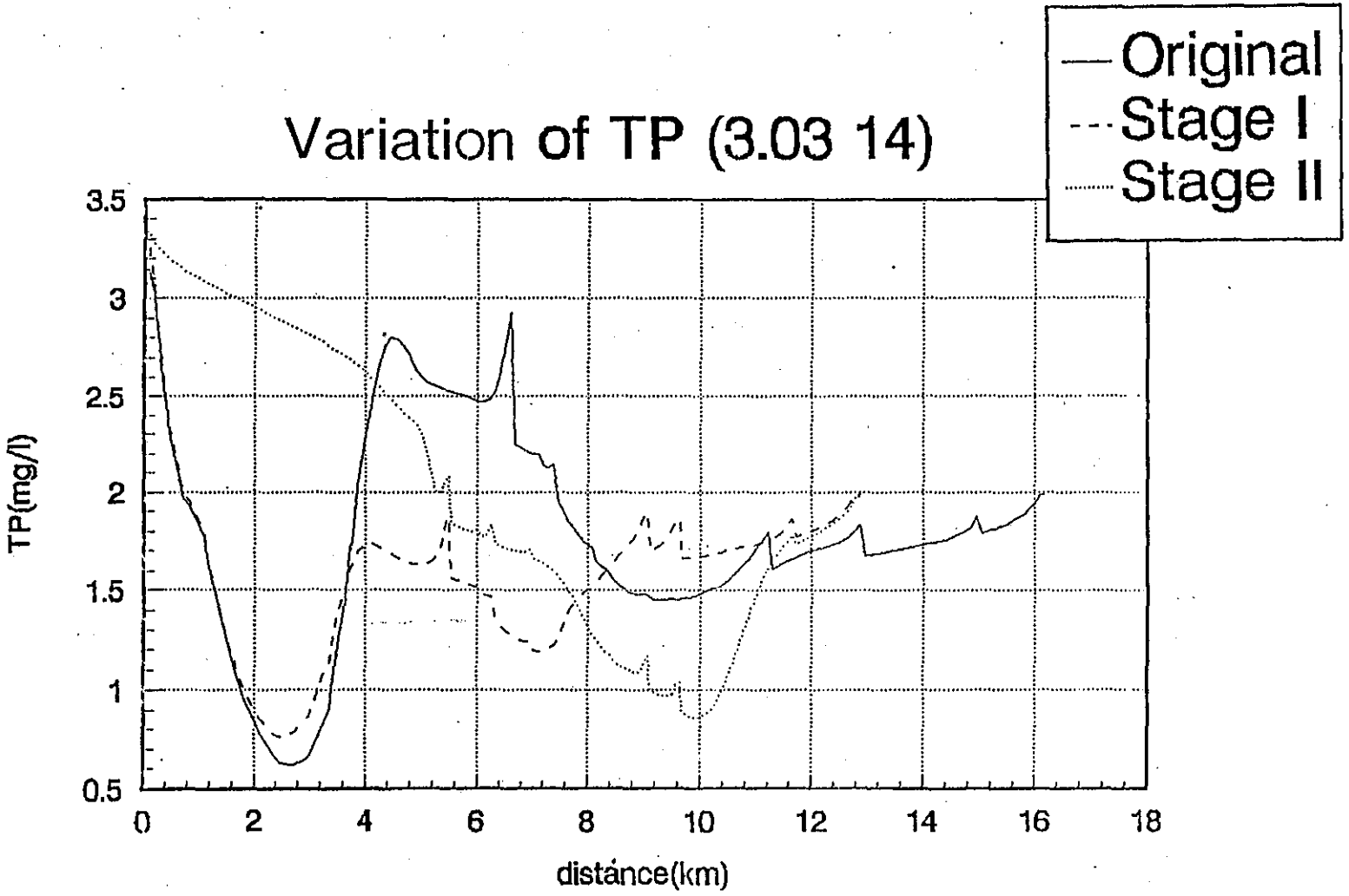

FIG. A7—62(c) TP variation before and after the works (3. 03 14)

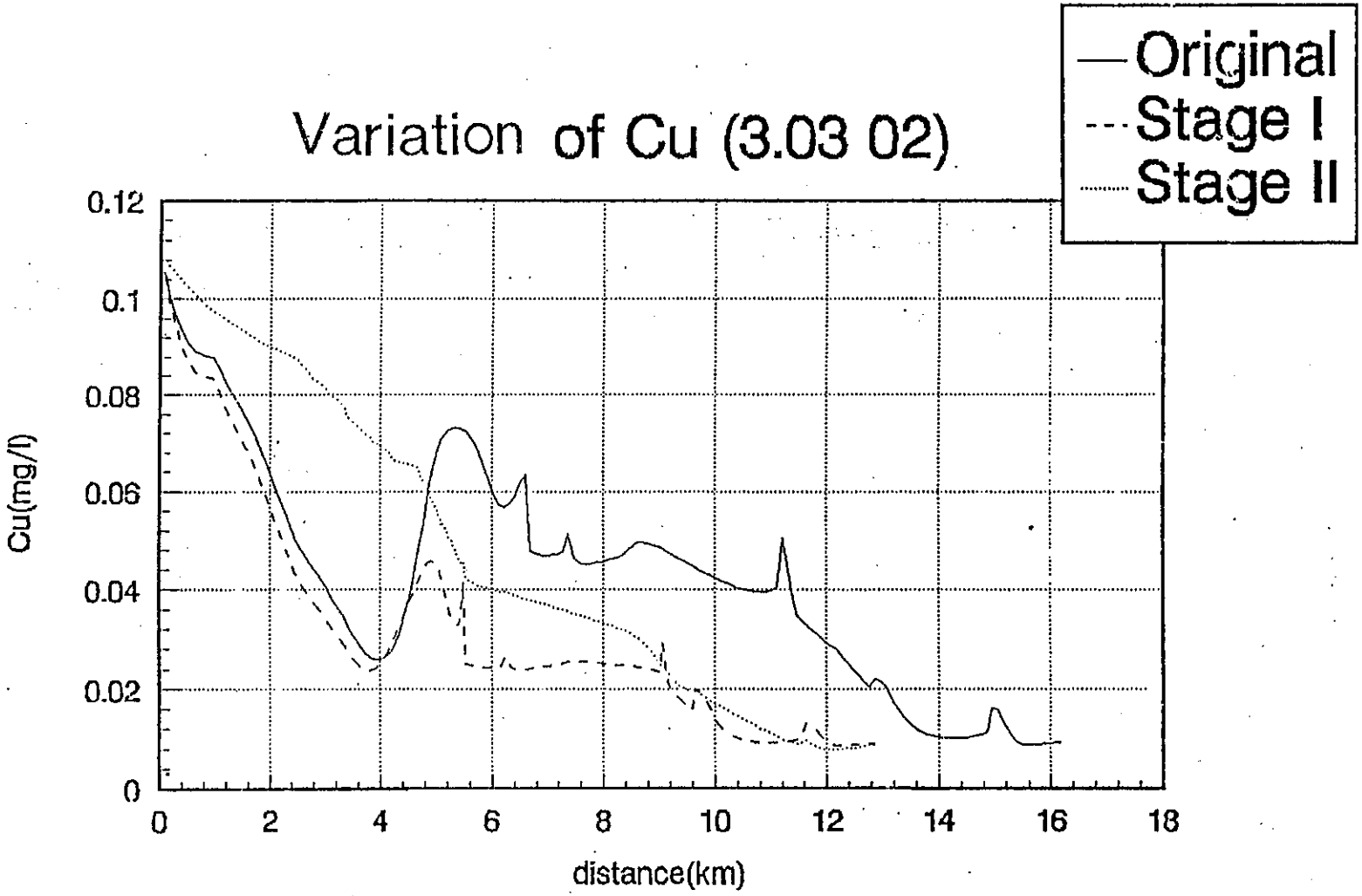

FIG. A7－63(a)　Cu variation before and after the works (3. 03 02)

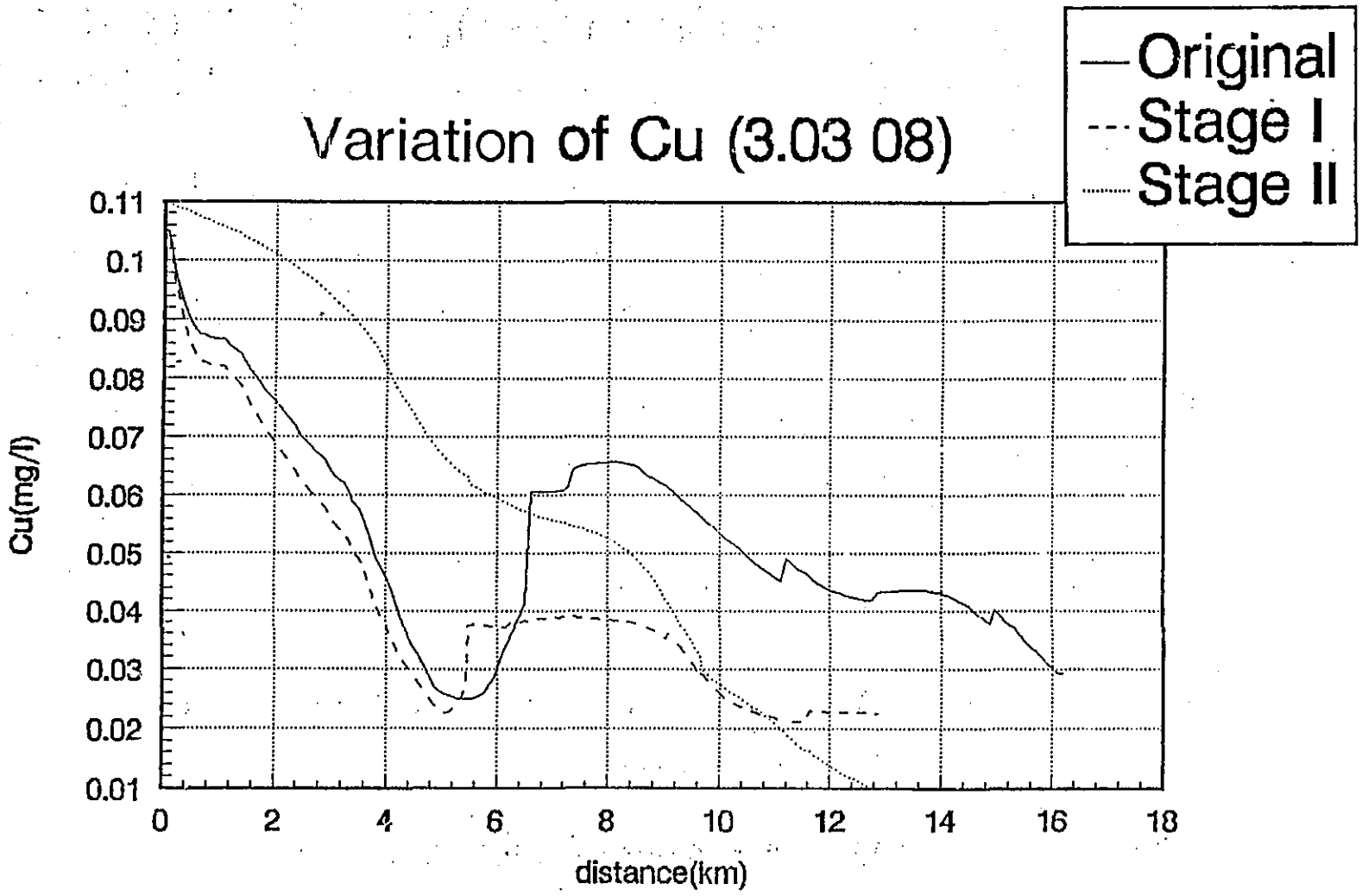

FIG. A7—63(b) **Cu variation before and after the works** (3. 03 08)

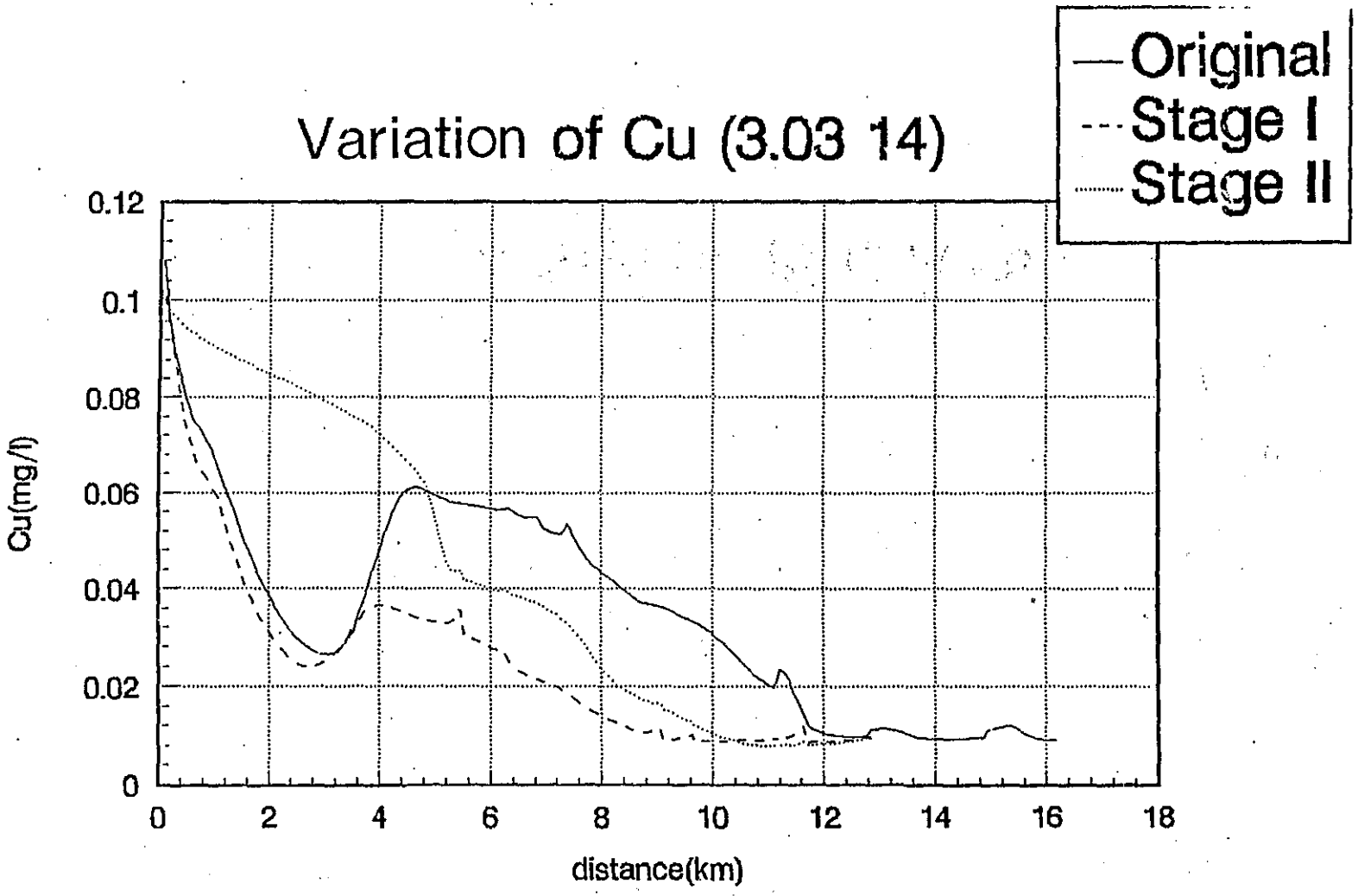

FIG. A7－63(c) **Cu variation before and after the works** (3. 03 14)

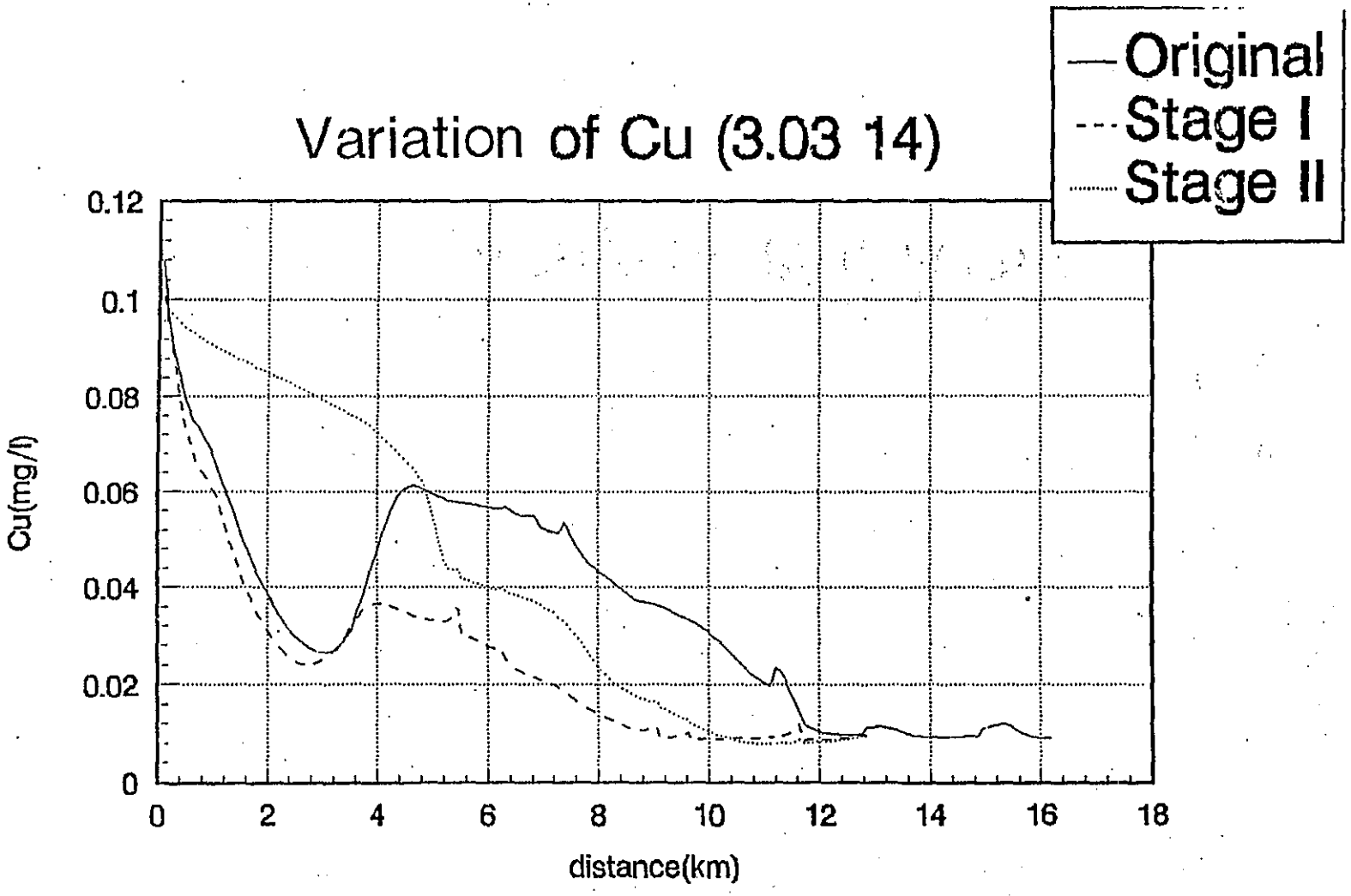

FIG. A7－63(c) **Cu variation before and after the works** (3. 03 14)

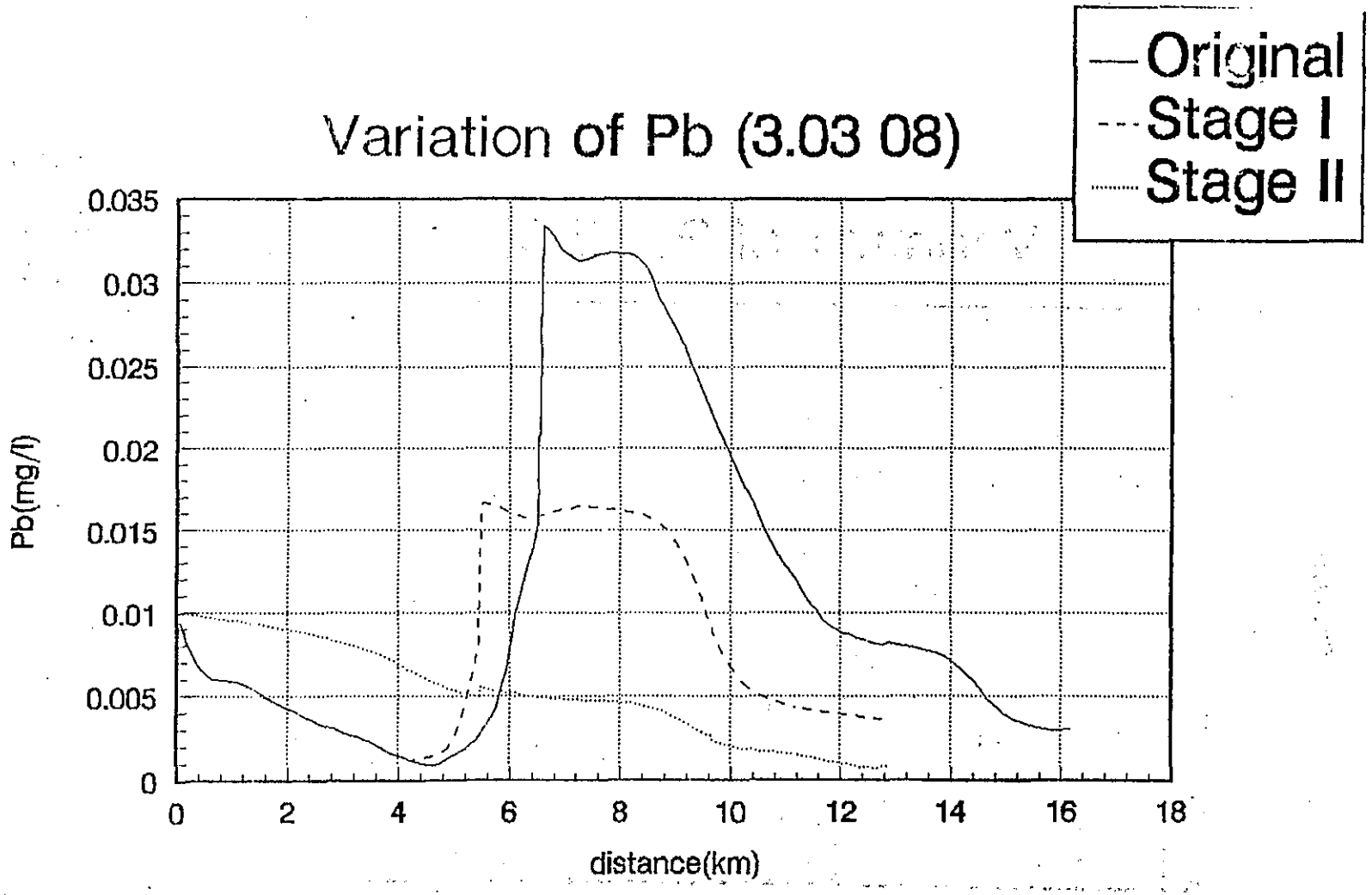

FIG. A7—64(b) Pb variation before and after the works (3.03 08)

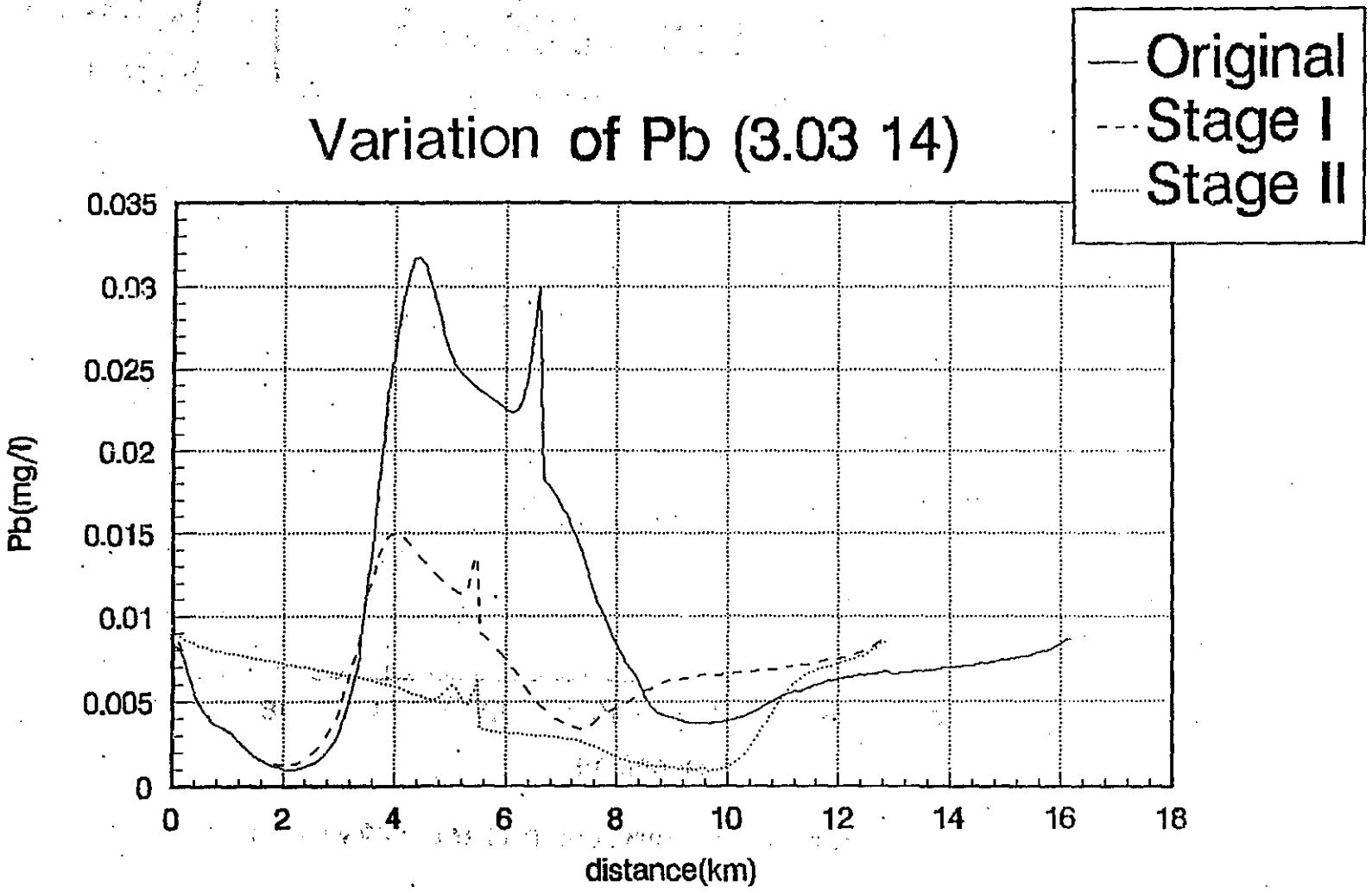

FIG. A7—64(c) **Pb variation before and after the works** (3.03 14)

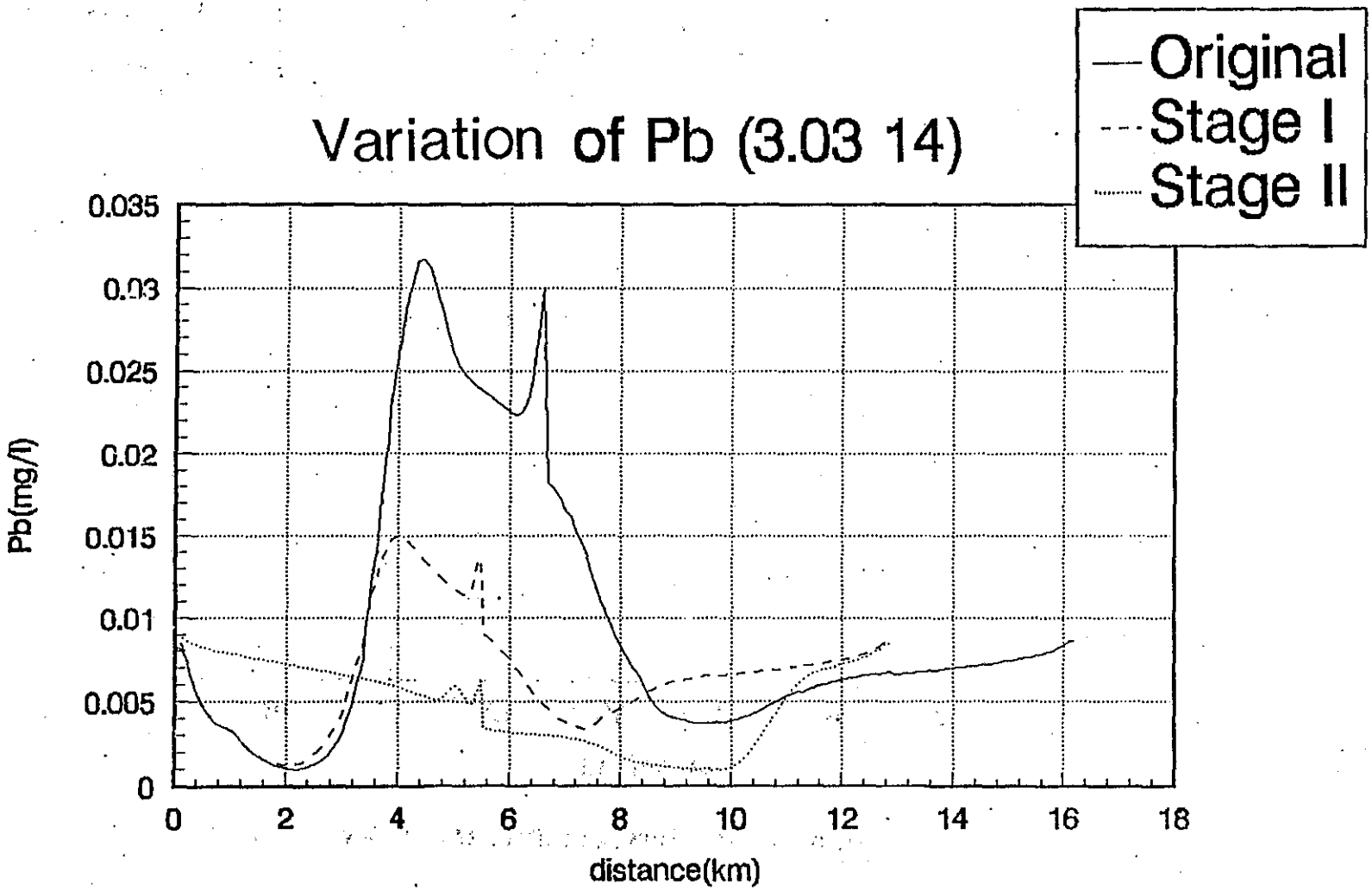

FIG. A7－64(c) Pb variation before and after the works (3.03 14)

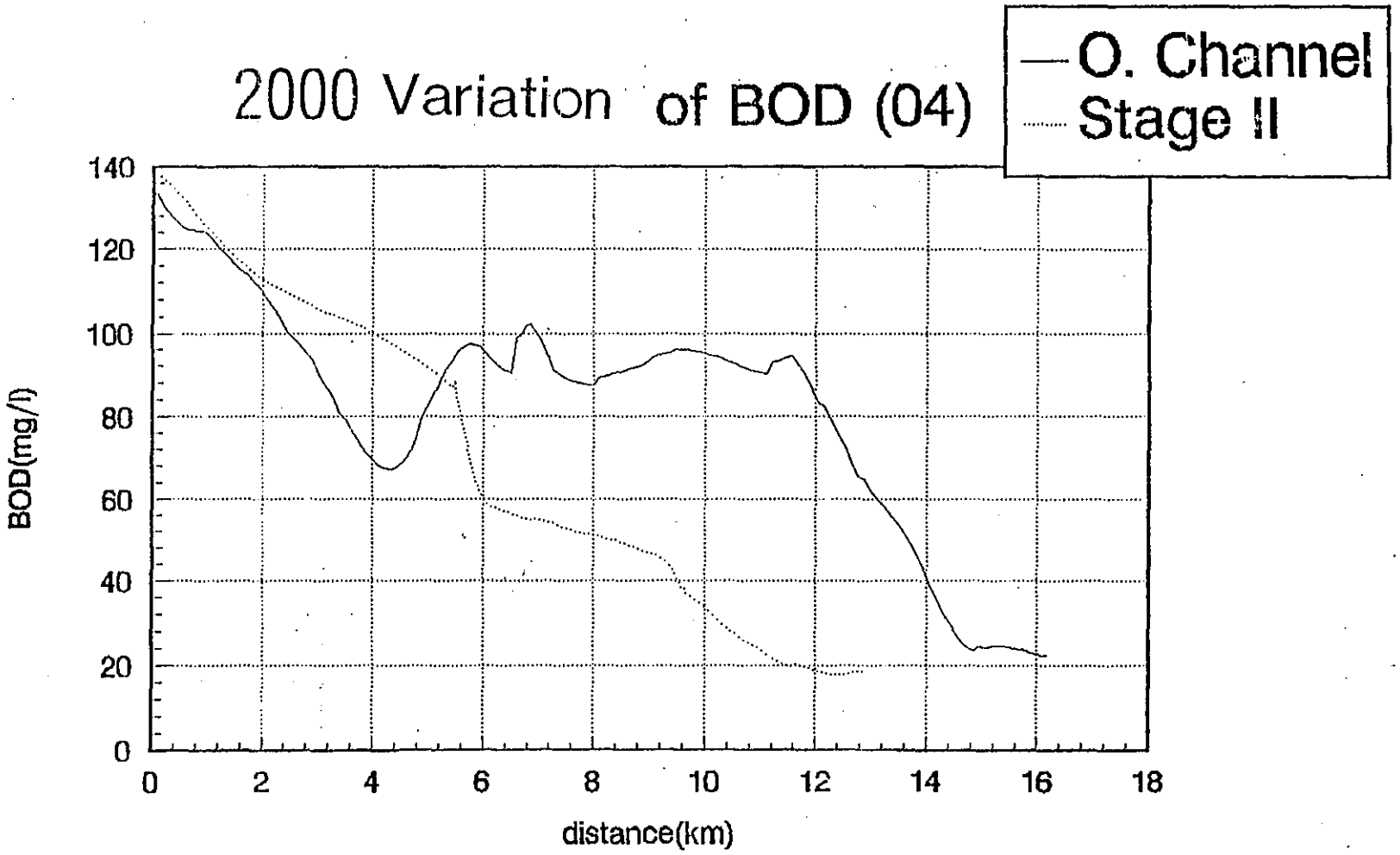

FIG. A7−65(a) **BOD variation in** 2000

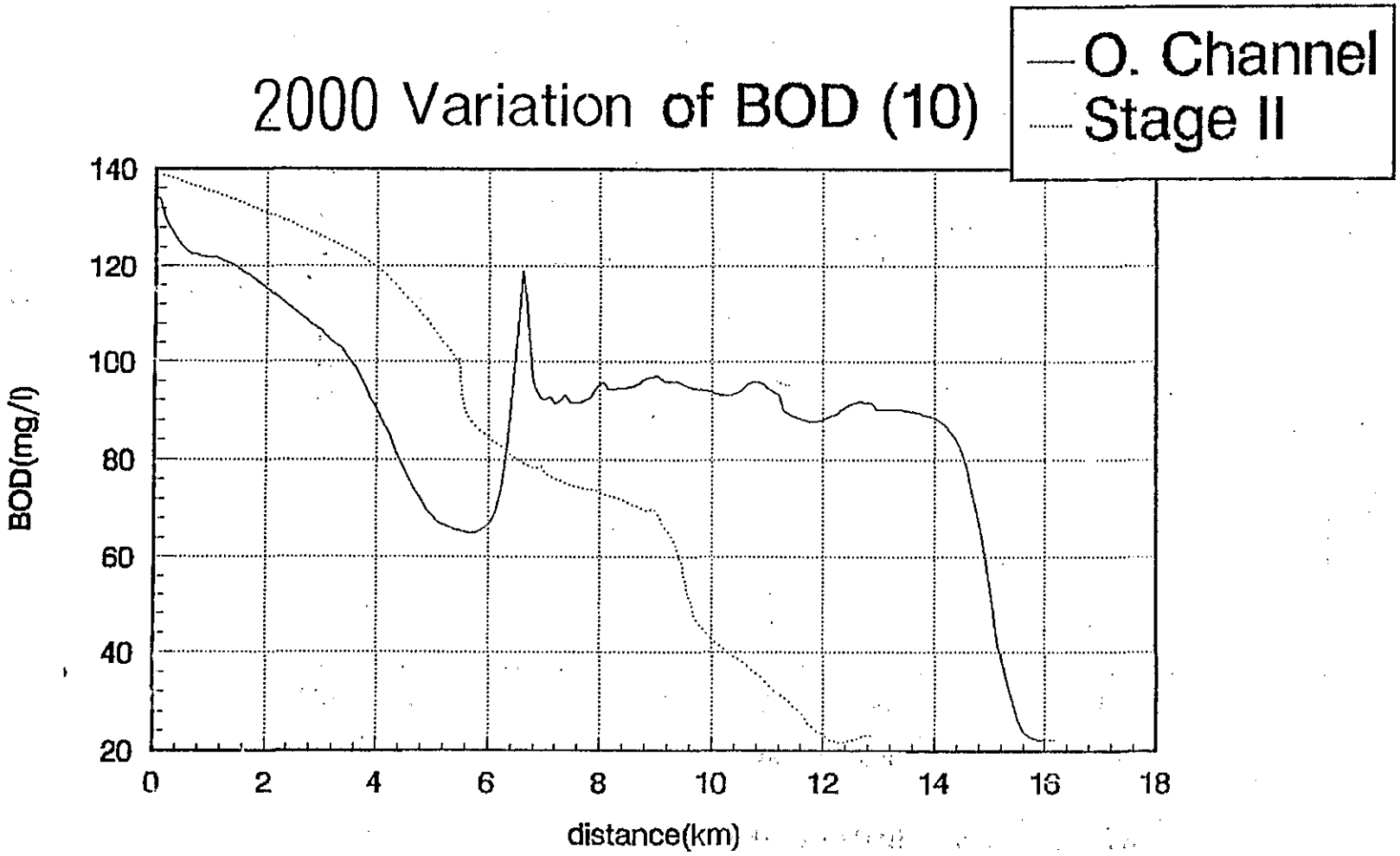

FIG. A7—65(b) BOD variation in 2000

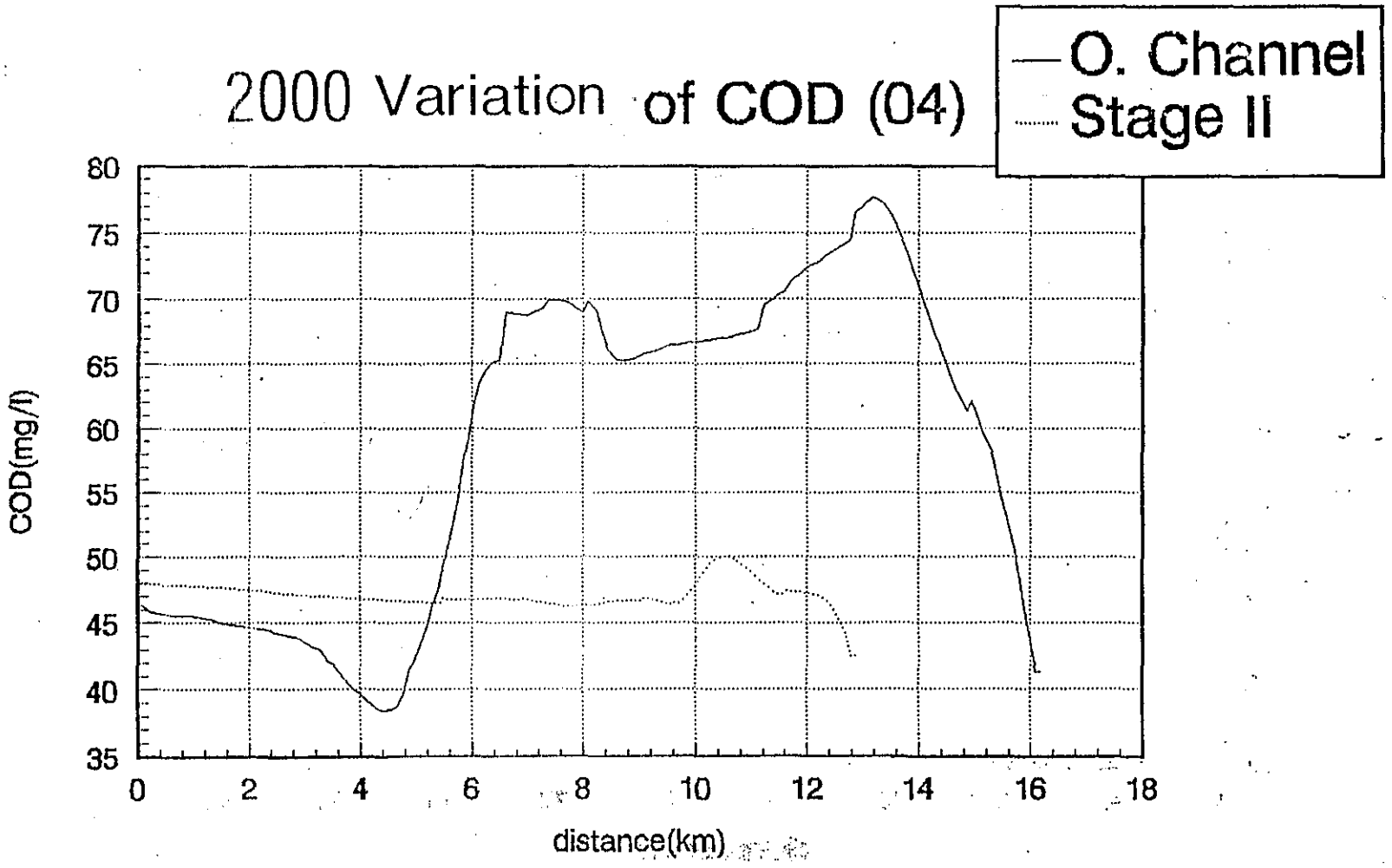

FIG. A7—66(a) COD variation in 2000

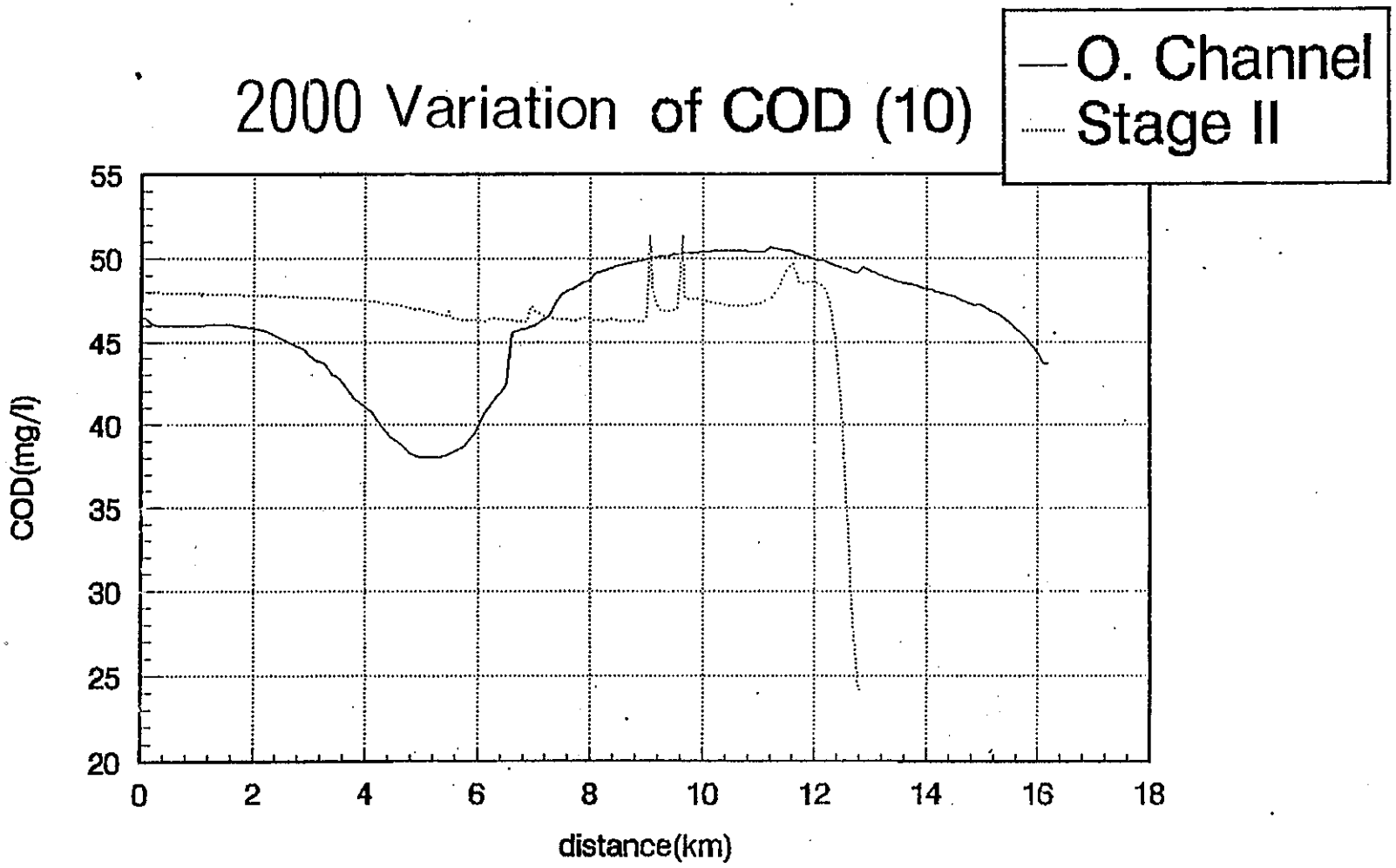

FIG. A7－66(b) COD variation in 2000

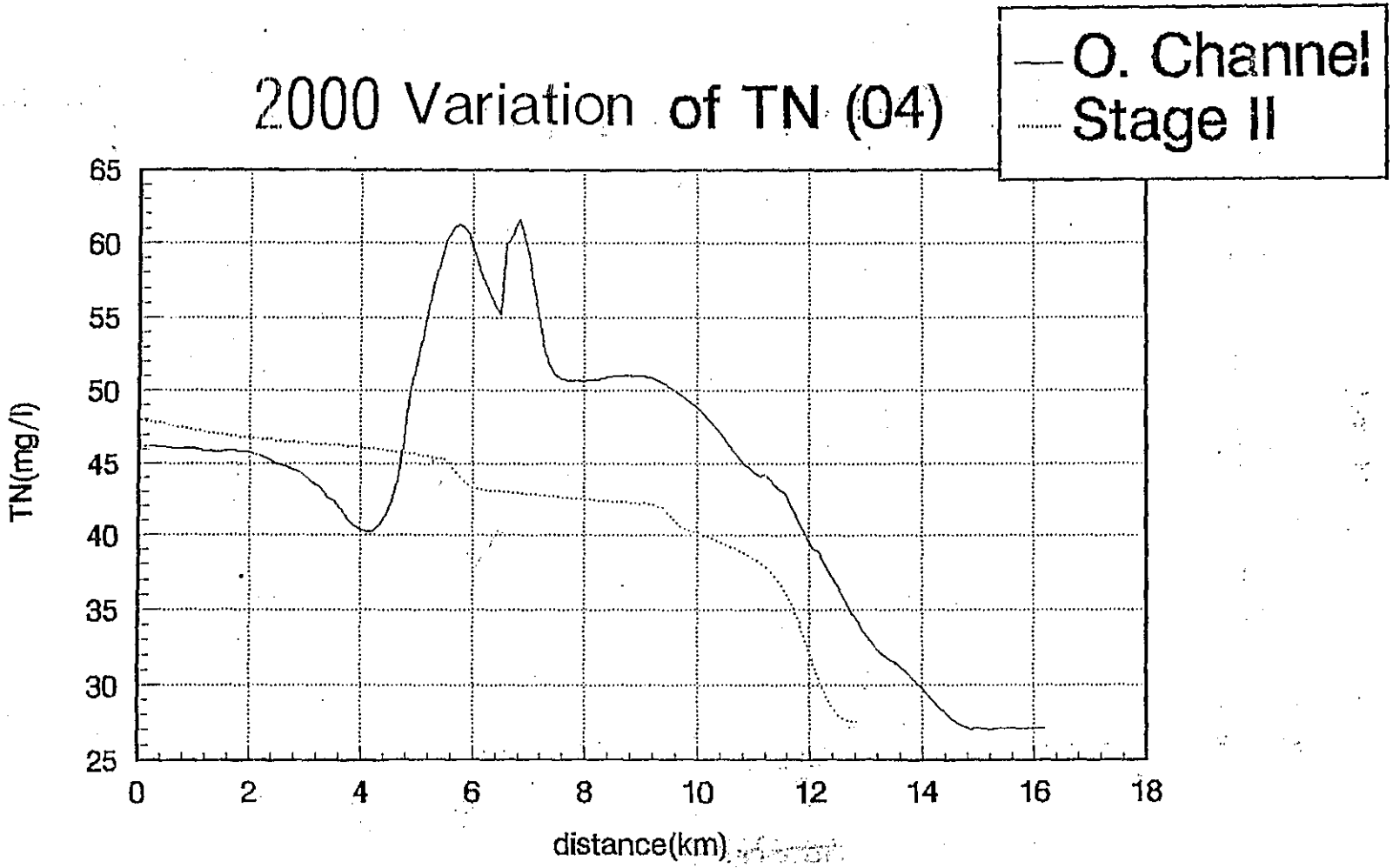

FIG. A7—67(a) TN variation in 2000

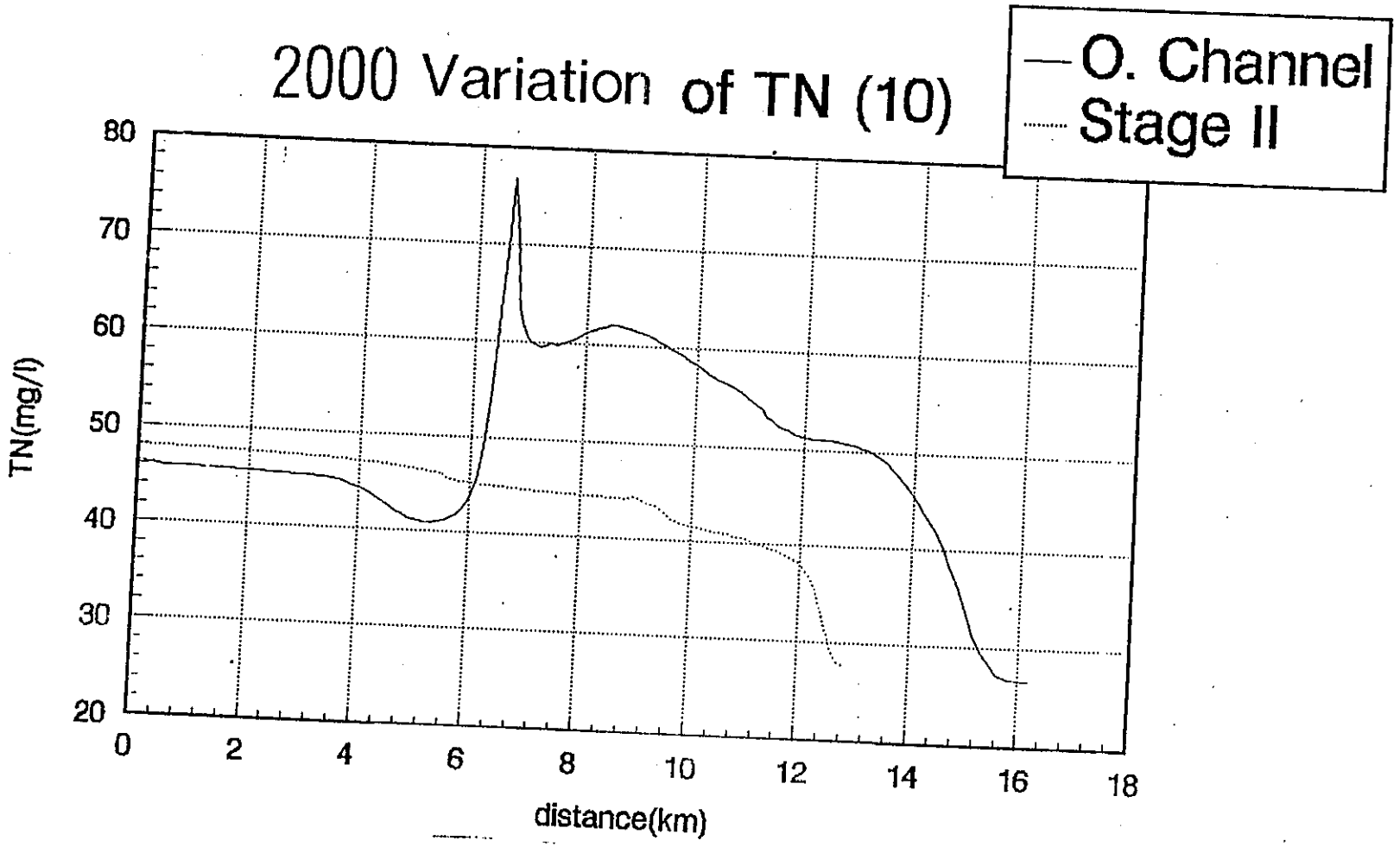

FIG. A7—67(b) TN variation in 2000

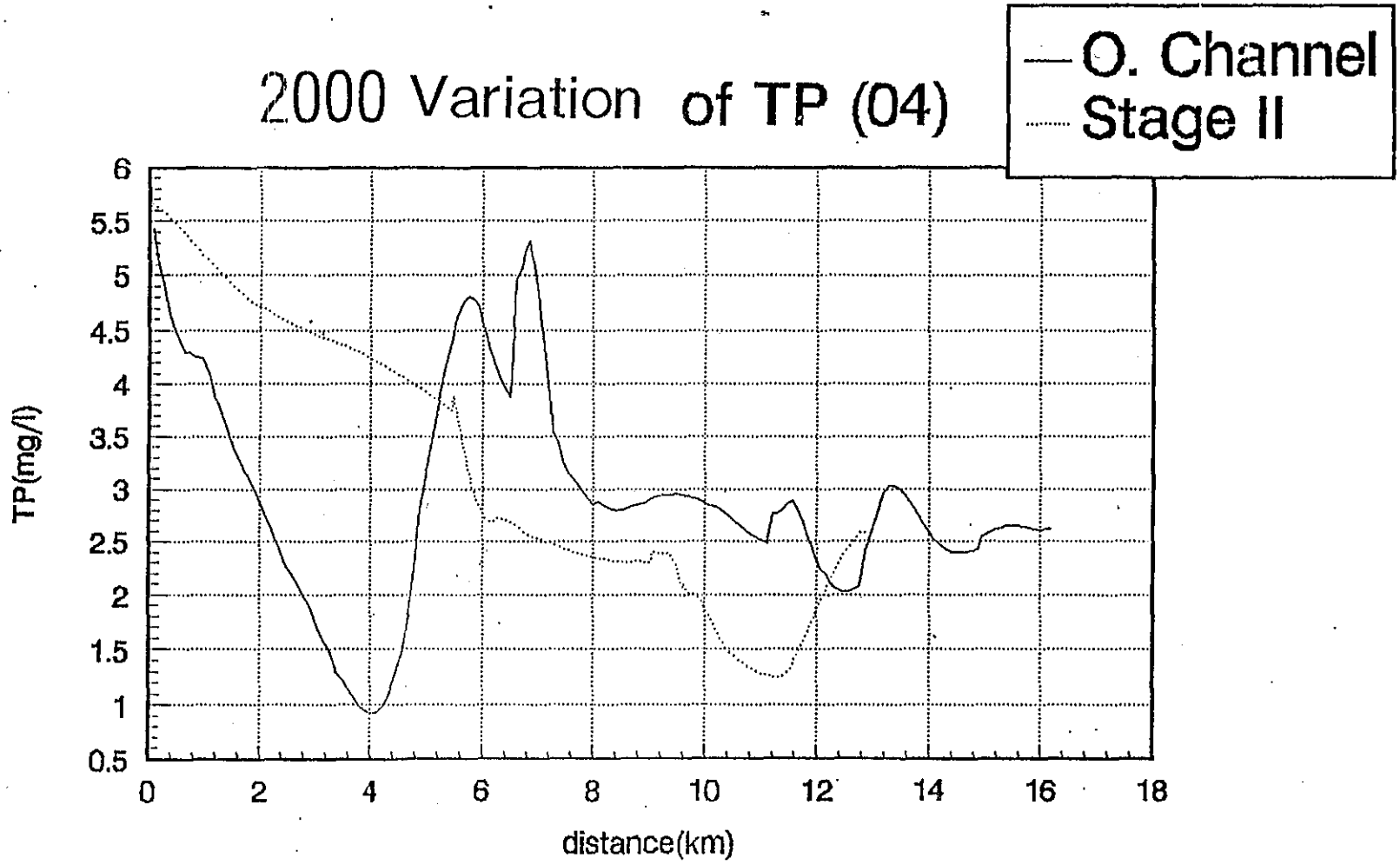

FIG. A7－68(a) TP variation in 2000

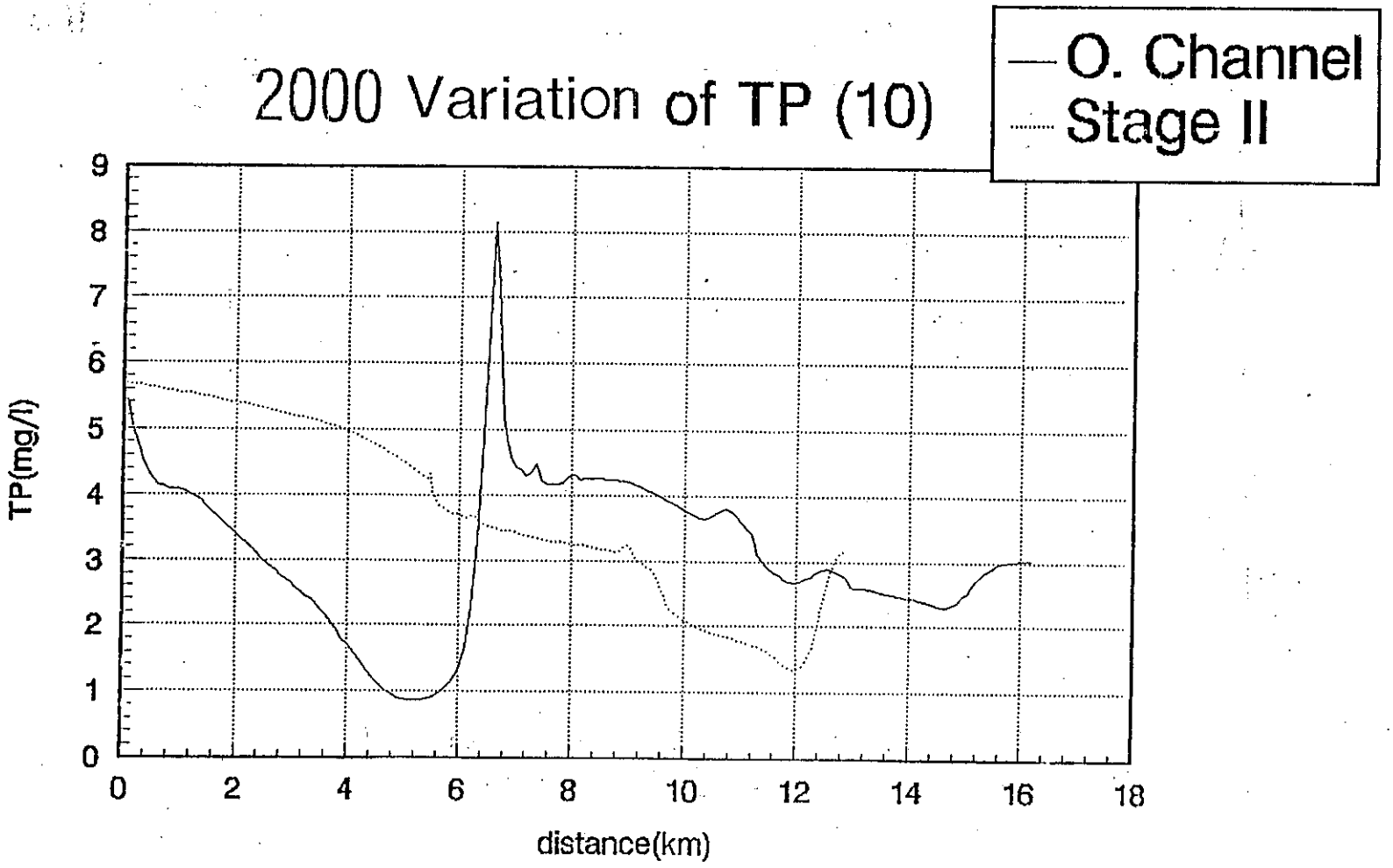

FIG. A7--68(b) · TP variation in 2000

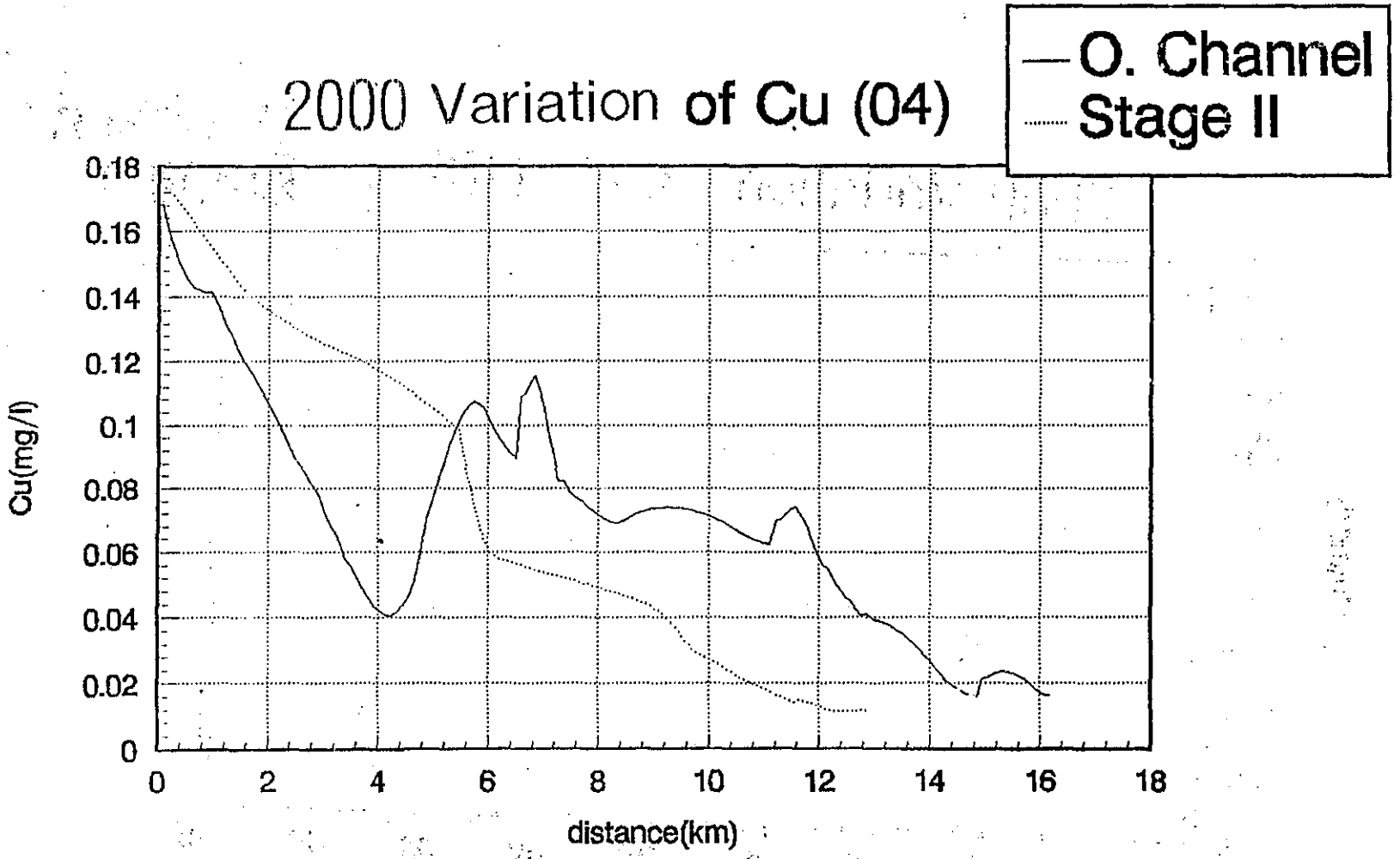

FIG. A7—69(a) Cu variation in 2000

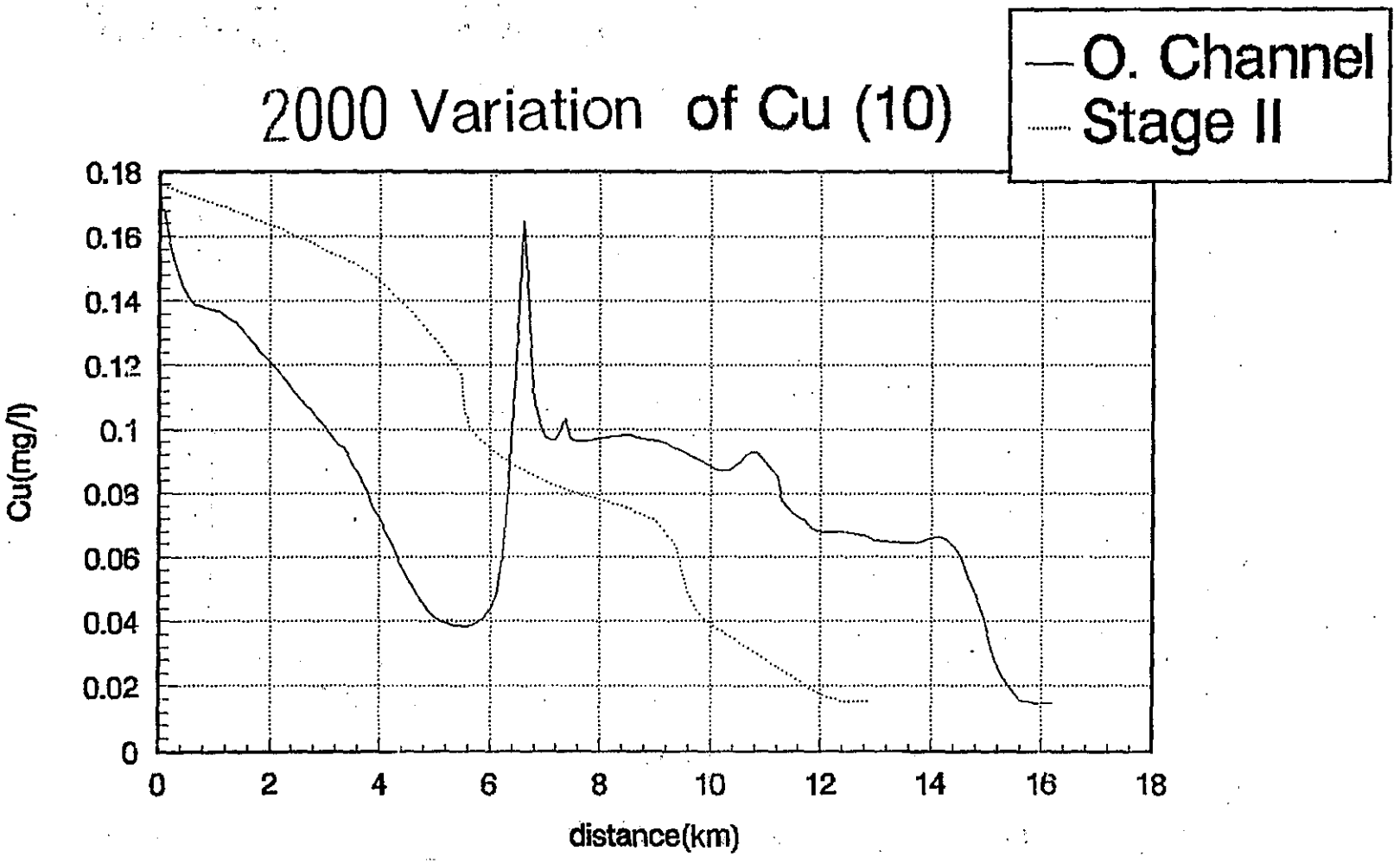

FIG. A7—69(b) Cu variation in 2000

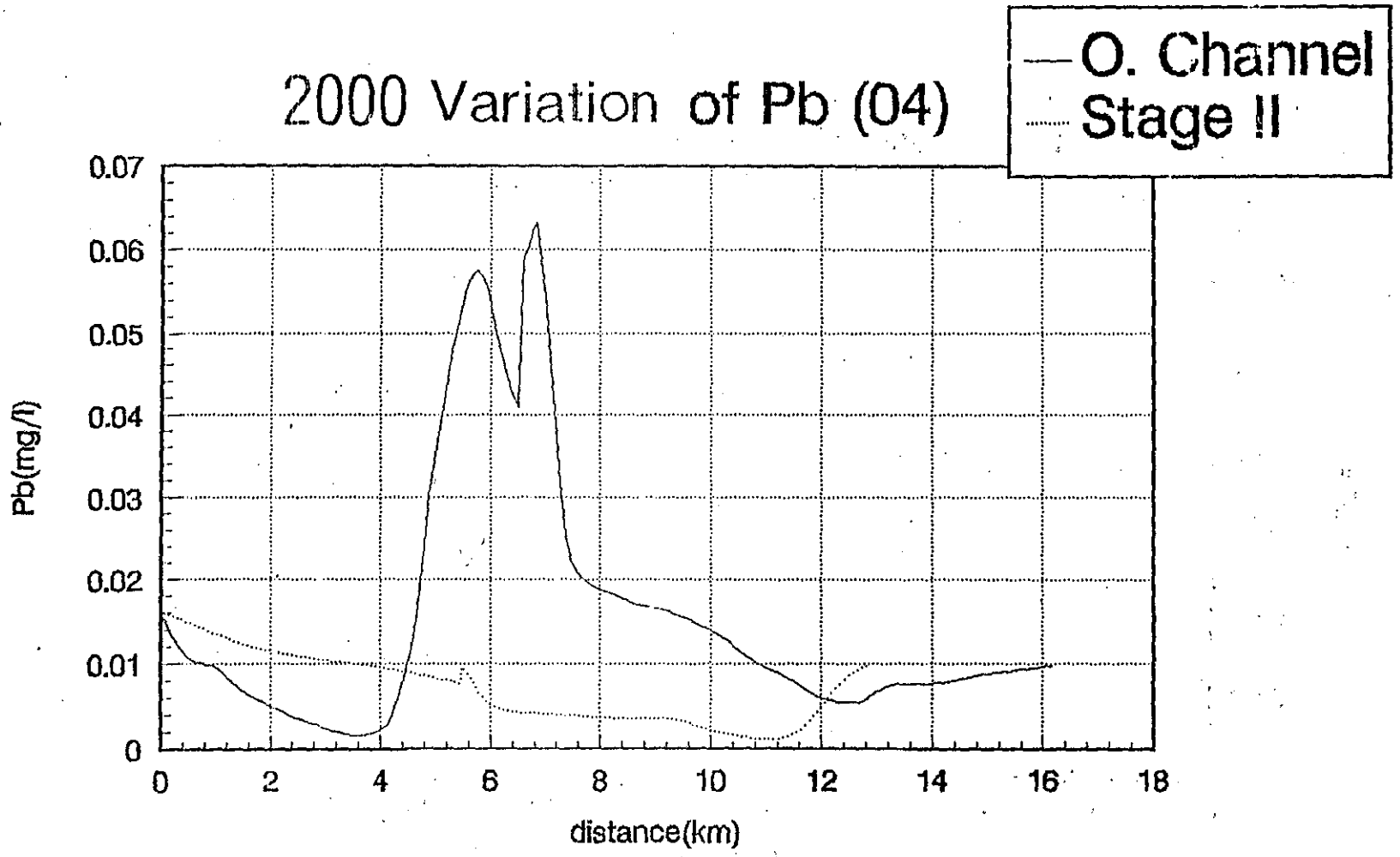

FIG. A7—70(a) Pb variation in 2000

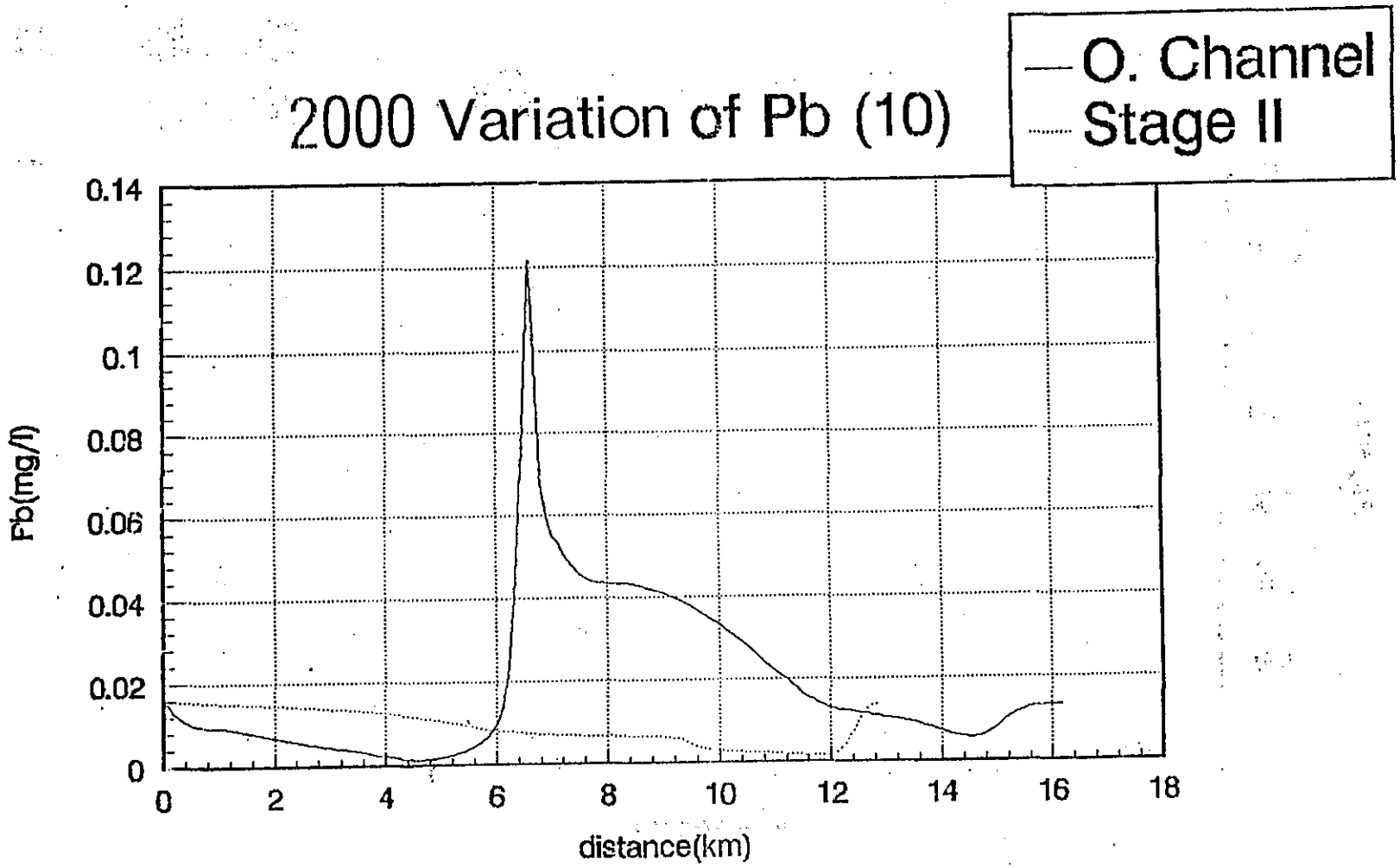

FIG. A7—70(b) Pb variation in 2000

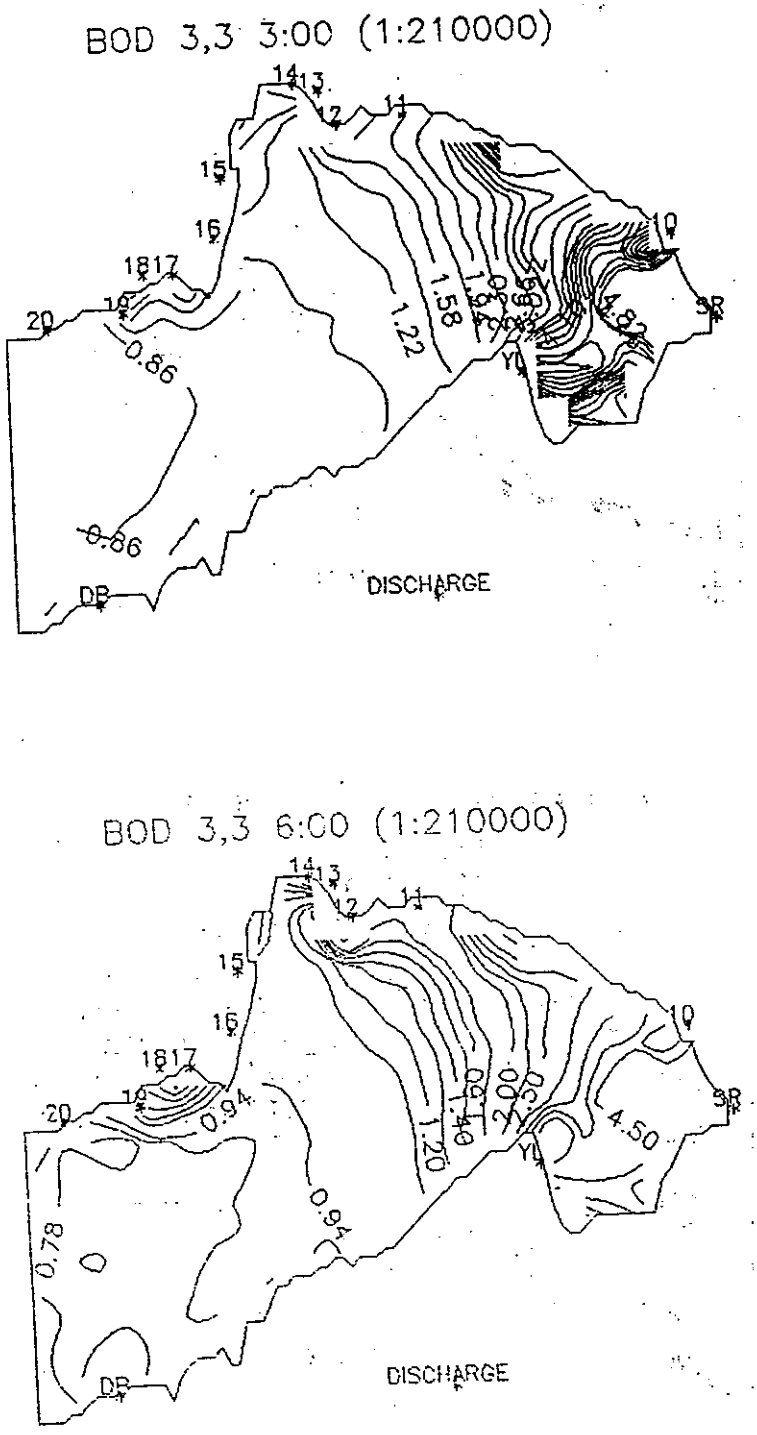

FIG. A7—71(a) Dynamic variation of BOD in Deep Bay (dry season)

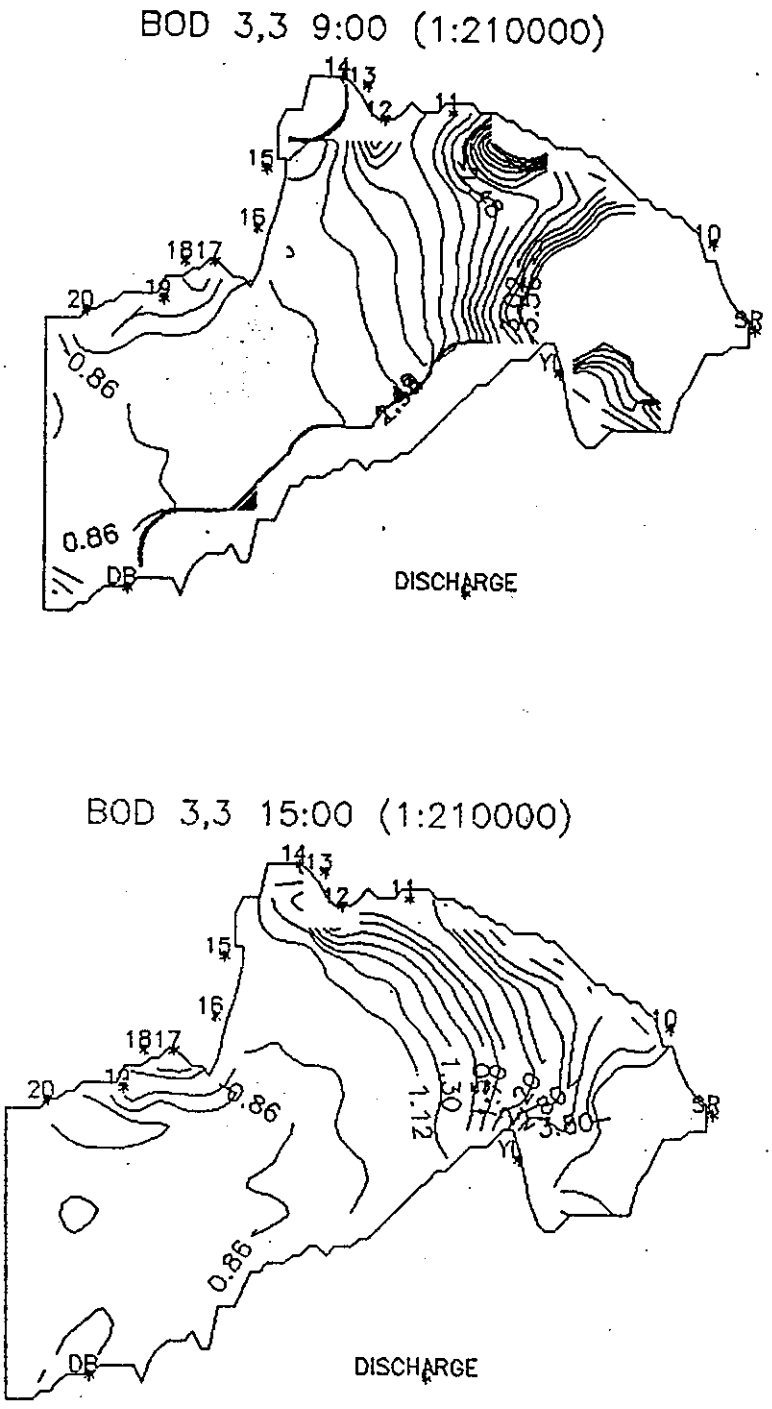

FIG. A7—71(b) Dynamic variation of BOD in Deep Bay (dry season)

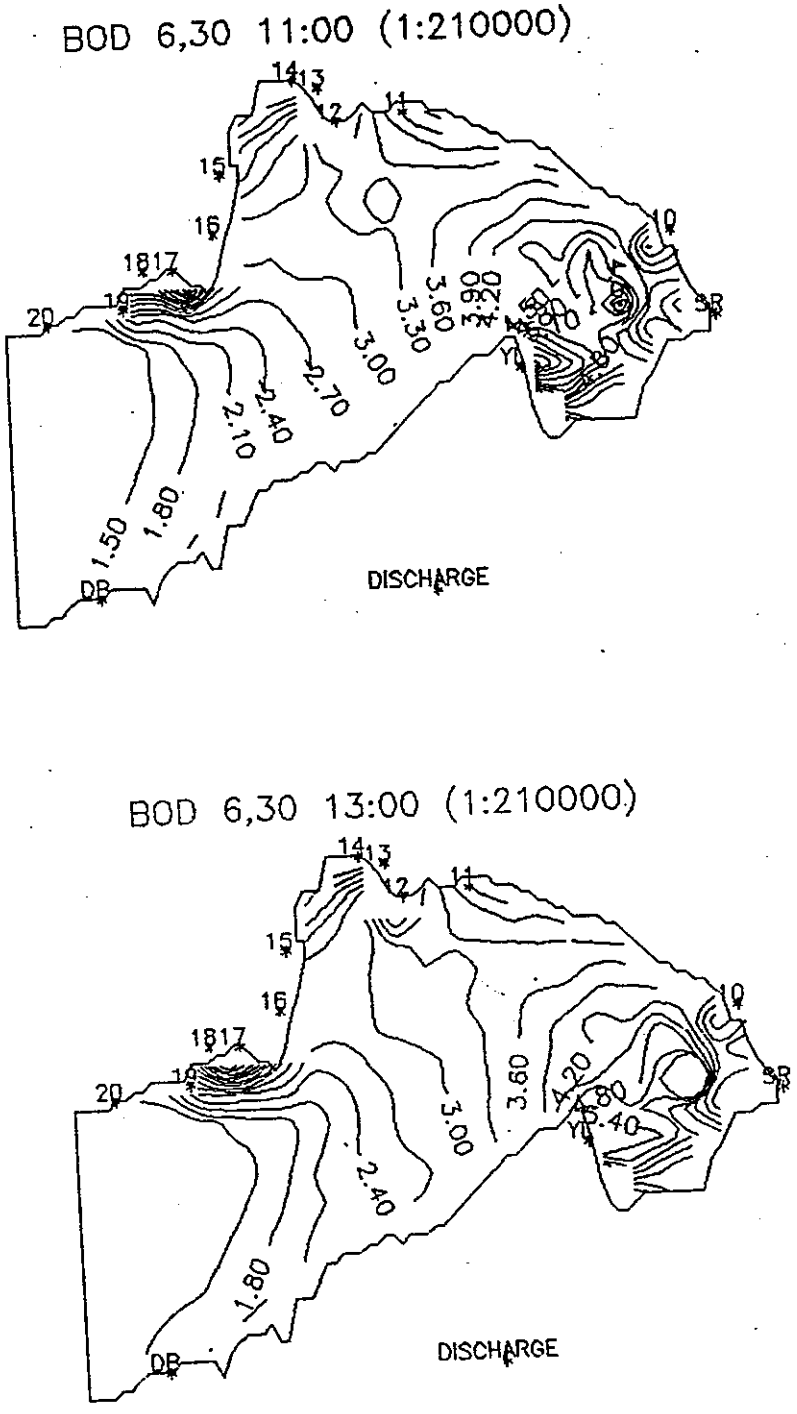

FIG. A7—71(c) Dynamic variation of BOD in Deep Bay (wet season)

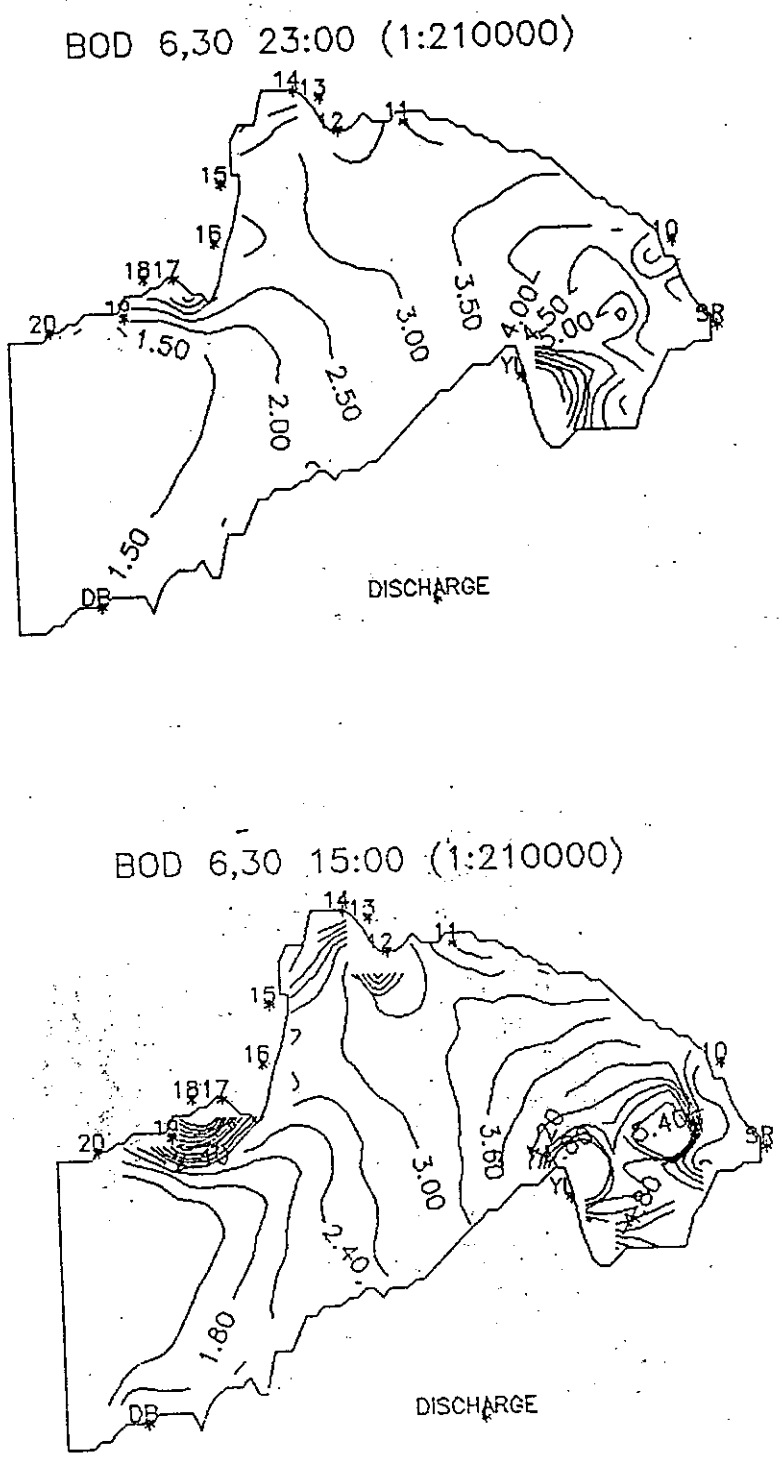

FIG. A7—71(d) Dynamic variation of BOD in Deep Bay (wet season)

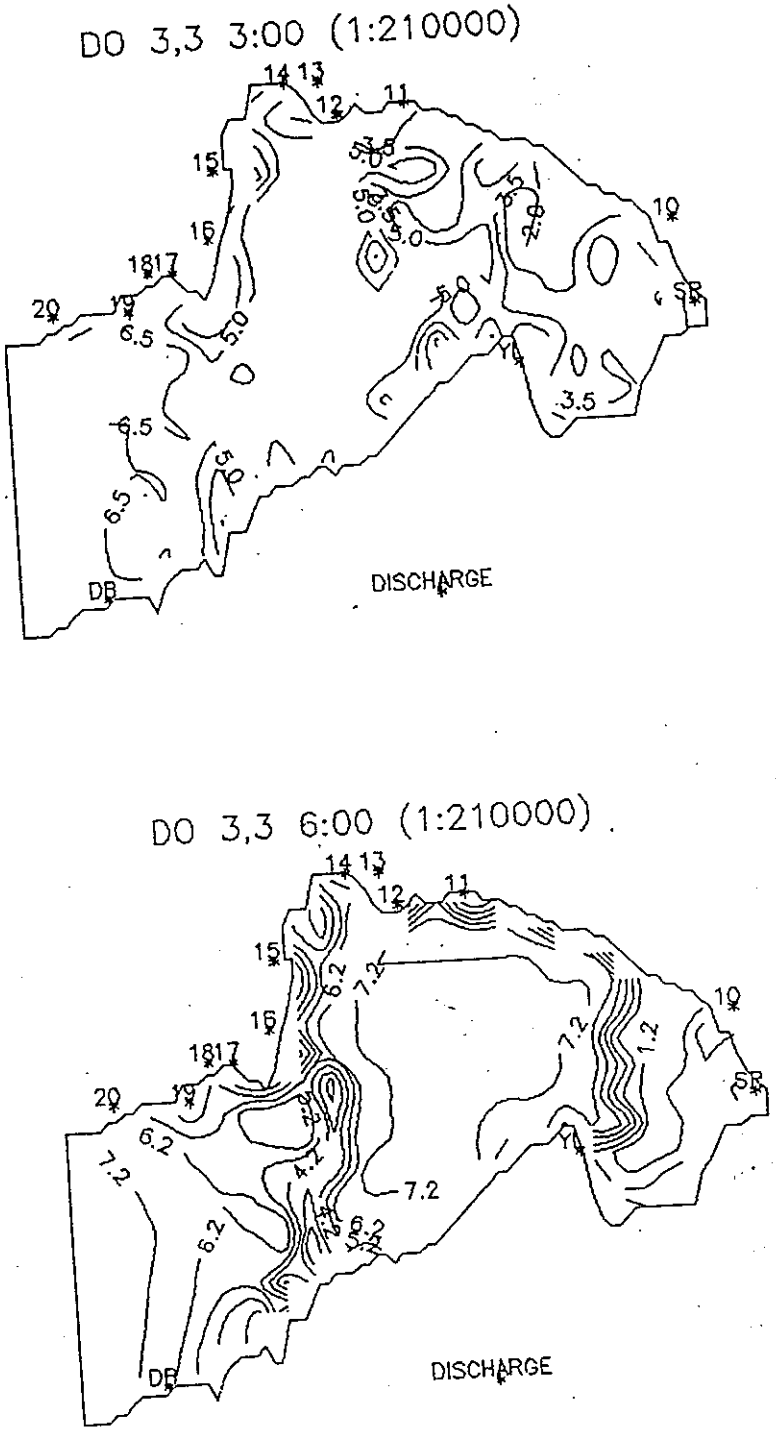

FIG. A7—72(a) Dynamic variation of DO in Deep Bay (dry season)

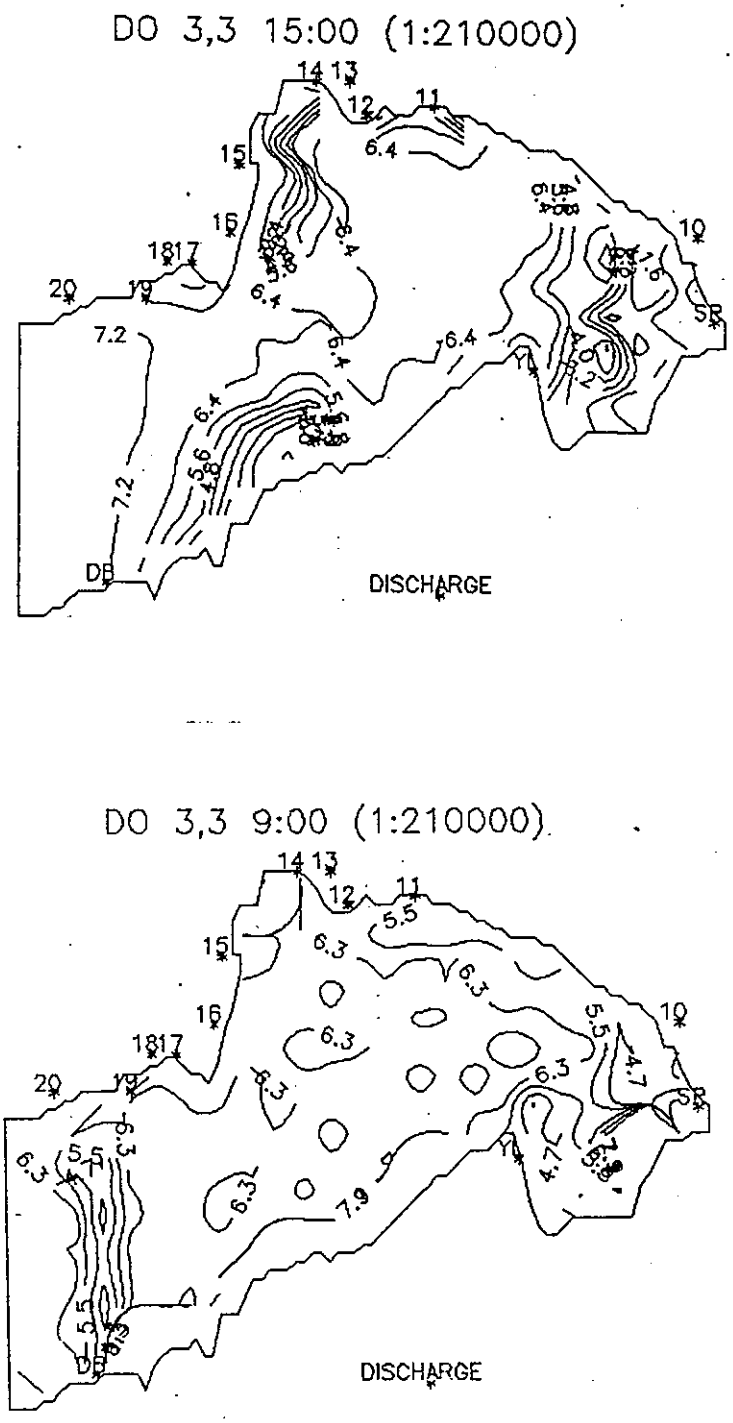

FIG. A7—72(b) Dynamic variation of DO in Deep Bay (dry season)

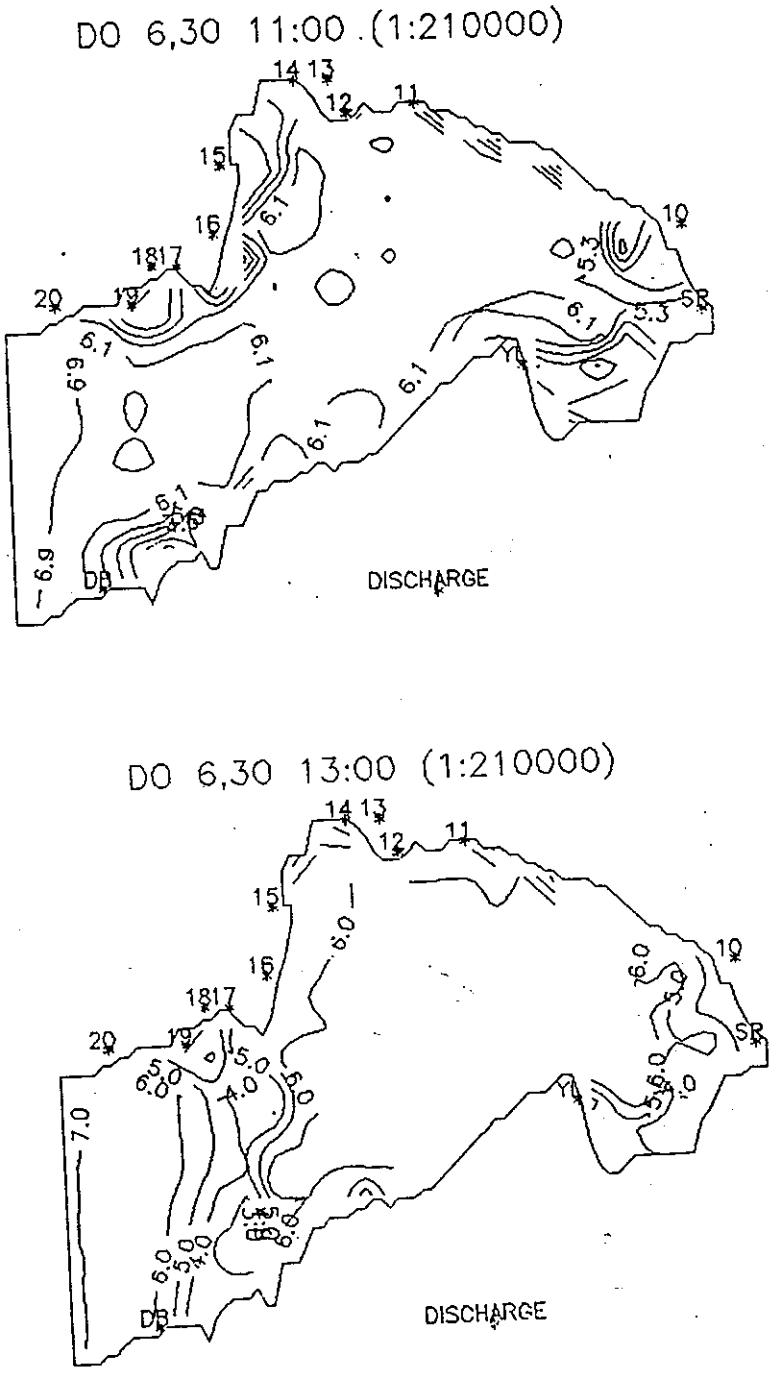

FIG. A7－72(c) Dynamic variation of DO in Deep Bay (wet season)

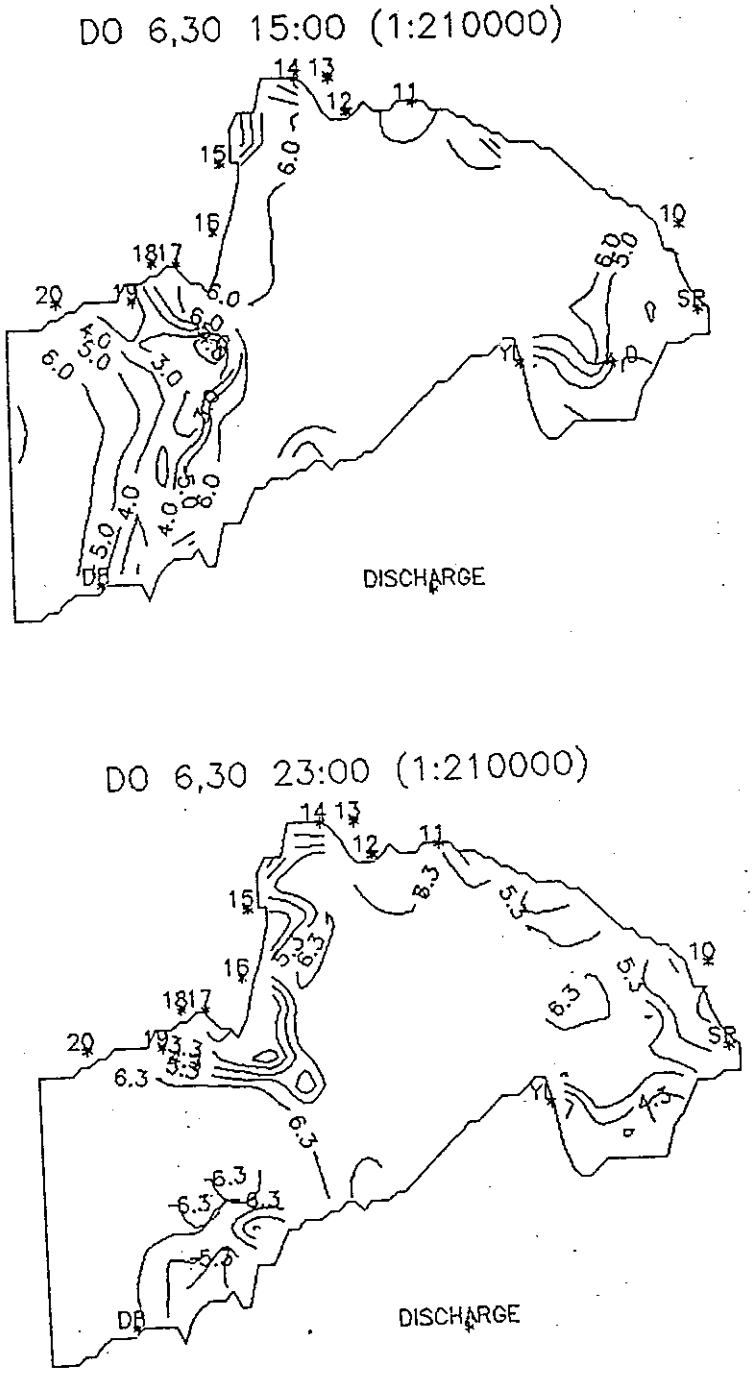

FIG. A7－72(d) Dynamic variation of DO in Deep Bay (wet season)

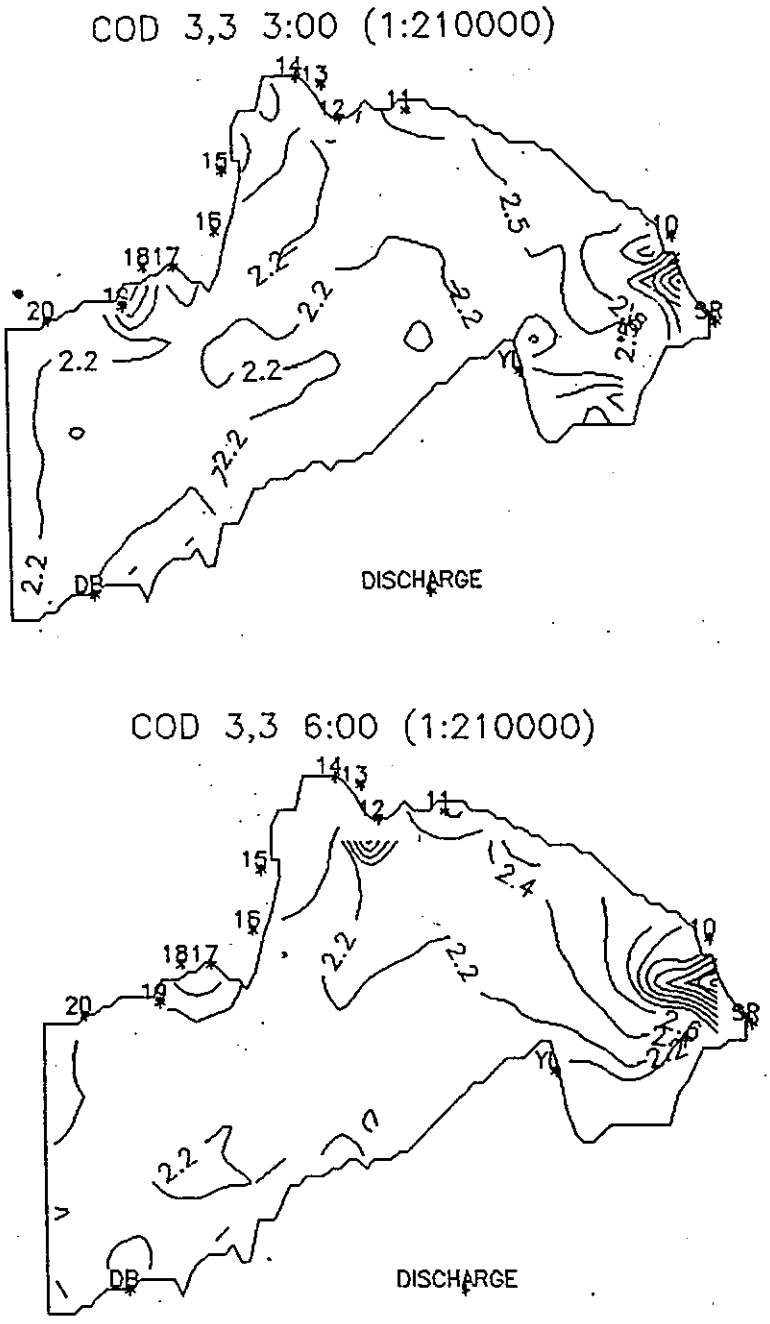

FIG. A7—73(a) Dynamic variation of COD in Deep Bay (dry season)

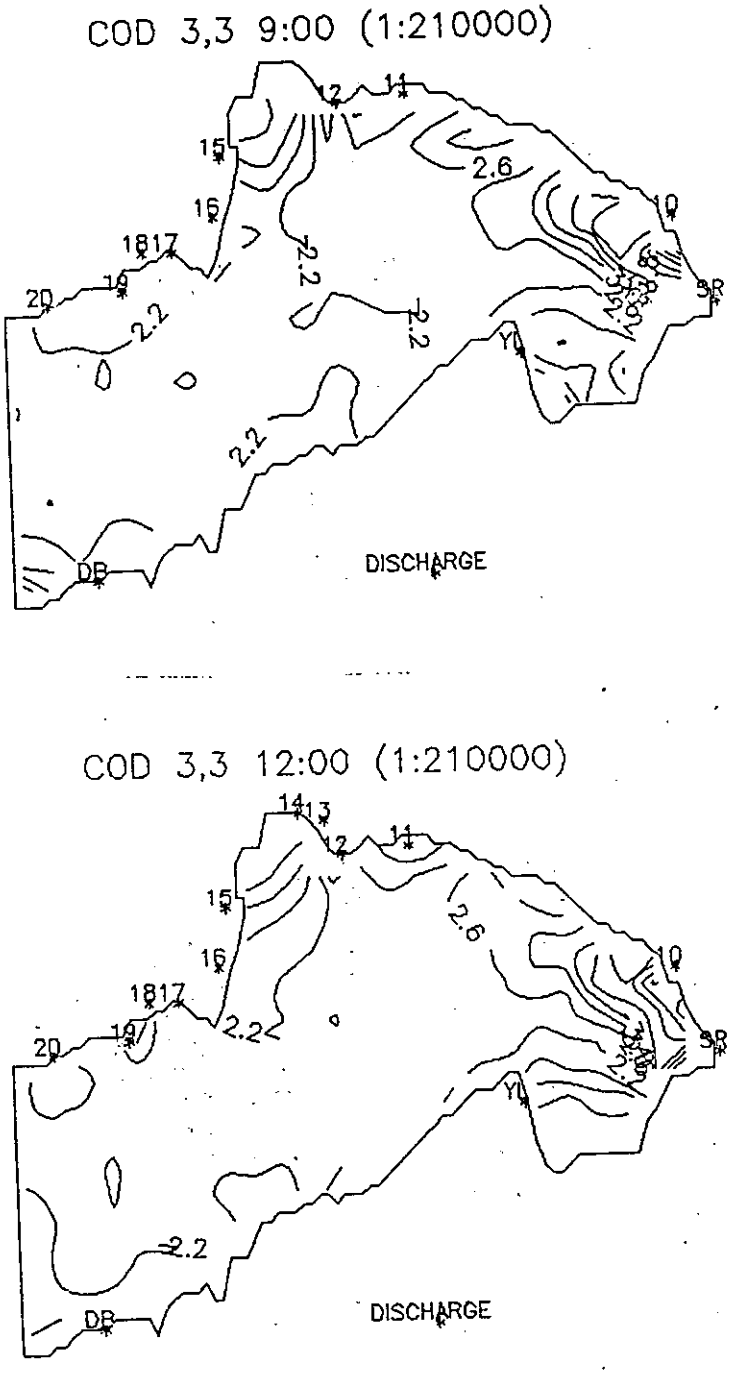

FIG. A7—73(b). Dynamic variation of COD in Deep Bay (dry season)

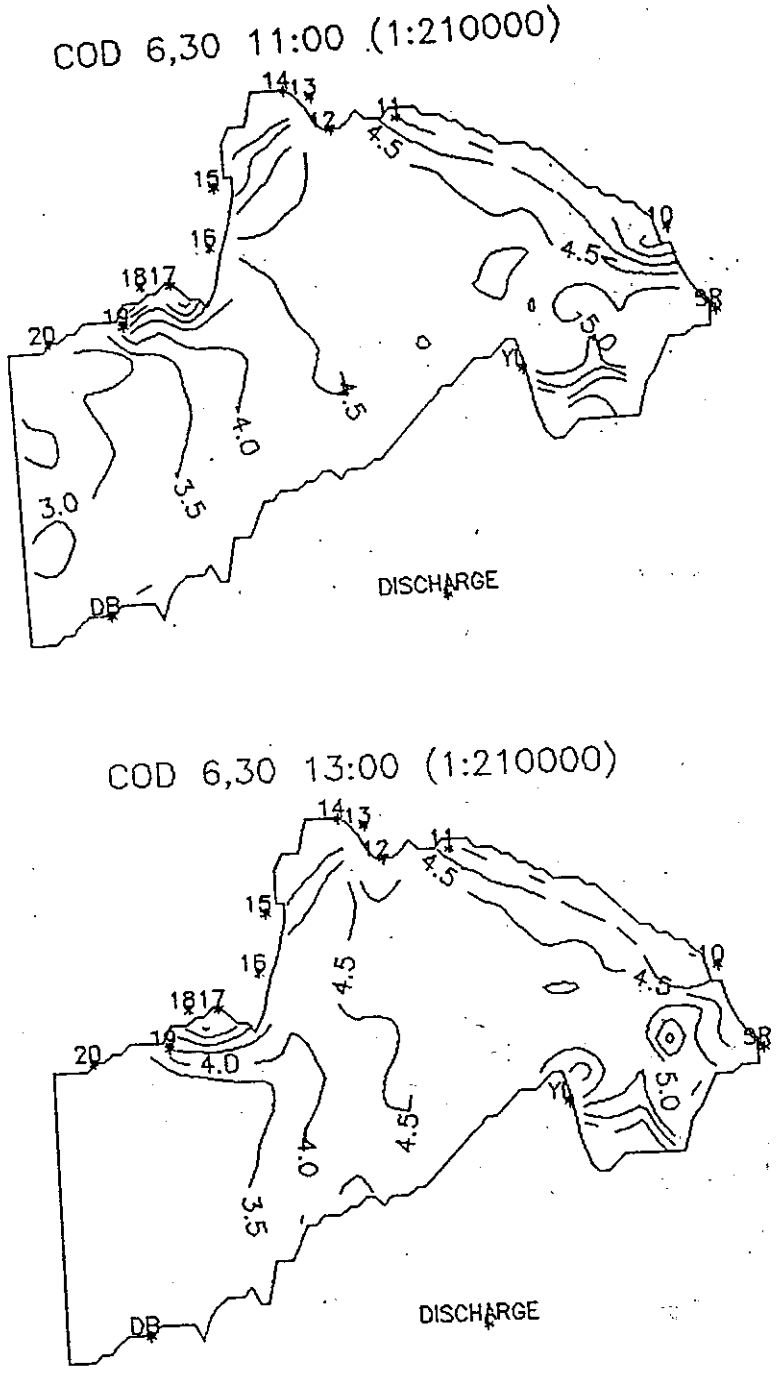

FIG. A7—73(c) Dynamic variation of COD in Deep Bay (wet season)

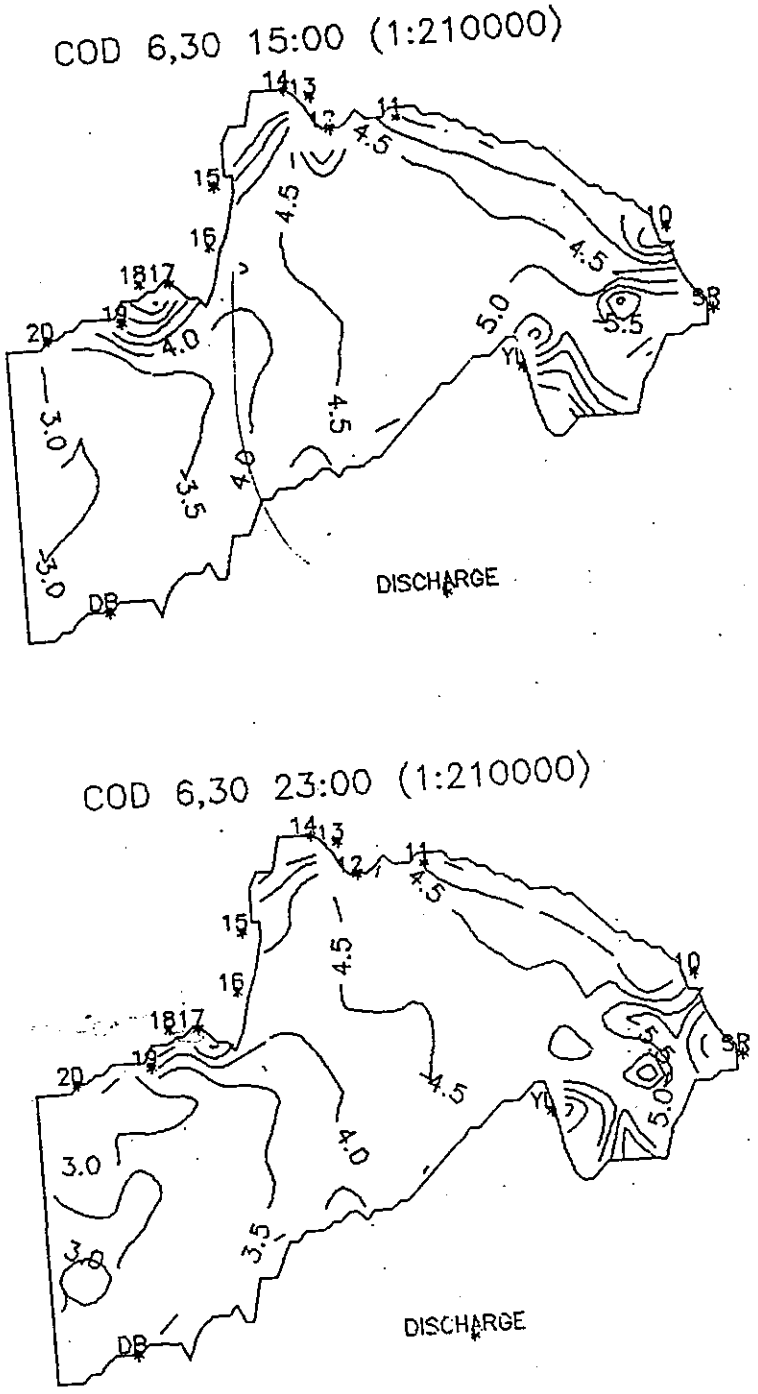

FIG. A7—73(d) Dynamic variation of COD in Deep Bay (wet season)

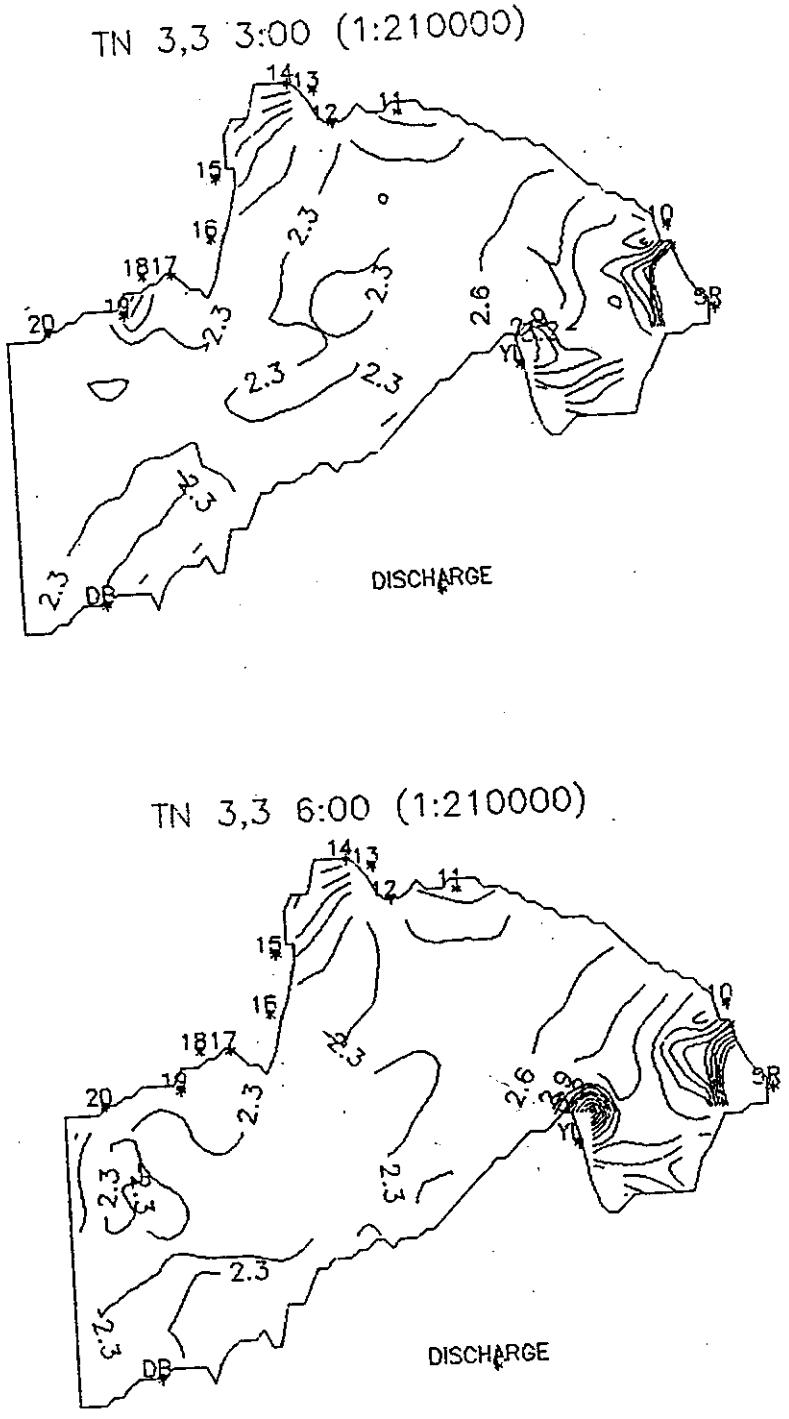

FIG. A7—74(a) **Dynamic variation of TN in Deep Bay (dry season)**

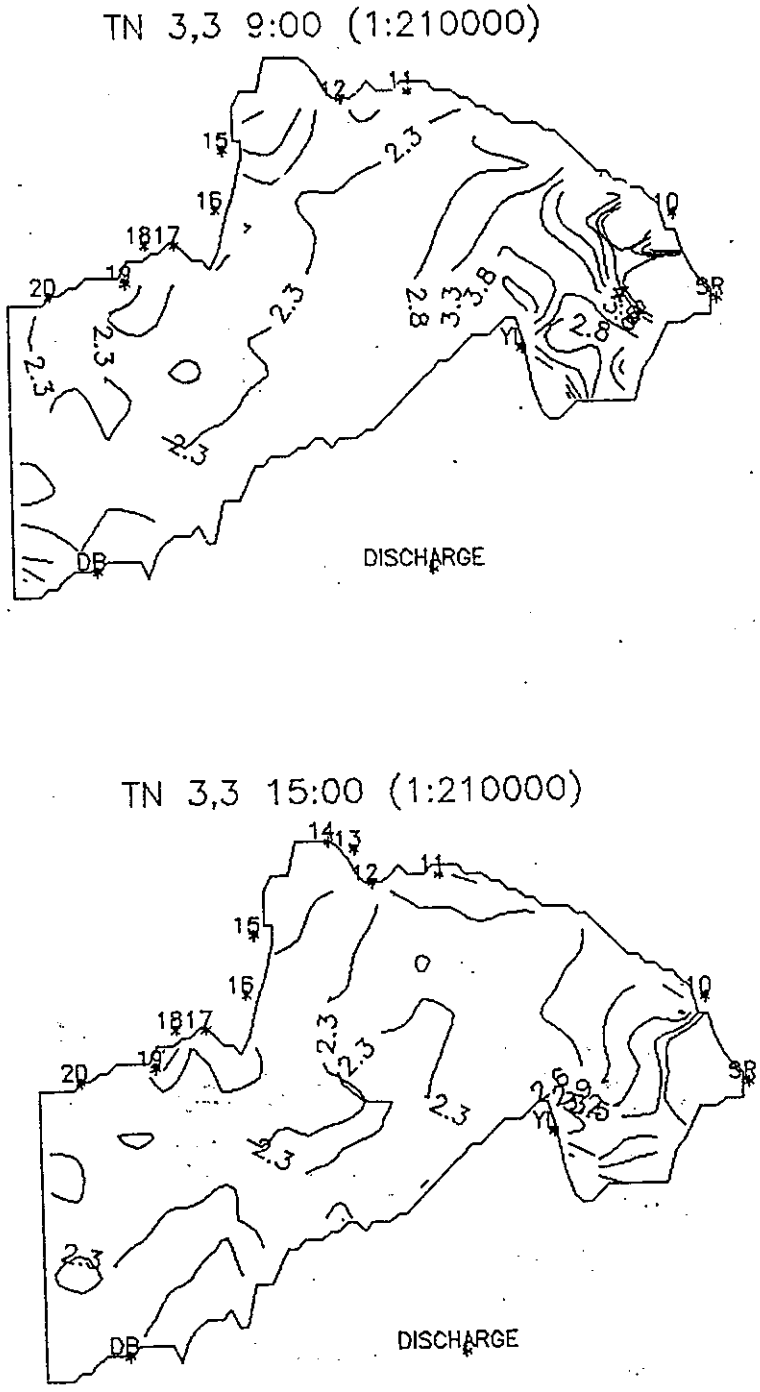

FIG. A7—74(b) Dynamic variation of TN in Deep Bay (dry season)

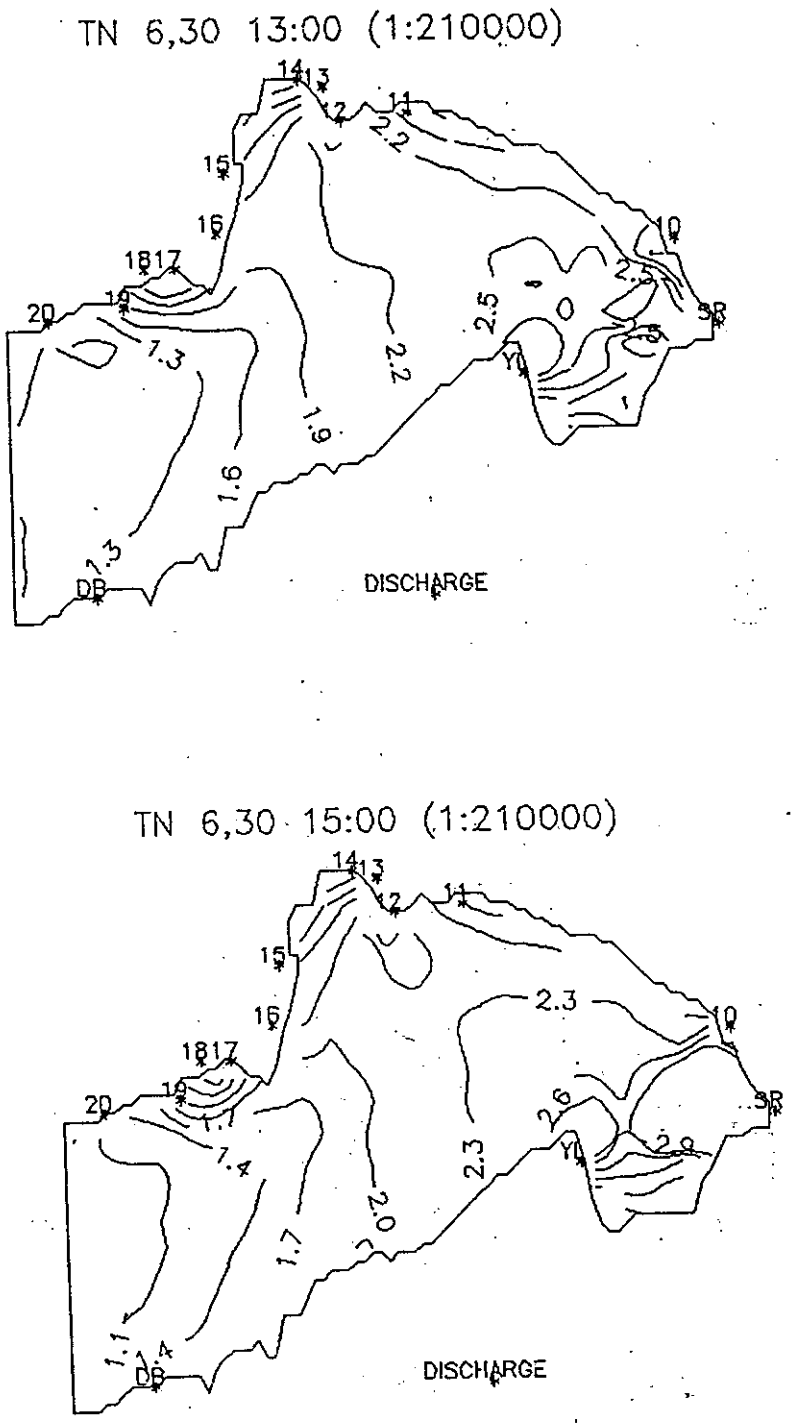

FIG. A7—74(c) Dynamic variation of TN in Deep Bay (wet season)

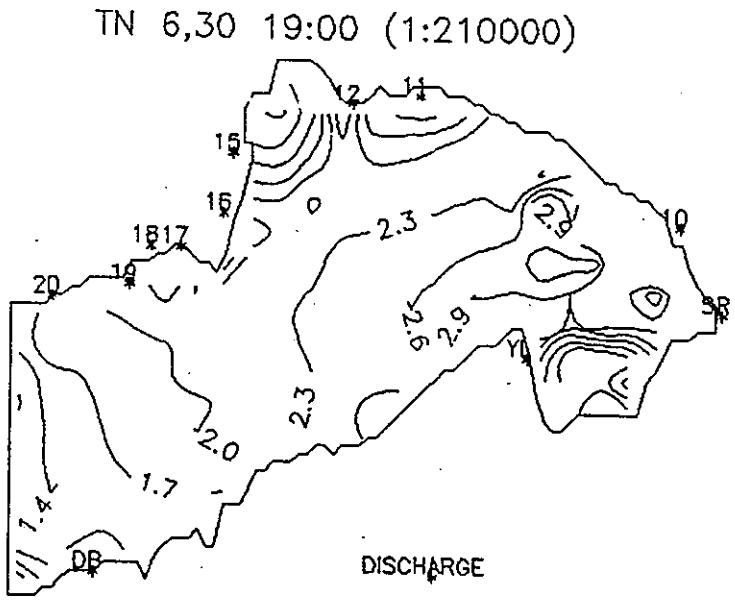

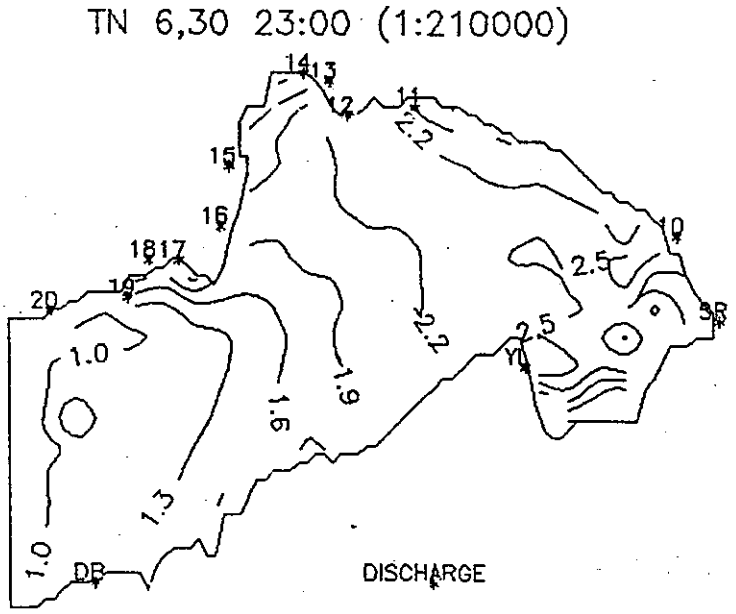

FIG. A7—74(d) Dynamic variation of TN in Deep Bay (wet season)

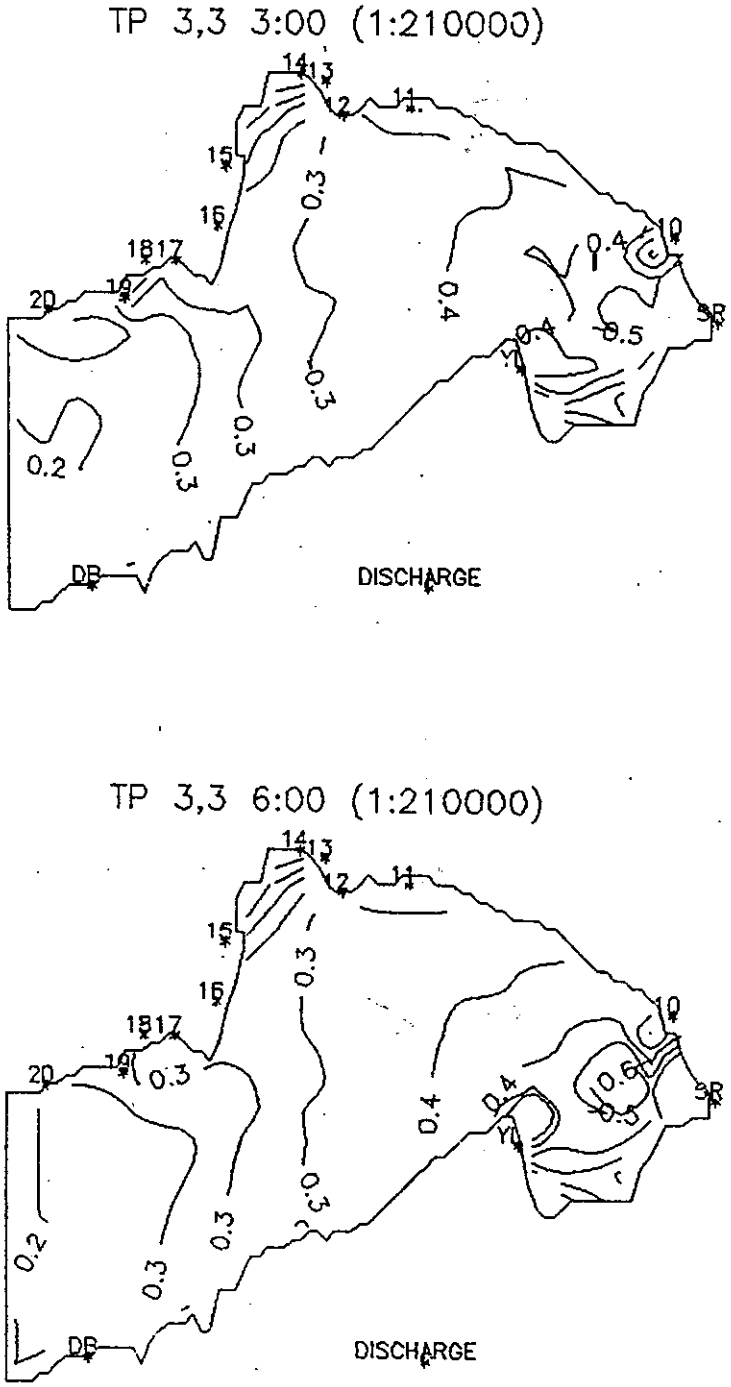

FIG. A7—75(a) **Dynamic variation of TP in Deep Bay (dry season)**

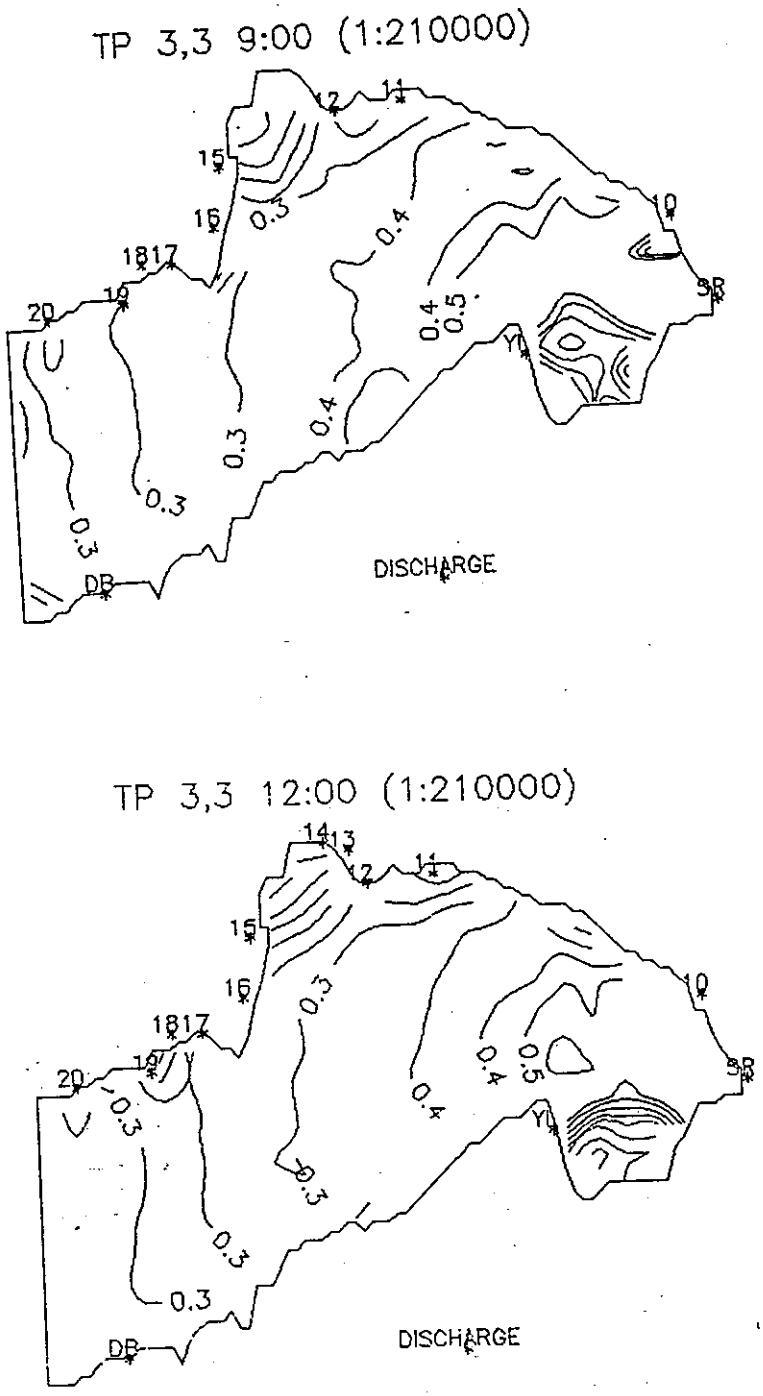

FIG. A7—75(b) Dynamic variation of TP in Deep Bay (dry season)

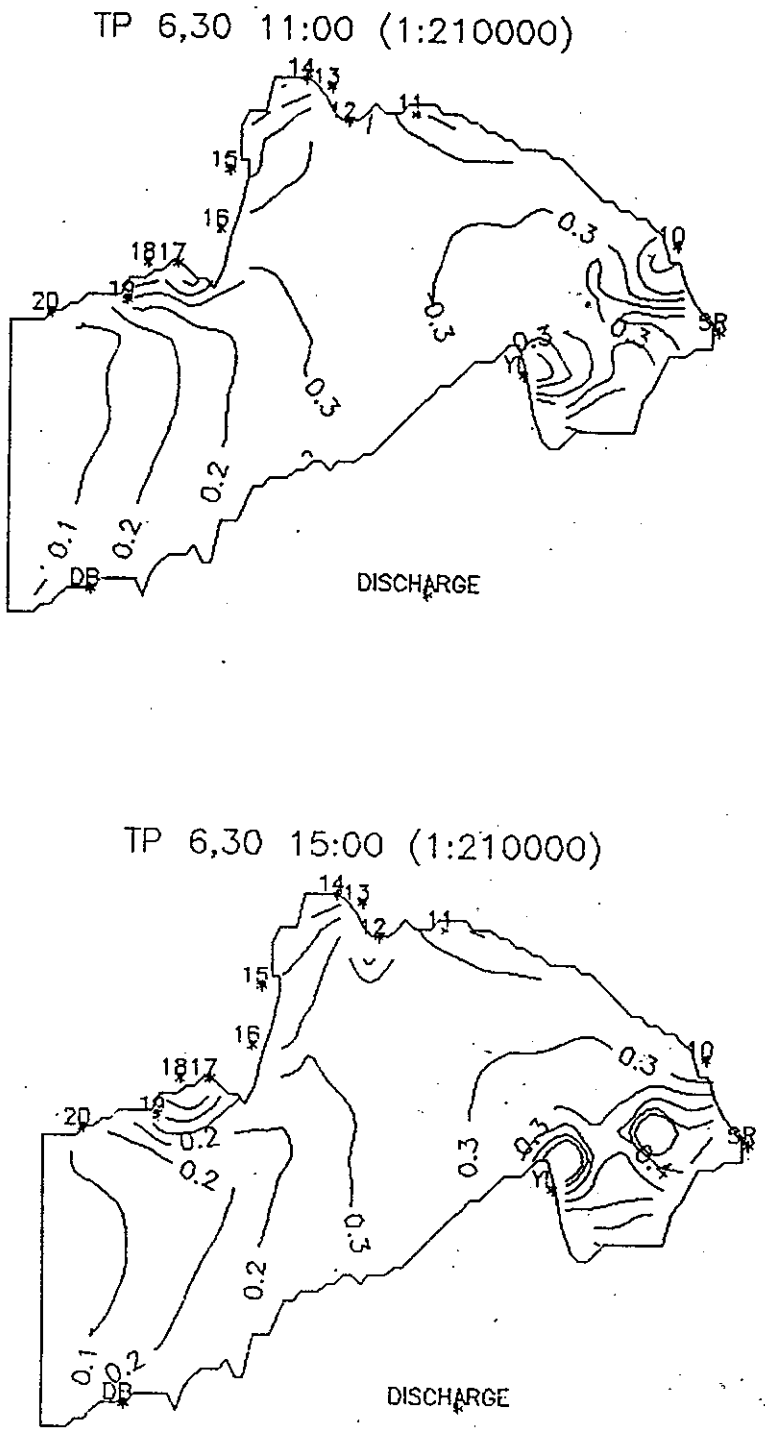

FIG. A7—75(c) **Dynamic variation of TP in Deep Bay (wet season)**

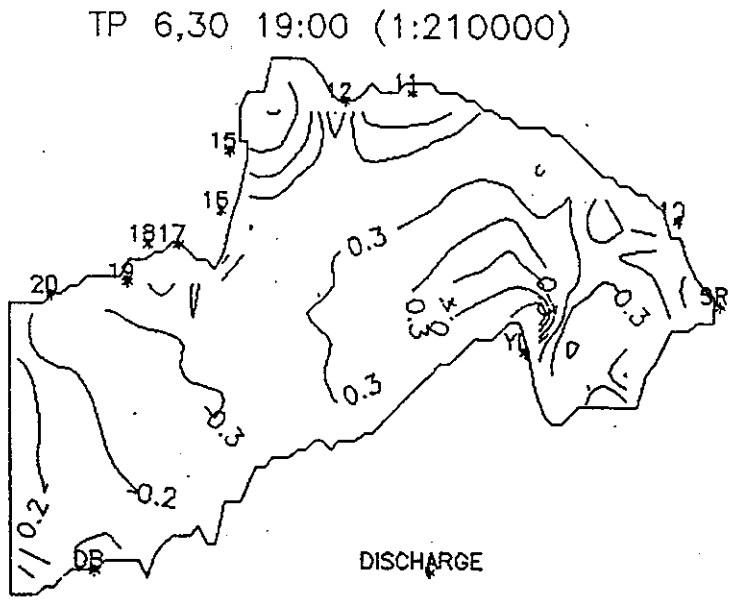

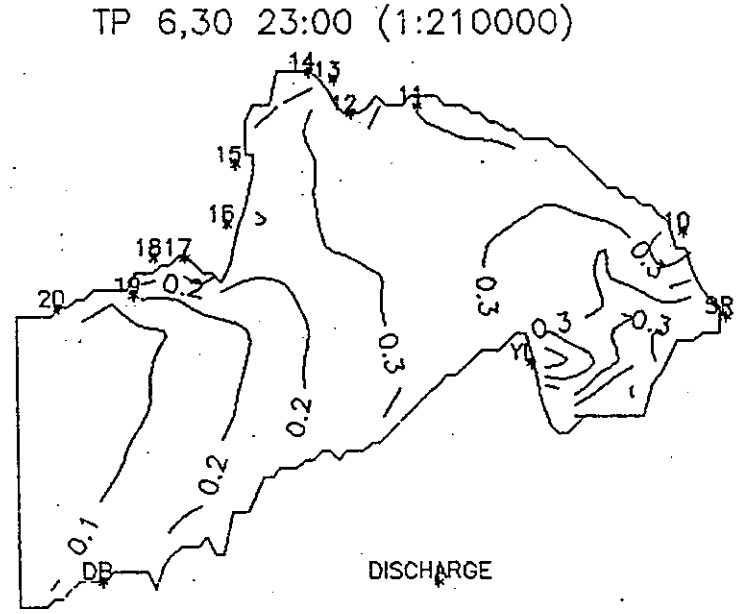

FIG. A7—75(d) Dynamic variation of TP in Deep Bay (wet season)

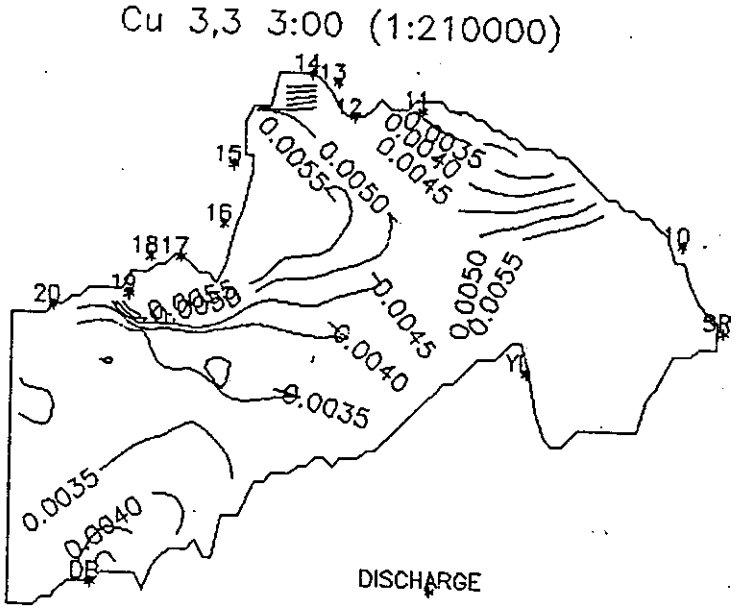

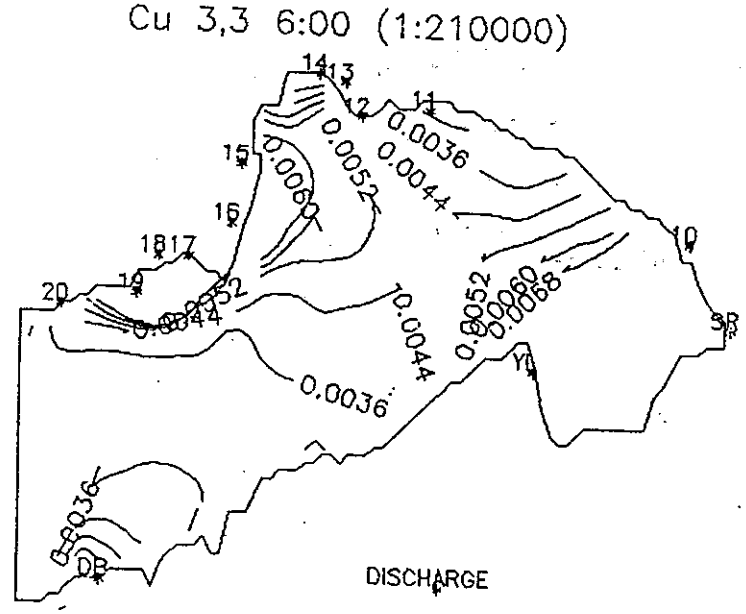

FIG. A7—76(a) Dynamic variation of Cu in Deep Bay (dry season)

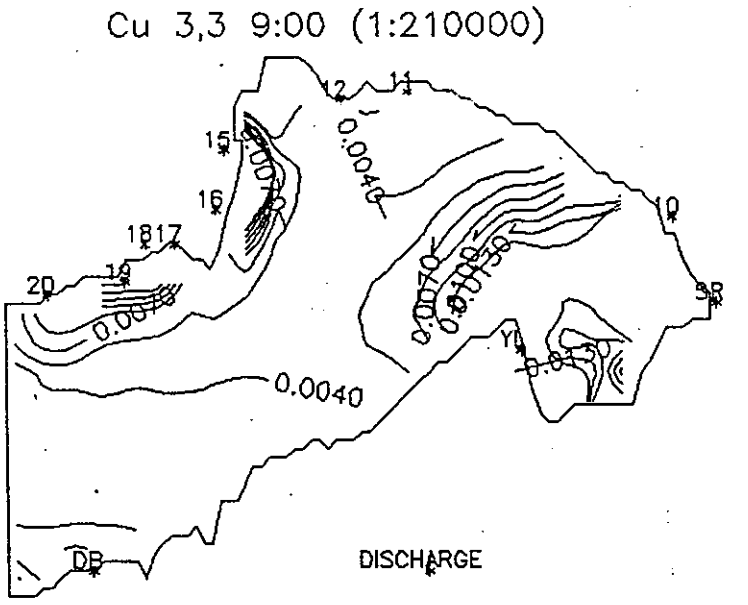

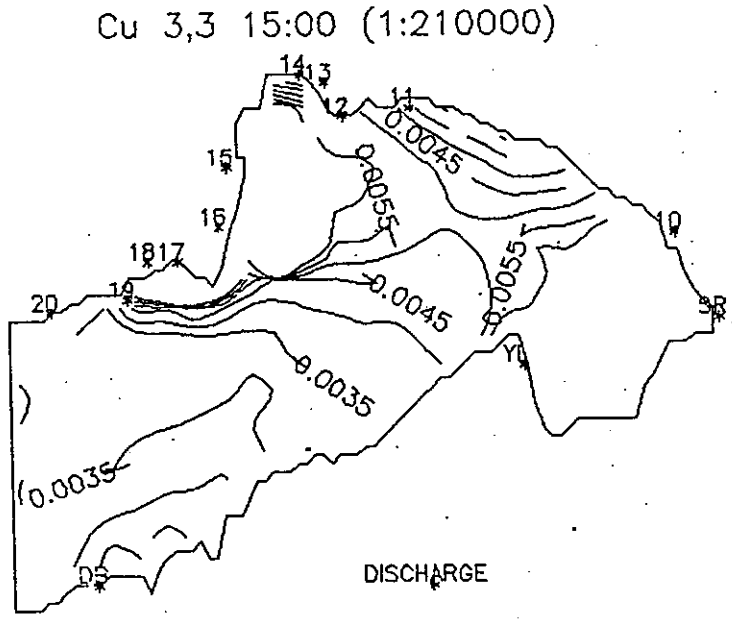

FIG. A7—76(b) **Dynamic variation of Cu in Deep Bay (dry season)**

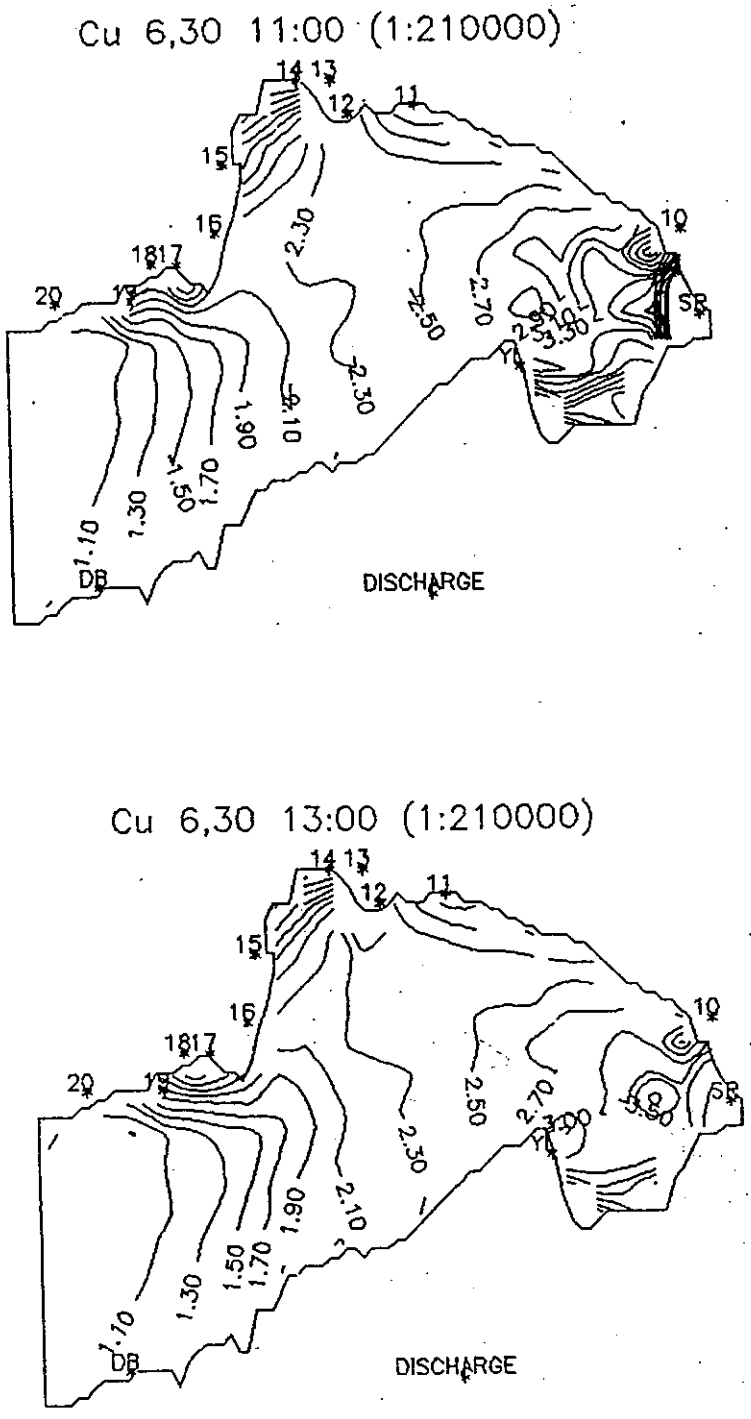

FIG. A7—76(c) Dynamic variation of Cu in Deep Bay (wet season)

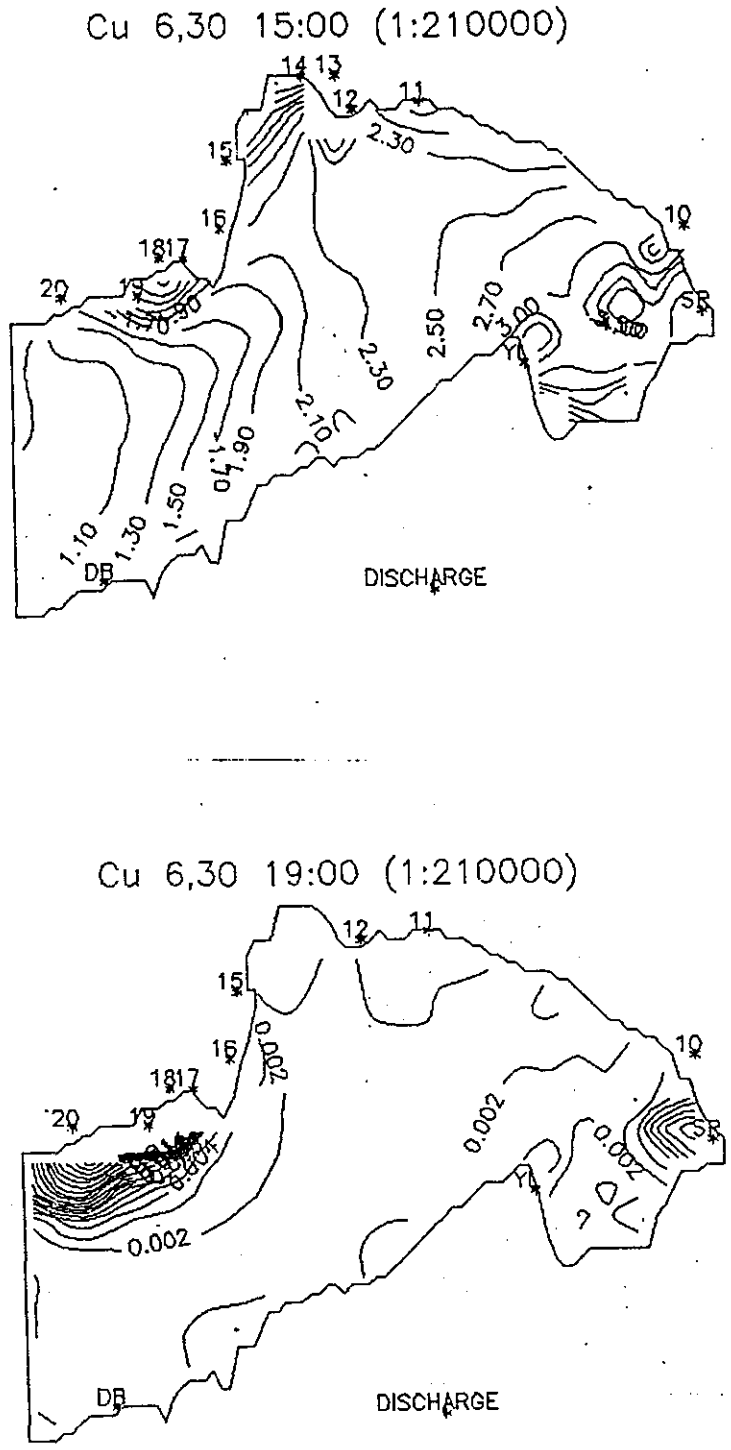

FIG. A7—76(d) Dynamic variation of Cu in Deep Bay (wet season)

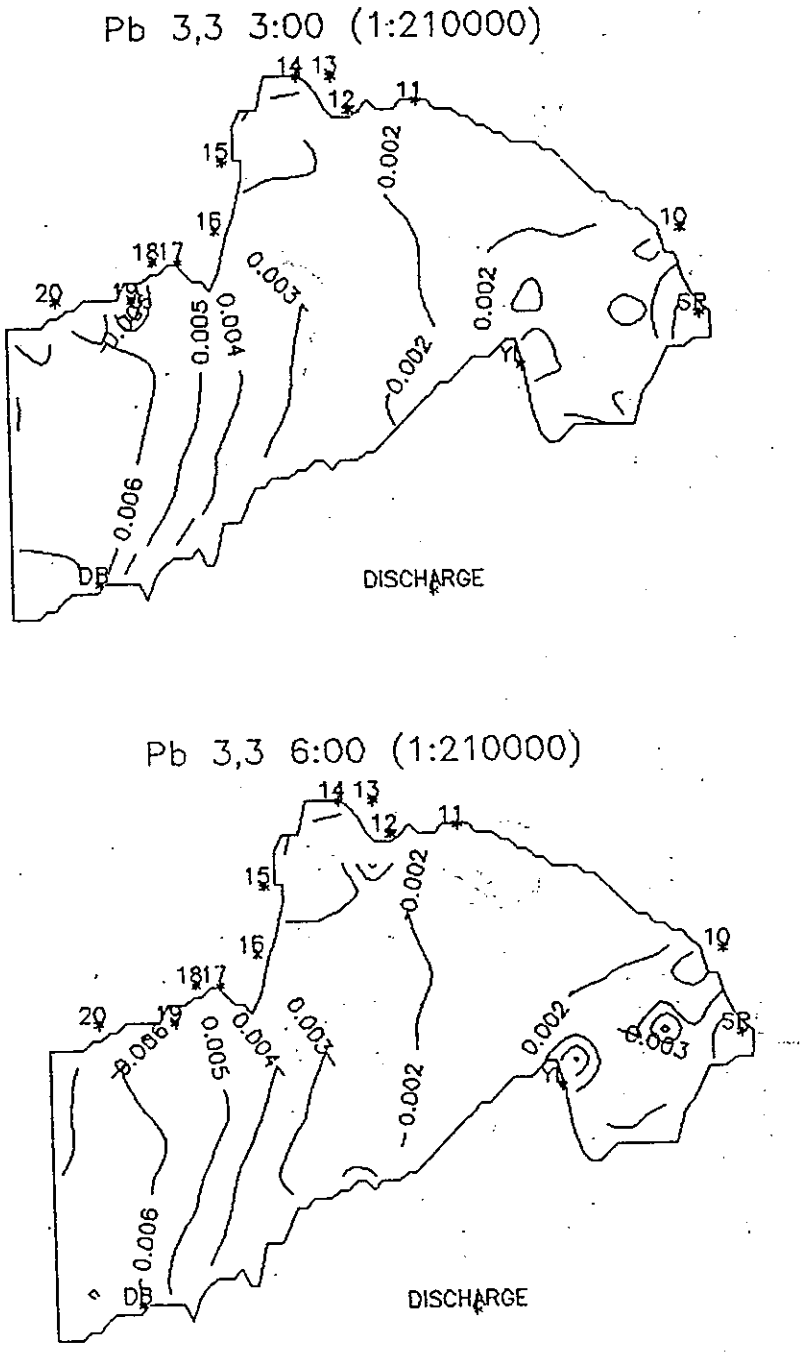

FIG. A7—77(a) Dynamic variation of Pb in Deep Bay (dry season)

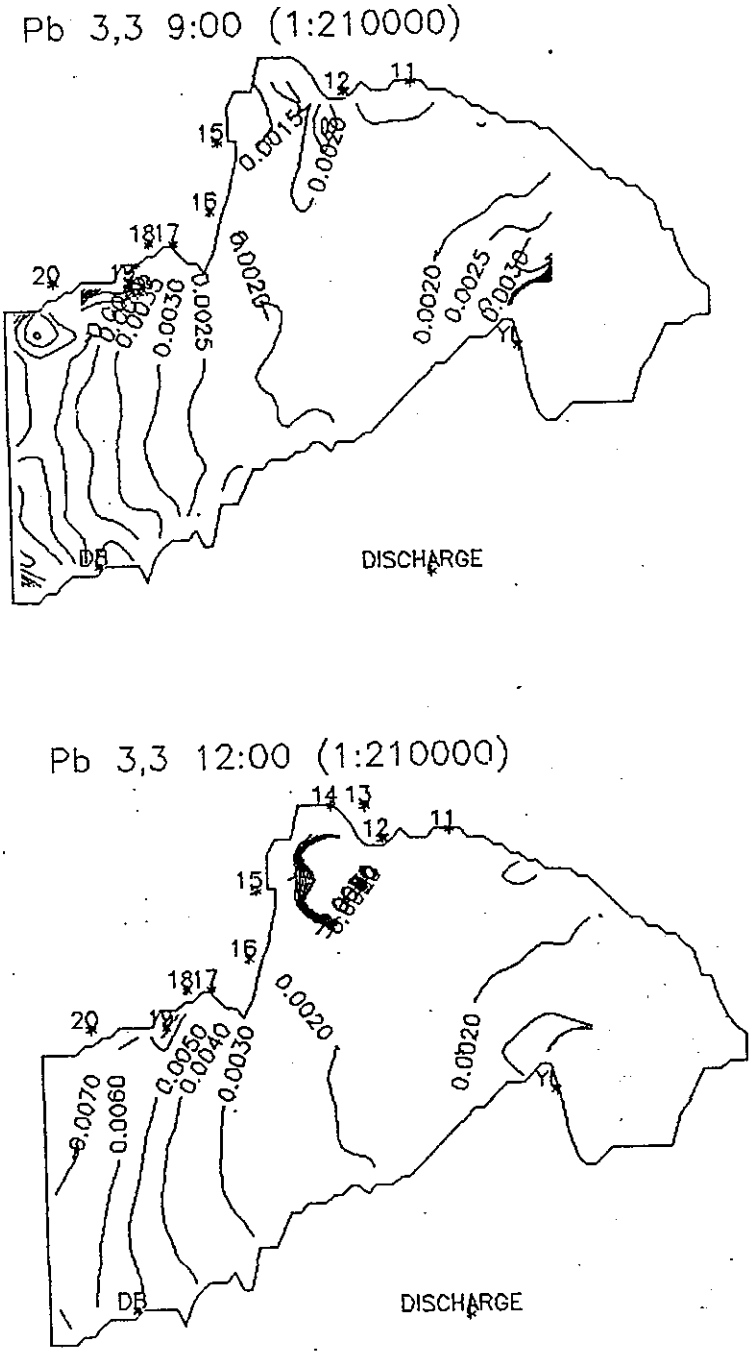

FIG. A7—77(b) Dynamic variation of Pb in Deep Bay (dry season)

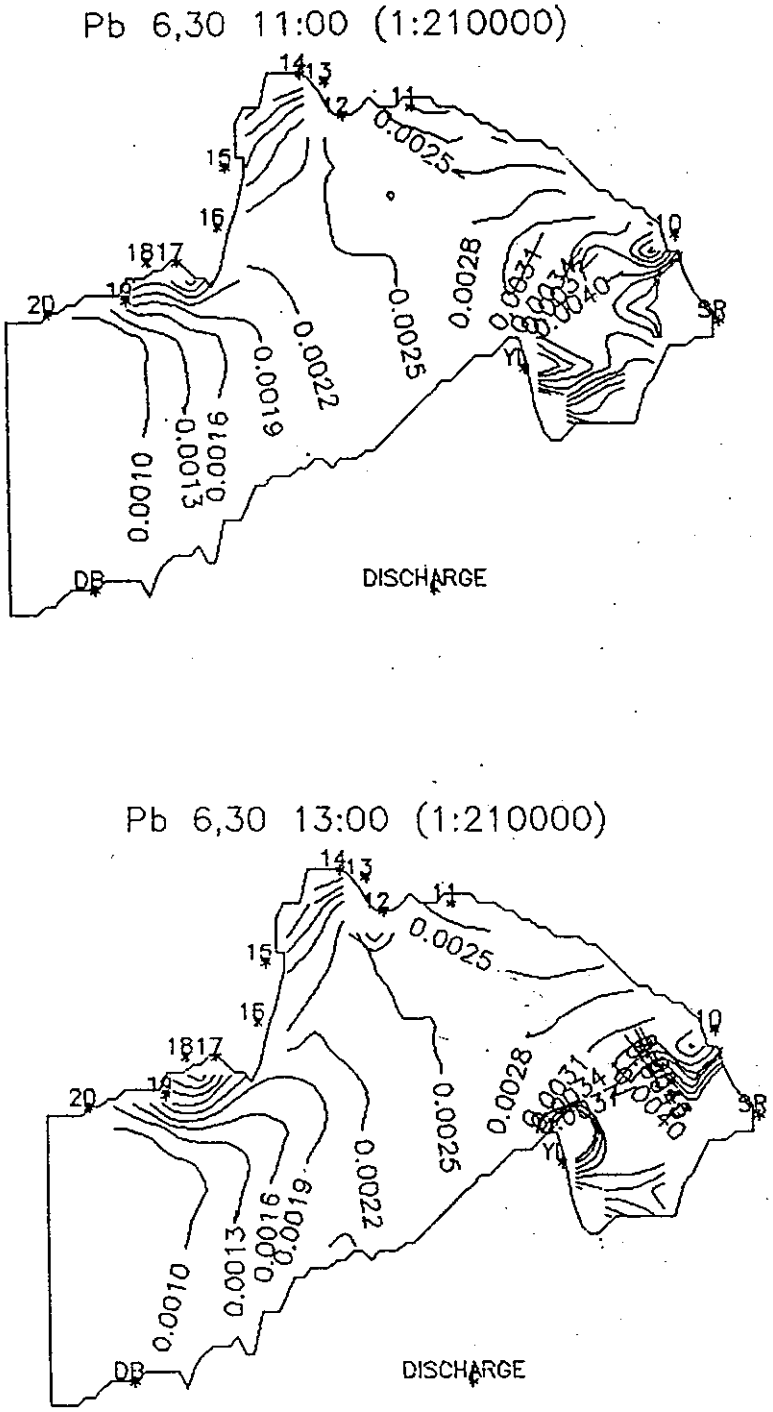

FIG. A7—77(c) **Dynamic variation of Pb in Deep Bay (wet season)**

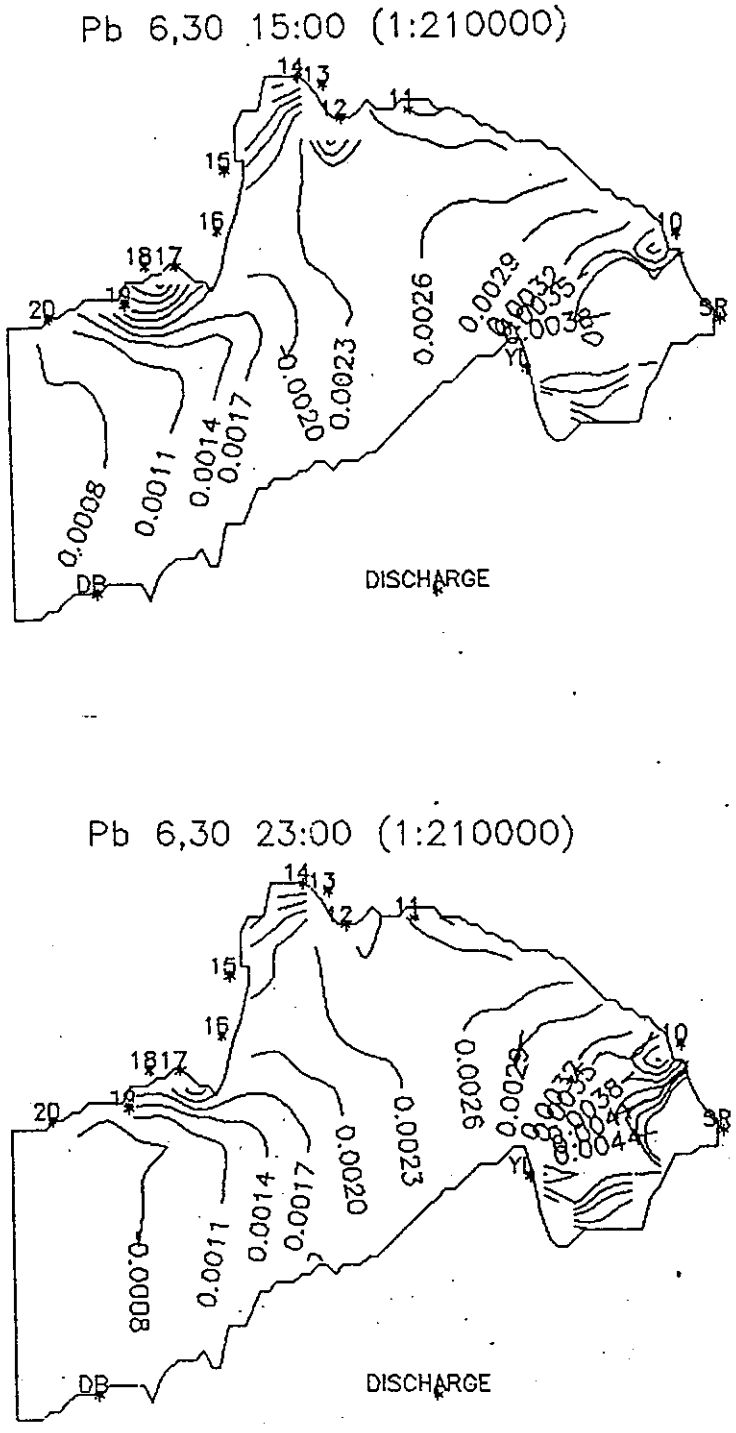

FIG. A7—77(d) Dynamic variation of PB in Deep Bay (wet season)

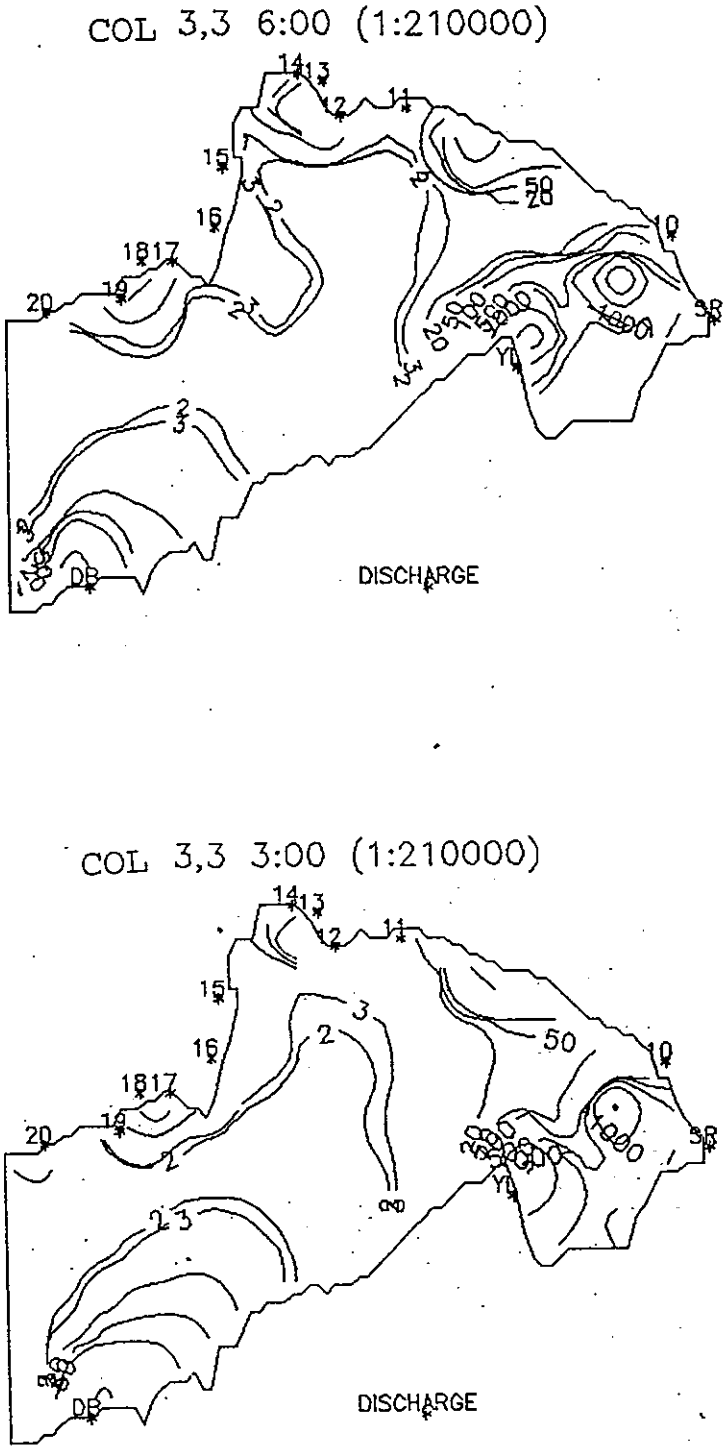

FIG. A7—78(a) Dynamic variation of Col. in Deep Bay (dry season)

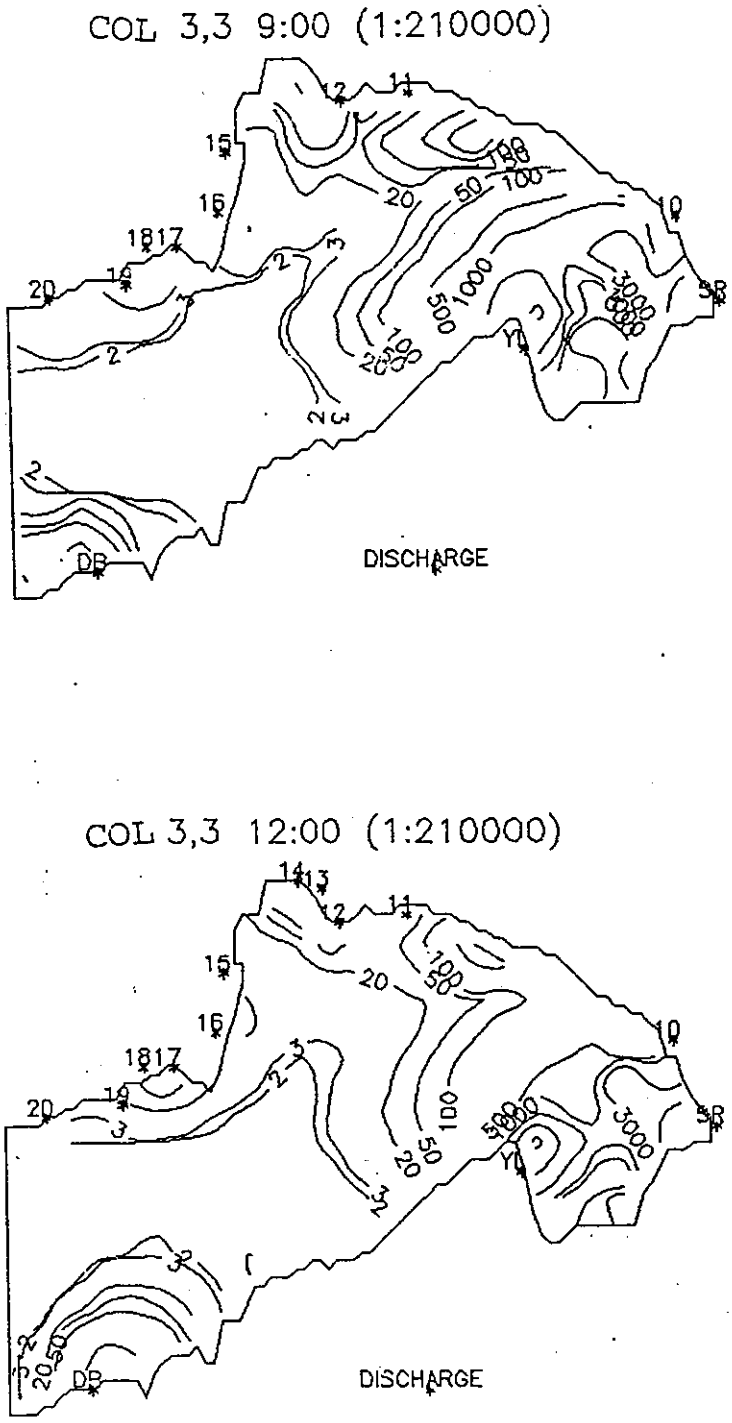

FIG. A7—78(b) Dynamic variation of Col. in Deep Bay (dry season)

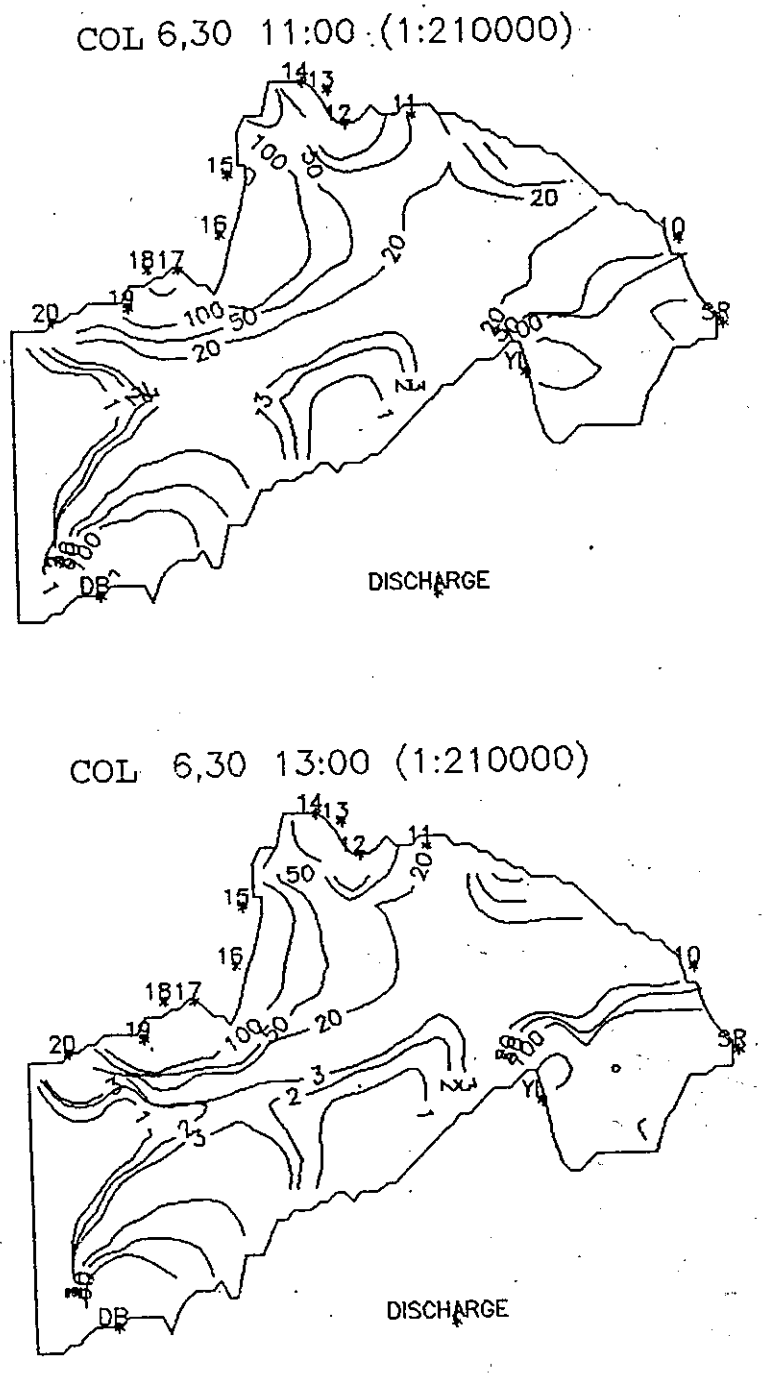

FIG. A7—78(c) Dynamic variation of Col. in Deep Bay (wet season)

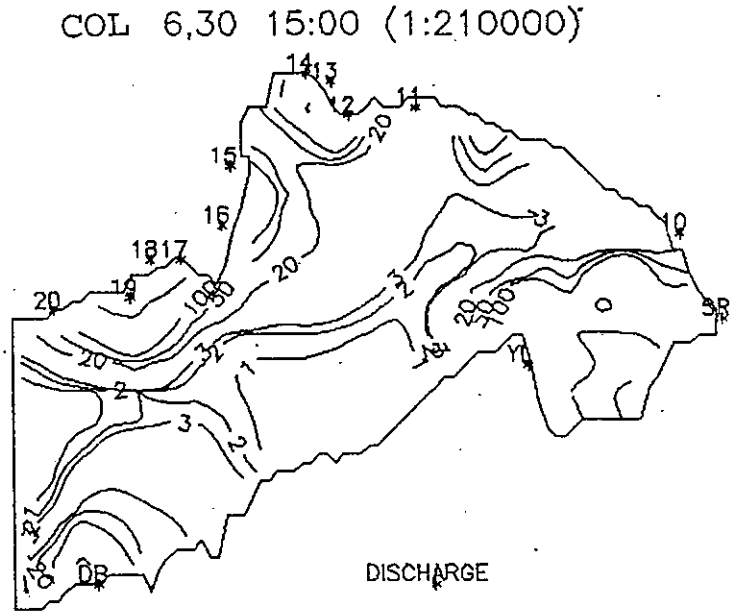

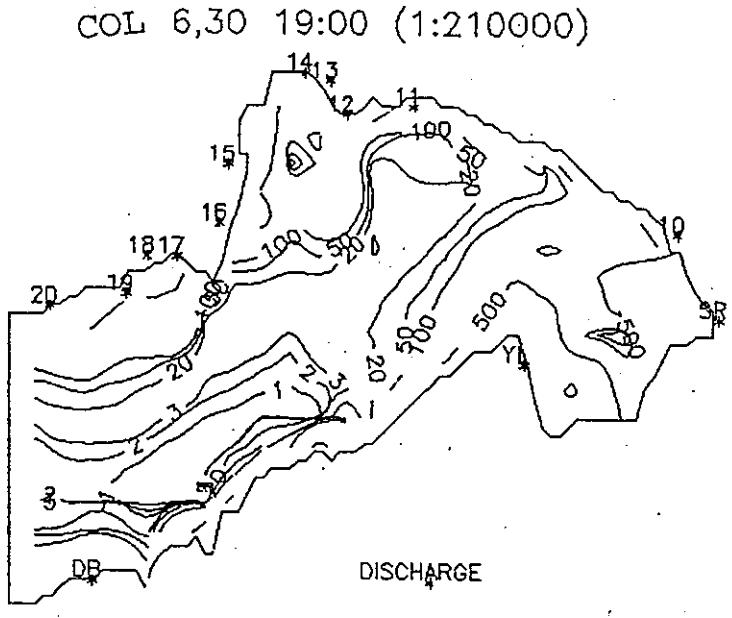

FIG. A7—78(d) Dynamic variation of Col. in Deep Bay (wet season)

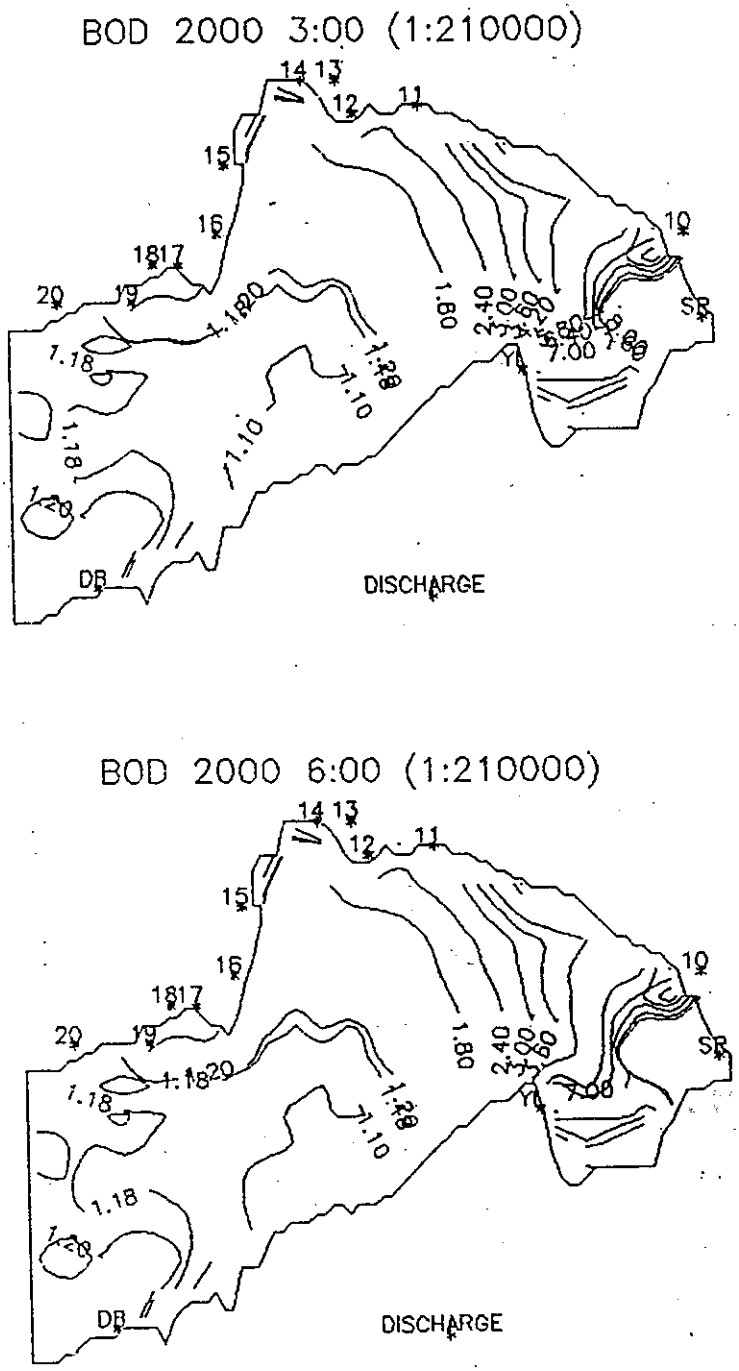

FIG. A7—79(a) Dynamic variation of BOD in Deep Bay in 2000

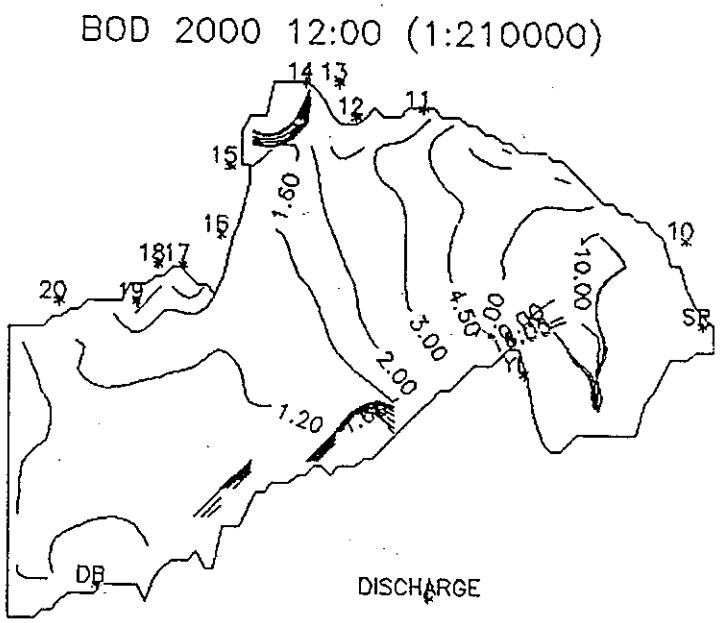

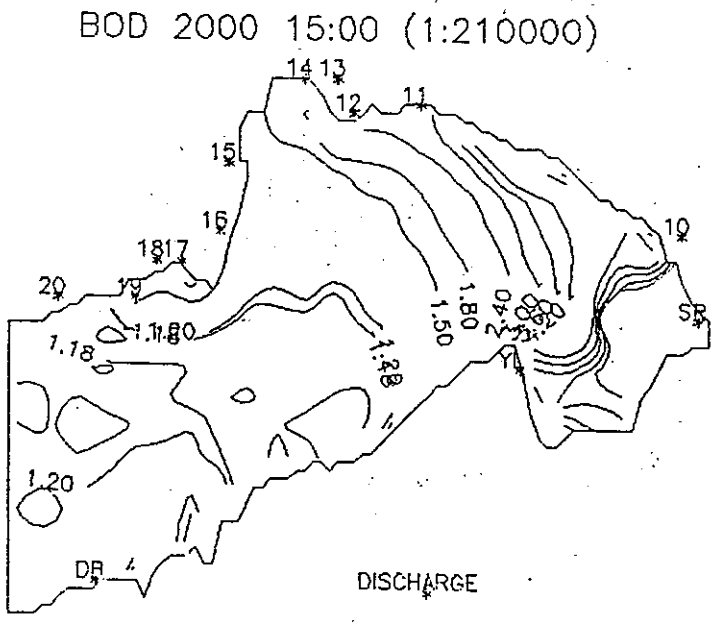

FIG. A7—79(b) **Dynamic variation of BOD in Deep Bay in** 2000

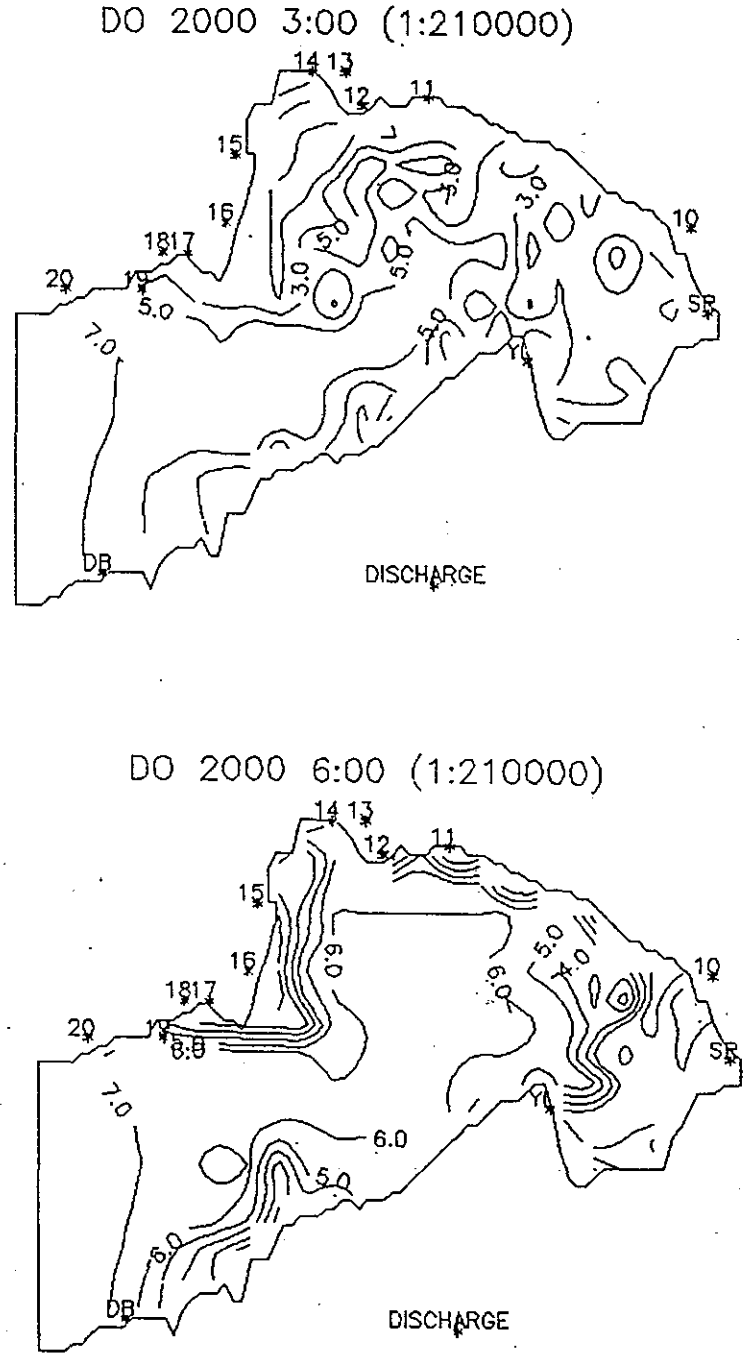

FIG. A7—80(a) Dynamic variation of DO in Deep Bay in 2000

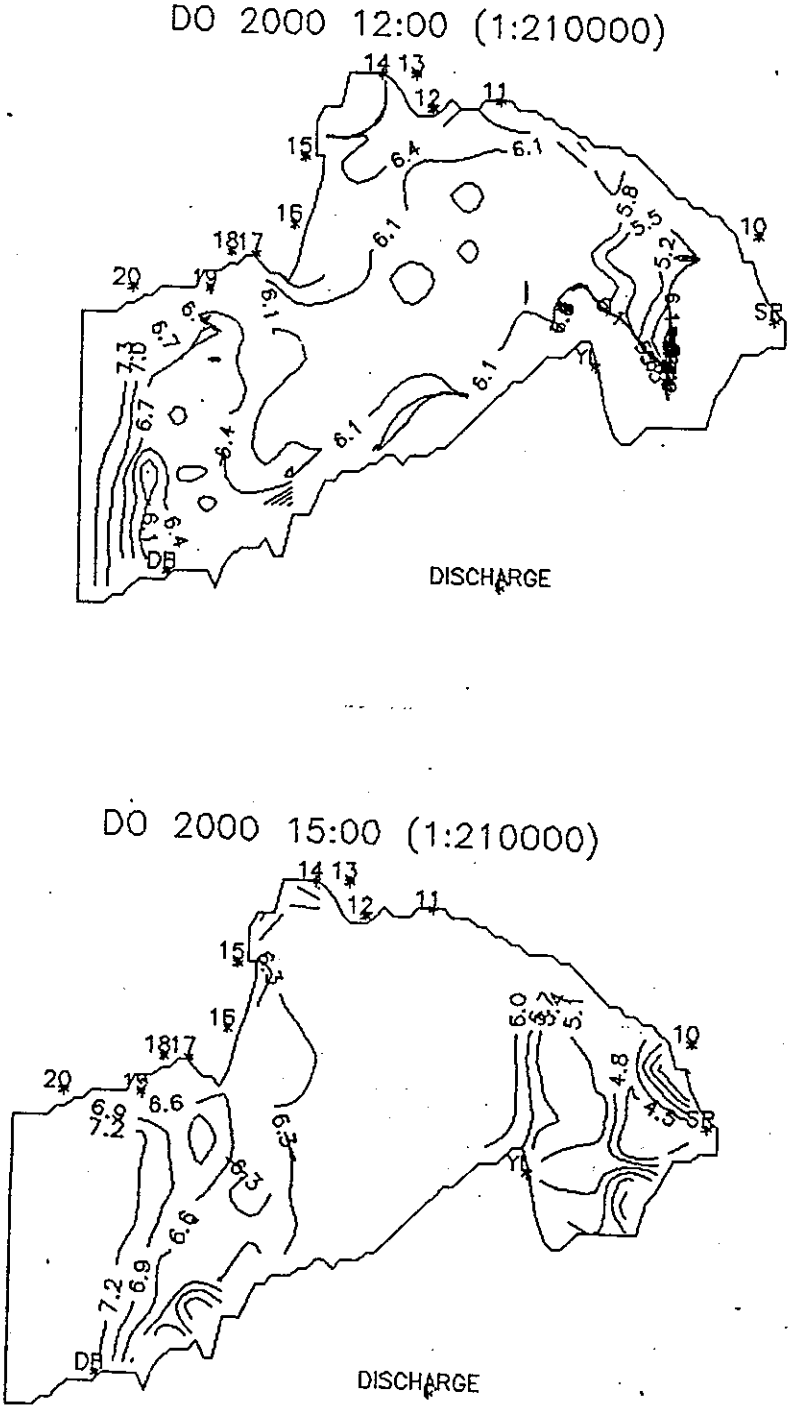

FIG. A7—80(b) Dynamic variation of DO in Deep Bay in 2000

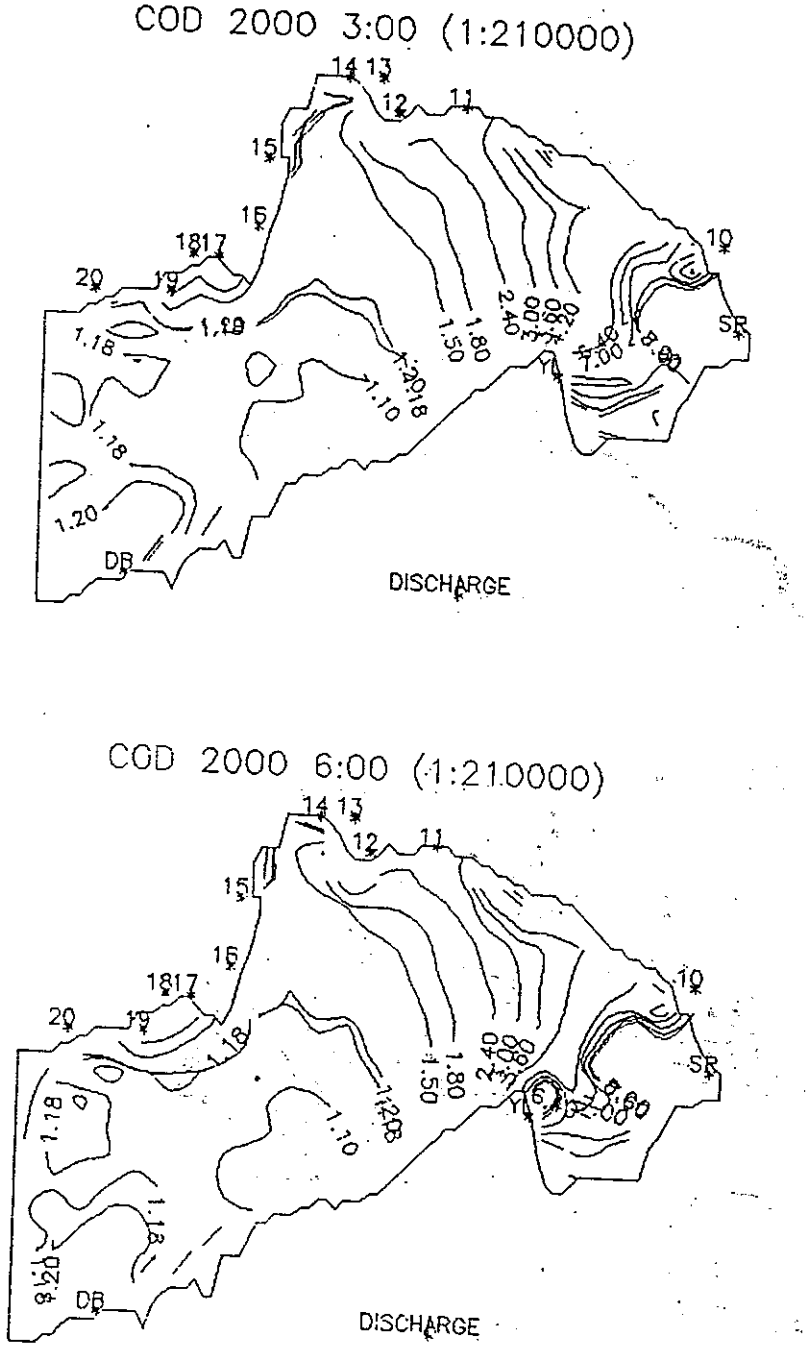

FIG. A7—81(a) Dynamic variation of COD in Deep Bay in 2000

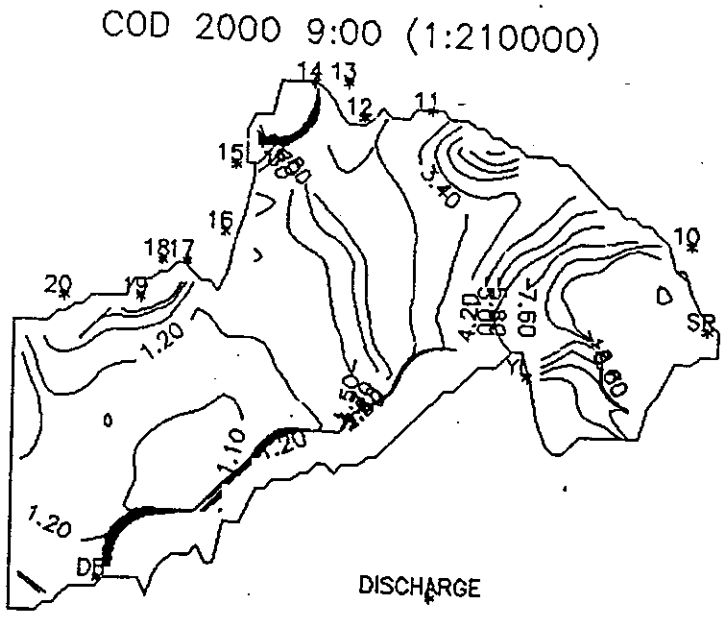

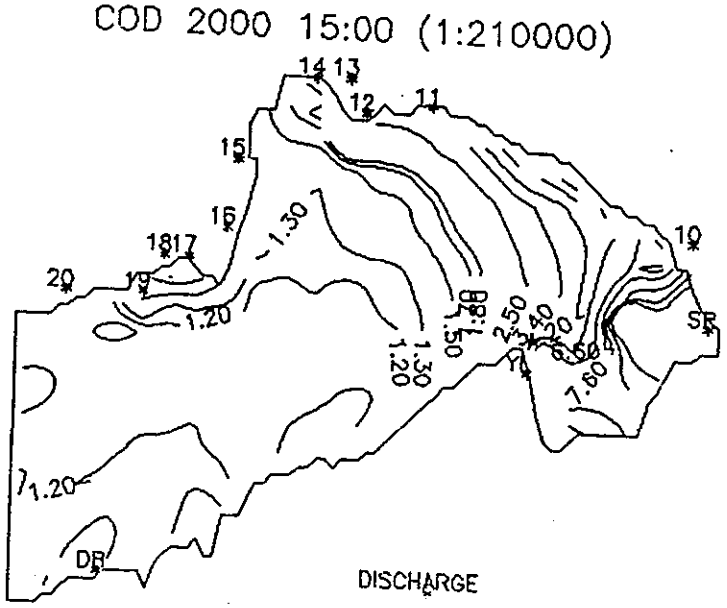

FIG. A7—81(b) Dynamic variation of COD in Deep Bay in 2000

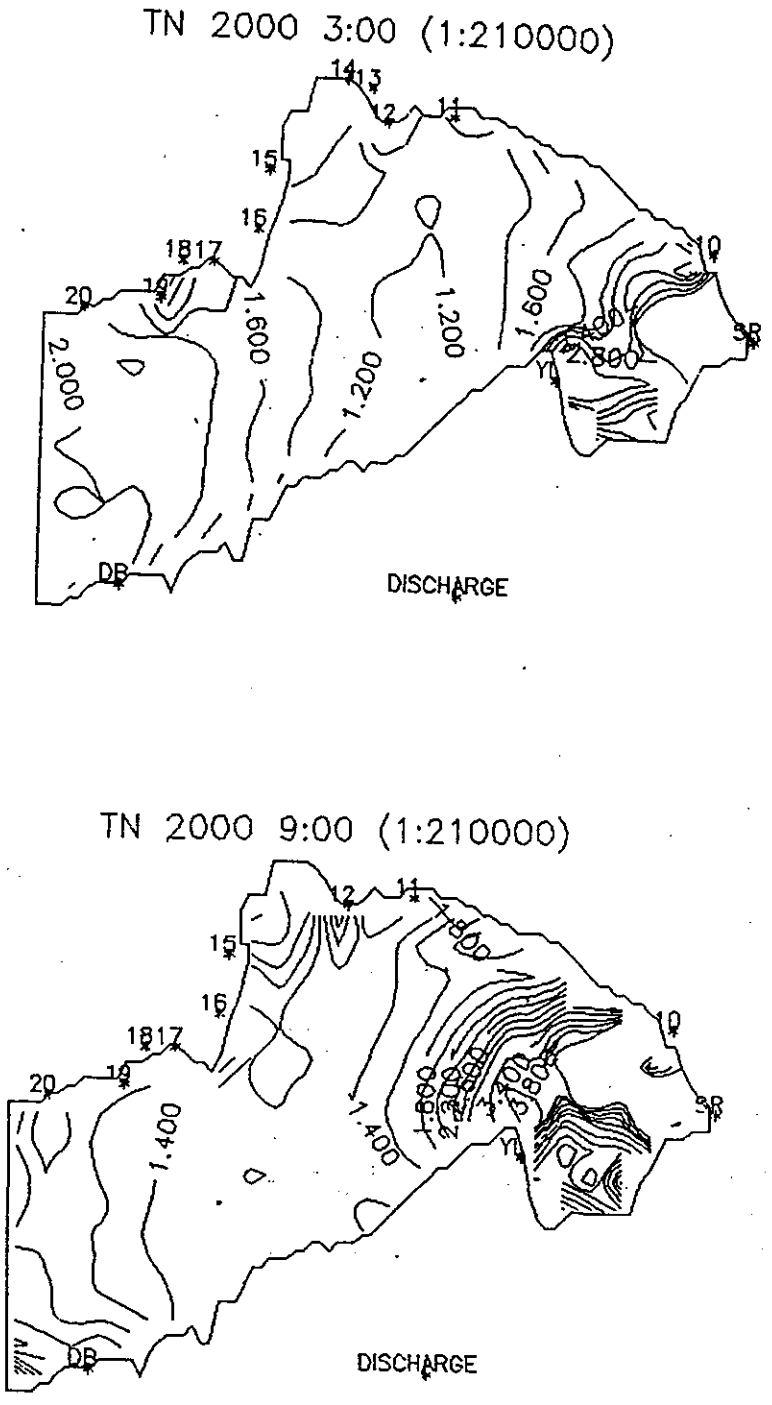

FIG. A7—82(a) Dynamic variation of TN in Deep Bay in 2000

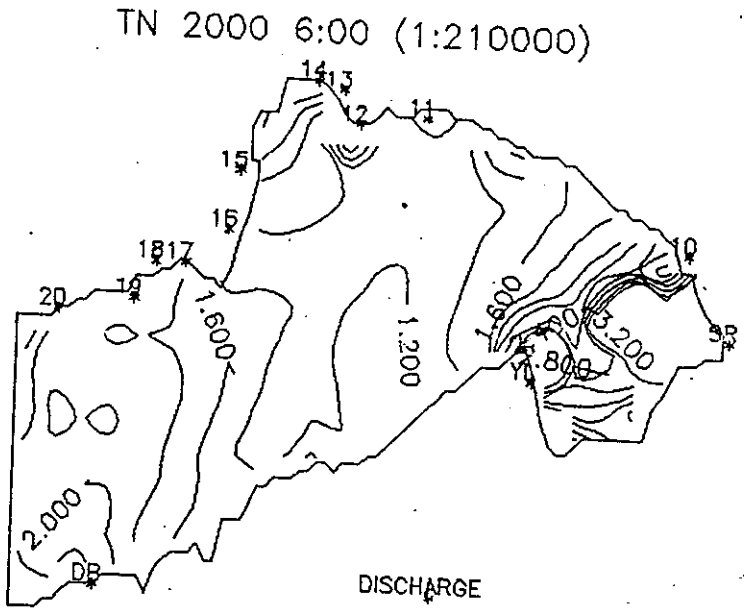

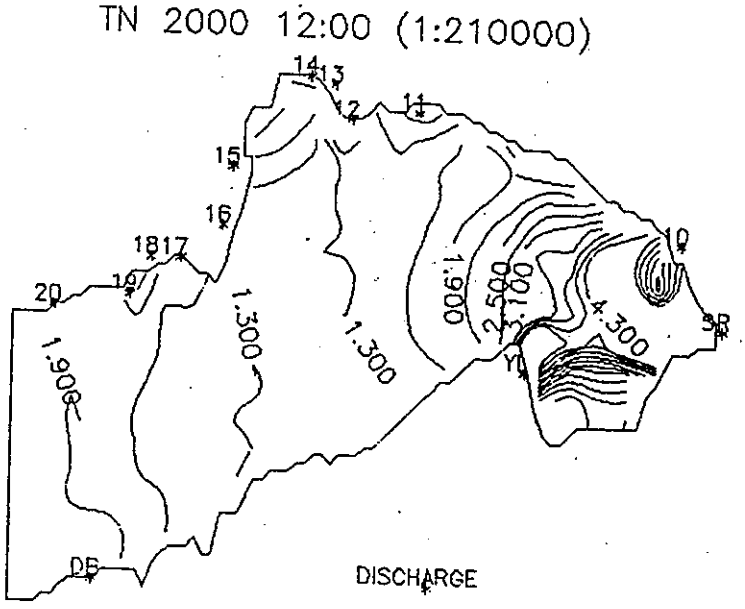

FIG. A7—82(b) Dynamic variation of TN in Deep Bay in 2000

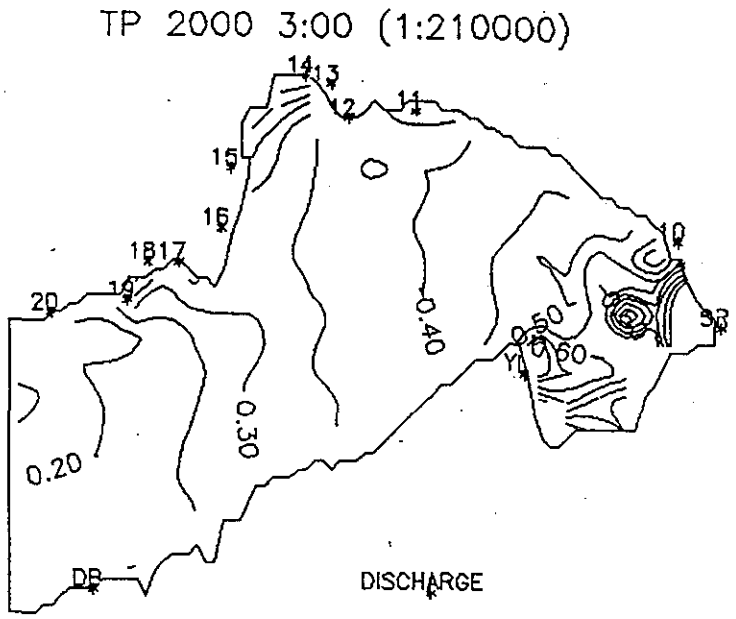

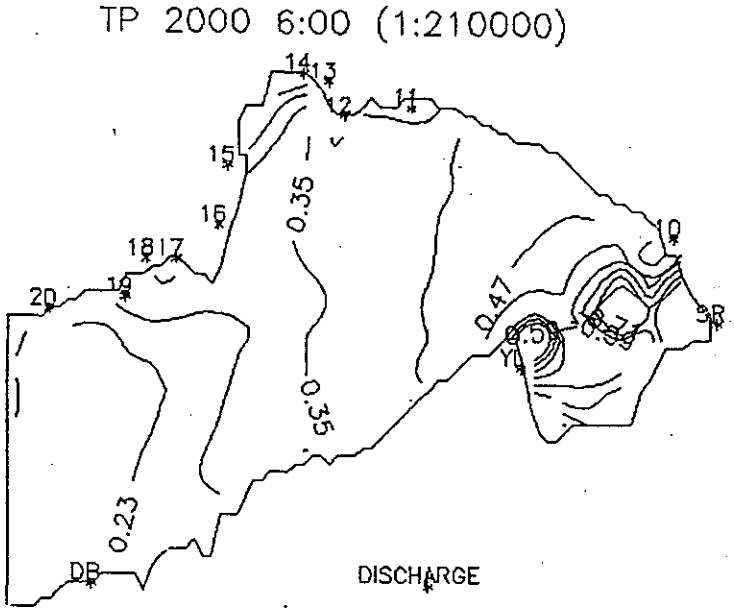

FIG. A7—83(a) Dynamic variation of TP in Deep Bay in 2000

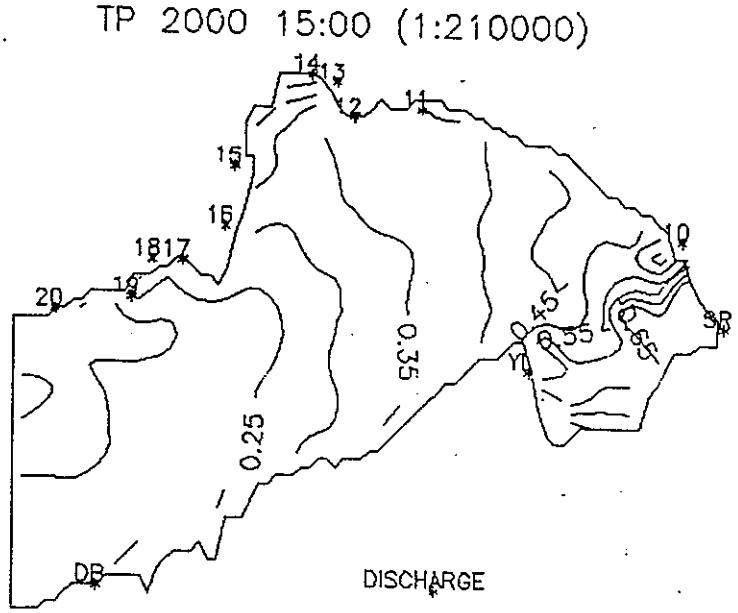

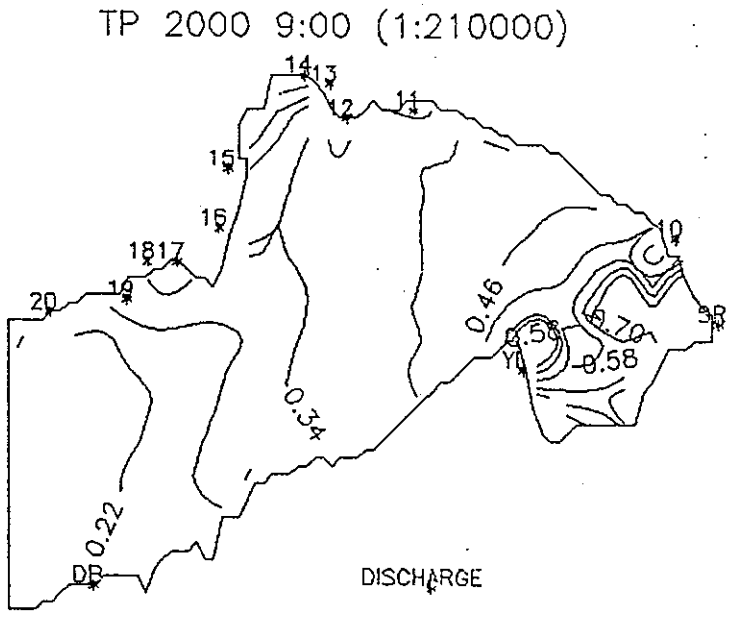

FIG. A7—83(b) **Dynamic variation of TP in Deep Bay in** 2000

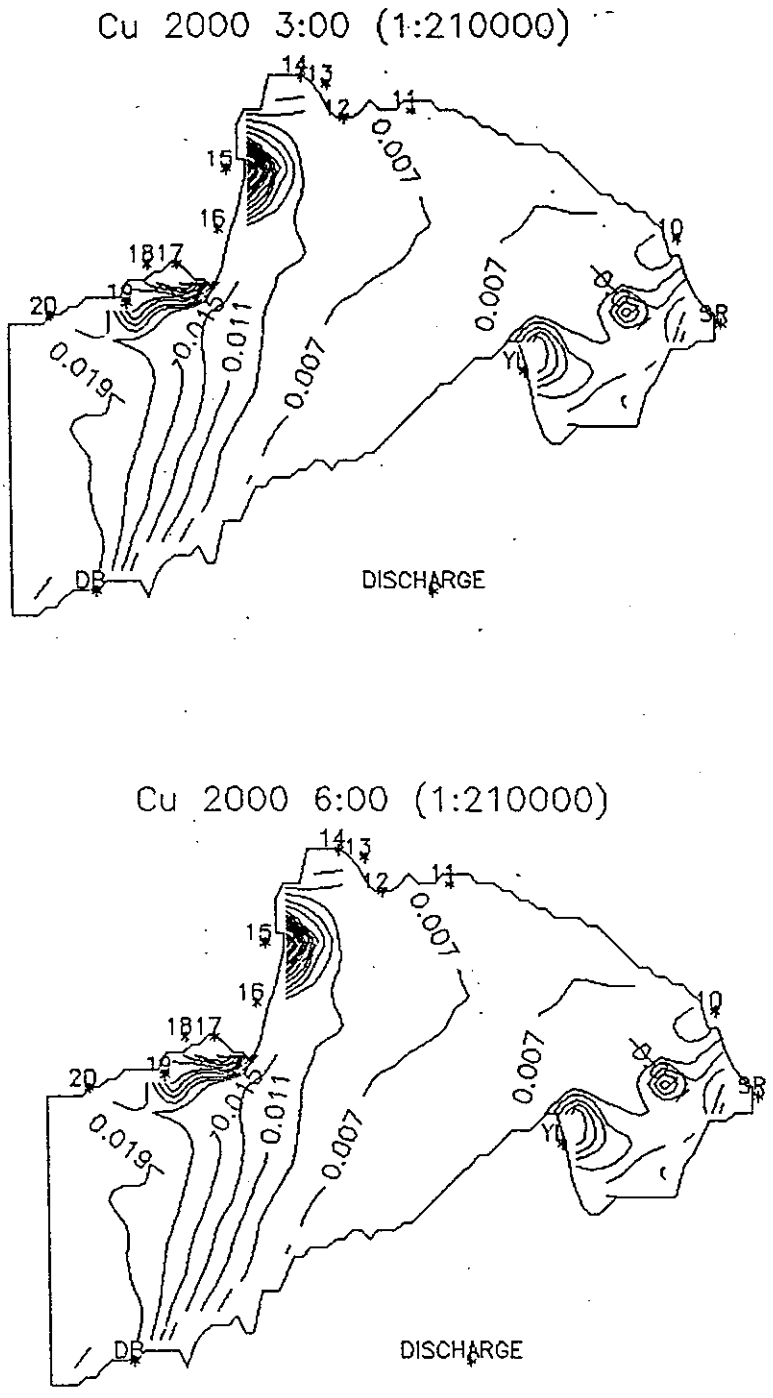

FIG. A7—84(a) **Dynamic variation of Cu in Deep Bay in** 2000

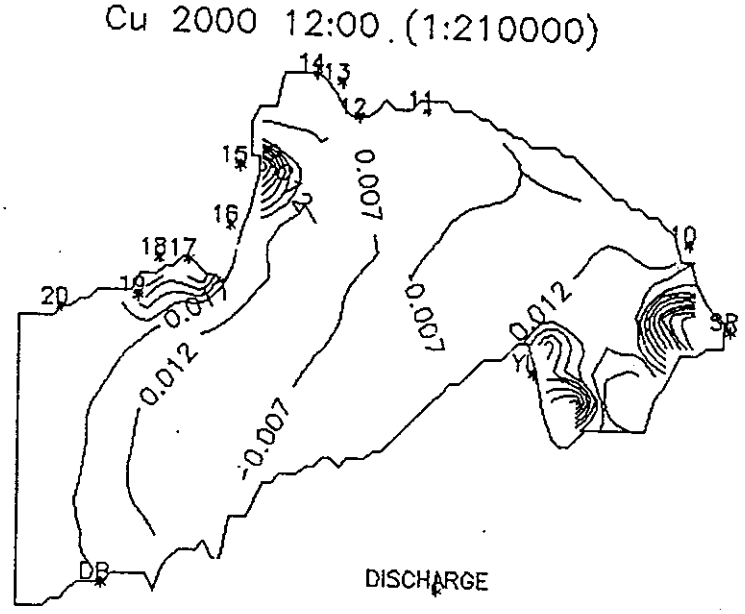

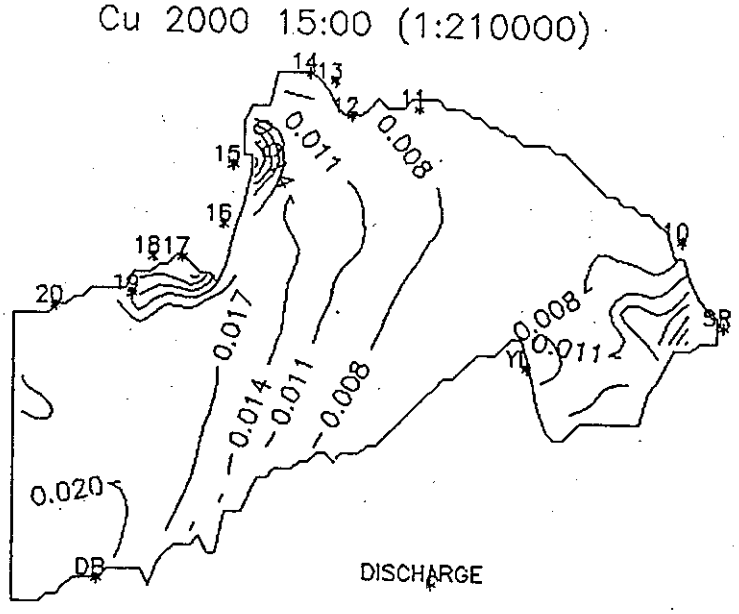

FIG. A7—84(b) Dynamic variation of Cu in Deep Bay in 2000

FIG. A7—85(a) Dynamic variation of Pb in Deep Bay in 2000

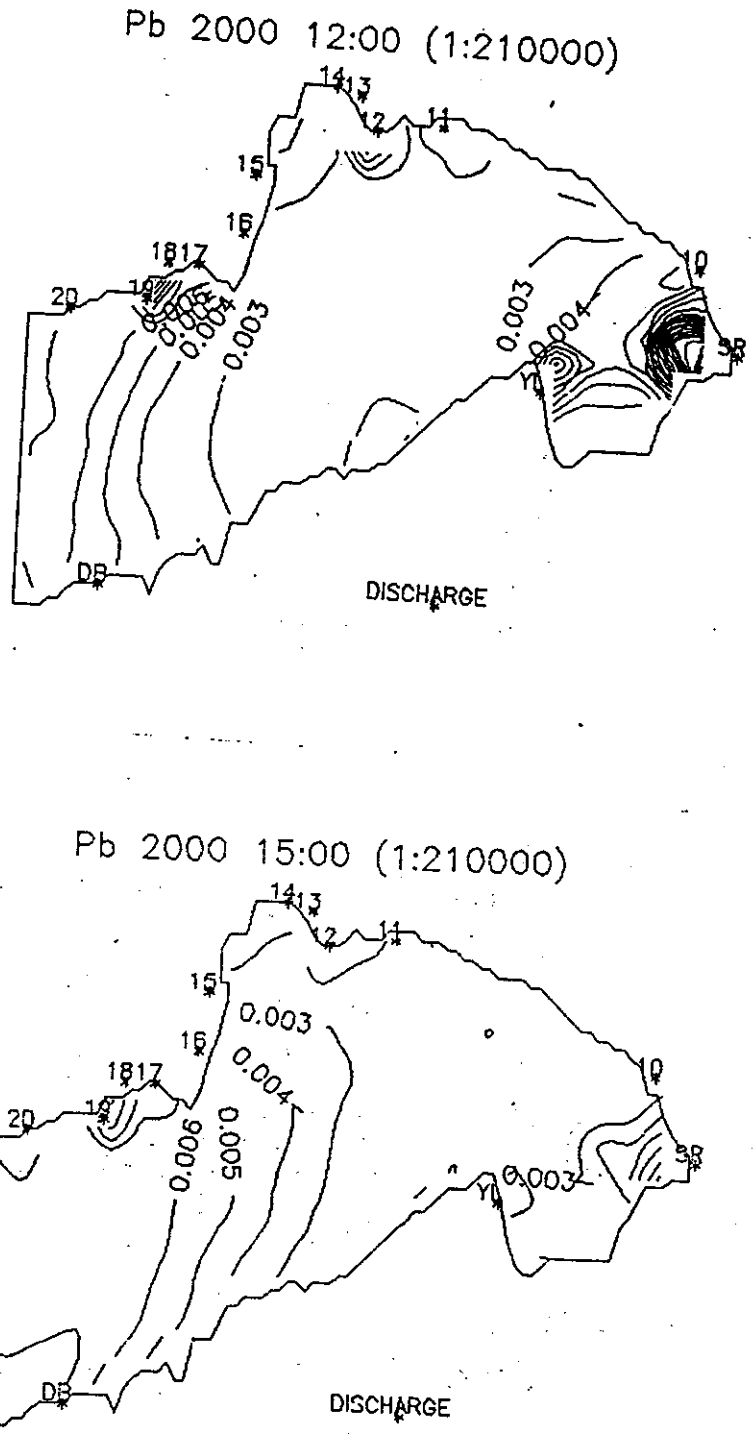

FIG. A7—85(b) Dynamic variation of Pb in Deep Bay in 2000

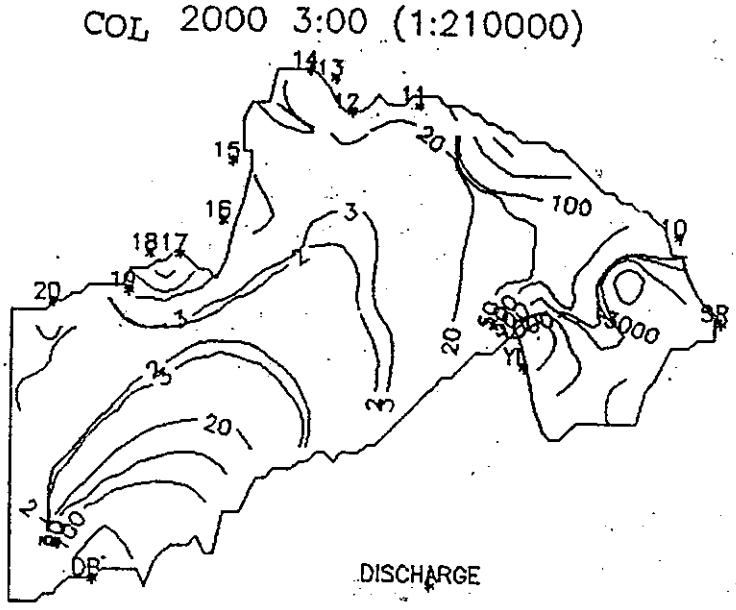

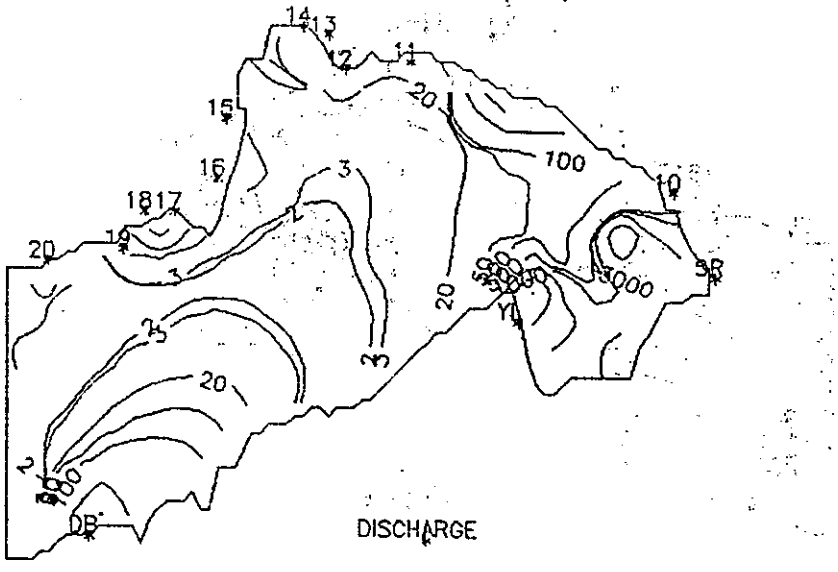

FIG. A7—86(a) Dynamic variation of Col. in Deep Bay in 2000

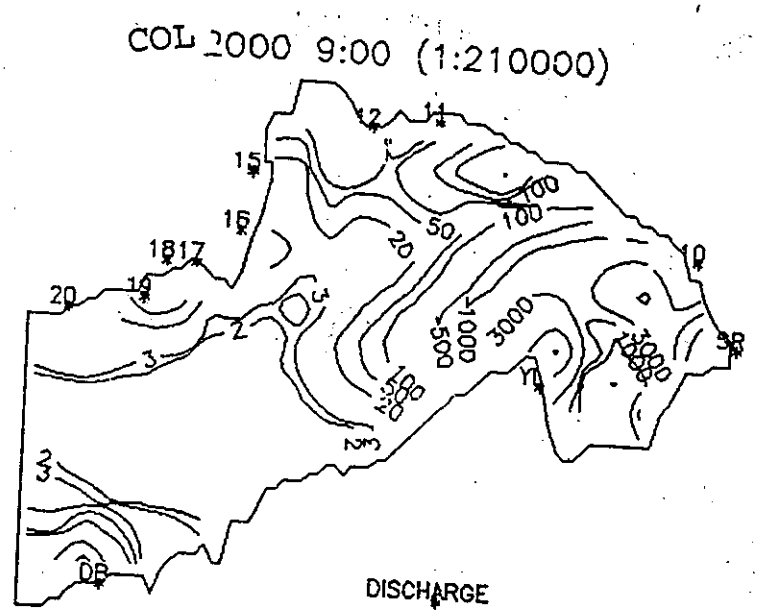

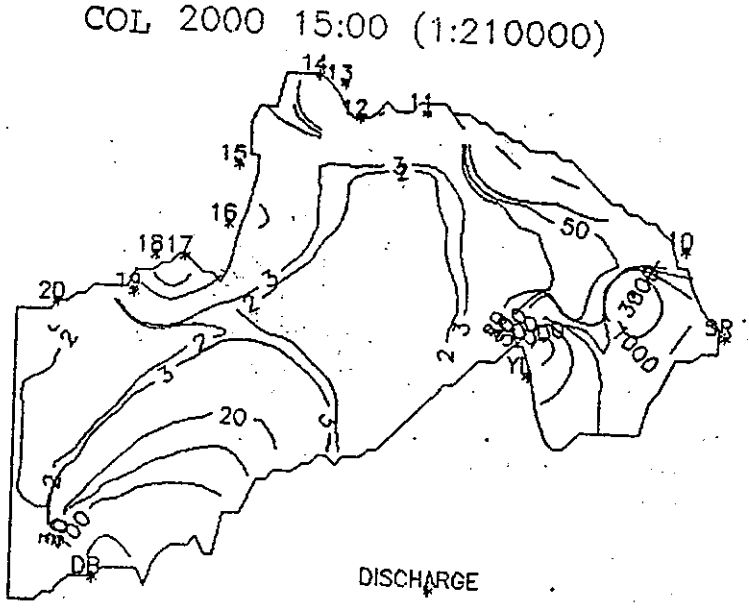

FIG. A7—86(b) Dynamic variation of Col. in Deep Bay in 2000

APPENDIX 8 WATER QUALITY BASELINE AND ASSESSMENT INDEX

A8.1 WATER QUALITY BASELINE OF DEEP BAY

Water quality of Deep Bay was monitored three times from January to October 1994 for dry, wet and normal seasons respectively. The raw data collected are stored in the Database Management System in a diskette attached to this report. The mean values of various parameters for three seasons are summarised in Table A8.1.

Table A8.1 Mean values of monitored parameters for three seasons, Deep Bay, 1994

Season		Wet	Normal	Dry
T	°C	28.4	22.7	18.7
pH		7.9	8.0	7.9
DO	mg/l	4.21	5.11	6.48
BOD_5	mg/l	5.29	2.59	1.97
COD	mg/l	4.85	3.81	1.56
SS	mg/l	54.4	26.5	13.7
turbidity	degree	34.0	39.0	15.3
chlorophyll a	μg/l	nd	1.96	1.78
salinity	g/l	8.4	20.5	26.9
conductivity	μs/cm	13328	32125	42925
NH_3-N	mg/l	2.03	3.91	2.04
NO_2-N	mg/l	0.08	0.08	0.05
NO_3-N	mg/l	0.54	0.13	0.13
TN	mg/l	3.11	8.53	4.13
TP	mg/l	0.51	0.40	0.26
DP	mg/l	0.12	0.19	0.21
Cu	μg/l	23.25	4.58	2.45
Zn	μg/l	na	10.75	2.48
Ni	μg/l	19.40	3.45	4.40
Cd	μg/l	0.17	0.17	0.13
Pb	μg/l	0.95	2.85	0.70
Hg	μg/l	nd	0.04	nd
Oil	mg/l	0.51	na	0.09
Coli.	10^7 c/l	4.0	0.75	0.23
Bacteria	10^3 c/l	nd	2.0	22

nd: under detection limits(see Monitoring Manual)
na: not available due to experimental failure

A8.2 WATER QUALITY BASELINE OF SHENZHEN RIVER

Water quality of Shenzhen was monitored six times from January to October 1994 for dry, wet and normal seasons respectively. The raw data collected are stored in the Database Management System in a diskette attached to this report. The mean values of various

parameters for three seasons are summarised in Table A8.2.

Table A8.2 Mean values of monitored parameters for three seasons, Shenzhen River, 1994

Season		Wet		Normal		Dry	
Tide		Low	High	Low	High	Low	High
T	°C	28.3	28.3	26.9	27.1	18.6	18.3
pH		7.2	7.2	7.3	7.3	7.2	7.4
DO	mg/l	0.48	0.61	0.44	0.55	1.07	0.75
BOD_5	mg/l	53.2	34.0	31.4	37.2	58.8	54.0
COD	mg/l	14.8	13.4	10.1	13.8	20.2	19.8
SS	mg/l	225.2	85.1	119.9	218.4	124.3	142.3
salinity	mg/l	105.6	301.7	95.5	741.2	327.7	1815.4
conductivity	μs/cm	886	3318	2950	6675	10049	8092
NH_3-N	mg/l	10.17	9.39	10.12	10.48	18.86	18.39
NO_2-N	mg/l	0.04	0.02	0.00	0.01	0.00	0.01
NO_3-N	mg/l	0.12	0.06	0.01	0.03	0.03	0.03
TN	mg/l	10.00	11.37	13.16	13.84	22.94	20.79
TP	mg/l	2.11	1.77	1.96	1.95	3.33	3.08
DP	mg/l	0.94	0.82	1.56	1.21	1.88	1.70
Cu	μg/l	18.4	18.4	37.3	53.9	22.5	26.2
Zn	μg/l	117	71	110	118	276	221
Ni	μg/l	29.0	99.3	12.0	14.3	60.0	62.0
Cd	μg/l	0.14	0.09	0.12	0.13	0.07	0.15
Pb	μg/l	14.6	6.08	9.06	16.6	12.6	18.3
Cr	μg/l	25.5	20.4	31.7	40.7	28.8	27.5
Hg	μg/l	0.16	0.21	0.25	0.21	0.19	0.19
As	μg/l	1.78	1.55	3.31	3.81	1.80	1.60
Oil	mg/l	2.81	2.14	2.31	1.43	2.86	2.68
Coli.	10^8 c/l	4	1	0.9	0.6	4	4

A8.3 POLLUTION SHARING RATE

Pollution Sharing Rate is adopted in Section 8 of this report for water quality assessment. It can be used to assess the contribution of various pollutants to the total pollution load. The Pollution Sharing Rate(K_i) can be calculated using following equation.

$$K_i(\%) = \frac{100P_{ij}}{P_j}$$

$$P_j = \sum_{i=1}^{n} P_{ij} \quad , \qquad P_{ij} = \frac{C_{ij}}{C_{io}}$$

where
K_i : Pollution Sharing Rate of ith pollutant
P_j : Integrated Pollution Index on section j
P_{ij} : pollution index of the ith pollutant on section j
C_{ij} : annual mean of the ith pollutant on section j
C_{io} : standard value for the ith pollutant
n : number of pollutants involved

A8.4 ESTIMATION OF DEEP BAY TOPOGRAPHY USING REMOTE SENSING AND GIS TECHNIQUE

A8.4.1 Deep Bay

The average annual precipitation is about 1900 mm. The area of Deep Bay is 115 km^2, with a average depth of 2.9 m and a volume of $3.3x10^8$ m^3. The main river discharges into the bay is Shenzhen River. The Yuan Lang River and Dasha River also afflux into the bay. The main character of the variation of depth in this bay is the northern part, also the inner part, is relatively shallow.

The remote sensing images and GIS technique were used for modelling Deep Bay topography. The results were used in hydrodynamics, sedimentation transport, and water quality modelling.

A8.4.2 Data and Data Process

The data of terrain was gathered from the channel map and terrain map published in 1984 with a scale of 1:50000 by digitalizing. TM images from Landsat were selected. The first set of images were photoed in Jan. 20, 1992, while the second set in Jan. 25, 1994 with a relatively higher tide. The TM sensor has 7 bands, with wavelength listed below:

Band Number	1	2	3	4	5	6	7
Wavelength(μm)	0.45-0.5	0.52-0.6	0.63-0.96	0.76-0.94	0.55-1.75	10.4-12.5	2.08-2.35

The first 3 bands reflect the submarine terrain. The values of these bands has some factional relationship with the depth of water. The main aim of the task was to find out the function between the depth of water and the values of these bands. The 4th and 5th bands are sensitive to the difference between land and water, they were used to determine the land-water boundary.

The data was processed in following steps:

1) Land-water boundary was determined by processing the image of band 4 and 5. value of 1 was assign to the water area and 0 to land area. By multiplying image of band 1,2 and 3 to this two-value image sequentially, three new images in which the land area has only value of 0 and the water area keeps the original value were obtained.

2) The image of band 1-3 was smoothed by smoothing average technique of 4x4 pixels. The effects of scanner line and sampling error of a few pixels were faded.

3) The depth of sample points were taken from terrain map and channel map, the correspondent R.S. values were taken from the R.S. image files. The principle of sampling is to cover all the depth that occur and stress the points where minimum or maximum depth occurs or the depth changes abruptly. 50 sample points were collected in which 30 were used for simulation (Table A8.3) and the remained 20 were used to verify the simulation result. The simulation was performed using polynomial fitting.

Table A8.3 Sample points

No	Depth(dm)	Value of Band 2	Value of Band 3
1	45	29	74
2	37	59	95
3	8	65	118
4	20	49	90
5	22	48	86
7	9	62	113
6	18	51	99
8	9	52	105
9	6	79	137
10	4	74	135
11	7	74	126
12	2	87	136
13	13	59	116
14	20	50	99
15	20	52	101
16	18	50	103
17	25	47	98
18	4	67	118
19	46	29	71
22	20	54	80
21	3	65	115
22	13	47	95
23	35	33	76
24	5	78	112
25	43	86	118
26	4	83	112
27	9	58	112
28	18	49	95
29	13	52	103
30	5	80	113

4) The result of polynomial fitting was rechecked by the method of goodness of fitting. The calculated depths were compared with the real values from terrain and channel maps. If the fitting results was not satisfied, additional sample points were taken and the fitting process was repeated. Table A8.4 shows the final result of polynomial fitting. The polynomial function is:

$$Z = -128.4255 - 9.3023x + 10.87y - 0.6399x^2 + 0.2510xy - 0.1846y^2 + 0.006568x^2y - 0.005102xy^2 + 0.001596y^3$$ (x is value of band 2 and y is value of band 3)

5) Two different mapping methods on the two set of images were used for comparison. Spaceman, a GIS system, was used to process the first set of images. The depth data were first transformed into to DEM format and 3-dimensional terrain map (VGA 16-color) was generated. As to the second set of images, GIS tools running under WINDOWS were employed to process the data (RGB True Color). Since the maximum depth is 6 m, the whole range of depth was divide into 12 classes each of which covers a range of 0.5 m. The RGB color tuning and color composition were then performed.

A8.4.3 Discussion

The digital map is able to reflects the submarine terrain. for example, the channel in SE part of the bay, the shoal in the northeastern part of the bay, and the river mouth bar are all clearly shown on the map. The map also matches the condition of water dynamic and provenance. The difference between the two maps shows the changes of submarine terrain with time.

The error of simulated depth is relatively larger at a small number of points, the maximum error is about 0.8 m. The reasons is:

a The terrain map, published in 1984, may not reflect the real situation today.

b Simulation is a method which minimizes total error on all points, so the simulated values at some location may have relatively larger error.

c There was inevitable error on the R.S. images, for example, the scanner lines.

In general, the digital maps represent the submarine terrain with a relatively high accuracy. The average error is about 0.1 to 0.2 m, the horizontal resolution is 30 m.

Table A8.4 The results of fitting (the goodness of fitting: 0.95905120, sample size: 30)

No	Depth Simulated	Real Depth	Error
1	45.187	45.000	0.187
2	18.864	27.000	-8.136
3	6.293	8.000	-1.707
4	21.484	20.000	1.484
5	23.500	22.000	1.500
6	8.216	9.000	-0.784
7	16.641	18.000	-1.359
8	14.724	9.000	5.724
9	4.506	6.000	-1.494
10	6.565	4.000	2.565
11	4.018	7.000	-2.982
12	2.076	2.000	0.076
13	9.587	13.000	-3.413
14	17.180	20.000	-2.820
15	15.455	20.000	-4.545
16	16.709	18.000	-1.291
17	19.922	25.000	-5.078
18	6.158	4.000	2.158
19	43.295	46.000	-2.705
20	21.147	20.000	1.147
21	7.322	3.000	4.322
22	20.311	13.000	7.311
23	37.616	35.000	2.616
24	9.212	5.000	4.212
25	1.083	3.000	-1.917
26	2.522	4.000	-1.478
27	9.860	9.000	0.860
28	19.117	18.000	1.117
29	14.916	13.000	1.916
30	7.513	5.000	2.513

APPENDIX 9 SEDIMENT QUALITY AND SEDIMENTATION RATE

A9.1 SOIL AND SEDIMENT QUALITY

Samples of sediment and bank soil in study area were collected and analyzed during this study. Sediment samples were collected from Shenzhen River, Deep Bay, fish pond, and gei wai. Sampling locations are indicated in Figure 4.3. Raw data can be found in Database Management System in diskette format which is attached to this report. The results are also tabulated Table A9.1 and A9.2, respectively. Metal contents of river sediment from routing monitoring conducted by Shenzhen Environmental Station from 1991 to 1993 are also presented in Table A9.3. Data in Table A9.4 are measured PAH contents in both soil and sediment samples.

Table A9.1 Bank soil quality of Shenzhen River (mg/kg)

Sample No.	S1	S2	S3
T (C°)	25.2	26.4	25.4
Org. Matter (%)	2.39	0.68	2.39
Eh (mv)	248.8	411.4	422.2
pH	5.70	6.30	6.15
Cu	77.9	17.2	24.1
Zn	567.8	117.8	124.0
Ni	34.4	24.5	24.3
Cd	0.664	0.081	0.059
Pb	80.2	59.6	55.7
Cr	84.3	46.9	51.5
Hg	0.290	0.039	0.123
As	9.267	9.158	7.046
DDT	nd	nd	nd
HBC	0.53	0.01	0.05

nd: under detection limits (DDT: 0.02mg/kg)

Table A9.2 Sediment monitoring results of Shenzhen River and Deep Bay(mg/kg)

Sample No.	B1	B2	B3	B4	B5	B6	B7	B8
T (C°)	26.0	26.0	25.8	26.4	26.0	25.5	na	na
Org. Matter (%)	5.84	1.67	2.59	2.65	2.76	0.83	3.43	3.43
Eh (mv)	-63.2	-157.6	-40.0	-154.4	-94.4	na	na	na
pH	7.3	7.12	7.31	8.10	8.02	6.67	6.80	6.80
Cu	133.4	36.9	78.1	86.7	57.7	21.7	31.2	29.9
Zn	545.2	171.7	268.5	261.7	221.7	122.7	168.0	164.7
Ni	53.9	28.8	39.5	36.8	38.7	23.1	42.3	42.3
Cd	0.397	0.259	0.214	0.300	0.137	0.079	0.104	0.087
Pb	79.3	38.7	70.3	68.8	72.6	49.0	71.7	79.3
Cr	135.9	69.8	82.5	85.9	93.2	53.0	95.0	95.6
Hg	0.357	0.150	0.209	0.491	0.195	0.071	0.140	0.159
As	8.937	7.320	4.584	6.306	7.591	5.711	12.159	13.482
DDT	nd	nd	nd	nd	nd	nd	nd	nd
HBC	nd	nd	nd	nd	nd	5.77	nd	nd

nd: under detection limits (DDT: 0.02mg/kg, HBC: 0.01mg/kg)
na: not available due to experimental failure

Table A9.3 Heavy metal contents in sediment (routine monitoring 1991-1993, mg/kg)

Year	Sample No.	As	Hg	Pb	Cd	Cu	Zn	Cr
1991	B2	9.9	0.64	85.1	0.26	178	366	61.9
	B4	9.9	0.19	83.8	0.31	138	286	71.2
1992	B2	13.1	0.44	110	0.83	269	566	63.6
	B4	14.1	0.19	109	0.99	102	721	38.4
1993	B2	16.5	0.3	102	0.43	207	523	106
	B4	13.1	0.14	82	0.24	99	308	65

Table A9.4 PAH concentrations in sediments from Shenzhen River (μg/kg)

Sample No.	S1	S2	S3	B1	B2	B3	B4	B5	B6	B7	B8
Naphthalene	20.6	26.4	20.7	7.4	8.7	7.9	24.2	9.4	24.6	16.7	1.7
Dibydroacenaphthene	15.7	22.5	15.8	9.8	1.4	17.6	22.3	28.4	21.6	2.3	nd
Acenaphthene	46.1	nd	34.5	nd	19.7	nd	79.5	56.7	43.3	13.9	nd
Fluorene	2.6	5.8	0.5	0.5	1.6	1.9	2.5	4.5	4.2	2.1	0.7
Phenanthrene	2.2	nd	2.8	nd	1.0	dn	nd	nd	2.6	1.3	0.9
Anthracene	1.1	34.0	3.3	0.6	2.2	0.4	nd	nd	2.3	0.7	nd
Fluorancene	11.8	7.5	6.9	nd	nd	nd	nd	nd	6.7	2.1	4.7
Pyrene	7.2	4.5	5.2	nd	nd	nd	nd	nd	3.6	1.6	1.5
Benzoanthracene	nd	2.7	2.8	6.2	0.9	8.6	nd	nd	nd	1.1	nd
Chrysene	nd	nd	nd	5.5	nd	7.2	4.6	2.6	nd	0.7	0.5
Benzofluoranthcene	nd	2.2	nd	8.3	nd	9.8	nd	nd	5.3	2.8	3.0
Benzopyrene	2.9	nd	2.2	nd	nd	nd	nd	nd	nd	1.7	1.7
Dibenzopyrene	nd	nd	nd	nd	nd	nd	nd	nd	nd	nd	nd
Indenopyrene	nd	nd	nd	nd	nd	nd	2.2	1.9	nd	nd	nd
Benzo(ghi)pyrene	nd	nd	nd	nd	nd	nd	4.9	nd	nd	nd	nd

nd: non-detectable

A9.2 VERTICAL DISTRIBUTION OF METAL AND PESTICIDE CONTENTS ALONG SEDIMENT PROFILE

Sediment core samples were collected from five locations along Shenzhen River (sampling locations are given in Figure 4.3). The depth of the cores were from 33mm to 60mm. Pb, Cd, Hg, Ni, Zn, Cr, and Cu contents were measured to determine the vertical variation in heavy metal contamination of the bottom sediment. The results are tabulated in Table A9.5.

Contents of HBC and DDT were measured for C2 and C3 profiles. The results are given in Table A9.6

Table A9.5 Vertical distribution of metal contents along sediment core profile (mg/kg)

Sample No.	Depth(cm)	Cd	Cr	Ni	Pb	Zn	Cu	Hg
C1	3	0.40	74.4	38.0	72.4	270.2	54.6	0.23
	9	0.36	36.7	13.0	70.8	152.4	28.1	0.33
	15	0.31	101.2	44.0	70.8	353.8	64.0	0.44
	21	0.40	64.4	36.0	67.2	342.0	96.6	0.40
	27	0.74	96.4	38.0	78.0	393.4	128.2	0.70
	33	0.67	99.6	42.0	78.6	408.4	98.6	0.50
C2	5	0.86	43.0	32.0	89.6	290.4	42.0	0.46
	10	0.89	55.0	28.0	95.4	330.8	56.8	0.36
	25	0.42	86.6	34.0	108.4	524.6	281.8	0.42
	35	0.39	64.0	26.0	132.8	619.0	126.8	0.44
	45	0.70	69.4	34.0	116.2	639.8	82.0	0.66
C3	6	0.33	55.4	20.0	73.4	258.2	53.2	0.25
	18	0.43	59.0	26.0	60.8	274.8	67.4	0.44
	30	0.41	46.1	19.0	80.4	269.5	50.2	0.20
	42	0.37	48.6	18.0	81.8	378.0	49.2	0.72
	60	0.31	56.8	22.0	49.0	242.8	73.4	0.25
C4	6	0.05	98.1	29.0	130.8	222.6	39.8	0.27
	18	0.22	98.6	25.0	117.5	199.7	38.6	0.38
	30	0.14	95.9	27.0	98.6	232.2	37.8	0.46
	42	0.51	93.6	16.0	81.2	154.2	32.8	0.19
	54	0.04	98.0	18.0	93.2	168.4	35.2	0.36
C5	6	0.03	94.6	22.0	98.8	263.8	558	0.34
	18	0.47	83.8	38.0	100.8	237.2	46.6	0.32
	30	0.89	74.6	26.0	111.9	315.9	50.5	0.32
	42	0.81	92.6	40.0	88.6	205.6	43.6	0.40
	54	0.78	91.0	28.0	97.6	213.0	42.2	0.40

Table A9.6 Vertical distribution of HBC and DDT contents along sediment core samples (μg/kg)

Sample No.	Depth (cm)	HBC-α	HBC-β	HBC-γ	HBC-δ	ΣHBC	p,p'-DDE	p,p'-DDD	p,p'-DDT	ΣDDT
C2	5	11.4	nd	nd	nd	5.5	4	nd	nd	4
	10	3.6	nd	nd	nd	6.6	2	nd	nd	2
	25	3.1	nd	nd	nd	7.9	nd	nd	nd	nd
	35	11.4	nd	5.7	nd	3.0	2	nd	nd	2
	45	2.8	nd	2.6	2.5	14.0	2	nd	nd	2
C3	6	5.5	nd	nd	nd	5.5	4	nd	nd	4
	18	6.5	nd	nd	nd	6.6	2	nd	nd	2
	30	7.0	nd	0.9	nd	7.9	nd	nd	nd	nd
	42	2.1	nd	0.9	nd	3.0	2	nd	nd	2
	60	8.8	nd	2.7	2.5	14.0	2	nd	nd	2
detection limit		0.2	6	0.4	0.5		2	6	10	

nd: non-detectable

A9.3 HAKANSON'S SEDIMENT ASSESSMENT METHOD

The method refers to Sweden scientist Hakanson's Potential Ecological Hazards Assessment (Hakanson, 1981). The Potential Ecological Risk Index (RI) calculated using this procedure is an integrated indicator to the potential hazards of the sediment to terrestrial ecosystem.

The Potential Ecological Risk Index is a sum of Potential Ecological Risk Factors (E_i) of individual heavy metals. RI and E_i can be calculated using following equations:

$$RI = \sum E_i \quad , \qquad E_i = T_i C_i \quad , \qquad C_i = \frac{C_{mi}}{C_{ri}}$$

where T_i, C_i, C_{mi}, and C_{ri}, are Toxic Response Factor, Factor of Contamination, measured content in the sediment, and Reference Value of the ith metal, respectively.

The preindustrialisation maximum background contents of heavy metals tabulated in Table A9.7 are commonly used as Reference Values. Toxic Response Factors suggested by Hakanson (Table A9.7) were derived based on results of toxicity tests and global abundances of the heavy metals.

Table A9.7 Reference values and toxic response factors used in Hakanson's method

Heavy Metal	Cu	Cd	Pb	Zn	Cr	As	Hg
Reference Value, C_{ri} (mg/kg)	50	1.0	70	175	90	15	0.25
Toxic Response Factor, T_i	5	30	5	1	2	10	40

Base on calculated Potential Ecological Risk Index, the potential impact of heavy metals in the sediment can be evaluated using criteria listed in Table A9.8.

Table A9.8 Criteria for sediment assessment based on RI

Potential Ecological Pollution Index	Degree of Ecological Hazard
<150	Mild Ecological Hazard
150-300	Medium Ecological Hazard
300-600	Serious Ecological Hazard
>600	Very Serious Ecological Hazard

A9.4 SEDIMENTATION RATES IN SHENZHEN RIVER ESTUARY

A9.4.1 Introduction

Interest in the history of recent sedimentological events has focused on applications of the naturally occurring radionuclide, ^{210}Pb, as a geochemical tracer to determine sedimentation rates in lakes, estuaries, and coastal marine sediments.

^{210}Pb occurs naturally as one of the radioisotopes in the ^{238}U decay series. Radioactive disequilibrium between ^{210}Pb and its parent isotope, ^{226}Ra (half-life 1,600 years), arises through the intermediate gaseous isotope ^{222}Rn. A proportion of the ^{222}Rn formed by ^{226}Ra decay in soils diffuses into the atmosphere where it decays to ^{210}Pb. This is precipitated onto the land or water surface and into lakes, estuaries, or coastal marine where it is adsorbed onto sedimentary particles. ^{210}Pb activity in sediments in excess of the fraction that derived from decay of the *in situ* ^{226}Ra is called unsupported ^{210}Pb. It declines in accordance with the exponential radioactive-decay law and can be used for age determinations provided there is an appropriate model for estimating the initial activity. The ^{210}Pb half-life of 22.26 years makes it suitable to dating sediments laid down over the past 100-150 years. Unsupported ^{210}Pb is measured by subtraction of ^{210}Pb supported by the parent ^{226}Ra from the total ^{210}Pb activity.

A9.4.2 Methodology

Five short sediment cores with length of 28-54 cm were taken from Shenzhen River Estuary during Oct. 11-14, 1994 (Figure 4-6). The cores were sampled at interval of 1 cm. Special attention has been paid to the area of mudflats near the river mouth. Low-background gamma counting procedure was used to measure naturally occurring levels of ^{210}Pb in sediment samples because sample preparation is simple and non-destructive.

A9.4.3 Results

Sedimentation rates at five locations were calculated based on measured ^{210}Pb. The results are tabulated in Table A9.9. The raw data of ^{210}Pb activities at various depth in sediment cores are given in Table A9.10. The sedimentation rate in the area is increasing from 0.95-1.81 cm/yr a decade ago to 2.84-3.68 cm/yr now. The maximum accumulation rate was observed at river mouth (SR5).

Table A9.9 ^{210}Pb activities measured in sediment cores

Core No.	SR1		SR2		SR3		SR4	SR5
Depth Interval (cm)	0-40	40-52	0-21	21-44.5	0-20	20-31	0-51	0-51
Mass-depth Interval (g/cm^2)	0-33.753	33.753-45.211	0-17.439	17.439-39.395	0-23.378	23.378-35.355	0-40.669	0-45.551
Age Interval (yr)	0-12.0	12.0-18.6	0-6.8	6.8-26.8	0-7.0	7.0-11.7	0-16.8	0-13.8
Accumulation Speed (cm/yr)	3.33	1.81	3.12	1.28	2.84	0.95	3.04	3.68
Accumulation Rate ($g/cm^2.yr$)	2.81	1.73	2.58	1.10	3.32	1.03	3.68	3.29

Table A9.10 Sediment accumulation rates at various locations

Core No.	Depth (cm)	Mass-Depth (g/cm^2)	Total ^{210}Pb (dpm/g)	^{210}Pb excess (dpm/g)
SR1	1-2	0.879	4.71	2.71
	4-5	2.905	4.20	2.20
	9-10	7.233	4.75	2.75
	14-15	11.342	4.25	2.25
	22-23	17.791	4.12	2.12
	29-30	24.016	3.99	1.99
	42-43	36.328	3.57	1.57
	46-47	41.015	3.50	1.50
	49-50	44.527	3.35	1.35
SR2	1-2	1.023	3.78	1.78
	4-5	3.240	3.40	1.40
	9-10	7.050	3.48	1.48
	14-15	11.274	3.47	1.47
	22-23	18.584	3.46	1.46
	26-27	22.148	2.84	0.84
	29-30	24.914	2.91	0.91
	34-35	29.130	2.16	0.16
	39-40	33.798	2.45	0.45
	41-42	35.822	3.37	1.37
	44-44.5	38.802	2.60	0.60
SR3	1-2	2.195	3.81	1.81
	4-5	5.723	4.18	2.18
	9-10	11.533	3.56	1.56
	14-15	17.143	3.76	1.76
	17-18	20.561	3.63	1.63
	22-23	25.890	3.45	1.45
	26-27	30.105	3.26	1.26
	28-29	32.524	3.16	1.16
	30-31	34.679	3.12	1.12
SR4	1-2	0.616	4.32	2.32
	4-5	3.059	3.96	1.96
	9-10	7.566	3.49	1.49
	14-15	12.572	3.24	1.24
	22-23	18.657	4.25	2.25
	29-30	24.368	3.02	1.02
	34-35	28.354	3.80	1.80
	42-43	34.455	3.50	1.50
	46-47	37.749	3.56	1.56
	49-50	40.004	2.80	0.80
SR5	1-2	1.044	3.80	1.80
	4-5	3.327	3.04	1.04
	9-10	7.788	3.06	1.06
	14-15	12.350	3.45	1.45
	22-23	19.151	3.23	1.23
	29-30	26.165	2.88	0.88
	34-35	31.455	2.83	0.83
	46-47	42.279	2.93	0.93
	50-51	45.198	3.03	1.03